frontiers | Research Topics

# Microbial response to a rapidly changing marine environment: Global warming and ocean acidification, volume II

**Edited by**
Mi Sun Yun, Jun Sun, Connie Lovejoy and Sang Heon Lee

**Published in**
Frontiers in Microbiology
Frontiers in Marine Science

ISSN 1664-8714
ISBN 978-2-83251-064-3
DOI 10.3389/978-2-83251-064-3

## About Frontiers

Frontiers is more than just an open access publisher of scholarly articles: it is a pioneering approach to the world of academia, radically improving the way scholarly research is managed. The grand vision of Frontiers is a world where all people have an equal opportunity to seek, share and generate knowledge. Frontiers provides immediate and permanent online open access to all its publications, but this alone is not enough to realize our grand goals.

## Frontiers journal series

The Frontiers journal series is a multi-tier and interdisciplinary set of open-access, online journals, promising a paradigm shift from the current review, selection and dissemination processes in academic publishing. All Frontiers journals are driven by researchers for researchers; therefore, they constitute a service to the scholarly community. At the same time, the *Frontiers journal series* operates on a revolutionary invention, the tiered publishing system, initially addressing specific communities of scholars, and gradually climbing up to broader public understanding, thus serving the interests of the lay society, too.

## Dedication to quality

Each Frontiers article is a landmark of the highest quality, thanks to genuinely collaborative interactions between authors and review editors, who include some of the world's best academicians. Research must be certified by peers before entering a stream of knowledge that may eventually reach the public - and shape society; therefore, Frontiers only applies the most rigorous and unbiased reviews. Frontiers revolutionizes research publishing by freely delivering the most outstanding research, evaluated with no bias from both the academic and social point of view. By applying the most advanced information technologies, Frontiers is catapulting scholarly publishing into a new generation.

## What are Frontiers Research Topics?

Frontiers Research Topics are very popular trademarks of the *Frontiers journals series*: they are collections of at least ten articles, all centered on a particular subject. With their unique mix of varied contributions from Original Research to Review Articles, Frontiers Research Topics unify the most influential researchers, the latest key findings and historical advances in a hot research area.

Find out more on how to host your own Frontiers Research Topic or contribute to one as an author by contacting the Frontiers editorial office: frontiersin.org/about/contact

# Microbial response to a rapidly changing marine environment: Global warming and ocean acidification, volume II

**Topic editors**

Mi Sun Yun — Tianjin University of Science and Technology, China
Jun Sun — China University of Geosciences Wuhan, China
Connie Lovejoy — Laval University, Canada
Sang Heon Lee — Pusan National University, South Korea

**Citation**

Yun, M. S., Sun, J., Lovejoy, C., Lee, S. H., eds. (2023). *Microbial response to a rapidly changing marine environment: Global warming and ocean acidification, volume II*. Lausanne: Frontiers Media SA. doi: 10.3389/978-2-83251-064-3

# Table of contents

frontiers | Frontiers in Microbiology

TYPE Editorial
PUBLISHED 01 December 2022
DOI 10.3389/fmicb.2022.1094511



OPEN ACCESS

EDITED AND REVIEWED BY
Rachel Ann Foster,
Stockholm University, Sweden

*CORRESPONDENCE
Mi Sun Yun
misunyun@pusan.ac.kr

SPECIALTY SECTION
This article was submitted to Aquatic Microbiology, a section of the journal Frontiers in Microbiology

RECEIVED 10 November 2022
ACCEPTED 21 November 2022
PUBLISHED 01 December 2022

CITATION
Yun MS, Sun J, Lovejoy C and Lee SH (2022) Editorial: Microbial Response to a Rapidly Changing Marine Environment: Global Warming and Ocean Acidification, Volume II. *Front. Microbiol.* 13:1094511. doi: 10.3389/fmicb.2022.1094511



# Editorial: Microbial Response to a Rapidly Changing Marine Environment: Global Warming and Ocean Acidification, Volume II

Mi Sun Yun[1]*, Jun Sun[1,2], Connie Lovejoy[3] and Sang Heon Lee[4]

[1]Institute for Advanced Marine Research, China University of Geosciences, Guangzhou, China, [2]College of Marine Science and Technology, China University of Geosciences, Wuhan, China, [3]Département de Biologie, Université Laval, Quebec, QC, Canada, [4]Department of Oceanography, Pusan National University, Busan, South Korea

KEYWORDS

**microbial community, marine environment, ecosystem, warming, ocean acidification**

Editorial on the Research Topic
Microbial response to a rapidly changing marine environment: Global warming and ocean acidification, volume II

## Introduction

Warming and acidification are representative of ongoing pronounced changes in the world's oceans today. Increasing sea water temperature adjusts basal metabolic rates or physiological status of marine organisms (Reid et al., 2019), and potentially forces some species to shift their distribution ranges (Benedetti et al., 2021). Ocean acidification results in physiological stress of organisms, inhibits their growth, and decreases biological calcification rates, although the degree and direction of these effects vary among taxonomic groups. For this Research Topic, we have focused on the responses of microbial communities. As a vital component of the marine ecosystem microbes play pivotal roles, not only in pathways of energy transfer through the food web but also in global biogeochemical cycles (e.g., Falkowski and Raven, 2013). This Research Topic was conceived to contribute to the understanding of present and future changes in microbial communities in recognition of ongoing warming and acidifying oceanic conditions.

The first volume of this Research Topic on *Microbial response to a rapidly changing marine environment: Global warming and ocean acidification* was launched in 2020 with a total of 10 articles published, covering the wide scope of physiological and ecological responses of diverse taxonomic groups to environmental changes in a range of geographic regions, as summarized in our Editorial (Yun et al., 2021). Due to the success of the first volume, we launched volume II of the Research Topic in 2021. We now add

a total of 11 new fascinating articles of which many expand our knowledge on specific aspects of physiological responses to environmental changes. Several articles focused on the alterations of dissolved organic matter (DOM) by bacteria and algae under warming and acidifying conditions, and other works used ecological and model based approaches to examine spatio-temporal dynamics.

## Overview of manuscripts in this Research Topic

Out of the 11 new contributions published, six are focused on the physiological or metabolic response of various microbial groups through field observations or laboratory trials. Billaud et al. demonstrated the effect of elevated seawater temperature on the expression of genes implicated in adhesion and biofilm formation on abiotic surfaces in a strain of *Vibrio parahaemolyticus*. The authors showed that increasing temperature triggers a rapid and transient expression of genes coding for adhesion to plastic surfaces and biofilm development, especially for free living cells. Liang et al. described the physiological and biochemical changes in *Nannochloropsis oceanica* in response to short- and long-term acidification conditions. They found that *N. oceanica* used specific mechanisms to adapt to acidification by regulating carbon and nitrogen metabolism, or changing cellular metabolic components (e.g., fatty acid synthesis). The composition, concentration, and production rates of phytoplankton pigments in the warming and oligotrophic Philippine Sea were investigated by Lee et al. They found that photosynthetic pigments had a significantly faster turnover rate at the surface to harness light energy to repair PSII subunits damaged by strong light. Their findings emphasized the importance of light conditions on phytoplankton physiology in warming ocean scenarios. The responses of phytoplankton photophysiology to nitrogen availability and light conditions at the Subsurface Chlorophyll Maximum (SCM) in the Arctic Ocean were described by Ko et al. The results showed a decrease in nutrient availability in the SCM reduces the photosynthetic activity and large size fraction of phytoplankton. They anticipated that alterations in nutrient flux and light conditions in the SCM in the future Arctic Ocean would be important for regulating phytoplankton photosynthesis and primary production. Calbet et al. presented the effect of thermal stress on the growth, ingestion, and respiration rates of three dinoflagellates. They discussed how the response of the different physiological rates to temperature is species- and strain dependent. The importance of distinguishing the effects of long-term adaptation vs. short-term acclimation of marine mixoplankton and protozooplankton to temperature was verified by Calbet and Saiz. They concluded that in protistan grazers, adaptation to temperature confers a selective advantage to warming within a narrow range (i.e., ca. +3°C). Attempts to adapt to much higher temperatures (i.e., +6°C) do not confer any clear physiological advantage within the temporal framework of their experiments (with few exceptions, e.g., the mixotroph *K. armiger*). Their work expanded our knowledge of protist response to predicted increases in ocean surface temperatures.

Other laboratory-based studies, discussed transformations of DOM derived from bacteria and algae under conditions of warming and acidification. For example, Liu et al. investigated the involvement of the bacterium *Bacillus pumilus* in the production and transformation of the DOM derived from cultures of the diatom *Skeletonema dohrnii*. The results showed that under higher temperature and partial pressure of carbon dioxide ($pCO_2$) conditions, *S. dohrnii*-derived DOM was dominated by a protein-like signal, which slowly waned over time, becoming increasingly humic-like. Zhang et al. presented data from *Synechococcous* sp., culture experiments, with and without bacteria present, to examine changes in DOM pools at different temperatures. The results showed that warming could enhance the bioavailability of the *Synechococcus* derived DOM, which may be tempered by the involvement of heterotrophic bacteria. The study provided insight into preservation or persistence of the organic carbon pool in the oceans.

Two studies showed details of spatio-temporal dynamics and environmental drivers related to biogeochemical cycles. Kim et al. conducted *in-situ* observations of the temporal dynamics of carbon and nitrogen uptake rates by phytoplankton in Marian Cove, Antarctica. Their results showed that the strong temporal shifts in phytoplankton carbon and nitrogen assimilation were influenced by wind stress. The response of planktonic ciliate communities in the Pacific Arctic Region was presented in the study of Wang et al. The authors suggested that temperature, which is influenced by hydrographic conditions, has a significant role in determining the aloricate and tintinnid ciliate species composition, with Pacific microzooplankton communities moving north with North Pacific waters. Finally, a model was used to assess the impact of ocean acidification on the size-specific growth of diatoms. Zhang and Luo constructed a theoretical model to understand size-specific growth of diatoms under increasing $CO_2$ scenarios. The model revealed a unimodal relationship between the simulated growth rate response (GRR) and cell size. The model further revealed that the "optimal" cell size corresponding to peak GRR increased with the magnitude of $CO_2$ increase. This metric then diminished with higher cellular carbon demand, leading to a projection of the smallest optimal cell size in the equatorial Pacific upwelling zone. Their study proposed a competitive advantage for middle-sized diatoms, which could be useful in forecasting changes in the diatom community in future acidified high-$CO_2$ oceans.

## Conclusion

In recent years, global attention has been turned toward ocean warming and acidification. As a result, studies reporting effects of these environmental perturbations have proliferated, but most of these studies have focused on single marine organisms and fewer on ecosystems (Raven and Beardall, 2021). This Research Topic was aimed to address this imbalance, to showcase how warming and acidification may alter marine microbial ecosystem structure and function. The studies in this Research Topic and similar studies of microbial responses to rapid environmental changes will contribute to understanding general responses of marine ecosystems to global climate change, including warming and acidification. In volume II of this Research Topic, we explored some of the diversity of physiological and metabolic responses of microbes to changing temperature and carbonate chemistry. Taken as a whole, the articles that make up these two volumes have shown that ongoing and future changes lead to profound consequences for microbial communities.

The mechanisms and processes employed by microbial communities and specific microbes to respond to environmental changes or gradients are highly diverse and complex (Dang et al., 2019). Articles in the Research Topic indicated some of the pressing issues and questions related to microbial response to changing ocean conditions. We, the editors, hope that the two volumes of this Research Topic will form the basis of further discussions and will foster future cross-disciplinary research on the effects of global warming and ocean acidification on marine microbes and ecosystems. Finally, we would like to emphasize the importance of long-term surveys, systematic analyses, and modeling to identify biological responses, feedback, and interactions that will continue to improve projections of microbial and ecosystem responses to climate change.

## Author contributions

MY wrote the draft, with input from JS, SL, and CL. The final version was revised by CL. All authors listed have made a substantial, direct, and intellectual contribution to the work and approved it for publication.

## Funding

MY and JS acknowledge funding from the National Key R&D Program of China (2019YFC1407805) and the National Nature Science Foundation of China (41876134). CL acknowledges funding from the Natural Sciences and Engineering Council (NSERC) Canada. Research support for SL was provided by the project titled KIOS (Korea Indian Ocean Study): Korea-US Joint Observation Study of the Indian Ocean, funded by the Korean Ministry of Oceans and Fisheries (20220548, PM63180).

## Acknowledgments

We thank all the contributing authors and reviewers to this Research Topic. Also, we would like to thank the Journal's Editorial Team for their professional support throughout.

## Conflict of interest

The authors declare that the research was conducted in the absence of any commercial or financial relationships that could be construed as a potential conflict of interest.

## Publisher's note



## References

Benedetti, F., Vogt, M., Elizondo, U. H., Righetti, D., Zimmermann, N. E., and Gruber, N. (2021). Major restructuring of marine plankton assemblages under global warming. *Nat. Commun.* 12, 1–15. doi: 10.1038/s41467-021-25385-x

Dang, H., Klotz, M. G., Lovell, C. R., and Sievert, S. M. (2019). Editorial: The responses of marine microorganisms, communities and ecofunctions to environmental gradients. *Front. Microbiol.* 10, 115. doi: 10.3389/fmicb.2019.00115

Falkowski, P. G., and Raven, J. A. (2013). *Aquatic Photosynthesis, 2nd Edn*. Princeton, NJ: Princeton University Press.

Raven, J. A., and Beardall, J. (2021). Influence of global environmental change on plankton. *J. Plankton Res.* 43, 779–800. doi: 10.1093/plankt/fbab075

Reid, G., Gurney-Smith, H., Marcogliese, D., Knowler, D., Benfey, T., Garber, A., et al. (2019). Climate change and aquaculture: considering biological response and resources. *Aquacult. Environ. Interact.* 11, 569–602. doi: 10.3354/aei0033310.3354/aei00332

Yun, M. S., Sun, J., Lovejoy, C., and Lee, S. H. (2021). Editorial: Microbial response to a rapidly changing marine environment: global warming and ocean acidification. *Front. Microbiol.* 12, 731732. doi: 10.3389/fmicb.2021.731732

frontiers in Microbiology

ORIGINAL RESEARCH
published: 25 February 2022
doi: 10.3389/fmicb.2022.833670

# Transformations of Diatom-Derived Dissolved Organic Matter by *Bacillus pumilus* Under Warming and Acidification Conditions

*Yang Liu*[1,2], *Xueru Wang*[2] *and Jun Sun*[2,3,4]*

[1] *Institute of Marine Science and Technology, Shandong University, Qingdao, China,* [2] *Research Center for Indian Ocean Ecosystem, Tianjin University of Science and Technology, Tianjin, China,* [3] *College of Marine Science and Technology, China University of Geosciences, Wuhan, China,* [4] *State Key Laboratory of Biogeology and Environmental Geology, China University of Geosciences, Wuhan, China*

Heterotrophic bacteria are assumed to play an important role in processing of phytoplankton-derived dissolved organic matter (DOM). Although the algae-derived organic matter is commonly studied, the transformation and processing of DOM by epiphytic bacteria for phytoplankton have rarely been investigated, especially under warming and acidification. In this study, *Bacillus pumilus* is used to explore the ecologically important marine diatom *Skeletonema dohrnii*-derived DOM under different conditions (temperature, 27°C and 31°C; $pCO_2$, 400 and 1,000 ppm), utilizing fluorescence excitation-emission matrix (EEM) combined with parallel factor analysis (EEM-PARAFAC). Fluorescence regional integration and the peak selecting method are used to generate B, T, N, A, M, and C peaks in the EEM fluorescence spectroscopy. The main known fluorophores including that protein-like components (peaks B and T), unknown components (peak N), and humic-like component (peaks A, M, and C). Our experimental results showed that under higher temperature and pressure of $CO_2$ ($pCO_2$) conditions, *S. dohrnii*-derived DOM fluorescence was dominated by a protein-like signal that slower waning throughout the experiment, becoming an increasingly humic-like substance, implying that processing by the epiphytic bacteria (*B. pumilus*) produced more complex molecules. In addition, spectroscopic indices (e.g., fluorescence index, biological index, freshness index β/α, and humification index) were changed in varying degrees. This study reveals and confirms the direct participation of heterotrophic bacteria in the transformation and generation of algae-derived DOM in the laboratory, underlining the influence of global warming and ocean acidification on this process.

**Keywords:** ***Skeletonema dohrnii*-derived DOM, *Bacillus pumilus*, EEM-PARAFAC, fluorophores, spectroscopic indices**

OPEN ACCESS

***Edited by:***
*Jin Zhou,*
*Tsinghua University, China*

***Reviewed by:***
*Guanghui Yu,*
*Tianjin University, China*
*Zhou Shilei,*
*Hebei University of Science and Technology, China*

***Correspondence:**
*Jun Sun*
*phytoplankton@163.com*

***Specialty section:***
*This article was submitted to Aquatic Microbiology, a section of the journal Frontiers in Microbiology*

***Received:*** *12 December 2021*
***Accepted:*** *10 January 2022*
***Published:*** *25 February 2022*

***Citation:***
*Liu Y, Wang X and Sun J (2022) Transformations of Diatom-Derived Dissolved Organic Matter by Bacillus pumilus Under Warming and Acidification Conditions. Front. Microbiol. 13:833670. doi: 10.3389/fmicb.2022.833670*

## INTRODUCTION

The primary type of organic matter in the oceanic environment is phytoplankton-derived dissolved organic matter (DOM), which contributes to the world's greatest carbon pool (662 Pg C) (Hansell et al., 2009, 2012). Diatoms, one of the most abundant and diverse groups of marine phytoplankton, contributing ∼20% of global primary productivity (Thangaraj and Sun, 2021). At a rate of 43 Tg per

year, more than 90% of dissolved organic carbon (DOC) could be generated, playing an essential role in the global carbon cycle (Thornton, 2014). The vast majority of DOC is changed, resulting in recalcitrant DOC, which is then exported to the deep sea (Hansell et al., 2012).

For almost 200 million years, algae and bacteria have coexisted in aquatic environments (Falkowski et al., 2004). Heterotrophic bacteria are key biogeochemical regulators in aquatic systems. The majority of the DOM metabolism produced by algae enters the microbial cycle, where it provides carbon and nutrients to heterotrophic bacteria (Pomeroy et al., 2007). Meanwhile, the bioreactivity and chemical composition of DOM have changed during/after microbial utilization (Liu et al., 2021a). Heterotrophic bacteria link biogeochemical cycles together by decomposing and producing organic matter. Most organic carbon fixed by photosynthesis is consumed by heterotrophic bacteria (Del Giorgio and Duarte, 2002). According to one study, increased $pCO_2$ will enhance vertical carbon flux (Siu et al., 2014), while another suggested that bacteria with high $pCO_2$ and temperature conditions have increased rates of polysaccharide degradation, protein production and enzymatic activity (Grossart et al., 2006). In brief, marine bacterioplankton play an important part in the carbon cycle. On the other hand, carbon consumption and transport rates of heterotrophic bacteria govern the efficacy of carbon sequestration in the ocean (Fuhrman, 2009).

The temperature and $CO_2$ concentrations have increased rapidly since the onset of the industrial revolution, led to global climate change (Meehl et al., 2007). Seawater, on the other hand, is becoming progressively acidified due to oceanic absorption of atmospheric $CO_2$ (Meehl et al., 2007; Pachauri et al., 2014). Marine ecosystems are particularly sensitive to environmental changes, as species are stressed by both warming and ocean acidification (Riebesell et al., 2018). The mean sea surface temperatures are forecast to rise by 4°C by the end of the twenty-first century, while $CO_2$ levels in the atmosphere are expected to treble (Meehl et al., 2007). The creatures and processes in the seas will surely suffer as a result of these cumulative impacts (Thangaraj and Sun, 2021). Ocean acidification and warming are seen as severe threats to the marine species (Stocker et al., 2014). Previous studies reported that ocean warming and acidification affect the physiological and biochemical state of diatoms (Thangaraj and Sun, 2020), but also have an impact on their photosynthesis and metabolism (Thangaraj and Sun, 2021). The potential response of the algae varies to the extent that the effect of bacterial utilization and transformation of algae-derived organic matter is uncertain. However, very few snapshots are available on the use of algae-derived organic matter by unibacteria under warming and acidification, let alone the combined effects of both factors.

Excitation-emission matrix (EEM) fluorescence spectroscopy is prevalent approaches for analyzing organic matter due to the vast quantity of visual maps, and three-dimensional information it gives (Rodríguez-Vidal et al., 2020). Recently, EEM spectroscopy combined with parallel factor analysis (PARAFAC) have been frequently employed to the characterization of DOM due to its remarkable sensitivity and selectivity (Lin et al., 2021; Liu et al., 2021d). Protein- and humic-like fluorophores have been found in previous studies, and their peak locations in EEM spectroscopy make it straightforward to distinguish between them (Coble, 1996; Coble et al., 1998).

In this study, we used single bacteria (*B. pumilus*) to investigate the role and preference for *S. dohrnii*-derived DOM under warming and acidification conditions. Our research builds upon laboratory-based studies over the 30-day timespan. We examined the characteristics of fluorescent organic matter by using EEM-PARAFAC methods. In addition, using different parameters (e.g., bacteria abundance, DOC, pH, fluorescence indices, peaks, and components) to further characterize the variation in organic matter *via* the processing of different bacterial under warming and acidification. We hypothesized that the DOM characteristics should be significantly correlated with bacterial utilization and transformation, and that they would exhibit different patterns.

# MATERIALS AND METHODS

## *Skeletonema dohrnii* Culture Conditions

Marine diatoms (e.g., *Skeletonema* spp.) are widely distributed in offshore China, especially, *S. dohrnii* have been found and isolated in China's Yellow Sea coastal waters, and subsequently preserved in our laboratory. *S. dohrnii* cells were pre-cultivated and transferred in artificial seawater (ASW) medium. The cultivation was conducted at 25°C with a light intensity of 100 μmol photons $m^{-2}$ $s^{-1}$ and a 14:10 h light:dark cycle. The cells were grown at least for three generations before the initiation of the experiment.

## Isolation and Identification of Epiphytic Bacteria

Epiphytic bacteria was isolated from the degradation growth stage of microalgae by gradient dilution method. The 2216E agar plates were used to isolate epiphytic bacteria, which cultured in transparent conical flasks (500 mL) in a shaking incubator (26°C, 150 rpm). To identify the epiphytic bacteria, the genomic DNA of bacteria was extracted by TIANamp Bacteria DNA Kit (Tiangen-Biotech, Beijing, China). For polymerase chain reaction (PCR) amplification of the 16S rDNA V3 region, a universal bacterial primer was used. The phylogenetic tree (Neighbor-Joining tree, N-J tree) was constructed using the bacteria sequences and closest related sequences from GenBank, and the genetic distances were calculated. Based on the results of analysis, the isolated bacterial strains (CA-35) shared 66.67% sequence identity to the valid species (*Bacillus pumilus*) from GenBank.

## Biochemical Characterization of Bacteria

The isolated positive colonies were identified by Gram staining reaction and biochemical tests (including arabinose test, glucose test, maltose test, urease test, Vogues Proskauer test, nitrate

reduction test, starch hydrolysis test, aesculin test, 7% NaCl test, and pH 5.7 test).

## Flow Cytometry of *B. pumilus* Abundance

The strains *B. pumilus* was cultured in 500 mL transparent conical flasks with pre-combusted (450°C, 5 h). As described in previous studies (Moens et al., 2016), the abundance of *B. pumilus* cells was measured by Accuri C6 flow cytometer (BD Biosciences, Erembodegem, Belgium). 0.01% SYBR Green I was applied to the sample to stain it for 30 min in the dark at 37°C. As an internal standard, 1 μm fluorescent beads (Polyscience, Warrington, PA, United States) were injected into each sample. Then, the samples were measured at a flow rate of 0.25 μL $s^{-1}$ for 1 min.

## Measurements of Dissolved Organic Carbon and pH

To avoid any carbon contamination, all glass materials were acid washed, rinsed with ultra-pure water, and precombusted (450°C for 5 h). A total organic carbon analyzer (TOC-3100, Germany) was used to detect the dissolved organic carbon (DOC). All DOC samples were gravity filtered using the GF/F glass fiber filters (0.7 μm pore size, 47 mm diameter, Whatman). GF/F glass fiber filters can be cleaned by high temperature combustion and can filter sufficient sample volumes without clogging, thus reducing potential sources of contamination. The pH variation of culture was measured using pH meter (Lab 850, SCHOTT Instruments).

## *Skeletonema dohrnii*-Derived Dissolved Organic Matter Collection and Experimental Setup

*Skeletonema dohrnii* cells were cultivated in ASW medium, and after reaching the degradation growth phase [algal concentration was around $(4.07 \pm 0.02) \times 10^7$ cells $L^{-1}$]. Microalgae liquid was filtered through a 0.2 μm polycarbonate membrane (Millipore, United States) to remove the particles. Then, the filtrate was regarded as the DOM fraction placed in 1 L conical flask with pre-combusted (450°C, 5 h).

To assess the effects of warming and acidification on the transformation of algae-derived DOM by epiphytic bacteria. Two different temperature (27 and 31°C) and $pCO_2$ (400 and 1,000 ppm) conditions were used in this work. The following four treatments were set up: (i) 27°C and 400 ppm (low temperature and low carbon, LL), (ii) 27°C and 1,000 ppm (low temperature and high carbon, LH), (iii) 31°C and 400 ppm (high temperature and low carbon, HL), and (iv) 31°C and 1,000 ppm (high temperature and high carbon, HH). *B. pumilus* were grown in above different growth conditions, which were gently bubbled with $CO_2$, and the gas-flow rate (0.5 L/min) was controlled using a Bronkhorst mass flow controller. In addition, the initial abundance of *B. pumilus* in each treatment group was approximately $(8.51 \pm 0.02) \times 10^9$ cells $L^{-1}$. All experiments were carried out in triplicate and under dark conditions.

## Excitation-Emission Matrix Combined With Parallel Factor Analysis Modeling

The fluorescence spectrophotometer (Hitachi F-7100, Tokyo, Japan) was used to take three-dimensional fluorescence spectroscopy measurements. The photomultiplier tube's voltage was set at 700 volts. Excitation (Ex) from 200 to 400 nm and emission (Em) from 250 to 550 nm were identified in successive scanning of fluorescence spectra. The scanning speed was adjusted at 8,000 nm min-1 and the Ex and Em slits were kept at 5 nm. Instrument adjustments were carried out the procedure recommended by the Hitachi F-7100 instruction manual. To eliminate the majority of the Raman scatter, each samples spectroscopy was blank subtracted using ultra-pure water. After that, Raman calibration was performed based on literature (Lawaetz and Stedmon, 2009), and Rayleigh scatter (1st and 2nd order) effects were removed using the manufacturer correction procedure. A PARAFAC analysis was conducted in Matlab 2018b (Mathworks, United States) with the DOMFluor toolbox (Stedmon and Bro, 2008).

Every component model may be tested using a split-half analysis residual analysis, and loadings to provide correct information about fluorescence components. All fluorescence components were described using water Raman units (RU). Fluorescence intensity arbitrary units (a.u.) were utilized to fluorescence peak intensity. Spectroscopic indices were further derived from the EEMs: fluorescence index (FI) is often used to indicate the origin of the DOM. Biological index (BIX) is a measure the degree of autochthonous pollution. The β/α (a ratio of two known fluorescing components, i.e., freshness index), and humification index (HIX) showed the humification degree (Parlanti et al., 2000; McKnight et al., 2001).

## Statistical Analysis

The correlation analysis and DOM associated parameters were obtained using the "corrplot" package in RStudio. To rigorously define the significance, the difference was determined significant at the levels of $p < 0.05$, $p < 0.01$, and $p < 0.001$. The measured value of the data is represented by the mean ± standard deviation (SD).

# RESULTS

## Bacterial Abundance, Dissolved Organic Carbon Concentration and pH

The abundance of *B. pumilus* strain growth in different treatment groups is shown in **Figure 1**. The initial abundance of *B. pumilus* was around $(8.51 \pm 0.02) \times 10^9$ cells $L^{-1}$ in every treatment groups. The *B. pumilus* abundance changed at 30 days in all conditions (**Figure 1A**). However, there were several differences for the abundance of these treatments. LH and HH achieved higher abundance of up to $(13.52 \pm 0.07) \times 10^9$ and $(13.08 \pm 0.05) \times 10^9$ cells $L^{-1}$, respectively. LL and HL had moderate abundance of $(11.48 \pm 0.04) \times 10^9$ and $(11.94 \pm 0.08) \times 10^9$ cells $L^{-1}$, respectively. This suggests that the significant increase of *B. pumilus* abundance was caused by

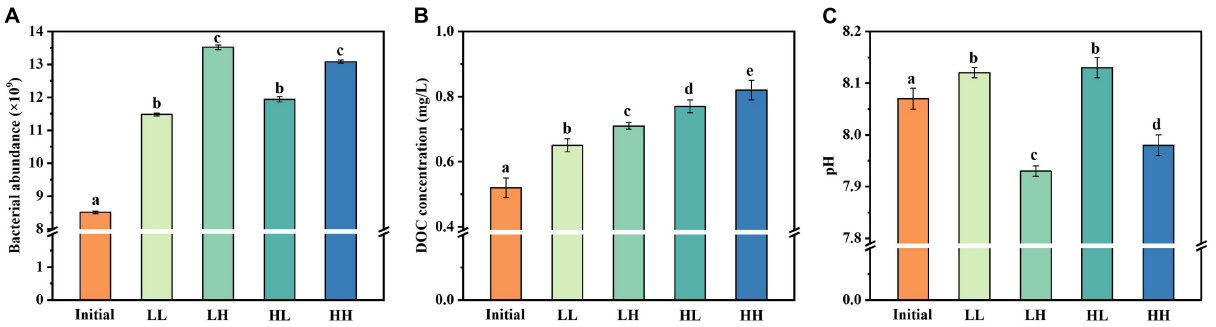


**FIGURE 1 |** Changes in **(A)** bacterial abundance, **(B)** DOC concentration, and **(C)** pH under warming and acidification conditions. Initial, initial value; LL, 27°C and 400 ppm; LH, 27°C and 1,000 ppm; HL, 31°C and 400 ppm; HH, 31°C and 1,000 ppm. All data are presented as mean ± SD ($n$ = 3). Error bars represent the standard error for duplicate cultures. Different letters (e.g., "a," "b," "c," "d," and "e") represented significant difference ($p < 0.05$), as determined by a one-way analysis of variance (ANOVA).

elevated temperature and $pCO_2$. The initial DOC concentration was (0.52 ± 0.03) mg $L^{-1}$ for the DOM treatment groups and increased at the end of the 30-day period (**Figure 1B**). The largest DOC increase occurred in the HH group, which rose by (0.82 ± 0.03) mg $L^{-1}$ DOC over the 30-day period. There were significant differences between each treatment group. The initial pH value of the sample was 8.07 ± 0.02 (**Figure 1C**). At the end of the experiment, the pH increased in LL and HL groups, conversely, decreased in LH and HH groups as a result of acidification.

## Identification of Bacterial Isolate and Biochemical Characterization

The culture labeled as CA-35 was identified as *Bacillus pumilus* (accession number SRR17041859) based on nucleotide homology and phylogenetic analysis. It was found that the strain CA-35 was Gram-positive rod. Results of various biochemical characteristics of CA-35 was shown in **Table 1**. The result shows that arabinose, glucose, 7% NaCl, malonate, starch hydrolysis, aesculin, pH 5.7 were positive at the initial phase of the experiment. The individual treatment groups showed different results under different incubation conditions. By contrast, warming and acidification caused changes in some characteristics such as arabinose, glucose, maltose, Voges-Prosk test.

**TABLE 1 |** Physiological and biochemical characteristics of *B. pumilus* under warming and acidification conditions.

| | Initial | LL | LH | HL | HH |
|---|---|---|---|---|---|
| Arabinose | + | − | − | + | − |
| Glucose | + | − | − | − | + |
| Maltose | − | − | + | + | − |
| 7% NaCl | + | + | + | + | + |
| Malonate | + | − | + | − | − |
| Urease test | − | − | − | − | − |
| pH 5.7 | + | + | + | + | + |
| Aesculin | + | + | + | + | + |
| Nitrate reduction | − | − | − | − | − |
| Starch hydrolysis | + | + | + | + | + |
| Voges-Prosk | − | + | + | − | − |

*A positive reaction is indicated by a plus sign (+), whereas a negative reaction is indicated by a minus sign (–). Initial, initial value; LL, 27°C and 400 ppm; LH, 27°C and 1,000 ppm; HL, 31°C and 400 ppm; HH, 31°C and 1,000 ppm.*

## Fluorescence Components

All DOM samples collected from the four different treatments were modeled and analyzed with EEM-PARAFAC. In this study, all of the components' spectral properties were compared to those previously reported in PARAFAC components (**Table 2**). As shown in **Figure 2**, one individual component (peak T, tryptophan-like) was identified by the PARAFAC analysis at initial stage. All components (protein-, tryptophan- marine humic-, and humic-like components) in this study have been successfully matched in the OpenFluor database. Component 1 (including A1, B1, C1, and D1; **Figure 2**) has two fluorescence peaks, located at the Ex/Em wavelength pairs of 225/300–400 and 275/300–400 nm, respectively (Coble, 1996; Coble et al., 1998). Similarly, double peaks have been found in other components. Component 2 (including A2, B2, C2, and D2; **Figure 2**) was distinguished as marine humic-like components (Ex/Em = 235 and 340/400 nm) (Yao et al., 2011). A humic-like component (peak A, Ex/Em = 250 and 325/425 nm) (Stedmon et al., 2003; Yamashita et al., 2011) associated to terrestrial substances was given to Component 3 (including B3, C3, and D3; **Figure 2**). Component 4 (including D4; **Figure 2**) corresponded to humic-like fluorescence (peak C, Ex/Em = 260 and 350/458 nm) (Yamashita and Tanoue, 2008).

## Fluorescence Indices and Peaks

The fluorescence index was further used as a parameter indicating changes in fluorescence characteristics (**Figure 3**). The origin of DOM is identified *via* FI. The three treatment groups had similar values for FI, which had no obvious change under warming and acidifying conditions. The freshness index was also calculated, with the β peak representing newly produced DOM and the α peak representing more decomposed DOM. All of the samples had β/α values between 1.12 and 1.16, whereas LL had maximum values of 1.16. For BIX, the values are almost appropriate (i.e.,

**TABLE 2 |** EEM fluorescence spectral features attributed to various organic matter sources.

| Traditional peak | Ex/Em | Description | Probable origin | References |
|---|---|---|---|---|
| Peak B | 225/305<br>275/305 | Protein-like | Autochthonous tyrosine-like fluorescence | Coble et al., 1998; Para et al., 2010 |
| Peak T | 225/330–340<br>275/330–340 | Protein-like<br>Tryptophan-like | Autochthonous | Coble, 1996; Coble et al., 1998 |
| Peak N | 280/360–370 | Unknown | Unknown | Coble et al., 1998 |
| Peak A | 250/425<br>325/425 | Humic-like | Terrestrial | Stedmon et al., 2003; Yamashita et al., 2011 |
| Peak M | 290–310/370–420 | Humic-like | Microbialprocessing of organic matter | Murphy et al., 2008 |
| Peak C | 320–360/430–460 | Humic-like | Terrestrial/Autochthonous | Murphy et al., 2008 |

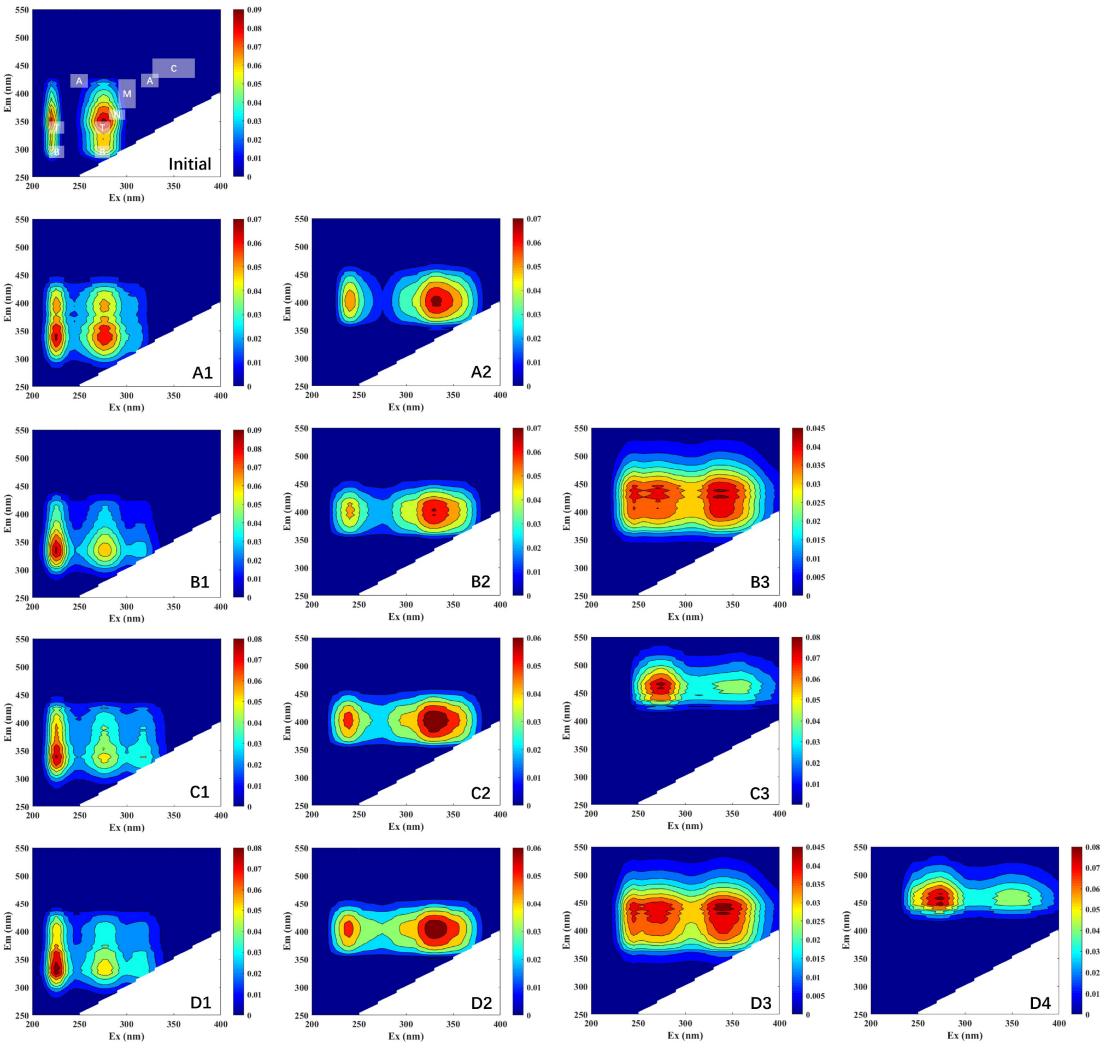


**FIGURE 2 |** EEM plots of the fluorescence components identified by PARAFAC model. Initial, initial component and intensity; **(A1–A2)**, LL group; **(B1–B3)**, LH group; **(C1–C3)**; HL group; **(D1–D4)**, HH group. Different scales of Raman units (RU) are used to characterize the fluorescence intensity.

1.28–1.32). The HIX is an indicator of how much organic matter has degraded. There are varying degrees of alteration in the degree of humification, especially in HH group.

The fluorescence intensity of the peaks was altered in all treatment groups after 30 days of incubation (**Figure 4**). Peak B (protein-like) and peak T (protein-like) maintained a high fluorescence intensity (3,000–4,000 a.u.) in the initial phases, with a similar degree of variation for treatment groups. There was minimal fluorescence intensity in the LL group, suggesting that warming and acidification slowed bacterial consumption

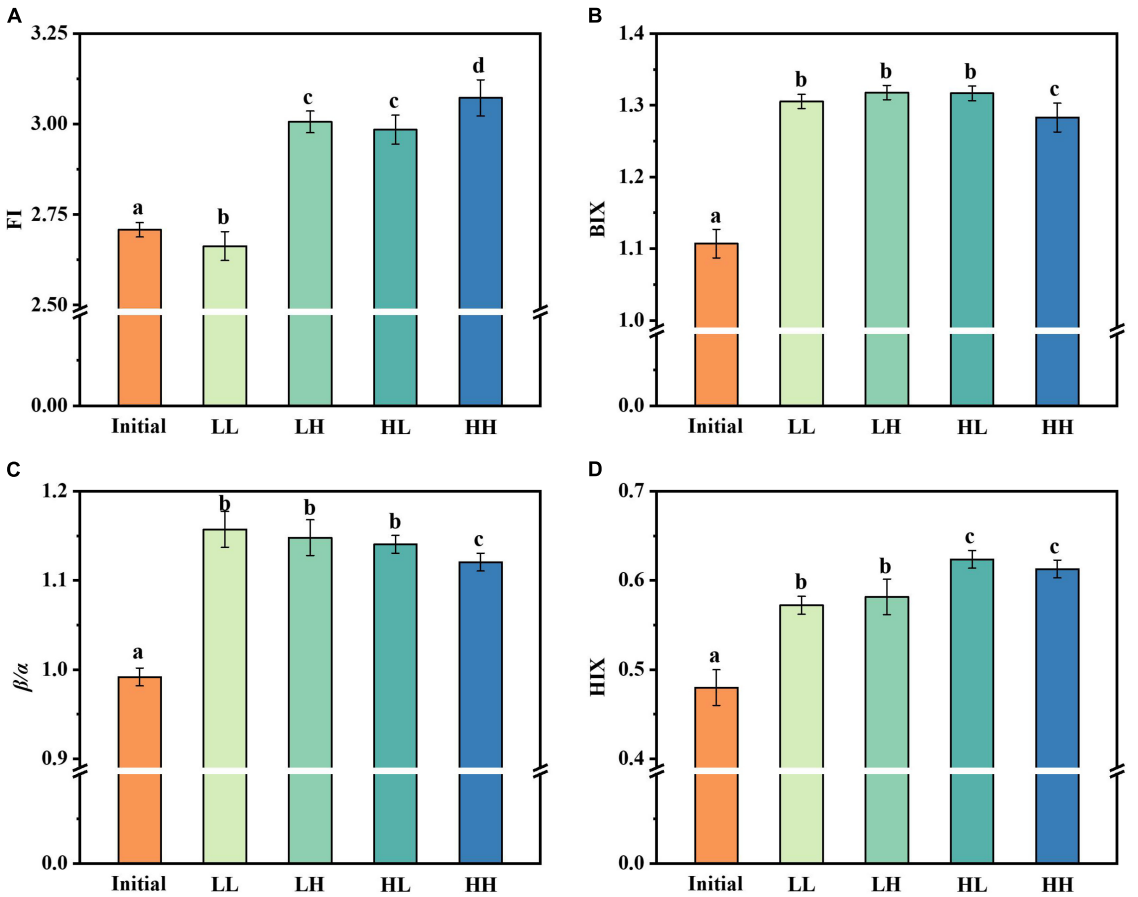


**FIGURE 3 |** Changes in fluorescence indices under warming and acidification conditions. **(A–D)** Represent FI, BIX, $\beta/\alpha$, and HIX respectively. Initial, initial value; LL, 27°C and 400 ppm; LH, 27°C and 1,000 ppm; HL, 31°C and 400 ppm; HH, 31°C and 1000 ppm. All data are presented as mean ± SD ($n$ = 3). Error bars represent the standard error for duplicate cultures. Different letters (e.g., "a," "b," "c," and "d") represented significant difference ($p < 0.05$), as determined by a one-way analysis of variance (ANOVA).

of protein-like substances. Additionally, peak N, an unknown component, followed a similar trend to peaks B and T, with generally lower values for all treatment groups. For peak A, acidification resulted in a reduction in the fluorescence intensity of the like-humic substances (i.e., LH and HH groups). However, the fluorescence intensity of peak M (like-humic) decreased and the warming slows down the utilization efficiency of peak M (i.e., HL and HH groups). The only difference is that the fluorescence intensity of peak C (like-humic) is generally increased in all groups.

## DISCUSSION

Phytoplankton-DOM (especially autochthonous DOM) is a highly more bioavailable and high-molecular-weight DOM (Hama and Yanagi, 2001). Heterotrophic bacteria prefer phytoplankton-derived DOM over terrestrial DOM as a substrate for catabolic activities when both are present (Kritzberg et al., 2004). A number of previous cultivation experiments have studied the dynamics of phytoplankton-derived DOM observed with carbon and nutrient additions (Romera-Castillo et al., 2010; Goto et al., 2017, 2020). It has also been shown that phytoplankton produce different characteristics of DOM under different conditions (Liu et al., 2021a,c). In order to better investigate the transformation of DOM by *B. pumilus*, *S. dohrnii*-derived DOM was used as the sole carbon sources. In addition, previously published data demonstrated that the characteristics of DOM produced by *S. dohrnii* are relatively single (Liu et al., 2021a,b). In this study, we have isolated and identified the epiphytic bacteria (*B. pumilus*) of *S. dohrnii*. We collected the *S. dohrnii*-derived DOM in the degradation, because of its enriched fluorescence characteristics and high fluorescence intensity. The results showed that *S. dohrnii*-derived DOM fluorescence is predominantly protein-like, which gradually becomes more and more humic-like within 30 days. This suggests that the *B. pumilus* transformed *S. dohrnii*-derived DOM into more complex substance under increasing temperature and acidification. Together, the present study highlights that warming and acidification affect the effectiveness of bacterial transformation of DOM.

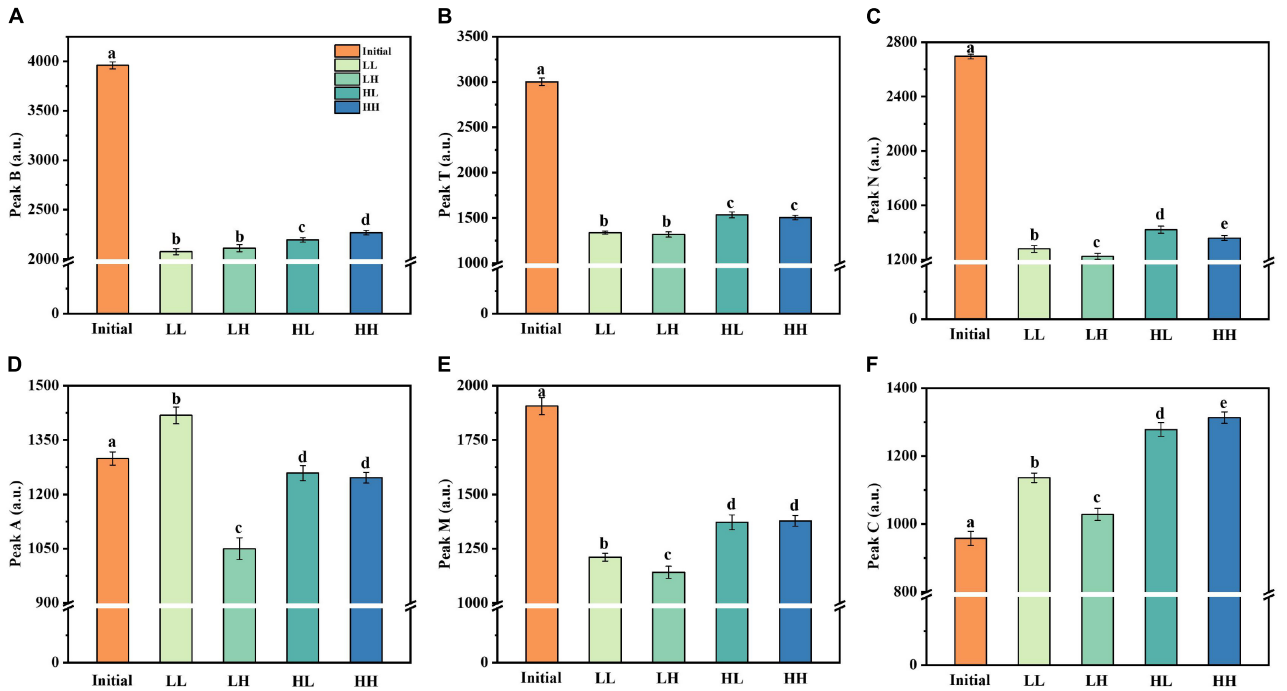


**FIGURE 4 |** Changes in fluorescence peaks (peaks B, T, N, A, M, and C) under warming and acidification conditions. **(A–F)** Represent peak B, peak T, peak N, peak A, peak M, and peak C respectively. Initial, initial value; LL, 27°C and 400 ppm; LH, 27°C and 1,000 ppm; HL, 31°C and 400 ppm; HH, 31°C and 1,000 ppm. All data are presented as mean ± SD ($n$ = 3). Error bars represent the standard error for duplicate cultures. Different letters (e.g., "a," "b," "c," "d," and "e") represented significant difference ($p < 0.05$), as determined by a one-way analysis of variance (ANOVA).

## Regulation of Phytoplankton-Derived Dissolved Organic Matter by Bacteria

According to Boyce et al. (2010) reported, total phytoplankton abundance is rapidly declining as a result of warming, with diatoms being the most impacted category (Toseland et al., 2013). Under stressed conditions like as warming, acidification, and nutrient scarcity, phytoplankton releases large amounts of DOM. Bacterial abundance was inversely proportional to phytoplankton abundance under these circumstances. Warming has been demonstrated to favor bacterial growing, which might be owing to two factors: (1) the favorable effect of temperature on bacteria, with more bacterial cells at higher temperatures (Apple et al., 2006), and (2) the availability of more enriched DOM for bacteria. Put simply, phytoplankton produces labile DOC, which heterotrophic bacteria can convert to recalcitrant DOC (Stoderegger and Herndl, 1998). Previous investigations have shown that the addition of $pCO_2$ had considerable impact on overall bacterial abundance (Baragi and Anil, 2016). However, in this study, algae-DOM was employed as the only carbon source and the LH group showed a relative increase in bacterial abundance. This is likely because high $pCO_2$ only slowed the rate of increase in bacterial abundance, but did not limit/inhibit it. Besides, the increase in *B. pumilus* abundance might be attributed to the effect of decreased pH, which increases respiration, as a result, the metabolic and energy cost of bacteria (Siu et al., 2014).

In the present study, a fixed amount of *S. dohrnii*-derived DOM was added at the initial phase. A considerable portion of the bioavailable fraction of DOM was reduced by bacterial respiration and absorption. However, the DOC concentration showed a distinct increase, suggesting that DOM components were transformed by bacteria to produce new DOC (i.e., production was higher than consumption) under warming and acidification. The DOM can be used as a substrate for remineralization of carbon by heterotrophic microorganisms. Microorganisms use enzymes to catalyze DOC into smaller molecules that can be transported to the environment through bacterial cell membranes (Arnosti, 2011). The organic carbon is subsequently absorbed into the biomass or expelled as DOC as metabolic products (Arnosti, 2011). This provides a new perspective for observing the transformation process of diatoms-derived DOM by epiphytic bacteria.

## Excitation-Emission Matrix Combined With Parallel Factor Analysis Components

To further understand the characteristics of DOM fluorophores, we built models with components and used a split-half analysis to validate them all. Four fluorescent components, including typically occurring protein- and humic-like components, were detected in *S. dohrnii*-derived DOM samples (**Figure 2**). At the initial phase, protein-like components (peak B and T) were detected. For example, peak T is typically connected to autochthonous tryptophan-like compounds, amino acids, and proteins. In aquatic ecosystems, peak T usually represents

the proteinaceous material produced by phytoplankton and bacteria. Moreover, the presence of visible components (peak T) could be attributed by energy transfer to tryptophan and quenching by adjacent groups suppressing tyrosine fluorescence (Lakowicz, 2013). Some of the components have previously been related to high molecular weight and aromatic humic material characterized as peaks A, M, and C in the literature (Wünsch et al., 2015).

All treatment groups essentially produced two-peak patter dominated by discrete *S. dohrnii*-derived DOM fluorophores, indicating that different compounds, such as protein- and humic-like have been described in the algae-DOM. Several studies have shown that protein peaks (e.g., tryptophan-like) are dominant in phytoplankton growth (Stedmon and Markager, 2005; Jørgensen et al., 2011; Liu et al., 2021b). In previous studies (Kinsey et al., 2018; Liu et al., 2021a), DOM produced in phytoplankton showed similar fluorescence patterns to presented here. As reported by Fukuzaki et al. (2014), the DOM spectra of algal cultures have also been studied. Although the DOM fluorophores are different, the DOM patterns produced are generally similar. The current results show that bacteria use and transform DOM to obtain different fluorescent components. Under elevated temperature and acidified conditions, more fluorescent components were identified, indicating that certain physicochemical characteristics of the bacteria were affected (**Table 1**), further leading to altered DOM utilization by the bacteria and more humic substances being produced.

In the current study, results showed that the fluorescence values of peak C increased on the whole, while peaks B, T, N, A, and M decreased comparably to the initial value. It suggested that the epiphytic bacteria utilize DOM, which leads to the increase of bacterial abundance, and then the DOM is transformed into recalcitrant DOM and gradual accumulation by epiphytic bacteria. It is noteworthy that on the time scale of deep ocean circulation, these humus-like substances have proven to be recalcitrant, whereas only a small fraction of humic-like substances were biodegradable (Catalá et al., 2015). Besides, the generally low fluorescence in the open ocean suggests that the degradation experiments were conducted over a longer period time than our and other studies (Gruber et al., 2006; Fukuzaki et al., 2014). Indeed, a prior study found that a single strains is incapable of entirely degrading high molecular weight DOM compounds, meaning that multiple bacterial species must work together (Horemans et al., 2013). Briefly, the utilization and transformation of DOM by a single bacterium take much longer.

The spectroscopic index provided a clear insight into the process of DOM-related substance changes. The values of FI were all greater than 1.8, demonstrating that bacteria were primarily responsible for the fluorescence component of DOM

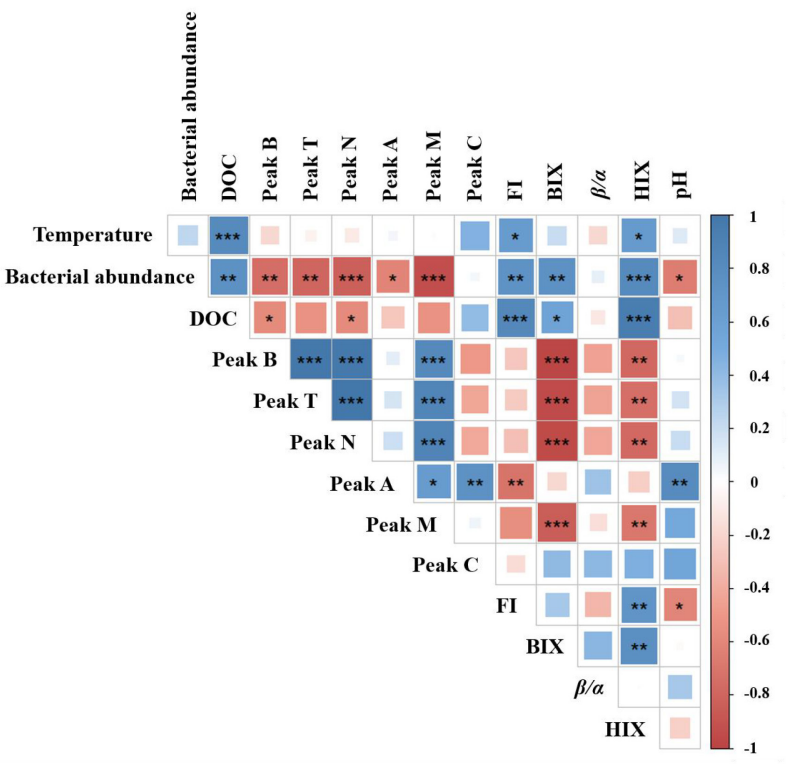


**FIGURE 5 |** Correlation analysis between DOM-associated parameters and temperature and pH potential impact. Pearson's correlation coefficients are shown by square colors and sizes. *, **, and *** represent significance degrees at $p < 0.05$, $p < 0.01$, and $p < 0.001$, respectively. A positive connection is represented by blue, whereas a negative correlation is shown by red.

transformation and production (Lavonen et al., 2015). In aquatic ecosystems, BIX could be used as a measurement of DOM traceability, with larger values indicating more DOM degradation. The significant changes in β/α and BIX values over a short period of time indicated that endogenous carbon products are most likely produced through bacterial processing of DOM. The HIX indicates the degree of degradation of organic matter, with higher values characteristic of higher molecular weight, aromatic compounds. In other words, the humic concentration of DOM is roughly proportional to HIX (Huguet et al., 2009).

Elevated temperature and acidification caused a general increase in FI and β/α values. Interestingly, we found that β/α values decreased in the HH group, which may be due to the fact that the highly decomposed DOM was higher than recently derived DOM. Besides, both warming and acidification led to a decrease in HIX value. From the current results, the effect of acidification was more prominent. However, the BIX value of each group was not significantly different.

### Transformations and Connections of Organic Matter

The overall DOM concentration increased by 9.23–26.15% in this study due to elevated temperature and acidification. This result indicates that warming promoted the accumulation of microbial-derived DOM and depressed the aromaticity of DOM. Previous studies have demonstrated that microbial-derived aliphatic carbon is the most labile DOM, which is more readily absorbed than plant-derived aromatic carbon (Yang et al., 2016). Changes in bacterial abundance and DOM properties such as pH, fluorophores, and fluorescence intensity could be explain the discrepancy. Acidification is linked to the decomposition of more refractory organic carbon (e.g., lignocelluloses), as compared to warming (Williamson et al., 1999). Specifically, pH increased the aromatic fractions in DOM (peak C), which are recognized as organic matter produced by bacteria. The bacterial abundance in our study was increased from $8.51 \times 10^9$ to $13.52 \times 10^9$ cells $L^{-1}$ under acidification conditions, besides, significant increase in DOC concentration. Thus, it is regarded as enhanced utilization of aromatic DOM by bacteria.

Pearson's correlation analysis showed significant variability between warming and acidification for DOM-associated parameters. As shown in **Figure 5**, temperature and DOC concentration had a significant positive correlation ($p < 0.001$). Besides, FI and HIX were positively correlated with temperature ($p < 0.05$), respectively. These results indicating that temperature affects microbial activity and production, which was consistent with results from previous studies (Thangaraj and Sun, 2021). The pH and peak A had a significant positive correlation ($p < 0.01$), and bacteria abundance and FI were significantly negatively correlated with pH ($p < 0.05$). Moreover, the formation of aromatic DOM or humic-like is thought to be facilitated by acidification-driven microorganisms. This appears to be corroborated by the fact that when the temperature rises, and pH decreases (0.09–0.14 units). Bacterial abundance and microbial activity have both been shown to increase when pH is raised (Han et al., 2022). This is overall consistent with our results.

As discussed above, elevated temperature and acidification showed different impacts on DOM utilization and transform by bacteria. This work has important implications for better understanding how microbes in the ocean transform and sequester DOM. Our findings show that warming and acidification conditions will exacerbate the accumulation of organic matter, particularly phytoplankton-derived aromatic substances. Given the crucial impacts and consequences of bacteria on the use of phytoplankton-DOM under warming and acidification conditions, further investigations regarding carbon transform and release process in natural environments (especially microbial environment) under global climate change deserves serious attention.

## CONCLUSION

This work provided direct evidences for bacterial utilization and transformation of phytoplankton-DOM under warming and acidification conditions. Our findings emphasized that warming reduced the efficiency of bacterial use of protein-like substances, while acidification promoted the transformation of humus-like substances (e.g., flavins and phenols, etc.). The simultaneous increment of warming and acidification accelerates the accumulation of recalcitrant DOM. Together, temperature and pH have important influence in the chemical composition and remineralization of DOM in marine microorganisms.

## DATA AVAILABILITY STATEMENT

The original contributions presented in the study are included in the article/supplementary material, further inquiries can be directed to the corresponding author/s.

## AUTHOR CONTRIBUTIONS

JS and YL contributed to conception and design of the study. YL and XW organized the database. YL performed the statistical analysis and wrote the first draft of the manuscript. All authors contributed to manuscript revision, read, and approved the submitted version.

## FUNDING

This research was financially supported by the National Key Research and Development Project of China (2019YFC1407805), the National Natural Science Foundation of China (41876134), the Changjiang Scholar Program of Chinese Ministry of Education (T2014253), and supported by State Key Laboratory of Biogeology and Environmental Geology, China University of Geosciences (No. GKZ21Y645) to JS.

## REFERENCES


Apple, J. K., Del Giorgio, P., and Kemp, W. M. (2006). Temperature regulation of bacterial production, respiration, and growth efficiency in a temperate salt-marsh estuary. *Aquat. Microb. Ecol.* 43:243. doi: 10.3354/ame043243

Arnosti, C. (2011). Microbial extracellular enzymes and the marine carbon cycle. *Annu. Rev. Mar. Sci.* 3, 401–425. doi: 10.1146/annurev-marine-120709-142731

Baragi, L. V., and Anil, A. C. (2016). Synergistic effect of elevated temperature, *p*CO2 and nutrients on marine biofilm. *Mar. Pollut. Bull.* 105, 102–109. doi: 10.1016/j.marpolbul.2016.02.049

Boyce, D. G., Lewis, M. R., and Worm, B. (2010). Global phytoplankton decline over the past century. *Nature* 466, 591–596. doi: 10.1038/nature09268

Catalá, T. S., Reche, I., Fuentes-Lema, A., Romera-Castillo, C., Nieto-Cid, M., Ortega-Retuerta, E., et al. (2015). Turnover time of fluorescent dissolved organic matter in the dark global ocean. *Nat. Commun.* 6:5986. doi: 10.1038/ncomms6986

Coble, P. G. (1996). Characterization of marine and terrestrial DOM in seawater using excitation-emission matrix spectroscopy. *Mar. Chem.* 51, 325–346. doi: 10.1016/0304-4203(95)00062-3

Coble, P. G., Del Castillo, C. E., and Avril, B. (1998). Distribution and optical properties of CDOM in the Arabian Sea during the 1995 Southwest Monsoon. *Deep Sea Res. Part II* 45, 2195–2223. doi: 10.1016/S0967-0645(98)00068-X

Del Giorgio, P. A., and Duarte, C. M. (2002). Respiration in the open ocean. *Nature* 420, 379–384. doi: 10.1038/nature01165

Falkowski, P. G., Katz, M. E., Knoll, A. H., Quigg, A., Raven, J. A., Schofield, O., et al. (2004). The evolution of modern eukaryotic phytoplankton. *Science* 305, 354–360. doi: 10.1126/science.1095964

Fuhrman, J. A. (2009). Microbial community structure and its functional implications. *Nature* 459, 193–199. doi: 10.1038/nature08058

Fukuzaki, K., Imai, I., Fukushima, K., Ishii, K. I., Sawayama, S., and Yoshioka, T. (2014). Fluorescent characteristics of dissolved organic matter produced by bloom-forming coastal phytoplankton. *J. Plankton Res.* 36, 685–694. doi: 10.1093/plankt/fbu015

Goto, S., Tada, Y., Suzuki, K., and Yamashita, Y. (2017). Production and reutilization of fluorescent dissolved organic matter by a marine bacterial strain, *Alteromonas macleodii*. *Front. Microbiol.* 8:507. doi: 10.3389/fmicb.2017.00507

Goto, S., Tada, Y., Suzuki, K., and Yamashita, Y. (2020). Evaluation of the production of dissolved organic matter by three marine bacterial strains. *Front. Microbiol.* 11:2553. doi: 10.3389/fmicb.2020.584419

Grossart, H. P., Allgaier, M., Passow, U., and Riebesell, U. (2006). Testing the effect of $CO_2$ concentration on the dynamics of marine heterotrophic bacterioplankton. *Limnol. Oceanogr.* 51, 1–11. doi: 10.4319/lo.2006.51.1.0001

Gruber, D. F., Simjouw, J. P., Seitzinger, S. P., and Taghon, G. L. (2006). Dynamics and characterization of refractory dissolved organic matter produced by a pure bacterial culture in an experimental predator-prey system. *Appl. Environ. Microbiol.* 72, 4184–4191. doi: 10.1128/AEM.02882-05

Hama, T., and Yanagi, K. (2001). Production and neutral aldose composition of dissolved carbohydrates excreted by natural marine phytoplankton populations. *Limnol. Oceanogr.* 46, 1945–1955. doi: 10.4319/lo.2001.46.8.1945

Han, Y., Qu, C., Hu, X., Wang, P., Wan, D., Cai, P., et al. (2022). Warming and humidification mediated changes of DOM composition in an Alfisol. *Sci. Total Environ.* 805:150198. doi: 10.1016/j.scitotenv.2021.150198

Hansell, D. A., Carlson, C. A., and Schlitzer, R. (2012). Net removal of major marine dissolved organic carbon fractions in the subsurface ocean. *Glob. Biogeochem. Cycles* 26:GB1016. doi: 10.1029/2011GB004069

Hansell, D. A., Carlson, C. A., Repeta, D. J., and Schlitzer, R. (2009). Dissolved organic matter in the ocean: a controversy stimulates new insights. *Oceanography* 22, 202–211. doi: 10.5670/oceanog.2009.109

Horemans, B., Vandermaesen, J., Smolders, E., and Springael, D. (2013). Cooperative dissolved organic carbon assimilation by a linuron-degrading bacterial consortium. *FEMS Microbiol. Ecol.* 84, 35–46. doi: 10.1111/1574-6941.12036

Huguet, A., Vacher, L., Relexans, S., Saubusse, S., Froidefond, J. M., and Parlanti, E. (2009). Properties of fluorescent dissolved organic matter in the Gironde Estuary. *Org. Geochem.* 40, 706–719. doi: 10.1016/j.orggeochem.2009.03.002

Jørgensen, L., Stedmon, C. A., Kragh, T., Markager, S., Middelboe, M., and Søndergaard, M. (2011). Global trends in the fluorescence characteristics and distribution of marine dissolved organic matter. *Mar. Chem.* 126, 139–148. doi: 10.1016/j.marchem.2011.05.002

Kinsey, J. D., Corradino, G., Ziervogel, K., Schnetzer, A., and Osburn, C. L. (2018). Formation of chromophoric dissolved organic matter by bacterial degradation of phytoplankton-derived aggregates. *Front. Mar. Sci.* 4:430. doi: 10.3389/fmars.2017.00430

Kritzberg, E. S., Cole, J. J., Pace, M. L., Granéli, W., and Bade, D. L. (2004). Autochthonous versus allochthonous carbon sources of bacteria: results from whole-lake $^{13}C$ addition experiments. *Limnol. Oceanogr.* 49, 588–596. doi: 10.4319/lo.2004.49.2.0588

Lakowicz, J. R. (2013). *Principles of Fluorescence Spectroscopy*. Berlin: Springer Science and Business Media.

Lavonen, E. E., Kothawala, D. N., Tranvik, L. J., Gonsior, M., Schmitt-Kopplin, P., and Köhler, S. J. (2015). Tracking changes in the optical properties and molecular composition of dissolved organic matter during drinking water production. *Water Res.* 85, 286–294. doi: 10.1016/j.watres.2015.08.024

Lawaetz, A. J., and Stedmon, C. A. (2009). Fluorescence intensity calibration using the Raman scatter peak of water. *Appl. Spectrosc.* 63, 936–940. doi: 10.1366/000370209788964548

Lin, H., Xu, H., Cai, Y., Belzile, C., Macdonald, R. W., and Guo, L. (2021). Dynamic changes in size-fractionated dissolved organic matter composition in a seasonally ice-covered Arctic River. *Limnol. Oceanogr.* 66, 3085–3099. doi: 10.1002/lno.11862

Liu, Y., Kan, J., He, C., Shi, Q., Liu, Y. X., Fan, Z. C., et al. (2021a). Epiphytic bacteria are essential for the production and transformation of algae-derived carboxyl-Rich alicyclic molecule (CRAM)-like DOM. *Microbiol. Spectrum* 9:e0153121. doi: 10.1128/Spectrum.01531-21

Liu, Y., Sun, J., Wang, X., Liu, X., Wu, X., Chen, Z., et al. (2021d). Fluorescence characteristics of chromophoric dissolved organic matter in the Eastern Indian Ocean: a case study of three subregions. *Front. Mar. Sci.* 8:742595. doi: 10.3389/fmars.2021.742595

Liu, Y., Liu, X., and Sun, J. (2021c). Response of chlorophyll fluorescence characteristics and dissolved organic matter for marine diatom *Skeletonema dohrnii* under stress from penicillin and $Zn^{2+}$. *Plants* 10:2684. doi: 10.3390/plants10122684

Liu, Y., Kan, J., Yang, J., Noman, M. A., and Sun, J. (2021b). Bacterial community composition and chromophoric dissolved organic matter differs with culture time of *Skeletonema dohrnii*. *Diversity* 13:150. doi: 10.3390/d13040150

McKnight, D., Boyer, E., Westerhoff, P. K., Doran, P. T., Kulbe, T., and Andersen, D. (2001). Spectrofluorometric characterization of dissolved organic matter for indication of precursor organic material and aromaticity. *Limnol. Oceanogr.* 46, 38–48. doi: 10.4319/lo.2001.46.1.0038

Meehl, G. A., Stocker, T. F., Collins, W. D., Friedlingstein, P., Gaye, T., Gregory, J. M., et al. (2007). "Global climate projections," in *Climate Change 2007: The Physical Science Basis. Contribution of Working Group I to the Fourth Assessment Report of the Intergovernmental Panel on Climate Change*, eds S. Solomon, D. Qin, M. Manning, Z. Chen, M. Marquis, K. B. Averyt, et al. (Cambridge: Cambridge University Press).

Moens, F., Weckx, S., and De Vuyst, L. (2016). Bifidobacterial inulin-type fructan degradation capacity determines cross-feeding interactions between bifidobacteria and *Faecalibacterium prausnitzii*. *Int. J. Food Microbiol.* 231, 76–85. doi: 10.1016/j.ijfoodmicro.2016.05.015

Murphy, K. R., Stedmon, C. A., Waite, T. D., and Ruiz, G. M. (2008). Distinguishing between terrestrial and autochthonous organic matter sources in marine environments using fluorescence spectroscopy. *Mar. Chem.* 108, 40–58. doi: 10.1016/j.marchem.2007.10.003

Pachauri, R. K., Allen, M. R., Barros, V. R., Broome, J., Cramer, W., Christ, R., et al. (2014). *Climate Change 2014: Synthesis Report. In Contribution of Working Groups I, II and III to the Fifth Assessment Report of the Intergovernmental Panel on Climate Change*. Geneva: IPCC.

Para, J., Coble, P. G., Charrière, B., Tedetti, M., Fontana, C., and Sempere, R. (2010). Fluorescence and absorption properties of chromophoric dissolved organic matter (CDOM) in coastal surface waters of the northwestern Mediterranean Sea, influence of the Rhône River. *Biogeosciences* 7, 4083–4103. doi: 10.5194/bg-7-4083-2010

Parlanti, E., Wörz, K., Geoffroy, L., and Lamotte, M. (2000). Dissolved organic matter fluorescence spectroscopy as a tool to estimate biological activity in a

coastal zone submitted to anthropogenic inputs. *Org. Geochem.* 31, 1765–1781. doi: 10.1016/S0146-6380(00)00124-8

Pomeroy, L. R., Williams, P. J. I., Azam, F., and Hobbie, J. E. (2007). The microbial loop. *Oceanography* 20, 28–33. doi: 10.5670/oceanog.2007.45

Riebesell, U., Aberle-Malzahn, N., Achterberg, E. P., Algueró-Muñiz, M., Alvarez-Fernandez, S., Arístegui, J., et al. (2018). Toxic algal bloom induced by ocean acidification disrupts the pelagic food web. *Nat. Clim. Change* 8, 1082–1086. doi: 10.1038/s41558-018-0344-1

Rodríguez-Vidal, F. J., García-Valverde, M., Ortega-Azabache, B., González-Martínez, Á, and Bellido-Fernández, A. (2020). Characterization of urban and industrial wastewaters using excitation-emission matrix (EEM) fluorescence: searching for specific fingerprints. *J. Environ. Manage.* 263:110396. doi: 10.1016/j.jenvman.2020.110396

Romera-Castillo, C., Sarmento, H., Álvarez-Salgado, X. A., Gasol, J. M., and Marrasé, C. (2010). Production of chromophoric dissolved organic matter by marine phytoplankton. *Limnol. Oceanogr.* 55, 446–454. doi: 10.4319/lo.2010.55.1.0446

Siu, N., Apple, J. K., and Moyer, C. L. (2014). The effects of ocean acidity and elevated temperature on bacterioplankton community structure and metabolism. *Open J. Ecol.* 4:434. doi: 10.4236/oje.2014.48038

Stedmon, C. A., and Bro, R. (2008). Characterizing dissolved organic matter fluorescence with parallel factor analysis: a tutorial. *Limnol. Oceanogr. Methods* 6, 572–579. doi: 10.4319/lom.2008.6.572

Stedmon, C. A., and Markager, S. (2005). Tracing the production and degradation of autochthonous fractions of dissolved organic matter by fluorescence analysis. *Limnol. Oceanogr.* 50, 1415–1426. doi: 10.4319/lo.2005.50.5.1415

Stedmon, C. A., Markager, S., and Bro, R. (2003). Tracing dissolved organic matter in aquatic environments using a new approach to fluorescence spectroscopy. *Marine Chem.* 82, 239–254. doi: 10.1016/S0304-4203(03)00072-0

Stocker, T., Qin, D., Plattner, G., Tignor, M., Allen, S., and Boschung, J. (2014). *Climate Change 2013: The Physical Science Basis: Working Group I Contribution to the Fifth Assessment Report of the Intergovernmental Panel on Climate Change*. Cambridge: Cambridge university press.

Stoderegger, K. E., and Herndl, G. J. (1998). Production and release of bacterial capsular material and its subsequent utilization by marine bacterioplankton. *Limnol. Oceanogr.* 43, 877–884. doi: 10.4319/lo.1998.43.5.0877

Thangaraj, S., and Sun, J. (2020). The biotechnological potential of the marine diatom *Skeletonema dohrnii* to the elevated temperature and $pCO_2$ concentration. *Mar. Drugs* 18:259. doi: 10.3390/md18050259

Thangaraj, S., and Sun, J. (2021). Transcriptomic reprogramming of the oceanic diatom *Skeletonema dohrnii* under warming ocean and acidification. *Environ. Microbiol.* 23, 980–995. doi: 10.1111/1462-2920.15248

Thornton, D. C. (2014). Dissolved organic matter (DOM) release by phytoplankton in the contemporary and future ocean. *Eur. J. Phycol.* 49, 20–46. doi: 10.1080/09670262.2013.875596

Toseland, A., Daines, S. J., Clark, J. R., Kirkham, A., Strauss, J., Uhlig, C., et al. (2013). The impact of temperature on marine phytoplankton resource allocation and metabolism. *Nat. Clim. Chang.* 3, 979–984. doi: 10.1038/nclimate1989

Williamson, C. E., Morris, D. P., Pace, M. L., and Olson, O. G. (1999). Dissolved organic carbon and nutrients as regulators of lake ecosystems: resurrection of a more integrated paradigm. *Limnol. Oceanogr.* 44, 795–803. doi: 10.4319/lo.1999.44.3_part_2.0795

Wünsch, U. J., Murphy, K. R., and Stedmon, C. A. (2015). Fluorescence quantum yields of natural organic matter and organic compounds: implications for the fluorescence-based interpretation of organic matter composition. *Front. Mar. Sci.* 2:98. doi: 10.3389/fmars.2015.00098

Yamashita, Y., and Tanoue, E. (2008). Production of bio-refractory fluorescent dissolved organic matter in the ocean interior. *Nat. Geosci.* 1, 579–582. doi: 10.1038/ngeo279

Yamashita, Y., Panton, A., Mahaffey, C., and Jaffé, R. (2011). Assessing the spatial and temporal variability of dissolved organic matter in Liverpool Bay using excitation-emission matrix fluorescence and parallel factor analysis. *Ocean Dyn.* 61, 569–579. doi: 10.1007/s10236-010-0365-4

Yang, Z., Wullschleger, S. D., Liang, L., Graham, D. E., and Gu, B. (2016). Effects of warming on the degradation and production of low molecular-weight labile organic carbon in an Arctic tundra soil. *Soil Biol. Biochem.* 95, 202–211. doi: 10.1016/j.soilbio.2015.12.022

Yao, X., Zhang, Y., Zhu, G., Qin, B., Feng, L., Cai, L., et al. (2011). Resolving the variability of CDOM fluorescence to differentiate the sources and fate of DOM in Lake Taihu and its tributaries. *Chemosphere* 82, 145–155. doi: 10.1016/j.chemosphere.2010.10.049

**Conflict of Interest:** The authors declare that the research was conducted in the absence of any commercial or financial relationships that could be construed as a potential conflict of interest.

**Publisher's Note:** All claims expressed in this article are solely those of the authors and do not necessarily represent those of their affiliated organizations, or those of the publisher, the editors and the reviewers. Any product that may be evaluated in this article, or claim that may be made by its manufacturer, is not guaranteed or endorsed by the publisher.

frontiers in Microbiology

ORIGINAL RESEARCH
published: 08 March 2022
doi: 10.3389/fmicb.2022.840628

# An Increase of Seawater Temperature Upregulates the Expression of *Vibrio parahaemolyticus* Virulence Factors Implicated in Adhesion and Biofilm Formation

*Mélanie Billaud[1], François Seneca[1], Eric Tambutté[2] and Dorota Czerucka[1]**

[1] Biomedical Department, Scientific Center of Monaco, Monaco, Monaco, [2] Marine Biology Department, Scientific Center of Monaco, Monaco, Monaco

OPEN ACCESS

**Edited by:**
*Connie Lovejoy, Laval University, Canada*

**Reviewed by:**
*CARO Audrey, Université Montpellier 2, France*
*Pendru Raghunath, Dr. VRK Women's Medical College, India*

***Correspondence:**
*Dorota Czerucka*
*dczerucka@centrescientifique.mc*

**Specialty section:**
*This article was submitted to Aquatic Microbiology, a section of the journal Frontiers in Microbiology*

**Received:** *21 December 2021*
**Accepted:** *24 January 2022*
**Published:** *08 March 2022*

**Citation:**
*Billaud M, Seneca F, Tambutté E and Czerucka D (2022) An Increase of Seawater Temperature Upregulates the Expression of Vibrio parahaemolyticus Virulence Factors Implicated in Adhesion and Biofilm Formation. Front. Microbiol. 13:840628. doi: 10.3389/fmicb.2022.840628*

Climate change driven seawater temperature (SWT) increases results in greater abundance and geographical expansion of marine pathogens, among which *Vibrio parahaemolyticus* (Vp) causes serious economic and health issues. In addition, plastic pollution in the ocean constitutes a vector for harmful pathogens dissemination. We investigate the effect of elevated SWT on the expression of genes implicated in adhesion and biofilm formation on abiotic surfaces in the clinical Vp strain RIMD2210633, which expresses hemolysins. Among the genes studied, the multivalent adhesion molecule-7 and the GlcNAc-binding protein A were involved in the adhesion of Vp to abiotic and biotic surfaces, whereas the type IV pili, the mannose-sensitive hemagglutinin, and the chitin-regulated pilins facilitate attachment and biofilm formation. Data presented here show that at 21°C, Vp is still viable but does not either proliferate or express the virulence factors studied. Interestingly, at 27°C and as early as 1 h of incubation, all factors are transiently expressed in free-living bacteria only and even more upregulated at 31°C. These results clearly show that increased SWT has an important impact on the adhesion properties of free-living Vp to plastic support and thus emphasize the role of climate change in the spread of this pathogenic bacteria.

**Keywords:** ***Vibrio parahaemolyticus*, climate change, virulence factors, biofilm, marine pathogen ecology**

## INTRODUCTION

*Vibrio parahaemolyticus* (Vp) is a marine bacterium including strains pathogenic to humans. It is mostly known to cause acute gastroenteritis from the consumption of contaminated and undercooked seafood (Daniels et al., 2000). In rare cases, septicemia and extraintestinal infections have been reported as a result of infected wounds from exposition to contaminated waters (Daniels et al., 2000).

*Vibrio* pathogenesis in humans is associated with the production of many virulence factors, among which thermostable direct hemolysin (TDH) and TDH-related hemolysin are considered

to be the main pathogenic factors of Vp (Baker-Austin et al., 2010; Mahoney et al., 2010). TDH acts directly on red blood cells and has hemolytic, enterotoxin, and cytotoxic activities. Epidemiological studies show that most clinical isolates of Vp contain genes coding for TDH and TDH-related hemolysin, whereas only a few environmental isolates contain these genes (Theethakaew et al., 2013). However, recent studies identified TDH in 48% of environmental strains indicating that hemolysin plays a role in bacterial fitness in the environment (Gutierrez West et al., 2013).

There are two major life stages in *Vibrio* species: free-living or planktonic and surface-associated. On the one hand, attachment to abiotic surfaces may be a survival strategy that allows bacteria to survive in a nutrient-poor natural environment by providing a selective advantage through access to nutrients that accumulate at the liquid–surface interface and promotes biofilm formation (Dawson et al., 1981). On the other hand, adhesion to host tissues is the initial step necessary to infection by Vp (Navarre and Schneewind, 1999). Both events, attachment and biofilm formation of Vp, are mediated by the bacterium's expression of functional type IV pili. The genome of Vp encodes two types of IV pilins: the mannose-sensitive hemagglutinin (MSHA) and the chitin-regulated (PilA) pilins (Makino et al., 2003). MSHA pilin facilitates adherence to abiotic and biotic (*e.g.*, chitin) surfaces, whereas PilA pilin enables cell aggregation and biofilm formation (Shime-Hattori et al., 2006). Vp is also capable of synthesizing another extracellular secreted protein that binds to chitin, the GlcNAc-binding protein A (GbpA; Makino et al., 2003). GbpA is involved in the attachment of Vp to chitin but also to human intestinal cells (Kirn et al., 2005; Zampini et al., 2005; Stauder et al., 2012). In addition, the multivalent adhesion molecule-7 (MAM-7) is a constitutively expressed surface protein that contributes to pathogen adhesion to host cells during the early stage of infection (Krachler et al., 2011). It binds two different proteins on the host's cell surface: fibronectin and phosphatidic acid (Krachler and Orth, 2011).

The incidence of Vp disease outbreaks is increasing, and the geographic range of serious infection is expanding, driven in large by rising seawater temperature (SWT) (Martinez-Urtaza et al., 2010). The expansion of *Vibrio* species distribution, from the Southern tropics to more Northern waters, has been reported (Vezzulli et al., 2012; Baker-Austin et al., 2017; Froelich and Daines, 2020). However, little is known about the effects of seawater warming on the expression of virulence factors or the bacterial adhesion to different substrates (*i.e.*, biotic or abiotic), although both represent great implications in the dissemination of Vp worldwide.

Plastic waste representing approximately 80% of all marine litter is now ubiquitous on the surface of oceans, coastlines, and even in most remote parts of the ocean (Carney Almroth and Eggert, 2019). As all new surfaces are introduced to the marine environment, microplastic is rapidly colonized by bacteria (Harrisson et al., 2014). According to the literature, some potentially pathogenic species, including Vp, are able to colonize a wide range of plastics, independently of their chemical composition, *e.g.*, polyethylene, polypropylene, or polystyrene (PS) (Kirstein et al., 2016; Laverty et al., 2020). Potentially pathogenic Vp originating from an estuarine environment were discovered on microplastics in the mid-North Atlantic Ocean and in the North Baltic Sea (Zettler et al., 2013; Kirstein et al., 2016). These findings suggest that harmful microbes that colonize plastics in the marine environment may use microplastics to travel long distances and expand their geographic range across oceans (Rech et al., 2018). In addition, bacteria-contaminated microplastics are ingested by filter-feeders such as oysters and mussels, which are in turn consumed by humans. Although the transfer of pathogens from plastic-containing seafood to humans is still speculative (Barboza et al., 2018), there are great concerns about the role of microplastics in increasing the threats of seafood-borne illnesses. The main goal of this study was to investigate the effects of SWT increase on the expression of virulence factors implicated in adhesion and biofilm formation. The temperatures studied were 21°C, corresponding to the annual average temperature of the Mediterranean Sea, 27°C as the average temperature of tropical waters, and 31°C as an estimated average temperature in the near future by the Intergovernmental Panel on Climate Change (Intergovernmental Panel on Climate Change [IPCC], 2019). In this study, we used a culture-dependent approach in the laboratory to carry out gene expression quantification of virulence factors in seawater at different temperatures in free-living bacteria (*i.e.*, in suspension) and in bacteria adhering to the PS-bottom of Petri dishes.

# MATERIALS AND METHODS

## Bacterial Strain and Growth Condition

The clinically isolated strain Vp RIMD2210633 serotype O3:K6 was provided by T. Honda from Osaka University Japan. To culture, Vp was routinely grown in a 5-ml tube at 37°C in Luria-Bertani LB medium containing 3% NaCl (standard condition).

## Bacterial Growth in Different Experimental Conditions

Overnight Vp culture in standard condition was centrifuged at 2,500 × *g* for 15 min at room temperature (RT). The pellet containing bacteria was suspended in 1 ml of 0.22-μm filtered seawater (FSW) to obtain a dilution corresponding to an optical density at a wavelength of 620 nm ($OD_{620}$) ∼0.8. Sixty microliters of the bacterial solution was put into six-well plates with 2 ml of FSW and incubated at different temperatures, 21, 27, and 31°C. Bacterial growth was followed by measurement of $OD_{620}$ until reaching the stationary phase.

## Bacterial Viability Test Determined by Fluorescence Intensity Measurement

For the viability measurement, overnight culture of bacteria was centrifuged at 2,500 × *g* for 15 min at RT. The pellets containing bacteria were suspended in 1 ml of FSW. Sixty microliters of the bacterial solution was put into six-well plates that were incubated at different temperatures, 21, 27, and 31°C, for 1 h. Samples were centrifuged at 2,500 × *g* for 15 min at RT. The pellet was suspended in a 0.85% NaCl Buffer. $OD_{620}$ was adjusted to ∼0.06.

The viability was measured using the LIVE/DEAD® BacLight™ bacterial viability kit according to the manufacturer's instructions using the Synergy H1 spectrophotometer. Bacterial samples were measured in triplicate. Each sample ratio obtained was compared with the standard curve. For the standard curve, alive Vps were conserved in 0.85% NaCl solution, and dead Vps were killed in 70% isopropyl alcohol solution. The standard curve was obtained by mixing Live/Dead bacteria in the following proportions: 0:100; 10:90; 50:50; 90:10; and 100:0.

## Scanning Electronic Microscopy

Vps were inoculated in 35-mm Petri dishes and maintained in 2 ml of seawater at different temperatures: 27 and 31°C. After 1 h incubation, the free-living bacteria were eliminated by successive washing with seawater, and bacteria adhering to the bottom of Petri dishes were fixed with 4% PFA/FSW (1v/2v). Samples were dehydrated by transfer through a graded series of ethanol, ending with a concentration of 100%. After dehydration, they were incubated for 30 min in hexamethyldisilazane (HMDS)/ethanol 100% (1v/2v), 30 min in HMDS/ethanol (v/v), and 2 × 30 min in HMDS 100% that was subsequently evaporated under a fume hood overnight. Samples were then coated with gold-palladium and observed at 3–5 kV with a JEOL JSM-6010LV.

## Measurement of the Amount of Biofilm

Vps were inoculated in a six-well plate dish in 1 ml of FSW. A volume of 180 μl was transferred into a 96-well plate. The plate with the bacterial suspension and the 96-ped Lid were incubated at different temperatures: 27 and 31°C for 1 h. Formation of biofilm was measured by crystal violet staining method using Biofilm Formation Assay Kit (Dojindo Laboratories) according to the manufacturer's instructions.

## RNA Extraction From Free-Living Bacteria and Bacteria Attached to the Well Bottom

Overnight VPs grown in standard condition were centrifuged, and the pellet containing bacteria were suspended in 1 ml of FSW corresponding to $OD_{620}$ ∼0.8. Sixty microliters of the bacterial solution was put into 1 ml of each medium per well of a six-well plate (Falcon- Ref 353046) and incubated at 21, 27, and 31°C. After 0.5, 1, 3, and 6 h, free-living bacteria were collected and pelleted by centrifugation at 4,500 × *g* for 15 min at RT. The supernatant is discarded. The pellet is suspended into 200 μl of Trizol max (Trizol Max Bacterial RNA Isolation Kit from Thermo Fisher Scientific).

For RNA extraction from bacteria attached to the plate bottom, 250 μl of Trizol max has been added directly into each well plate. The bacteria layer is scrapped, and approximately 200 μl is recovered. All samples are incubated at 95°C for 4 min. We added 1 ml of Trizol Reagent (Invitrogen) to each sample, mixed thoroughly, and waited 5 min at RT.

All the samples obtained from free-swimming and attached bacteria are grinding with Zirconium beads thanks to a Precellys Homogenizer at 2600 revolution two times for 30 s at RT. RNA was purified using columns from the DirectZol kit (Zymo Research) following the manufacturer's instructions. Total RNA was quantified at 260-nm wavelength using a Synergy H1M spectrophotometer.

## Quantitative Reverse Transcription-Polymerase Chain Reaction

Bacterial RNA was used for the determination of the expression of virulence factors. Complementary DNA (cDNA) was constructed using the RevertAid First Strand cDNA Synthesis Kit (Fermentas/Thermoscientific, K1622) according to the manufacturer's instructions.

The quantitative reverse transcription-polymerase chain reaction (RT-qPCR) was performed using the Applied Biosystems Real-Time PCR instrument. Fifteen nanograms of cDNA was placed in triplicate in each well of the qPCR plate, and a solution was added containing: 10 μM of forward primer, 10 μM of reverse primer, 0.1 μl of carboxy-X-rhodamine, which is a dye, 4.9 μl of RNAse free water, and 10 μl of SYBR, which is completed to obtain a final volume of 20 μl per well. The primers used are listed in **Supplementary Table 1**. The plate is then centrifuged. Efficiencies of the primers were in the range of 95–105%. Machine parameters are set to "Comparative Ct," "SYBR Green Reagents" detected, including dissociation curves and on standard cycles (approximately 2 h). Quantification was determined using the comparative cycle threshold ($C_T$) method relative to housekeeping gene RecA, which is highly conserved and implicated in DNA repair or genetic recombination. The average expression obtained after 30-min incubation of bacteria in different media was normalized to 1 for relative quantification expression (RQ).

## Statistical Analysis

The results are expressed as the mean ± standard error. Statistical studies were performed by analysis of means (*T*-test). The p-values $< 0.05$ are considered to be significantly different.

# RESULTS

## Correlation Between *Vibrio parahaemolyticus* Growth and Viability Maintained in Different Seawater Temperatures

We measured the growth and viability of Vp maintained at different SWT (21, 27, and 31°C). At 21°C, Vp did not grow (**Figure 1A**) over all the time of the experimentation (8 h), and after 1 h of exposure, only a small percentage of bacterium (around 40%) were viable (**Figure 1B**). By contrast, when maintained at 27°C, Vp grows and reaches a stationary phase after 7 h of incubation with $OD_{620}$ ∼0.15. The bacterium growth was significantly faster at 31°C when compared with 27°C. It begins after 1 h of incubation at 31°C *versus* 3 h at 27°C. In both conditions (27 and 31°C), the estimated numbers of Vp ($OD_{620}$ of 0.15) in the stationary phase were low (**Figure 1A**). These numbers represent 10% of the bacteria

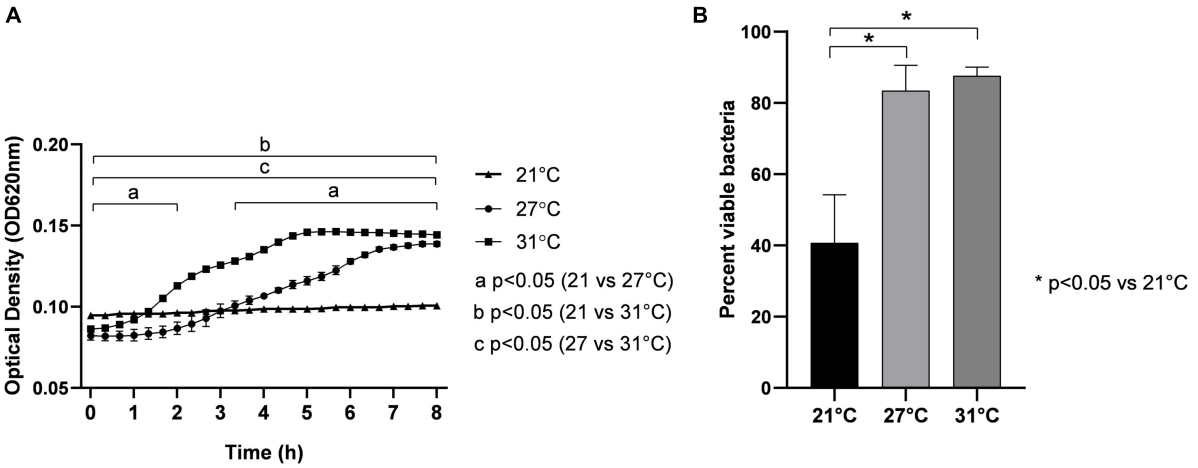


**FIGURE 1 |** Effect of temperature on growth by optical density measurement at 620 nm ($OD_{620}$) **(A)** and viability **(B)** of *V. parahaemolyticus* maintained in seawater at different temperatures: 21, 27, and 31°C. Bacteria were seeded in FSW at $OD_{620}$ ~0.1, corresponding to $3.4 \times 10^7$ CFU/ml. Results are expressed as means ± standard deviations from experiments performed with three replicate samples.

estimated in the stationary phase when maintained in LB NaCl 3% (**Supplementary Figure 1**). This indicates that seawater represents environmental conditions rather than the optimal medium to grow Vp. However, in both conditions (27 and 31°C), cell viability reaches values close to 90% (**Figure 1B**), similar to environmental conditions.

## Adhesion of *Vibrio parahaemolyticus* to the Bottom of Petri Dishes Is Influenced by Temperature

Vps were inoculated in 35-mm Petri dishes and maintained in 2 ml of seawater at different temperatures: 27 and 31°C. Images illustrating adherent bacteria by scanning microscopy are presented in **Figure 2A** for 27°C and **Figure 2B** for 31°C. Bacterial clusters are larger in size at 31°C (**Figure 2B**). The effect of temperature on biofilm formation was confirmed by biofilm quantification (**Figure 2C**) significatively higher at 31°C ($n$ = 8). This observation led us to investigate the effect of temperature on the expression of genes implicated in adhesion and biofilm formation.

## Increasing Seawater Temperature Upregulates Genes Expression Implicated in Adhesion and Biofilm Formation

Adhesion is the first step necessary for biofilm formation on abiotic surfaces or host infection. MAM-7 and GbpA play a role in the adhesion of Vp to abiotic and biotic surfaces (Zampini et al., 2005; Krachler et al., 2011; Stauder et al., 2012). After different times of incubation indicated in **Figure 3**, MAM-7 and GbpA genes expressions were estimated in free-living bacteria (**Figure 3A**) and in adherent bacteria (**Figure 3B**). In free-living bacteria, MAM-7 and GbpA gene expressions were transiently upregulated over kinetics with a maximal expression after 1 h at both temperatures. However, at this time point, the expression of both genes was significantly higher at 31°C compared with 27°C. After 1 h of incubation, the expression of both genes dropped significantly. In adherent bacteria (**Figure 3B**), we did not observe any significant modification in the expression of MAM-7 and GbpA at the early time of incubation, but we observed an overexpression of these genes in both conditions (27 and 31°C) after 6 h of incubation.

In Vp, the MSHA pili facilitate attachment to abiotic surfaces and biofilm formation, whereas PilA pili mediate cell-to-cell interactions and the binding of one bacterium to another (Shime-Hattori et al., 2006). After different incubation times, their expressions were estimated in free-living bacteria (**Figure 4A**) and in adherent bacteria (**Figure 4B**). The profile of their expression is similar to those found for MAM-7 and GbpA. In free-living bacteria, MSHA and PilA expressions were overexpressed after 1 h of incubation when compared with the first time point 0.5 h, and their expressions were significantly higher at 31°C compared with 27°C. After 3 and 6 h of incubation, the expression of both genes significantly dropped. In adherent bacteria (**Figure 4B**), we did not observe a significant modification in the expression of MSHA and PilA between the two temperatures 27 and 31°C in the early time of incubation, but we observed overexpression in both conditions at 6 h of incubation.

Note that the expression of all these genes is not upregulated at 21°C in free-living bacteria (**Supplementary Figure 2**) nor in adherent bacteria (**Supplementary Figure 3**).

## Increasing Seawater Temperature Induces the Expression of Thermostable Direct Hemolysin

Thermostable direct hemolysin is a hemolysin involved in the pathogenesis of Vp strains that infect humans. As the strain 03:K6 was isolated from a patient, we looked at whether these

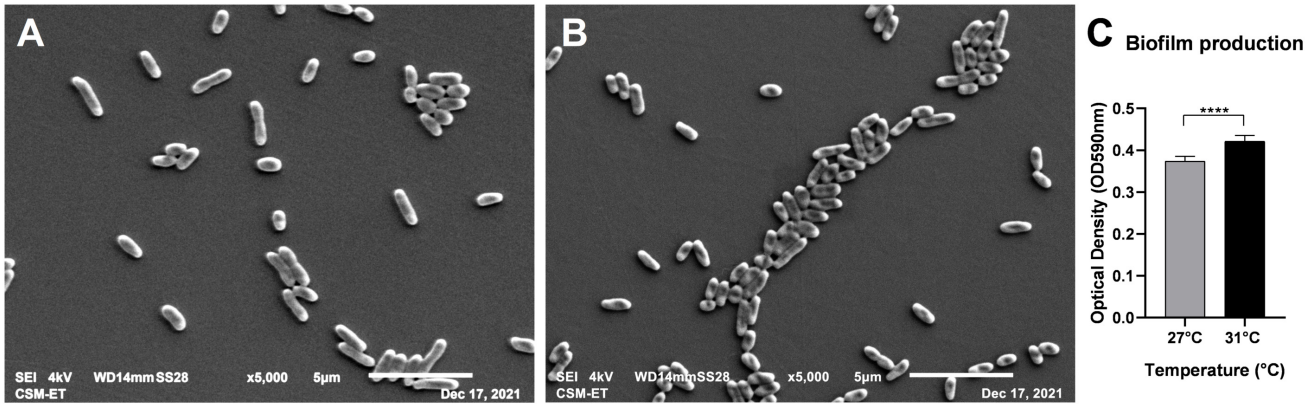


**FIGURE 2 |** Scanning electron micrographs presenting adhering *V. parahaemolyticus* at 27°C **(A)** and 31°C **(B)**. (Magnification × 5,000). Biofilm quantification of adhering bacteria to plastic **(C)**. ****p*-values < 0.0001.

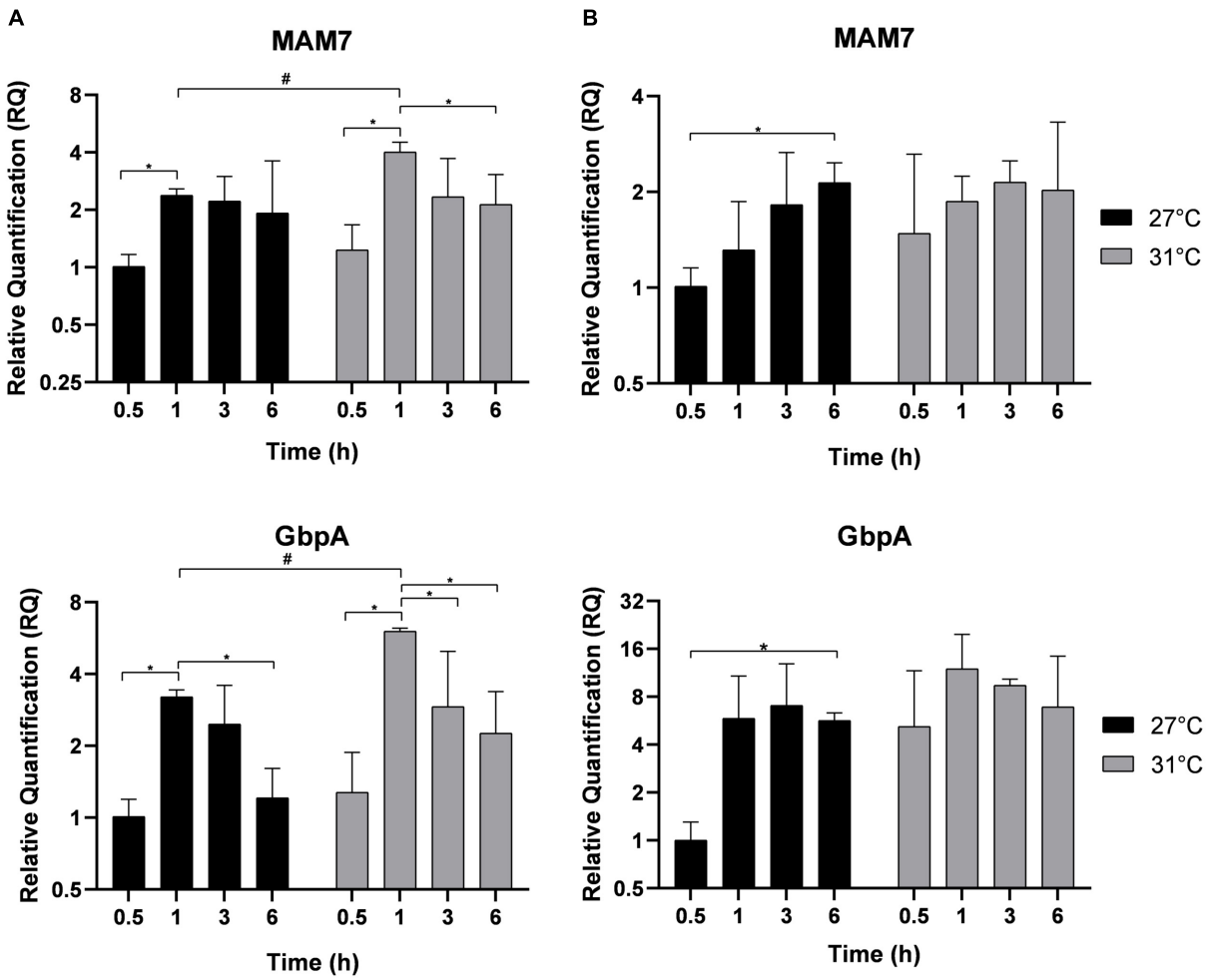


**FIGURE 3 |** Adhesion genes expression MAM-7 and GbpA in free-living *V. parahaemolyticus* **(A)** and adherent bacteria **(B)** incubated at 27°C (black) and 31°C (gray). Bacteria were maintained 0.5, 1, 3, and 6 h in different conditions before RNA extraction from free-living bacteria and adherent bacteria for same well. Relative quantification expressions are expressed as means ± standard deviations of results from experiments performed with three replicate samples. #Significant difference between temperatures. *Significant difference between time points.

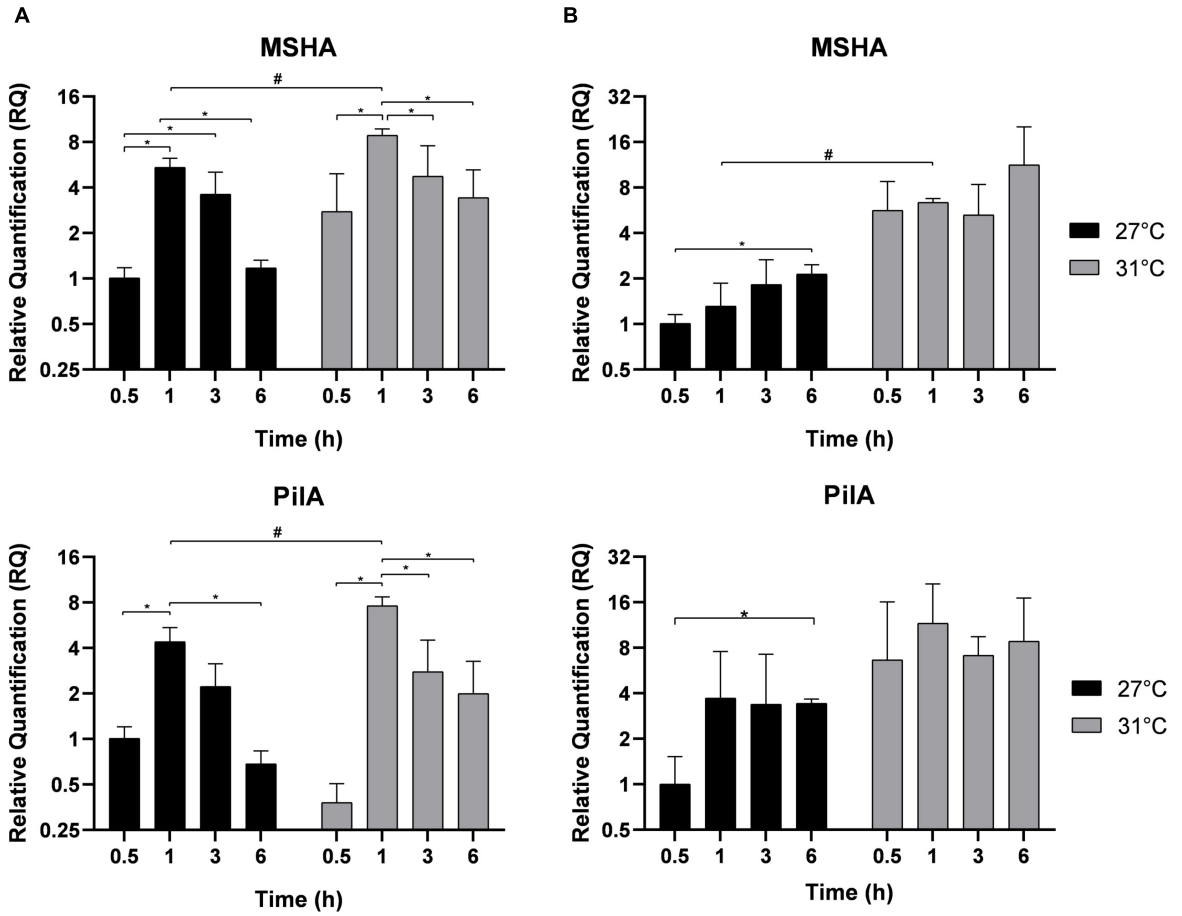


**FIGURE 4 |** Biofilm genes expression MSHA and PilA in free-living *V. parahaemolyticus* **(A)** and adherent bacteria **(B)** incubated at 27°C (black) and 31°C (gray). Bacteria were maintained 0.5, 1, 3, and 6 h in different conditions before RNA extraction from free-living bacteria and adherent bacteria in same well. Relative quantification expressions are expressed as means ± standard deviations of results from experiments performed with three replicate samples. #Significant difference between temperatures. *Significant difference between time points.

bacteria synthesize TDH in seawater and whether the increase in temperature can influence its expression level. After different incubation times, TDH gene expression was estimated in free-living bacteria (**Figure 5A**) and in adherent bacteria (**Figure 5B**). In free-living bacteria, a significant increase in TDH gene expression was observed at 27°C after 1 and 3 h of incubation compared with the first time point at 0.5 h. In comparison, no significant increase in TDH expression was observed over time at 31°C. Similarly, the TDH transcript level was not modified at 21°C in both bacterial populations (**Supplementary Figure 4**). However, after 1 h of incubation, TDH expression was significantly upregulated at 31°C compared with 27°C (**Figures 5A,B**) in both free-living and adherent bacteria.

## DISCUSSION

Bacterial adhesion is essential to the colonization of biotic and abiotic surfaces and represents a link between the behavior of bacteria in natural environments and their pathogenicity potential. Data presented in this study show that elevated SWTs can affect the expression of genes involved in adhesion and biofilm formation in Vp and favor its adhesion to plastics. Warmer temperatures also promote Vp's pathogenicity by inducing the synthesis of the TDH toxin. Interestingly, bacterial cultures in the laboratory consisting of suspended and adherent populations (*i.e.*, similar to free-living planktonic and sedentary in the environment) show differences in the kinetics and induction rates of all these genes.

Pathogenic bacteria must detect and respond to changes in their local environment parameters (*i.e.*, temperature, pH, salinity, and nutrient availability) to successfully colonize and invade their host (Gode-Potratz et al., 2011). Among pathogens, vibrios show a broad tolerance to several environmental parameters, including temperature. In this study, SWT significantly influences the growth of the clinical Vp strain O3:K6, which is latent at 21°C but begins to grow at 27 and 31°C. This result confirms previous observations that under adverse conditions, including cold temperature, Vp is able to enter a viable but not culturable state that supports long-term survival

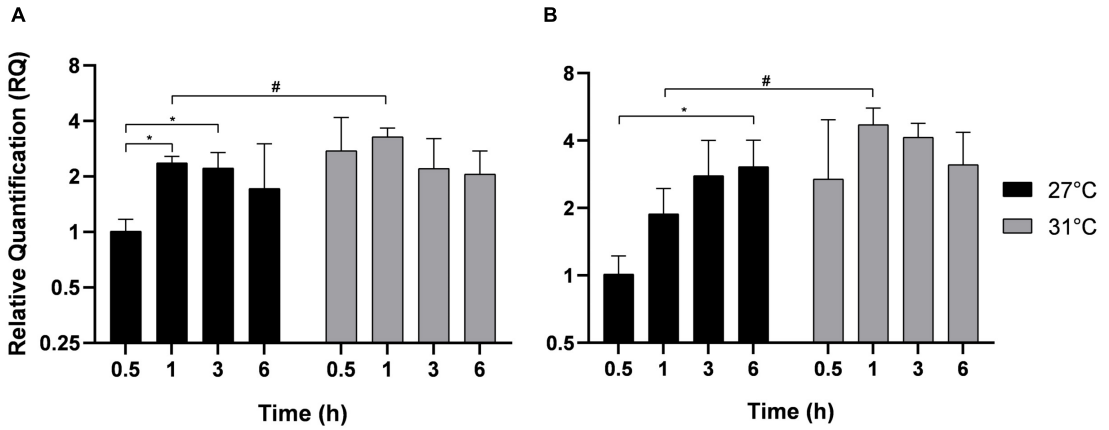


**FIGURE 5 |** Thermostable direct hemolysin gene expression in free-living *V. parahaemolyticus* **(A)** and adherent bacteria **(B)** incubated at 27°C (black) and 31°C (gray). Bacteria were maintained 0.5, 1, 3, and 6 h in different conditions before RNA extraction from free-living bacteria and adherent bacteria in same well. Relative quantification expressions are expressed as means ± standard deviations of results from experiments performed with three replicate samples. #Significant difference between temperatures. *Significant difference between time points.

(Xu et al., 1982; Oliver, 2005; Burnham et al., 2009). Entering a partial dormant state is one of the ways Vp can persist in cold environments. Attachment to substrates such as plankton has also been proposed as another mechanism of environmental persistence (Sarkar et al., 1983).

Because adhesion and biofilm formation is the first step in the colonization of surfaces and pathogenesis, we studied the influence of temperature on the expression of genes essential to these mechanisms: adhesins and pilins. Our data show a quick induction of the expression of genes in free-living bacteria coding for adhesins (MAM-7 and GbpA) and the type IV pilins (MSHA and PilA) occurring after 1 h of incubation at 27°C. Warmer temperature exerts a stimulating effect, as these genes are upregulated at 31°C when compared with 27°C. After 3 and 6 h of incubation, expression levels of GbpA, PilA, and MSHA are downregulated. Interestingly, the quick increase in gene expression at 1 h is observed only in suspended bacteria. In adherent bacteria, all the genes mentioned earlier are upregulated after 6 h of incubation, but the increased temperature has no impact on their expressions. Our data show that an adaptation of Vp to temperature fluctuations results in the regulation of adhesin and pilin genes. However, this temperature-dependent regulation only occurs in suspended and not in adherent bacteria.

Differences in gene expression between free-living and sedentary lifestyles have been described for many pathogenic bacteria and involve surface sensing (Gode-Potratz et al., 2011). In the case of flagellated rod-shaped bacteria (*e.g.*, *E. coli* and vibrios), surface sensing takes place *via* a two-step process: (1) reversible attachment characterized by polarly attached bacteria and (2) irreversible attachment, which results in microcolonies and biofilm formation (Armbruster and Parsek, 2018). Vp senses the surface *via* rotation of the flagella and can stimulate a specific program of genes depending on whether the surface is favorable to colonization and pathogenesis. The OpaR gene has been described as a quorum-sensing regulator that negatively regulates polar flagellum in Vp (Lu et al., 2021). Here, OpaR is upregulated in suspended Vp after 1 h of incubation (**Supplementary Figure 5A**) and suggests repression of Vp's motility by regulating the expression of its flagella. Noteworthy, this gene is also overexpressed at 31°C compared with 27°C, further supporting our previous observation on the increased adhesion at elevated temperature.

The two pilin genes studied play different roles in the adhesion process. MSHA pilin is crucial to arresting cell motion in near-surface swimming bacteria and allows the transition to irreversible attachment and colony formation, whereas PilA pilin mediates cell-to-cell interactions and binding of one bacterium to another (Frischkorn et al., 2013; Utada et al., 2014). Both pilins, MSHA and PilA, worked synergistically and were involved in biofilm formation in Vp on abiotic PS, synthetic chitin, and biological diatom-derived chitin (Frischkorn et al., 2013). Data presented here clearly show that these two pilin genes are synergistically expressed in suspended Vp. We also observed a significant increase in expression for these two genes at 31°C, which could potentially also promote the attachment and the formation of colonies.

The role of adhesins in colony formation on plastics is less studied. GbpA and MAM-7 were mainly implicated in the virulence processes. GbpA contributes to the adhesion on culture epithelial cells by interacting with GlcNAC residues of mucin and interacting with natural polymers, *e.g.*, chitin present on marine hosts (Zampini et al., 2005; Bhowmick et al., 2008). MAM-7 constitutes an adhesin especially found in mammal infection cases (Krachler et al., 2011). This adhesin binds with high affinity to phosphatidic acid and low affinity to fibronectin (Krachler and Orth, 2011). To our knowledge, there are no reports on the binding of GbpA and MAM-7 to synthetic polymers. Curiously, this adhesin is upregulated in seawater in free-living bacteria only, and its expression is positively influenced by elevated temperature. The role of GbpA and MAM-7 in biofilm formation on synthetic polymers, *e.g.*, PS of the bottom of Petri dishes, requires further investigation.

As the body temperature of mammals is often higher than the temperature of their external environment, many bacterial virulence factors are thermally regulated. TDH is a virulence factor mainly present in clinical isolates of Vp. The Vp strain O3:K6 used in this study is isolated from a patient, and this strain was reported to synthesize TDH at 37°C (Mahoney et al., 2010). Data presented here show that this strain expresses TDH in seawater at higher levels at 31°C when compared with 27°C. These data first illustrate that this clinical strain can express TDH in seawater and, second, that its expression is temperature-dependent. Thermoregulation of the expression of known and putative virulence-associated traits, including hemolysin, motility, and biofilm formation, has only been reported in environmental and clinical strains maintained in a heart infusion medium (Mahoney et al., 2010). To our knowledge, this is the first study to demonstrate the effect of temperature on the upregulation of TDH expression in a clinical Vp strain maintained in seawater. It is also interesting to point out that this toxin is synthesized in free-living and adherent bacteria.

A direct link between infection of marine animals and temperature-dependent expression of virulence factors was recently reported in the case of *Vibrio coralliilyticus* that was isolated from the coral *Acropora cytherea* during a bleaching outbreak due to thermal stress (Ushijima et al., 2016). In the case of this vibrio, mutation of MSHA reduces its virulence. Another mutation in ToxR also decreases the pathogenicity of this bacterium. The ToxR gene encodes a regulatory protein under the control of quorum-sensing and is involved in regulating the expression of virulence genes in vibrios (Zhang et al., 2018). Here, ToxR is overexpressed in suspended Vp during the early time of incubation and is upregulated at 31°C when compared with 27°C (**Supplementary Figure 5B**). These results support the correlation between SWT and Vp's virulence.

As plastic debris in the environment continues to increase, an emerging concern is the potential for microplastics to act as vectors in pathogen dissemination. Zettler et al. (2013) showed that microbial communities on marine plastic debris differ consistently from the surrounding seawater communities and coined the term "Plastisphere" for this new habitat, which is now acting as a "mobile ecological niche." Numerous reports describe the presence of pathogenic bacteria on both macro- and microplastic surfaces found across oceans (Amaral-Zettler et al., 2020). Among marine bacteria, *Vibrio* spp. have been found in high abundances within the "plastisphere," in particular during summer months (Bowley et al., 2021). This observation is in agreement with the findings reported in this study, showing that elevated SWTs favor the expression of genes implicated in the adhesion of *Vibrio* to plastic and, consequently, the number of adhering bacteria. In addition, several studies demonstrate that microplastic surfaces represent favorable environments for biofilm formation. Living within a biofilm is highly beneficial for adhering bacteria to become more infectious than free-living bacteria. When compared with free-living bacteria, adhering bacteria have shown significant elevation in metabolic pathways that contributes to pathogenesis and favor horizontal gene transfer that may contribute to the development of resistance to antibiotics (Bowley et al., 2021). These observations also support our results showing different gene expressions for adhesins between free-living and adhering bacteria.

Altogether, the findings presented in this study clearly show the impact of increased temperature on the virulence of Vp in seawater environments. Warmer temperatures promote growth and the expression of virulence factors implicated in biofilm formation on abiotic surfaces and the synthesis of toxins. These factors play an important role in the pathogenesis of Vp and therefore represent a mechanism by which increased SWT and plastic pollution can promote the spread of plastic-associated pathogenic Vp and the intensification of their virulence.

## DATA AVAILABILITY STATEMENT

The original contributions presented in the study are included in the article/**Supplementary Material**, further inquiries can be directed to the corresponding author/s.

## AUTHOR CONTRIBUTIONS

DC conceived and designed the experiments. MB and ET performed the experimentation. DC, MB, and FS analyzed the data. DC wrote the first draft. FS and MB revised the manuscript. All authors contributed to the article and approved the submitted version.

## FUNDING

Funding was provided by the government of Monaco. MB was financially supported by a Ph.D. fellowship funded by Lady Monika Bacardi and the association "les Amis du CSM."

## ACKNOWLEDGMENTS

We are grateful to Maria Luiza Pedrotti and Patrick Munro for their participation in discussions on the experimental design. We also thank Rodolphe Pontier-Bres for their help in the laboratory.

## SUPPLEMENTARY MATERIAL

The Supplementary Material for this article can be found online at: https://www.frontiersin.org/articles/10.3389/fmicb.2022.840628/full#supplementary-material

**Supplementary Figure 1 |** Growth of Vp in LB NaCl 3%. Overnight *V. parahaemolyticus* culture in standard condition was centrifuged at 2500 x g during 15 min at room temperature (RT). The pellet containing bacteria was suspended in 1 mL of LB NaCl 3% to obtain a dilution corresponding to $OD_{620}$ ~ 0.8. 60 µl of the bacterial solution was put into 6 well plates with 2 mL of LB NaCl 3% and incubated at different temperatures 21, 27, 31, and 37°C. Bacterial growth was followed by measurement of $OD_{620}$ until reaching the stationary phase.

**Supplementary Figure 2 |** Adhesion and biofilm genes expression at 21°C in free-living Vp maintained in FSW.

**Supplementary Figure 3 |** Adhesion and biofilm genes expression at 21°C in adhering Vp maintained in FSW.

**Supplementary Figure 4 |** TDH expression in free-living **(A)** or adhering **(B)** Vp maintained in FSW at 21°C.

**Supplementary Figure 5 |** OpaR **(A)** and Tox R **(B)** expression in free-living Vp maintained in FSW at 27 and 31°C.

**Supplementary Table 1 |** Primers and sequences used in this study.

## REFERENCES


Amaral-Zettler, L. A., Zettler, E. R., and Mincer, T. (2020). Ecology of the plastisphere. *Nat. Rev. Microbiol.* 18, 139–151. doi: 10.1038/s41579-019-0308-0

Armbruster, C. R., and Parsek, M. R. (2018). New insight into the early stages of biofilm formation. *Proc. Natl. Acad. Sci. U. S. A.* 115, 4317–4319. doi: 10.1073/pnas.1804084115

Baker-Austin, C., Stockley, L., Rangdale, R., and Martinez-Urtaza, J. (2010). Environmental occurrence and clinical impact of *Vibrio vulnificus* and *Vibrio parahaemolyticus*, a European perspective. *Environ. Microbiol. Rep.* 2, 7–18. doi: 10.1111/j.1758-2229.2009.00096.x

Baker-Austin, C., Trinanes, J., Gonzales-Escalona, N., and Martinez-Urtaza, J. (2017). Non-cholera vibrios: the microbial barometer of climate change. *Trends Microbiol.* 25, 76–84. doi: 10.1016/j.tim.2016.09.008

Barboza, L. G. A., Vethaak, A. D., Lavorante, B. R. B. O., Lundebye, A.-K., and Guilhermino, L. G. (2018). Marine microplastic debris: an emerging issue for food security, food safety and human health. *Mar. Pollut. Bull.* 133, 336–348. doi: 10.1016/j.marpolbul.2018.05.047

Bowley, J., Baker-Austin, C., Porter, A., Hartnell, R., and Lewis, C. (2021). Oceans-hitchhikers-assessing pathogen risks from marine microplastic. *Trends Microbiol.* 29, 107–116. doi: 10.1016/j.tim.2020.06.011

Bhowmick, R., Ghosal, A., Das, B., Koley, H., Saha, D. R., Ganguly, S., et al. (2008). Intestinal adherence of *Vibrio cholerae* involves a coordinated interaction between colonization factors GpbA and mucin. *Infect. Immun.* 76, 4968–4977. doi: 10.1128/IAI.01615-07

Burnham, V. E., Janes, M. E., Jakus, K. L. A., Supan, J., DePaola, A., and Bell, J. (2009). Growth and survival differences of *Vibrio vulnificus* and *Vibrio parahaemolyticus* strains during cold storage. *J Food Sci. Dis.* 181, 1661–1666. doi: 10.1111/j.1750-3841.2009.01227.x

Carney Almroth, B., and Eggert, H. (2019). Marine plastic pollution: source impacts and policy issues. *Rev. Environ. Econ. Policy* 13, 317–326.

Daniels, N. A., MacKinnon, L., Bishop, R., Alterkruse, S., Ray, B., Hammond, R. M., et al. (2000). *Vibrio parahaemolyticus* infections in the United States 1973-1998. *J. Inf. Dis.* 181, 1661–1666. doi: 10.1086/315459

Dawson, M. P., Humphrey, B. A., and Marshall, K. C. (1981). Adhesion: a tactic in the survival strategy of a marine Vibrio during starvation. *Curr. Microbiol.* 6, 195–199. doi: 10.1007/bf01566971

Frischkorn, K. R., Stojanovski, A., and Paranjpye, R. (2013). *Vibrio parahaemolyticus* type IV pili mediate interactions with diatom-derived chitin and point to an unexplored mechanism of environmental persistence. *Environ. Microbiol.* 15, 1416–1427. doi: 10.1111/1462-2920.12093

Froelich, B. A., and Daines, D. A. (2020). In hot water: effects of climate change on Vibrio-human interactions. *Environ. Microbiol.* 22, 4101–4111. doi: 10.1111/1462-2920.14967

Gode-Potratz, C. J., Kustusch, R. J., Breheny, P. J., Weiss, D. S., and McCarter, L. L. (2011). Surface sensing in *Vibrio parahaemolyticus* triggers a program of gene expression that promotes colonization and virulence. *Mol. Microbiol.* 79, 240–263. doi: 10.1111/j.1365-2958.2010.07445.x

Gutierrez West, C. K., Klein, S. L., and Lovell, C. K. (2013). High frequency of virulence factor genes tdh, trh, and tlh in *Vibrio parahaemolyticus* strains isolated from a pristine estuary. *Appl. Environ. Microbiol.* 79, 2247–2252. doi: 10.1128/AEM.03792-12

Harrisson, J. P., Schratzberger, M., Sapp, M., and Osborn, M. A. (2014). Rapid bacterial colonization of low-density polyethylene microplastics in coastal sediment microcosms. *BMC Microbiol.* 14:232. doi: 10.1186/s12866-014-0232-4

Intergovernmental Panel on Climate Change [IPCC] (2019). *The Special Reports on the Ocean and Cryosphere in a Changing Climate*. Geneva: intergovernmental Panel on climate change (IPCC), 1–44.

Kirn, T. J., Jude, B. A., and Taylor, R. K. (2005). A colonization factor links *Vibrio cholerae* environmental survival and human infection. *Nature* 438, 863–866. doi: 10.1038/nature04249

Kirstein, I. V., Kirmizi, S., Wichels, A., Garin-Fernandez, A., Erle, R., Loder, M., et al. (2016). Dangerous hitchhikers? Evidence for potentially pathogenic Vibrio spp. On plastic particles. *Mar. Environ. Res.* 120, 1–8. doi: 10.1016/j.marenvres.2016.07.004

Krachler, A. M., Ham, H., and Orth, K. (2011). Outer membrane adhesion factor multivalent adhesion molecule 7 initiates host cell binding during infection by gram negative pathogens. *Proc. Natl. Acad. Sci. U. S. A.* 108, 11614–11619. doi: 10.1073/pnas.1102360108

Krachler, A. M., and Orth, K. (2011). Functional characterization of the interaction between bacterial adhesins multivalent adhesion molecule 7 (MAM7) proteins and its host. *J. Biol. Chem.* 286, 38939–38947. doi: 10.1074/jbc.M111.291377

Laverty, A. L., Primpke, S., Lorenz, C., Gerdts, G., and Dobbs, F. C. (2020). Bacterial biofilms colonizing plastics in estuarine waters, with an emphasis on *Vibrio* spp. and bacterial resistance. *PLoS One* 15:e0237704. doi: 10.1371/journal.pone.0237704

Lu, R., Sun, J., Qiu, Y., Zhang, M., Xue, X., Li, X., et al. (2021). The quorum sensing regulator OpaR is a repressor of polar flagellum genes in *Vibrio parahaemolyticus*. *J. Microbiol.* 59, 651–657. doi: 10.1007/s12275-021-0629-3

Mahoney, J. C., Gerding, M. J., Jones, S. H., and Whistler, C. A. (2010). Comparison of the pathogenic potentials of environmental and clinical *Vibrio parahaemolyticus* strains indicates a role for temperature regulation of virulence. *App. Environ. Microbiol.* 76, 7459–7465. doi: 10.1128/AEM.01450-10

Makino, K., Oshima, K., Kurokawa, K., Yokoyama, K., Uda, T., Tagomori, K., et al. (2003). Genome sequence of *Vibrio parahaemolyticus*: a pathogenic mechanism distinct from that of *V. cholerae*. *Lancet* 361, 743–749. doi: 10.1016/S0140-6736(03)12659-1

Martinez-Urtaza, J., Bowers, J. C., Trinanes, J., and DePaola, A. (2010). Climate anomalies and increasing risk of *Vibrio parahaemolyticus* and *Vibrio vulnificus* illnesses. *Food Res. Int.* 43, 1780–1790.

Navarre, W. W., and Schneewind, O. (1999). Surface proteins of gram-positive bacteria and mechanisms of their targeting to the cell wall envelope. *Microbiol. Mol. Biol. Rev.* 63, 174–229. doi: 10.1128/MMBR.63.1.174-229.1999

Oliver, J. (2005). The viable but nonculturable state in bacteria. *J. Microbiol.* 43, 93–100.

Rech, S., Thiel, M., Borrell Pichs, Y. J., and Garcia-Vazquez, E. (2018). Travelling light: fouling biota on microplastics arriving on beaches of remote Rapa Nui (Easter Island) in the South pacific subtropical gyre. *Mar. Pollut. Bull.* 137, 119–128. doi: 10.1016/j.marpolbul.2018.10.015

Sarkar, B. L., Balakrish, N. G., Sircar, B. K., and Pal, S. C. (1983). Incidence and level of *Vibrio parahaemolyticus* associated with freshwater plankton. *Appl. Environ. Microbiol.* 46, 288–290. doi: 10.1128/aem.46.1.288-290.1983

Shime-Hattori, A., Iida, T., Arita, M., Park, K. S., Kodama, T., and Honda, T. (2006). Two type IV pili of *Vibrio parahaemolyticus* play different roles in biofilm formation. *FEMS Microbiol. Lett.* 264, 89–97. doi: 10.1111/j.1574-6968.2006.00438.x

Stauder, M., Huq, A., Pezzati, E., Grim, C. J., Ramoino, P., Pane, L., et al. (2012). Role of GbpA protein, an important virulence-related colonization factor, for *Vibrio cholerae*'s survival in the aquatic environment. *Environ. Microbiol. Rep.* 4, 439–445. doi: 10.1111/j.1758-2229.2012.00356.x

Theethakaew, C., Feil, E. J., Castillo-Ramírez, S., Aanensen, D. M., Suthienkul, O., Neil, D. M., et al. (2013). Genetic relationships of *Vibrio parahaemolyticus* isolates from clinical, human carrier, and environmental sources in Thailand, determined by multilocus sequence analysis. *Appl. Environ. Microbiol.* 79, 2358–2370. doi: 10.1128/AEM.03067-12

Ushijima, B., Videau, P., Poscablo, D., Stengel, J. W., Beurmann, S., Burger, A. H., et al. (2016). Mutation of the tox R or mshA genes from *Vibrio coralliilyticus*

strain OCN014 reduces infection of the coral *Acropora Cytherea*. *Environ. Microbiol.* 18, 4055–4067. doi: 10.1111/1462-2920.13428

Utada, A. S., Bennet, R. R., Fong, J. C. N., Gibiansky, M. L., Yildiz, H. Y., Golestanian, R., et al. (2014). *Vibrio cholerae* use pili and flagella synergistically to effect motility and conditional surface attachment. *Nat. Commun.* 5, 4913–4928. doi: 10.1038/ncomms5913

Vezzulli, L., Brettar, I., Pezzati, E., Reid, P. C., Colwell, R., Hofle, M. G., et al. (2012). Long-term effects of ocean warming on the prokaryotic community: evidence from the vibrios. *ISME J.* 6, 21–30. doi: 10.1038/ismej.2011.89

Xu, H. S., Roberts, N., Singleton, F. L., Attwell, R. W., Grimes, D. J., and Colwell, R. R. (1982). Survival and viability of nonculturable *Escherichia coli* and *Vibrio cholerae* in the estuarine and marine environment. *Microbiol. Ecol.* 8, 313–323. doi: 10.1007/BF02010671

Zampini, M., Pruzzo, C., Bondre, V. P., Tarsi, R., Cosmo, M., Bacciaglia, A., et al. (2005). *Vibrio cholerae* persistence in aquatic environments and colonization of intestinal cells: involvement of a common adhesion mechanism. *FEMS Microbiol. Lett.* 244, 267–273. doi: 10.1016/j.femsle.2005.01.052

Zettler, E. R., Mincer, T. J., and Amaral-Zettler, L. A. (2013). Life in the "plastisphere": microbial communities on plastic marine debris. *Environ. Sci. Technol.* 47, 7137–7146. doi: 10.1021/es401288x

Zhang, Y., Hu, L., Osei-Adjei, G., Zhang, Y., Yang, W., Yin, Z., et al. (2018). Autoregulation of ToxR and its regulatory actions on major virulence gene loci in *Vibrio parahaemolyticus*. *Cell. Infect. Microbiol.* 8:291. doi: 10.3389/fcimb.2018.00291

**Conflict of Interest:** The authors declare that the research was conducted in the absence of any commercial or financial relationships that could be construed as a potential conflict of interest.

**Publisher's Note:** All claims expressed in this article are solely those of the authors and do not necessarily represent those of their affiliated organizations, or those of the publisher, the editors and the reviewers. Any product that may be evaluated in this article, or claim that may be made by its manufacturer, is not guaranteed or endorsed by the publisher.

frontiers in Microbiology

ORIGINAL RESEARCH
published: 23 March 2022
doi: 10.3389/fmicb.2022.832810

# Thermal Acclimation and Adaptation in Marine Protozooplankton and Mixoplankton

*Albert Calbet**† and Enric Saiz†*

*Institut de Ciències del Mar, CSIC, Barcelona, Spain*

Proper thermal adaptation is key to understanding how species respond to long-term changes in temperature. However, this is seldom considered in protozooplankton and mixoplankton experiments. In this work, we studied how two heterotrophic dinoflagellates (*Gyrodinium dominans* and *Oxyrrhis marina*), one heterotrophic ciliate (*Strombidium arenicola*), and one mixotrophic dinoflagellate (*Karlodinium armiger*) responded to warming. To do so, we compared strains adapted at 16, 19, and 22°C and those adapted at 16°C and exposed for 3 days to temperature increases of 3 and 6°C (acclimated treatments). Neither their carbon, nitrogen or phosphorus (CNP) contents nor their corresponding elemental ratios showed straightforward changes with temperature, except for a modest increase in P contents with temperature in some grazers. In general, the performance of both acclimated and adapted grazers increased from 16 to 19°C and then dropped at 22°C, with a few exceptions. Therefore, our organisms followed the "hotter is better" hypothesis for a temperature rise of 3°C; an increase of >6°C, however, resulted in variable outcomes. Despite the disparity in responses among species and physiological rates, 19°C-adapted organisms, in general, performed better than acclimated-only (16°C-adapted organisms incubated at +3°C). However, at 22°C, most species were at the limit of their metabolic equilibrium and were unable to fully adapt. Nevertheless, adaptation to higher temperatures allowed strains to maintain physiological activities when exposed to sudden increases in temperature (up to 25°C). In summary, adaptation to temperature seems to confer a selective advantage to protistan grazers within a narrow range (i.e., ca. 3°C). Adaptation to much higher increases of temperatures (i.e., +6°C) does not confer any clear physiological advantage (with few exceptions; e.g., the mixotroph *K. armiger*), at least within the time frame of our experiments.

**Keywords: microzooplankton, protist, mixotroph, temperature, grazing, growth, climate change, adaptation**

OPEN ACCESS

***Edited by:***
*Jun Sun,*
*China University of Geosciences Wuhan, China*

***Reviewed by:***
*Casey Michael Godwin,*
*University of Michigan, United States*
*Sophie Charvet,*
*American Museum of Natural History, United States*

****Correspondence:***
*Albert Calbet*
*acalbet@icm.csic.es*

*† These authors have contributed equally to this work*

***Specialty section:***
*This article was submitted to Aquatic Microbiology, a section of the journal Frontiers in Microbiology*

***Received:*** *10 December 2021*
***Accepted:*** *21 February 2022*
***Published:*** *23 March 2022*

***Citation:***
*Calbet A and Saiz E (2022) Thermal Acclimation and Adaptation in Marine Protozooplankton and Mixoplankton. Front. Microbiol. 13:832810. doi: 10.3389/fmicb.2022.832810*

## INTRODUCTION

The progressive increase of temperature due to anthropogenic sources (Intergovernmental Panel on Climate Change [IPCC], 2014) will certainly affect planktonic communities in the coming future. This is because temperature is a major factor driving biological activity; the resulting changes in the fitness of a species in response to temperature may provide a selective advantage/disadvantage in comparison to other coexisting species (Halsband-Lenk et al., 2002). This rule applies to all marine

organisms, including protistan grazers, such as microzooplankton (pure heterotrophic protists) and mixoplankton (autotrophic protists with phagotrophic capability). Both groups of protistan grazers, which encompass many ciliates and dinoflagellates, are key components of marine pelagic food webs because of their functions as major grazers of phytoplanktonic primary production and as very important prey for larger zooplankton (Calbet, 2001; Calbet and Saiz, 2005; Flynn et al., 2019; Traboni et al., 2021).

Despite the relevance of temperature, most ecophysiological studies addressing its direct effects on protistan grazers do not include multigenerational effects and typically only address short-term responses to variations in environmental temperature [see review by Montagnes et al. (2003)]. Therefore, the actual response of protist grazers to gradual and longer-term temperature changes in marine systems remains essentially unexplored. Conversely, long-term adaptations to temperature have been studied in planktonic algae, and the results have been very revealing and occasionally opposite to those that were expected. For instance, the accepted faster thermal response of respiration vs. photosynthesis, predicted by the metabolic theory of ecology (López-Urrutia et al., 2006; Rose and Caron, 2007), may not be the same after proper adaptation (>100 generations) to environmental conditions (Padfield et al., 2016; Barton et al., 2020). This is because basal metabolism diminishes after genetic adaptation to temperature (Padfield et al., 2016; Barton et al., 2020). Other observed changes in temperature-adapted species are stoichiometric (lower C:N ratios) and related to more efficient use of carbon (Padfield et al., 2016; Aranguren-Gassis et al., 2019). The elemental composition of an organisms is the result of the balance between its metabolic demands and the relative supply of elements in the environment (Sterner and Elser, 2002). It is assumed that phytoplankton exhibit wide variations in their elemental composition and protozoans are more homoeostatic, showing a narrower range of variation (Sterner and Elser, 2002; Klausmeier et al., 2004). However, several studies have shown that the elemental stoichiometry of protozoans may vary significantly in response to the environment and prey composition (Hantzsche and Boersma, 2010; Malzahn et al., 2010; Meunier et al., 2012), and may affect the energy transfer to upper trophic levels (Traboni et al., 2021). The incorporation of elemental ratios and absolute elemental contents (dependent on cellular volume) of different planktonic groups into ecosystem models could improve our ability to predict the response of planktonic communities to environmental threats, and help to understand their influence on the biogeochemistry of the ocean (Litchman et al., 2013; Meunier et al., 2017). Little is known, however, about protistan grazers, both mixotrophic and heterotrophic, in this respect.

We hypothesize that because of the different activation energies between physiological processes, a rise in temperature will favor phagotrophy over photosynthetic carbon acquisition in mixotrophs (Wilken et al., 2013; Lin et al., 2018). We could also hypothesize that following the von Bertalanffy-Perrin model, which states that catabolism is more affected by temperature than anabolism (Perrin, 1995; Li et al., 2011), higher temperatures will enhance respiratory losses to a larger extent than ingestion in protozooplankton (at least for short-term responses). This imbalance should result in a reduction of gross growth efficiency (GGE; Straile, 1997; Li et al., 2011) and perhaps in lower cellular C:N and C:P ratios, depending on the temperature-sensitivity of the excretion response (Alcaraz et al., 2013). We cannot discard, however, that fully temperature-adapted species may not show such differences, as previously reported for algae (Padfield et al., 2016; Barton et al., 2020). This hypothesis, if true, could have very relevant consequences for understanding the functioning of the marine food web and for biochemical modeling ecosystems.

In this study, we aim to explore the responses (volume, stoichiometry growth, and grazing) of different protistan grazers to temperature rise after a short-term exposure (acclimation) and compare them to the performances of long-term adapted organisms. By working with temperature-adapted species, we will also be able to test whether protistan grazers follow the "hotter is better hypothesis" (Bennett, 1987), which predicts that organisms adapted to lower temperatures will have lower maximum performances than those adapted to higher temperatures (Knies et al., 2009). Finally, we also aim to investigate the response of the strains adapted to different temperatures to an extreme temperature episode, here represented by a sudden increase in temperature to 25°C. Heatwaves may become a relevant instrument of species selection in a future scenario of a warmer ocean, where many species will likely be at the edge of their physiological limits. The reported increases of temperature during heatwaves do not reach >6.5°C (Hobday et al., 2016). However, we wanted to go one step further and expose the experimental organisms to relatively extremer temperatures (up to +9°C), to evaluate their survival and performance under critical conditions, and how temperature-adaptation would modify this response. Overall, understanding the processes involved in the thermal adaptation of protozooplankton and mixoplankton and their response to warming will improve the accuracy of climate change models in predicting ecological or biogeochemical effects of temperature projections in the near future.

# MATERIALS AND METHODS

## Experimental Organisms

For the experiments, we used cultures of two heterotrophic dinoflagellates (*Gyrodinium dominans* and *Oxyrrhis marina*), one heterotrophic ciliate (*Strombidium arenicola*), and one mixotrophic dinoflagellate (*Karlodinium armiger*), all of which originated from the NW Mediterranean. *G. dominans* (ICM-ZOO-GD001) was isolated in February 2011, then kept at 19°C, and transferred to 16°C in June 2019 and to 22°C in November 2020. *O. marina* (ICM-ZOO-OM001) was isolated in 1995 and kept at 19°C; then, it was transferred to 16°C in June 2019 and from 19 to 22°C in November 2020. *S. arenicola* (ICM-ZOO-SA001) was isolated in April 2017, kept at 19°C, and transferred to 16°C in July 2020 and from 19 to 22°C in November 2020. Finally, *K. armiger* (ICM-ZOO-KA001) was isolated in winter 2013, kept at 19°C, and transferred to 16°C in June 2019 and from 19 to 22°C in November 2020. The cultures were kept in

temperature-controlled incubators in 260 mL untreated tissue culture PTE flasks with autoclaved 0.1-μm filtered seawater, at a salinity of 38, ca. 35 μmol photons $m^{-2}$ $s^{-1}$, and they were fed exponentially growing *Rhodomonas salina* (K-0294) every 1–2 weeks. We made sure that all the species were kept at the selected temperatures for at least 7 months before conducting the experiments.

## Elemental Analysis

We prepared stock cultures of the adapted strains of all species and starved them. Once no prey was detected both visually and with the aid of a Multisizer IV Coulter Counter, we waited for an additional 24 h to ensure digestion of any remaining prey in the food vacuoles. To evaluate the changes in the stoichiometry of prey during the incubations, we also incubated cultures of *R. salina* (grown at 19°C) at 16, 19, 22, and 25°C for 24 and 48 h. Then, we filtered aliquots of known grazer and prey concentrations onto pre-combusted (450°C, 5 h) GF/F filters (Whatman, 25 mm) for determination of the carbon (C), nitrogen (N), and phosphorus (P) elemental compositions. The filters for CN analysis were dried at 60°C for 48–72 h and then stored in a desiccator until processing with a Flash EA1112 (Thermo Finnigan, München, Germany) CHNS analyzer. The filters for P analysis were immediately frozen at −80°C until processing. We processed P samples with the acid persulfate digestion method and posterior conversion to dissolved inorganic P with a Seal Analytical AA3 (Bran + Luebbe) analyzer. We calculated stoichiometric ratios as molar ratios, and we considered error propagation (square root law) in the calculation of the CP and NP ratios (Saiz et al., 2020).

## Acclimation vs. Adaptation Responses Experimental Setup

We compared strains grown for multiple generations (>7 months) at 16, 19, and 22°C (adapted treatments) with those from 16°C exposed for a short period (2 days preconditioning and 1 day experiment) to a temperature rise of either 3°C (19°C) or 6°C (22°C) (acclimated treatments). These temperatures are within the range of annual oscillation in the area of study and isolation of the microbial grazers used (Calbet et al., 2001). The protocol used was the same for all species and temperatures; i.e., adapted strains incubated at their respective long-term temperature and those incubated at a different temperature followed the same 2d + 1d protocol. The 2-days acclimation took place in 620 mL Pyrex glass bottles submerged in a temperature-controlled bath at the previously noted temperatures. Light conditions were a 10:14 light/dark cycle at 15–20 μmol photons $m^{-2}$ $s^{-1}$. We used saturating prey concentrations for the experiments. Thus, *G. dominans* and *K. armiger* were incubated with 50,000 *R. salina* $mL^{-1}$ (Calbet et al., 2013; Martínez and Calbet, unpublished), whereas *O. marina* and *S. arenicola* were supplied with 100,000–120,000 *R. salina* $mL^{-1}$ (Calbet et al., 2013; Arias and Calbet, unpublished). We added 20 mL of f/2 medium per liter of suspension in all treatments to avoid nutrient deficiency. After the 2 days of acclimation grazers usually had grown and prey were partially depleted. Therefore, we readjusted the prey and grazer concentrations to the ones indicated before, added nutrients again (20 mL f/2 $L^{-1}$), and sequentially transferred the organisms to triplicate 75 mL untreated tissue culture flasks (Falcon), where they were incubated for another 24 h (experiment). The grazer concentrations were chosen to allow a decrease in prey between 10–20%. We also set triplicate control bottles with only *R. salina* at each temperature. Initial and final samples were quantified using a Multisizer IV Coulter Counter, which provided data on abundance and cell volume (Multisizer$^{TM}$ user's manual, 2010). Predator growth rates were calculated in cell numbers assuming exponential growth. To obtain grazing rates and average prey concentrations during the incubations, we used Frost's (1972) equations; we calculated per capita values using the average concentration of grazers in each replicate according to Heinbokel (1978). GGEs were calculated as the quotient between carbon-based specific growth and ingestion rates x 100.

## Extreme Thermal Exposure Experimental Setup

We used the same experimental setup described before. However, here, we exposed all the temperature-adapted strains to 25°C for 3 days (two pre-conditioning and one experiment). This temperature is around the maximum average summer temperatures experienced in the area of origin of the species (Calbet et al., 2001). Then, we compared the growth, grazing, and GGEs of the adapted strains at their normal temperature with those after exposure to 25°C. Similar to the previous experiment, we used Frost's (1972) equations to obtain ingestion rates.

## Statistical Analysis

We used GraphPad Prism 7.0 software to conduct the statistical analysis. For stoichiometric effects of temperature, we sought for significant linear responses in the relationship between temperature and elemental composition or elemental ratio. Regarding experiments, our main objective was to investigate whether the physiological response of temperature-adapted organisms was different from that of only acclimated ones. To do such comparisons, we conducted ANOVA tests, with Tukey's test to compare the treatments at each temperature, and assuming a $p < 0.05$ for significant differences. Our experimental design rendered more information, such as the different response of both adapted and acclimated organisms to temperature; the effects of temperature on each physiological activity were evaluated by ANOVA, with Tukey's test to compare the response of each temperature. The differences in the slope of the relationship between temperature (16–19°C) and growth rates ($d^{-1}$) for the different species were evaluated with ANCOVA tests (see Section Acclimation vs. Adaptation). Error propagation, when necessary, was calculated using the square root law (Saiz et al., 2020).

# RESULTS

## Elemental Composition

**Table 1** presents the elemental compositions of the temperature-adapted predators. No statistically significant relationship

**TABLE 1 |** Elemental contents and molar stoichiometric ratios of the temperature-adapted grazers.

| Species | Adaptation T (°C) | pgC $\mu m^{-3}$ | SE | pgN $\mu m^{-3}$ | SE | pgP $\mu m^{-3}$ | SE | C:N | SE | C:P | SE | N:P | SE |
|---|---|---|---|---|---|---|---|---|---|---|---|---|---|
| *G. dominans* | 16 | 0.11 | 0.005 | 0.017 | 0.001 | 0.0026 | 0.00016 | 7.7 | 0.05 | 113 | 2.0 | 14.7 | 0.33 |
| *G. dominans* | 19 | 0.09 | 0.001 | 0.016 | 0.0002 | 0.0028 | 0.00001 | 7.1 | 0.08 | 86 | 0.6 | 12.2 | 0.18 |
| *G. dominans* | 22 | 0.12 | 0.003 | 0.020 | 0.001 | 0.0032 | 0.00002 | 7.0 | 0.14 | 96 | 2.6 | 13.7 | 0.61 |
| *O. marina* | 16 | 0.11 | 0.003 | 0.025 | 0.0007 | 0.0040 | 0.0001 | 5.2 | 0.03 | **71.0** | 3.2 | 13.7 | 0.70 |
| *O. marina* | 19 | 0.11 | 0.004 | 0.025 | 0.0007 | 0.0044 | 0.0002 | 5.3 | 0.07 | **67.3** | 1.5 | 12.8 | 0.37 |
| *O. marina* | 22 | 0.10 | 0.001 | 0.023 | 0.0005 | 0.0040 | 0.0001 | 5.1 | 0.04 | **64.4** | 2.0 | 12.7 | 0.48 |
| *S. arenicola* | 16 | n.d. | n.d. | n.d. | n.d. | n.d. | n.d. | n.d. | n.d. | n.d. | n.d. | n.d. | n.d. |
| *S. arenicola* | 19 | 0.09 | 0.003 | 0.019 | 0.0008 | 0.0034 | 0.00007 | 5.2 | 0.09 | 67.0 | 2.2 | 12.8 | 0.46 |
| *S. arenicola* | 22 | 0.10 | 0.003 | 0.024 | 0.0008 | 0.0038 | 0.00007 | 5.0 | 0.02 | 70.0 | 2.3 | 14.0 | 0.49 |
| *K. armiger* | 16 | 0.21 | 0.005 | 0.033 | 0.0007 | **0.0030** | 0.00002 | 7.3 | 0.01 | 178 | 5.3 | 24.2 | 0.72 |
| *K. armiger* | 19 | 0.13 | 0.004 | 0.027 | 0.0008 | **0.0034** | 0.00004 | 5.7 | 0.10 | 99 | 1.8 | 17.3 | 0.44 |
| *K. armiger* | 22 | 0.18 | 0.004 | 0.026 | 0.0004 | **0.0039** | 0.00001 | 8.2 | 0.08 | 121 | 2.8 | 14.7 | 0.23 |

*Statistically significant linear relationships with temperature are indicated in bold. n.d. not determined because loss of samples.*

between temperature and either elemental composition or elemental molar ratios was observed in any of the grazers (simple linear regression analysis, $P > 0.05$), with only two exceptions. The P contents of *K. armiger* slightly increased with temperature (from 0.0030 to 0.0039 pgP $\mu m^{-3}$), and the C:P ratio of *O. marina* diminished with temperature to some degree (from 71 to 64). **Table 2** presents the volume and elemental composition of *R. salina* after exposure for 24 and 48 h to the experimental temperatures. This information is relevant for detecting any change in the nutritional composition that the temperature may have produced during the incubations. The volume and CNP composition of *R. salina* were relatively stable and unaffected by exposure at the different temperatures within the incubation periods (variations always <20% with respect to 16°C, and no statistically significant pattern with temperature).

## Acclimation vs. Adaptation

Our goal was to compare the physiologies and behaviors of the thermal-adapted strains with those of the parental 16°C strains when exposed to warmer temperatures (acclimated treatment). The focus was on cell volume, growth rates ($d^{-1}$), ingestion rates (in cells $ind^{-1}$ $d^{-1}$), and GGE. For simplicity, we present the significance of the comparison between temperature-adapted strains with their acclimated counterparts in the figures (asterisks indicating $p < 0.05$), whereas the significance of the differences between the response to the different temperatures for adapted and acclimated strains is shown in **Table 3**. Compared to the 16°C strain, *G. dominans* and *O. marina* cell volumes slightly (although not significantly) augmented with a 3°C temperature increase (19°C), and warmer conditions (+6°C) resulted in a decrease in volume (not statistically significant either), both in adapted and acclimated strains (**Figures 1A,B** and **Table 3**). The effect of temperature on *S. arenicola* cell volume was weak for both acclimated and adapted strains (**Figure 1C** and **Table 3**). The treatments of 16°C-adapted *S. arenicola* incubated at +3°C (19°C-acclimated treatment) was the only one significantly different from its adapted counterpart (**Figure 1C**). Finally, the acclimated strains of *K. armiger* decreased in volume at higher temperatures (19 and 22°C) compared to the adapted counterparts (**Figure 1D** and **Table 3**). Among the adapted strains of this species, the ones at warmer temperatures showed higher cell volumes than those at 16°C (**Table 3**), and their volumes were larger than their temperature-acclimated counterparts (**Figure 1D**; $p < 0.001$).

*Gyrodinium dominans* cell-based growth rates increased exponentially with temperature from 0.19 $d^{-1}$ at 16°C to 0.48 $d^{-1}$ at 22°C for only the acclimated strains (**Figure 2A** and **Table 3**). Adapted strains showed higher growth rates than acclimated strains at 19°C ($p < 0.001$), but it was the opposite at 22°C ($p < 0.001$; **Figure 2A**). The growth rates of *O. marina*

**TABLE 2 |** Cell volume, elemental contents and molar stoichiometric ratios of *Rhodomonas salina* after 24 and 48 of exposure to the experimental temperatures.

| Exposure time | T | Volume ($\mu m^3$) | SE | pgC $\mu m^{-3}$ | SE | pgN $\mu m^{-3}$ | SE | pgP $\mu m^{-3}$ | SE | C:N | SE | C:P | SE | N:P | SE |
|---|---|---|---|---|---|---|---|---|---|---|---|---|---|---|---|
| 24 h | 16 | 208 | 0.51 | 0.18 | 0.002 | 0.039 | 0.0006 | 0.0036 | 0.00002 | 5.4 | 0.02 | 128 | 2.3 | 23.5 | 0.49 |
| 24 h | 19 | 198 | 0.26 | 0.17 | 0.008 | 0.036 | 0.0020 | 0.0036 | 0.00004 | 5.5 | 0.04 | 120 | 5.1 | 21.6 | 1.06 |
| 24 h | 22 | 202 | 0.49 | 0.17 | 0.003 | 0.037 | 0.0009 | 0.0041 | 0.00015 | 5.4 | 0.02 | 108 | 3.8 | 20.0 | 0.68 |
| 24 h | 25 | 209 | 0.66 | 0.16 | 0.001 | 0.034 | 0.0003 | 0.0028 | 0.00000 | 5.7 | 0.02 | 153 | 1.0 | 27.0 | 0.23 |
| 48 h | 16 | 211 | 0.94 | 0.18 | 0.004 | 0.039 | 0.0011 | 0.0040 | 0.00003 | 5.4 | 0.04 | 117 | 3.3 | 21.8 | 0.79 |
| 48 h | 19 | 202 | 0.52 | 0.18 | 0.010 | 0.038 | 0.0029 | 0.0038 | 0.00003 | 5.5 | 0.11 | 118 | 6.0 | 21.7 | 1.51 |
| 48 h | 22 | 207 | 2.00 | 0.17 | 0.007 | 0.036 | 0.0016 | 0.0039 | 0.00004 | 5.5 | 0.04 | 115 | 4.9 | 20.9 | 1.03 |
| 48 h | 25 | 212 | 1.66 | 0.20 | 0.004 | 0.042 | 0.0012 | 0.0050 | 0.00001 | 5.7 | 0.09 | 105 | 2.3 | 18.5 | 0.51 |

*No significant relationship was found between temperature and any of the variables analyzed.*

**TABLE 3 |** Probability values of the ANOVA tests comparing the response to temperature in Volume ($\mu m^3$), Growth rates ($d^{-1}$), Ingestion rates (cells $grazer^{-1}$ $d^{-1}$), and GGE (gross-growth efficiency) of the four species of protistan grazers studied.

| | *G. dominans* | | | | *O. marina* | | | |
|---|---|---|---|---|---|---|---|---|
| **Treatment** | **Volume** | **Growth rates** | **Ingestion rates** | **GGE** | **Volume** | **Growth rates** | **Ingestion rates** | **GGE** |
| ANOVA temperature-acclimated | ns | 0.002 | <0.0001 | <0.0001 | 0.034 | 0.016 | 0.0004 | ns |
| Adapted to 16°C vs. Acclimated to +3°C | ns | ns | 0.0003 | 0.007 | ns | 0.028 | 0.002 | ns |
| Adapted to 16°C vs. Acclimated to +6°C | ns | 0.003 | <0.0001 | <0.0001 | ns | 0.021 | 0.0004 | ns |
| Acclimated to +3°C vs. Acclimated to +6°C | ns | 0.007 | 0.0002 | 0.002 | 0.030 | ns | ns | ns |
| ANOVA temperature-adapted | ns | 0.009 | <0.0001 | 0.0002 | ns | <0.0001 | <0.0001 | ns |
| Adapted to 16°C vs. Adapted to 19°C | ns | 0.010 | <0.0001 | 0.004 | ns | <0.0001 | <0.0001 | ns |
| Adapted to 16°C vs. Adapted to 22°C | ns | 0.026 | <0.0001 | 0.0001 | ns | 0.026 | 0.003 | ns |
| Adapted to 19°C vs. Adapted to 22°C | ns | ns | ns | 0.0078 | ns | 0.0006 | 0.0004 | ns |
| | *S. arenicola* | | | | *K. armiger* | | | |
| | **Volume** | **Growth rates** | **Ingestion rates** | **GGE** | **Volume** | **Growth rates** | **Ingestion rates** | **GGE** |
| ANOVA temperature-acclimated | 0.007 | 0.0002 | <0.0001 | ns | 0.001 | 0.004 | 0.001 | 0.001 |
| Adapted to 16°C vs. Acclimated to +3°C | ns | 0.0002 | <0.0001 | ns | 0.001 | 0.017 | 0.002 | 0.001 |
| Adapted to 16°C vs. Acclimated to +6°C | 0.006 | 0.001 | <0.0001 | ns | 0.002 | ns | 0.001 | ns |
| Acclimated to +3°C vs. Acclimated to +6°C | ns | 0.108 | ns | ns | ns | 0.004 | ns | 0.002 |
| ANOVA temperature-adapted | 0.029 | <0.0001 | <0.0001 | ns | 0.001 | 0.009 | 0.002 | ns |
| Adapted to 16°C vs. Adapted to 19°C | ns | <0.0001 | <0.0001 | ns | 0.001 | 0.011 | 0.006 | ns |
| Adapted to 16°C vs. Adapted to 22°C | ns | 0.0002 | <0.0001 | ns | 0.002 | 0.022 | 0.003 | ns |
| Adapted to 19°C vs. Adapted to 22°C | 0.030 | <0.0001 | <0.0001 | ns | ns | ns | ns | ns |

*For each comparison, we provide first the overall probability of the ANOVA test and next the posteriori Tukey's test for each combination of temperature responses. Temperature acclimated corresponds to the results of organisms adapted to 16°C and then incubated at +3 and +6°C. Temperature adapted correspond to the comparison of the performance of each species incubated at the temperature they have been cultivated for multiple generations. The actual data appears in* ***Figures 1****,* ***2****,* ***4****,* ***5****. ns = not significant.*

increased from 0.66 $d^{-1}$ at 16°C to 0.89 $d^{-1}$ and 1.07 $d^{-1}$ at 19°C for the acclimated and adapted organisms, respectively (**Figure 2B** and **Table 3**). At 22°C, the rates either remained the same (acclimated) or dropped to 0.8 $d^{-1}$ in the adapted *O. marina* (**Figure 2B** and **Table 3**). There were differences in the growth rates between the acclimated and adapted *O. marina*, but they were statistically significant only at 22°C (**Figure 2C**, $p < 0.05$). *S. arenicola* showed a similar pattern to that of *O. marina*, with clear enhancements in growth rates at 19°C, acutely in the acclimated strains (up to 1.8 $d^{-1}$), compared to a drop in growth rates at 22°C (**Figure 2C** and **Table 3**). Overall, the growth rates of *S. arenicola* were consistently higher for the temperature-acclimated strains than for the adapted ones (**Figure 2C**). The *K. armiger* thermal response was also similar to the previously described ones; however, the drop in growth rates at 22°C for the acclimated organisms was more severe than that for the adapted organisms (**Figure 2D**). Conversely, the growth rates for the 22°C-adapted strains of *K. armiger* were similar to those at 19°C (**Table 3**).

Because most species responded negatively to 22°C in both the adapted and acclimated strains, we restricted the calculation of thermal-driven enhancement of the grazer growth rates to the 16–19°C interval. Given the expected linear (not exponential) relationship between temperature (°C) and growth rates ($d^{-1}$) in protozoans shown by Montagnes et al. (2003), in **Figure 3**, we present the slope of this relationship for acclimated and adapted organisms. Temperature-adapted organisms always showed higher slopes than those of their interacting counterparts; however, the differences between slopes were only statistically significant for *S. arenicola* (ANCOVA, $p < 0.0001$).

There was a consistent increase in the number of cells consumed daily by *G. dominans* and *O. marina* in their acclimated strains, from 16 to 22°C (**Figures 4A,B** and **Table 3**). This pattern was mirrored by the adapted organisms at 19°C in both species, with only significantly higher rates for the adapted vs. the acclimated strains in *G. dominans* (**Figures 4A,B** and **Table 3**). The ingestion rates dropped for the 22°C-adapted *O. marina* strain, while they remained high for *G. dominans* (**Figures 4A,B** and **Table 3**). The ciliate *S. arenicola* ingested *R. salina* at increasing rates with temperature up to 19°C (**Figure 4C** and **Table 3**); above this temperature, the rates were steady for acclimated organisms and dropped for the adapted organisms (**Figure 4C** and **Table 3**). In contrast, *K. armiger*-acclimated strains reduced their ingestion performance at increasing temperatures (**Figure 4D** and **Table 3**). This trend did not occur in the adapted strains, which showed higher rates at 19 and 22°C (**Table 3**).

There was an overall tendency to decrease GGE at increasing temperatures for both adapted and acclimated *G. dominans* and *O. marina* (**Figures 5A,B** and **Table 3**). However, *S. arenicola* and *K. armiger* showed slightly increasing tendencies in GGEs with increasing temperature, and those were significant only in few occasions (**Figures 5C,D** and **Table 3**). Both species responded positively to a short term increase of 3°C (acclimation

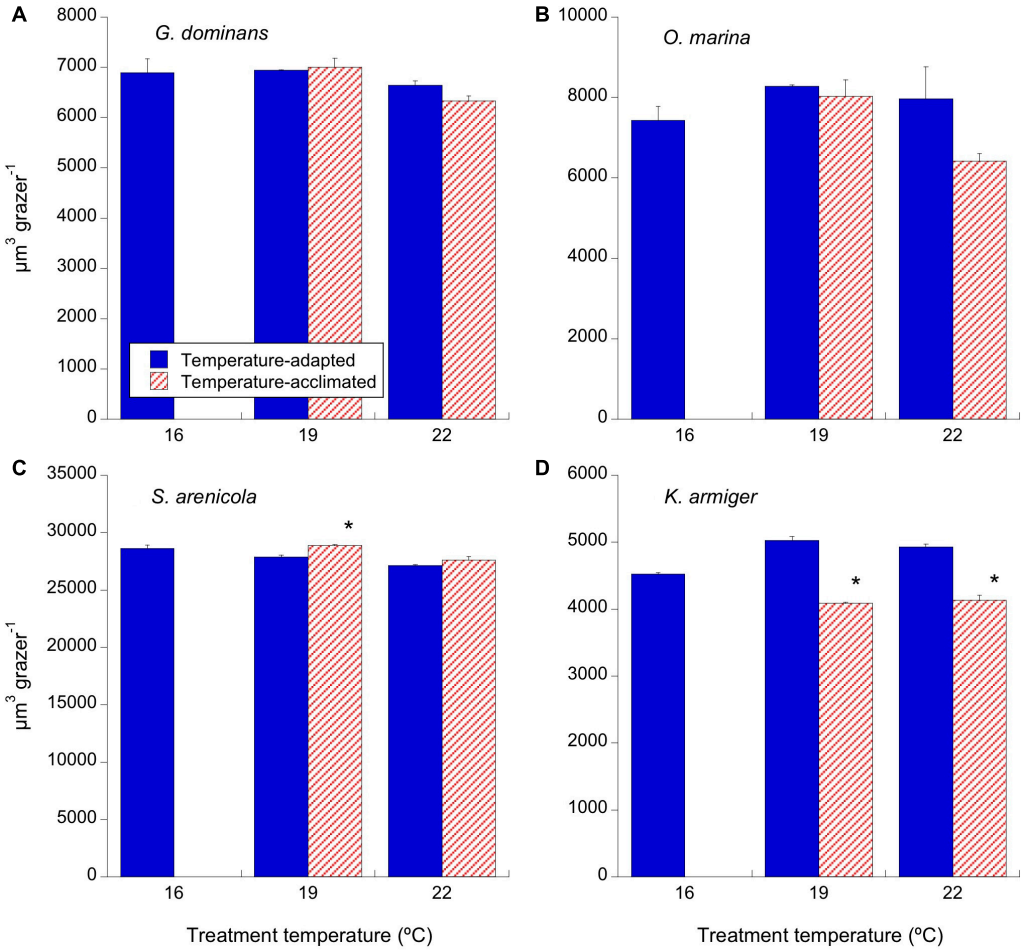


**FIGURE 1 |** Effects of temperature on cell volume ($\mu m^3$) of the different grazers. Solid blue bars correspond to the temperature-adapted organisms incubated at their standard temperature. Stripped red bars correspond to those organisms adapted at 16°C and exposed to either +3°C (19°C) or +6°C (22°C) temperature raise (2 days acclimation plus 1-day experimental incubation). **(A)** *G. dominans*, **(B)** *O. marina*, **(C)** *S. arenicola*, and **(D)** *K. armiger*. Asterisks denote differences ($p < 0.05$) between acclimated and adapted treatments. The statistics corresponding to differences between temperature treatments of adapted and acclimated organisms can be found in **Table 3**. The error bars are SE.

experiment), and in the case of the *S. arenicola*, also to an increase of 6°C (**Figures 5C,D** and **Table 3**).

## Response to an Extreme Temperature Episode

We present data about the response to a sudden temperature increase (**Figure 6**) only for *G. dominans*, *O. marina*, and *K. armiger* because the 16°C-adapted *S. arenicola* strains quickly died (within 24 h) when exposed to 25°C, and the remaining strains of this species (those adapted to higher temperatures) died after 48 h of incubation. The growth rates of *G. dominans* exposed to 25°C were very similar irrespective of the origin of the strain, although the growth rate of the strain adapted to 16°C was 26% higher than those of the other 19 and 22°C adapted ones (ANOVA and Tukey's test, $p < 0.001$; **Figure 6A**). The opposite was apparent for *O. marina* adapted to 16°C, which at 25°C exhibited the lowest growth rates followed by the 22 and 19°C adapted strains (ANOVA $p < 0.001$; Tukey's test: 16°C was different from 19°C, $p < 0.01$; 19°C different from 22°C, $p < 0.05$, and 16°C was different from 22°C, $p < 0.05$; **Figure 6A**). Similarly, when exposed to 25°C, the *K. armiger* 16°C-adapted strain also showed the lowest (even negative) growth rates compared to the other two strains that grew at higher and rather similar rates (ANOVA and Tukey's test $p < 0.01$; **Figure 6A**). Overall, the growth rates of *K. armiger* at 25°C were low compared to the strains adapted and incubated at 19 and 22°C (**Figure 2D**).

The effects of incubation at 25°C on ingestion rates are presented in **Figure 6B**. *G. dominans* did not present any difference between the ingestion rates at 25°C, irrespective of the strain. In contrast, in *O. marina* and *K. armiger,* the strains adapted to 19°C (Tukey's test for both $p < 0.05$) always showed the highest feeding rates, followed by those adapted to 22°C, and finally, the lowest rates were exhibited for the strains adapted to 16°C. *K. armiger* ingestion rates at 25°C were near zero for the

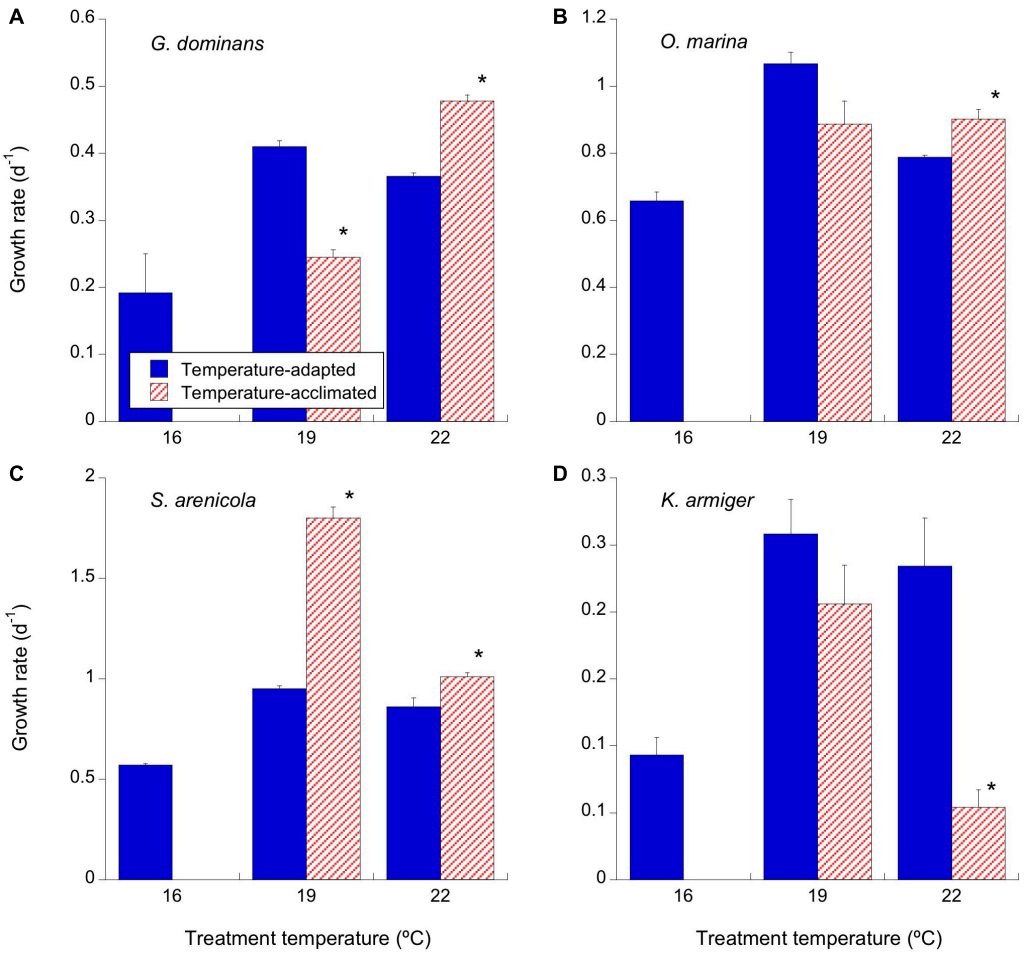


**FIGURE 2 |** Effects of temperature on the growth rates ($d^{-1}$) of the experimental protistan grazers. Solid blue bars correspond to the temperature-adapted organisms incubated at their standard temperature. Stripped red bars correspond to those organisms adapted at 16°C and exposed to either +3°C (19°C) or +6°C (22°C) temperature raise (2 days acclimation plus 1-day experimental incubation). **(A)** *G. dominans*, **(B)** *O. marina*, **(C)** *S. arenicola*, and **(D)** *K. armiger*. Asterisks denote differences ($p < 0.05$) between acclimated and adapted treatments. The statistics corresponding to differences between temperature treatments of adapted and acclimated organisms can be found in **Table 3**. The error bars are SE.

strain adapted to 16°C (**Figure 6B**). The combination of ingestion and growth rates determine the values of GGE (**Figure 6C**). *G. dominans* grown at 19°C showed a lower GGE than that of the remaining strains of this species. All *O. marina* strains, on the other hand, showed similar GGEs at 25°C, irrespective of the temperature of adaptation. Finally, the *K. armiger* GGE was a direct function of adaptation to temperature, with the strains grown at higher temperatures showing more elevated GGEs (**Figure 6C**).

## DISCUSSION

We evaluated the adaptive responses of four species of protistan grazers, including both heterotrophs and mixotrophs, to temperature. We started with several hypotheses that proved to be partially wrong. For instance, we did not find any robust evidence of lower C:N or C:P ratios resulting from temperature adaptation in either heterotrophs or mixotrophs. On the other hand, we found lower GGEs with increasing temperatures for some species, but others showed the opposite pattern. We also discovered evidence partially supporting the "hotter is better hypothesis" (Bennett, 1987), but only for a range of temperatures.

### Temperature Effects on Stoichiometry

For autotrophs, one would expect that at short time intervals (acclimation) and given the higher $Q_{10}$ of respiration than photosynthesis predicted by the metabolic theory of ecology (López-Urrutia et al., 2006; Rose and Caron, 2007), the C:N and C:P ratios would diminish with warming. The elemental ratio decrease is explained because increased respiration over photosynthesis would make C use proportionally more favored by warming than C assimilation, reducing the overall C pool over other elements. In contrast to expectations, this pattern in elemental ratios is not commonly found for well-adapted species to temperature, particularly in terms

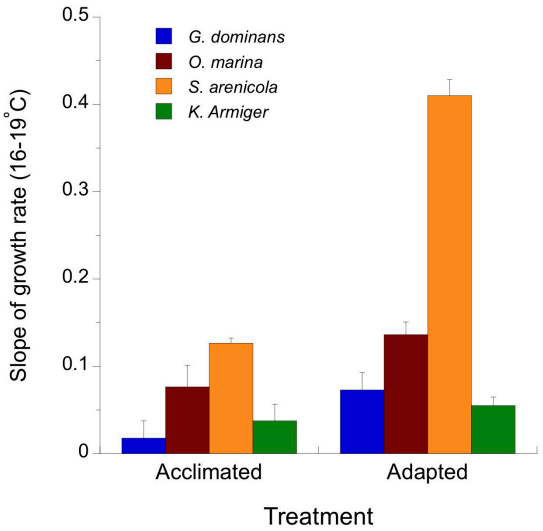


**FIGURE 3 |** Slopes of the simple linear regression fit between growth rate and temperature for temperature-acclimated and temperature-adapted grazers. The slopes were calculated using the data showed in **Figure 2** between 16 and 19°C.

of C:P (Yvon-Durocher et al., 2017). For heterotrophs, the stoichiometric response to temperature is not straightforward because it is impossible to separate the direct effects of temperature from those of their prey. In their meta-analysis, Woods et al. (2003) concluded that P and N contents were higher in cold vs. warm environments across various animal groups, except for prokaryotes. However, generalizations are not always corroborated by individual experiments. For instance, copepod C:P ratios decreased with temperature in nauplii and copepodites under no limitation of this element in their diets; nevertheless, when P is limiting, copepodites increased their C:P with temperature, whereas nauplii kept it low (Mathews et al., 2018). For *Daphnia* spp., the P content is negatively related to temperature, as predicted, although this relationship is species-specific and dependent on the P contents of the prey (McFeeters and Frost, 2011). For protistan grazers, unfortunately, there is an obvious need for data. Our results show that the variations in the elemental composition per unit of cell volume in adapted protistan grazers due to temperature are minor. We should consider that equal stoichiometry combined with a hypothetic reduction in volume due to temperature may nevertheless result in a lower CNP transfer (*via* mesozooplankton grazing) to higher trophic levels. Therefore, the overall effects of temperature on nutrient transfer through the food web should be considered, even if the stoichiometry of the protistan grazers does not change much.

## Does Size Matter?

Some organisms used in this study have been shown to present high body plasticity, modifying their cellular volume depending on the amount of ingested prey (Calbet et al., 2013). This fact could have masked the patterns of cell volume variations related to temperature. This does not seem to be the case because the experiments were conducted under satiating food conditions. Therefore, any change in volume during the incubations was because of a direct effect of temperature. It is surprising, then, that we did not observe a decrease in size between organisms adapted to 16°C and those adapted to 19°C. On the other hand, most of the strains adapted to 22°C, appeared smaller than those adapted at 19°C, although the differences were not significant in most of the occasions.

A decrease in the volume of autotrophs at higher temperatures, with its consequent increase in the surface/volume relationship, may favor the acquisition of dissolved inorganic nutrients. For heterotrophs, a size reduction does not seem to provide any advantage in terms of the acquisition of prey. A higher surface/volume relationship may also help obtain more oxygen, which availability is reduced by increased temperatures (Atkinson et al., 2003). Another advantage associated with the size decrease that accompanies temperature for unicellular organisms is to reduce settling rates (Atkinson, 1994; Atkinson et al., 2003). In our case, all the species considered swim, and size reduction would have only offered limited advantages. It has also been suggested that because an increased temperature will favor higher growth rates, a reduction in cell size at higher temperatures may be a response to increased population growth rates because cells that divide early will make up a more significant fraction of the total population (Atkinson et al., 2003). However, the only decrease in size we observed in our experiments (even though not significant) occurred at 22°C, and at that temperature, only *G. dominans* showed increased growth rates. In summary, our results do not clearly support the hypothesis of consistent decrease in size motivated by temperature in protozoans (Atkinson et al., 2003).

## Acclimation vs. Adaptation

Most global theories about temperature effects on plankton are mainly based on acclimated-only organisms [e.g., Rose and Caron (2007)]. Therefore, it is critical to assess whether temperature-adapted organisms show the same response than acclimated organisms. Our data showed that this is not the case for many of the variables tested. Based on growth rates, we could conclude that our organisms adapted at 16°C followed the hypothesis "hotter is better" (Bennett, 1987; Knies et al., 2009) when exposed to a moderate temperature rise (+3°C). Increases of 6°C, however, compromised the physiological performance of most of the species, except for *G. dominans*, which continued to show an enhancement in growth rates.

When considering the GGE, however, we observed that this species showed a decrease in this variable with temperature, indicating a lower efficiency of converting food into growth at high temperatures. This is not unexpected because for zooplankton, the GGE at saturated prey concentrations usually decreases with increasing temperatures (Straile, 1997; Li et al., 2011), probably due to an imbalance between physiological rates. Surprisingly, the ciliate *S. arenicola* showed higher GGEs when exposed for a short period of time to a 3 and 6°C increase. This result could suggest that this species might be favored under a future climate change scenario. However, the lack of

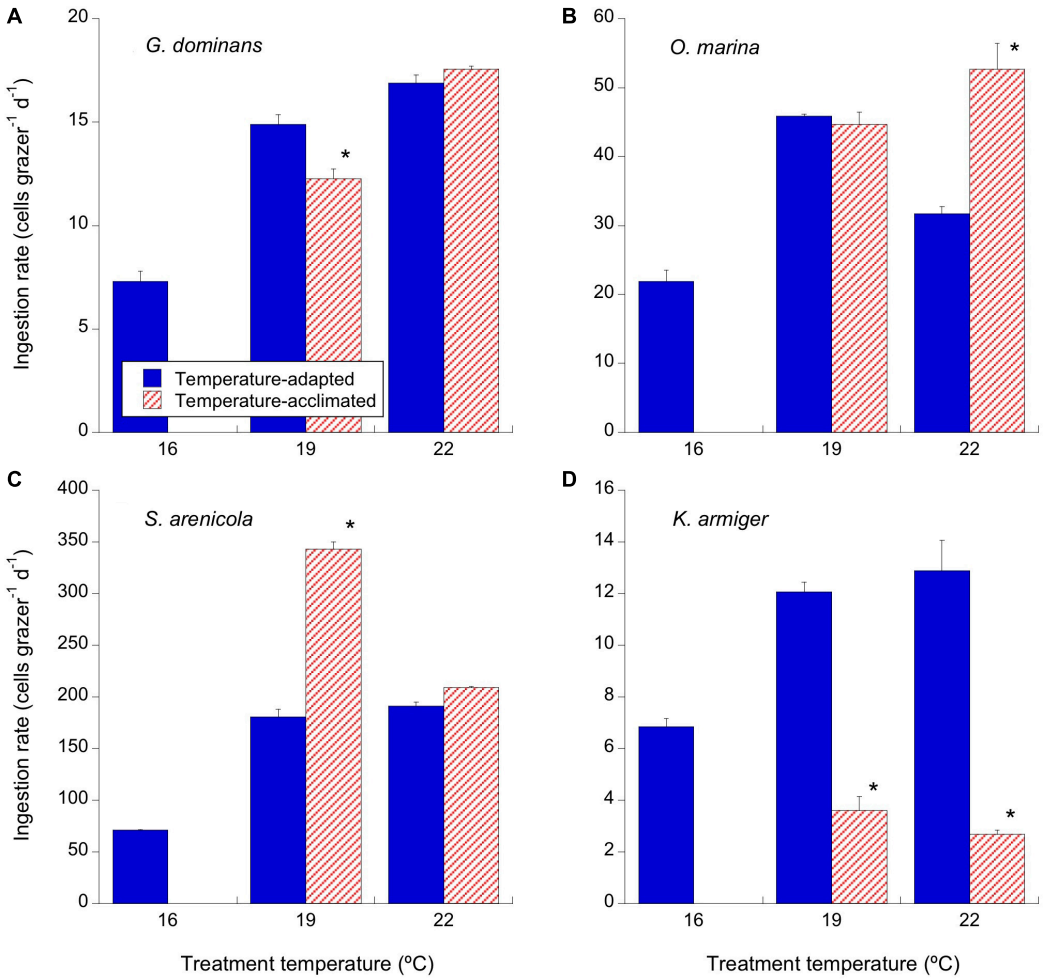


**FIGURE 4 |** Effects of temperature on the ingestion rates (cells consumed per grazer and day) of the experimental protistan grazers. Solid blue bars correspond to the temperature-adapted organisms incubated at their standard temperature. Stripped red bars correspond to those organisms adapted at 16°C and exposed to either +3°C (19°C) or +6°C (22°C) temperature raise (2 days acclimation plus 1 day experimental incubation). Asterisks denote differences ($p < 0.05$) between acclimated and adapted treatments. **(A)** *G. dominans*, **(B)** *O. marina*, **(C)** *S. arenicola*, and **(D)** *K. armiger*. The statistics corresponding to differences between temperature treatments of adapted and acclimated organisms can be found in **Table 3**. The error bars are SE.

response to temperature in the adapted strains, and the collapse of the population when exposed to 25°C, indicate that 22°C was close to its physiological thermal limit, at least for the given temporal exposure.

Finally, we want to call attention to the fact that some GGEs found in this study were at the higher limit of those reported previously (Straile, 1997). Regarding *K. armiger*, it is important to note that the very high GGE found at 19°C for the acclimated organisms may have been a combination of its autotrophic and mixotrophic metabolism. Nevertheless, for the remaining grazers, this explanation does not apply. We believe the reason for such elevated GGEs may be a consequence of the body plasticity of protozoans, in many instances a direct function of the prey ingested (Calbet et al., 2013). When considering the specific growth used to calculate GGE, we could not discern between the actual increase in biomass due to cell growth and that derived from an accumulation of prey inside the grazer's cell. Nevertheless, even though the absolute values may be somewhat high, we feel that the comparison between treatments should be correct.

## Response to a Sudden Extreme Rise in Temperature: 25°C Experiment

The Intergovernmental Panel on Climate Change [IPCC] (2014) predicts an increase of ocean surface temperature from 0.3 to 4.8°C by the end of the twenty first century relative to 1986–2005. We have seen that many species will tolerate this increase, if gradual. However, climate change is also associated with abrupt temperature rises, known as heatwaves (Müren et al., 2005; Hayashida et al., 2020). The increase in temperature experienced by the 19 and 22°C adapted strains in the 25°C treatment was within the maximum range expected to occur in nature [up to 6.5°C, Hobday et al. (2016)], but maybe was unrealistically

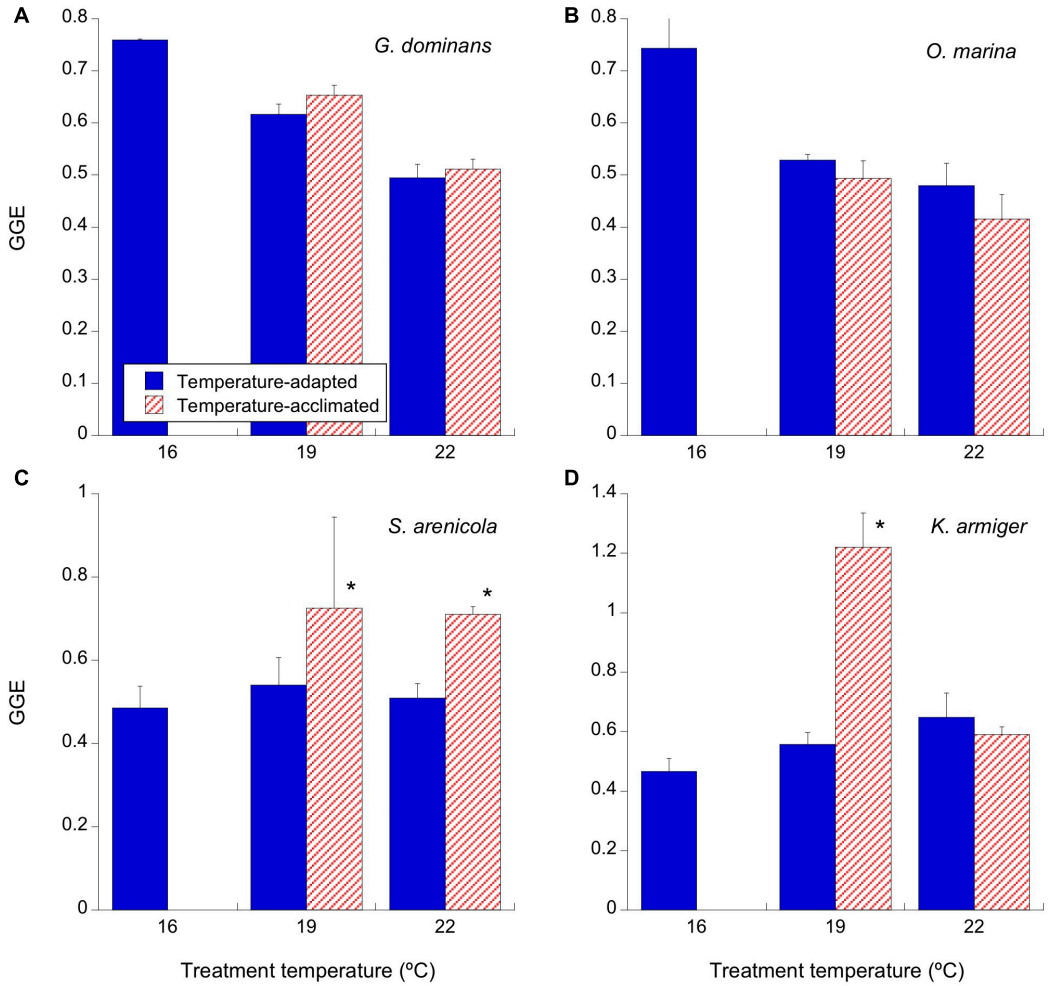


**FIGURE 5 |** Effects of temperature on the gross growth efficiency (GGE; as the percentage of carbon produced out the one ingested) of the experimental protistan grazers ($d^{-1}$). Given we did not have carbon data for *S. sulcatum* at 16°C, we used the values at the closest temperature (19°C). Solid blue bars correspond to the temperature-adapted organisms incubated at their standard temperature. **(A)** *G. dominans*, **(B)** *O. marina*, **(C)** *S. arenicola*, and **(D)** *K. armiger*. Stripped red bars correspond to those organisms adapted at 16°C and exposed to either +3°C (19°C) or +6°C (22°C) temperature raise (2 days acclimation plus 1-day experimental incubation). Asterisks denote differences ($p < 0.05$) between acclimated and adapted treatments. The statistics corresponding to differences between temperature treatments of adapted and acclimated organisms can be found in **Table 3**. The error bars are SE.

high for the 16°C adapted strains (+9°C). Despite this fact, however, the 16°C-adapted strains of *G. dominans* and *O. marina* showed higher growth and ingestion rates when incubated at 25°C than at 16°C (**Figures 2**, **4**, and **6**). Nevertheless, it is worth mentioning that the GGEs of the 16°C-adapted strains of all the species investigated were lower at 25°C than at 16°C, and that the maximum growth and ingestion rates of *O. marina* and *K. armiger* at 25°C were found for the 19°C-adapted strains (**Figure 6**). Particularly, the mixotrophic dinoflagellate seemed quite susceptible to abrupt exposure to high temperatures, dying at 25°C if adapted to 16°C, but thriving relatively well when adapted to higher temperatures. For this species, adaptation conferred clear resistance to sudden increases of temperature because the performance under 25°C was greatly improved when adapted to warmer temperatures. *S. arenicola* was the most extreme case of weak resistance to high temperature not surviving the acclimation period, and with even the 16°C adapted strain dying in less than 24 h. In summary, adaptation to warmer temperatures, even if not always fully developing the potential of the species, helps overcome the effects of short-term abrupt increases in temperature in some cases.

## Were the Strains Fully Adapted to the Experimental Temperatures?

We define acclimation as the reversible physiological changes that improve an organism's function in the environment, whereas adaptation involves more profound genetic changes (Bennett and Lenski, 1997). In phytoplankton, previous reports suggest that a few hundred generations are enough for thermal adaptation (Listmann et al., 2016; O'Donnell et al., 2018; Aranguren-Gassis et al., 2019). However, we are not aware of similar data for protistan grazers. As these organisms also have fast

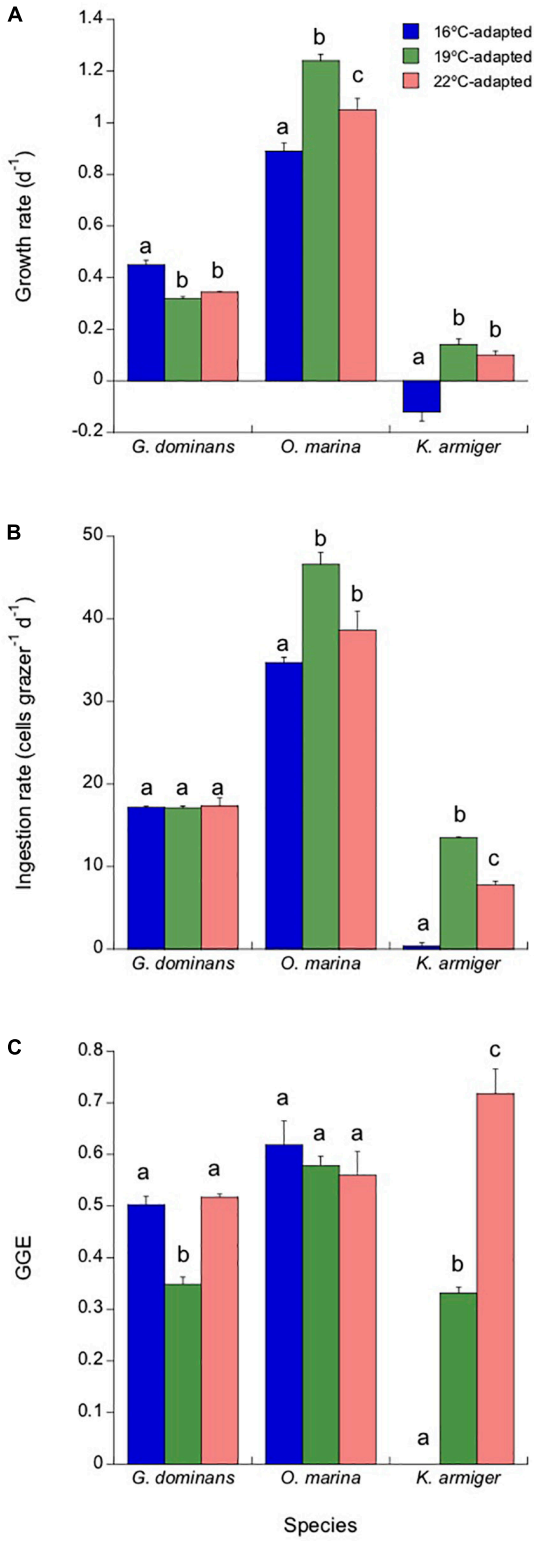


**FIGURE 6 |** Response of the different adapted grazers (16, 19, and 22°C) to a sudden exposure to 25°C (2 days acclimation plus 1-day experimental incubation), simulating a heatwave episode. Growth rates **(A)**, ingestion rates **(B)**, and GGEs **(C)** are presented. Statistical differences ($p < 0.05$) within each species are indicated by different letters. The error bars are SE.

generation times, one could assume a similar rule may apply. The minimum time interval the adapted strains were reared at a given temperature was 7 months, and this occurred at the highest temperature tested (22°C), meaning shorter generation times. The growth rates found in our study at 22°C ranged from 0.23 $d^{-1}$ in *K. armiger* to 1.0 $d^{-1}$ in *S. arenicola*, which represents less than one doubling per day for the mixotrophs and over one doubling per ciliate. It can be argued that at least *K. armiger* at 22°C may not have gone through enough generations (one hundred at most, assuming food was not always in excess) to ensure a genotypic change.

However, it is precisely in this species where we found the highest performances (i.e., growth rates) at 22°C of the adapted strains compared to those of the merely acclimated strains (**Figure 2**). Thus, we can conclude that even if there is likely still room to adapt to warmer temperatures, the species showed clear evidence of adaptation to high temperatures. Similarly, Huertas et al. (2011) also concluded that not all phytoplankton adapt to the temperature at the same speed. Some species are much faster than others; i.e., some algae can adapt to tolerate high temperatures after only 45 days (Padfield et al., 2016). Perhaps, the changes shown in these responses to temperature did not involve mutation but are epigenetic, and therefore, reversible. In this respect, we should be aware that despite 16°C was closer to the temperature of origin of most of our strains, after so many years in the laboratory at 19°C under a controlled environment, different from what we find in nature (no predators, minor fluctuations in the physicochemical variables, etc.), our 16°C-adapted clones could be different from the wild specimens originating the cultures. Natural selection forces in nature are different than those in the laboratory. Therefore, we cannot expect wild protists to behave the same way as our cultures. Clear evidence of this is the results of Arias et al. (2021), who found the ciliate *S. arenicola* lost its diel feeding rhythm after prolonged periods of laboratory cultivation and partially recovered it when exposed to predators chemical cues.

It can also be questioned whether our food scenario during the cultivation of the organisms could have interfered with the adaptative process. The experiments presented here were conducted at saturating food concentrations to ease the comparison between treatments. However, the thermal adaptation of the strains took place in periods of variable food conditions. Routine maintenance of cultures is designed to feed the protistan grazers every 1 or 2 weeks, allowing them consume most of the available prey. Some researchers have suggested that nutrient limitation impairs the ability of algae to adapt to lethal temperatures because of a trade-off between increased temperature tolerance and higher N requirements (Aranguren-Gassis et al., 2019). Perhaps, this situation may also be similar for heterotrophs. In our study, the range of temperatures used was below those considered lethal for the selected species, except for 25°C, which was not used to adapt any strain. We cannot discount, however, that intermittent starvation could have affected our results, explaining why our 22°C-adapted strains did not perform better than those at 19°C. Given that constant food is seldom found in nature and that food fluctuations seem to be normal (Haury et al., 1978; Mackas et al., 1985), we believe our

adaptative process mimics natural communities much better than constantly fed organisms in typical experimental setups.

## Final Remarks

We can conclude that in protistan grazers, adaptation to temperature confers a selective advantage to warming within a reasonable limit (i.e., ca. +3°C), at least under food satiating conditions. Attempts to adapt to much higher temperatures (i.e., +6°C) do not confer any clear physiological advantage within the temporal framework of our experiments. Perhaps, the most remarkable exception to this was *K. armiger*, the only mixotroph that showed higher growth and grazing rates at 22°C in the adapted strains than in the acclimated strains. *S. arenicola* also showed this pattern in growth rates but not in ingestion rates. We cannot generalize with one single species that mixotrophs will thrive more than heterotrophs at higher temperatures. However, it is notable that the metabolic theory of ecology (López-Urrutia et al., 2006; Rose and Caron, 2007) predicts that heterotrophs may do better than autotrophs under a future global change scenario. Mixotrophs, showing a dual mode of nutrition, may then become more heterotrophic at higher temperatures and be favored. Interestingly, for short-term (24 h) responses to temperature, Ferreira et al. (submitted)[1] found that in mixoplankton (including our strain of *K. armiger*), grazing was impaired at warmer temperatures, whereas photosynthesis increased. We can corroborate the results for grazing; our acclimated *K. armiger* did not respond well to warming in terms of ingestion rates. However, after proper adaptation, the ingestion rates were remarkably high (although we have no information on photosynthetic rates). Overall, this particular observation, even if not conclusive, calls for further research on the subject and a cautious interpretation of the interaction of marine protists and temperature when sufficient time to develop adaptive responses does not occur. Finally, we also want to emphasize that our experiments were conducted under excess of food and feeding on prey that were nutrient repleted. Other food scenarios would securely render different outcomes. This is particularly important because experimental assessments of temperature costs on fitness may be more evident when resources are limiting, and the other way around, food-limited organisms may have higher problems adapting to high temperatures (Aranguren-Gassis et al., 2019).

[1] Ferreira, G. D., Grigoropoulou, A., Saiz, E., and Calbet, A. (submitted). The effect of short-term temperature exposure on critical physiological processes of mixoplankton and protozooplankton.

## DATA AVAILABILITY STATEMENT

he raw data supporting the conclusions of this article can be found at the open repository (DigitalCSIC, http://hdl.handle.net/10261/262244).

## AUTHOR CONTRIBUTIONS

AC wrote the manuscript and ES contributed to the manuscript revision. Both authors contributed to the conception and design of the study and approved the submitted version.

## FUNDING

This research was funded by Grant CTM2017–84288-R by Fondo Europeo de Desarrollo Regional (FEDER)/Ministerio de Ciencia, Innovación y Universidades—Agencia Estatal de Investigacioìn (AEI), and by Grant PID2020-118645RB-I00 by Ministerio de Ciencia e innovación (MCIN)/AEI/10.13039/501100011033 and by ERDF A way of making Europe. It is a contribution of the Marine Zooplankton Ecology Group (2017 SGR 87). With the institutional support of the Severo Ochoa Centre of Excellence accreditation (CEX2019-000928-S). The open-access publication fee was partially covered by the CSIC Open Access Publication Support Initiative through its Unit of Information Resources for Research (URICI).

## ACKNOWLEDGMENTS

We thank all the people from the lab involved in keeping the cultures alive during all the months the experiment lasted, particularly during the restrictive and dangerous confinement period of the pandemic COVID-19. We also thank C. Traboni for preparing the CNP samples for analysis.

## REFERENCES

Alcaraz, M., Almeda, R., Saiz, E., Calbet, A., Duarte, C. M., Agusti, S., et al. (2013). Effects of temperature on the metabolic stoichiometry of Arctic zooplankton. *Biogeoscien* 10, 689–697. doi: 10.5194/bg-10-689-2013

Aranguren-Gassis, M., Kremer, C. T., Klausmeier, C. A., Litchman, E., and Bates, A. (2019). Nitrogen limitation inhibits marine diatom adaptation to high temperatures. *Ecol. Lett.* 22, 1860–1869. doi: 10.1111/ele.13378

Arias, A., Selander, E., Saiz, E., and Calbet, A. (2021). Predator chemical cue effects on the diel feeding behaviour of marine protists. *Microb. Ecol.* 82, 356–364. doi: 10.1007/s00248-020-01665-9

Atkinson, A. (1994). Diets and feeding selectivity among the epipelagic copepod community near South Georgia in summer. *Polar Biol.* 14, 551–560.

Atkinson, D., Ciotti, B. J., and Montagnes, D. J. (2003). Protists decrease in size linearly with temperature: ca. 2.5% degrees $C^{-1}$. *Proc. Biol. Sci.* 270, 2605–2611. doi: 10.1098/rspb.2003.2538

Barton, S., Jenkins, J., Buckling, A., Schaum, C. E., Smirnoff, N., Raven, J. A., et al. (2020). Evolutionary temperature compensation of carbon fixation in marine phytoplankton. *Ecol. Lett.* 23, 722–733. doi: 10.1111/ele.13469

Bennett, A. F. (1987). "Evolution of the control of body temperature: is warmer better?," in *Comparative Physiology: Life in Water and on Land*, eds L. B. P. Dejours, C. R. Taylor, and E. R. Weibel (Padova: IX-Liviana Press).

Bennett, A. F., and Lenski, R. E. (1997). Evolutionary adaptation to temperature. VI. Phenotypic acclimation and its evolution in *Escherichia Coli*. *Evolution* 51, 36–46. doi: 10.1111/j.1558-5646.1997.tb02386.x

Calbet, A. (2001). Mesozooplankton grazing effect on primary production: a global comparative analysis in marine ecosystems. *Limnol. Oceanogr.* 46, 1824–1830.

Calbet, A., Garrido, S., Saiz, E., Alcaraz, M., and Duarte, C. M. (2001). Annual zooplankton succession in coastal NW Mediterranean waters: the importance of the smaller size fractions. *J. Plankton Res.* 23, 319–331.

Calbet, A., Isari, S., Martínez, R. A., Saiz, E., Garrido, S., Peters, J., et al. (2013). Adaptations to feast and famine in different strains of the marine heterotrophic

dinoflagellates *Gyrodinium dominans* and *Oxyrrhis marina*. *Mar. Ecol. Prog. Ser.* 483, 67–84. doi: 10.3354/meps10291

Calbet, A., and Saiz, E. (2005). The ciliate-copepod link in marine ecosystems. *Aquat. Microb. Ecol.* 38, 157–167. doi: 10.3354/ame038157

Flynn, K. J., Mitra, A., Anestis, K., Anschütz, A. A., Calbet, A., Ferreira, G. D., et al. (2019). Mixotrophic protists and a new paradigm for marine ecology: where does plankton research go now? *J. Plankton Res.* 41, 375–391. doi: 10.1093/plankt/fbz026

Frost, B. W. (1972). Effects of size and concentration of food particles on the feeding behavior of the marine planktonic copepod Calanus pacificus. *Limnol. Oceanogr.* 17, 805–815. doi: 10.4319/lo.1972.17.6.0805

Halsband-Lenk, C., Hirche, H. J., and Carlotti, F. (2002). Temperature impact on reproduction and development of congener copepod populations. *J. Exp. Mar. Biol. Ecol.* 271, 121–153. doi: 10.1016/s0022-0981(02)00025-4

Hantzsche, F. M., and Boersma, M. (2010). Dietary-induced responses in the phagotrophic flagellate *Oxyrrhis marina*. *Mar. Biol.* 157, 1641–1651. doi: 10.1007/s00227-010-1437-1

Haury, L. R., Mcgowan, J. A., and Wiebe, P. H. (1978). "Patterns and processes in the time-scales of plankton distributions," in *Spatial Patterns in Plankton Communities. Plenum NATO Conference Series IV. Marine Sciences 3*, ed. J. H. Steel (Berlin: Springer), 277–327. doi: 10.1007/978-1-4899-2195-6_12

Hayashida, H., Matear, R. J., and Strutton, P. G. (2020). Background nutrient concentration determines phytoplankton bloom response to marine heatwaves. *Glob. Chang. Biol.* 26, 4800–4811. doi: 10.1111/gcb.15255

Heinbokel, J. F. (1978). Studies on the functional role of tintinnids in the Southern California Bight. I. Grazing and growth rates in laboratory cultures. *Mar. Biol.* 47, 177–189. doi: 10.1007/bf00395638

Hobday, A. J., Alexander, L. V., Perkins, S. E., Smale, D. A., Straub, S. C., Oliver, E. C. J., et al. (2016). A hierarchical approach to defining marine heatwaves. *Prog. Oceanogr.* 141, 227–238. doi: 10.1016/j.pocean.2015.12.014

Huertas, I. E., Rouco, M., Lopez-Rodas, V., and Costas, E. (2011). Warming will affect phytoplankton differently: evidence through a mechanistic approach. *Proc. Biol. Sci.* 278, 3534–3543. doi: 10.1098/rspb.2011.0160

Intergovernmental Panel on Climate Change [IPCC] (2014). *Climate Change 2014: Synthesis Report. Contribution of Working Groups I, II and III to the Fifth Assessment Report of the Intergovernmental Panel on Climate Change*. Geneva: IPCC.

Klausmeier, C. A., Litchman, E., Daufresne, T., and Levin, S. A. (2004). Optimal nitrogen-to-phosphorus stoichiometry of phytoplankton. *Nature* 429, 171–174. doi: 10.1038/nature02454

Knies, J. L., Kingsolver, J. G., and Burch, C. L. (2009). Hotter is better and broader: thermal sensitivity of fitness in a population of bacteriophages. *Am. Nat.* 173, 419–430. doi: 10.1086/597224

Li, C. C., Xu, K. D., and Lei, Y. L. (2011). Growth and grazing responses to temperature and prey concentration of Condylostoma spatiosum, a large benthic ciliate, feeding on *Oxyrrhis marina*. *Aquat. Microb. Ecol.* 64, 97–104. doi: 10.3354/ame01521

Lin, C.-H., Flynn, K. J., Mitra, A., and Glibert, P. M. (2018). Simulating effects of variable stoichiometry and temperature on mixotrophy in the harmful dinoflagellate *Karlodinium veneficum*. *Front. Mar. Sci.* 5:320. doi: 10.3389/fmars.2018.00320

Listmann, L., Leroch, M., Schluter, L., Thomas, M. K., and Reusch, T. B. (2016). Swift thermal reaction norm evolution in a key marine phytoplankton species. *Evol. Appl.* 9, 1156–1164. doi: 10.1111/eva.12362

Litchman, E., Ohman, M. D., and Kiørboe, T. (2013). Trait-based approaches to zooplankton communities. *J. Plankton Res.* 35, 473–484. doi: 10.1093/plankt/fbt019

López-Urrutia, A., San Martin, E., Harris, R. P., and Irigoien, X. (2006). Scaling the metabolic balance of the oceans. *Proc. Natl. Acad. Sci. U.S.A.* 103, 8739–8744. doi: 10.1073/pnas.0601137103

Mackas, D. L., Denman, K. L., and Abbott, M. R. (1985). Plankton patchiness: biology in the physical vernacular. *Bull. Mar. Sci.* 37, 652–674.

Malzahn, A. M., Hantzsche, F., Schoo, K. L., Boersma, M., and Aberle, N. (2010). Differential effects of nutrient-limited primary production on primary, secondary or tertiary consumers. *Oecologia* 162, 35–48. doi: 10.1007/s00442-009-1458-y

Mathews, L., Faithfull, C. L., Lenz, P. H., and Nelson, C. E. (2018). The effects of food stoichiometry and temperature on copepods are mediated by ontogeny. *Oecologia* 188, 75–84. doi: 10.1007/s00442-018-4183-6

McFeeters, B. J., and Frost, P. C. (2011). Temperature and the effects of elemental food quality on Daphnia. *Freshw. Biol.* 56, 1447–1455. doi: 10.1007/s00442-009-1452-4

Meunier, C. L., Alguero-Muniz, M., Horn, H. G., Lange, J. A. F., and Boersma, M. (2017). Direct and indirect effects of near-future pCO(2) levels on zooplankton dynamics. *Mar. Freshwater Res.* 68, 373–380. doi: 10.1071/mf15296

Meunier, C. L., Haafke, J., Oppermann, B., Boersma, M., and Malzahn, A. M. (2012). Dynamic stoichiometric response to food quality fluctuations in the heterotrophic dinoflagellate Oxyrrhis marina. *Mar. Biol.* 159, 2241–2248. doi: 10.1007/s00227-012-2009-3

Montagnes, D. J. S., Kimmance, S. A., and Atkinson, D. (2003). Using Q10: can growth rates increase linearly with temperature? *Aquat. Microb. Ecol.* 32, 307–313. doi: 10.3354/ame032307

Multisizer$^{TM}$ user's manual. (2010). *MultisizerTM User's Manual. Beckman Coulter, Inc. 250 Kraemer Blvd. Brea, CA 92821*. Brea, CA: Beckman Coulter, Inc.

Müren, U., Berglund, J., Samuelsson, K., and Andersson, A. (2005). Potential effects of elevated sea-water temperature on pelagic food webs. *Hydrobiologia* 545, 153–166. doi: 10.1007/s10750-005-2742-4

O'Donnell, D. R., Hamman, C. R., Johnson, E. C., Kremer, C. T., Klausmeier, C. A., and Litchman, E. (2018). Rapid thermal adaptation in a marine diatom reveals constraints and trade-offs. *Glob. Chang. Biol.* 24, 4554–4565. doi: 10.1111/gcb.14360

Padfield, D., Yvon-Durocher, G., Buckling, A., Jennings, S., Yvon-Durocher, G., and Hillebrand, H. (2016). Rapid evolution of metabolic traits explains thermal adaptation in phytoplankton. *Ecol. Lett.* 19, 133–142. doi: 10.1111/ele.12545

Perrin, N. (1995). About Berrigan and Charnov's life history puzzle. *Oikos* 73, 137–139. doi: 10.1111/1365-2656.12183

Rose, J. M., and Caron, D. A. (2007). Does low temperature constrain the growth rates of heterotrophic protists? Evidence and implications for algal blooms in cold waters. *Limnol. Oceanogr.* 52, 886–895. doi: 10.4319/lo.2007.52.2.0886

Saiz, E., Griffell, K., and Calbet, A. (2020). Ontogenetic changes in the elemental composition and stoichiometry of marine copepods with different life history strategies. *J. Plankton Res.* 42, 320–333. doi: 10.1093/plankt/fbaa018

Sterner, R., and Elser, J. (2002). *Ecological Stoichiometry: the Biology of Elements From Molecules to the Biosphere*. Princeton, NJ: Princeton University Press.

Straile, D. (1997). Gross growth efficiencies of protozoan and metazoan zooplankton and their dependence on food concentration, predator-prey weight ratio, and taxonomic group. *Limnol. Oceanogr.* 42, 1375–1385. doi: 10.4319/lo.1997.42.6.1375

Traboni, C., Calbet, A., and Saiz, E. (2021). Mixotrophy upgrades food quality for marine calanoid copepods. *Limnol. Oceanogr.* 66, 4125–4139. doi: 10.1002/lno.11948

Wilken, S., Huisman, J., Naus-Wiezer, S., and Van Donk, E. (2013). Mixotrophic organisms become more heterotrophic with rising temperature. *Ecol. Lett.* 16, 225–233. doi: 10.1111/ele.12033

Woods, H. A., Makino, W., Cotner, J. B., Hobbie, S. E., Harrison, J. F., Acharya, K., et al. (2003). Temperature and the chemical composition of poikilothermic organisms. *Funct. Ecol.* 17, 237–245.

Yvon-Durocher, G., Schaum, C. E., and Trimmer, M. (2017). The temperature dependence of phytoplankton stoichiometry: investigating the roles of species sorting and local adaptation. *Front. Microbiol.* 8:2003. doi: 10.3389/fmicb.2017.02003

**Conflict of Interest:** The authors declare that the research was conducted in the absence of any commercial or financial relationships that could be construed as a potential conflict of interest.

**Publisher's Note:** All claims expressed in this article are solely those of the authors and do not necessarily represent those of their affiliated organizations, or those of the publisher, the editors and the reviewers. Any product that may be evaluated in this article, or claim that may be made by its manufacturer, is not guaranteed or endorsed by the publisher.

frontiers | Frontiers in Microbiology

ORIGINAL RESEARCH
published: 19 April 2022
doi: 10.3389/fmicb.2022.838707

# Temperature Rise Increases the Bioavailability of Marine *Synechococcus*-Derived Dissolved Organic Matter

*Jiajie Zhang[1,2], Jihua Liu[1,2,3]*, Daixi Liu[1,2], Xiao Chen[1,2], Quan Shi[4], Chen He[4] and Gang Li[5]*

[1] Institute of Marine Science and Technology, Shandong University, Qingdao, China, [2] Joint Lab for Ocean Research and Education at Dalhousie University, Shandong University and Xiamen University, Qingdao, China, [3] Southern Marine Science and Engineering Guangdong Laboratory, Zhuhai, China, [4] State Key Laboratory of Heavy Oil Processing, China University of Petroleum, Beijing, China, [5] Key Laboratory of Tropical Marine Bio-resources and Ecology, South China Sea Institute of Oceanology, Chinese Academy of Sciences, Guangzhou, China

OPEN ACCESS

**Edited by:**
Jun Sun,
China University of Geosciences, China

**Reviewed by:**
Yonghui Zeng,
University of Copenhagen, Denmark
Peter Leslie Croot,
National University of Ireland Galway, Ireland

***Correspondence:**
Jihua Liu
liujihua1982@sdu.edu.cn

**Specialty section:**
This article was submitted to Aquatic Microbiology, a section of the journal Frontiers in Microbiology

**Received:** 18 December 2021
**Accepted:** 18 February 2022
**Published:** 19 April 2022

**Citation:**
Zhang J, Liu J, Liu D, Chen X, Shi Q, He C and Li G (2022) Temperature Rise Increases the Bioavailability of Marine Synechococcus-Derived Dissolved Organic Matter. Front. Microbiol. 13:838707. doi: 10.3389/fmicb.2022.838707

*Synechococcus* is one group of main primary producers and plays a key role in oceanic carbon fixation and transformation. To explore how the temperature rise affects the bioavailability of *Synechococcus*-derived dissolved organic matter (SOM) and whether this effect would be altered by the involvement of heterotrophic bacteria, we compared the optical and molecular properties of the SOM of axenic *Synechococcus* sp. PCC7002 culture (*Syn*) to that with associated heterotrophic bacteria (*Syn*B) under 15, 18, and 21°C growth temperatures at exponential and decay growth phases. Our results showed that the temperature rise increased the bioavailability of the SOM of both *Syn* and *Syn*B cultures by lowering the proportion of the hydrogen-poor and double-bond structure-rich humus-like components and highly unsaturated substances, as indicated by the increase of spectral slope ratio ($S_R$) and biological index (BIX) and decrease of humification index (HIX). Moreover, the involvement of heterotrophic bacteria modified the *Synechococcus*-derived SOM, together with its intracellular dissolved organic matter (DOM) excludes, lowering the SOM bioavailability. Our results indicated that the warming in climate change scenario may enhance the bioavailability of the *Synechococcus*-derived SOM although it may be tempered by the involvement of heterotrophic bacteria, providing an insight for preservation of the organic carbon pool in global oceans.

**Keywords: dissolved organic matter (DOM), bioavailability, temperature rise, heterotrophic bacteria, exponential and decay phases, *Synechococcus* sp. PCC7002**

## INTRODUCTION

*Synecchococcus* is a significant group of photosynthetic carbon sequestration organisms that are widely distributed in coastal and oceanic environments, and is thus of great value in marine ecosystem (Huang et al., 2011; Jiao et al., 2011). Previous studies predicted that ocean warming will promote the importance of *Synechococcus* in the oceanic carbon cycle through expanding their

distribution range and increasing their cell abundance (Morán et al., 2010; Flombaum et al., 2013). The *Synechococcus*-derived dissolved organic matter (SOM) that is released into surroundings via secretion, natural cell death, viral lysis, and predation (Jiao et al., 2010; Fiore et al., 2015; Xiao et al., 2020) largely contributes to the marine dissolved organic matter (DOM) pool (Jiao et al., 2011; Gontikaki et al., 2013), and is thus one of the main drivers for the oceanic carbon cycle (Dufresne et al., 2008). The ultimate fate of SOM is usually determined by the associated heterotrophic bacteria in the ocean, and the bioavailability of SOM influences its persistence and the development of DOM pools (Jiao et al., 2010; Sarmento et al., 2016). Generally, the bioavailability of DOM refers to the consumed or/and utilized degrees of DOM compounds by associated heterotrophic bacteria, which primarily depends on their chemical composition (Berggren and Giorgio, 2015). Contrary to common belief, the DOM produced by algae did not always have high bioavailability (Koch et al., 2014). For example, a study by Koch et al. (2014) showed that only 20% of organic carbon from marine algae was degraded during the 2-year cultivation. Moreover, the DOM induced by viral lysis from cyanobacteria was detected to have similar optical properties with that from natural deep-ocean, indicating a great possibility that the cyanobacteria-derived DOM directly contributes to the refractory DOM (RDOM) formation (Zhao et al., 2017).

Ocean warming is accelerating, with surface seawater temperature being expected to increase by 1–7°C by the end of this century (Kattsov et al., 2001; Levitus et al., 2005; Gleick et al., 2010; Cheng et al., 2019). Previous studies indicated that global warming enhances the bioavailability of marine DOM (Segschneider and Bendtsen, 2013). The available evidence also indicated the possible effects of ocean warming on the bioavailability of SOM. For instance, many studies reported the temperature rise deeply affected the physiology, biochemical compositions, and carbon fixation of *Synechococcus* (Fu et al., 2007; Paerl and Huisman, 2008; Flombaum et al., 2013; Harvey et al., 2013; Paul et al., 2018). Furthermore, the elevated temperature has been observed to accelerate the production of phytoplankton fluorescent DOM (FDOM) (Yang et al., 2020). The temperature rise was also observed to be tightly coupled with the amount of extracellular microcystin (Walls et al., 2018), heterocyst glycolipid ketone alcohols (Bauersachs et al., 2014), and fatty acid (Nalley et al., 2018) produced by cyanobacteria. However, it is unclear about the effects of temperature rise on the molecular properties of SOM.

The exudations of both healthy and dead *Synechococcus* cells contribute to the SOM within surroundings (Agustí et al., 1998; Marañón et al., 2004; López Sandoval et al., 2013; Becker et al., 2014). Approximately, 25–65% of environmental DOM is released by cell lyse, viral lysis, or grazing activity, and is considered as intracellular DOM (Hygum et al., 1997; Myklestad and Swift, 1998; Møller et al., 2003; Malits et al., 2021). Compared with the intracellular DOM released due to cell death, the extracellular DOM secreted during cell growing, e.g., chromophoric DOM (CDOM) and FDOM, were more photolabile, with faster photochemical removal (Bittar et al., 2015). In addition, the molecular weight, double bond equivalents (DBE), hydrogen to carbon ratio (H/C), and modified aromatic index (AImod) of the algae-associated DOM often increase with algae cell growing or decay durations, indicating the transformation from active to refractory DOM (Liu et al., 2021). Apart from that, heterotrophic bacteria also play an important role in both the growth of *Synechococcus* and transformation of SOM (Zheng et al., 2017, 2019). Experiments assessing the SOM without the effects of heterotrophic bacteria have so far been scarce. In return for utilization of the organic carbon fixed by cyanobacteria, the heterotrophic bacteria benefit them by providing complex and unidentified substances like vitamins and bioavailable trace metals (Amin et al., 2009; Kazamia et al., 2012). Because of this, rendering axenic cyanobacteria is difficult for laboratorial cultures. Therefore, few studies have so far focused on how temperature affects the bioavailability of DOM in *Synechococcus*, especially under different growth phases and with/without heterotrophic bacteria transformations.

It is of great significance to study the bioavailability change of SOM under elevated temperature when considering its contribution to the oceanic carbon pool. Cyanobacteria like *Synechococcus* are one group of the dominating photoautotrophic microorganisms in the middle and low latitudinal coastal waters (Flombaum et al., 2013), while the *Synechococcus* sp. PCC7002 is a model strain and mainly distributed in the coastal waters (Mou et al., 2017, 2018). Therefore, in this study we examined the changes of the properties of DOM from *Synechococcus* sp. PCC7002 with and without the associated heterotrophic bacteria effects under different growth temperatures (15, 18, and 21°C) at exponential and decay growth phases. This study intended to elucidate how the increased temperature influences the persistence of SOM pool in global oceans.

# MATERIALS AND METHODS

## Experimental Design

The marine *Synechococcus* sp. PCC7002 culture with microbes was obtained from Xiamen University Center for Marine Phytoplankton. In this culture, 30 mainly associated bacteria strains belonging to six species (**Supplementary Table 1**) were identified with agar 2216 medium. Among them the *Halomonas* sp. that belongs to class *Gammaproteobacteria* was dominant and isolated with streak plate methods and used in the following experiments. The axenic *Synechococcus* sp. PCC7002 was isolated by streaking onto the $A^+$ agar plate and purified by repeatedly culturing in solid and liquid media (Zhang et al., 2021).

To probe how heterotrophic bacteria affect the bioavailability of SOM, we cultured both axenic *Synechococcus* sp. PCC7002 (*Syn*) and that with *Halomonas* sp. (*Syn*B) in $A^+$ medium with the Fe-EDTA, Tris-HCl, and vitamin B12 concentrations being adjusted to 7.5 μM, 4 mM, and 3 nM, respectively (Stevens and Porter, 1980; Ludwig and Bryant, 2011). Such an adjustment was to eliminate the influence of external organic carbon while maintaining the growth of *Synechococcus* sp. PCC7002. Both the *Syn* and *Syn*B cultures were grown in 300-ml conical flasks (50-ml cultures) under the temperatures of 15, 18, and 21°C in a light incubator (ZQZYCGF8, Shanghai, China). Continuous growth

light was provided by a panel of LEDs (Light Emitting Diodes) on top of the incubator with light intensity of 20 ± 1.0 μmol photons $m^{-2}$ $s^{-1}$, that was measured with a microscopically quantum sensor (QRT1, Hansatech, United Kingdom) in a culture flask filled with medium. Such a low growth light was chosen to limit the photodegradation or photo transformation of the *Synechococcus*-derived SOM, as well as maintain the favorable growth of *Synechococcus* sp. PCC7002 (Mackey et al., 2017). Under each temperature, 20 replicate flasks for each *Syn* and *Syn*B culture were maintained for the subsequent determination of growth, SOM absorption, and fluorescence and molecular compositions. In each flask, the initial *Synechococcus* sp. PCC7002 cell density was adjusted to $\sim 10^7$ cells $ml^{-1}$, and extra *Halomonas* sp. isolated above was co-inoculated in *Syn*B culture to the density of $\sim 10^6$ cells $ml^{-1}$ (Zhang et al., 2021). Before inoculating to the *Syn* culture, the bacteria was pre-cultured 2 days in marine broth 2216 at 33°C and washed twice with the modified $A^+$ medium. All the glassware used in this experiment was pre-combusted at 450°C for 5 h to eliminate the effects of external organic carbon.

## Growth Phase Determination

Growth of *Synechococcus* sp. PCC7002 in *Syn* and *Syn*B cultures was tracked through monitoring the changes in cell abundance using a flow cytometer (Accuri§ C6, Becton-Dickinson, Franklin Lakes, NJ, United States). Every 1–3 days, 1-ml culture was taken out from random three flasks of *Syn* and *Syn*B cultures under each temperature, and the cell abundance was measured. In addition, the decay phase can be primarily identified with the visible color changes, i.e., from blue-green to yellow-green.

We identified the exponential growth phase at Days 10–32 in *Syn* and at Days 14–35 in *Syn*B cultures following Mou et al. (2018), and calculated the specific growth rate ($\mu_{max}$, $d^{-1}$) with the equation:

$$\mu_{\max} = [LN(N_t) - LN(N_{t0})] / (t - t_0)$$

where $N_t$ and $N_{t0}$ are the culture cell abundance at the time t and t0, respectively.

## Dissolved Organic Matter Absorption and Fluorescence Measurements

In the exponential growth phase, random three replicate flasks of *Syn* and *Syn*B cultures were taken out from the incubator to measure DOM absorption and fluorescence. From each flask, 5 ml culture was taken out and filtrated through a pre-combusted (450°C, 5 h) GF/F filter (Whatman, 25 mm in diameter), and the filtration was collected, dispensed into a brown glass tube, and stored at 4°C after 10-time dilution until later measurements of absorption and fluorescence within 3 days. After sampling, these flasks were discarded to eradicate contamination. At the end of cultivation, such a sampling process was performed again, for the DOM determinations in decay growth phase.

To measure the DOM absorption, the filtration was put into a 1-cm quartz cuvette of spectrophotometer. The DOM absorption spectrum was scanned from 250 to 600 nm with a 1-nm increment, referencing to Milli-Q water. Mean absorptions from 575 to 600 nm were used to correct the effects of scattering and baseline fluctuation (Helms et al., 2008). The absorption coefficient of CDOM was calculated (Bricaud et al., 1981) as:

$$a_{CDOM}(\lambda) = 2.303 * A_{CDOM}(\lambda)/L$$

where $a_{CDOM}(\lambda)$ is the corrected CDOM absorption coefficient at wavelength λ, $A_{CDOM}$ (λ) is the corrected optical density at wavelength λ, and L is the path length (m).

The spectral slope was calculated using a non-linear least squares fitting routine over the range of 275–295 nm ($S_{275-295}$) and 350–400 nm ($S_{350-400}$) (Nvdv, 2002) as:

$$a_{CDOM}(\lambda) = a_{CDOM}(\lambda 0)\ exp[S((\lambda 0 - \lambda))]$$

where λ*o* is a reference wavelength and S is the spectral slope parameter.

The spectral slope ratio ($S_R$) was defined as the ratio of the spectral slope of 275–295 nm to that of 350–400 nm. Generally, the average molecular weight and aromaticity of CDOM are inversely proportional to $S_R$: Lower $S_R$ indicates higher aromaticity, while higher $S_R$ indicates lower aromaticity and thus easier biological degradation (Helms et al., 2008).

To measure excitation emission matrix (EEM), the DOM sample was dispensed into a 1-cm quartz cuvette and measured using a fluorescence spectrophotometer (Cary Eclipse, Agilent, Santa Clara, CA, United States) with the excitation and emission wavelengths of 250–550 nm and 250–600 nm, respectively. The excitation and emission slit widths were set as 10 nm, with the scan speed of 1,200 nm $min^{-1}$. Parallel factor analysis (PARAFAC) was performed in MATLAB 2021a with the drEEM toolbox 0.6.3 (Murphy et al., 2013). Moreover, the Milli-Q water was used as blank to calibrate the EEMs data (Lawaetz and Stedmon, 2009; Guo et al., 2011), and all the fluorescent data were presented in Raman Units (RU), from which the humification index (HIX) (Ohno, and Tsutomu., 2002), and biological index (BIX) (Huguet et al., 2009) were calculated.

## Molecular Signature Determinations

After measuring DOM absorption and fluorescence, the remaining cultures (~40 ml in each of three replicate flasks) were mixed together, filtered through a GF/F filter, and collected into a pre-combusted glass bottle. The collected filtrate was extracted through methanol-rinsed and formic acid-acidified PPL solid-period extraction cartridges (500 mg, Agilent Technologies) with the speed of ~5 ml $min^{-1}$. After extraction, the cartridges were washed with 15 ml formic acid (Sigma-Aldrich, Darmstadt, Germany, 98%), dried, and stored at -20°C for later DOM molecular signature analysis with a Fourier transform ion cyclotron resonance mass spectrometry (FT-ICR MS). The DOM molecular signature analysis was conducted by a 9.4 Tesla Apex-ultra FT-ICR MS in the Heavy Oil Key Laboratory, School of Chemical Engineering, China University of Petroleum, Beijing, China (He et al., 2020). To determine molecular properties, the DOM in PPL was eluted with 10 ml chromatographically pure methanol (Sigma-Aldrich, Darmstadt, Germany) and

injected into instrument at speed of 180 μl $h^{-1}$. The operating conditions for negative formation were set as: 3.0 kV emitter voltage, 3.5 kV capillary column introduce voltage, and -320 V capillary column end voltage, and the samples were scanned over an *m/z* range of 200–800. Then, based on the AImod index (Qiao et al., 2020) and H/C, the DOM compounds were grouped into five classes (Seidel et al., 2014): polycyclic aromatics (AImod > 0.66), polyphenols (0.5 < AImod < 0.66), highly unsaturated and phenolic compounds (AImod ≤ 0.5 and H/C < 1.5), aliphatic compounds (1.5 ≤ H/C < 2), and saturated compounds (AImod < 0.5 and H/C > 2). The intensity of molecular formula is also taken into account when calculating the percentage of each class. The DBE values were calculated (Koch and Dittmar, 2006) to characterize the number of double bonds in molecules.

## Statistical Analyses

All the parameters were presented with mean and standard deviations (mean ± SD) of three independent biological replicate cultures except for the FT-ICR MS data from a mixture of the three replicates. Paired *t*-test was performed with OriginPro 2021 software (Origin Lab Corporation, Northampton, MA, United States), and a linear regression was applied to test the correlation of measured parameters to temperature. The significance level was set as $p = 0.05$.

# RESULTS AND DISCUSSION

## *Synechococcus* Growth

Growth of *Synechococcus* sp. PCC7002 in the *Syn* and *Syn*B cultures under different temperatures is shown in **Figure 1**. The $\mu_{max}$ of *Synechococcus* in the axenic culture were 0.12 ± 0.02, 0.15 ± 0.04, and 0.17 ± 0.03 $d^{-1}$ under 15, 18, and 21°C, while that in *Syn*B culture were 0.09 ± 0.02, 0.18 ± 0.02, and 0.18 ± 0.01 $d^{-1}$, indicating the inhibitory effect of adding bacteria upon the growth merely occurred at low temperature. By contrast, symbiotic heterotrophic bacterial bacteria often promote the growth of algae by providing them with micronutrients like vitamins or bioavailable trace metals (Amin et al., 2009). Such a positive effect is closely related to temperature according to our results. Although adding bacteria showed a limited effect on the growth of *Synechococcus* at higher temperatures, it indeed induced approximately 50% promotion in cell density at both 18 and 21°C at stationary phase if comparing the cell abundance of *Syn* culture to that of *Syn*B culture (i.e., $1.21 \times 10^9 \pm 2.02 \times 10^7$ vs. $2.67 \times 10^9 \pm 5.52 \times 10^7$ at 18°C; and $1.26 \times 10^9 \pm 1.46 \times 10^7$ vs. $2.80 \times 10^9 \pm 2.13 \times 10^7$ at 21°C). Consistent with this finding, a model result by Flombaum et al. (2013) showed that the abundance of *Synechococcus* increases in the future oceans. It was worth noting that the final cell density of *Synechococcus* at 15°C was insignificant between *Syn* and *Syn*B cultures. This may be explained that the heterotrophic bacteria may have activated the growth of *Synechococcus* through providing them essential micronutrients (Hayashi et al., 2011; Kazamia et al., 2012), but such an activated function just started when temperature is over a threshold of e.g., higher than 18°C (**Figure 1**).

## Common Chromophoric Dissolved Organic Matter Properties

Chromophoric dissolved organic matter is an important component of DOM and its vital role in the marine carbon cycle has been widely acknowledged (Yamashita et al., 2010; Andrew et al., 2013). To explore the impacts of temperature on the common CDOM properties of SOM, we measured the absorbance ($S_R$) and fluorescence indicators (HIX and BIX) of the *Syn* and *Syn*B cultures under three different temperatures (**Figure 2**), which are well-known to closely correlate with the bioavailability of DOM (Cory and McKnight, 2005; Helms et al., 2008; Huguet et al., 2009; Yuan et al., 2017).

In axenic *Syn* culture, the $S_R$ of SOM increased from 3.73 ± 0.64 at 15°C to 5.71 ± 0.69 at 21°C at exponential growth phase, while it increased from 1.55 ± 0.12 to 3.30 ± 0.27 at decay phase (**Figure 2A**). Higher $S_R$ values are generally associated with the lower DOM molecular weight and aromaticity (Helms et al., 2008), while the DOM with lower aromaticity is often less stable and more likely to be utilized by heterotrophic microorganisms (Zhou et al., 2020). Therefore, the elevated temperature may have reduced the molecular weight and aromaticity, leading to the better bioavailability of SOM. Moreover, the $S_R$ value at exponential phase was significantly higher than that at decay phase, no matter under what temperatures (Paired *t*-test, 15°C, $t = 6.94$, $p < 0.05$; 18°C, $t = 8.82$, $p < 0.05$; 21°C, $t = 4.38$, $p < 0.05$), indicating the bioavailability of SOM is higher in former than latter growth phases. A possible explanation is that the more permeability of cell membrane at decay phase allowed the release of intracellular matters like pigments to surroundings, while these metabolites may contribute to the humic-like fluorescent groups (Zhao et al., 2017). It may thus be speculated that the addition of such a humic substance results in the decrease of the bioavailability of SOM. Evidence that elevated temperature enhanced the bioavailability may also be inferred from the HIX and BIX values of SOM, which decreased from 0.99 ± 0.00 to 0.96 ± 0.01 and increased from 0.53 ± 0.03 to 0.61 ± 0.01 with temperature increasing from 15 to 21°C at exponential phase (**Figures 2C,E**). At decay phase, the HIX was similar to that at exponential phase, but the BIX was significantly lower (paired *t*-test, 15°C, $t = 4.61$, $p < 0.05$; 18°C, $t = 6.98$, $p < 0.05$; 21°C, $t = 13.48$, $p < 0.05$), and both HIX and BIX presented similar temperature-dependent changes. HIX values correspond to the ratio of fluorescence intensity between humic and protein-like components at long excitation wavelengths (Ohno, and Tsutomu., 2002), and higher HIX values thus indicate the presence of complex molecules like high molecular weight aromatics (Senesi et al., 1991). It is generally believed that the DOM that can persist for a long time in deep sea often contains large amounts of humic substances that are not easily utilized by microorganisms (Zhao et al., 2017); in contrast, protein-like components have a rapid turnover rate and cannot retain for a long time in marine

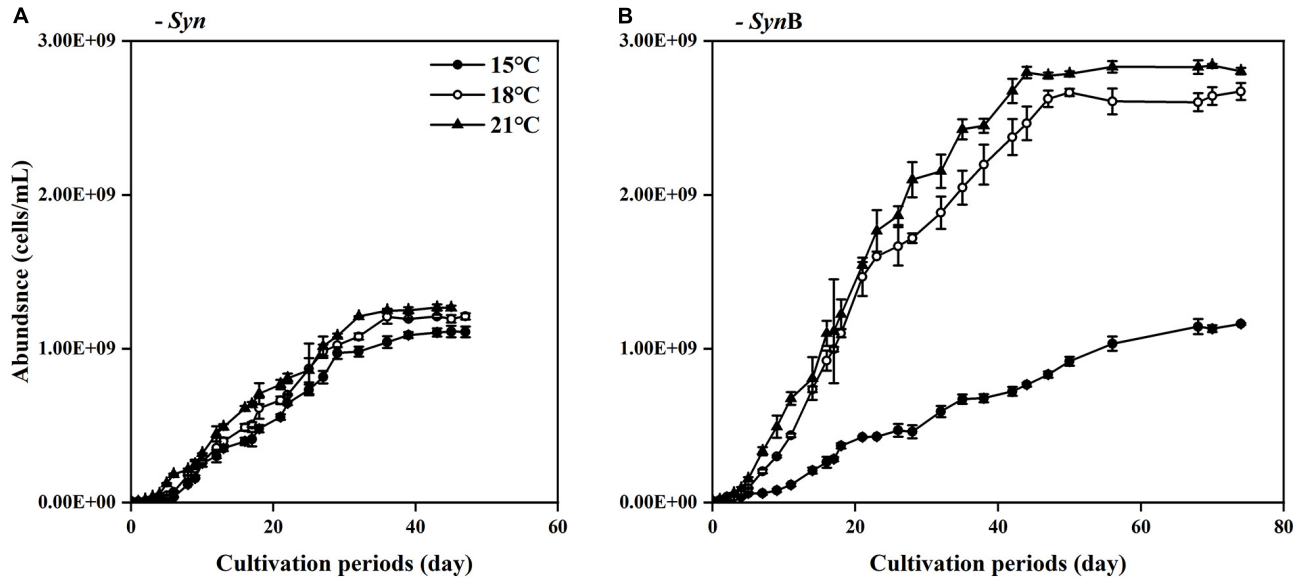


**FIGURE 1 |** Changes of cell density (indicated by adjusted $OD_{730}$) of *Synechococcus* sp. PCC7002 in cultures without [**(A)**, *Syn*] and with heterotrophic bacteria [**(B)**, *Syn*B] during cultivation periods under temperatures of 15, 18, and 21°C. Points show averages of measurements on three independent cultures and vertical bars show standard deviations ($n$ = 3).

environment (Zhang and Wang, 2017). The BIX characteristics of autochthonous biological activity in water (Huguet et al., 2009) essentially reflects the ratio of fluorescence intensity of humic-like component peaks at short wavelengths to that at long wavelengths. The fluorescence emission spectra usually move toward longer wavelengths with increasing aromaticity (Senesi, 1990). Therefore, the accumulation of more fluorescent substances at short wavelengths means the higher BIX values and the DOM being more easily utilized; the higher BIX values, the more fresh and higher bioavailability of DOM (Cory and McKnight, 2005; Huguet et al., 2009). Given the lower HIX and higher BIX at 21°C condition, the SOM from the cultures under higher temperature have a lower degree of humification and can be retained for a shorter time period. Again, these SOM were inferred from higher bioavailability. The mechanisms underlying this phenomenon need to be studied further. Moreover, consistent with $S_R$, the lower BIX at exponential than decay phases (**Figures 2A,E**) also indicated the higher bioavailability of SOM in former than latter phases.

All of the above results appeared to suggest that higher temperature favors higher bioavailability of SOM. Does the heterotrophic bacterial biological process change this? As compared to axenic *Syn* culture, the $S_R$ of SOM of non-axenic *Syn*B culture was significantly lower among all temperatures in both exponential and decay growth phases (Paired $t$-test, $t = 5.69$, $p < 0.05$), and with an insignificant increase of increasing temperature (**Figure 2B**). Similar to $S_R$, the decrease effect by adding heterotrophic bacteria also occurred in the BIX (**Figure 2F**). The heterotrophic bacteria addition significantly enhanced the BIX at 18 and 21°C, but not at 15°C (**Figure 2F**), indicating the modification of heterotrophic bacteria on bioactivity of SOM. Consistently, previous studies demonstrated that heterotrophic bacterial processes can make the DOM more resistant to further degradation (Liu et al., 2021). According to Ogawa et al. (2001),Jiao et al. (2010),Jiao et al. (2011), and Benner (2011), most of the SOM modified by heterotrophic bacteria were converted into inorganic carbon and returned to environments, and the others were converted into more complex organic structures and retained in the environments for the extended time-periods, which was also illustrated in this study.

## Fluorescent Components of *Synechococcus*-Derived Dissolved Organic Matter

During calculation process of the above fluorescence parameters, the limited data such as a single point fluorescence signal (e.g., BIX) or the segment of fluorescence signal at a single excitation wavelength (e.g., HIX) were considered, which inevitably introduced into the deviations. The PARAFAC component analysis was thus performed to validate the changes of the bioavailability of SOM. To characterize the structures of SOM, we detailed its fluorescence and identified a total of five main components (C1–C5) from all samples according to EEM-PARAFAC model (**Supplementary Figure 1**), being detailed in **Table 1**. Components 1–3 and 5 have been evidenced as humus-like substances (Stedmon et al., 2003; Stedmon and Markager, 2005a,b; Murphy et al., 2008; Yamashita et al., 2008; Zhang et al., 2009), and the Component 4 as protein-like substances (Yu et al., 2015). Components 1–3 are usually considered as terrestrially derived humic substances (Coble, 1996); while some studies have also identified these components as algae-derived DOM (Mou et al., 2017; Zhao et al., 2017), also in this

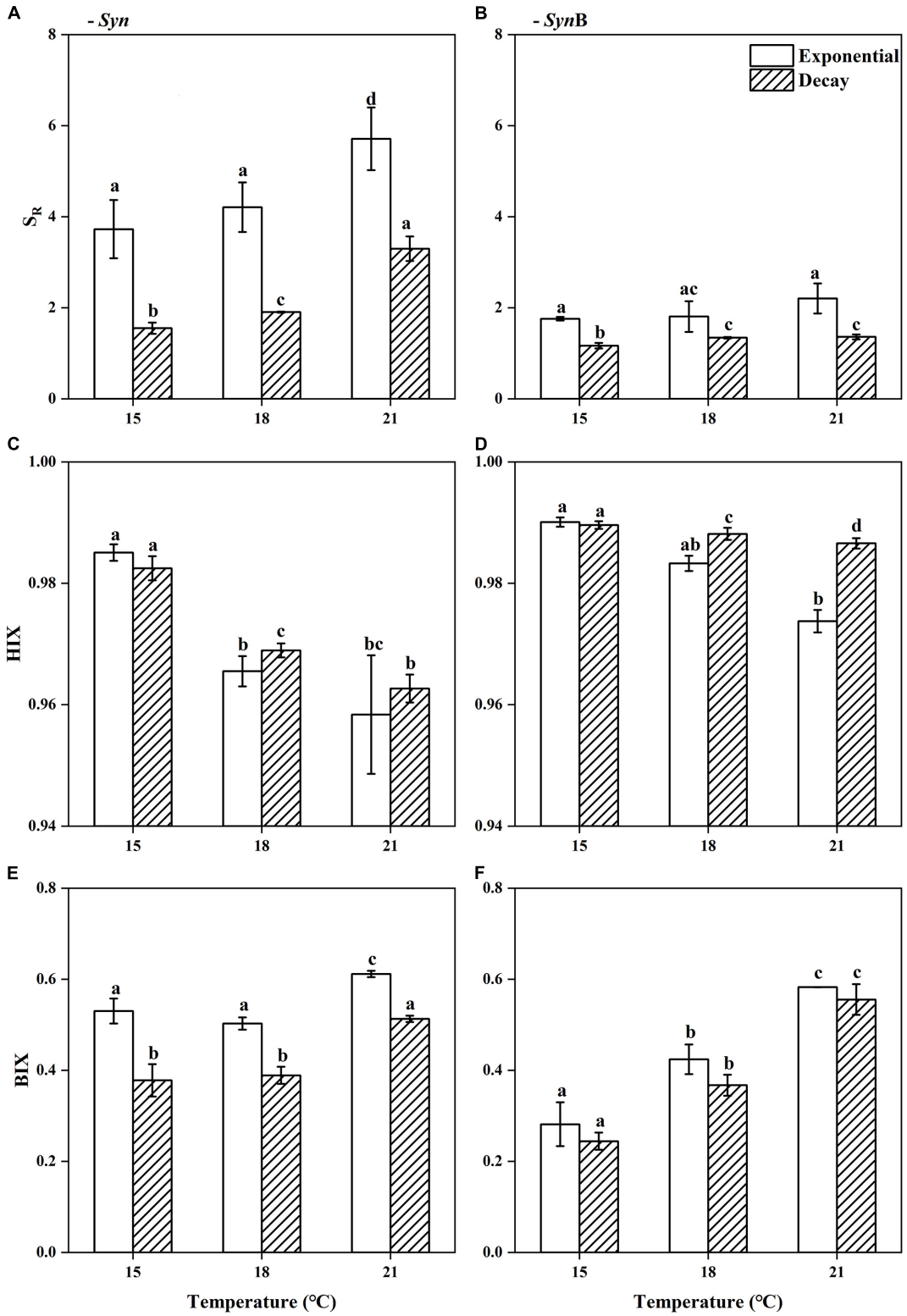


**FIGURE 2 |** Spectral slope ratio [**(A,B)**, $S_R$], humification index [**(C,D)**, HIX], and biological index [**(E,F)**, BIX] of *Synechococcus*-derived dissolved organic matter (SOM) at exponential and decay phases, in *Synechococcus* sp. PCC7002 cultures without [**(A,C,E)**, *Syn*] and with heterotrophic bacteria [**(B,D,F)**, *Syn*B] under temperatures of 15, 18, and 21°C. Vertical bars indicate standard deviations ($n$ = 3), and different letters on top of bars indicate significant difference (paired $t$-test, $p < 0.05$).

study (**Supplementary Figure 1**). Component 5 has also been reported to be associated with heterotrophic microbial processes (Zhang et al., 2009). But we found it not only presented in *Syn*B culture, but also in axenic culture of *Synechococcus*; it suggested the participation of heterotrophic bacteria was not necessary to produce Component 5. Furthermore, component 1 displayed similar optical properties as the fluorescent component BATS1 from deep sea [ex| em: 250 (340)| 460 nm], while the component 5 was similar to component BATS2 [ex| em: 250 (310)| 400 nm] (Zhao et al., 2017). Our results again confirmed the conclusion that *Synechococcus* is one of an important source of deep-sea autochthonous FDOM (Zhao et al., 2017; Zheng et al., 2020). Previous studies have also identified the protein-like components including tyrosine- and tryptophan-like fluorophores (Stedmon and Markager, 2005a,b), and Component 4 in this study could be identified as autochthonous tyrosine-like fluorophores (Yu et al., 2015). In general, it is speculated that all the fluorescent components identified in this study could be produced by *Synechococcus* that may do the contribution in field oceans.

Difference in contribution of the five components to total CDOM fluorescence intensity in each DOM sample is shown in **Figure 3** (the data quality as indicated by the SD versus mean value of three biological replicates is shown in **Supplementary Figure 2**). In general, the humus-like fluorescent substances (C1–3 and C5) are dominant in SOM (i.e., 87–95%). A similar result was also reported by Zheng et al. (2020). Furthermore, the humus-like fluorescent components derived from both *Syn* and *Syn*B cultures were mainly the components 1 and 2 (over 70%). Similar results have also been found in some other *Synechococcus* cultures, such as *Synechococcus* CB0101 and *Synechococcus* sp. YX04-3 (Zhao et al., 2017; Zheng et al., 2019). In *Syn* culture, the sum of humus-like substances (C1, C2, C3, and C5) significantly decreased with increasing temperature in both exponential ($R^2 = 0.99$, $p < 0.05$) and decay growth phases ($R^2 = 0.97$, $p < 0.05$), although no clear trend was observed in each component (**Figure 3A**). In protein-like component (C4), however, this trend contrarily increased. The protein-like component has simpler cellular structure and could be utilized more easily

**TABLE 1 |** Fluorescent components identified by parallel factor analysis (PARAFAC).

| Components | Ex/Em maximum wavelength (nm) | Descriptions | References |
|---|---|---|---|
| C1 | 250/455 | Humic-like substances | Stedmon et al., 2003; |
| C2 | 260 (360)/450 | | Stedmon and Markager, 2005a,b; |
| C3 | 250 (380)/480 | | Murphy et al., 2008; |
| C5 | 330(< 250)/400 | | Yamashita et al., 2008; Zhang et al., 2009 |
| C4 | 275/300 | Tyrosine-like fluorescence | Yu et al., 2015 |

*The secondary peaks are shown in parentheses.*

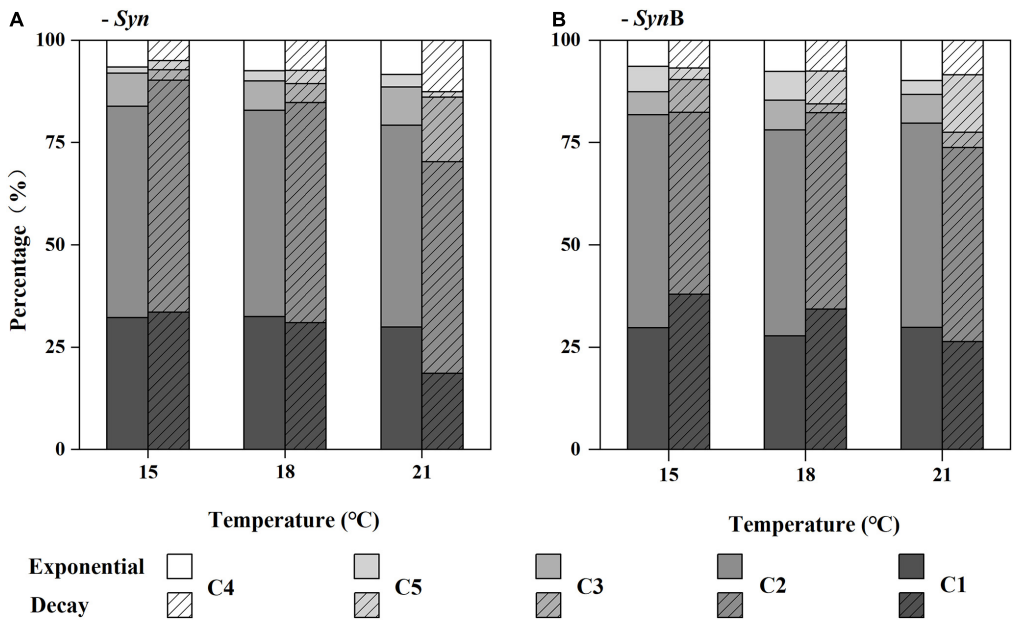


**FIGURE 3 |** Relative contribution (%) of the main fluorescence components (C1, C2, C3, C4, and C5) to total chromophoric dissolved organic matter (CDOM) fluorescence (Raman Units, RU) of *Synechococcus*-derived dissolved organic matter (SOM) at exponential and decay phases, in *Synechococcus* sp. PCC7002 cultures without [**(A)**, *Syn*] and with heterotrophic bacteria [**(B)**, *Syn*B] under temperatures of 15, 18, and 21°C.

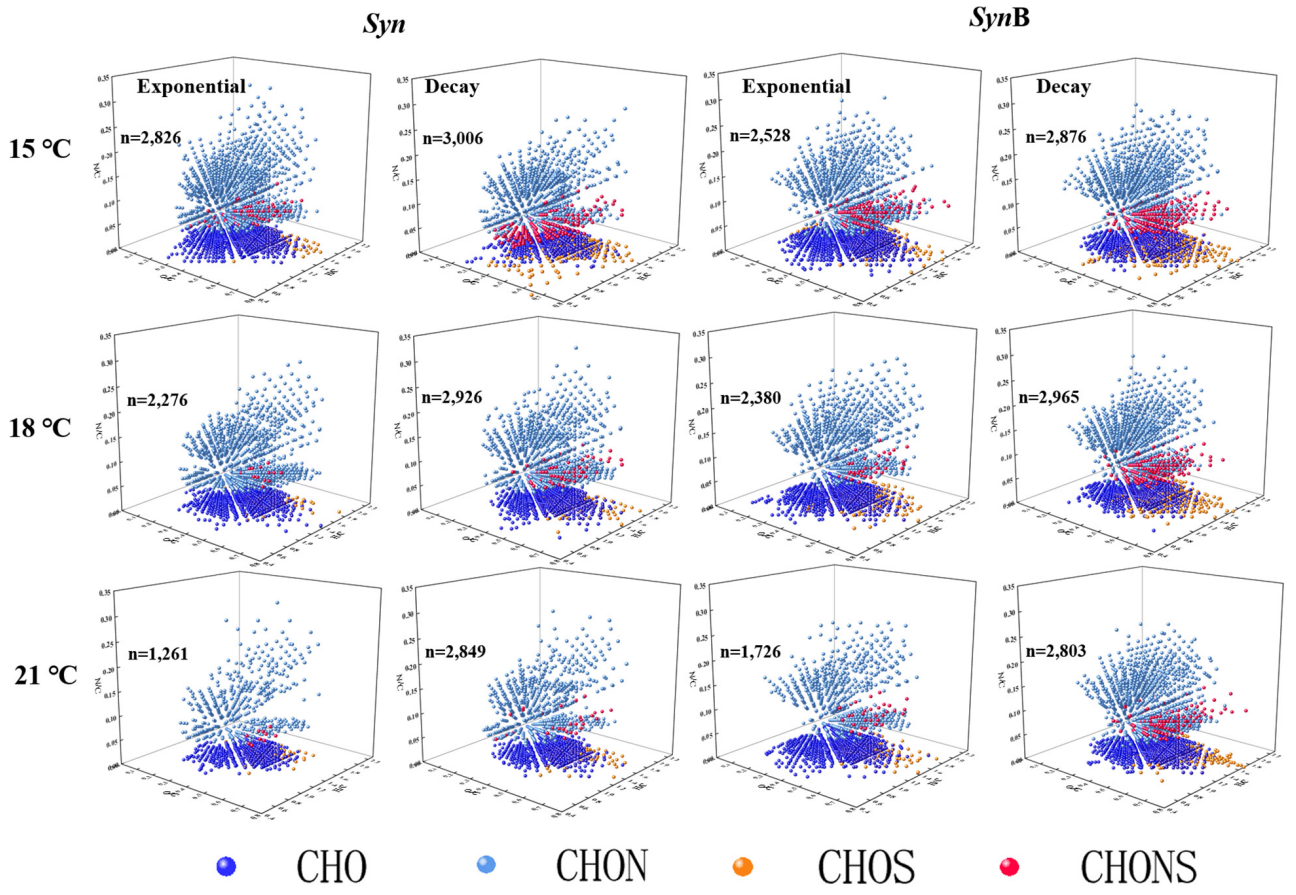


**FIGURE 4 |** 3D Van Krevelen diagram showing the characteristics of each molecule identified by Fourier transform ion cyclotron resonance mass spectrometry (FT-ICR MS). Each ball represents a molecular formula and "*n*" is the total number of molecular formulae. Dark blue, light blue, orange, and red colors indicate the formulae containing element CHO, CHON, CHOS, and CHONS, respectively.

by heterotrophic bacteria, as compared with the humus-like component (Zheng et al., 2020). Therefore, the increased protein-like component could be responsible for the increase of the bioavailability of SOM at elevated temperature. In addition, reliability of the results about the changes of SOM bioavailability from optical indicators was also considered. However, based on the FDOM data, the reasons why the higher bioavailability of SOM occurred in exponential growth phase and was not modified by heterotrophic bacteria could not be explained at present (**Figure 3**); this would be further explained by the molecular composition of the SOM identified with FT-ICR-MS.

## Chemical Composition of *Synechococcus*-Derived Dissolved Organic Matter

The FT-ICR-MS analysis can provide information about the molecular compositions of DOM (Martínez-Pérez et al., 2017; Zark and Dittmar, 2018) that may indicate its bioavailability through revealing the large diversity of organic compounds (**Figure 4** and **Supplementary Figure 3**). Due to the limitation of extraction efficiency of PPL cartridge, here we just analyzed the extractable and ionizable components of DOM. The 3D Van Krevelen diagram showed the detailed information of SOM molecules in terms of element compositions, i.e., oxygen to carbon ratio (O/C), H/C and nitrogen to carbon ratio (N/C) (**Figure 4**). Based on the element compositions (CHO, CHNO, CHOS, and CHNOS), the SOM can be classified into four groups. Apart from C, H, and O, they also contained abundant nitrogen and sulfur, consistent with previous studies that reported the DOM released by marine *Synechococcus* was a substantial source of *in situ* nitrogen- and sulfur-containing compounds (Zhao et al., 2017; Zheng et al., 2019, 2020). In *Syn* culture at 15°C temperature, 2,826 and 2,528 molecular formulas were identified in SOM in exponential and decay growth phases, and the numbers were 2,276 and 2,380 at 18°C, and 1,261 and 1,726 at 21°C, respectively (**Supplementary Figure 3**). The types of identified molecular formulas of SOM were more simplified at higher temperatures, indicating the ocean warming may make the SOM composition more and more simplification. Moreover, the bacteria addition has increased the diversity of SOM molecules (**Supplementary Figure 3**), suggesting the associated heterotrophic bacteria have contrarily changed this phenomenon.

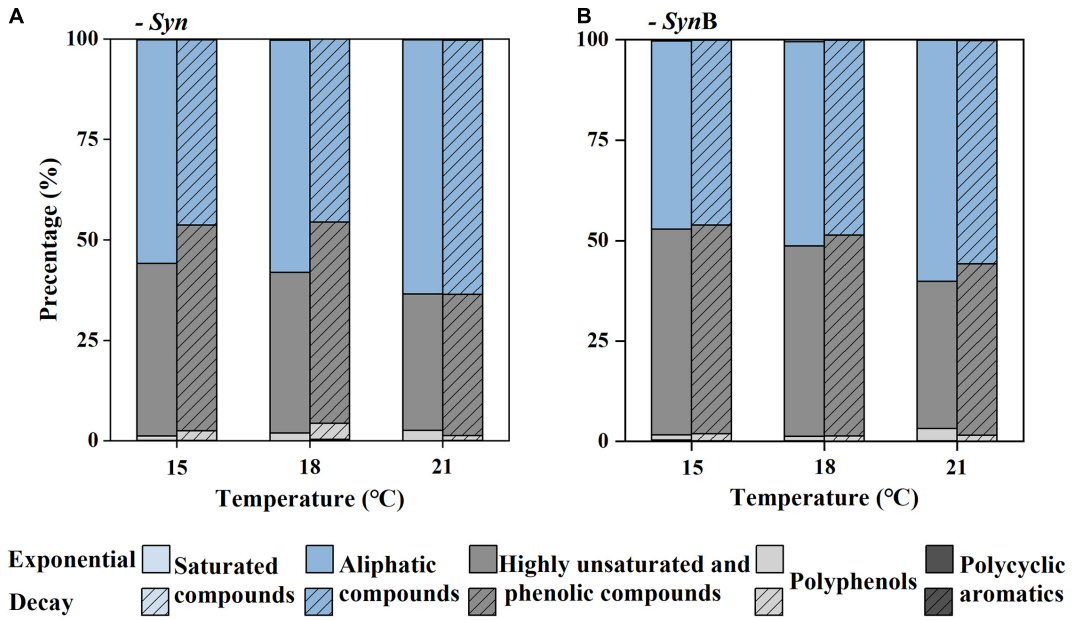


**FIGURE 5 |** Relative abundance (%) of classification classes based on the modified aromatic index (Almod) values and hydrogen to carbon ratio (H/C) of *Synechococcus*-derived dissolved organic matter (SOM) at exponential and decay phases, in *Synechococcus* sp. PCC7002 cultures without [**(A)**, *Syn*] and with heterotrophic bacteria [**(B)**, *Syn*B] under temperatures of 15, 18, and 21°C. The polycyclic aromatics are defined as Almod > 0.66, polyphenols as 0.5 < Almod < 0.66, highly unsaturated and phenolic compounds as Almod ≤ 0.5 and H/C < 1.5, aliphatic compounds as 1.5 ≤ H/C < 2, and saturated compounds as Almod < 0.5 and H/C > 2.

To further explore the compositions of SOM, the DOM compounds were divided into five classifications according to AImod value and H/C ratio, among which the sum of highly unsaturated and phenolic compounds and aliphatic compounds accounted for more than 95%, while the remaining (i.e., sum of polycyclic aromatics, polyphenols, and saturated compounds) accounted for less than 5% (**Figure 5**). According to Liu and co-authors the algal-derived DOM are lack of compounds with the AImod > 0.67 (Liu et al., 2021). Our study further indicated that the proportion of compounds with AImod > 0.5 (polycyclic aromatics and polyphenols) was low in SOM. The saturated compounds were shown with low abundance in various DOM samples (Seidel et al., 2014, 2015; Qiao et al., 2020), consistent with this study. As below, we focused on two more abundant compounds (i.e., highly unsaturated and phenolic compounds and aliphatic compounds). The proportion of aliphatic compounds in *Syn* cultures increased from 46.14 to 63.24% as temperature increased from 15 to 21°C at exponential growth phase. At decay phase, a similar temperature-dependent increase trend occurred. In contrast, the proportion of highly unsaturated and phenolic compounds decreased with increasing temperature. The modification of cellular fatty acid composition has been widely reported to maintain the normal cell growth across temperatures (Thompson, 1996). Compared with highly unsaturated and phenolic compounds, the aliphatic compounds had higher biodegradability and more rapidly turnover rate (Kellerman et al., 2018). Therefore, it is likely that the increase of aliphatic compounds in SOM caused by elevated temperature was responsible for the increase of its bioavailability. Moreover, the proportion of aliphatic compounds was 1–12% higher in exponential than decay phases among all temperature treatments (**Figure 5**). It may also explain why the bioavailability of SOM in the exponential growth phase was relatively high due to the lower proportion of highly unsaturated and phenolic compounds and higher aliphatic compounds. This result is consistent with the findings of Liu et al. (2021) that the amount of more recalcitrant compounds increased with the growth and degradation of algal cells. Most of SOM in exponential growth phase was secreted by *Synechococcus* cells, while in decay growth phase it was a mixture with intracellular substances exuded by cell death. It could be speculated that the bioavailability of intracellular SOM was lower than that being secreted during cell growth. In *Syn*B cultures, the proportion of highly unsaturated and phenolic compounds in culture *Syn*B was about 3–9% higher than that in culture *Syn* in both growth phases (**Figure 5**). It is possible that heterotrophic bacterial modifications play an important role in formation of highly unsaturated and phenolic compounds. The heterotrophic bacteria usually prefer to utilize the relatively well-used aliphatic compounds rather than highly unsaturated and phenolic compounds, during which part of aliphatic compounds were transformed into inorganic matters by respiration and the remaining may be modified to other components and retained in cultures (Jiao et al., 2010; Hach et al., 2020). So, the proportion of highly unsaturated and phenolic compounds was higher and that of aliphatic compounds lower in *Syn*B cultures, thus suggesting that heterotrophic bacteria modify the bioavailability of SOM by altering their molecular composition.

Overlap and difference of molecular formulas of SOM among different treatments are illustrated in **Supplementary Figure 4**: the similarities and differences among different growth phases or cultures without or with bacteria (**Supplementary Figure 4A**) and among different growth temperatures (**Supplementary Figure 4B**). Approximately two-thirds of molecular formulas of SOM in different cultures or growth phases were shared, and no unique part was observed, while they varied greatly with temperature changes. So, we pooled all the SOM at each temperature together and found the molecular formulas that were shared by three growth temperatures accounted for 54.56% (**Supplementary Figure 4B**), indicating these molecules were insensitive to temperature changes. The temperature-sensitive molecules accounted for 13.71, 9.78, and 3.59% at 15, 18, and 21°C, respectively, consistent with the result that the most identified molecular formulas presented at 15°C.

By further analyzing the O/C, H/C, AImod, and DBE of these unique molecular formulas, we found these molecular formulas tended to have higher H/C and lower O/C, AImod, and DBE values at higher temperatures (**Figure 6**). The averaged O/C values for specific molecules were 0.40, 0.39, and 0.36 at 15, 18, and 21°C, while the averaged H/C values were 1.21, 1.34, and 1.48, respectively. Such a decrease in O-containing compounds and increase in H-containing compounds suggested that the bioavailability of organic matters increased and became more well-used by heterotrophic bacteria with increasing temperature (Ohno et al., 2014; Qiao et al., 2020). Moreover, the lower aromaticity in formulas of specific molecules that was higher at higher temperatures (6.71 at 18°C, 6.37 at 21°C) than lower temperatures (8.30 at 15°C) also supported the bioavailability increased with increasing temperatures (Zheng et al., 2019). It was reported that cell membranes typically incorporate more unsaturated compounds at lower temperature, but more saturated substances at higher temperature (Hilditch, 1949; Jacobson et al., 1959). In this study, we confirmed that elevated temperature resulted in the more saturated SOM (**Figure 6D**).

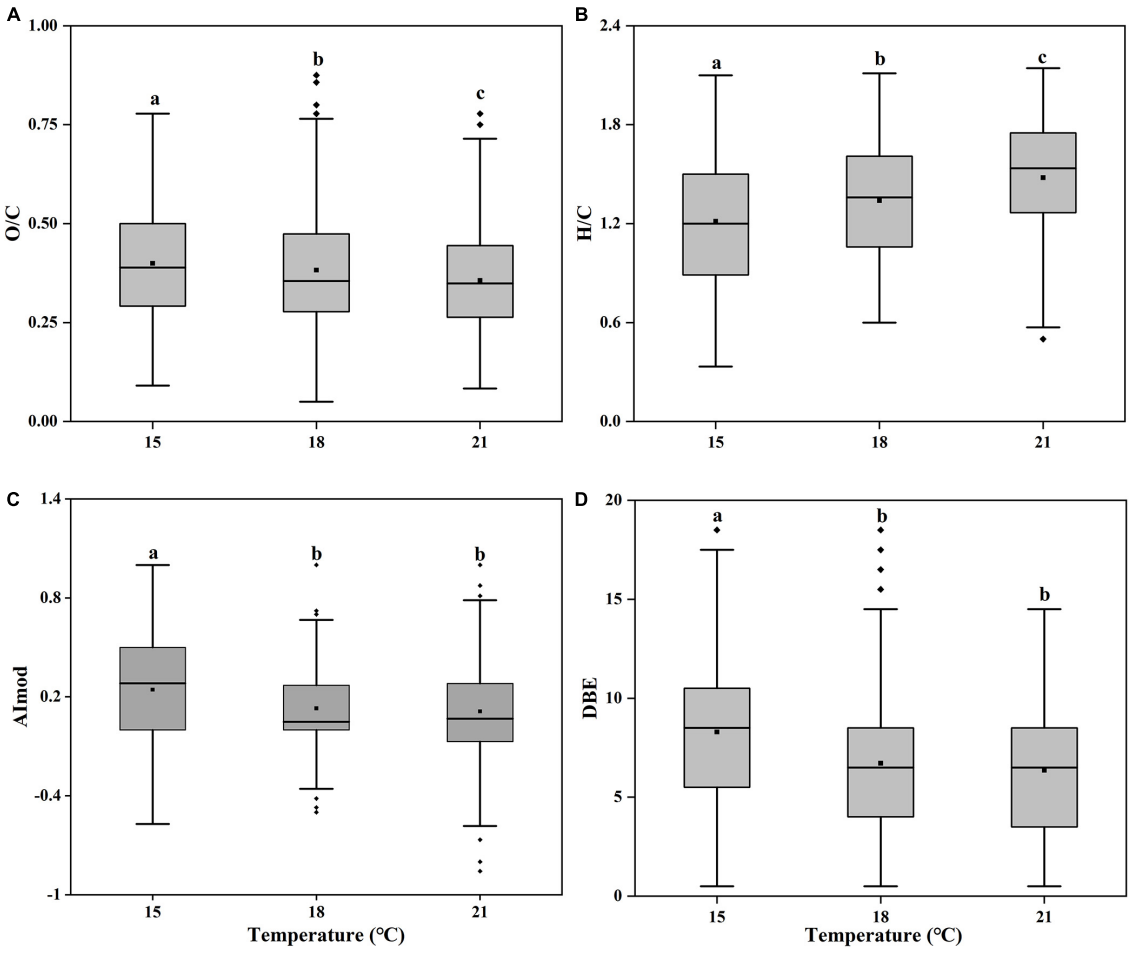


**FIGURE 6 |** Box plots of pooled oxygen to carbon ratio [**(A)**, O/C], hydrogen to carbon ratio [**(B)**, H/C], modified aromatic index [**(C)**, AImod] and double bond equivalents [**(D)**, DBE] of unique molecular formulas of the *Synechococcus*-derived dissolved organic matter (SOM) of *Synechococcus* sp. PCC7002 cultures without and with heterotrophic bacteria at both exponential and decay phases under temperatures of 15, 18, and 21°C. Bottom and top of the box correspond to 25th and 75th percentiles, and the line in box shows the median. Black squares represent the mean values. Vertical lines outside the box represent 10th and 90th percentiles, and filled diamonds denote the outliers. Different letters represent significant differences (paired *t*-test, $p < 0.05$).

The averaged DBE value decreased from 0.24 to 0.11 from 15 to 21°C. The low value of DBE represents the more saturated structure of molecules and could be considered as an indicative of the substances with high bioavailability (Koch and Dittmar, 2006). In general, SOM at elevated temperature were H-richer, with a higher aromaticity and relatively saturated (lower DBE value), indicating higher bioavailability.

## CONCLUSION

Heterotrophic bacteria are of great significance to the growth of marine *Synechococcus* (Zheng et al., 2017); therefore, there have been few studies focused on the SOM that is not modified by bacteria so far. Our study filled this gap and found that the bioavailability of SOM significantly increased with increasing temperatures. Furthermore, through analyzing photochemical properties and molecular compositions, we found the possible reasons for this bioavailability increase of SOM are as follows: (1) the increase of protein-like components; (2) the increase of relatively well-used aliphatic compounds; (3) the increase of hydrogen-containing molecules; and decrease of the unsaturation and aromaticity degrees. In addition, the heterotrophic bacterial processes and intracellular DOM release may decrease the bioavailability, but it did not change the increased trend of the SOM bioavailability with increasing temperatures. Considering the wide distribution of *Synechococcus* and its abundance increase with increasing temperature (Morán et al., 2010), our results gave a perspective that warming may enhance the bioavailability of certain SOM in global oceans.

## DATA AVAILABILITY STATEMENT

The original contributions presented in the study are included in the article/**Supplementary Material**, further inquiries can be directed to the corresponding author/s.

## AUTHOR CONTRIBUTIONS

JL and GL were in charge of experimental guidance and manuscript revision. JZ was in charge of cultivating experiments and manuscript writing. JZ and XC were in charge of data analysis. DL was in charge of maintenance of laboratory equipment and guidance of cultivating experiments. Molecular determination of the samples was performed by CH and QS. All authors designated in this manuscript contributed to the article and approved the submitted version.

## FUNDING

This work was supported by the National Key Research and Development Program of China (2018YFA0605800), the Key Research and Development Program of Shandong Province (2020ZLYS04), the Innovation Group Project of Southern Marine Science and Engineering Guangdong Laboratory (Zhuhai) (No. 311021006), and National Key Research and Development Program of China (2019YFA0606704).

## ACKNOWLEDGMENTS

We are very grateful to the two reviewers for their helpful comments and suggestions and would like to thank Yongle Xu for providing the marine *Synechococcus* sp. PCC7002.

## SUPPLEMENTARY MATERIAL

The Supplementary Material for this article can be found online at: https://www.frontiersin.org/articles/10.3389/fmicb.2022.838707/full#supplementary-material

## REFERENCES

Agustí, S., Satta, M. P., Mura, M. P., and Benavent, E. (1998). Dissolved esterase activity as a tracer of phytoplankton lysis: Evidence of high phytoplankton lysis rates in the northwestern Mediterranean. *Limnol. Oceanogr.* 43, 1836–1849. doi: 10.4319/LO.1998.43.8.1836

Amin, S. A., Green, D. H., Hart, M., Küpper, F. C., Sunda, W. G., and Carrano, C. J. (2009). Photolysis of iron–siderophore chelates promotes bacterial–algal mutualism. *Proc. Natl. Acad. Sci. U.S.A.* 106, 17071–17076. doi: 10.1073/pnas.0905512106

Andrew, A. A., Vecchio, R. D., Subramaniam, A., and Blough, N. V. (2013). Chromophoric dissolved organic matter (CDOM) in the Equatorial Atlantic Ocean: Optical properties and their relation to CDOM structure and source. *Mar. Chem.* 148, 33–43. doi: 10.1016/J.MARCHEM.2012.11.001

Bauersachs, T., Stal, L. J., Grego, M., and Schwark, L. (2014). Temperature induced changes in the heterocyst glycolipid composition of N2-fixing heterocystous cyanobacteria. *Org. Geochem.* 69, 98–105. doi: 10.1016/j.orggeochem.2014.02.006

Becker, J. W., Berube, P. M., Follett, C. L., Waterbury, J. B., Chisholm, S. W., Delong, E. F., et al. (2014). Closely related phytoplankton species produce similar suites of dissolved organic matter. *Front. Microbiol.* 5:111. doi: 10.3389/fmicb.2014.00111

Benner, R. (2011). Biosequestration of carbon by heterotrophic microorganisms. *Nat. Rev. Microbiol.* 9:75. doi: 10.1038/nrmicro2386-c3

Berggren, M., and Giorgio, P. A. (2015). Distinct patterns of microbial metabolism associated to riverine dissolved organic carbon of different source and quality. *J. Geophys. Res.* 120, 989–999. doi: 10.1002/2015JG002963

Bittar, T. B., Vieira, A. A. H., Stubbins, A., and Mopper, K. W. (2015). Competition between photochemical and biological degradation of dissolved organic matter from the cyanobacteria Microcystis aeruginosa. *Limnol. Oceanogr.* 60, 1172–1194. doi: 10.1002/LNO.10090

Bricaud, A., Morel, A., and Prieur, L. (1981). Absorption by dissolved organic matter of the sea (yellow substance) in the UV and visible domains1. *Limnol. Oceanogr.* 26, 43–53. doi: 10.4319/LO.1981.26.1.0043

Cheng, L., Abraham, J., Hausfather, Z., and Trenberth, K. E. (2019). How fast are the oceans warming? *Science* 363, 128–129. doi: 10.1126/science.aav7619

Coble, P. (1996). Characterization of marine and terrestrial DOM in seawater using excitation-emission matrix spectroscopy. *Mar. Chem.* 51, 325–346. doi: 10.1016/0304-4203(95)00062-3

Cory, R., and McKnight, D. (2005). Fluorescence spectroscopy reveals ubiquitous presence of oxidized and reduced quinones in dissolved organic matter. *Environ. Sci. Technol.* 39, 8142–8149. doi: 10.1021/ES0506962

Dufresne, A., Ostrowski, M., Scanlan, D., Garczarek, L., Mazard, S., Palenik, B., et al. (2008). Unraveling the genomic mosaic of a ubiquitous genus of marine cyanobacteria. *Genom. Biol.* 9, R90–R90. doi: 10.1186/gb-2008-9-5-r90

Fiore, C. L., Longnecker, K., Soule, M., and Kujawinski, E. B. (2015). Release of ecologically relevant metabolites by the cyanobacterium Synechococcus elongatusCCMP 1631. *Environ. Microbiol.* 17, 3949–3963. doi: 10.1111/1462-2920.12899

Flombaum, P., Gallegos, J. L., Gordillo, R. A., Rincón, J., and Martiny, A. C. (2013). Present and future global distributions of the marine Cyanobacteria Prochlorococcus and Synechococcus. *Proc. Natl. Acad. Sci. U.S.A* 110, 9824–9829. doi: 10.1073/pnas.1307701110

Fu, F., Warner, M. E., Zhang, Y., Feng, Y., and Hutchins, D. (2007). Effects of increased temperature and CO2 on photosynthesis, growth, and elemental ratios in marine Synechococcus and Prochlorococcus (cyanobacteria). *J. PHYCOL.* 43, 485–496. doi: 10.1111/j.1529-8817.2007.00355.x

Gleick, P. H., Adams, R. M., Amasino, R. M., Anders, E., Anderson, D. J., Anderson, W. W., et al. (2010). Climate change and the integrity of science. *Science* 328, 689–690. doi: 10.1126/science.328.5979.689

Gontikaki, E., Thornton, B., Huvenne, V. A. I., and Witte, U. (2013). Negative Priming Effect on Organic Matter Mineralisation in NE Atlantic Slope Sediments. *PLoS One* 8:e67722. doi: 10.1371/journal.pone.0067722

Guo, W., Yang, L., Hong, H., Stedmon, C. A., Wang, F., Xu, J., et al. (2011). Assessing the dynamics of chromophoric dissolved organic matter in a subtropical estuary using parallel factor analysis. *Mar. Chem.* 124, 125–133. doi: 10.1016/J.MARCHEM.2011.01.003

Hach, P. F., Marchant, H., Krupke, A., Riedel, T., Meier, D. V., Lavik, G., et al. (2020). Rapid microbial diversification of dissolved organic matter in oceanic surface waters leads to carbon sequestration. *Sci. Rep.* 10:13025. doi: 10.1038/s41598-020-69930-y

Harvey, B. P., Gwynn-Jones, D., and Moore, P. (2013). Meta-analysis reveals complex marine biological responses to the interactive effects of ocean acidification and warming. *Ecol. Evol.* 3, 1016–1030. doi: 10.1002/ece3.516

Hayashi, S., Itoh, K., and Suyama, K. (2011). Growth of the cyanobacterium Synechococcus leopoliensis CCAP1405/1 on agar media in the presence of heterotrophic bacteria. *Microb. Environ.* 26, 120–127. doi: 10.1264/JSME2.ME10193

He, C., Zhang, Y., Li, Y., Zhuo, X., Li, Y., Zhang, C., et al. (2020). In-House Standard Method for Molecular Characterization of Dissolved Organic Matter by FT-ICR Mass Spectrometry. *ACS Omega* 5, 11730–11736. doi: 10.1021/acsomega.0c01055

Helms, J. R., Stubbins, A., Ritchie, J., Minor, E., Kieber, D. J., and Mopper, K. (2008). Absorption spectral slopes and slope ratios as indicators of molecular weight, source, and photobleaching of chromophoric dissolved organic matter. *Limnol. Oceanogr.* 53, 955–969. doi: 10.4319/LO.2008.53.3.0955

Hilditch, T. P. (1949). The Chemical Constitution of Natural Fats. *Br. J. Nutr.* 3, 347–354. doi: 10.1079/BJN19490048

Huang, S., Wilhelm, S. W., Harvey, H. R., Taylor, K., Jiao, N., and Chen, F. (2011). Novel lineages of Prochlorococcus and Synechococcus in the global oceans. *ISME J.* 6:285. doi: 10.1038/ismej.2011.106

Huguet, A., Vacher, L., Relexans, S., Saubusse, S., Froidefond, J.-M., and Parlanti, É (2009). Properties of fluorescent dissolved organic matter in the Gironde Estuary. *Org. Geochem* 40, 706–719. doi: 10.1016/j.orggeochem.2009.03.002

Hygum, B. H., Petersen, J., and Søndergaard, M. (1997). Dissolved organic carbon released by zooplankton grazing activity - a high-quality substrate pool for bacteria. *J. Plankton Res.* 19, 97–111. doi: 10.1093/PLANKT/19.1.97

Jacobson, B. S., Jaworski, J. G., and Stumpf, P. K. (1959). Fat Metabolism in Higher Plants. *Plant Physiol.* 49, 497–501. doi: 10.1146/annurev.pp.10.060159.001213

Jiao, N., Herndl, G., Hansell, D. A., Benner, R., Kattner, G., Wilhelm, S., et al. (2010). Microbial production of recalcitrant dissolved organic matter: long-term carbon storage in the global ocean. *Nat. Rev. Microbiol.* 8, 593–599.

Jiao, N., Herndl, G. J., Hansell, D. A., Benner, R., Kattner, G., Wilhelm, S. W., et al. (2011). The microbial carbon pump and the oceanic recalcitrant dissolved organic matter pool. *Nat. Rev. Microbiol.* 9, 555–555. doi: 10.1038/nrmicro2386-c5

Kattsov, Z., Joussaume, S., Covey, C., McAvaney, B., Ogana, W., et al. (2001). *Climate Change 2001, the Scientific Basis, Chap. 8: Model Evaluation. Contribution of Working Group I to the Third Assessment Report of the Intergovernmental Panel on Climate Change IPCC*. Cambridge: Cambridge University Press

Kazamia, E., Czesnick, H., Nguyen, T. T. V., Croft, M., Sherwood, E., Sasso, S., et al. (2012). Mutualistic interactions between vitamin B12 -dependent algae and heterotrophic bacteria exhibit regulation. *Environ. Microbiol.* 14, 1466–1476. doi: 10.1111/j.1462-2920.2012.02733.x

Kellerman, A., Guillemette, F., Podgorski, D., Aiken, G., Butler, K., and Spencer, R. (2018). Unifying Concepts Linking Dissolved Organic Matter Composition to Persistence in Aquatic Ecosystems. *Environ. Sci. Technol.* 52, 2538–2548. doi: 10.1021/acs.est.7b05513

Koch, B., and Dittmar, T. (2006). From mass to structure: an aromaticity index for high resolution mass data of natural organic matter. *Rapid Commun. Mass Spectrom.* 20, 926–932. doi: 10.1002/RCM.2386

Koch, B., Kattner, G., Witt, M., and Passow, U. (2014). Molecular insights into the microbial formation of marine dissolved organic matter: recalcitrant or labile? *Biogeosciences* 11, 4173–4190. doi: 10.5194/BG-11-4173-2014

Lawaetz, A. J., and Stedmon, C. A. (2009). Fluorescence Intensity Calibration Using the Raman Scatter Peak of Water. *Appl. Spectrosc.* 63, 936–940. doi: 10.1366/000370209788964548

Levitus, S., Antonov, J., and Boyer, T. (2005). Warming of the world ocean, 1955–2003. *Geophys. Res. Lett.* 32:L02604. doi: 10.1029/2004GL021592

Liu, Y., Kan, J., He, C., Shi, Q., Liu, Y.-X., Fan, Z.-C., et al. (2021). Epiphytic Bacteria Are Essential for the Production and Transformation of Algae-Derived Carboxyl-Rich Alicyclic Molecule (CRAM)-like DOM. *Microbiol. Spectr.* 9:e0153121. doi: 10.1128/Spectrum.01531-21

López Sandoval, D. C., Rodríguez-Ramos, T., Cermeño, P., and Marañón, E. (2013). Exudation of organic carbon by marine phytoplankton: Dependence on taxon and cell size. *Mar. Ecol. Prog. Ser.* 477, 53–60. doi: 10.3354/MEPS10174

Ludwig, M., and Bryant, D. A. (2011). Transcription Profiling of the Model Cyanobacterium Synechococcus sp. Strain PCC 7002 by Next-Gen (SOLiD) Sequencing of cDNA. *Front. Microbiol.* 2:41. doi: 10.3389/fmicb.2011.00041

Mackey, K., Post, A. F., McIlvin, M. R., and Saito, M. A. (2017). Physiological and proteomic characterization of light adaptations in marine Synechococcus. *Environ. Microbiol.* 19, 2348–2365. doi: 10.1111/1462-2920.13744

Malits, A., Boras, J. A., Balagué, V., Calvo, E., Gasol, J. M., Marrasè, C., et al. (2021). Viral-Mediated Microbe Mortality Modulated by Ocean Acidification and Eutrophication: Consequences for the Carbon Fluxes Through the Microbial Food Web. *Front. Microbiol.* 12:635821. doi: 10.3389/fmicb.2021.635821

Marañón, E., Cermeño, P., Fernández, E., Rodríguez, J., and Zabala, L. (2004). Significance and mechanisms of photosynthetic production of dissolved organic carbon in a coastal eutrophic ecosystem. *Limnol. Oceanogr.* 49, 1652–1666. doi: 10.4319/LO.2004.49.5.1652

Martínez-Pérez, A. M., Osterholz, H., Nieto-Cid, M., Álvarez, M., Dittmar, T., and Álvarez-Salgado, X. A. (2017). Molecular composition of dissolved organic matter in the Mediterranean Sea. *Limnol. Oceanogr.* 62, 2699–2712. doi: 10.1002/LNO.10600

Møller, E. F., Thor, P., and Nielsen, T. G. (2003). Production of DOC by Calanus finmarchicus, C-glacialis and C-hyperboreus through sloppy feeding and leakage from fecal pellets. *Mar. Ecol. Prog. Ser.* 262, 185–191. doi: 10.3354/MEPS262185

Morán, X., Lopez-Urrutia, A., Calvo-Díaz, A., and Li, W. K. W. (2010). Increasing importance of small phytoplankton in a warmer ocean. *Glob. Chang. Biol.* 16, 1137–1144. doi: 10.1111/J.1365-2486.2009.01960.X

Mou, S., Li, G., Li, H., Li, F., Shao, Z., Li, J., et al. (2018). Differential physiological responses of the coastal cyanobacterium Synechococcus sp. PCC7002 to elevated pCO2 at lag, exponential, and stationary growth phases. *Sci. China Earth Sci.* 61, 1397–1405. doi: 10.1007/s11430-017-9206-5

Mou, S., Zhang, Y., Li, G., Li, H., Liang, Y., Tang, L., et al. (2017). Effects of elevated CO2 and nitrogen supply on the growth and photosynthetic physiology of a marine cyanobacterium, Synechococcus sp. PCC7002. *J. Appl. Psychol.* 29, 1755–1763. doi: 10.1007/s10811-017-1089-3

Murphy, K. R., Stedmon, C. A., Graeber, D., and Bro, R. (2013). Fluorescence spectroscopy and multi-way techniques. *PARAFAC. Anal. Methods* 5, 6557–6566. doi: 10.1039/C3AY41160E

Murphy, K. R., Stedmon, C. A., Waite, T. D., and Ruiz, G. M. (2008). Distinguishing between terrestrial and autochthonous organic matter sources in marine environments using fluorescence spectroscopy. *Mar. Chem.* 108, 40–58. doi: 10.1016/j.marchem.2007.10.003

Myklestad, S. M., and Swift, E. (1998). A new method for measuring soluble cellular organic content and a membrane property. *Tm, of planktonic algae. Eur. J. Phycol.* 33, 333–336. doi: 10.1080/09670269810001736823

Nalley, J. O., O'Donnell, D. R., and Litchman, E. (2018). Temperature effects on growth rates and fatty acid content in freshwater algae and cyanobacteria. *Algal. Res.* 35, 500–507. doi: 10.1016/j.algal.2018.09.018

Nvdv, R. B. (2002). *Chromophoric DOM in the Coastal Environment*. San Diego, CA: Academic Press.

Ogawa, H., Amagai, Y., Koike, I., Kaiser, K., and Benner, R. (2001). Production of Refractory Dissolved Organic Matter by Bacteria. *Science* 292, 917–920. doi: 10.1126/science.1057627

Ohno, T., Parr, T. B., Gruselle, M. C. I., Fernandez, I. J., Sleighter, R. L., and Hatcher, P. G. (2014). Molecular Composition and Biodegradability of Soil Organic Matter: A Case Study Comparing Two New England Forest Types. *Environ. Sci. Technol.* 48, 7229–7236. doi: 10.1021/es405570c

Ohno, and Tsutomu. (2002). Fluorescence inner-filtering correction for determining the humification index of dissolved organic matter. *Environ. Sci. Technol.* 36, 742–746. doi: 10.1021/ES015527

Paerl, H., and Huisman, J. (2008). Blooms Like It Hot. *Science* 320, 57–58. doi: 10.1126/science.1155398

Paul, A., Sommer, U., Paul, C., and Riebesell, U. (2018). Baltic Sea diazotrophic cyanobacterium is negatively affected by acidification and warming. *Mar. Ecol. Prog. Ser.* 598, 49–60. doi: 10.3354/meps12632

Qiao, W., Guo, H., He, C., Shi, Q., and Zhao, B. (2020). Unraveling roles of dissolved organic matter in high arsenic groundwater based on molecular and optical signatures. *J. Hazard. Mater.* 406:124702. doi: 10.1016/j.jhazmat.2020.124702

Sarmento, H., Morana, C., and Gasol, J. M. (2016). Bacterioplankton niche partitioning in the use of phytoplankton-derived dissolved organic carbon: quantity is more important than quality. *ISME J.* 10, 2582–2592. doi: 10.1038/ismej.2016.66

Segschneider, J., and Bendtsen, J. (2013). Temperature dependent remineralization in a warming ocean increases surface pCO2 through changes in marine ecosystem composition. *Glob. Biogeochem. Cycl.* 27, 1214–1225. doi: 10.1002/2013GB004684

Seidel, M., Beck, M., Riedel, T., Waska, H., Suryaputra, I., Schnetger, B., et al. (2014). Biogeochemistry of dissolved organic matter in an anoxic intertidal creek bank. *Geochim. Cosmochim. Acta.* 140, 418–434. doi: 10.1016/J.GCA.2014.05.038

Seidel, M., Yager, P. L., Ward, N. F. D., Carpenter, E. J., Gomes, H.d.R, Krusche, A. V., et al. (2015). Molecular-level changes of dissolved organic matter along the Amazon River-to-ocean continuum. *Mar. Chem.* 177, 218–231. doi: 10.1016/j.marchem.2015.06.019

Senesi, N. (1990). Molecular and quantitative aspects of the chemistry of fulvic acid and its interactions with metal ions and organic chemicals : Part II. The fluorescence spectroscopy approach. *Anal. Chim. Acta* 232, 77–106. doi: 10.1016/S0003-267081226-X

Senesi, N., Miano, T., Provenzano, M. R., and Brunetti, G. (1991). Characterization, differentiation and classification of humic substances by fluorescence spectroscopy. *Soil Sci.* 152:271. doi: 10.1097/00010694-199110000-00004

Stedmon, C., Markager, S., and Bro, R. (2003). Tracing dissolved organic matter in aquatic environments using a new approach to fluorescence spectroscopy. *Mar. Chem.* 82, 239–254. doi: 10.1073/pnas.77.10.6052

Stedmon, C. A., and Markager, S. (2005a). Resolving the variability in dissolved organic matter fluorescence in a temperate estuary and its catchment using PARAFAC analysis. *Limnol. Oceanogr.* 50, 686–697. doi: 10.4319/LO.2005.50.2.0686

Stedmon, C. A., and Markager, S. (2005b). Tracing the production and degradation of autochthonous fractions of dissolved organic matter by fluorescence analysis. *Limnol. Oceanogr.* 50, 1415–1426. doi: 10.4319/LO.2005.50.5.1415

Stevens, S. E., and Porter, R. D. (1980). Transformation in Agmenellum quadruplicatum. *Proc. Natl. Acad. Sci. U.S.A.* 77, 6052–6056. doi: 10.1073/pnas.77.10.6052

Thompson, G. A. (1996). Lipids and membrane function in green algae. *Biochim. Biophys. Acta.* 1302, 17–45. doi: 10.1016/0005-2760(96)00045-8

Walls, J. T., Wyatt, K. H., Doll, J. C., Rubenstein, E. M., and Rober, A. R. (2018). Hot and toxic: Temperature regulates microcystin release from cyanobacteria. *Environ. Sci. Technol.* 61, 786–795. doi: 10.1016/j.scitotenv.2017.08.149

Xiao, X., Guo, W., Li, X., Wang, C., and Zhang, R. (2020). Viral lysis alters the optical properties and biological availability of dissolved organic matter derived from picocyanobacteria Prochlorococcus. *Appl. Environ. Microbiol.* 87:e02271-20. doi: 10.1128/AEM.02271-20

Yamashita, Y., Cory, R. M., Nishioka, J., Kuma, K., Tanoue, E., and Jaffé, R. (2010). Fluorescence characteristics of dissolved organic matter in the deep waters of the Okhotsk Sea and the northwestern North Pacific Ocean. *Deep Sea Res. Part II Top. Stud. Oceanogr.* 57, 1478–1485. doi: 10.1016/J.DSR2.2010.02.016

Yamashita, Y., Jaffeé, R., Maie, N., and Tanoue, E. (2008). Assessing the dynamics of dissolved organic matter (DOM) in coastal environments by excitation emission matrix fluorescence and parallel factor analysis (EEM-PARAFAC). *Limnol. Oceanogr.* 53, 1900–1908. doi: 10.4319/LO.2008.53.5.1900

Yang, X., Yuan, J., Yue, F., Li, S. L., Wang, B., Mohinuzzaman, M., et al. (2020). New insights into mechanisms of sunlight- and dark-mediated high-temperature accelerated diurnal production-degradation of fluorescent DOM in lake waters. *Environ. Sci. Technol.* 760:143377. doi: 10.1016/j.scitotenv.2020.143377

Yu, H., Liang, H., Qu, F., Han, Z.-s, Shao, S., Chang, H., et al. (2015). Impact of dataset diversity on accuracy and sensitivity of parallel factor analysis model of dissolved organic matter fluorescence excitation-emission matrix. *Sci. Rep.* 5:10207. doi: 10.1038/srep10207

Yuan, Z., He, C., Shi, Q., Xu, C., Li, Z., Wang, C., et al. (2017). Molecular Insights into the Transformation of Dissolved Organic Matter in Landfill Leachate Concentrate during Biodegradation and Coagulation Processes Using ESI FT-ICR MS. *Environ. Sci. Technol.* 51, 8110–8118. doi: 10.1021/acs.est.7b02194

Zark, M., and Dittmar, T. (2018). Universal molecular structures in natural dissolved organic matter. *Nat. Commun.* 9:3178. doi: 10.1038/s41467-018-05665-9

Zhang, T., and Wang, X. (2017). Release and microbial degradation of dissolved organic matter (DOM) from the macroalgae Ulva prolifera. *Mar. Pollut. Bull.* 125, 192–198. doi: 10.1016/j.marpolbul.2017.08.029

Zhang, Y., van Dijk, M. A., Liu, M., Zhu, G., and Qin, B. (2009). The contribution of phytoplankton degradation to chromophoric dissolved organic matter (CDOM) in eutrophic shallow lakes: field and experimental evidence. *Water Res.* 43, 4685–4697. doi: 10.1016/j.watres.2009.07.024

Zhang, Z., Nair, S., Tang, L., Zhao, H., Hu, Z., Chen, M., et al. (2021). Long-Term Survival of Synechococcus and Heterotrophic Bacteria without External Nutrient Supply after Changes in Their Relationship from Antagonism to Mutualism. *mBio* 12:e0161421. doi: 10.1128/mBio.01614-21

Zhao, Z., Gonsior, M., Luek, J., Timko, S., Ianiri, H., Hertkorn, N., et al. (2017). Picocyanobacteria and deep-ocean fluorescent dissolved organic matter share similar optical properties. *Nat. Commun.* 8:15284. doi: 10.1038/ncomms15284

Zheng, Q., Chen, Q., Cai, R., He, C., Guo, W., Wang, Y., et al. (2019). Molecular characteristics of microbially mediated transformations of Synechococcus-derived dissolved organic matter as revealed by incubation experiments. *Environ. Microbiol.* 21(7), 2533-2543. doi: 10.1111/1462-2920.14646

Zheng, Q., Lin, W., Wang, Y., Li, Y., He, C., Shen, Y., et al. (2020). Highly enriched N containing organic molecules of Synechococcus lysates and their rapid transformation by heterotrophic bacteria. *Limnol. Oceanogr.* 66, 335–348. doi: 10.1002/LNO.11608

Zheng, Q., Wan, Y., Xie, R., Lan, A. S., Liu, Y., Lu, J., et al. (2017). Dynamics of Heterotrophic Bacterial Assemblages within Synechococcus Cultures. *Appl. Environ. Microbiol.* 84(3), e01517-17. doi: 10.1128/AEM.01517-17

Zhou, L., Zhou, Y., Tang, X., Zhang, Y., Jang, K. S., Székely, A. J., et al. (2020). Resource aromaticity affects bacterial community successions in response to different sources of dissolved organic matter. *Water Res.* 190:116776. doi: 10.1016/j.watres.2020.116776

**Conflict of Interest:** The authors declare that the research was conducted in the absence of any commercial or financial relationships that could be construed as a potential conflict of interest.

**Publisher's Note:** All claims expressed in this article are solely those of the authors and do not necessarily represent those of their affiliated organizations, or those of the publisher, the editors and the reviewers. Any product that may be evaluated in this article, or claim that may be made by its manufacturer, is not guaranteed or endorsed by the publisher.

frontiers | Frontiers in Microbiology

ORIGINAL RESEARCH
published: 18 May 2022
doi: 10.3389/fmicb.2022.838629

# A Competitive Advantage of Middle-Sized Diatoms From Increasing Seawater $CO_2$

*Qi Zhang*† *and Ya-Wei Luo**

*State Key Laboratory of Marine Environmental Science, College of Ocean and Earth Sciences, Xiamen University, Xiamen, China*

Diatoms, one of the most important phytoplankton groups, fulfill their carbon demand from seawater mainly by obtaining passively diffused carbon dioxide ($CO_2$) and/or actively consuming intracellular energy to acquire bicarbonate ($HCO_3^-$). An anthropogenically induced increase in seawater $CO_2$ reduces the $HCO_3^-$ requirement of diatoms, potentially saving intracellular energy and benefitting their growth. This effect is commonly speculated to be most remarkable in larger diatoms that are subject to a stronger limitation of $CO_2$ supply because of their smaller surface-to-volume ratios. However, we constructed a theoretical model for diatoms and revealed a unimodal relationship between the simulated growth rate response (GRR, the ratio of growth rates under elevated and ambient $CO_2$) and cell size, with the GRR peaking at a cell diameter of ~7 μm. The simulated GRR of the smallest diatoms was low because the $CO_2$ supply was nearly sufficient at the ambient level, while the decline of GRR from a cell diameter of 7 μm was simulated because the contribution of seawater $CO_2$ to the total carbon demand greatly decreased and diatoms became less sensitive to $CO_2$ increase. A collection of historical data in $CO_2$ enrichment experiments of diatoms also showed a roughly unimodal relationship between maximal GRR and cell size. Our model further revealed that the "optimal" cell size corresponding to peak GRR enlarged with the magnitude of $CO_2$ increase but diminished with elevating cellular carbon demand, leading to projection of the smallest optimal cell size in the equatorial Pacific upwelling zone. Last, we need to emphasize that the size-dependent effects of increasing $CO_2$ on diatoms are multifaceted, while our model only considers the inorganic carbon supply from seawater and optimal allocation of intracellular energy. Our study proposes a competitive advantage of middle-sized diatoms and can be useful in projecting changes in the diatom community in the future acidified high-$CO_2$ ocean.

**Keywords: ocean acidification, diatom, $CO_2$-concentrating mechanism, growth rate response, cell size, eco-physiological modeling**

OPEN ACCESS

***Edited by:***
*Jun Sun,*
*China University of Geosciences Wuhan, China*

***Reviewed by:***
*Kam W. Tang,*
*Swansea University, United Kingdom*
*Jin Zhou,*
*Tsinghua University, China*
*Alex J. Poulton,*
*Heriot-Watt University, United Kingdom*

***Correspondence:**
*Ya-Wei Luo*
*ywluo@xmu.edu.cn*

†***Present address:***
*Qi Zhang*
*Earth and Atmospheric Sciences, Georgia Institute of Technology, Atlanta, GA, USA*

***Specialty section:***
*This article was submitted to Aquatic Microbiology, a section of the journal Frontiers in Microbiology*

***Received:*** *18 December 2021*
***Accepted:*** *12 April 2022*
***Published:*** *18 May 2022*

***Citation:***
*Zhang Q and Luo Y-W (2022) A Competitive Advantage of Middle-Sized Diatoms From Increasing Seawater $CO_2$. Front. Microbiol. 13:838629. doi: 10.3389/fmicb.2022.838629*

## INTRODUCTION

Diatoms are one of the most important marine phytoplankton groups. They contribute 40% of primary production (e.g., Nelson et al., 1995; Tréguer and De La Rocha, 2013) and are one of the major contributors to organic carbon export in the global ocean (Buesseler, 1998; Jin et al., 2006). Marine diatoms fix carbon dioxide ($CO_2$) into organic carbon through photosynthesis, which

is catalyzed by ribulose-1,5-bisphosphate carboxylase/oxygenase (RuBisCO) in the Calvin cycle. However, RuBisCO has a low affinity for $CO_2$, and its carboxylation is inefficient in fixing $CO_2$ due to photorespiration unless its surrounding $CO_2$ concentration is sufficiently high (Reiskind et al., 1989; Badger et al., 1998; Reinfelder, 2011). Meanwhile, due to the slow diffusion of $CO_2$ in aqueous environments (10,000 times slower than that in air) and sluggish dehydration of bicarbonate ($HCO_3^-$) to $CO_2$ (Wolf-Gladrow and Riebesell, 1997; Reinfelder, 2011), the $CO_2$ concentration in contemporary surface oceans (~10–30 μM) often limits the growth of diatoms (Reinfelder, 2011; Wu et al., 2014). Diatoms therefore use a series of processes termed the $CO_2$-concentrating mechanism (CCM) to achieve high $CO_2$ concentrations near RuBisCO at the cost of metabolic energy that is otherwise available for growth (Giordano et al., 2005; Raven et al., 2008; Hopkinson et al., 2011). As one of the key processes of CCM, many diatoms evolve to consume energy to acquire $HCO_3^-$, which is then catalyzed by carbonic anhydrase (CA) and converted to $CO_2$ to maintain a high $CO_2$ concentration near RuBisCO, leading to a high leakage of $CO_2$ into seawater (Burkhardt et al., 2001; Cassar et al., 2002; Reinfelder, 2011). Some diatoms can also actively release extracellular CA (eCA) to catalyze the conversion of $HCO_3^-$ to $CO_2$ in seawater (Martin and Tortell, 2008; Tortell et al., 2008; Chrachri et al., 2018).

The ocean absorbs approximately 26% of anthropogenic $CO_2$ emissions (Friedlingstein et al., 2019), causing a significant increase in $CO_2$ concentrations and a decrease in pH in seawater, collectively termed ocean acidification (Orr et al., 2005). It influences marine ecosystems with wide-ranging impacts, such as community structure, diversity, and carbon export (Sabine et al., 2004; Doney, 2009; Feng et al., 2009; Finkel et al., 2009; Endo et al., 2013; Mouw et al., 2016; Deppeler et al., 2018; Doney et al., 2020). The increasing $CO_2$ concentration in surface seawater, predicted to double within this century under business-as-usual scenarios (Lerman et al., 2011), will mitigate $CO_2$ limitation on phytoplankton and downregulate CCM to save intracellular energy and potentially enhance cell growth (Taylor et al., 2012; McMinn et al., 2014; Cyronak et al., 2016; Biswas et al., 2017; Gafar et al., 2018). This stimulation has been observed in $CO_2$ enrichment experiments of diatoms when they were cultured under favorable nutrient and light conditions (e.g., Kroeker et al., 2013; Wu et al., 2014).

Diatoms vary greatly in cell size, from a minimal reported dimension $< 1$ μm to a maximal reported dimension of $>5{,}000$ μm in a global marine diatom database (Leblanc et al., 2012a,b). However, large diatoms are usually less abundant in the community, mainly because of their decreasing growth rates with cell size (Mizuno, 1991; Sarthou et al., 2005). For example, in 515 diatom species sampled along the Swedish coast and the Gulf of Finland, those with a cell volume larger than 1,000 $\mu m^3$, an equivalent spherical diameter equivalent (ESD) of 12 μm, accounted for only approximately half (57%) of the total species (Snoeijs et al., 2002). In this study, we followed that study and define the "large" diatoms by ESD of larger than 12 μm. We further defined the "small" and "middle-sized" diatoms by ESD of $< 5$ μm and 5–12 μm, respectively.

The relationship between diatom cell size and the degree of their growth rate response (GRR), defined here as the ratio of the growth rates under elevated and ambient $CO_2$ concentrations, remains unclear. If $CO_2$ was the only carbon source for diatoms, their GRR would increase with cell size because larger cells have smaller surface-to-volume ratios and are limited more severely by $CO_2$ supply (Wirtz, 2011). However, $HCO_3^-$ is the secondary carbon source of diatoms, and its concentration in seawater ($\sim 10^3$ μM) is 2 orders of magnitude higher than that of $CO_2$. It is worth further evaluating how diatoms respond differently to increasing $CO_2$ when they also acquire substantial amounts of $HCO_3^-$.

Although the increase in GRR with cell size has been shown in a $CO_2$ enrichment experiment of diatoms (Wu et al., 2014), the interpretation of the results can be complex, such as the high light intensity of 350 μmol photons/$m^2$/s used in that experiment. Indeed, high light can inhibit the photosynthesis of diatoms, which can be exacerbated when cells grow in acidified, high-$CO_2$ environments. For example, the effect of increasing $CO_2$ on the growth of three diatom species shifted from positive to negative when the incubation light increased from 150 to 250 μmol photons/$m^2$/s (Gao et al., 2012). It is therefore possible that the higher GRR seen in larger diatoms in Wu et al. (2014) can be partly a result that larger cells were less susceptible to the inhibition of high light (Key et al., 2010) instead of a sole effect of mitigated $CO_2$ limitation.

In this study, we constructed a theoretical model to simulate the GRR as a function of cell size and magnitude of seawater $CO_2$ increase. The model calculated the $CO_2$ supply rate to diatom cells as a result of physical diffusion and carbonate equilibrium in seawater, represented $CO_2$ leakage from cells, and solved an optimal energy allocation between $HCO_3^-$ acquisition and biomass synthesis. The model results were compared to historical data from diatom $CO_2$ enrichment experiments. We also evaluated the robustness of our model and further explored the underlying mechanisms by performing a series of model sensitivity experiments. We finally applied our model to the global ocean under a $CO_2$ release scenario (Representative Concentration Pathway RCP 8.5), illuminating possible spatial variations in the cell size–dependent responses of diatom growth.

# MATERIALS AND METHODS

## Model Overview

We constructed a model of a spherical diatom cell to quantify its acquisition rates of $CO_2$ and/or $HCO_3^-$ and to solve for the optimal allocation of metabolic energy between $HCO_3^-$ uptake and biomass synthesis (i.e., growth) over a day (**Figure 1**). Given cell radius $R$ (μm) and $CO_2$ concentration in bulk water $[CO_2]_{bulk}$ (μM), the model simulates a daily growth rate $g$ /day:

$$g = f(R, [CO_2]_{bulk}) \quad (1)$$

Note that although the model uses the cell radius to simplify calculations, the results are conventionally reported using the cell diameter.

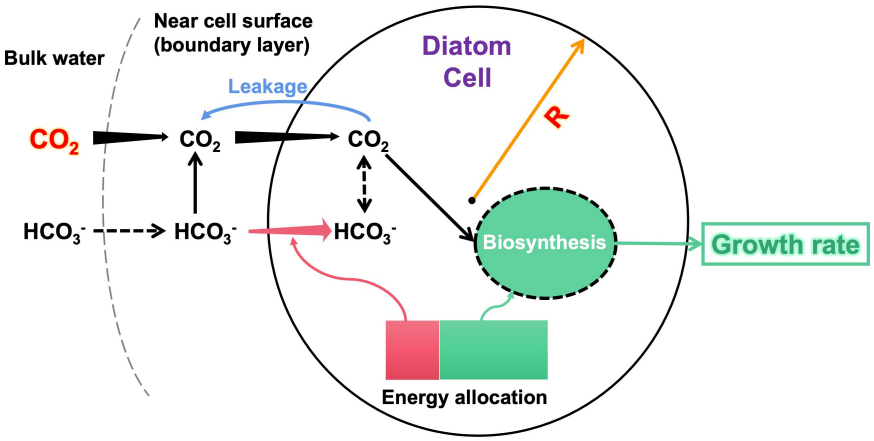


**FIGURE 1 |** Illumination of the model structure. The input variables of the model are diatom cell radius R and bulk-water $CO_2$ concentration. The model estimates the $CO_2$ supply (black arrows) to the cell considering both $CO_2$ diffusion and $HCO_3^-$ dehydration near the cell surface, energy-consuming $HCO_3^-$ transport (pink arrows), and $CO_2$ leakage (blue arrow) across cell membranes. The model finally calculates an optimal allocation of metabolic energy between $HCO_3^-$ acquisition and biomass synthesis, which derives the growth rate as the model output. An arrow with increasing (decreasing) width along the direction represents that the flux increases (decreases) with the cell radius. The dashed arrows are not explicitly simulated by the model. More details of the model are described in the text.

The model first calculates the cell-specific acquisition rate of $CO_2$ under given $R$ and $[CO_2]_{bulk}$. The model then counted the $CO_2$ leakage from the cell. The model reaches a maximal growth rate if the net acquisition of $CO_2$ is sufficient; otherwise, it lowers the growth rate to save metabolic energy for actively acquiring $HCO_3^-$ as a carbon complement. The lowered growth also reduces the total carbon demand, partly relieving the requirement for $HCO_3^-$. Note that we set a minimum $HCO_3^-$ acquisition at 20% of the total carbon demand even if the $CO_2$ supply is sufficient, reflecting findings that even very small diatoms also take $HCO_3^-$ (e.g., Burkhardt et al., 2001; Shi et al., 2019). Therefore, there exists a solution for the modeled growth rate at which cellular energy is optimally allocated between $HCO_3^-$ acquisition and growth.

The parameter values of the model (**Supplementary Table 1**) were set up based on the literature as described below. Our model only represents fundamental metabolic processes of cell growth and focuses on the responses of diatom growth to increasing $CO_2$, particularly the dynamics of $HCO_3^-$ acquisition as the secondary inorganic carbon source, while ignoring other complex physiological processes.

## Model Scheme of the $CO_2$ Supply

Our model scheme of the $CO_2$ supply rate to the cell ($F_T$, μmol/cell/day) is established by improving those of previous studies (Gavis and Ferguson, 1975; Wolf-Gladrow and Riebesell, 1997; Reinfelder, 2011) in which both $CO_2$ diffusion and $CO_2$ dehydrated from $HCO_3^-$ near the cell surface are included

$$F_T = 3.456 \times 10^{-10} \cdot \pi DR \left(1 + R\sqrt{\frac{k'}{D}}\right) \left([CO_2]_{bulk} - [CO_2]_{sfc}\right) \quad (2)$$

where $3.456 \times 10^{-10} = 4 \times 10^{-15}$ L · μm$^{-3}$ × 86,400 s/day, in which the constant of 4 is from the original equation (Gavis and Ferguson, 1975), $10^{-15}$ is the factor to convert μm$^3$ to L for consistency with the unit used in $CO_2$ concentrations, and 86,400 is the factor to convert day to second; $D$ (μm$^2$/s) is the diffusivity of $CO_2$ in water $k'$ (s$^{-1}$) is a combined rate constant for the hydration of $CO_2$ with $H_2O$ and $OH^-$, with its value estimated at 15°C, pH of 8.1 and salinity of 35 PSU (**Supplementary Table 1**; Wolf-Gladrow and Riebesell, 1997; Reinfelder, 2011), and $[CO_2]_{sfc}$ (μM = μmol L$^{-1}$) is the seawater $CO_2$ concentration near the cell surface. Although $[CO_2]_{sfc}$ can be effectively eliminated from the equation by assuming that it was 1/3 of $[CO_2]_{bulk}$, as done in a previous study (Reinfelder, 2011), $[CO_2]_{sfc}$ is likely to decline with increasing cell size (Flynn et al., 2012). In this study, we further solve $[CO_2]_{sfc}$ by assuming a balance between $CO_2$ supply to the cell surface ($F_T$) and $CO_2$ permeation across the cell membrane ($F_P$, μmol/cell/day):

$$F_T = F_P = 3.456 \times 10^{-10} \cdot \pi R^2 P \Delta_{CO2} [CO_2]_{sfc} \quad (3)$$

where $P$ (μm/s) is the $CO_2$ permeability coefficient of the cell membrane, $\Delta_{CO2}$ = 10% is the relative reduction in $CO_2$ concentration from near the cell surface to the cytoplasm (Hopkinson et al., 2016), that is, $\Delta_{CO2}[CO_2]_{sfc}$ is the difference in $CO_2$ concentration between the two sides of the cell membrane, and $3.456 \times 10^{-10} = 4 \times 10^{-15}$ L · μm$^{-3}$ × 86,400 s/day. From Eqs. 2 and 3, $[CO_2]_{sfc}$ can be solved as a function of input variables $R$ and $[CO_2]_{bulk}$:

$$[CO_2]_{sfc} = \frac{D'[CO_2]_{bulk}}{RP\Delta_{CO2} + D'} \quad (4)$$

where $D' = D \cdot (1 + R\sqrt{k'/D})$. This equation generates a declining $[CO_2]_{sfc}$ with increasing cell size, as expected (**Supplementary Figure 1**). $F_T$ can then be obtained by substituting Eq. 2 into either Eq. 3 or Eq. 4.

This scheme introduces a new parameter $P$, for which the maximal value of 560 μm/s found in experiments of several diatom species (Hopkinson et al., 2011) is used in the model (**Supplementary Table 1**). The assumption of $F_T = F_P$ used in the scheme (Eq. 3) implies that $CO_2$ supplied to the cell surface is completely acquired by the cell, and the $CO_2$ supply rate is solved at its maximal potential, which we annotate as $F_{T,max}$.

## Model Scheme of Energy Constraint

The energetic cost of growth is estimated by adding the theoretical requirements of ATP when synthesizing particulate organic carbon (POC) from $CO_2$ [3 mol ATP (mol C) $^{-1}$] (Raven, 1991) and synthesizing particulate organic nitrogen (PON) from nitrate [2 mol ATP (mol N) $^{-1}$] (Eichner et al., 2014), which is equivalent to ∼ 0.30 ATP (mol C) $^{-1}$ by using a Redfieldian molar C:N ratio of 106:16. By further assuming small additional energy of 0.2 mol ATP (mol C) $^{-1}$ used in other cellular processes, the energy cost rate for growth, $e_g$, is set at 3.5 ATP (mol C) $^{-1}$ (**Supplementary Table 1**).

The intracellular energy production rate $E_0$ [ATP/mol C/day] is set at:

$$E_0 = g_0 \cdot e_g \tag{5}$$

where the maximal daily average growth rate $g_0$ = 3.0/day represents those maximal rates found in previous experiments culturing diatoms under saturating light and nutrients (Sarthou et al., 2005). The instantaneous maximal growth rate (and consequently, $E_0$) is further set to vary in a 12:12 h light–dark cycle in which the rate peaks for 6 h around noon to represent light saturation, while its daily average is kept at $g_0$ (**Supplementary Figure 2**). This setup can improve the model performance to mimic the diel variation of inorganic carbon demand. For example, a model cell that would have sufficient $CO_2$ supply, should its maximal growth rate be set constant at $g_0$, may become, after implementing the diel cycle, $CO_2$-limiting and have to acquire $HCO_3^-$ around noon when the instantaneous maximal growth rate is 8/3 times higher than $g_0$ (**Supplementary Figure 2**).

ATP expenditure by CCM is generally high in diatoms (Raven, 1991), which may be partially satisfied by the Mehler reaction (Behrenfeld et al., 2008). The energy cost for diatoms to transport 1 $HCO_3^-$ molecule has been estimated at 0.5 ATP to cross the cytoplasmic membrane (Liu et al., 2017) and 1 ATP to cross the chloroplast membrane to reach pyrenoids (Raven et al., 2000). Therefore, we set the energy cost rate for $HCO_3^-$ acquisition, $e_{bc}$, at 1.5 ATP (mol C) $^{-1}$ (**Supplementary Table 1**).

## Model Scheme of Growth Rate

The net inorganic carbon acquisition rate $F$ (μmol/cell/day) is

$$F = (F_T + F_{bc}) \cdot (1 - l_k) \tag{6}$$

where $F_{bc}$ (μmol/cell/day) is the $HCO_3^-$ acquisition rate, and $l_k$ = 30% is the fraction of acquired carbon leaking from the cell based on a previously reported $CO_2$ efflux for diatoms (Burkhardt et al., 2001). Note that the leakage in the model does not count the exudation, which, however, could be small (∼5% of primary production) in exponentially growing phytoplankton (Nagata, 2000). The model sensitivity to $l_k$ was also tested (see below).

If both $F_T$ and $F_{bc}$ are determined (discussed below), $F$ can be solved (Eq. 6), and the growth rate is then

$$g = F/q_c \tag{7}$$

where $q_c$ is the cell carbon quota (μmol cell$^{-1}$) estimated by adopting an empirical relationship with the cell volume of diatoms (Menden-Deuer and Lessard, 2000):

$$q_c = 2.4 \times 10^{-8} \cdot \left(\frac{4}{3}\pi R^3\right)^{0.811} \tag{8}$$

$F_T$ and $F_{bc}$ are optimally solved under the constraint of intracellular energy production $E_0$. The intracellular energy requirement is:

$$E = E_g + E_{bc} \tag{9}$$

in which

$$E_g = e_g \cdot g = e_g \cdot (F_T + F_{bc}) \cdot (1 - l_k)/q_c \tag{10}$$

$$E_{bc} = e_{bc} \cdot F_{bc}/q_c \tag{11}$$

A trial rate of $HCO_3^-$ acquisition ($F_{bc}$) is first set to be the minimal fraction ($f_{min}^{bc}$) of total carbon uptake ($F_{T,max} + F_{bc}$) so that:

$$F_{bc} = F_{T,max} \cdot f_{min}^{bc}/(1 - f_{min}^{bc}) \tag{12}$$

Then, a trial energy requirement $E$ is calculated using Eqs. 10–12 and setting $F_T = F_{T,max}$ (see section "Model Scheme of the $CO_2$ Supply"). When $E > E_0$, energy production limits growth and the total carbon supply is more than sufficient. Therefore, the effective $F_T$ and $F_{bc}$ must be smaller than their trial rates while their ratio holds. Therefore, a factor of $E_0/E$ is multiplied by $F_{T,max}$ and the trial $F_{bc}$ to obtain the effective $F_T$ and $F_{bc}$, which ensures $E = E_0$.

However, a trial rate of $E$ larger than $E_0$ indicates that the inorganic carbon supply is insufficient, additional acquisition of $HCO_3^-$ is needed, and the effective $F_T$ is at its maximal allowed rate $F_{T,max}$. The effective $F_{bc}$ is calculated from Eqs. 9–11 by setting $E = E_0$ (Eq. 9) and $F_T = F_{T,max}$ (Eq. 10).

Once the effective $F_T$ and $F_{bc}$ are determined in either case, the growth rate $g$ can be calculated from Eqs. 6, 7. Noting that the intracellular energy produced is fully used, the scheme described here solves an optimal allocation of intracellular energy to estimate $g$ at its maximal potential.

## Model Simulation

The cell growth rate was simulated at two levels of bulk-water $CO_2$ concentrations of 10 μM (low carbon condition, LC) and 20 μM (high carbon condition, HC) over a diameter range of 2–200 μm. LC was selected at 10 μM to represent the typical condition of subtropical surface ocean waters. GRR is calculated as the ratio of the simulated growth rates under HC and LC. We also calculated two key indicators, the value of the peak GRR over the simulated diameter range and the corresponding cell diameter at the peak GRR (namely, the optimal cell diameter).

## Sensitivity Tests

Our model does not represent other factors, such as light and nutrient concentrations, that can limit the diatom growth rate. Instead, the model parameter $g_0$ can be considered to represent collective effects from multiple limiting factors. We then conducted model experiments by setting $g_0$ at 0.1, 0.5, 1.0, and 2.0/day.

We also compared the model sensitivity, in terms of the peak GRR and the optimal cell diameter, to 6 model parameters, including $P$, $l_k$, $e_{bc}$, $g_0$, $\triangle_{CO2}$, and $f_{min}^{bc}$. These parameters were tested in a range of ± 50% of their default values. The model was also tested over 12–30 μM of the input variable $[CO_2]_{bulk}$ in HC.

## Analysis of Historical Data of Diatom $CO_2$ Enrichment Experiments

We collected 85 pairs of growth rate data from published $CO_2$ enrichment experiments culturing diatoms, among which 5 pairs of data were removed due to extremely high culturing $CO_2$ concentrations (**Supplementary Table 2**). Due to different magnitudes of $CO_2$ enrichment, we linearly adjusted the originally reported GRR ($GRR_{orig}$) cultured under high ($[CO_2]_H$) and low ($[CO_2]_L$) $CO_2$ concentrations to $GRR_{adj}$ at a $CO_2$-enrichment factor ($f_{CO2}$) of 200%:

$$\frac{\mathbf{GRR_{adj}-100\%}}{\mathbf{f_{CO2}-100\%}} = \frac{\mathbf{GRR_{orig}-100\%}}{\mathbf{[CO_2]_H/[CO_2]_L-100\%}} \quad (13)$$

The cell diameters of the diatoms were either reported in the experiments or estimated using the average diameters of the same species collected in a global diatom database (Leblanc et al., 2012a). Considering the purpose of this study, for nonspherical diatom species, we simply used the length of their shortest dimension as the cell diameter because it was the shortest distance that inorganic carbon was transported to the cell center, admitting that this simplification slightly overestimated the $CO_2$ supply rate.

## Global Prediction

We projected the peak GRR and optimal cell size of diatoms to $CO_2$ increase in global surface seawater over the 21st century. We first obtained projected results from the Community Earth System Model (CESM) 1.0-BGC module under the RCP8.5 scenario, including the annual climatology of $CO_2$ partial pressure, pH, temperature, diatom carbon fixation rate, and diatom carbon biomass during the historical (1990–2000) and future (2090–2100) periods[1]. The $CO_2$ partial pressure, pH, and temperature were used to calculate the $CO_2$ concentration using CO2SYS (Lewis and Wallace, 1998). The diatom growth rates were calculated as the ratio of the diatom carbon fixation rate to the diatom carbon biomass.

The cellular model ran using historical and future $CO_2$ concentrations to estimate monthly peak GRR and optimal cell size at a resolution of 1° × 1° in the global ocean, in which historical diatom growth rates were used to set location specificity $g_0$. Because CESM did not simulate diatom sizes, our results can only be regarded as a demonstration of the spatial variations in the responses of diatoms impacted by the magnitude of $CO_2$ increase and environmental favorability (such as nutrients, temperature, and light), with the latter collectively represented here by the CESM-projected diatom growth rate.

The scientific color map batlow was used in the plot of the global prediction to prevent visual distortion of the data and exclusion of readers with color-vision deficiencies (Crameri et al., 2020).

[1]https://www.earthsystemgrid.org/dataset/ucar.cgd.ccsm4.CESM_CAM5_BGC_LE.ocn.proc.monthly_ave.html

# RESULTS

## Model Results

The modeled cell growth rate declines with increasing cell diameter under LC, while the modeled growth under HC remains at a maximal rate of 2.67/day before it starts to decline when its diameter is larger than 7 μm (**Figure 2A**). As the ratio of the modeled growth rate under HC to that under LC, the GRR increases with cell diameter, reaches a peak value of 1.14 at an optimal cell diameter of 7 μm, and then gradually decreases to 1.02 at the modeled maximal cell diameter (**Figure 2B**).

We then analyze the inorganic carbon ($C_i$) budget of the model cell in two cell diameter ranges. As expected, the model simulates a decreasing $CO_2$ supply rate with increasing cell diameter (**Figure 3**). First, for cells with a diameter < 7 μm, $CO_2$ and minimum $HCO_3^-$ supply under LC are insufficient to meet the requirements of both growth and leakage, causing $HCO_3^-$ acquisition to increase with cell size (**Figure 3A**). However, under HC, $CO_2$ and minimum $HCO_3^-$ supply are sufficient, and cells do not acquire additional $HCO_3^-$ (**Figure 3B**). Second, for cells

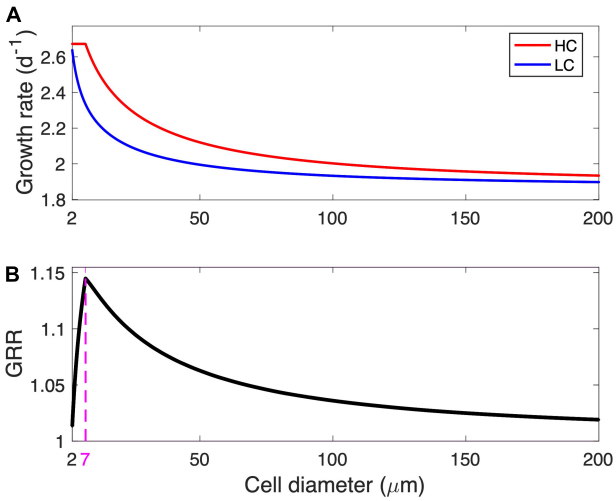


**FIGURE 2 |** Modeled growth rate and growth rate response (GRR). **(A)** Modeled growth rate under low-$CO_2$ (LC, 10 μM) and high-$CO_2$ (HC, 20 μM) conditions and **(B)** the corresponding GRR from LC to HC as a function of cell diameter. The magenta dashed line and number in **(B)** represent the optimal cell diameter at peak GRR.

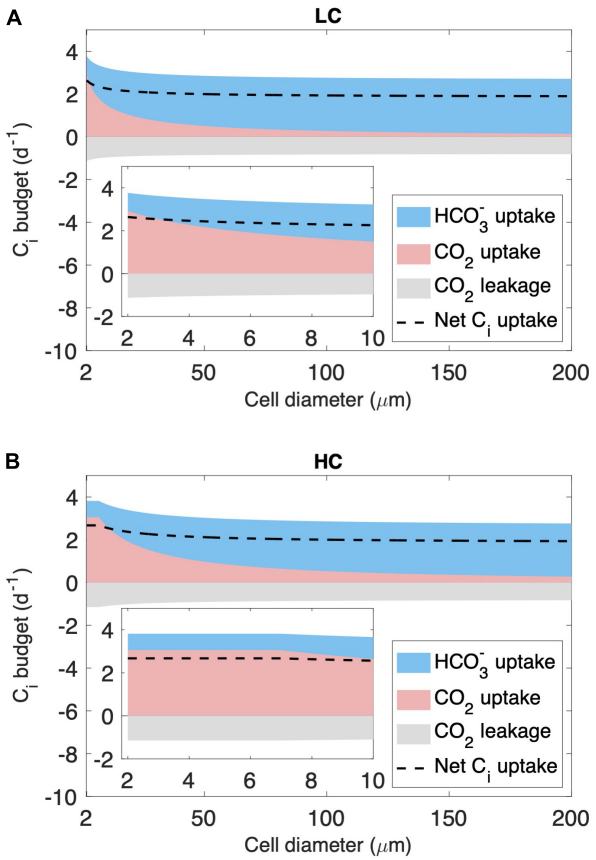


**FIGURE 3 |** Modeled inorganic carbon (Ci) budget (normalized to cell carbon biomass) across the cytoplasmic membrane. The results shown include those under **(A)** the low-$CO_2$ (LC, 10 μM) and **(B)** high-$CO_2$ (HC, 20 μM) conditions in the cell diameter of the full modeled range and zoomed in to 2–10 μm. Ci is acquired in the form of $HCO_3^-$ (blue area) and $CO_2$ (pink area), and part of the $CO_2$ leaks out of the cell (gray area), resulting in a net Ci uptake used for cell growth (dashed line).

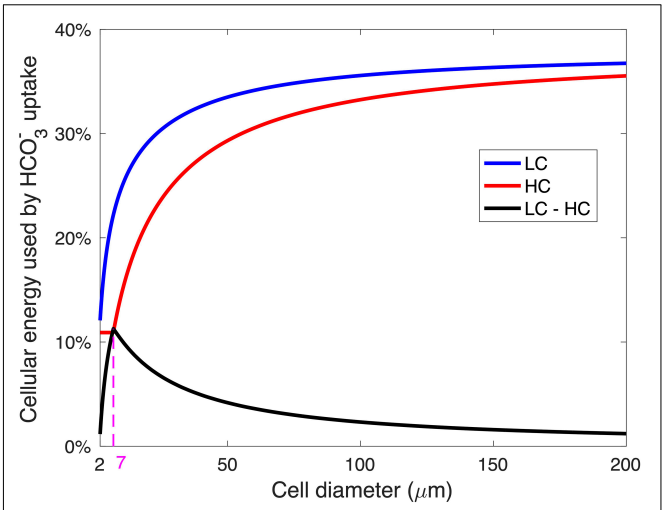


**FIGURE 4 |** The relationship between the modeled energy consumption for $HCO_3^-$ acquisition and the cell diameter. The energy for $HCO_3^-$ acquisition is shown as the fraction of total cellular metabolic energy under the low-$CO_2$ (LC, 10 μM) (blue) and high-$CO_2$ (HC, 20 μM) (red) conditions, as well as the saved energy in $HCO_3^-$ acquisition when the condition changed from LC to HC (black). The magenta dashed line and number represent the optimal cell diameter at maximal energy savings from LC and HC.

with a diameter > 7 μm, $CO_2$ and minimum $HCO_3^-$ supply become insufficient even under HC (**Figure 3B**), and the modeled $HCO_3^-$ acquisition increases with cell size under both HC and LC (**Figure 3**).

The modeled pattern between GRR and cell size (**Figure 2B**) is mainly determined by the magnitude of energy savings on $HCO_3^-$ acquisition from LC to HC (**Figure 4**). In the cell diameter range < 7 μm, the energy expenditure on $HCO_3^-$ increases greatly with increasing cell size under LC but is unchanged under HC, resulting in substantial energy savings that increase with cell size (**Figure 4**). In the cell diameter range > 7 μm, however, the energy used in $HCO_3^-$ acquisition increases with cell size under both HC and LC, leading to a narrowed difference between the two (**Figure 4**). This can be explained by the decrease in the relative contribution of $CO_2$ to the total $C_i$ acquisition with increasing cell size (**Figure 3**): The fraction of $HCO_3^-$ acquisition that can be substituted by the same magnitude of the elevated $CO_2$ supply decreases in larger diatoms. In other words, larger cells become less sensitive to the $CO_2$ increase.

The model reveals a general pattern in which (1) the smallest diatoms respond weakly to the increase in seawater $CO_2$ because $CO_2$ supply fulfills most of the cell demand even without that increase, (2) the response intensifies with a moderate enlargement in cell size, while (3) large cells are insensitive to the $CO_2$ increase because $CO_2$ supply is a small contribution to total $C_i$ acquisition. There exists an optimal, intermediate cell size in which the modeled cell growth rate is enhanced the most by the same magnitude of $CO_2$ increase. Our model shows that the optimal cell size corresponds to a point where the model cell under HC just starts to use $HCO_3^-$.

## Sensitivity Tests

The maximal growth rate ($g_0$) has been set at a high level assuming that the modeled diatom grows at optimal conditions. We then conduct the model experiments with lowered $g_0$, representing that the growth of the modeled diatom is limited by other factors. The results show that the modeled diatom starts to benefit from the $CO_2$ increase at larger cell sizes when $g_0$ decreases, so that the optimal cell size also increases (**Figure 5A**). This result is expected because the modeled diatom needs less inorganic carbon at a lowered $g_0$, and the $CO_2$ supply alone becomes sufficient for larger diatoms. At very low $g_0$ values, such as 0.1/day, the $CO_2$ supply is even sufficient at the maximal cell diameter simulated in our model (200 μm), and diatoms do not respond to the $CO_2$ increase in the whole model domain (**Figure 5A**). Additionally, $g_0$ does not impact the modeled peak GRR (**Figure 5A**), the reason for which is discussed below. These results indicate that the optimal cell size of diatoms in response

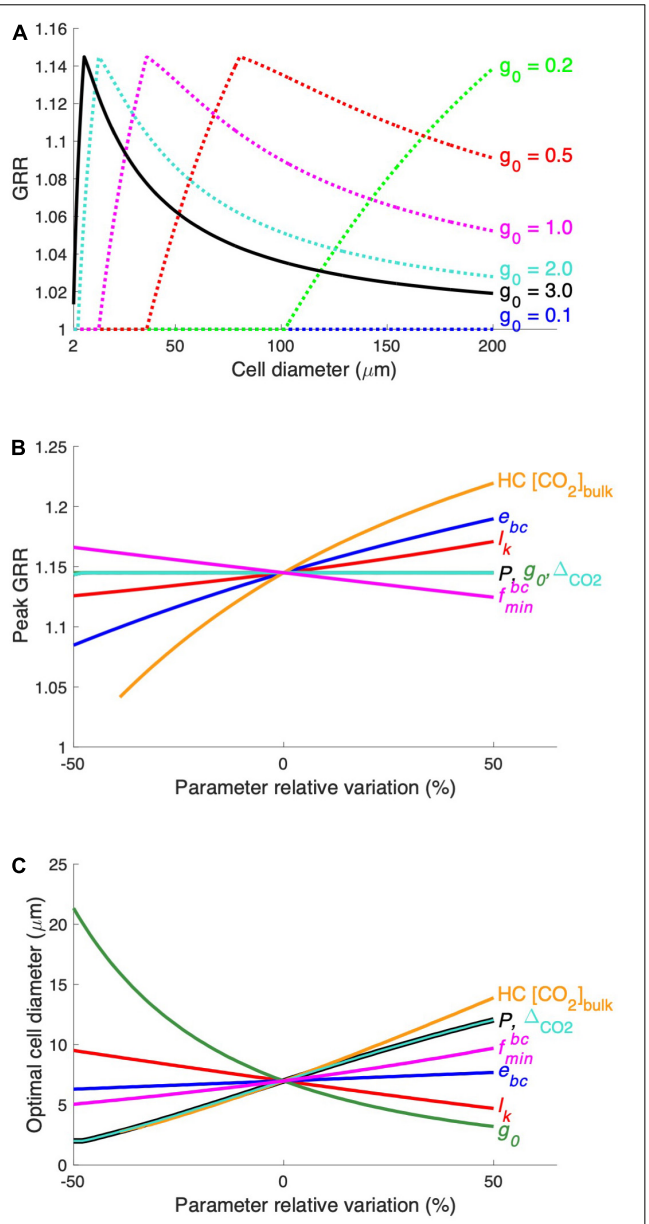


**FIGURE 5 |** Results of the parameter sensitivity experiment. **(A)** The modeled relationship between GRR and cell diameter is tested at different levels of the model parameter $g_0$ (maximal growth rate). The modeled peak GRR **(B)** and the optimal cell diameter **(C)** were tested against ± 50% of the default values of the parameters. See **Supplementary Table 1** for parameter symbols and their default values. The range of HC $CO_2$ concentrations (HC $[CO_2]_{bulk}$) tested in this experiment was 12–30 μM.

to the $CO_2$ increase tends to be small when the environmental conditions favor their growth but can be larger when other factors are also limiting.

We also compared the sensitivity of the modeled peak GRR (**Figure 5B**) and optimal cell size (**Figure 5C**) to various model parameters. The $CO_2$ supply rate, mainly determined by the production of the $CO_2$ permeability ($P$) and $CO_2$ gradient across the cytoplasmic membrane ($\triangle_{CO2}$) (Eqs. 3, 4), has a positive relationship with the optimal cell size but does not impact the GRR. This can be more clearly understood from a model experiment with a 50% higher $P$ (**Supplementary Figure 3A**): The cell needs to use additional $HCO_3^-$ at large cell sizes with increased $CO_2$ supply. Hence, the curves of $HCO_3^-$ acquisition energy under both HC and LC move toward larger cell sizes without noticeable changes in the magnitude of the energy cost, leading to a moderately elevated optimal cell size but unchanged peak GRR (**Figures 5B,C**; **Supplementary Figure 3A**). Similarly, a smaller maximal daily growth rate ($g_0$) also leads to a larger optimal cell size but no effect on peak GRR (**Figure 5** and **Supplementary Figure 3B**) because the lowered carbon demand also allows larger cells to only use $CO_2$. In contrast, reduced $CO_2$ leakage ($l_k$) lowers the requirement of $HCO_3^-$ acquisition and shrinks the difference in energy cost between HC and LC, causing a decreased GRR and enlarged optimal cell size (**Figure 5** and **Supplementary Figure 3C**).

The elevated energy cost rate of $HCO_3^-$ acquisition ($e_{bc}$) substantially increases the peak GRR but has little effect on the optimal cell size (**Figures 5B,C**) because it mainly determines the energy allocation and not the cell size at which $HCO_3^-$ acquisition is needed. The high bulk-water $CO_2$ concentration of HC (HC $[CO_2]_{bulk}$) greatly increases both the peak GRR and the optimal cell size (**Figures 5B,C**), which is expected because the cell under HC benefits more from higher $CO_2$ while starting to use $HCO_3^-$ at a larger size. The minimum $HCO_3^-$ uptake proportion ($f_{min}^{bc}$) slightly impacts both the peak GRR and the optimal cell size: a higher $f_{min}^{bc}$ leads to a reduced model sensitivity to the change in $CO_2$ and results in a lower peak GRR and a larger optimal cell size.

Our model sensitivity tests reveal that the peak GRR is largely determined by the magnitude of the seawater $CO_2$ increase and the energy consumption rate in $HCO_3^-$ acquisition. Meanwhile, the optimal cell diameter increases with increasing $CO_2$ supply (higher membrane permeability to $CO_2$ and larger increase in seawater $CO_2$) but decreases with cellular carbon demand, such as higher growth and leakage rates.

# DISCUSSION

## Unimodal Relationship Between Growth Rate Response and Cell Size

Our theoretical model reveals a unimodal relationship between the GRR and diatom cell size. Although the increased $CO_2$ concentration and acidified seawater can have multiple physiological effects on diatoms, our model considers the most direct effect: the variations in species and rates of inorganic carbon acquired by diatoms. The absolute rates of growth do not solely determine the competition among phytoplankton because they can also be controlled by other factors, such as zooplankton grazing and viral lysis, which is also suggested by the fact that phytoplankton with different growth rates coexist in the ocean. A phytoplankton species with a stronger enhancement in the growth rate from the $CO_2$ increase, can have a better advantage and reach higher biomass when competing with other

phytoplankton, which is also confirmed by a modeling study (Dutkiewicz et al., 2015). Therefore, the unimodal relationship between GRR and diatom cell size shown by our model suggests a competitive advantage for middle-sized diatoms of ∼7 μm in the future high-$CO_2$ ocean.

It is generally true that organisms limited more strongly by a resource should benefit more from its repletion, but only if there are no substitute resources. $CO_2$, for example, is not the only carbon resource for phytoplankton and can be complemented by, although not preferentially, $HCO_3^-$ when $CO_2$ is insufficient. This is the important reason why our model reveals that middle-sized diatoms can have a competitive advantage over larger diatoms from elevated $CO_2$, even though the latter is limited more strongly by $CO_2$.

We also explored the GRR–cell size relationship using historical data from $CO_2$ manipulation experiments of diatoms. The originally reported GRR in those experiments was first interpolated to the same degree of $CO_2$ enrichment (**Supplementary Figure 4** and **Supplementary Table 2**, see section "Materials and Methods"). The adjusted GRRs varied greatly (0.7–1.4) and did not support the previous speculation that the GRR should increase with cell size (Spearman's correlation, $p = 0.59$) (**Figure 6**). The GRRs also did not directly show the same pattern as that proposed by our model. However, all GRRs higher than 1.2 were only found in cell diameters of 3–7 μm, while the GRRs at other cell diameters were mostly lower than 1.1 (**Figure 6**). This may indicate that the growth rate of diatoms in this middle cell size range had the greatest potential to respond to increasing seawater $CO_2$. Additionally, the GRRs in the same size range also varied the most (**Figure 6**), suggesting that the GRR of middle-sized diatoms can be impacted by different factors and mechanisms and/or be species specific. Interestingly, considering the species in the genus *Thalassiosira* that had the largest cell diameter range (3.9–47 μm) in our dataset, their GRRs decreased with cell diameter (Spearman's correlation = −0.45, $p < 0.05$), with GRRs in cell diameter ≤ 7 μm (1.14 ± 0.13, mean ± s.d.; $n = 11$) significantly higher than those in cells > 7 μm in diameter (1.00 ± 0.06, mean ± s.d.; $n = 10$) ($t$-test, $p < 0.01$). Nevertheless, these historical data showed some consistency with our model, while the GRR can be a synergistic result impacted not only by cell size but also by other physiological and ecological characteristics and culturing conditions. More studies are needed to reveal complex mechanisms controlling the GRR.

Other studies may directly or indirectly support our model. Hancock et al. (2018) cultured a near-shore Antarctic community over a gradient of $CO_2$ levels, showing that the abundance of nanosized diatoms (2–20 μm in diameter) increased with $CO_2$, while larger microplanktonic diatoms (>20 μm in diameter) and smaller discoid centric diatoms of 1–2 μm in diameter had no significant response to $CO_2$. Other studies also showed that middle-sized diatom species (∼8 μm) had an increased contribution to the community under increased $CO_2$ (Hoppe et al., 2013; Eggers et al., 2014).

We also constructed a new scheme of the maximal seawater $CO_2$ supply rate to diatom cells as a function of cell size. Compared to other studies (Milligan et al., 2009; Reinfelder, 2011), the new scheme solves a cell size–dependent $CO_2$ concentration near the cell surface (**Supplementary Figure 1**). Our scheme introduces a new constant parameter, the $CO_2$ permeability of the cell membrane. Although elevated seawater $CO_2$ can lead to a saturated $CO_2$ supply and reduce the effective $CO_2$ permeability (e.g., Sultemeyer and Rinast, 1996), our scheme is constructed to study the maximal effect of seawater $CO_2$ increase and therefore uses the maximal potential of $CO_2$ permeability, which theoretically is determined by the number of channels such as pores and aquaporins (Matsui et al., 2018; Blanco-Ameijeiras et al., 2020) allowed per unit area of the cell membrane and should be independent of cell size. Limited data on diatom $CO_2$ permeability (Hopkinson et al., 2011) also do not show a clear relationship to cell size. Our model scheme therefore can be more suitable to quantify the relationship between phytoplankton cell size and their maximal potential for $CO_2$ uptake.

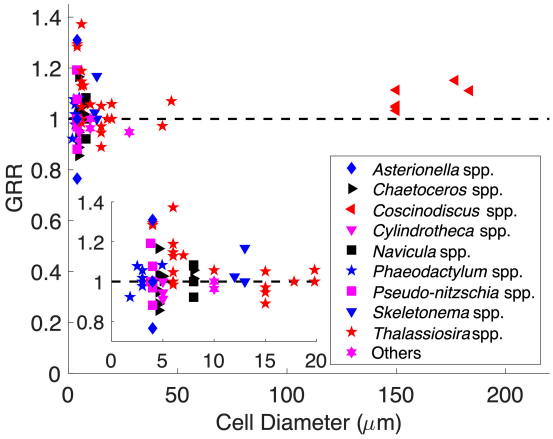


**FIGURE 6 |** Historical data of diatom $CO_2$ enrichment experiments showing the growth rate response (GRR) over cell diameter. The dashed line represents no response (GRR = 1). The inset is magnified to a cell range of 1–20 μm.

## Model Experiments of Additional Processes

The growth rates of diatoms are generally inversely related to cell sizes (Cosper, 1982; Sarthou et al., 2005; Marañón, 2015), which could result from a lower $CO_2$ supply rate to larger diatoms, as observed in this study, and/or other size-dependent physiological characteristics of diatoms. This implies that the constant model parameter of maximal growth rate $g_0$ can in reality decline with increasing cell size. We then conducted a model experiment by using an empirical function for diatoms (Sarthou et al., 2005):

$$g_0 = 3.4V^{-0.13} \quad (14)$$

where $V$ was the cell volume (μm$^3$). In the results, the unimodal pattern between GRR and cell size remained (**Supplementary Figure 5**), although the optimal cell size increased to 45 μm, which was expected because of the negative relationship between the optimal cell size and $g_0$ (**Figure 5B**).

As eCA can be potentially important in particularly large phytoplankton in converting $HCO_3^-$ to $CO_2$ extracellularly (Martin and Tortell, 2008; Tortell et al., 2008; Chrachri et al., 2018) and therefore saving energy on $HCO_3^-$ acquisition, we tested its role by increasing the conversion rate of $HCO_3^-$ to $CO_2$ in the model by an enhancement factor ($f_{eCA}$) of 2–10 (Tortell et al., 2008). As the ratio of the chemical conversion between $HCO_3^-$ and $CO_2$ to the $CO_2$ diffusivity is $R\sqrt{k'/D}$ (Eq. 2) (Reinfelder, 2011), the $CO_2$ supply ($F_T$) was then enhanced to a new rate:

$$F_T' = \frac{1 + f_{eCA} R\sqrt{k'/D}}{1 + R\sqrt{k'/D}} F_T \quad (15)$$

In the model experiments, although the GRR was elevated in the large cells, the unimodal pattern between the GRR and cell size, the optimal cell diameter, and the magnitude of peak GRR were barely changed (**Supplementary Figure 6A**). We also conducted another model experiment by linearly increasing $f_{eCA}$ from 1 (i.e., no enhancement) at the smallest cell diameter (2 μm) to 10 at a cell diameter of 200 μm to mimic a hypothetical scenario of stronger eCA of larger cells, and still obtained a similar pattern between the GRR and cell size, except that the GRR remained at a constant low level when the cell diameter was >100 μm (**Supplementary Figure 6B**).

The two parameters $D$ and $k'$ used in the $CO_2$ reaction–diffusion kinetics (Eq. 2) are fixed in our model, while in reality, they change with temperature (Wolf-Gladrow and Riebesell, 1997). A sensitivity test of temperature-dependent $D$ and $k'$, however, showed no obvious effect on the model results (**Supplementary Figure 7**).

The above experiments can partly support the robustness of our model results, suggesting that the negative correlation between diatom growth rates and cell size, the extracellular conversion of $HCO_3^-$ to $CO_2$, and temperature do not change the unimodal relationship between the GRR and the cell size of diatoms.

## Global Prediction

Our model sensitivity experiments reveal that the modeled optimal cell size enlarges with stronger seawater $CO_2$ supplies associated with its higher concentration and permeability across the cell membrane, but diminishes with elevating cellular carbon demand determined by higher rates of cell growth potential (**Figure 5**). Among these factors, the magnitude of future $CO_2$ increase and the maximal growth rate of diatoms can vary substantially in the global ocean. Particularly, as already discussed, our model does not represent the effects of other factors that can limit diatom growth. We then ran our model in the global ocean using the projected levels of these two variables in this century under the RCP8.5 scenario from an Earth system model (see section "Materials and Methods"), in which multiple limiting factors on diatom growth were simulated. The spatial variation in the modeled peak GRR was generally small in the global ocean, with the lowest value in the tropical Pacific upwelling zone (**Figure 7A**) associated with its smallest magnitude of $CO_2$ increase (**Figure 7C**). The modeled optimal cell size, however, varied greatly from < 20 μm in tropical oceans to the highest modeled cell diameter (i.e., GRR increases monotonically with cell size) in the subpolar regions (**Figure 7B**). The modeled optimal cell size was systematically smaller than what was predicted in our theoretical model (**Figures 2**, **5B**) because the CESM-simulated diatom growth rates incorporated other limiting factors and were mostly below 1.0/day (**Figure 7D**), much lower than those found in laboratories with ideal culturing conditions (Sarthou et al., 2005). The lowest optimal cell size was also in the tropical Pacific upwelling zone (**Figure 7B**), contributed synergistically by the high growth rates of diatoms and low magnitude of $CO_2$ increase (**Figures 7C,D**).

Our projection for diatoms in the global ocean should be regarded at most as the first-order estimation. However, some interesting implications emerged from the projection. Diatoms are one of the important contributors to carbon export to the deep ocean (Falkowski et al., 2004), particularly in tropical oceans (Siegel et al., 2014, 2016). The relatively small optimal cell size projected in these regions (**Figure 7B**) implies that, without considering other effects, the size structure of the diatom community would not shift to larger species in the future high-$CO_2$ ocean, which consequently would not lead to an increase in the sinking speed of organic particles and carbon export.

## Model Limitations

Carbonic anhydrase in diatoms can convert $CO_2$ to $HCO_3^-$ in the cytoplasm and result in much-increased $HCO_3^-$ transport further into chloroplasts, as found for diatom *Phaeodactylum tricornutum* (Hopkinson et al., 2011; Hopkinson, 2014). Additionally, a high leakage of $CO_2$ from the chloroplast to the cytoplasm has been suggested (Hopkinson et al., 2011), although it is unclear how much of the leaked $CO_2$ further leaks to the environment or is converted to $HCO_3^-$ in the cytoplasm and transported back to the chloroplast. The $CO_2$ leakage from the cell to the environment was already counted in the model. However, if there is substantial recycling of the leaked $CO_2$ to $HCO_3^-$ in the cytoplasm, the rate of $HCO_3^-$ transfer across the chloroplast membrane can be further elevated. In other words, $e_{bc}$ can possibly be higher for at least some diatoms, leading to higher GRRs (**Figure 5A**) but small changes in the optimal cell size (**Figure 5B**).

There are some limitations in our model that can be investigated in future studies. First, our model does not include the negative effects of the lower pH concomitant with elevated $CO_2$, which can be important to some species or functional groups of phytoplankton (e.g., Taylor et al., 2012; McMinn et al., 2014; Cyronak et al., 2016; Hong et al., 2017; Gafar et al., 2018; Luo et al., 2019; Shi et al., 2019). If there is no relationship between the negative effects of lower pH and diatom cell sizes, which, however, is unclear, our modeled pattern between GRR and diatom cell sizes can still hold.

Second, RuBisCO in different diatoms shows greater variation in the Michaelis constant for $CO_2$ (23–68 μM) (Young et al., 2016), indicating diverse patterns of CCM, RuBisCO kinetics, and catalytic features in diatoms. Our model does not separate diatom species but focuses on the general response of diatoms of different sizes to seawater $CO_2$ increases. Nevertheless, the

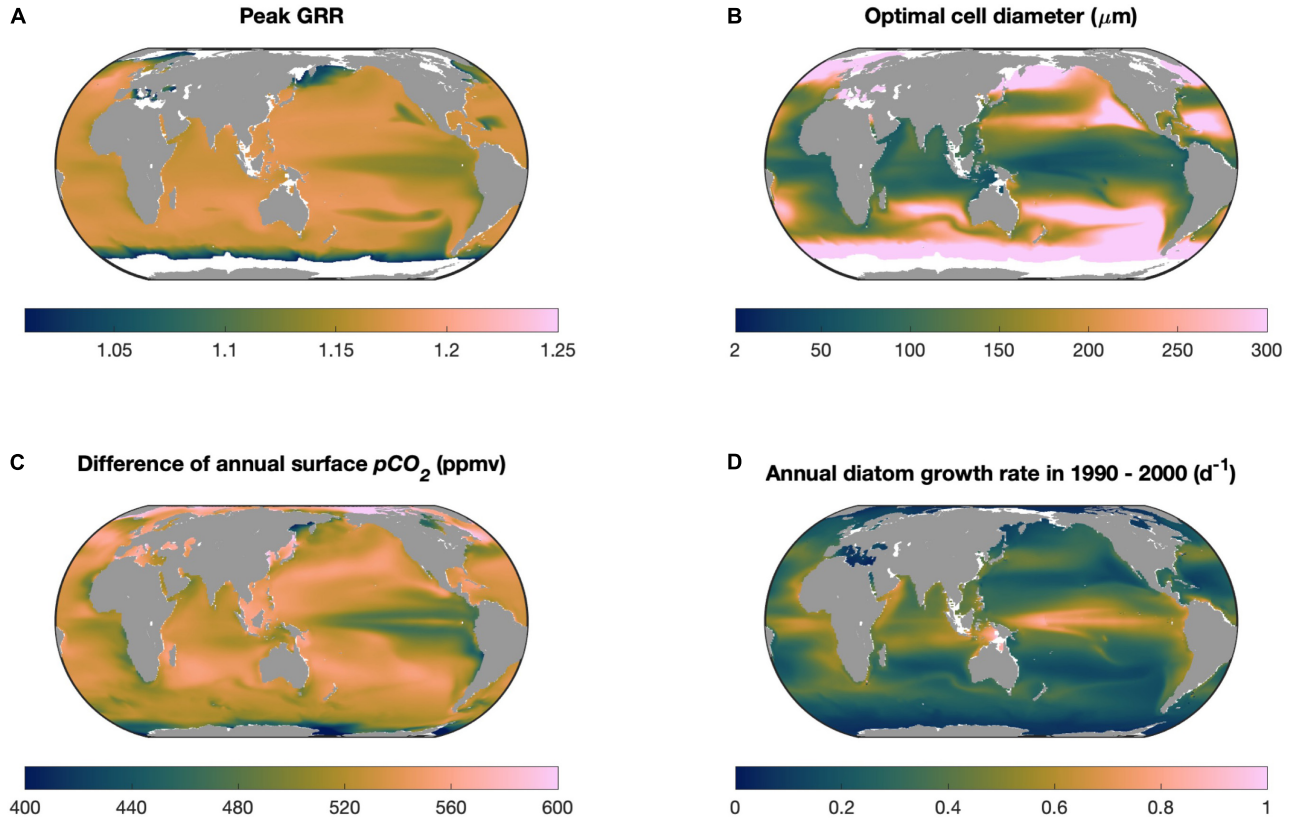


**FIGURE 7 |** Model projections in the global ocean. **(A)** Modeled peak growth rate response (GRR) and **(B)** optimal cell size within this century under the CESM-predicted RCP8.5 scenario, including **(C)** the increase in partial pressure of $CO_2$ and **(D)** annual average diatom growth rate. White areas in **(A,B)** represent the locations where the modeled GRR is very weak (<1.01).

variation of these factors can change model parameters of the cell membrane permeability to $CO_2$ ($P$) and the energy cost rate in $HCO_3^-$ uptake ($e_{bc}$), among which a ± 50% change in the former can vary the optimal cell size in a range of 2–13 μm while that in the latter has no substantial effect (**Figure 5C**). That is, if the $CO_2$ permeability is substantially lower than that used in our model, the GRR can be highest in the smallest diatoms and then decreases with increasing cell size.

Third, light appears to interact with elevated $CO_2$ in determining the collective effect in cell size–dependent responses of diatoms, such as that we already discussed for the stronger response of larger diatoms to $CO_2$ increase under very high light. Another study also proposed a light-based maximal benefit of CCM in middle-sized phytoplankton: The depletion of light near the center of large cells depresses photosynthesis and reduces the energy available for CCM, making CCM economically less efficient in large cells (Wirtz, 2011). This effect and our proposed mechanism, if valid, can synergistically intensify the competitive advantage of middle-sized diatoms under the $CO_2$ increase.

Last, cultured diatoms also often respond differently to $CO_2$ increases depending on the availability of nutrients such as nitrogen (Li et al., 2012), phosphorus (Sun et al., 2011), and silicon (Tatters et al., 2012), while these nutrients are not simulated in our model. Instead, our model experiments implicitly represent the limitation of these nutrients by applying a lower model parameter $g_0$, showing that middle-sized diatoms are more likely to have better competition from the $CO_2$ increase when these nutrients are not severely limiting (**Figures 5**, **7**). Nevertheless, our model does not simulate the cell size–dependent limitation of nutrients on diatoms. In the future warmer and more stratified oceans, nutrients can become more limiting, and smaller diatoms may gain another competitive advantage because of their lower surface-to-volume ratios. Considering this effect, the increasing trend of GRR from small to middle-sized diatoms can be weakened or even reversed. However, the decreasing trend of GRR from middle-sized to large-sized diatoms may be even stronger.

Overall, despite the limitations of our model, the discussions above suggest that the GRR in the future high-$CO_2$ ocean, in general, likely decreases from middle-sized to large-sized diatoms, except in the regions where the light is substantially high or nutrients are substantially limiting on diatoms. The GRR may also increase from small to middle-sized diatoms unless the cell membrane permeability to $CO_2$ is low or nutrients become severely limiting, particularly on middle-sized diatoms.

In summary, this study constructed a theoretical model and revealed a competitive advantage of middle-sized diatoms of

~7 μm over both small and large diatoms when seawater $CO_2$ increases. Although the model is mostly based only on the basic principles of the carbonate equilibrium system and inorganic carbon diffusion with constraints on cellular energy allocations, it appears to be a robust pattern, although the exact cell size of which diatoms benefit most from the $CO_2$ increase can change substantially. If the mechanism proposed in this study dominates, the diatom community in the future high-$CO_2$ ocean may not shift toward larger cells, and carbon export by sinking diatoms may not be substantially stimulated, while we admit that other known and unknown factors can also influence the cell size–dependent responses of marine diatoms to the $CO_2$ increase. Our simplified physiological model processes, or even more simply the size-dependent pattern revealed by our model, can be integrated into marine ecosystem models to improve the predictions of the size composition of diatoms, phytoplankton community structure, and productivity for future high-$CO_2$ oceans.

## DATA AVAILABILITY STATEMENT

The original contributions presented in the study are included in the article/**Supplementary Material**, further inquiries can be directed to the corresponding author.

## AUTHOR CONTRIBUTIONS

Y-WL originated the concept for the study. Y-WL and QZ designed the numerical model, analyzed the results, and improved the numerical model. QZ coded the initial version of the model and performed numerical modeling. Both authors contributed to writing the manuscript.

## FUNDING

This study was funded by the National Natural Science Foundation of China (41890802 and 42076153) and the National Key R&D Program of China (2016YFA0601404).

## ACKNOWLEDGMENTS

We thank Ruiping Huang, Xin Lin, Chris Bowler, Richard Dorrell, and Xia Gao for very useful discussions.

## SUPPLEMENTARY MATERIAL

The Supplementary Material for this article can be found online at: https://www.frontiersin.org/articles/10.3389/fmicb.2022.838629/full#supplementary-material

## REFERENCES

Badger, M. R., Andrews, T. J., Whitney, S. M., Ludwig, M., Yellowlees, D. C., Leggat, W., et al. (1998). The diversity and coevolution of Rubisco, plastids, pyrenoids, and chloroplast-based $CO_2$-concentrating mechanisms in algae. *Can. J. Bot.* 76, 1052–1071. doi: 10.1139/b98-074

Behrenfeld, M. J., Halsey, K. H., and Milligan, A. J. (2008). Evolved physiological responses of phytoplankton to their integrated growth environment. *Philos. Trans. R. Soc. B* 363, 2687–2703. doi: 10.1098/rstb.2008.0019

Biswas, H., Shaik, A. U. R., Bandyopadhyay, D., and Chowdhury, N. (2017). $CO_2$ induced growth response in a diatom dominated phytoplankton community from SW Bay of Bengal coastal water. *Estuar. Coast. Shelf Sci.* 198, 29–42. doi: 10.1016/j.ecss.2017.07.022

Blanco-Ameijeiras, S., Stoll, H. M., Zhang, H., and Hopkinson, B. M. (2020). Influence of temperature and $CO_2$ on plasma-membrane permeability to $CO_2$ and $HCO_3^-$ in the marine haptophytes *Emiliania huxleyi* and *Calcidiscus leptoporus* (Prymnesiophyceae). *J. Phycol.* 56, 1283–1294. doi: 10.1111/jpy.13017

Buesseler, K. O. (1998). The decoupling of production and particulate export in the surface ocean. *Glob. Biogeochem. Cycles* 12, 297–310. doi: 10.1029/97GB03366

Burkhardt, S., Amoroso, G., Riebesell, U., and Sueltemeyer, D. (2001). $CO_2$ and $HCO_3^-$ uptake in marine diatoms acclimated to different $CO_2$ concentrations. *Limnol. Oceanogr.* 46, 1378–1391. doi: 10.4319/lo.2001.46.6.1378

Cassar, N., Laws, E. A., Popp, B. N., and Bidigare, R. R. (2002). Sources of inorganic carbon for photosynthesis in a strain of *Phaeodactylum tricornutum*. *Limnol. Oceanogr.* 47, 1192–1197. doi: 10.4319/lo.2002.47.4.1192

Chrachri, A., Hopkinson, B. M., Flynn, K., Brownlee, C., and Wheeler, G. L. (2018). Dynamic changes in carbonate chemistry in the microenvironment around single marine phytoplankton cells. *Nat. Commun.* 9:74. doi: 10.1038/s41467-017-02426-y

Cosper, E. (1982). Influence of light intensity on diel variations in rates of growth, respiration and organic release of a marine diatom: comparison of diurnally constant and fluctuating light. *J. Plankton. Res.* 4, 705–724. doi: 10.1093/plankt/4.3.705

Crameri, F., Shephard, G. E., and Heron, P. J. (2020). The misuse of colour in science communication. *Nat. Commun.* 11:5444. doi: 10.1038/s41467-020-19160-7

Cyronak, T., Schulz, K. G., and Jokiel, P. L. (2016). The Omega myth: what really drives lower calcification rates in an acidifying ocean. *ICES J. Mar. Sci.* 73, 558–562. doi: 10.1093/icesjms/fsv075

Deppeler, S., Petrou, K., Schulz, K. G., Westwood, K., Pearce, I., McKinlay, J., et al. (2018). Ocean acidification of a coastal Antarctic marine microbial community reveals a critical threshold for $CO_2$ tolerance in phytoplankton productivity. *Biogeosciences* 15, 209–231. doi: 10.5194/bg-15-209-2018

Doney, S. (2009). The consequences of human-driven ocean acidification for marine life. *F1000 Biol. Rep.* 1:36. doi: 10.3410/B1-36

Doney, S. C., Busch, D. S., Cooley, S. R., and Kroeker, K. J. (2020). The impacts of ocean acidification on marine ecosystems and reliant human communities. *Annu. Rev. Environ. Resour.* 45, 83–112. doi: 10.1146/annurev-environ-012320-083019

Dutkiewicz, S., Morris, J. J., Follows, M. J., Scott, J., Levitan, O., Dyhrman, S. T., et al. (2015). Impact of ocean acidification on the structure of future phytoplankton communities. *Nat. Clim. Change* 5, 1002–1006. doi: 10.1038/nclimate2722

Eggers, S. L., Lewandowska, A. M., Barcelos e Ramos, J., Blanco-Ameijeiras, S., Gallo, F., and Matthiessen, B. (2014). Community composition has greater impact on the functioning of marine phytoplankton communities than ocean acidification. *Glob. Chang. Biol.* 20, 713–723. doi: 10.1111/gcb.12421

Eichner, M., Kranz, S. A., and Rost, B. (2014). Combined effects of different $CO_2$ levels and N sources on the diazotrophic cyanobacterium *Trichodesmium*. *Physiol. Plant.* 152, 316–330. doi: 10.1111/ppl.12172

Endo, H., Yoshimura, T., Kataoka, T., and Suzuki, K. (2013). Effects of $CO_2$ and iron availability on phytoplankton and eubacterial community compositions in the northwest subarctic Pacific. *J. Exp. Mar. Bio. Ecol.* 439, 160–175. doi: 10.1016/j.jembe.2012.11.003

Falkowski, P. G., Koblfzek, M., Gorbunov, M., and Kolber, Z. (2004). "Development and application of variable chlorophyll fluorescence techniques in marine ecosystems," in *Chlorophyll a Fluorescence: A Signature of Photosynthesis*, eds

G. C. Papageorgiou and Govindjee (Dordrecht: Springer), 757–778. doi: 10.1007/978-1-4020-3218-9_30

Feng, Y., Hare, C. E., Leblanc, K., Rose, J. M., Zhang, Y., DiTullio, G. R., et al. (2009). Effects of increased $pCO_2$ and temperature on the North Atlantic spring bloom. I. The phytoplankton community and biogeochemical response. *Mar. Ecol. Prog. Ser.* 388, 13–25. doi: 10.3354/meps08133

Finkel, Z. V., Beardall, J., Flynn, K. J., Quigg, A., Rees, T. A. V., and Raven, J. A. (2009). Phytoplankton in a changing world: cell size and elemental stoichiometry. *J. Plankton Res.* 32, 119–137. doi: 10.1093/plankt/fbp098

Flynn, K. J., Blackford, J. C., Baird, M. E., Raven, J. A., Clark, D. R., Beardall, J., et al. (2012). Changes in pH at the exterior surface of plankton with ocean acidification. *Nat. Clim. Change* 2, 510–513. doi: 10.1038/nclimate1489

Friedlingstein, P., Jones, M. W., O'Sullivan, M., Andrew, R. M., Hauck, J., Peters, G. P., et al. (2019). Global carbon budget 2019. *Earth Syst. Sci. Data* 11, 1783–1838. doi: 10.5194/essd-11-1783-2019

Gafar, N. A., Eyre, B. D., and Schulz, K. G. (2018). A conceptual model for projecting coccolithophorid growth, calcification and photosynthetic carbon fixation rates in response to global ocean change. *Front. Mar. Sci.* 4:433. doi: 10.3389/fmars.2017.00433

Gao, K., Xu, J., Gao, G., Li, Y., Hutchins, D. A., Huang, B., et al. (2012). Rising $CO_2$ and increased light exposure synergistically reduce marine primary productivity. *Nat. Clim. Change* 2, 519–523. doi: 10.1038/nclimate1507

Gavis, J., and Ferguson, J. F. (1975). Kinetics of carbon dioxide uptake by phytoplankton at high pH. *Limnol. Oceanogr.* 20, 211–221. doi: 10.4319/lo.1975.20.2.0211

Giordano, M., Beardall, J., and Raven, J. A. (2005). $CO_2$ concentrating mechanisms in algae: mechanisms, environmental modulation, and evolution. *Annu. Rev. Plant Biol.* 56, 99–131. doi: 10.1146/annurev.arplant.56.032604.144052

Hancock, A. M., Davidson, A. T., McKinlay, J., McMinn, A., Schulz, K. G., and van den Enden, R. L. (2018). Ocean acidification changes the structure of an Antarctic coastal protistan community. *Biogeosciences* 15, 2393–2410. doi: 10.5194/bg-15-2393-2018

Hong, H., Shen, R., Zhang, F., Wen, Z., Chang, S., Lin, W., et al. (2017). The complex effects of ocean acidification on the prominent $N_2$-fixing cyanobacterium *Trichodesmium*. *Science* 356, 527–531. doi: 10.1126/science.aal2981

Hopkinson, B. M. (2014). A chloroplast pump model for the $CO_2$ concentrating mechanism in the diatom *Phaeodactylum tricornutum*. *Photosynth. Res.* 121, 223–233. doi: 10.1007/s11120-013-9954-7

Hopkinson, B. M., Dupont, C. L., Allen, A. E., and Morel, F. M. M. (2011). Efficiency of the $CO_2$-concentrating mechanism of diatoms. *Proc. Natl. Acad. Sci. U. S. A.* 108, 3830–3837. doi: 10.1073/pnas.1018062108

Hopkinson, B. M., Dupont, C. L., and Matsuda, Y. (2016). The physiology and genetics of $CO_2$ concentrating mechanisms in model diatoms. *Curr. Opin. Plant Biol.* 31, 51–57. doi: 10.1016/j.pbi.2016.03.013

Hoppe, C. J. M., Hassler, C. S., Payne, C. D., Tortell, P. D., and Rost, B. (2013). Iron limitation modulates ocean acidification effects on Southern Ocean phytoplankton communities. *PLoS One* 8:e79890. doi: 10.1371/journal.pone.0079890

Jin, X., Gruber, N., Dunne, J. P., Sarmiento, J. L., and Armstrong, R. A. (2006). Diagnosing the contribution of phytoplankton functional groups to the production and export of particulate organic carbon, CaCO3, and opal from global nutrient and alkalinity distributions. *Glob. Biogeochem. Cycles* 20:GB2015. doi: 10.1029/2005GB002532

Key, T., McCarthy, A., Campbell, D. A., Six, C., Roy, S., and Finkel, Z. V. (2010). Cell size trade-offs govern light exploitation strategies in marine phytoplankton. *Environ. Microbiol.* 12, 95–104. doi: 10.1111/j.1462-2920.2009.02046.x

Kroeker, K. J., Kordas, R. L., Crim, R., Hendriks, I. E., Ramajo, L., Singh, G. S., et al. (2013). Impacts of ocean acidification on marine organisms: quantifying sensitivities and interaction with warming. *Glob. Chang. Biol.* 19, 1884–1896. doi: 10.1111/gcb.12179

Leblanc, K., Arístegui, J., Armand, L., Assmy, P., Beker, B., Bode, A., et al. (2012a). A global diatom database – abundance, biovolume and biomass in the world ocean. *Earth Syst. Sci. Data* 4, 149–165. doi: 10.5194/essd-4-149-2012

Leblanc, K., Arístegui Ruiz, J., Armand, L. K., Assmy, P., Beker, B., Bode, A., et al. (2012b). *Global Distributions of Diatoms Abundance, Biovolume and Biomass - Gridded Data Product (NetCDF) - Contribution to the MAREDAT World Ocean Atlas of Plankton Functional Types.* Pangaea. doi: 10.1594/PANGAEA.777384

Lerman, A., Guidry, M., Andersson, A. J., and Mackenzie, F. T. (2011). Coastal ocean last glacial maximum to 2100 $CO_2$-carbonic acid-carbonate system: a modeling approach. *Aquat. Geochem.* 17, 749–773. doi: 10.1007/s10498-011-9146-z

Lewis, E., and Wallace, D. W. (1998). *Program Developed for $CO_2$ System Calculations*. Oak Ridge, Ten: Oak Ridge National Laboratory.

Li, W., Gao, K., and Beardall, J. (2012). Interactive effects of ocean acidification and nitrogen-limitation on the diatom *Phaeodactylum tricornutum*. *PLoS One* 7:e51590. doi: 10.1371/journal.pone.0051590

Liu, N., Beardall, J., and Gao, K. (2017). Elevated $CO_2$ and associated seawater chemistry do not benefit a model diatom grown with increased availability of light. *Aquat. Microb. Ecol.* 79, 137–147. doi: 10.3354/ame01820

Luo, Y.-W., Shi, D., Kranz, S. A., Hopkinson, B. M., Hong, H., Shen, R., et al. (2019). Reduced nitrogenase efficiency dominates response of the globally important nitrogen fixer *Trichodesmium* to ocean acidification. *Nat. Commun.* 10:1521. doi: 10.1038/s41467-019-09554-7

Marañón, E. (2015). Cell size as a key determinant of phytoplankton metabolism and community structure. *Ann. Rev. Mar. Sci.* 7, 241–264. doi: 10.1146/annurev-marine-010814-015955

Martin, C. L., and Tortell, P. D. (2008). Bicarbonate transport and extracellular carbonic anhydrase in marine diatoms. *Physiol. Plant.* 133, 106–116. doi: 10.1111/j.1399-3054.2008.01054.x

Matsui, H., Hopkinson, B. M., Nakajima, K., and Matsuda, Y. (2018). Plasma membrane-type aquaporins from marine diatoms function as $CO_2$/$NH_3$ channels and provide photoprotection. *Plant Physiol.* 178, 345–357. doi: 10.1104/pp.18.00453

McMinn, A., Muller, M. N., Martin, A., and Ryan, K. G. (2014). The response of Antarctic sea ice algae to changes in pH and $CO_2$. *PLoS One* 9:e86984. doi: 10.1371/journal.pone.0086984

Menden-Deuer, S., and Lessard, E. J. (2000). Carbon to volume relationships for dinoflagellates, diatoms, and other protist plankton. *Limnol. Oceanogr.* 45, 569–579. doi: 10.4319/lo.2000.45.3.0569

Milligan, A. J., Mioni, C. E., and Morel, F. M. M. (2009). Response of cell surface pH to $pCO_2$ and iron limitation in the marine diatom *Thalassiosira weissflogii*. *Mar. Chem.* 114, 31–36. doi: 10.1016/j.marchem.2009.03.003

Mizuno, M. (1991). Influence of cell-volume on the growth and size-reduction of marine and estuarine diatoms. *J. Phycol.* 27, 473–478. doi: 10.1111/j.0022-3646.1991.00473.x

Mouw, C. B., Barnett, A., McKinley, G. A., Gloege, L., and Pilcher, D. (2016). Phytoplankton size impact on export flux in the global ocean. *Glob. Biogeochem. Cycles* 30, 1542–1562. doi: 10.1002/2015gb005355

Nagata, T. (2000). "Production mechanisms of dissolved organic matter," in *Microbial Ecology of the Oceans*, ed. D. L. Kirchman (New York: Wiley-Liss), 121–152.

Nelson, D. M., Treguer, P., Brzezinski, M. A., Leynaert, A., and Queguiner, B. (1995). Production and dissolution of biogenic silica in the ocean - revised global estimates, comparison with regional data and relationship to biogenic sedimentation. *Glob. Biogeochem. Cycles* 9, 359–372. doi: 10.1029/95gb01070

Orr, J. C., Fabry, V. J., Aumont, O., Bopp, L., Doney, S. C., Feely, R. A., et al. (2005). Anthropogenic ocean acidification over the twenty-first century and its impact on calcifying organisms. *Nature* 437, 681–686. doi: 10.1038/nature04095

Raven, J. A. (1991). Physiology of inorganic C acquisition and implications for resource use efficiency by marine phytoplankton: relation to increased $CO_2$ and temperature. *Plant Cell Environ.* 14, 779–794. doi: 10.1111/j.1365-3040.1991.tb01442.x

Raven, J. A., Cockell, C. S., and De La Rocha, C. L. (2008). The evolution of inorganic carbon concentrating mechanisms in photosynthesis. *Philos. Trans. R. Soc. B* 363, 2641–2650. doi: 10.1098/rstb.2008.0020

Raven, J. A., Kübler, J. E., and Beardall, J. (2000). Put out the light, and then put out the light. *J. Mar. Biol. Assoc. UK* 80, 1–25. doi: 10.1017/S0025315499001526

Reinfelder, J. R. (2011). Carbon concentrating mechanisms in eukaryotic marine phytoplankton. *Ann. Rev. Mar. Sci.* 3, 291–315. doi: 10.1146/annurev-marine-120709-142720

Reiskind, J. B., Beer, S., and Bowes, G. (1989). Photosynthesis, photorespiration and ecophysiological interactions in marine macroalgae. *Aquat. Bot.* 34, 131–152. doi: 10.1016/0304-3770(89)90053-3

Sabine, C. L., Feely, R. A., Gruber, N., Key, R. M., Lee, K., Bullister, J. L., et al. (2004). The oceanic sink for anthropogenic $CO_2$. *Science* 305, 367–371.

Sarthou, G., Timmermans, K. R., Blain, S., and Tréguer, P. (2005). Growth physiology and fate of diatoms in the ocean: a review. *J. Sea Res.* 53, 25–42. doi: 10.1016/j.seares.2004.01.007

Shi, D., Hong, H., Su, X., Liao, L., Chang, S., and Lin, W. (2019). The physiological response of marine diatoms to ocean acidification: differential roles of seawater $pCO_2$ and pH. *J. Phycol.* 55, 521–533. doi: 10.1111/jpy.12855

Siegel, D. A., Buesseler, K. O., Behrenfeld, M. J., Benitez-Nelson, C. R., Boss, E., Brzezinski, M. A., et al. (2016). Prediction of the export and fate of global ocean net primary production: the EXPORTS science plan. *Front. Mar. Sci.* 3:22. doi: 10.3389/fmars.2016.00022

Siegel, D. A., Buesseler, K. O., Doney, S. C., Sailley, S. F., Behrenfeld, M. J., and Boyd, P. W. (2014). Global assessment of ocean carbon export by combining satellite observations and food-web models. *Glob. Biogeochem. Cycles* 28, 181–196. doi: 10.1002/2013gb004743

Snoeijs, P., Busse, S., and Potapova, M. (2002). The importance of diatom cell size in community analysis. *J. Phycol.* 38, 265–281. doi: 10.1046/j.1529-8817.2002.01105.x

Sultemeyer, D., and Rinast, K. A. (1996). The $CO_2$ permeability of the plasma membrane of *Chlamydomonas reinhardtii*: mass-spectrometric $^{18}O$-exchange measurements from $^{13}C^{18}O_2$ in suspensions of carbonic anhydrase-loaded plasma-membrane vesicles. *Planta* 200, 358–368.

Sun, J., Hutchins, D. A., Feng, Y., Seubert, E. L., Caron, D. A., and Fu, F.-X. (2011). Effects of changing $pCO_2$ and phosphate availability on domoic acid production and physiology of the marine harmful bloom diatom *Pseudo-nitzschia multiseries*. *Limnol. Oceanogr.* 56, 829–840. doi: 10.4319/lo.2011.56.3.0829

Tatters, A. O., Fu, F.-X., and Hutchins, D. A. (2012). High $CO_2$ and silicate limitation synergistically increase the toxicity of *Pseudo-nitzschia fraudulenta*. *PLoS One* 7:e32116. doi: 10.1371/journal.pone.0032116

Taylor, A. R., Brownlee, C., and Wheeler, G. L. (2012). Proton channels in algae: reasons to be excited. *Trends Plant Sci.* 17, 675–684. doi: 10.1016/j.tplants.2012.06.009

Tortell, P. D., Payne, C., Gueguen, C., Strzepek, R. F., Boyd, P. W., and Rost, B. (2008). Inorganic carbon uptake by Southern Ocean phytoplankton. *Limnol. Oceanogr.* 53, 1266–1278. doi: 10.4319/lo.2008.53.4.1266

Tréguer, P. J., and De La Rocha, C. L. (2013). The world ocean silica cycle. *Ann. Rev. Mar. Sci.* 5, 477–501. doi: 10.1146/annurev-marine-121211-172346

Wirtz, K. W. (2011). Non-uniform scaling in phytoplankton growth rate due to intracellular light and CO2 decline. *J. Plankton Res.* 33, 1325–1341. doi: 10.1093/plankt/fbr021

Wolf-Gladrow, D., and Riebesell, U. (1997). Diffusion and reactions in the vicinity of plankton: a refined model for inorganic carbon transport. *Mar. Chem.* 59, 17–34. doi: 10.1016/S0304-4203(97)00069-8

Wu, Y., Campbell, D. A., Irwin, A. J., Suggett, D. J., and Finkel, Z. V. (2014). Ocean acidification enhances the growth rate of larger diatoms. *Limnol. Oceanogr.* 59, 1027–1034. doi: 10.4319/lo.2014.59.3.1027

Young, J. N., Heureux, A. M. C., Sharwood, R. E., Rickaby, R. E. M., Morel, F. M. M., and Whitney, S. M. (2016). Large variation in the Rubisco kinetics of diatoms reveals diversity among their carbon-concentrating mechanisms. *J. Exp. Bot.* 67, 3445–3456. doi: 10.1093/jxb/erw163

**Conflict of Interest:** The authors declare that the research was conducted in the absence of any commercial or financial relationships that could be construed as a potential conflict of interest.

**Publisher's Note:** All claims expressed in this article are solely those of the authors and do not necessarily represent those of their affiliated organizations, or those of the publisher, the editors and the reviewers. Any product that may be evaluated in this article, or claim that may be made by its manufacturer, is not guaranteed or endorsed by the publisher.

frontiers | Frontiers in Marine Science

ORIGINAL RESEARCH
published: 03 June 2022
doi: 10.3389/fmars.2022.901096

# Effects of Temperature on the Bioenergetics of the Marine Protozoans *Gyrodinium dominans* and *Oxyrrhis marina*

*Albert Calbet*[1*], *Rodrigo Andrés Martínez*[1,2], *Enric Saiz*[1] *and Miquel Alcaraz*[1†]

[1] Institut de Ciències del Mar, CSIC, Barcelona, Spain, [2] Instituto de Fomento Pesquero (IFOP), Puerto Montt, Chile

We exposed *Gyrodinium dominans* and two strains of *Oxyrrhis marina* to temperatures well above (25°C) and below (12°C) their maintenance temperature (18°C) to study the mechanisms controlling the overall physiological response to thermal stress. As variables, we measured growth, ingestion, and respiration rates (this latter with and without food). The growth rates of *O. marina* strains plotted as a function of temperature showed maximum values at the maintenance temperature, as expected in a typical unimodal functional response. However, *G. dominans* showed similar growth rates at 12 and 18°C, and even a marked decrease in growth rates at 25°C, happened to be not significant. *G. dominans* ingestion rates were not significantly different at all temperatures (although apparently decreased at 25°C), whereas both *O. marina* strains showed higher ingestion rates at 18°C. The respiration rates of *G. dominans* were unaffected by temperature, but those of *O. marina* strains increased with temperature. The specific dynamic action (respiration increase produced by feeding activity) ranged from 2 to 20% of the daily carbon ingestion for all organisms investigated. The calculated energetic budget indicated that the responses to temperature were diverse, even between in strains of the same species. *G. dominans* maintained similar growth at all temperatures by balancing metabolic gains and losses. In *O. marina* strains, on the other hand, the decrease in growth rates at the lowest temperature was driven mainly by reduced ingestion rates. However, increased respiration seemed the primary factor affecting the decrease in growth rates at the highest temperature. These results are discussed in the light of previous studies and on its suitability to understand the response of wild organisms to fluctuations in temperature.

**Keywords: growth, grazing, respiration, specific dynamic action, energetic budget, temperature, *Gyrodinium dominans*, *Oxyrrhis marina***

OPEN ACCESS

***Edited by:***
*Jun Sun,*
*China University of Geosciences Wuhan, China*

***Reviewed by:***
*Andrew J. Irwin,*
*Dalhousie University, Canada*
*Se Hyeon Jang,*
*Chonnam National University, South Korea*
*Wonho Yih,*
*Kunsan National University, South Korea*

***Correspondence:**
*Albert Calbet*
*acalbet@icm.csic.es*

[†]*Deceased*

***Specialty section:***
*This article was submitted to Aquatic Microbiology, a section of the journal Frontiers in Marine Science*

***Received:*** *21 March 2022*
***Accepted:*** *09 May 2022*
***Published:*** *03 June 2022*

***Citation:***
*Calbet A, Martínez RA, Saiz E and Alcaraz M (2022) Effects of Temperature on the Bioenergetics of the Marine Protozoans Gyrodinium dominans and Oxyrrhis marina. Front. Mar. Sci. 9:901096. doi: 10.3389/fmars.2022.901096*

## INTRODUCTION

Temperature is a key variable affecting most physiological rates of all organisms (Huey and Kingsolver, 1989; Alcaraz et al., 2014; Sinclair et al., 2016). Thus, climate-driven distribution shifts of microplankton, copepod species, and fish have been related to their different thermal sensitivities (Helaouët and Beaugrand, 2007; Takasuka et al., 2008; Wilson et al., 2015). Usually, the changes in

survival and physiological rates of an organism due to temperature are represented by a unimodal function (Huey and Kingsolver, 1989; Schulte et al., 2011; Alcaraz et al., 2014; Sinclair et al., 2016), commonly shaped by a progressive increase up to a peak (optimum temperature) from where the decline is more or less abrupt (Van Der Have, 2002; Angilletta, 2006; Sinclair et al., 2016). This graphical representation of the changes in an organism physiology with temperature is the result of the coupling/uncoupling among the different thermal sensitivities of key ecophysiological activities (e.g., feeding, respiration, assimilation, excretion, molting, growth; Alcaraz et al., 2014; Saiz et al., 2022). Thus, understanding how the uncoupling between physiological rates ultimately translates into growth and survival is crucial in predicting organisms' responses to temperature (Pörtner, 2002; Pörtner and Farrell, 2008; Alcaraz et al., 2014).

For marine protozoans, while the effects of temperature on vital rates are well studied (Hansen et al., 1997; Montagnes et al., 2003; Rose and Caron, 2007), the subjacent processes behind this response are poorly investigated (Kimmance et al., 2006). Marine protozoans, also referred to as microzooplankton, are key components of the marine pelagic food webs because of their role as the main link between primary producers (daily consuming ca. 75% of the oceans' overall phytoplankton primary production) and higher trophic levels (Calbet, 2001; Calbet and Saiz, 2005; Schmoker et al., 2013), and because their relevance as remineralizers of inorganic nutrients, supporting regenerated primary production (Ikeda et al., 1982; Alcaraz et al., 1994; Alcaraz et al., 1998). Because of these functions in the marine ecosystem, and considering the threat of global change, it is crucial to gather a deeper understanding of how temperature affects the different physiological rates. Only with a better knowledge of these processes we will be able to conduct accurate predictions about the performance, fate, and role in the ecosystem of the different species that assemble marine microzooplankton. In this respect, it will be under thermal stress where the different process rates, with different Arrhenius breakpoints (Alcaraz et al., 2014), may become uncoupled, resulting in overall detrimental effects on growth rates. We can hypothesize that the mechanisms acting at each side of the equilibrium temperature, at which species are adapted, may be different. Given the exponential nature of the relationship between temperature and respiration activity ($Q_{10}$ concept; e.g., Caron et al., 1986; López-Urrutia et al., 2006) and the physiological upper bounds for ingestion (Aelion and Chisholm, 1985; Kimmance et al., 2006), we can hypothesize that respiration rates will mostly drive the resulting growth rates at high temperatures. At lower temperatures, on the other hand, both respiration and ingestion rates find zero at their lower bound, and it will be the different $Q_{10}$ of both rates the ones depicting the overall growth response.

To demonstrate this hypothesis, we designed a series of experiments that simultaneously compared the physiological responses of three marine heterotrophic protozoans (*Gyrodinium dominans*, and two strains of *Oxyrrhis marina* originated from different locations) at their maintenance temperature (18°C) with those at 12 and 25°C. We chose these temperatures to be apart enough to theoretically show different physiological responses (Calbet and Saiz, 2022), being within reasonable limits of the temperature fluctuation likely experienced by the species in nature (Estrada et al., 1993; Calbet et al., 2015; Hobday et al., 2016; Oliver et al., 2018).

# METHODS

## The Cultures

As experimental organisms we used one strain of *Gyrodinium dominans* isolated by H.H. Jakobsen in 1996 from the northern part of Øresund (Denmark; Hansen and Daugbjerg, 2004), one strain of *Oxyrrhis marina* MED isolated by A. Calbet off Barcelona coast (NW Mediterranean) in 1996, and one strain *O. marina* CRB (purchased from the SCCAP Denmark; code SCCAP-0592) that originates from the Great Bay Salt Pond in St Maarten (Dutch Caribbean). All were kept in autoclaved 0.2-µm filtered seawater with added trace metals and EDTA (0.003 mL of f/2 metal stock solution per liter of suspension, Guillard1975), at 18°C and 38 salinity, under dim light and fed with *Rhodomonas salina.* The strains that originated from places with different temperatures and salinity from our laboratory standard conditions (Mediterranean waters) had been gradually adjusted for months. The prey, *R. salina* strain K-0294 (RHO; range ESD: 6.3-6.5 µm), was obtained from the Scandinavian Culture Collection of Algae and Protozoa at the University of Copenhagen, and it has been growing in our laboratory for years. The prey were kept in f/2 medium (Guillard, 1975), under exponential growth conditions, at 18°C, 38 salinity, 100-200 µE $m^{-2}$ $s^{-1}$, and a light:dark cycle of 12h.

## The Experimental Setup

We concurrently estimated the protozoan growth, ingestion, and respiration rates from the same incubation bottles incubated at 12, 18, and 25°C, being 18°C the maintenance temperature for all the cultures. Prior to the experiments, the grazers were kept in 2-4 L Pyrex glass bottles fed ad libitum with *R. salina* at their maintenance temperature (18°C). We calculated the amount of prey offered on the last day of feeding to be mostly depleted after 24h. Then, we gently concentrated the dinoflagellates by gravity filtration through a 3-µm polycarbonate filter to remove the excess of bacteria and detritus, re-suspended them in 0.2-µm filtered seawater, and pre-conditioned them (without food) for 24 hours to the experimental temperature (12, 18 and 25°C). All incubations were conducted in quadruplicate 130 mL Pyrex glass bottles, in darkness, at 16, 18, and 25°C (in temperature-controlled incubator baths), and lasted for 24 hours. Dinoflagellate density in the incubations was ca. 3000-4000 ind $mL^{-1}$. In the treatments with food, *R. salina* was added at a concentration of ca. 100000 cells $mL^{-1}$ to ensure saturated food conditions (Calbet et al., 2013). In parallel, we set suspensions only with the prey at the same concentration as the previous one (grazer + prey) to serve as controls for the

growth of the algae. We added 10 mL of f/2 per liter of suspension (i.e., a final nutrient concentration equivalent to f/200) to override microzooplankton excretion effects on the algae. The concentrations and cellular volumes of prey and grazer were estimated with a Multisizer III particle counter. To calculate grazing rates and average prey concentrations, we used Frost's equations (Frost, 1972), and *per capita* values were calculated using the average concentration of grazers in each replicate (Heinbokel, 1978). The corresponding volume to carbon (C) equivalence was obtained from Calbet et al. (2013), which provides elemental content/volume for the same strains in similar degree of starvation as in our treatments (Table 5 of Calbet et al., 2013).

Oxygen concentration was monitored using optical oxygen sensors (Oxygen Dipping Probe DP-PSt3, Presens®), at a measuring frequency of 15 min, with a setup similar to the one described in Almeda et al. (2011). The respiration activity of the three dinoflagellates was measured in the presence and in the absence of food. The previously described control bottles with only *R. salina* were used to account for changes in oxygen concentration due to the presence of prey alone, whereas an additional set of bottles filled with only 0.2 μm filtered seawater served as background control. In the case of both the prey and the grazers incubated alone in filtered seawater, oxygen consumption rates (μmol $O_2$ $d^{-1}$) were estimated as the slopes of the linear regression equations relating incubation time and dissolved oxygen concentration, after correcting for any changes in dissolved $O_2$ observed in the extra bottles with only filtered seawater. Cell-specific respiration rates (μmol $O_2$ $cell^{-1}$ $d^{-1}$) were then calculated by dividing the experimental oxygen consumption rates per bottle by the average cell concentration during the incubation.

In the case of the grazers incubated with prey, the oxygen consumption observed in the bottles resulted from the combined respiration of the grazers (heterotrophic dinoflagellates) and the prey. For this reason, before calculating the actual per capita consumption by the feeding dinoflagellates, we had to subtract the decline in oxygen concentration (incubations were in darkness) due to the presence of *R. salina*. To do so, we first determined the *R. salina* growth rates based on the initial and final cell concentrations using an exponential growth model; then, we estimated the average cell concentrations at each oxygen-measurement time interval. Next, we applied the cell-specific *R. salina* respiration rates from the incubations in filtered seawater to the actual *R. salina* concentration in the grazing bottles, estimated at each measuring time interval, and computed the expected oxygen concentration decrease in the incubations with feeding grazers due to the presence of *R. salina*. We then subtracted the oxygen consumption by *R. salina* from the time series of oxygen concentrations in the incubation bottles with the mixture of predator and prey, and estimated the oxygen respiration rates of the feeding dinoflagellates from the slope of changes in the remaining dissolved oxygen through time. The per capita respiration rate of the dinoflagellates under the presence of food was calculated taking into account the mean number of dinoflagellates incubated assuming exponential growth.

To calculate $Q_{10}$ coefficients, we first conducted a simple linear regression analysis between the inverse of temperature (1/T, in Kelvin degrees) and the natural logarithm of the carbon-specific physiological rate (i.e., the Arrhenius plot). Then, the activation energy was calculated from the slopes of the linear fit as Ea = –slope x R, where R is the universal gas constant (8.3145 J $mol^{-1}$ $K^{-1}$). Finally, $Q_{10}$ coefficients were calculated from Ea as $Q_{10} = \exp(Ea/R \times 10/T_m^2)$, where $T_m$ is the mean for the range of temperatures over which the organisms have been exposed (i.e., between 12 and 25°C) (Raven and Geider, 1988).

The oxygen consumption rates were converted into C losses using a respiratory quotient of 0.97 (Omori and Ikeda, 1984). Gross-growth efficiency (GGE) was calculated as in Kiørboe et al. (1985), dividing the growth rates by the ingestion rates in specific C units and expressed as percentage. Assimilation efficiency (AE) was calculated as $AE = 100 \times (\mu_C+R_C)/I_C$ (where $\mu_C$ and $I_C$ are the C-specific growth and ingestion rates, respectively, and $R_C$ is the respiratory carbon losses also expressed as C specific; Kiørboe et al., 1985). Specific dynamic action (SDA; the increase of respiration rates produced in the presence of food) was calculated as the difference between C-specific respiratory losses between feeding and non-feeding grazers, and expressed as % of C ingested daily.

# RESULTS

## Growth and Ingestion Rates, and Gross-Growth Efficiency

The growth rates of *G. dominans* were not significantly different at any of the temperatures tested (ANOVA and Tukey's test), although the rates dropped to less than half at 25°C (**Figure 1A**). *O. marina* MED showed growth rates higher at 18°C, and reduced at 12°C (albeit not significantly different from 18°C, Tukey's test) and 25°C ($p<0.01$, **Figure 1A**). In the case of *O. marina* CRB, 12°C drastically decreased the growth rates to negative values (mortality); on the other hand, at 18°C the growth rates were reasonably high (more than one doubling per day), while they dropped significantly at 25°C (ANOVA, Tukey's test, $p<0.01$; **Figure 1A**).

All the strains studied showed a similar pattern of ingestion rates, with peaks at 18°C and lower rates at 12 and 25°C (**Figure 1B**). However, only *O. marina* strains showed significant differences in ingestion rates between temperatures (ANOVA, Tukey's tests, $p<0.01$). Regarding GGE, there was a tendency to be inversely related to temperature for *G. dominans* and *O. marina* MED, but it was not statistically significant due to the high associated error (**Figure 1C**). There were significant differences for *O. marina* CRB, between the GGE at 12°C (zero because of the lack of growth at this temperature) and the rest of the values at higher temperatures (ANOVA, Tukey's tests, $p<0.01$; **Figure 1C**).

## Respiratory Activity

The respiration rates of *G. dominans* were not significantly different at the temperatures investigated, neither for starved

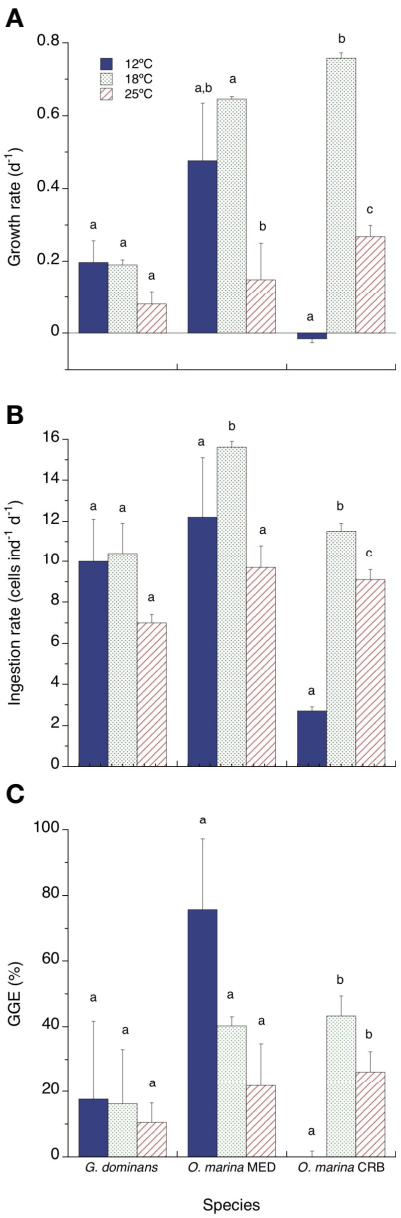


**FIGURE 1** | Growth rates (**A**, $d^{-1}$), ingestion rates (**B**, cells $ind^{-1}$ $d^{-1}$) and growth gross efficiencies (**C**, GGE %) of the three protozoans investigated at 12, 18 and 25°C. Statistical differences ($p<0.05$) within each species are indicated by different letters. The error bars are SE. For GGE, the SE have been calculated using the square root formula for error propagation.

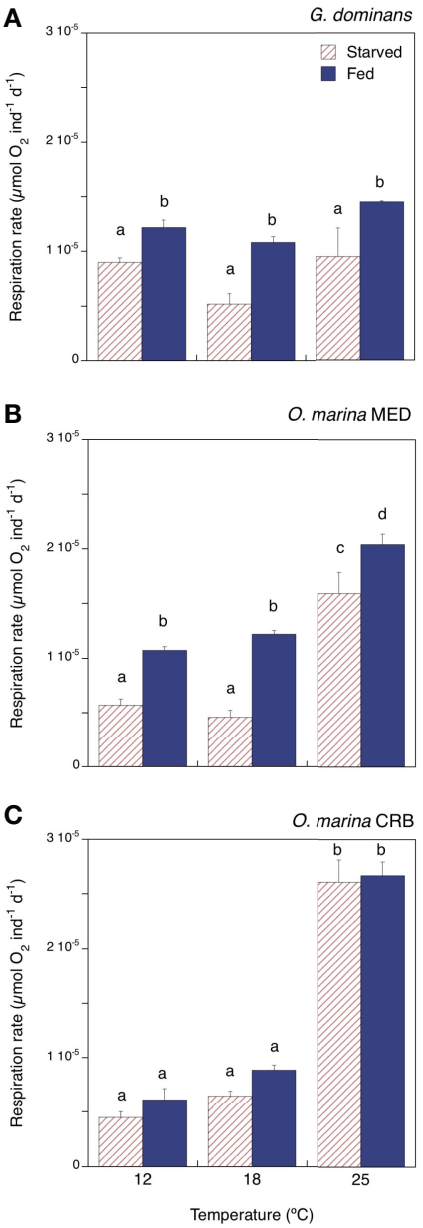


**FIGURE 2** | Respiration rates (µmol $O_2$ $ind^{-1}$ $d^{-1}$) of starved and fed **(A)** *G dominans*, **(B)** *O. marina* MED, and **(C)** *O. marina* CRB at the different temperatures investigated. Statistical differences ($p<0.05$) within each species are indicated by different letters. The error bars are SE.

nor for fed organisms (**Figure 2A**; Two-way ANOVA, Tukey's tests). However, respiration rates of this species with food were always significantly higher than those without food (**Figure 2A**; Two-way ANOVA, $p< 0.001$). *O. marina* MED respiration rates were significantly different between starved and fed organisms, and the rates at 12 and 18°C were different from those at 25°C, both in starving and fed treatments (Two-way ANOVA, Tukey's test, $p<0.001$; **Figure 2B**). The respiration rates for starving and fed *O. marina* CRB were not statistically different (Two-way ANOVA; **Figure 2B**), and within treatment, the rates were different between 12 and 25°C and between 18 and 25°C (Tukey's test, $p<0.001$; **Figure 2C**).

The respiratory activity of the grazers under starving conditions rendered 8 to 82% of the C biomass respired daily, the highest for *O. marina* CRB at 25°C and the lowest for *O. marina* MED at 12°C (**Table 1**). The metabolic cost associated with the feeding process (SDA) ranged from 2 to 20% of the C ingested, with the maximum

for *G. dominans* at 25°C, and the minimum for *O. marina* CRB at the same temperature (**Table 1**). *G. dominans* showed an increase of SDA with temperature, whereas in *O. marina* strains this pattern was not evident. In the case of *O. marina* CRB, we provide SDA values in **Table 1**, even if the presence of food during the incubations did not significantly enhance respiratory activity. The $Q_{10}$ values of the respiration rates between 12 and 25°C for starved and fed organisms are also provided in **Table 1**. *G. dominans* was the species showing the lowest $Q_{10}$ coefficients; *O. marina* MED showed intermedium values, with $Q_{10}$ higher for starved organisms than for fed ones (**Table 1**). Overall, the maximum $Q_{10}$ found in the study corresponded to *O. marina* CRB starved, followed by fed organisms.

## Energetic Budget

The allocation of the C ingested per organism and temperature is presented in **Table 2**. Approximately half of the C ingested (46-69%, depending on temperature) was assimilated by *G. dominans*. From the C biomass incorporated per day, roughly 2/3 were respired at 12 and 18°C (85% at 25°C), and 15-36% was converted into somatic growth at all temperatures (**Table 2**). *O. marina* MED assimilated nearly all C ingested at the highest and lowest temperatures (approx. 60% at 18°C; **Table 2**), incorporating an equivalent to about its biomass per day at 18°C and half of it at the highest and lowest temperatures. Only 25-35% of the C assimilated was respired at 12 and 18°C, and 73% at 25°C. The remaining C was allocated to growth (**Table 2**). Finally, the combination of ingestion rates and assimilation efficiencies of *O. marina* CRB resulted in daily C incorporations equivalent to, and even slightly more than, its C biomass at 18 and 25°C, but this quantity reduced to 16% of its biomass at 12°C. The low amount of C ingested at 12°C by this protozoan was respired completely, about 1/3 was respired at 18° C, and a about 82% at 25°C. The C used for growth was lower at 25° C compared to 18°C (**Table 2**).

To stress the relative effects of temperature on the different physiological rates, we show in **Figure 3** a graphical summary of the results presented in **Figures 1**, **2**. This figure does not intend to report the effects of temperature on the different rates again, but to provide a snapshot of the magnitude and sign of the effects of low and high temperatures on the different physiological variables measured, compared to those at 18°C. This analysis will be instrumental to understand each variable's weight in explaining the effects on growth rates due to temperature changes. *G. dominans* was the species showing the lowest effects of temperature, these being only evident (although not significant) at 25°C. *O. marina* CRB is the species showing larger variations in the different physiological rates with temperature variations, particularly at 25°C (**Figure 3C**). In general, ingestion rates are always negatively affected by higher and lower temperatures, compared to the control at 18°C, and respiration only clearly increases at 25°C (**Figure 3**). Regarding these two last variables, the effect of an increase of temperature on respiration rates is always more acute than that on ingestion rates for *O. marina* strains (**Figures 3B, C**); at the lowest temperature, the effect seems to be the opposite (**Figures 3B, C**). Finally, AEs are often increased when the temperature is higher and lower than 18°C.

With knowledge of the different physiological parameters of all species pooled together, we attempted to find relationships between specific ingestion rates, respiration rates, and growth rates ($d^{-1}$). We only found significant relationship for specific ingestion rates (ING) and growth rates (GR). The linear regression of this variable with growth rates explained 62% of the variance on growth rates (GR = 0.431 x ING - 0.126).

**TABLE 1** | Basal respiration of starved organisms as % of the cell carbon, specific dynamic action (SDA) as % of the carbon ingested, and $Q_{10}$ for starved and fed organisms at the three temperatures investigated.

| Species | Temperature (°C) | Basal respiration (% cell C) | SDA (% C ing) | $Q_{10}$ starved | $Q_{10}$ fed |
|---|---|---|---|---|---|
| *G. dominans* | 12 | 28.5 | 9.0 | 1.1 | 1.2 |
| | 18 | 16.4 | 15.2 | | |
| | 25 | 29.4 | 20.1 | | |
| *O. marina* MED | 12 | 8.3 | 11.5 | 2.3 | 1.7 |
| | 18 | 13.2 | 13.8 | | |
| | 25 | 31.3 | 13.0 | | |
| *O. marina* CRB | 12 | 11.5 | 17.2 | 3.9 | 3.1 |
| | 18 | 27.7 | 6.0 | | |
| | 25 | 82.4 | 1.7 | | |

**TABLE 2** | Metabolic balance of the three protozoans studied at the three selected temperatures.

| Species | Temp. (°C) | Ingested (% body C $d^{-1}$) | Assimilation efficiency (% ingested C) | C Assimilated (% body C $d^{-1}$) | Respired (% assimilated C $d^{-1}$) | Growth (% assimilated C $d^{-1}$) |
|---|---|---|---|---|---|---|
| *G. dominans* | 12 | 112.1 | 52.0 | 58.2 | 66.2 | 33.8 |
| | 18 | 116.7 | 45.5 | 53.1 | 64.2 | 35.8 |
| | 25 | 77.3 | 68.6 | 53.0 | 84.8 | 15.2 |
| *O. marina* MED | 12 | 63.0 | 100.0 | 63.0 | 24.6 | 75.4 |
| | 18 | 160.6 | 62.2 | 99.9 | 35.4 | 64.6 |
| | 25 | 68.2 | 80.8 | 55.1 | 72.9 | 27.1 |
| *O. marina* CRB | 12 | 24.1 | 64.9 | 15.7 | 100.0 | 0.0 |
| | 18 | 175.0 | 65.1 | 113.9 | 33.5 | 66.5 |
| | 25 | 102.1 | 100.0 | 102.1 | 82.4 | 26.2 |

*We provide data on specific ingestion rates, assimilation efficiency of the ingested carbon, amount of carbon assimilated, % of carbon respired out of the one assimilated, and % of the carbon assimilated allocated to growth.*

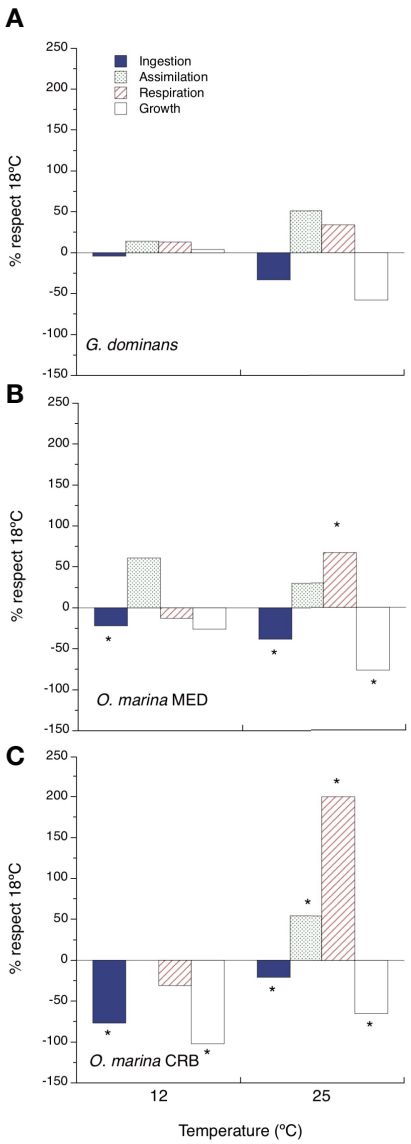


**FIGURE 3** | Relative effects of temperature on the metabolic balance. The figure shows the percentage of change respect to 18°C for different metabolic rates at 12 and 25°C. **(A)** *G dominans*, **(B)** *O. marina* MED, and **(C)** *O. marina* CRB. Asterisks indicate significant differences ($p<0.05$, ANOVA).

# DISCUSSION

## Unveiling the Processes Behind Growth at Different Temperatures

The main objective of this work was to shed light on the different metabolic processes acting under temperature stress in marine protozoans. To do so, we chose some representative species and exposed them to temperatures above and below that of maintenance. Overall, it seems the direct effects of temperature on ingestion rates are the major driver of growth in the species tested, but a closer look at the effects of temperature on both sides of the maintenance temperature gives some clues on the actual mechanisms taking place there.

*G. dominans* was the species less responsive to temperature changes. This protozoan was able to balance the variations in ingestion rates by modifying the assimilation efficiency (AE) and kept the respiration relatively stable despite the variations of temperature, balancing the metabolic gains and losses to maintain roughly similar growth at all the temperatures. For the *O. marina* strains, the adverse effects of both higher and lower temperatures were too strong to be dampened by increasing AE. In these strains, the decrease in growth rates at the lowest temperature was driven mainly by reduced ingesta. However, increased respiration was the primary factor affecting growth rates at the highest temperature. Interestingly, the growth of the Caribbean strain of *O. marina* (CRB) was more impaired by lower temperatures, whereas the Mediterranean one (MED) was more affected by higher temperatures. Also, Calbet et al. (2013) stressed the phenotypic differences between these strains in terms of feeding rates, gross growth efficiency (GGE), and biochemical composition. Our results point towards deeply rooted adaptations at each environment inhabited by the different strains of *O. marina* that were not modified by the long-term conditioning to our laboratory conditions. It can, then, be concluded that diversity among strains, originating from different habitats, can be as significant as species themselves when responding to temperature changes. Several authors also reached a similar conclusion for other variables and found significant differences in behavior, toxic capacity, and biochemical composition among different strains of dinoflagellates (Loret et al., 2002; Adolf et al., 2008; Calbet et al., 2011).

One variable that we did not consider relevant when placing our hypotheses was AE. We had previous knowledge that AE depended on ingestion rates; higher ingestions tended to lower the AE and the other way around (Kiørboe et al., 1985; Straile, 1997; Schmoker et al., 2011). We did not expect this variable to depend on temperature (Rogerson, 1981; Caron et al., 1986). We should keep in mind, however, that if AE is not directly measured but calculated based on ingestion, respiration, and growth rates, and these rates are dependent on temperature, a relationship between AE and temperature could theoretically arise. This was not our case, likely because of the opposite effects of ingestion and respiration on growth.

Specific Dynamic Action (SDA) was another important variable of our study for which we did not find a relationship with temperature, except for *G. dominans*. It was surprising that this energetic expenditure was not related to feeding because, theoretically, it results from feeding activity (Kiørboe et al., 1985). However, given the large number of physiological processes involved in the SDA energetic budget: feeding, digestion, absorption, biomass formation, etc. (Krebs and Allison, 1964; Bayne and Scullard, 1977; Tandler and Beamish, 1979), all of them with its particular response to temperature, it may well be any relationship between SDA and ingestion rates being masked by the effects of temperature. Actually, Kiørboe et al. (1985) suggested for marine copepods that SDA is largely

related to biosynthesis and transport, and that other processes, such as feeding, gut activity, amino acid oxidation, and excretion are of minor importance. SDA, therefore, represents the 'cost of growth' rather than the 'cost of feeding'.

## Previous Studies and a Caution Note on the Use of Biomass for Calculations

To our knowledge, there is no previous report including the many physiological rates for several protozoan species at various temperatures shown here. However, there are references to particular data to compare with ours. For instance, Calbet et al. (2013) reported comparable growth, grazing, and respiration rates at 18°C for the same species studied here. Likewise, they found similar AEs and GGEs. On the other hand, on a latter study with the same species adapted to 16, 19, and 22°C, Calbet and Saiz (2022) found slightly higher growth and ingestion rates. Schmoker et al. (2011) calculated the metabolic balance of *G. dominans* at 17°C under different food conditions. The growth, ingestion, and respiration rates found in that study were somehow higher than ours, but their estimated GGEs and AEs are within the range found here. Kimmance et al. (2006) exposed *O. marina* to different concentrations of prey (*Isochrysis galbana*) and temperatures. For well-fed organisms, they observed a bell-shaped response for specific growth rates, although with maximum around 25°C; this maximum shifted towards lower temperatures when food was not so abundant. Overall, their reported specific growth and ingestion rates were slightly higher than ours. Finally, the $Q_{10}$ values we report for respiration are within the average for marine protozoa (Verity, 1985; Caron et al., 1986). We did not find literature on SDA of protozoans, but our data fit well within the limits found for ectotherms (Kiørboe et al., 1985; Secor, 2009).

When comparing our results with previous reports, we should consider the distinct methodologies, strains, and previous history of the organisms used in the different experiments, which may introduce variability and explain some of the differences between studies. Therefore, perfect matches are not expected. Another source of variability between studies is found in the biomass assessment. For such purpose, it is common to use previously published volume-to-C relationships (e.g., Menden-Deuer and Lessard, 2000) or even simply take the average C contents per organism from other studies. As stated in the methods section, our calculations on metabolic budgets are based on volumetric conversion factors obtained for the same strains in our laboratory (Calbet et al., 2013). The selection of the conversion factors will undoubtedly affect the final data. Therefore, it is always advisable to conduct specific elemental content analyses for each particular experiment. We must be aware, however, of another important aspect seldom considered that relates to the C-conversion factors. Protozoans that show a certain degree of body plasticity tend to increase their volume when feeding (Calbet et al., 2013). This augmentation of the cellular volume could be misinterpreted as growth, but in fact it is produced by an accumulation of undigested prey in the cell vacuoles and not by an actual increase in the biomass of the grazer. For growth calculations, then, it is important to avoid using the volume of fed organisms, and rely only on cell abundance. If conversion to biomass is required, our advice is to use the biomass of the protozoans that have had time to empty the cell vacuoles (Calbet et al., 2013; Calbet and Saiz, 2022).

## Concluding Remarks: Are Our Results of Any Ecological or Predictive Use?

We have shown how the response of the different physiological rates to temperature is species- and strain-dependent. Despite so, some overall conclusions can be reached. It seems temperature-mediated effects on ingestion rates are relatively well translated into growth in marine protozooplankton. In this regard, ingestion rates seem to be driving the growth rates at lower-than-equilibrium temperatures. However, respiration rates appeared largely uncoupled at higher temperatures and are likely an important factor responsible for the observed decrease in growth rates.

Notwithstanding the effect we observed of high temperatures on the performance of protozooplankton, it is important to stress that our intention was not to address the effects of climate change on physiological rates of this group of organisms. For such purpose, long-term adaptations and narrower ranges of temperatures are advised (Calbet and Saiz, 2022). We limited our study to a narrow range of temperatures that the organisms could naturally experience. Oscillations of 5-6°C below and above a given temperature can be found in nature. For one side, in temperate and tropical seas, the differences between upper and lower layers of the thermocline can encompass (and surpass) such thermal gradient (Estrada et al., 1993; Calbet et al., 2015); vertical water masses displacements, eddies, and even vertical migration in some species may produce, then, these thermal exposures in short periods. Moreover, temperature rises of 1-5°C and durations of at least five consecutive days are expected during heatwave episodes (Hobday et al., 2016; Oliver et al., 2018). In the Mediterranean Sea, the increases are exceptionally high, 2-4°C, and are expected to increase in amplitude along with the water temperature rise due to climate change (Oliver et al., 2019). Therefore, even if not our original intention, the data presented in this study may help answering particular questions about the future effects of climate change on marine planktonic ecosystems.

# DATA AVAILABILITY STATEMENT

Publicly available datasets were analyzed in this study. This data can be found here: https://doi.org/10.20350/digitalCSIC/14561.

# AUTHOR CONTRIBUTIONS

AC and RM contributed to the conception and design of the study. RM conducted the experiments. All the authors contributed to the data analysis and interpretation of the results. AC wrote the manuscript and all the authors

contributed to the manuscript revision. All authors contributed to the article and approved the submitted version.

## FUNDING

This research was funded by Grant PID2020-118645RB-I00 by Ministerio de Ciencia e innovación (MCIN)/AEI/10.13039/501100011033 and by "ERDF A way of making Europe". The open access publication fee was partially covered by the CSIC Open Access Publication Support Initiative through its Unit of Information Resources for Research (URICI). It is a contribution of the Marine Zooplankton Ecology Group (2017 SGR 87). With the institutional support of the 'Severo Ochoa Centre of Excellence' accreditation (CEX2019-000928-S).

## ACKNOWLEDGMENTS

We thank Dr. H. H. Jakobsen for providing the strain of *G. dominans*, and the reviewers for greatly improving the manuscript with their comments.

## REFERENCES

Adolf, J. E., Bachvaroff, T., and Place, A. R. (2008). Can Cryptophyte Abundance Trigger Toxic Karlodinium Veneficum Blooms in Eutrophic Estuaries? *Harmful Algae* 8 (1), 119–128. doi: 10.1016/j.hal.2008.08.003

Aelion, C. M., and Chisholm, S. W. (1985). Effect of Temperature on Growth and Ingestion Rates of Favella Sp. *J. Plankton Res.* 7 (6), 821–830. doi: 10.1093/plankt/7.6.821

Alcaraz, M., Felipe, J., Grote, U., Arashkevich, E., and Nikishina, A. (2014). Life in a Warming Ocean: Thermal Thresholds and Metabolic Balance of Arctic Zooplankton. *J. Plankton Res.* 36, 3–10. doi: 10.1093/plankt/fbt111

Alcaraz, M., Saiz, E., and Estrada, M. (1994). Excretion of Ammonia by Zooplankton and its Potential Contribution to Nitrogen Requeriments for Primary Production in the Catalan Sea (NW Mediterranean). *Mar. Biol.* 119, 69–76. doi: 10.1007/BF00350108

Alcaraz, M., Saiz, E., Fernandez, J. A., Trepat, I., Figueiras, F., Calbet, A., et al. (1998). Antarctic Zooplankton Metabolism: Carbon Requirements and Ammonium Excretion of Salps and Crustacean Zooplankton in the Vicinity of the Bransfield Strait During January 1994. *J. Mar. Syst.* 17, 347–359. doi: 10.1016/S0924-7963(98)00048-7

Almeda, R., Alcaraz, M., Calbet, A., and Saiz, E. (2011). Metabolic Rates and Carbon Budget of Early Developmental Stages of the Marine Cyclopoid Copepod *Oithona Davisae*. *Limnol. Oceanogr.* 56 (1), 403–414. doi: 10.4319/lo.2011.56.1.0403

Angilletta, M. J. (2006). Estimating and Comparing Thermal Performance Curves. *J. Therm. Biol.* 31 (7), 541–545. doi: 10.1016/j.jtherbio.2006.06.002

Bayne, B. L., and Scullard, C. (1977). An Apparent Specific Dynamic Action of *Mytilus Edulis*. *J. Mar. Biol.* 57, 371–378. doi: 10.1017/S0025315400021810

Calbet, A. (2001). Mesozooplankton Grazing Effect on Primary Production: A Global Comparative Analysis in Marine Ecosystems. *Limnol. Oceanogr.* 46 (7), 1824–1830. doi: 10.4319/lo.2001.46.7.1824

Calbet, A., Agersted, M. D., Kaartvedt, S., Mohl, M., Moller, E. F., Enghoff-Poulsen, S., et al. (2015). Heterogeneous Distribution of Plankton Within the Mixed Layer and its Implications for Bloom Formation in Tropical Seas. *Sci. Rep.* 5, 11240. doi: 10.1038/srep11240

Calbet, A., Bertos, M., Fuentes-Grunewald, C., Alacid, E., Figueroa, R., Renom, B., et al. (2011). Intraspecific Variability in *Karlodinium Veneficum*: Growth Rates, Mixotrophy, and Lipid Composition. *Harmful Algae* 10 (6), 654–667. doi: 10.1016/j.hal.2011.05.001

Calbet, A., Isari, S., Martínez, R. A., Saiz, E., Garrido, S., Peters, J., et al. (2013). Adaptations to Feast and Famine in Different Strains of the Marine Heterotrophic Dinoflagellates *Gyrodinium Dominans* and *Oxyrrhis Marina*. *Mar. Ecol. Prog. Ser.* 483, 67–84. doi: 10.3354/meps10291

Calbet, A., and Saiz, E. (2005). The Ciliate-Copepod Link in Marine Ecosystems. *Aquat. Microb. Ecol.* 38 (2), 157–167. doi: 10.3354/ame038157

Calbet, A., and Saiz, E. (2022). Thermal Acclimation and Adaptation in Marine Protozooplankton and Mixoplankton. *Front. Microbiol.* 13. doi: 10.3389/fmicb.2022.832810

Caron, D. A., Goldman, J. C., and Dennett, M. R. (1986). Effect of Temperature on Growth, Respiration, and Nutrient Regeneration by an Omnivorous Microflagellate. *Appl. Environ. Microb.* 52 (6), 1340–1347. doi: 10.1128/aem.52.6.1340-1347.1986

Estrada, M., Marrasé, C., Latasa, M., Berdalet, E., Delgado, M., and Riera, T. (1993). Variability of Deep Chlorophyll Maximum Characteristics in the Northwestern Mediterranean. *Mar. Ecol. Prog. Ser.* 92, 289–300. doi: 10.3354/meps092289

Frost, B. W. (1972). Effects of Size and Concentration of Food Particles on the Feeding Behavior of the Marine Planktonic Copepod *Calanus Pacificus*. Limnol. *Oceanography* 17, 805–815. doi: 10.4319/lo.1972.17.6.0805

Guillard, R. R. L. (1975). "Culture of Phytoplankton for Feeding Marine Invertebrates," in *Culture of Marine Invertebrate Animals*. Eds. W. L. Smith and M. H. Chanley (New York: Plenum Press), 29–60.

Hansen, P. J., Bjornsen, P. K., and Hansen, B. W. (1997). Zooplankton Grazing and Growth: Scaling Within the 2-2,000- Mu M Body Size Range. *Limnol. Oceanogr.* 42 (4), 687–704. doi: 10.4319/lo.1997.42.4.0687

Hansen, G., and Daugbjerg, N. (2004). Ultrastructure of Gyrodinium Spirale, the Type Species of *Gyrodinium (dinophyceae)*, Including a Phylogeny of *G. dominans*, *G. rubrum* and *G. spirale* Deduced From Partial LSU rDNA Sequences. *Protist* 155, 271–294.

Heinbokel, J. F. (1978). Studies on the Functional Role of Tintinnids in He Southern California Bight. II. Grazing Rates of Field Populations. *Mar. Biol.* 47, 191–197. doi: 10.1007/BF00395639

Helaouët, P., and Beaugrand, G. (2007). Macroecology of *Calanus finmarchicus* and *C-helgolandicus* in the North Atlantic Ocean and Adjacent Seas. *Mar. Ecol. Prog. Ser.* 345, 147–165.

Hobday, A. J., Alexander, L. V., Perkins, S. E., Smale, D. A., Straub, S. C., Oliver, E. C. J., et al. (2016). A Hierarchical Approach to Defining Marine Heatwaves. *Prog. Oceanogr.* 141, 227–238. doi: 10.1016/j.pocean.2015.12.014

Huey, R. B., and Kingsolver, J. G. (1989). Evolution of Thermal Sensitivity of Ectotherm Performance. *Trends Ecol. Evol.* 4, 131–135. doi: 10.1016/0169-5347(89)90211-5

Ikeda, T., Carleton, J. H., Mitchell, A. W., and Dixon, P. (1982). Ammonia and Phosphate Excretion by Zooplankton From the Inshore Waters of the Great Barrier Reef. 2. Their *in Situ* Contributions to Nutrient Regeneration. *Aust. J. Mar. Freshwater Res.* 33 (4), 683–698. doi: 10.1071/MF9820683

Kiørboe, T., Mohlenberg, F., and Hamburger, K. (1985). Bioenergetics of the Planktonic Copepod *Acartia Tonsa*: Relation Between Feeding, Egg Production and Respiration and Composition of Specific Dynamic Action. *Mar. Ecol. Prog. Ser.* 26, 85–97. doi: 10.3354/meps026085

Kimmance, S., Atkinson, D., and Montagnes, D. J. S. (2006). Do Temperature-Food Interactions Matter? Responses of Production and its Components in the Model Heterotrophic Flagellate Oxyrrhis Marina. *Aquat. Microb. Ecol.* 42, 63–73. doi: 10.3354/ame042063

Krebs, H. A., and Allison, J. B. (1964). "The Metabolic Fate of Amino Acids," in *Mammalian Protein Metabolism*. Ed. H. N. Munro (London: Academic Press), 125–176.

López-Urrutia, A., San Martin, E., Harris, R. P., and Irigoien, X. (2006). Scaling the Metabolic Balance of the Oceans. *Proc. Natl. Acad. Sci. U. S. A.* 103 (23), 8739–8744. doi: 10.1073/pnas.0601137103

Loret, P., Tengs, T., Villareal, T. A., Singler, H., Richardson, B., McGuire, P., et al. (2002). No Difference Found in Ribosomal DNA Sequences From Physiologically Diverse Clones of *Karenia Brevis* (Dinophyceae) From the Gulf of Mexico. *J. Plankton Res.* 24 (7), 735–739. doi: 10.1093/plankt/24.7.735

Menden-Deuer, S., and Lessard, E. J. (2000). Carbon to Volume Relationships for Dinoflagellates, Diatoms, and Other Protist Plankton. *Limnol. Oceanogr.* 45 (3), 569–579. doi: 10.4319/lo.2000.45.3.0569

Montagnes, D. J. S., Kimmance, S. A., and Atkinson, D. (2003). Using $Q_{10}$: Can Growth Rates Increase Linearly With Temperature? *Aquat. Microb. Ecol.* 32 (3), 307–313. doi: 10.3354/ame032307

Oliver, E. C. J., Burrows, M. T., Donat, M. G., Sen Gupta, A., Alexander, L. V., Perkins-Kirkpatrick, S. E., et al. (2019). Projected Marine Heatwaves in the 21st Century and the Potential for Ecological Impact. *Front. Mar. Scien.* 6. doi: 10.3389/fmars.2019.00734

Oliver, E. C. J., Donat, M. G., Burrows, M. T., Moore, P. J., Smale, D. A., Alexander, L. V., et al. (2018). Longer and More Frequent Marine Heatwaves Over the Past Century. *Nat. Commun.* 9 (1), 1324. doi: 10.1038/s41467-018-03732-9

Omori, M., and Ikeda, T. (1984). *Methods in Marine Zooplankton Ecology* (New York: John Wiley and Sons: New York).

Pörtner, H. O. (2002). Climate Variations and the Physiological Basis of Temperature Dependent Biogeography: Systemic to Molecular Hierarchy of Thermal Tolerance in Animals. *Comp. Biochem. Physiol.* 132, 739–761. doi: 10.1016/S1095-6433(02)00045-4

Pörtner, H. O., and Farrell, A. P. (2008). Physiology and Climate Change. *Science* 322, 690–692. doi: 10.1126/science.1163156

Raven, J. A., and Geider, R. J. (1988). Temperature and Algal Growth. *New Phytol.* 110, 441–461. doi: 10.1111/j.1469-8137.1988.tb00282.x

Rogerson, A. (1981). The Ecological Energetics of *Amoeba Proteus* (Protozoa). *Hydrobiologia* 85 (2), 117. doi: 10.1007/BF00006621

Rose, J. M., and Caron, D. A. (2007). Does Low Temperature Constrain the Growth Rates of Heterotrophic Protists? Evidence and Implications for Algal Blooms in Cold Waters. *Limnol. Oceanogr.* 52 (2), 886–895. doi: 10.4319/lo.2007.52.2.0886

Saiz, E., Griffell, K., Olivares, M., Solé, M., Theodorou, I., and Calbet, A. (2022). Reduction in Thermal Stress of Marine Copepods After Physiological Acclimation. *J. Plankton Res.* doi: 10.1093/plankt/fbac017

Schmoker, C., Hernéndez-León, S., and Calbet, A. (2013). Microzooplankton Grazing in the Oceans: Impacts, Data Variability, Knowledge Gaps and Future Directions. *J. Plankton Res.* 35 (4), 691–706. doi: 10.1093/plankt/fbt023

Schmoker, C., Thor, P., Hernández-León, S., and Hansen, B. W. (2011). Feeding, Growth and Metabolism of the Marine Heterotrophic Dinoflagellate *Gyrodinium Dominans*. *Aquat. Microb. Ecol.* 65 (1), 65–73. doi: 10.3354/ame01533

Schulte, P. M., Healy, T. M., and Fangue, N. A. (2011). Thermal Performance Curves, Phenotypic Plasticity, and the Time Scales of Temperature Exposure. *Integr. Comp. Biol.* 51, 691–702.

Secor, S. M. (2009). Specific Dynamic Action: A Review of the Postprandial Metabolic Response. *J. Comp. Physiol. B.* 179 (1), 1–56. doi: 10.1007/s00360-008-0283-7

Sinclair, B. J., Marshall, K. E., Sewell, M. A., Levesque, D. L., Willett, C. S., Slotsbo, S., et al. (2016). Can We Predict Ectotherm Responses to Climate Change Using Thermal Performance Curves and Body Temperatures? *Ecol. Lett.* 19 (11), 1372–1385. doi: 10.1111/ele.12686

Straile, D. (1997). Gross Growth Efficiencies of Protozoan and Metazoan Zooplankton and Their Dependence on Food Concentration, Predator-Prey Weight Ratio, and Taxonomic Group. *Limnol. Oceanogr.* 42 (6), 1375–1385. doi: 10.4319/lo.1997.42.6.1375

Takasuka, A., Oozeki, Y., and Kubota, H. (2008). Multi-Species Regime Shifts Reflected in Spawning Temperature Optima of Small Pelagic Fish in the Western North Pacific. *Mar. Ecol. Prog. Ser.* 360, 211–217. doi: 10.3354/meps07407

Tandler, A., and Beamish, F. W. H. (1979). Mechanical and Biochemical Components of Apparent Specific Dynamic Action in Large Mouth Bass. *Muopterus Salmoides* Lacépède. *J. Fish Biol.* 14, 343–350. doi: 10.1111/j.1095-8649.1979.tb03529.x

Van Der Have, T. (2002). A Proximate Model for Thermal Tolerance in Ectotherms. *Oikos* 98, 141–155.

Verity, P. G. (1985). Grazing, Respiration, Excretion and Growth Rates of Tintinnids. *Limnol. Oceanogr.* 30, 1268–1282. doi: 10.4319/lo.1985.30.6.1268

Wilson, R. J., Speirs, D. C., Heath, M. R., Rlotti F, L., and Oceanography, V. P. (2015). On the Surprising Lack of Differences Between Two Congeneric Calanoid Copepod Species, *Calanus Finmarchicus* and C. Helgolandicus. *Progr. Oceanogr.* 134, 413–431. doi: 10.1016/j.pocean.2014.12.008

**Conflict of Interest:** The authors declare that the research was conducted in the absence of any commercial or financial relationships that could be construed as a potential conflict of interest.

**Publisher's Note:** All claims expressed in this article are solely those of the authors and do not necessarily represent those of their affiliated organizations, or those of the publisher, the editors and the reviewers. Any product that may be evaluated in this article, or claim that may be made by its manufacturer, is not guaranteed or endorsed by the publisher.

frontiers | Frontiers in Microbiology

ORIGINAL RESEARCH
published: 09 June 2022
doi: 10.3389/fmicb.2022.881048

# Hydrographic Feature Variation Caused Pronounced Differences in Planktonic Ciliate Community in the Pacific Arctic Region in the Summer of 2016 and 2019

*Chaofeng Wang[1,2,3†], Mengyao Yang[4†], Yan He[5], Zhiqiang Xu[2,6], Yuan Zhao[1,2,3], Wuchang Zhang[1,2,3*] and Tian Xiao[1,2,3]*

[1] CAS Key Laboratory of Marine Ecology and Environmental Sciences, Institute of Oceanology, Chinese Academy of Sciences, Qingdao, China, [2] Laboratory for Marine Ecology and Environmental Science, Qingdao National Laboratory for Marine Science and Technology, Qingdao, China, [3] Center for Ocean Mega-Science, Chinese Academy of Sciences, Qingdao, China, [4] College of Marine Life Sciences and Institute of Evolution and Marine Biodiversity, Ocean University of China, Qingdao, China, [5] First Institute of Oceanography, Ministry of Natural Resources, Qingdao, China, [6] Jiaozhou Bay Marine Ecosystem Research Station, Institute of Oceanology, Chinese Academy of Sciences, Qingdao, China

OPEN ACCESS

**Edited by:**
*Jun Sun,*
*China University of Geosciences Wuhan, China*

**Reviewed by:**
*Sophie Charvet,*
*American Museum of Natural History, United States*
*Ya-Wei Luo,*
*Xiamen University, China*

***Correspondence:**
*Wuchang Zhang*
*wuchangzhang@qdio.ac.cn*

*† These authors have contributed equally to this work and share first authorship*

**Specialty section:**
*This article was submitted to Aquatic Microbiology, a section of the journal Frontiers in Microbiology*

**Received:** *22 February 2022*
**Accepted:** *11 May 2022*
**Published:** *09 June 2022*

**Citation:**
*Wang C, Yang M, He Y, Xu Z, Zhao Y, Zhang W and Xiao T (2022) Hydrographic Feature Variation Caused Pronounced Differences in Planktonic Ciliate Community in the Pacific Arctic Region in the Summer of 2016 and 2019. Front. Microbiol. 13:881048. doi: 10.3389/fmicb.2022.881048*

Planktonic ciliates are an important component of microzooplankton, but there is limited understanding of their responses to changing environmental conditions in the Pacific Arctic Region. We investigated the variations of ciliate community structure and their relationships with environmental features in the Pacific Arctic Region in the summer of 2016 and 2019. The Pacific water was warmer and more saline in 2019 than in 2016. The abundance and biomass of total ciliate and aloricate ciliate were significantly higher in 2019 than those in 2016, while those of tintinnid were significantly lower. The dominant aloricate ciliate changed from large size-fraction (> 30 μm) in 2016 to small size-fraction (10–20 μm) in 2019. More tintinnid species belonging to cosmopolitan genera were found in 2019 than in 2016, and the distribution of tintinnid species (*Codonellopsis frigida*, *Ptychocylis obtusa*, and *Salpingella* sp.1) in 2019 expanded by 5.9, 5.2, and 8.8 degrees further north of where they occurred in 2016. The environmental variables that best-matched tintinnid distributions were temperature and salinity, while the best match for aloricate ciliate distributions was temperature. Therefore, the temperature might play a key role in ciliate distribution. These results provide basic data on the response of the planktonic ciliate community to hydrographic variations and implicate the potential response of microzooplankton to Pacification as rapid warming progresses in the Pacific Arctic Region.

**Keywords: planktonic ciliate, community structure, hydrographic variations, pacification, microzooplankton, Pacific Arctic Region**

## INTRODUCTION

The Pacific Arctic Region, extending from the northern Bering Sea into the Chukchi Sea and adjacent Arctic seas, is recognized as one of the region most sensitive to global climate changes (Grebmeier and Maslowski, 2014). In recent decades, rapid changes have been found in the Arctic, such as sea ice retreat (Stroeve et al., 2012), near-surface air temperature increase

(Screen and Simmonds, 2010), and increasing Pacific Inflow Water (Pacific water transport from the Bering Sea to the Arctic Ocean, including Alaskan Coastal Water, Bering Shelf Water, and Anadyr Water) (Woodgate, 2018; Lalande et al., 2021; Woodgate and Peralta-Ferriz, 2021). Pacific currents flow from the Bering Sea and transport plankton to the Arctic Ocean through the Bering Strait (Springer et al., 1996; Steele et al., 2004). A long-term increase in the annual mean transport of Pacific Inflow Water into the Arctic has been recorded in year-round, *in situ* Bering Strait mooring data, and this increase may bring more fresh water and heat fluxes into the Arctic Ocean (Woodgate and Peralta-Ferriz, 2021). As a major source of oceanic nutrients (Torres-Valdés et al., 2013), the Bering Strait through flow may also exert a profound effect on ecosystems in the Chukchi Sea, the western Arctic Ocean, and even in outflows in the Canadian Arctic Archipelago (Woodgate, 2018; Woodgate and Peralta-Ferriz, 2021).

The increasing Pacific Inflow Water has changed local hydrographic features in the Arctic Ocean and transported more Pacific-origin species into the Arctic: a process called Pacification (Woodgate, 2018; Polyakov et al., 2020). Studies on the Pacific Arctic Region Pacification have mainly focused on mesozooplankton and phytoplankton communities (Ershova et al., 2015; Wassmann et al., 2015; Hunt et al., 2016; Wang et al., 2018; Xu et al., 2018; Lewis et al., 2020; Wang Y. et al., 2020; Mueter et al., 2021; Zhuang et al., 2021). By analyzing mesozooplankton data from 1946 to 2012, Ershova et al. (2015) found that the distribution of Pacific copepods (*Eucalanus bungii*, *Metridia pacifica*, and *Neocalanus* spp.) in 2012 extend about 5 further north than in 1946. Wang Y. et al. (2020) found that Pacific-origin phytoplankton species can be transported into the Chukchi Sea. These results indicated that the pelagic ecosystem in the Pacific Arctic Region is experiencing rapid Pacification. Despite their important contribution to microzooplankton, there have not been any studies about the pacification of ciliate communities.

Taxonomically, planktonic ciliates belong to phylum Ciliophora, class Spirotrichea, subclass Oligotrichia, and Choreotrichia (Lynn, 2008), and morphologically consist of aloricate ciliate and tintinnid. Planktonic ciliates (belonging to microzooplankton) are primary consumers of pico- (0.2–2 μm) and nano- (2–20 μm) sized plankton and are important food items of metazoans and fish larvae (Stoecker et al., 1987; Dolan et al., 1999; Gómez, 2007). They play an important role in material circulation and energy flow from the microbial food web into the classical food chain (Azam et al., 1983; Pierce and Turner, 1992; Calbet and Saiz, 2005). Furthermore, ciliates have been widely used as a useful bioindicator of different water masses owing to their simple, short life cycle and sensitive response to environmental changes (Kato and Taniguchi, 1993; Kim et al., 2012; Jiang et al., 2013; Wang et al., 2021a, 2022a).

As for planktonic ciliates, Taniguchi (1984) found that aloricate ciliates and tintinnids were dominant taxa in the Bering Sea and Bering Strait, but their abundance showed increasing and decreasing trends from the Bering Sea to Bering Strait, respectively. Subsequent studies found a similar phenomenon and further realized that the Bering Sea, Bering Strait, and Arctic Ocean had their endemic species (Dolan et al., 2014, 2016; Wang et al., 2019). During the summer of 2020, Pacific species (*Salpingella* sp.1) had intruded into the Canada Basin with a higher abundance than Arctic endemic species (Wang et al., 2022a). These previous studies mainly researched ciliate (especially tintinnid) vertical distribution patterns and northward transported trends at a specific time. However, there are still no studies about planktonic ciliates community variations correlated with hydrographic features (temperature, salinity, and Chlorophyll-*a* concentrations) in different years.

As an important trophic link between mesozooplankton and phytoplankton, we hypothesize that the planktonic ciliate community in the Pacific Arctic Ocean is also experiencing rapid Pacification progress under environmental variations induced by global warming. By comparing environmental factors and planktonic ciliate community structure (e.g., abundance proportion of tintinnid to total ciliate, aloricate ciliate size-fraction, tintinnid richness, and latitudinal distribution variations) of 2016 and 2019 in this region, we aim to determine how variations in environmental factors affect ciliate communities. Our results will help monitor changes in the Pacific Arctic Ocean pelagic ecosystem in response to global warming.

# MATERIALS AND METHODS

## Study Area and Sample Collection

Sampling was conducted during two cruises performed from July 18 to September 10, 2016 (Transect A), during the 7th Chinese National Arctic Research Expedition aboard *R.V.* "Xuelong," and from August 24 to September 2, 2019 (Transects B), during the 10th Chinese National Arctic Research Expedition aboard *R.V.* "Xiangyanghong 01" from the Bering Sea to the Arctic Ocean (**Figure 1**). Water samples were collected at 45 stations (St.) along two transects (Tr.): Tr. A (Sts. 1–20) and B (Sts. 1–26) (**Figure 1** and **Supplementary Table 1**). Stations A1 to A5, A19, A20, B1 to B6, and B24 to B26 were located over depths exceeding 200 m (**Supplementary Table 1**). We treated A1 to A5, B1 to B6 as the Bering Sea stations, A19, A20, B24 to B26 as the Arctic Ocean stations, and A6 to A18 and B7 to B23 as the Bering Strait stations (depths shallower than 200 m).

Vertical profiles of temperature and salinity were obtained at each station from the surface (3 m) to the bottom (or 200 m, where the bottom is deeper than 200 m) using an SBE911-conductivity-temperature-depth (CTD) unit. Water samples were taken from three to eight depths (from surface to bottom or 200 m depth with stations deeper than 200 m) at each station using 12 L Niskin bottles attached to a rosette wheel of the CTD (sampling points). A total of 251 water samples (1 L) were collected for planktonic ciliate community structure analysis. Samples were fixed with acid Lugol's (1% final concentration) and stored in darkness at 4°C during the cruise. All the stations were free of sea ice. Chlorophyll *a* (Chl *a*) concentration was determined by filtering 500 mL of seawater through a Whatman GF/F glass fiber filter. Plankton retained on the filter was extracted in 90% ($vv^{-1}$) acetone. Fluorescence was measured

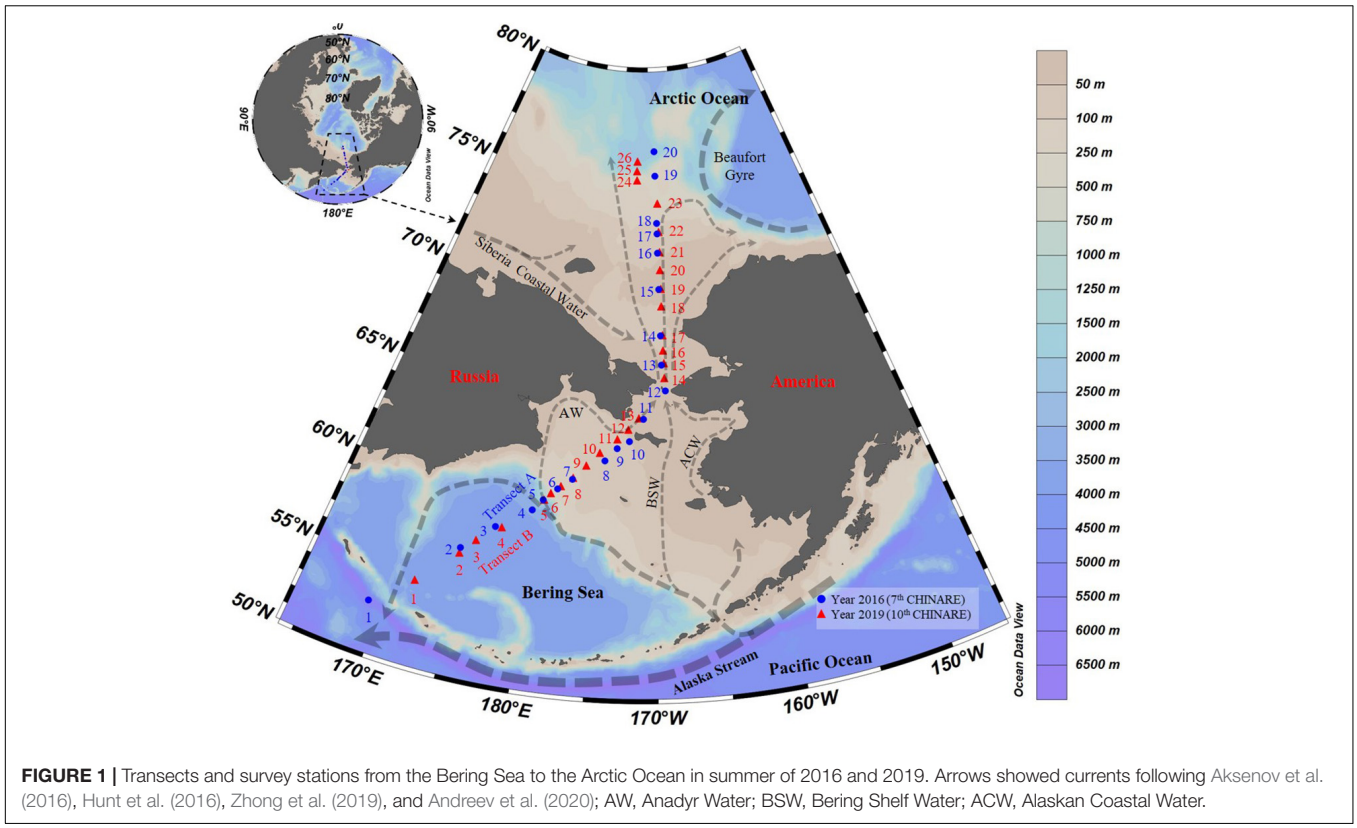


**FIGURE 1 |** Transects and survey stations from the Bering Sea to the Arctic Ocean in summer of 2016 and 2019. Arrows showed currents following Aksenov et al. (2016), Hunt et al. (2016), Zhong et al. (2019), and Andreev et al. (2020); AW, Anadyr Water; BSW, Bering Shelf Water; ACW, Alaskan Coastal Water.

according to the Joint Global Ocean Flux Study (JGOFS) protocol (Knap et al., 1996) using a Turner Trilogy fluorometer Model 10.

## Sample Analysis and Species Identification

In the laboratory, water samples were concentrated to ∼200 mL by siphoning off the supernatant after settling the sample for 60 h. This settling and siphoning process was repeated until a final concentrated volume of 50 mL was achieved, which was then settled in two Utermöhl counting chambers (25 mL per chamber) (Utermöhl, 1958) for at least 24 h. Planktonic ciliates were counted using an Olympus IX 73 inverted microscope (100 × or 400 ×) according to the process of Lund et al. (1958) and Utermöhl (1958).

For each species, the size (length, width, and according to shape) of the cell (aloricate ciliate) or lorica (tintinnid, especially length and oral diameter) were measured for at least 20 individuals if possible. Aloricate ciliates were categorized into size-fractions in increments of 10 μm for maximum body length for each individual following Lessard and Murrell (1996), Taylor et al. (2011), and Wang C. F. et al. (2020). The size-fractions were further clustered into small (10–20 μm), medium (20–30 μm), and large (>30 μm) (Sohrin et al., 2010). Tintinnid taxa were identified to the species level according to the size and shape of loricae following Taniguchi (1976), Davis (1977, 1981), Zhang et al. (2012), Dolan et al. (2014, 2017), Li et al. (2016), and Wang et al. (2019, 2022a,b). Because mechanical and chemical disturbance during collection and fixation can detach the tintinnid protoplasm from the loricae (Paranjape and Gold, 1982; Alder, 1999), we included empty tintinnid loricae in cell counts.

## Data Processing

Ciliate volumes were estimated using appropriate geometric shapes (cone, ball, and cylinder). Tintinnid carbon biomass was estimated using the equation:

$$C = V_i \times 0.053 + 444.5 \text{ (Verity and Lagdon, 1984)}.$$

Where $C$ (μg C $L^{-1}$) was the carbon and $V_i$ ($\mu m^3$) was the lorica volume. We used a conversion factor of carbon biomass for aloricate ciliates of 0.19 pg/$\mu m^3$ (Putt and Stoecker, 1989). Calculation of ciliate depth-integrated abundance and biomass in water column following Yu et al. (2014). Biogeographically, the classification of tintinnid genera (Neritic, species largely restricted to nearshore waters; Boreal, species restricted to Arctic and Subarctic waters; Cosmopolitan, species distributed widely in the world ocean) was based on Pierce and Turner (1993) and Dolan and Pierce (2013). The threshold for Pacific Inflow Water was 4°C as Yamashita et al. (2019) in our results. Data of total surface heat flux (SHF = net solar radiation + net longwave radiation + sensible heat flux + latent heat flux) were obtained from the European Centre for Medium-Range Weather Forecasts (ECMWF).[1]

[1]https://www.ecmwf.int/en/forecasts/datasets/reanalysis-datasets/era5

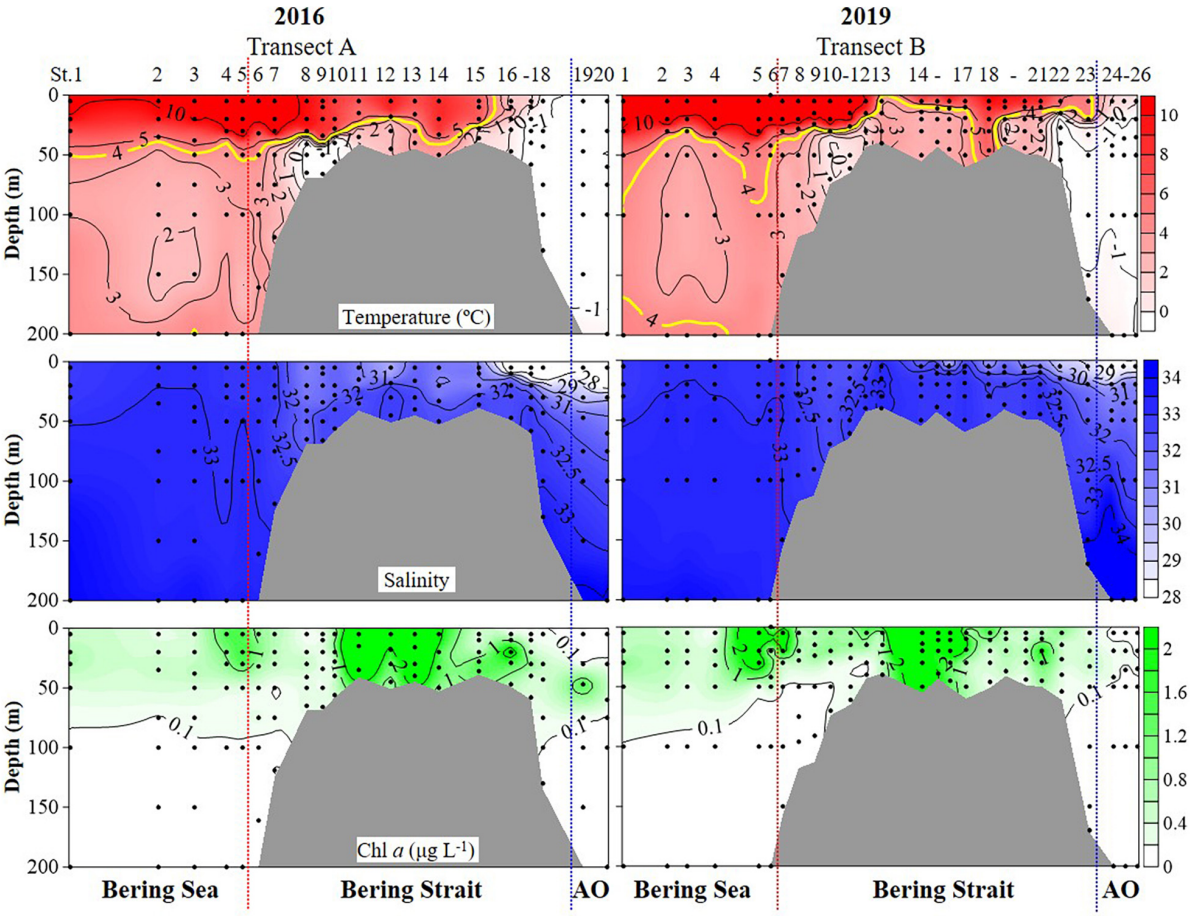


**FIGURE 2 |** Temperature, salinity, and Chlorophyll *a* (Chl *a*) profiles from surface to bottom (or 200 m). Black dots, sampling points; red dotted line, boundary between the Bering Sea and Bering Strait; blue dotted line, boundary between the Bering Strait and Arctic Ocean (AO).

Horizontal and vertical distribution of environment and ciliate data are presented by ODV (Ocean Data View, Version 5.0, Reiner Schlitzer, Alfred Wegener Institute, Bremerhaven, Germany), Surfer (Version 13.0, Golden Software Inc., Golden, CO., United States), OriginPro 2021 (Version 9.6, OriginLab Corp., United States), and Grapher (Version 12.0, Golden Software Inc., Golden, CO., United States). RELATE analysis was conducted based on Spearman's correlation between square root-transformed abundance data and log-transformed abiotic parameters (normalized the abiotic parameters, including temperature, salinity, and Chlorophyll-*a*) to explore whether the environment had an effect on organisms, which is a function in PRIMER (Version 6.0, Plymouth Routes in Multivariate Ecological Research). Biota-Environment (BIOENV) analysis was performed based on Spearman's correlation between log-transformed abiotic parameters and square root-transformed abundance data using PRIMER. The significance for grouping in the environment and ciliate community (aloricate ciliate and tintinnid) was tested by PERMANOVA analysis in PERMANOVA + of PRIMER 6 (Anderson et al., 2008; Jiang et al., 2016). SIMPER (Clarke and Warwick, 1994) analysis was conducted with a criterion of tintinnid dominant species/aloricate ciliate three size-fractions by cutting off for low contributions: 90.00% in 2016 and 2019 using PRIMER.

**TABLE 1 |** Results of PERMANOVA based on Euclidean distance matrices derived from log-transformed environmental data between 2016 and 2019.

| PERMANOVA table of results | | | | |
|---|---|---|---|---|
| | **df** | **MS** | **Pseudo-*F*** | ***P*** |
| Groups | 1 | 8.8788 | 2.9832 | 0.043 |
| Residual | 248 | 2.9763 | | |
| Total | 249 | | | |

# RESULTS

## Hydrographic Feature Variations

Hydrographic features (temperature, salinity, and Chlorophyll *a* (Chl *a*) concentrations) showed significant variations during cruises in the summers of 2016 and 2019 (PERMANOVA

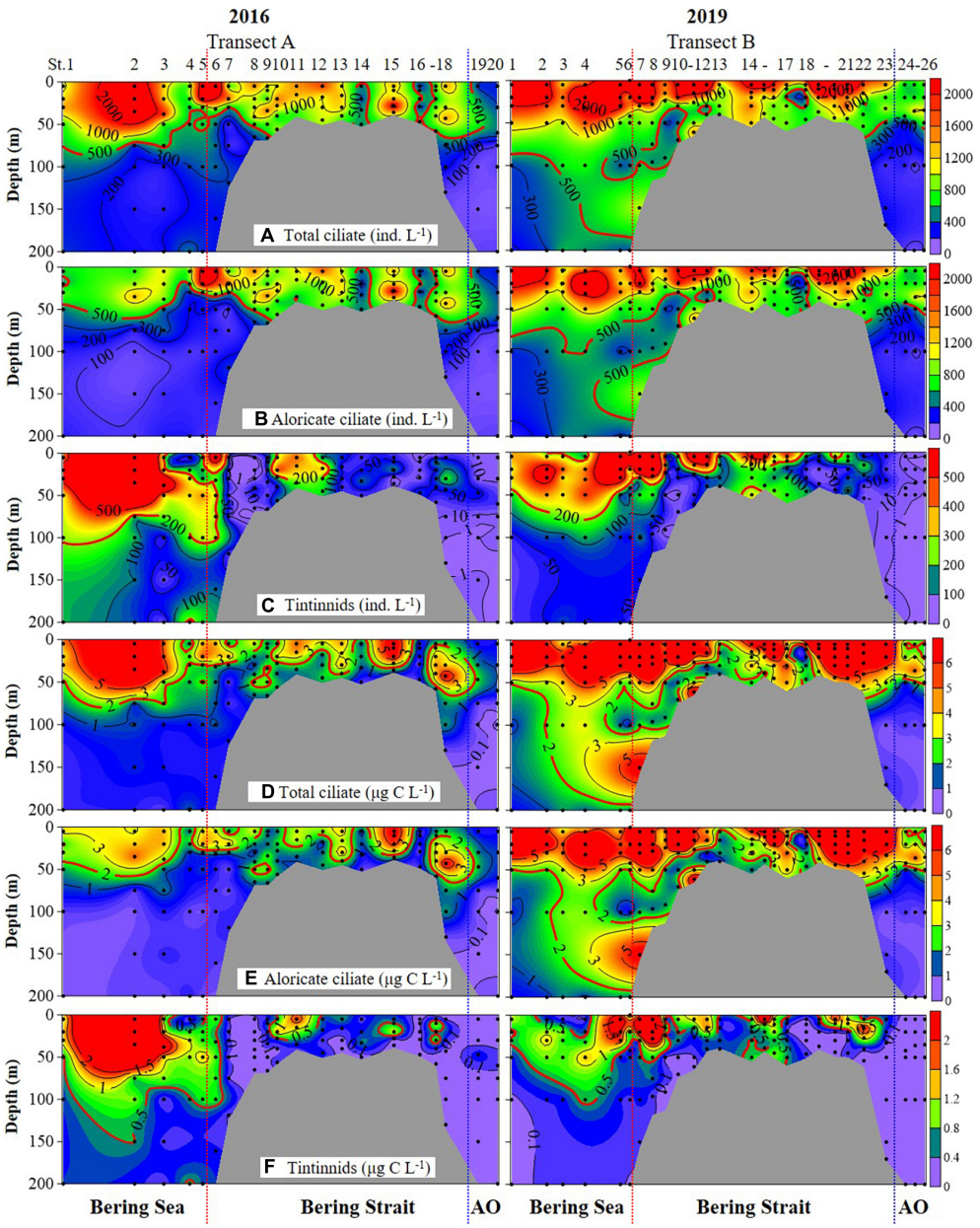


**FIGURE 3 |** Vertical distribution of total ciliate, aloricate ciliate, and tintinnid abundance **(A–C)** and biomass **(D–F)** from surface to bottom (or 200 m). Black dots, sampling depths; red dotted line, boundary between the Bering Sea and Bering Strait; blue dotted line, boundary between the Bering Strait and Arctic Ocean (AO).

pseudo-$F$ = 2.9832, $P$ = 0.043) (**Figure 2** and **Supplementary Figure 1** and **Table 1**). Horizontally, temperature continually decreased northward in 2016. While in 2019, the temperature first decreased to St. B13, increased to St. B17, and eventually decreased to the Arctic Ocean (**Figure 2**). The average temperature in surface layers of 2019 (10.85 ± 0.31°C, 8.22 ± 2.43°C, and 0.48 ± 0.43°C) were 0.40°, 1.73°, and 1.82°C higher than that in 2016 (10.45 ± 0.41°, 6.49 ± 3.67°, and −1.34 ± 0.01°C) in the Bering Sea, Bering Strait, and the Arctic Ocean, respectively (**Supplementary Figure 1**). Vertically, temperature first decreased, then increased to 200 m layers in the Bering Sea in both 2019 and 2016, while the average temperature from 50 to 200 m layers in 2019 was higher than that in 2016. In the Bering Strait, the temperature decreased from surface to bottom in both 2019 and 2016. In the Arctic Ocean, temperature showed almost no change from surface to 200 m depth in 2016. However, temperature first decreased from surface to 50 m layers, then increased to 200 m layers in 2019 (**Figure 2** and **Supplementary Figure 1**).

Horizontally, salinity continually decreased northward in both 2016 and 2019, while the average salinity in surface layers of 2019

(32.88 ± 0.11, 31.54 ± 1.24, and 28.25 ± 0.28) were 0.06, 1.08, 0.76 higher than that in 2016 (32.82 ± 0.13, 30.46 ± 2.03, and 27.49 ± 0.70) in the Bering Sea, Bering Strait, and the Arctic Ocean, respectively (**Figure 2** and **Supplementary Figure 1**). Vertically, salinity increased from the surface to 200 m layers or bottom in the Bering Sea, Bering Strait, and Arctic Ocean (**Figure 2**). Except for 200, 100, and 50 m layers, the average salinity value in other layers in 2019 was higher than that in 2016 (**Supplementary Figure 1**).

Chl *a* showed similar distribution characteristics in both 2016 and 2019, but there were still several differences (**Figure 2** and **Supplementary Figure 1**). Horizontally, Chl *a* increased from the Bering Sea to Bering Strait, then decreased northward in both 2016 and 2019, while the average Chl *a* in surface layers of 2019 ($0.96 \pm 1.49\ \mu g\ L^{-1}$, $2.43 \pm 4.36\ \mu g\ L^{-1}$, and $0.40 \pm 0.01\ \mu g\ L^{-1}$) were higher than that in 2016 ($0.78 \pm 0.60\ \mu g\ L^{-1}$, $1.28 \pm 1.51\ \mu g\ L^{-1}$, and $0.04 \pm 0.01\ \mu g\ L^{-1}$) in the Bering Sea, Bering Strait, and the Arctic Ocean, respectively (**Figure 2** and **Supplementary Figure 1**). For vertical distribution, Chl *a* decreased from surface to 200 m or bottom generally in the Bering Sea and Bering Strait in both 2016 and 2019. While in the Arctic Ocean, deep Chl *a* maximum (DCM) layers in 2019 (40 m) were shallower than that in 2016 (50 m) and the average Chl *a* in DCM of 2019 ($0.14 \pm 0.12\ \mu g\ L^{-1}$) was lower than that in 2016 ($0.93 \pm 0.74\ \mu g\ L^{-1}$) (**Figure 2** and **Supplementary Figure 1**).

The total surface heat flux in the Pacific Arctic Region showed that the ocean gained heat from air both in August and September, but the heat from the atmosphere to the ocean in 2019 was lower than that in 2016 in most stations of our study area (**Supplementary Figure 2**).

## Variations in Planktonic Ciliate Abundance and Biomass in 2016 and 2019

Ciliate abundance and biomass generally decreased northward (from the Bering Sea to the Arctic Ocean) in both 2016 and 2019, with some significant differences (**Figure 3** and **Supplementary Figure 3**). PERMANOVA tests indicated significant differences between 2 years of aloricate ciliate (pseudo-$F$ = 17.272, $P$ = 0.001) and tintinnid (pseudo-$F$ = 9.2666, $P$ = 0.001) abundance data (**Table 2**). In the Bering Sea, ciliate high abundance (total ciliate and aloricate ciliate: ≥ 500 ind. $L^{-1}$, tintinnids: 200 ind. $L^{-1}$) and biomass (total ciliate and aloricate ciliate: ≥ 2 μg C $L^{-1}$, tintinnids: 0.5 μg C $L^{-1}$) mainly occurred in upper 100 m in 2019, while these values mainly appeared in upper 50 m in 2016 (**Figure 3**). Although vertical distribution patterns of ciliate abundance and biomass were the same in both 2016 and 2019, the highest average total abundance (2025.67 ± 1628.80 ind. $L^{-1}$) and biomass (9.66 ± 4.80 μg C $L^{-1}$) at 20 m in 2019 were 1.21 and 1.79 folds higher than that in 2016 (1679.20 ± 1034.85 ind. $L^{-1}$; 5.39 ± 3.87 μg C $L^{-1}$) (**Supplementary Figure 3**). The proportion of tintinnid abundance and biomass to total ciliate in 2019 (18.68 ± 3.29%, 12.75 ± 2.46%) was much lower than that in 2016 (41.79 ± 8.96%, 46.15 ± 10.33%) (**Supplementary Figure 3**).

In the Bering Strait, ciliate abundance and biomass decreased from surface to bottom in both 2016 and 2019, while the highest average total abundance (2224.92 ± 1131.25 ind. $L^{-1}$) and biomass (11.02 ± 8.56 μg C $L^{-1}$) at 5 m in 2019 were 2.11 and 4.11 folds higher than that in 2016 (1053.29 ± 692.03 ind. $L^{-1}$; 2.68 ± 2.08 μg C $L^{-1}$) (**Figure 3** and **Supplementary Figure 3**). The proportion of tintinnid abundance and biomass to total ciliate in 2019 (10.53 ± 4.40%, 9.03 ± 4.13%) was lower than that in 2016 (14.88 ± 5.42%, 17.69 ± 4.88%) (**Supplementary Figure 3**).

In the Arctic Ocean, ciliate abundance and biomass increased from surface to DCM layers, then decreased to 200 m, but the highest average total abundance (876.67 ± 277.29 ind. $L^{-1}$) and biomass (3.71 ± 1.15 μg C $L^{-1}$) in DCM layers of 2019 were 1.73 and 2.81 folds higher than in 2016 (507.50 ± 177.48 ind. $L^{-1}$; 1.32 ± 0.63 μg C $L^{-1}$) (**Figure 3** and **Supplementary Figure 3**). Tintinnid had low abundance and biomass in both 2019 and 2016, while the proportion of tintinnid abundance and biomass to total ciliate in 2019 (0.38 ± 0.25%, 0.31 ± 0.30%) were lower than that in 2016 (3.18 ± 3.02%, 6.93 ± 6.20%) (**Supplementary Figure 3**).

Latitudinally, ciliate integrated abundance and biomass increased from the Bering Sea to Bering Strait, then decreased to the Arctic Ocean in both 2016 and 2019. However, those values in the Bering Sea ($0.86 \pm 0.25 \times 10^6$ ind. $m^{-2}$, 3.09 ± 0.93 mg C $m^{-2}$), Bering Strait ($1.24 \pm 0.54 \times 10^6$ ind. $m^{-2}$, 6.20 ± 3.81 mg C $m^{-2}$), and Arctic Ocean ($0.29 \pm 0.06 \times 10^6$ ind. $m^{-2}$, 0.99 ± 0.15 mg C $m^{-2}$) in 2019 were higher than that in 2016 (Bering Sea $0.59 \pm 0.16 \times 10^6$ ind. $m^{-2}$, 1.86 ± 0.87 mg C $m^{-2}$; Bering Strait 0.82 ± 0.34 × $10^6$ ind. $m^{-2}$, 2.14 ± 1.39 mg C $m^{-2}$; Arctic Ocean 0.20 ± 0.06 × $10^6$ ind. $m^{-2}$, 0.46 ± 0.13 mg C $m^{-2}$), respectively (**Supplementary Figure 4** and **Supplementary Table 1**).

**TABLE 2 |** Results of PERMANOVA based on Bray Curtis similarity matrices derived from Square root-transformed abundance data of aloricate ciliates and tintinnids between 2016 and 2019.

| | df | MS | Pseudo-*F* | *P* |
|---|---|---|---|---|
| **PERMANOVA between aloricate ciliates** | | | | |
| Groups | 1 | 11,004 | 17.272 | 0.001 |
| Residual | 248 | 637.13 | | |
| Total | 249 | | | |
| **PERMANOVA between tintinnids** | | | | |
| Groups | 1 | 28,998 | 9.2666 | 0.001 |
| Residual | 215 | 3129.3 | | |
| Total | 216 | | | |

## Aloricate Ciliate Size-Fraction Abundance and Abundance Proportion Variations

Aloricate ciliates were the main contributors to the observed increase in ciliate abundance in the summer of 2019, compared with 2016 (**Figure 4** and **Supplementary Figure 3**). The average abundance and abundance proportion of aloricate ciliate small (10–20 μm) size-fraction in the upper 50 m layers of the Bering Sea, Bering Strait, and the Arctic Ocean in 2019 were higher

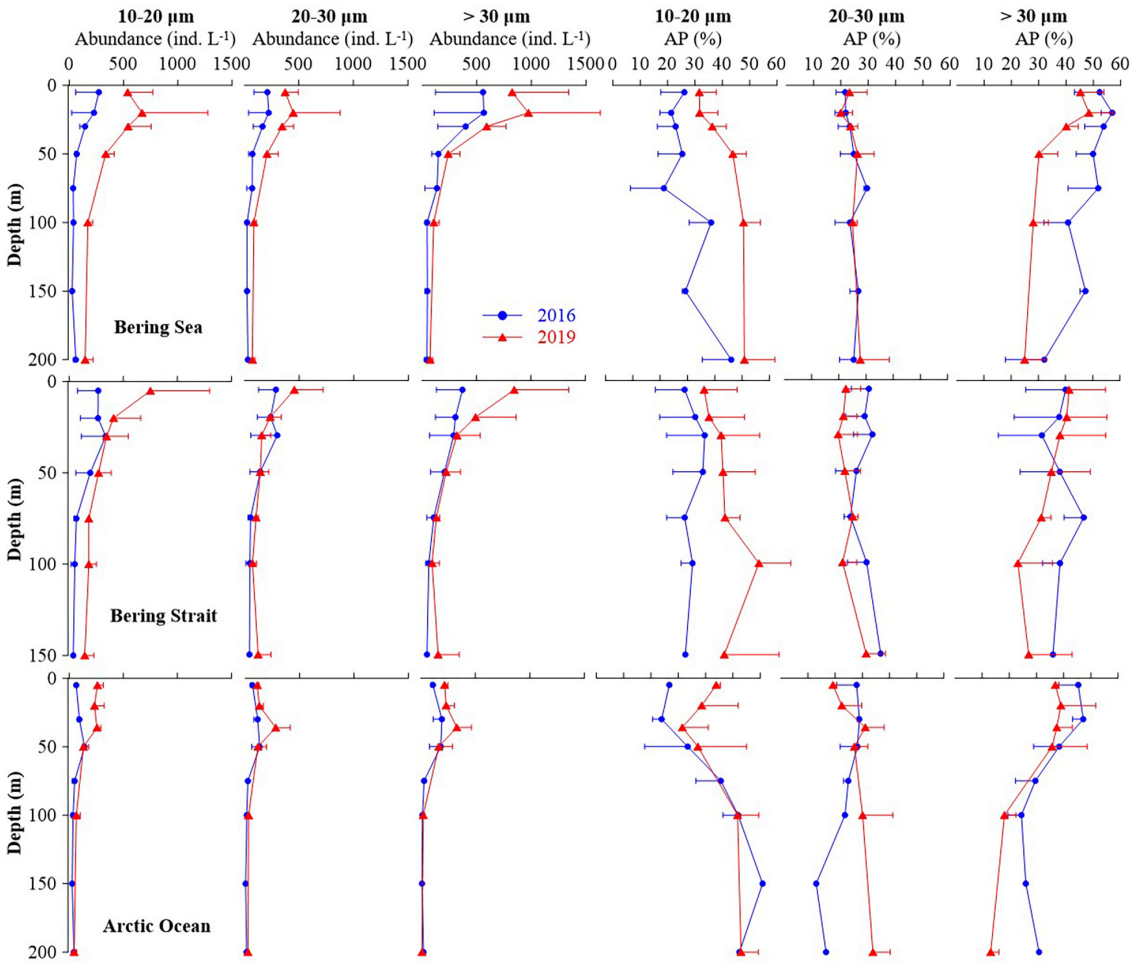


**FIGURE 4 |** Average abundance and abundance proportion of each aloricate ciliate size-fraction at each layers in the Bering Sea, Bering Strait, and Arctic Ocean.

than that in 2016. The average abundance of large (> 30 μm) size-fraction in the upper 50 m layers of three seas in 2019 was higher than that in 2016, but the average abundance proportion was lower in the Bering Sea and Arctic Ocean (**Figure 4**). For integrated abundance of small, medium (20–30 μm), and large size-fraction groups, an increase occurred in the Bering Sea, Bering Strait, and the Arctic Ocean in 2019 compared with 2016, respectively. In 2016, the most abundant group was the large size-fraction in the Bering Sea (50.77 ± 3.31%), Bering Strait (36.88 ± 10.80%), and Arctic Ocean (39.19 ± 5.05%). While in 2019, the small size-fraction was the most abundant (Bering Sea 39.94 ± 3.71%, Bering Strait 38.87 ± 8.82%, and Arctic Ocean 39.70 ± 11.12%) (**Supplementary Figure 5**).

## Tintinnid Composition and Latitudinal Distribution Variations in 2016 and 2019

A total of 49 tintinnid species belonging to 15 genera were identified (**Supplementary Figure 6** and **Supplementary Table 2**). Tintinnid species richness in 2019 (45 species) was higher than that in 2016 (35 species). All tintinnid species were classified into abundant and rare species according to their maximum abundance ($A_{max}$) and occurrence frequency (OF). We defined abundant species as those with $A_{max} \geq 100$ ind. $L^{-1}$ and OF ≥ 40% (**Table 1**). Other species were defined as rare species (**Supplementary Table 2**).

Geographical distribution trends of the average integrated abundance of tintinnid were different in 2016 and 2019. In 2016, this value gradually decreased from the Bering Sea to the Arctic Ocean, while in 2019, the average integrated abundance in the Bering Sea was similar to that in the Bering Strait, then decreased sharply to the Arctic Ocean (**Figure 5** and **Supplementary Table 3**). Oceanic genera (cosmopolitan and boreal) were distributed in all three seas. Neritic genera (neritic) mainly occurred in the Bering Strait (**Figure 5**).

The distribution trend of average integrated abundance and the relative proportion of each biogeographical category were similar in both 2016 and 2019, while there were still some differences (**Figure 5** and **Supplementary Table 3**). In the Bering Sea and the Arctic Ocean, an average integrated abundance of

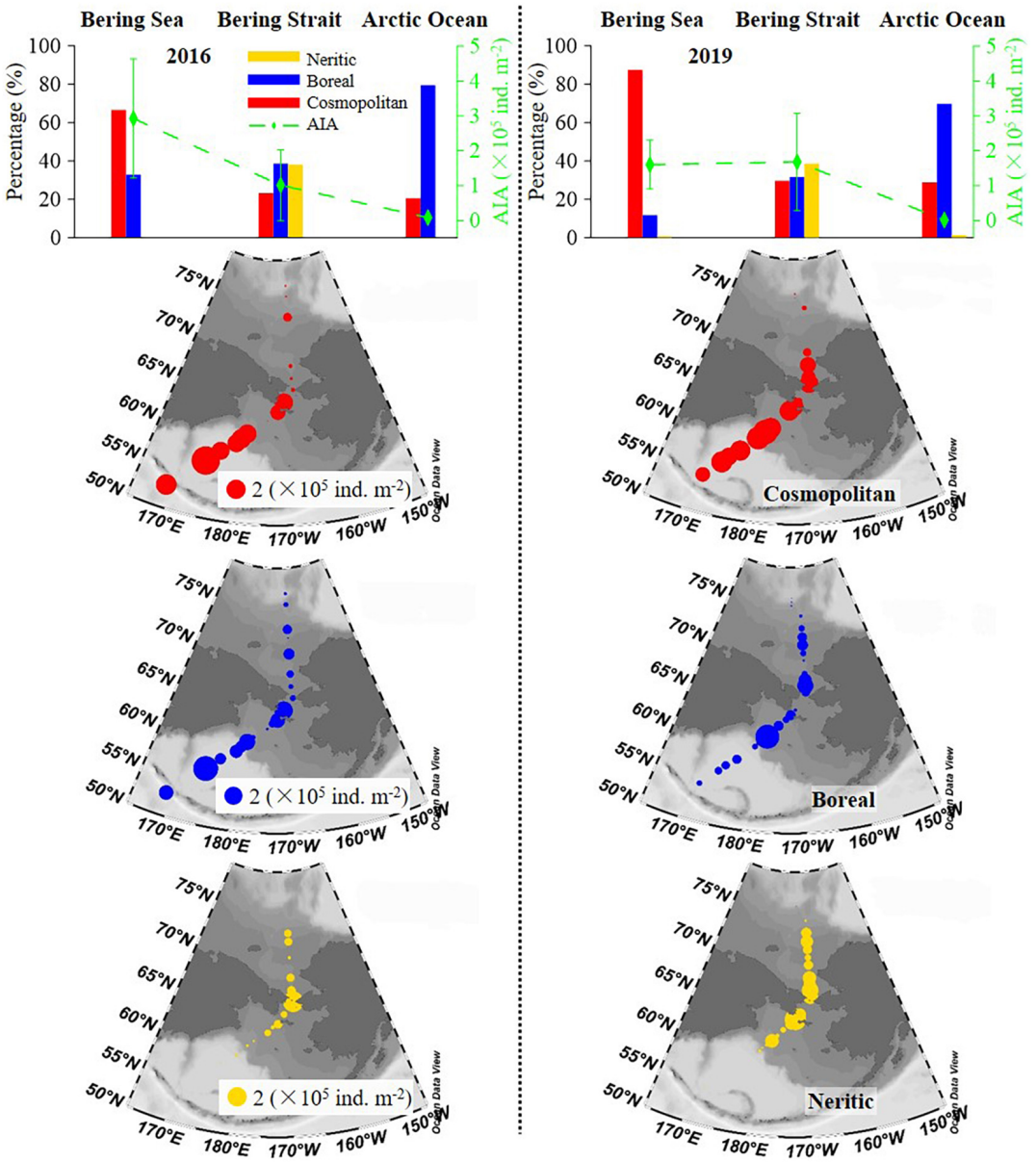


**FIGURE 5 |** Latitudinal variation of cosmopolitan, neritic, and boreal tintinnid (average) integrated abundance and its percentage. AIA, average integrated abundance.

cosmopolitan and boreal genera in 2019 was lower than in 2016, respectively. But in the Bering Strait, cosmopolitan and boreal genera were 2.03 and 1.15 folds higher than in 2016, respectively. The average integrated abundance of neritic genera in 2019 was also higher than in 2016 (**Supplementary Table 3**). As for average integrated abundance proportions in the Bering Sea, Bering Strait, and the Arctic Ocean, cosmopolitan genera in 2019 were 20.72, 6.45, and 8.30% higher than in 2016, respectively. However, boreal genera in 2019 were lower than in 2016, respectively (**Supplementary Table 3**).

The latitudinal distribution of abundant oceanic tintinnids was different from the Bering Sea to the Arctic Ocean between 2 years (**Figure 6** and **Supplementary Figure 7**). *Codonellopsis frigida*, *Ptychocylis obtusa*, genus *Parafavella*, *Salpingella* sp.1, and *Acanthostomella norvegica* were abundant in the Bering Sea in 2016 or 2019. Among them, the distribution of *C. frigida*, *P. obtusa*, and *Salpingella* sp.1 in 2019 have expanded north to 68.2°N, 69.5°N, and 69.5°N, respectively, which were 5.9, 5.2, and 8.8 degrees further north of where they occurred in 2016. While genus *Parafavella* distributed southward in 2019 (66.9°N) compared to 2016 (70.3°N). *P. acuta* was an abundant oceanic tintinnid in the Bering Strait, and its distribution in 2019 was wider than in 2016. In the Arctic Ocean, the distribution range of oceanic tintinnid *P. urnula* was narrower in 2019 than in 2016 (**Figure 6** and **Supplementary Figure 7**).

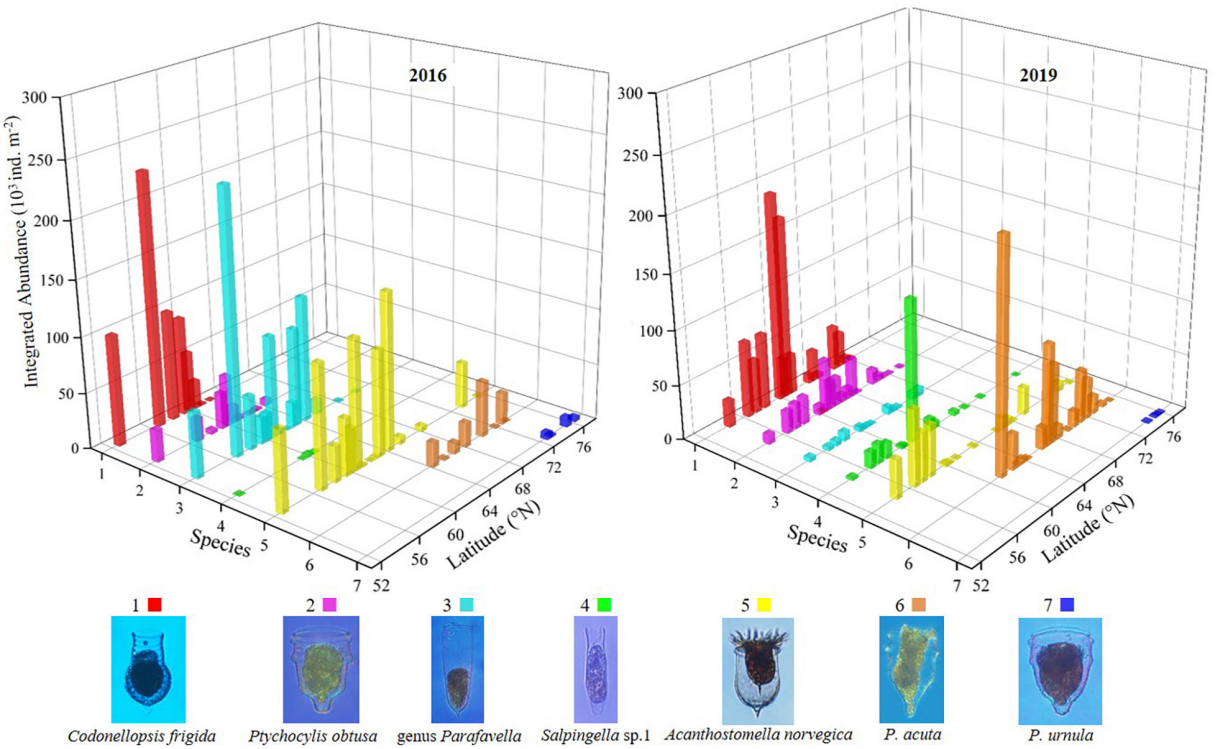


**FIGURE 6 |** Latitudinal distribution variation of dominant oceanic tintinnid integrated abundance.

## Relationship Between Ciliates and Environmental Factors

Correlations between ciliates (aloricate ciliates and tintinnids) and environmental variables (temperature, salinity, and Chl *a*) were different. The routine RELATE test showed that there were significant correlations between changes in environmental variables and tintinnids (*Rho* = 0.318, *P* = 0.001), while the impact of the environment on aloricate ciliates (*Rho* = 0.126, *P* = 0.001) was smaller. In addition, the multivariate biota-environment (BIOENV) analysis was conducted to select the combination of environmental factors (temperature, salinity, and Chl *a*) that have the greatest impact on the ciliate community structure. The analysis showed that the best match with tintinnids was a combination of temperature and salinity (*Rho* = 0.430, *P* = 0.01), while aloricate ciliates were most impacted by temperature alone (*Rho* = 0.163, *P* = 0.01) (**Table 3**).

**TABLE 3 |** Summary of results from BIOENV (biota-environment) analysis showing the best matches of combinations of environmental variables with variations in aloricate ciliate and tintinnid abundance.

| Rank | Best combination of variables | Correlation coefficient |
|---|---|---|
| **Aloricate ciliate** | | |
| 1 | T | 0.163 |
| 2 | T, Chl *a* | 0.152 |
| 3 | T, SAL, Chl *a* | 0.126 |
| 4 | T, SAL | 0.125 |
| 5 | Chl *a* | 0.121 |
| 6 | SAL, Chl *a* | 0.074 |
| 7 | SAL | 0.019 |
| **Tintinnid** | | |
| 1 | T, SAL | 0.430 |
| 2 | T | 0.369 |
| 3 | T, SAL, Chl *a* | 0.318 |
| 4 | SAL | 0.276 |
| 5 | SAL, Chl *a* | 0.241 |
| 6 | SAL, Chl *a* | 0.148 |
| 7 | Chl *a* | −0.021 |

*T, Temperature; SAL, Salinity; Chl a, Chlorophyll a.*

For the three aloricate ciliate size-fractions (10–20 μm, 20–30 μm, and > 30 μm) in the Bering Sea, Bering Strait, and the Arctic Ocean, SIMPER analysis revealed that the small size-fraction was more dominant in 2019 (contrib% = 38.37) than that in 2016 (contrib% = 33.52) (**Table 4**). As for oceanic abundant tintinnid in the Bering Sea (genus *Parafavella*, *C. frigida*, *P. obtusa,* and *A. norvegica*) and Bering Strait (*P. acuta*), SIMPER analysis indicated that the composition of Bering Sea dominant tintinnid species changed significantly between 2016 and 2019. In 2016, genus *Parafavella* (Contrib% = 32.71) dominated, then followed by *A. norvegica* (Contrib% = 27.72), *C. frigida* (Contrib% = 15.54), and *P. obtusa* (Contrib% = 10.05). While in 2019, *C. frigida* (Contrib% = 34.63) became the most dominant species and the contribution rate of the genus *Parafavella* was the lowest (<9.68%) (**Table 4**). No abundant oceanic species were detected in the Arctic Ocean in either 2016 or 2019.

**TABLE 4 |** Results from SIMPER analysis based on Bray Curtis similarity showing community composition of aloricate ciliate and tintinnid whose cumulative contribution rate was higher than 90% in 2016 and 2019, respectively.

| Aloricate ciliate | | | | Tintinnids | | | |
|---|---|---|---|---|---|---|---|
| **Size-fraction (μm)** | **Av.Abund** | **Contrib%** | **Cum.%** | **Species** | **Av.Abund** | **Contrib%** | **Cum.%** |
| **2016** | | | | **2016** | | | |
| >30 | 14.17 | 35.88 | 35.88 | Genus *Parafavella* | 3.87 | 32.71 | 32.71 |
| 10–20 | 12.44 | 33.52 | 69.39 | *Acanthostomella norvegica* | 3.56 | 27.72 | 60.43 |
| 20–30 | 11.84 | 30.61 | 100.00 | *Codonellopsis frigida* | 3.33 | 15.54 | 75.97 |
| | | | | *Ptychocylis obtusa* | 1.72 | 10.05 | 86.02 |
| | | | | *P. acuta* | 0.86 | 8.02 | 94.04 |
| **2019** | | | | **2019** | | | |
| 10–20 | 18.29 | 38.37 | 38.37 | *C. frigida* | 3.85 | 34.63 | 34.63 |
| >30 | 18.20 | 33.09 | 71.46 | *P. acuta* | 2.26 | 25.69 | 60.32 |
| 20–30 | 14.02 | 28.54 | 100.00 | *P. obtusa* | 2.09 | 17.41 | 77.73 |
| | | | | *A. norvegica* | 1.93 | 12.58 | 90.32 |

## Temperature-Salinity-Plankton Diagrams for Abundant Tintinnid Species

Temperature-salinity-plankton diagrams showed that seven abundant tintinnid species had different temperature and salinity ranges (**Figure 7**). In the Bering Sea, high abundance (≥ 100 ind. $L^{-1}$) of *C. frigida*, *P. obtusa,* and *A. norvegica* mainly occurred in relatively higher temperatures (2.0–11.8°C) but narrower salinity range (32.7–33.3) in both 2016 and 2019. In contrast, the genus *Parafavella* had a narrower salinity range and *Salpingella* sp.1 had a wider temperature range in 2019 than in 2016, respectively. In the Bering Strait and the Arctic Ocean, *P. acuta* had a wider temperature range and *P. urnula* had a narrower salinity range in 2019 than in 2016, respectively (**Figure 7**).

# DISCUSSION

The Pacific Inflow Water (PIW) brings heat and fresh water to the Arctic Ocean in summer, resulting in sea ice melt and renewal of the nutrients, and supporting Arctic ecosystems (Grebmeier et al., 2006; Woodgate and Peralta-Ferriz, 2021). In recent years, significant warming in the annual mean temperatures of the PIW has been observed (Woodgate and Peralta-Ferriz, 2021). The atmosphere has significant effects on the heat budget of upper waters in the Pacific Arctic Region. After calculating the total surface heat flux in the Pacific Arctic Region, we found that the heat from the atmosphere to the ocean in 2019 was lower than that in 2016 (**Supplementary Figure 2**). Therefore, we conclude that the higher sea temperature in 2019 was due to warm advection from PIW, bringing heat to the Arctic Ocean.

Planktonic ciliates, as an important component of microzooplankton, have been extensively investigated for their important ecological roles in the Pacific Arctic Region (e.g., Jiang et al., 2015; Dolan et al., 2016, 2021; Li et al., 2016; Xu et al., 2018a,b; Wang et al., 2019, 2022b; Wang C. F. et al., 2020). However, studies related to ciliate Pacification are still scant. After comparing hydrographic features at similar locations and sampling times in 2016 and 2019, we found warmer Pacific Inflow Water in 2019 (**Supplementary Figure 1**), and propose potential identification of ciliate Pacification characteristics.

## Rapid Pacification Progress of Ciliates in the Pacific Arctic Region

The abundance proportion of tintinnids to total ciliates has been described in tropical, subtropical, and polar seas (Sherr et al., 1997; Yang et al., 2004; Gómez, 2007; Sohrin et al., 2010; Wang et al., 2019, 2021b; Wang C. F. et al., 2020). In the tropical West Pacific, North Pacific, and the Arctic Ocean, average abundance proportions of tintinnids to total ciliates tend to be about 0–10% (Sohrin et al., 2010; Wang et al., 2019, 2021b; Wang C. F. et al., 2020), 10–20% (Gómez, 2007; Sohrin et al., 2010; Wang et al., 2021a), and <2% (Sherr et al., 1997; Wang C. F. et al., 2020), respectively. The highest value was shown to occur in the Bering Sea, where it reaches ∼50% (Taniguchi, 1984). Our results showed that this value in 2019 (18.68 ± 3.29%) was much lower than in 2016 (41.79 ± 8.96%), indicating that warmer and more saline Bering Sea waters result in a similar abundance proportion of tintinnids to total ciliates to that found in the North Pacific (Sohrin et al., 2010; Wang et al., 2021a). The warm Alaska Stream was the main current and transported plankton from the North Pacific to the Bering Sea (Andreev et al., 2020). Therefore, we speculated that the abundance proportion of tintinnids to total ciliates in the Bering Sea will be closer to that in the North Pacific (beginning of the Pacification).

Abundance proportions of different aloricate ciliate size-fractions have rarely been reported in the Pacific Arctic Region. In the tropical West Pacific and North Pacific (Yang et al., 2004; Wang et al., 2021a,b), average abundance proportions of small aloricate ciliate (10–20 μm) to total ciliates ranged from 38 to 50% and this size-fraction was the dominant group at each depth in most stations. While in the Bering Sea, dominance shifted to the large (>30 μm) size-fraction group (Wang C. F. et al., 2020). Although our results showed that the average

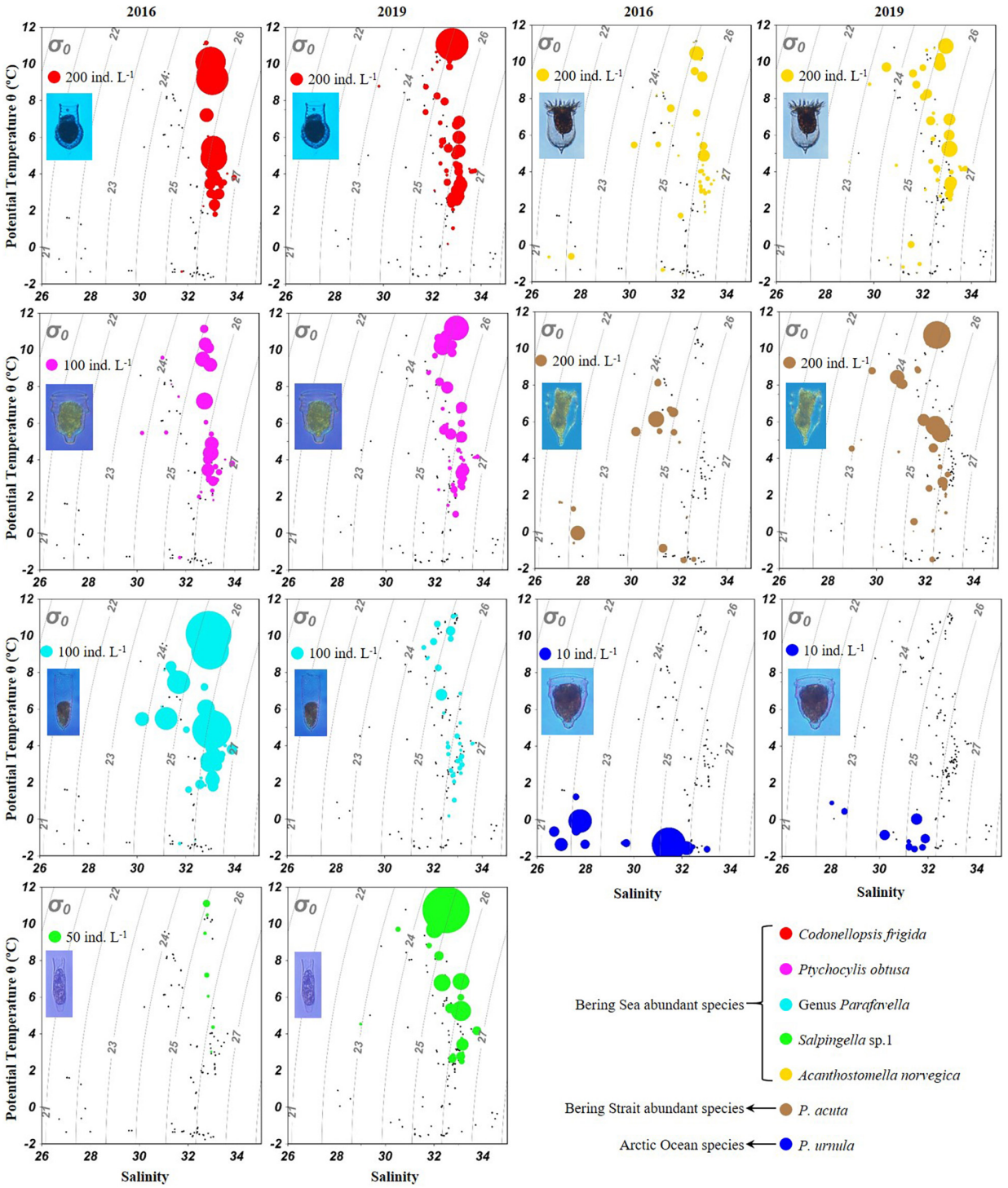


**FIGURE 7 |** Temperature-salinity-plankton diagrams for abundant oceanic tintinnids in 2016 and 2019.

abundance of the large size-fraction group increased in 2019 compared to 2016 (**Figure 4**), the average integrated abundance and the proportion of dominant groups changed to small size-fraction (**Supplementary Figure 4**). A similar phenomenon was previously observed in the North Pacific (Yang et al., 2004; Wang et al., 2021a). With rapid Pacification progress, aloricate ciliate small size-fraction might be more abundant in the Pacific Arctic Region in the future.

The latitudinal diversity gradient in tintinnids appears to be closely related to temperature over a wide variety of time

scales (Yasuhara et al., 2012; Dolan et al., 2016), suggesting that temperature has a preponderant role in determining species richness. These studies also showed a decrease in tintinnid richness from the tropical to polar seas (Dolan et al., 2016; Wang C. F. et al., 2020). In our study, tintinnid richness in warmer waters was higher in 2019 than in 2016. This phenomenon was consistent with Yasuhara et al. (2012), Dolan et al. (2016), and Wang C. F. et al. (2020). In addition, new tintinnid species belonging to the cosmopolitan genera which we detected in the Bering Sea in 2019 also appeared in the North Pacific (Li et al., 2021; Wang et al., 2021a). Therefore, we speculate that those new species originating from the North Pacific might be transported by the Alaska Stream (Springer et al., 1996; Andreev et al., 2020).

There have been numerous studies on tintinnid horizontal and vertical distribution (Taniguchi, 1984; Dolan et al., 2016; Li et al., 2016; Xu et al., 2018a,b; Wang et al., 2019), but there is limited information on tintinnid northward transportation. As for the Bering Sea species, *Salpingella* sp.1, *C. frigida,* and *P. obtusa* were reported to successively disappear with a northward progression and did not pass the Bering Strait (Taniguchi, 1984; Li et al., 2016; Wang et al., 2019). However, in our results, those species extended further north to south side of the Chukchi Sea in 2019. The Bering Strait species (*P. acuta*) also extended further north, and the Arctic species (*P. urnula*) distribution range was narrower in 2019 than in 2016. We conclude that stronger Pacific Inflows in 2019 further alter the hydrographic feature of the Chukchi Sea and Arctic Ocean (Woodgate and Peralta-Ferriz, 2021), which will eventually become suitable for the Bering Sea and Bering Strait species to live in, simultaneously reducing the living space of Arctic native species.

## Possible Response of Ciliate to Ongoing Global Warming

In the Pacific Arctic Region, the PIW carries more warm water into the Arctic Ocean in recent years. From 1990 to 2019, Woodgate and Peralta-Ferriz (2021) reported increasing northward flow (0.010 ± 0.006 Sv/yr) and annual mean temperatures (0.05 ± 0.02°C/yr), with faster change (∼0.1°C/yr) in warming (June/July) and cooling (October/November) months, which were 2°–4°C above climatology. The maximum temperature of the Pacific Water Layer increased by ∼0.5°C between 2009 and 2013 in the Canada Basin (Timmermans et al., 2014), with a doubling in integrated heat content from 1987 to 2017 (Timmermans et al., 2018). From 2001 to 2014, heat transport associated with Bering Strait inflow increased by 60%, from around 10 TW in 2001 to 16 TW in 2014 (due to increase in both volume flux and temperature) (Woodgate, 2018), which further alter the hydrographical environment of the Arctic Ocean.

Previous studies have shown that macrozooplankton abundance and biomass increase significantly in warmer waters in recent years compared to historical studies (Ershova et al., 2015; Xu et al., 2018; Kim et al., 2022). During each August from 2016 to 2020, macrozooplankton abundance was highest in the Bering Strait with higher water temperature (Kim et al., 2022). As important food items of macrozooplankton, we speculate that higher ciliate abundance and biomass in warmer waters of 2019 might be the main reason for higher macrozooplankton abundance.

In the Pacific Arctic Region, Pacific-origin tintinnids were transported from the Bering Sea to the Arctic Ocean mainly in waters > 4°C (Li et al., 2016; Wang et al., 2019, 2022b). For this reason, they probably could not survive in cold Arctic waters (<0°C). This phenomenon does not apply completely to all tintinnids. For example, *Salpingella* sp.1 was first recorded in the northwest Pacific and mainly lived in water temperature > 2°C in 2014 (Li et al., 2016) and our results. In 2020, this species was transported into the warmer Pacific Summer Water (compared to 2016, Wang et al., 2019) with a temperature range from −0.3° to 0.9°C in the Canada Basin of the Arctic Ocean (Wang et al., 2022a). Although our present study did not find PIW sink into the subsurface layers of the Canada Basin, we speculate that, given sustained intrusion trends of warmer waters, more Pacific-origin tintinnids will be found in the future Arctic Ocean. Comparable studies in the Atlantic Gateway are needed to discover whether Atlantic-origin species are being similarly transported into the High Arctic.

The size-fraction for aloricate ciliate or lorica oral diameter (LOD) for tintinnid is related to its preferred food item size, for example, the preferred food item for a tintinnid is about 25% of the LOD (Dolan, 2010). Our results showed a clear increase in abundance and biomass of aloricate ciliate of small size-fraction in warmer Pacific Inflows. This phenomenon revealed that the preferred food item size for aloricate ciliate is getting smaller, and this was consistent with the decreasing trend of phytoplankton size classes (Li et al., 2009; Zhuang et al., 2021). We hypothesize that, as rapid Arctic Pacification progresses, more aloricate ciliate small size-fraction and Pacific-origin tintinnids (belonging to cosmopolitan genera) may be transported into the Arctic Ocean by increasing warm Pacific Inflow Water in the future. Our results only present a "snapshot" phenomenon about ciliate Pacification in 2016 and 2019. Further investigations in the Arctic Ocean are needed to test our hypothesis.

# CONCLUSION

The present study reported planktonic ciliate community structure variations, relationship with environmental factors in similar locations, and sampling time in the Pacific Arctic Region in 2016 and 2019. In 2019, both temperature and salinity were higher than in 2016, which increased both total ciliate and aloricate ciliate abundance and biomass and a decrease for tintinnids. More aloricate ciliate small size-fraction and Pacific-origin tintinnids (belonging to cosmopolitan genera) occurred in warmer and more saline waters of the Pacific Arctic Region in 2019, and community structure characteristics were more similar to the North Pacific, which suggested the rapid Pacification of Arctic microzooplankton. Multivariate correlation analysis between ciliate communities and environmental variables revealed that temperature has a preponderant role in determining both aloricate ciliate and tintinnid composition.

## DATA AVAILABILITY STATEMENT

The original contributions presented in this study are included in the article/**Supplementary Material**, further inquiries can be directed to the corresponding author.

## AUTHOR CONTRIBUTIONS

CW: tintinnid taxonomy and counting, data analysis, and writing—original draft. MY: data analysis. YH and ZX: field sampling and writing—original draft. YZ and TX: conceptualization. WZ: field sampling, conceptualization, and writing—original draft. All authors contributed to the article and approved the submitted version.

## FUNDING

This research was funded by the China Postdoctoral Science Foundation (Grant No. 2020M672149), the Basic Scientific Fund for National Public Research Institutes of China (Grant No. 2021Q08), the Applied Research Project for Postdoctoral in Qingdao, and the National Natural Science Foundation of China (Grant No. 42176228).

## ACKNOWLEDGMENTS

We thank the captain and crews of R.V. "Xuelong" and R.V. "Xiangyanghong 01" for their great help in sampling during the 7th and 10th Chinese National Arctic Research Expedition, respectively. We also thank Liwen Bianji (Edanz) (https://www.liwenbianji.cn) for editing the language of a draft of this manuscript. We greatly appreciate the constructive comments by two reviewers, which dramatically improve the quality of the manuscript.

## SUPPLEMENTARY MATERIAL

The Supplementary Material for this article can be found online at: https://www.frontiersin.org/articles/10.3389/fmicb.2022.881048/full#supplementary-material

## REFERENCES

Aksenov, Y., Karcher, M., Proshutinsky, A., Gerdes, R., de Cuevas, B., Golubeva, E., et al. (2016). Arctic pathways of Pacific Water: Arctic Ocean Model Intercomparison experiments. *J. Geophys. Res. Oceans* 121, 27–59. doi: 10.1002/2015JC011299

Alder, V. A. (1999). "Tintinnoinea," in *South Atlantic Zooplankton*, ed. D. Boltovskoy (Leiden: Backhuys), 321–384.

Anderson, M. J., Gorley, R. N., and Clarke, K. R. (2008). *PERMANOVA+ for PRIMER: Guide to Software and Statistical Methods*. Plymouth, MA: PRIMER-E.

Andreev, A. G., Budyansky, M. V., Khen, G. V., and Uleysky, M. Y. (2020). Water dynamics in the western Bering Sea and its impact on chlorophyll a concentration. *Ocean Dyn.* 70, 593–602. doi: 10.1007/s10236-020-01347-7

Azam, F., Fenchel, T., Field, J. G., Gray, J. S., Meyer-Reil, L. A., and Thingstad, F. (1983). The ecological role of water column microbes in the sea. *Mar. Ecol. Prog. Ser.* 10, 257–263. doi: 10.3354/meps010257

Calbet, A., and Saiz, E. (2005). The ciliate-copepod link in marine ecosystems. *Aquat. Microb. Ecol.* 38, 157–167. doi: 10.3354/ame038157

Clarke, K. R., and Warwick, R. M. (1994). *Changes in Marine Communities: An Approach to Statistical Analyses and Interpretation*. Plymouth: Natural Environment Research Council.

Davis, C. C. (1977). Variations of the lorica in the genus *Parafavella* (Protozoa: Tintinnida) in northern Norway waters. *Can. J. Zool.* 56, 1822–1827. doi: 10.1139/z78-248

Davis, C. C. (1981). Variations of lorica shape in the genus *Ptychocylis* (Protozoa: Tintinnina) in relation to species identification. *J. Plankton Res.* 3, 433–443. doi: 10.1093/plankt/3.3.433

Dolan, J. R. (2010). Morphology and ecology in tintinnid ciliates of the marine plankton: correlates of lorica dimensions. *Acta Protozool.* 49, 235–244.

Dolan, J. R., and Pierce, R. W. (2013). "Diversity and distributions of tintinnid ciliates," in *The Biology and Ecology of Tintinnid Ciliates: Models for Marine Plankton*, eds J. R. Dolan, S. Agatha, and D. W. Coats (Oxford: WileyBlackwell), 214–243. doi: 10.1002/9781118358092.ch10

Dolan, J. R., Moon, J. K., and Yang, E. J. (2021). Notes on the occurrence of tintinnid ciliates, and the nasselarian radiolarian *Amphimelissa setosa* of the marine microzooplankton, in the Chukchi Sea (Arctic Ocean) sampled each August from 2011 to 2020. *Acta Protozool.* 60, 1–243. doi: 10.4467/16890027AP.21.001.14061

Dolan, J. R., Pierce, R. W., and Yang, E. J. (2017). Tintinnid ciliates of the marine microzooplankton in Arctic Seas: a compilation and analysis of species records. *Polar Biol.* 40, 1247–1260. doi: 10.1007/s00300-016-2049-0

Dolan, J. R., Vidussi, F., and Claustre, H. (1999). Planktonic ciliates in the Mediterranean Sea: longitudinal trends. *Deep Sea Res. I.* 46, 2025–2039. doi: 10.1016/S0967-0637(99)00043-6

Dolan, J. R., Yang, E. J., Kang, S. H., and Rhee, T. S. (2016). Declines in both redundant and trace species characterize the latitudinal diversity gradient in tintinnid ciliates. *ISME J.* 10, 2174–2183. doi: 10.1038/ismej.2016.19

Dolan, J. R., Yang, E. J., Kim, T. W., and Kang, S. H. (2014). Microzooplankton in warming Arctic: a comparison of tintinnids and radiolarians from summer 2011 and 2012 in the Chukchi Sea. *Acta Protozool.* 52, 101–113.

Ershova, E. A., Hopcroft, R. R., Kosobokova, K. N., Matsuno, K., Nelson, R. J., Yamaguchi, A., et al. (2015). Long-term changes in summer zooplankton communities of the western Chukchi Sea, 1945-2012. *Oceanography* 28, 100–115. doi: 10.5670/oceanog.2015.60

Gómez, F. (2007). Trends on the distribution of ciliates in the open Pacific Ocean. *Acta Oecol.* 32, 188–202. doi: 10.1016/j.actao.2007.04.002

Grebmeier, J. M., and Maslowski, W. (2014). "The Pacific Arctic Region: an introduction," in *The Pacific Arctic Region*, eds J. Grebmeier and W. Maslowski (Dordrecht: Springer).

Grebmeier, J. M., Cooper, L. W., Feder, H. M., and Sirenko, B. I. (2006). Ecosystem dynamics of the Pacific-influenced Northern Bering and Chukchi Seas in the Amerasian Arctic. *Prog. Oceanogr.* 71, 331–361. doi: 10.1016/j.pocean.2006.10.001

Hunt, G. L., Drinkwater, K. F., Arrigo, K., Berge, J., Daly, K. L., Danielson, S., et al. (2016). Advection in polar and sub-polar environments: impacts on high latitude marine ecosystems. *Prog. Oceanogr.* 149, 40–81. doi: 10.1016/j.pocean.2016.10.004

Jiang, Y., Xu, G., and Xu, H. (2016). Use of multivariate dispersion to assess water quality based on species composition data. *Environ. Sci. Pollut. Res.* 23, 3267–3272. doi: 10.1007/s11356-015-5583-3

Jiang, Y., Yang, E. J., Min, J. O., Kang, S. H., and Lee, S. H. (2013). Using pelagic ciliated microzooplankton communities as an indicator for monitoring environmental condition under impact of summer sea-ice reduction in western Arctic Ocean. *Ecol. Indic.* 34, 380–390. doi: 10.1016/j.ecolind.2013.05.026

Jiang, Y., Yang, E. J., Min, J. O., Kim, T. W., and Kang, S. H. (2015). Vertical variation of pelagic ciliate communities in the western Arctic Ocean. *Deep Sea Res. II* 120, 103–113. doi: 10.1016/j.dsr2.2014.09.005

Kato, S., and Taniguchi, A. (1993). Tintinnid ciliates as indicator species of different water masses in the western North Pacific Polar Front. *Fish. Oceanogr.* 2, 166–174.

Kim, J. H., La, H. S., Cho, K. H., Jung, J., Kang, S. H., Lee, K., et al. (2022). Spatial and interannual patterns of epipelagic summer mesozooplankton community structures in the western Arctic Ocean in 2016–2020. *J. Geophys. Res. Oceans.* 127:e2021JC018074. doi: 10.1029/2021JC018074

Kim, Y. O., Shin, K., Jang, P. G., Choi, H. W., Noh, J. H., Yang, E. J., et al. (2012). Tintinnid species as biological indicators for monitoring intrusion of the warm oceanic waters into Korean coastal waters. *Ocean Sci. J.* 47, 161–172. doi: 10.1007/s12601-012-0016-4

Knap, A. H., Michaels, A., Close, A. R., Ducklow, H., and Dickson, A. G. (1996). Protocols for the joint global ocean flux study (JGOFS) core measurements. *JGOFS Rep.* 19, 155–162.

Lalande, C., Grebmeier, J. M., McDonnell, A. M. P., Hopcroft, R. R., O'Daly, S., and Danielson, S. L. (2021). Impact of a warm anomaly in the Pacific Arctic region derived from time-series export fluxes. *PLoS One* 16:e0255837. doi: 10.1371/journal.pone.0255837

Lessard, E. J., and Murrell, M. C. (1996). Distribution, abundance and size composition of heterotrophic dinoflagellates and ciliates in the Sargasso Sea near Bermuda. *Deep Sea Res. I* 43, 1045–1065.

Lewis, K. M., Dijken, G., and Arrigo, K. R. (2020). Changes in phytoplankton concentration now drive increased Arctic Ocean primary production. *Science* 369, 198–202. doi: 10.1126/science.aay8380

Li, H. B., Xu, Z. Q., Zhang, W. C., Wang, S., Zhang, G. T., and Xiao, T. (2016). Boreal tintinnid assemblage in the Northwest Pacific and its connection with the Japan Sea in summer 2014. *PLoS One* 11:e0153379. doi: 10.1371/journal.pone.0153379

Li, H. B., Xuan, J., Wang, C. F., Chen, Z. H., Grégori, G., Zhao, Y., et al. (2021). Summertime tintinnid community in the surface waters across the North Pacific Transition Zone. *Front. Microbiol.* 12:697801. doi: 10.3389/fmicb.2021.697801

Li, W., Mclaughlin, F. A., Lovejoy, C., and Carmack, E. C. (2009). Smallest algae thrive as the Arctic Ocean freshens. *Science* 326, 539–539. doi: 10.1126/science.1179798

Lund, J. W. G., Kipling, C., and Cren, E. D. L. (1958). The inverted microscope method of estimating algal numbers and the statistical basis of estimations by counting. *Hydrobiologia* 11, 143–170. doi: 10.1007/BF00007865

Lynn, D. H. (2008). *Ciliated Protozoa: Characterization, Classification, and Guide to the Literature*, 3rd Edn. Berlin: Springer.

Mueter, F. J., Iken, K., Cooper, L., Grebmeier, J. M., Kuletz, K. J., Hopcroft, R. R., et al. (2021). Changes in diversity and species composition across multiple assemblages in the eastern Chukchi Sea during two contrasting years are consistent with borealization. *Oceanography* 34, 38–51. doi: 10.5670/oceanog.2021.213

Paranjape, M. A., and Gold, K. (1982). Cultivation of marine pelagic protozoa. *Ann. Inst. Oceanogr. Paris.* 58, 143–150. doi: 10.1128/AEM.67.5.2145-2155.2001

Pierce, R. W., and Turner, J. T. (1992). Ecology of planktonic ciliates in marine food webs. *Rev. Aquat. Sci.* 6, 139–181.

Pierce, R. W., and Turner, J. T. (1993). Global biogeography of marine tintinnids. *Mar. Ecol. Prog. Ser.* 94, 11–26. doi: 10.3354/meps094011

Polyakov, I., Alkire, M. B., Bluhm, B. A., Brown, K. A., and Wassmann, P. (2020). Borealization of the Arctic Ocean in response to anomalous advection from sub-Arctic seas. *Front. Mar. Sci.* 7:491. doi: 10.3389/fmars.2020.00491

Putt, M., and Stoecker, D. K. (1989). An experimentally determined carbon: volume ratio for marine "oligotrichous" ciliates from estuarine and coastal waters. *Limnol. Oceanogr.* 34, 1097–1103. doi: 10.4319/lo.1989.34.6.1097

Screen, J., and Simmonds, I. (2010). The central role of diminishing sea ice in recent Arctic temperature amplification. *Nature* 464, 1334–1337. doi: 10.1038/nature09051

Sherr, E. B., Sherr, B. F., and Fessenden, L. (1997). Heterotrophic protists in the Central Arctic Ocean. *Deep Sea Res. II* 44, 1665–1673.

Sohrin, R., Imazawa, M., Fukuda, H., and Suzuki, Y. (2010). Full-depth profiles of prokaryotes, heterotrophic nanoflagellates, and ciliates along a transect from the equatorial to the subarctic central Pacific Ocean. *Deep Sea Res. II* 57, 1537–1550. doi: 10.1016/j.dsr2.2010.02.020

Springer, A. M., Mcyro, C. P., and Flint, M. V. (1996). Bering Sea Green Belt: shelf-edge processes and ecosystem production. *Fish. Oceanogr.* 5, 205–223. doi: 10.1111/j.1365-2419.1996.tb00118.x

Steele, M., Morison, J., Ermold, W., Rigor, I., Ortmeyer, M., and Shimada, K. (2004). Circulation of summer Pacific halocline water in Arctic Ocean. *J. Geophys. Res.* 109:C02027. doi: 10.1029/2003JC002009

Stoecker, D. K., Michaels, A. E., and Davis, L. H. (1987). Grazing by the jellyfish, *Aurelia aurita*, on microzooplankton. *J. Plankton Res.* 9, 901–915. doi: 10.1093/plankt/9.5.901

Stroeve, J. C., Serreze, M. C., Holland, M. M., Kay, J. E., Malanik, J., and Barrett, A. P. (2012). The Arctic's rapidly shrinking sea ice cover: a research synthesis. *Clim. Change* 110, 1005–1027. doi: 10.1007/s10584-011-0101-1

Taniguchi, A. (1976). Microzooplankton and seston in Akkeshi Bay. Japan. *Hydrobiologia* 50, 195–204. doi: 10.1007/BF00020992

Taniguchi, A. (1984). Microzooplankton biomass in Arctic and subarctic Pacific Ocean in summer. *Mem. Natl. Inst. Polar Res. Spec. Issue* 32, 63–80.

Taylor, A. G., Landry, M. R., Selph, K. E., and Yang, E. J. (2011). Biomass, size structure and depth distributions of the microbial community in the eastern equatorial Pacific. *Deep Sea Res. II* 58, 342–357. doi: 10.1016/j.dsr2.2010.08.017

Timmermans, M. L., Proshutinsky, A., Golubeva, E., Jackson, J. M., Krishfield, R., McCall, M., et al. (2014). Mechanisms of Pacific summer water variability in the Arctic's Central Canada basin. *J. Geophys. Res. Oceans* 119, 7523–7548. doi: 10.1002/2014JC010273

Timmermans, M. L., Toole, J., and Krishfield, R. (2018). Warming of the interior Arctic Ocean linked to sea ice losses at the basin margins. *Sci. Adv.* 4:eaat6773. doi: 10.1126/sciadv.aat6773

Torres-Valdés, S., Tsubouchi, T., Bacon, S., Naveira-Garabato, A. C., Sanders, R., McLaughlin, F. A., et al. (2013). Export of nutrients from the Arctic Ocean. *J. Geophys. Res. Oceans* 118, 1625–1644. doi: 10.1002/jgrc.20063

Utermöhl, H. (1958). Zur vervollkommnung der quantitativen phytoplankton Methodik. *Mit. Int. Ver. Theor. Angew. Limnol.* 9, 1–38. doi: 10.1080/05384680.1958.11904091

Verity, P. G., and Lagdon, C. (1984). Relationships between lorica volume, carbon, nitrogen, and ATP content of tintinnids in Narragansett Bay. *J. Plankton Res.* 6, 859–868. doi: 10.1093/plankt/6.5.859

Wang, C. F., Li, H. B., Xu, Z. Q., Zheng, S., Hao, Q., Dong, Y., et al. (2020). Difference of planktonic ciliate communities of the tropical West Pacific, the Bering Sea and the Arctic Ocean. *Acta Oceanol. Sin.* 39, 9–17. doi: 10.1007/s13131-020-1541-0

Wang, C. F., Xu, M. Q., Xuan, J., Li, H. B., Zheng, S., Zhao, Y., et al. (2021a). Impact of the warm eddy on planktonic ciliate, with an emphasis on tintinnids as bioindicator species. *Ecol. Indic.* 133:108441. doi: 10.1016/j.ecolind.2021.108441

Wang, C. F., Li, H. B., Dong, Y., Zhao, L., Grégori, G., Zhao, Y., et al. (2021b). Planktonic ciliate trait structure variation over Yap, Mariana and Caroline seamounts in the tropical western Pacific Ocean. *J. Oceanol. Limnol.* 39, 1705–1717. doi: 10.1007/s00343-021-0476-4

Wang, C. F., Wang, X. Y., Xu, Z. Q., Hao, Q., Zhao, Y., Zhang, W. C., et al. (2022a). Planktonic tintinnid community structure variations in different water masses of the Arctic Basin. *Front. Mar. Sci.* 8:775653. doi: 10.3389/fmars.2021.775653

Wang, C. F., Xu, Z. Q., He, Y., Yuan, C., Li, H. B., Zhao, Y., et al. (2022b). Neritic tintinnid community structure and mixing with oceanic tintinnids in shelf waters of the Pacific Arctic Region during summer. *Cont. Shelf Res.* 239:104720. doi: 10.1016/j.csr.2022.104720

Wang, C. F., Xu, Z. Q., Liu, C. G., Li, H. B., Liang, C., Zhao, Y., et al. (2019). Vertical distribution of oceanic tintinnid (Ciliophora: Tintinnida) assemblages from the Bering Sea to Arctic Ocean through Bering Strait. *Polar Biol.* 42, 2105–2117.

Wang, Y., Kang, J., Xiang, P., Wang, W., and Lin, M. (2020). Short timeframe changes of environmental impacts on summer phytoplankton in the Chukchi Sea and surrounding areas in a regional scaling. *Ecol. Indic.* 117:106693. doi: 10.1016/j.ecolind.2020.106693

Wang, Y., Xiang, P., Kang, J. H., Ye, Y. Y., Lin, G. M., and Yang, Q. L. (2018). Environmental controls on spatial variability of summer phytoplankton structure and biomass in the Bering Sea. *J. Sea Res.* 131, 1–11. doi: 10.1016/j.seares.2017.08.008

Wassmann, P., Kosobokova, K. N., Slagstad, D., Drinkvvater, K. F., Hoperoft, R. R., Moore, S. E., et al. (2015). The contiguous domains of Arctic Ocean advection: trails of life and death. *Prog. Oceanogr.* 139, 42–65. doi: 10.1016/j.pocean.2015.06.011

Woodgate, R. A. (2018). Increasing in the Pacific inflow to the Arctic from 1990 to 2015, and insights into seasonal trends and driving mechanisms from

yearround Bering Strait mooring data. *Prog. Oceanogr.* 160, 124–154. doi: 10.1016/j.pocean.2017.12.007

Woodgate, R. A., and Peralta-Ferriz, C. (2021). Warming and freshening of the Pacific inflow to the Arctic from 1990-2019 implying dramatic shoaling in Pacific Winter Water ventilation of the Arctic water column. *Geophys. Res. Lett.* 48:e2021GL092528. doi: 10.1029/2021GL092528

Xu, G., Yang, E., Jiang, Y., Cho, K., Jung, J., Lee, Y., et al. (2018a). Can pelagic ciliates indicate vertical variation in the water quality status of western Arctic pelagic ecosystems? *Mar. Pollut. Bull.* 133, 182–190. doi: 10.1016/j.marpolbul.2018.05.017

Xu, G., Yang, E., Lee, Y., and Kang, S. (2018b). Vertical shift in ciliate body-size spectrum and its environmental drivers in western Arctic pelagic ecosystems. *Environ. Sci. Pollut. Res.* 25, 19082–19091. doi: 10.1007/s11356-018-2094-z

Xu, Z. Q., Zhang, G. T., and Sun, S. (2018). Inter-annual variation of the summer zooplankton community in the Chukchi Sea: spatial heterogeneity during a decade of rapid ice decline. *Polar Biol.* 41, 1827–1843. doi: 10.1007/s00300-018-2324-3

Yamashita, Y., Yagi, Y., Ueno, H., Ooki, A., and Hirawake, T. (2019). Characterization of the water masses in the shelf region of the Bering and Chukchi Seas with fluorescent organic matter. *J. Geophys. Res. Oceans* 124, 7545–7556. doi: 10.1029/2019JC015476

Yang, E. J., Choi, J. K., and Hyun, J. H. (2004). Distribution and structure of heterotrophic protist communities in the northeast equatorial Pacific Ocean. *Mar. Biol.* 146, 1–15. doi: 10.1007/s00227-004-1412-9

Yasuhara, M., Hunt, G., Dowsett, H. J., Robinson, M. M., and Stoll, D. K. (2012). Latitudinal species diversity gradient of marine zooplankton for the last three million years. *Ecol. Lett.* 15, 1174–1179. doi: 10.1111/j.1461-0248.2012.01828.x

Yu, Y., Zhang, W. C., Zhang, C. X., Zhou, F., Zhao, N., and Xiao, T. (2014). Basin-scale variation in planktonic ciliate distribution: a detailed temporal and spatial study of the Yellow Sea. *Mar. Biol. Res.* 10, 641–654. doi: 10.1080/17451000.2013.852683

Zhang, W. C., Feng, M. P., Yu, Y., Zhang, C. X., and Xiao, T. (2012). *An Illustrated Guide to Contemporary Tintinnids in the World*. Beijing: Science Press.

Zhong, W., Steele, M., Zhang, J., and Cole, S. T. (2019). Circulation of Pacific winter water in the Western Arctic Ocean. *J. Geophys. Res. Oceans* 124, 863–881. doi: 10.1029/2018JC014604

Zhuang, Y., Jin, H., Zhang, Y., Li, H., Zhang, T., Li, Y., et al. (2021). Incursion of Alaska coastal water as a mechanism promoting small phytoplankton in the western Arctic Ocean. *Prog. Oceanogr.* 197:102639. doi: 10.1016/j.pocean.2021.102639

**Conflict of Interest:** The authors declare that the research was conducted in the absence of any commercial or financial relationships that could be construed as a potential conflict of interest.

**Publisher's Note:** All claims expressed in this article are solely those of the authors and do not necessarily represent those of their affiliated organizations, or those of the publisher, the editors and the reviewers. Any product that may be evaluated in this article, or claim that may be made by its manufacturer, is not guaranteed or endorsed by the publisher.

frontiers | Frontiers in Marine Science

ORIGINAL RESEARCH
published: 22 July 2022
doi: 10.3389/fmars.2022.863262

# Elevated $pCO_2$ Induced Physiological, Molecular and Metabolic Changes in *Nannochloropsis Oceanica* and Its Effects on Trophic Transfer

*Chengwei Liang*[1], *Yufei Zhang*[1], *Zipeng Gu*[1], *Yudong Ren*[1], *Xiaowen Zhang*[2,3], *Dong Xu*[2,3] *and Naihao Ye*[2,3]*

[1] College of Marine Science and Biological Engineering, Qingdao University of Science and Technology, Qingdao, China, [2] Yellow Sea Fisheries Research Institute, Chinese Academy of Fishery Sciences, Qingdao, China, [3] Laboratory for Marine Fisheries and Aquaculture, Qingdao National Laboratory for Marine Science and Technology, Qingdao, China

The rise of dissolution of anthropogenic $CO_2$ into the ocean alters marine carbonate chemistry and then results in ocean acidification (OA). It has been observed that OA induced different effects on different microalgae. In this study, we explored the physiological and biochemical changes in *Nannochloropsis oceanica* in response to increased atmospheric carbon dioxide and tested the effect of ocean acidification (OA) on the food web through animal feeding experiments at a laboratory scale. We found that the levels of C, N, C/N, *Fv/Fm*, and photosynthetic carbon fixation rate of algae cells were increased under high carbon dioxide concentration. Under short-term acidification, soluble carbohydrate, protein, and proportion of unsaturated fatty acids in cells were significantly increased. Under long-term acidification, the proportion of polyunsaturated fatty acids (PUFAs) (~33.83%) increased compared with that in control (~30.89%), but total protein decreased significantly compared with the control. Transcriptome and metabonomics analysis showed that the differential expression of genes in some metabolic pathways was not significant in short-term acidification, but most genes in the Calvin cycle were significantly downregulated. Under long-term acidification, the Calvin cycle, fatty acid biosynthesis, TAG synthesis, and nitrogen assimilation pathways were significantly downregulated, but the fatty acid β-oxidation pathway was significantly upregulated. Metabolome results showed that under long-term acidification, the levels of some amino acids increased significantly, while carbohydrates decreased, and the proportion of PUFAs increased. The rotifer *Brachionus plicatilis* grew slowly when fed on *N. oceanica* grown under short and long-term acidification conditions, and fatty acid profile analysis indicated that eicosapentaenoic acid (EPA) levels increased significantly under long-term acidification in both *N. oceanica* (~9.48%) and its consumer *B. Plicatilis* (~27.67%). It can be seen that *N. oceanica* formed a specific adaptation mechanism to OA by regulating carbon and nitrogen metabolism, and at the same time caused changes of cellular metabolic components. Although PUFAs were increased, they still had adverse effects on downstream consumers.

**Keywords:** ***Nannochloropsis oceanica*, elevated $pCO_2$, long-term acidification, metabolomics, transcriptomics, *Brachionus plicatilis***

OPEN ACCESS

***Edited by:***
*Mi Sun Yun,*
*Tianjin University of Science and Technology, China*

***Reviewed by:***
*Yandu Lu,*
*Hainan University, China*
*Carole Anne Llewellyn,*
*Swansea University, United Kingdom*
*Rishiram Ramanan,*
*Central University of Kerala, India*

***Correspondence:**
*Naihao Ye*
*Yenh@ysfri.ac.cn*

***Specialty section:***
*This article was submitted to Aquatic Microbiology, a section of the journal Frontiers in Marine Science*

***Received:*** *27 January 2022*
***Accepted:*** *16 June 2022*
***Published:*** *22 July 2022*

***Citation:***
*Liang C, Zhang Y, Gu Z, Ren Y, Zhang X, Xu D and Ye N (2022) Elevated $pCO_2$ Induced Physiological, Molecular and Metabolic Changes in Nannochloropsis Oceanica and Its Effects on Trophic Transfer. Front. Mar. Sci. 9:863262. doi: 10.3389/fmars.2022.863262*

# 1 INTRODUCTION

Anthropogenic emissions of carbon dioxide ($CO_2$) have steadily increased the global partial pressure of $CO_2$ ($pCO_2$) from 280 ppm in pre-industrial times to around 400 ppm at present, with the level predicted to reach 1,000 ppm by 2100 (IPCC 2013). The accelerated rise of $CO_2$ concentration in the atmosphere also accelerates the absorption of $CO_2$ by the ocean, which leads to a decrease of the pH value in seawater and the formation of ocean acidification (OA) (Caldeira and Wickett, 2003; Hopkins et al., 2020). The pH of the surface ocean has dropped by ~0.1 since pre-industrial times and will drop by ~0.4 by the end of this century (Gattuso et al., 2015), which may directly or indirectly affect marine life (Hurd et al., 2018). Marine microalgae are a key link in the marine ecosystem because they are responsible for more than 50% of global primary carbon production (Field et al., 1998; Falkowski, 2012). During OA, changes in the carbon chemistry of the water trigger regulatory changes at the physiological, biochemical, and molecular levels, as well as in the evolution, of microalgae (Jin et al., 2013; Li et al., 2014; Jin et al., 2015). The effects of OA on microalgae may be diverse: positive, negative, and even neutral (Gao & Campbell, 2014). For example, elevated $pCO_2$ reflects the light-dependent downregulation of carbon-concentrating mechanisms in *Phaeodactylum tricornutum*, thus energy saved from carbon-concentrating downregulation is used to enhance the growth of diatoms (Li et al., 2014). *P. tricornutum* grown for about 80 generations at 1,000 ppm $CO_2$ had an increased growth rate compared with that growth at 390 ppm (Li et al., 2014). At elevated $CO_2$ concentrations, the growth and photosynthesis of *Skeletonema costatum*, *Chaetoceros debilis*, and *Fragilariopsis kerguelensis* are inhibited (Chen and Gao, 2004a; Chen and Gao 2004b; Trimborn et al., 2017). Long-term conditioning to elevated $pCO_2$ influences the fatty and amino acid compositions of the diatom *Cylindrotheca fusiformis* (Bermúdez et al., 2015). Previous studies have shown that increased $CO_2$ concentration could significantly promote the utilization efficiency of inorganic carbon in *Nannochloropsis* cells and may increase the eicosapentaenoic acid (EPA) levels in algae cells (Hu and Gao, 2003). The biomass and lipid content of *Nannochloropsis oculate* increase as $CO_2$ concentration increases (Chiu et al., 2009; Razzak et al., 2015). Our previous studies have also shown that elevated $pCO_2$ could increase the growth and photosynthetic efficiency of microalgae and change the contents of total protein and soluble carbohydrates, as well as the compositions of fatty acid and amino acids (Liang et al., 2020a; Liang et al., 2020b; Liang et al., 2020c).

Studies have shown that most of the genes involved in glycolysis, the TCA cycle, and oxidative phosphorylation in polar chlorophyte *Coccomyxa subellipsoidea* C169 were significantly upregulated under elevated $pCO_2$ concentrations. In addition, the significant downregulation of fatty acid degradation genes and the upregulation of fatty acid synthesis genes may be one of the causes of fat accumulation (Peng et al., 2016). The physiological responses of the psychrophilic sea ice diatom *Nitzschia lecointei* to long-term adaptation (194 d, ~60 asexual generations) in high $pCO_2$ levels were different in growth rate and total fatty acid content from the short-term physiological responses to increased $pCO_2$ (Torstensson et al., 2015).

Because some metabolites such as essential fatty acids (FAs) play an important role in growth, development, and in the reproductive success in heterotrophs (Müler-Navarra et al., 2004; Glencross, 2009). However, they cannot be synthesized *de novo* by heterotrophic organisms and have to be acquired through the diet. Rossoll et al. (2012) showed that elevated $pCO_2$ affected the FA composition of the diatom that constrained the growth performance of copepods as consumers. In addition, OA-induced effects on metabolic of primary producers may influence the nutrient transfer efficiency (Cripps et al., 2016). However, the consequences of OA in food web interactions remain poorly understood, because OA-induced effects on the food quality of primary producers is different among different phytoplankton species and natural fluctuations in $pCO_2$ (Jin et al., 2020).

*N. oceanica* is a unicellular alga of the class Eustigmatophyceae found in the marine environment. Based on its rapid growth, oil productivities and high contents of proteins, *N. oceanica* is widely used as a feed and dietary supplement for aquaculture. Previous studies on the acidification of *N. oceanica* only focused on the accumulation of lipid (Chiu et al., 2009; Razzak et al., 2015; Ma et al., 2016), but ignored the physiological and biochemical responses of *N. oceanica* to the increased dissolved inorganic carbon, as well as the changes in the main metabolic pathways under acidification conditions, and the impacts on consumers. In this study, the physiological and biochemical response of *N. oceanica* to a short-term (7 days) acidification and its adaptive evolution to long-term (1,460 days) acidification were studied on a laboratory scale, and the impact of the changes on the food chain during the process of OA was analyzed. Our study will provide more evidence on the effect of OA on the microalga *N. oceanica* and associated food webs.

# 2 MATERIALS AND METHODS

## 2.1 *N. Oceanica* Strains and Culture Conditions

The *N. oceanica* IMET1 strain was maintained at the Yellow Sea Fisheries Research Institute, Microalgae Culture Centre, Chinese Academy of Fishery Sciences. *N. oceanica* was semi-continuously cultured at ambient (400 ppm $CO_2$, $pH_{NBS}$ 8.16, LC) and the near-future elevated $pCO_2$ concentration predicted for the end of this century (1,000 ppm $CO_2$, $pH_{NBS}$ 7.86, HC) gradients for 1,460 days (about 1,368 generations) in f/2 medium (Guillard & Ryther, 1962), respectively. We used the indoor air as a control, which might be slightly higher than a $CO_2$ concentration of 400 ppm. The cultures were diluted with fresh sterilized f/2 medium every 6 days to maintain a cell concentration below $1.0 \times 10^6$ cells $mL^{-1}$ and to maintain a steady carbonate system. Chemical carbonate system parameters were measured by 848 Titrino plus automatic titrator (Metrohm, Riverview, FL, USA) and calculated using the $CO_2$ SYS Package in the MS Excel based on pH, temperature, $CO_2$ concentration, salinity, and total alkalinity (**Table 1**) (Pierrot et al., 2006). The preservation conditions were cultured in 100 mL conical flasks containing 75 mL f/2 medium in a $CO_2$ plant

**TABLE 1 |** Parameters of the seawater carbonate system under CK, ST and LT treatments.

| Treatment | $CO_2$(ppm) | $pH_{NBS}$ | DIC (μmol $kg^{-1}$) | $HCO_3^{2-}$ (μmol $kg^{-1}$) | $CO_3^{2-}$ (μmol $kg^{-1}$) | $CO_2$ (μmol $kg^{-1}$) | Total Alkalinity (μmol $kg^{-1}$) |
|---|---|---|---|---|---|---|---|
| CK | 400 | 8.16 ± 0.02[a] | 2348 ± 152[b] | 2135 ± 141[b] | 197 ± 11[a] | 16 ± 1[b] | 2607 ± 159[a] |
| ST | 1000 | 7.86 ± 0.02[b] | 2574 ± 79[ab] | 2426 ± 77[a] | 112 ± 1[b] | 36 ± 2[a] | 2693 ± 75[a] |
| LT | 1000 | 7.85 ± 0.01[b] | 2677 ± 127[a] | 2524 ± 121[a] | 115 ± 4[b] | 38 ± 3[a] | 2797 ± 127[a] |

*These parameters were calculated based on salinity, pH, temperature, and total alkalinity with CO2SYS software. The different superscript letters indicate significant differences among treatments at $p < 0.05$. CK, control; ST, short-term acidification; LT, long-term acidification.*

growth chamber (GXZ, Ruihua, Wuhan, China), in which the $CO_2$ concentration was continuously monitored and maintained at 400 ± 20 ppm or 1000 ± 40 ppm, at 100 μmol photons·$m^{-2}$·$s^{-1}$, in 20 ± 0.1°C and a 12 h light/12 h dark photoperiod cycle.

## 2.2 Experimental Treatments

In this assay, the algal cells grown at 400 ppm and 1,000 ppm were cultured to logarithmic phase and the initial optical density (OD, 680 nm) (Das et al., 2011) of two algal solutions were diluted to 0.02 by using an ultraviolet spectrophotometer (UV-2000, UNICO, Suzhou, China). For the control (CK), algal cells were cultured in 400 ppm $CO_2$ with bubbling of LC; for short-term acidification (ST), algal cells were cultured at 400 ppm $CO_2$ and transferred to 1,000 ppm $CO_2$ for continuous bubbling of HC; for long-term acidification (LT), algal cells in 1,000 ppm $CO_2$ were inoculated and cultured with bubbling of HC. The initial cell concentrations of the three treatments were (2.15 ± 0.02) × $10^5$ cells $mL^{-1}$ (CK), (2.12 ± 0.05) × $10^5$ cells $mL^{-1}$ (ST), and (2.24 ± 0.10) × $10^5$ cells $mL^{-1}$ (LT). The conditions of aeration were processed according to the method described by (Zhang et al., 2021). Algal cells were harvested by centrifugation (5804R, Eppendorf, Hamburg, Germany) at 6,000× g for 5 min at specific times and washed twice with distilled water to remove the effects of impurities and salts (Rocha et al., 2003). For each of the three cultures for each treatment three sample replicates were taken, with the culture conditions the same as before.

## 2.3 Measurement of Cell Growth and Carbon Biofixation Rate

Algal cell density was measured by using a combination of spectrophotometry and hemocytometry every other day. For each of the three cultures for each treatment three sample replicates were taken. Each sample was diluted to an OD680 value between 0.1 to 1.0 if the OD of the algal solution was greater than 1.0. For the measurement of cell dry weight (g $L^{-1}$), each 50 mL sample was centrifuged at 6,000 × g for 5 min to remove the supernatant and then washed twice with distilled water to remove excess salts. Then it was transferred to a dried and weighed tin foil square box, dried in the oven at 60°C for 24 h, and the change in cell dry weight was determined.

We measured the $OD_{680}$ value, cell concentration, and dry weight of every sample according to the methods described by Tang et al. (2011) and Das et al. (2011). Linear regression was used to obtain the relationship between cell dry weight and OD (**Figure S1**), and the relationship between cell concentration and OD (**Figure S2**).

Specific growth rate μ ($d^{-1}$) was calculated as follows:

$$\mu = \frac{\ln(C_f / C_0)}{\Delta t} \quad (1)$$

where $C_f$ and $C_o$ were the final and initial cell concentrations (cells $mL^{-1}$), respectively, and Δt was the cultivation time in days (Liang et al., 2020c).

Biomass productivity $P$ (g $L^{-1}$ $d^{-1}$) was calculated from the following equation:

$$P = \frac{X_1 - X_0}{t_1 - t_0} \quad (2)$$

where $X_1$ and $X_0$ were the biomass concentration (g $L^{-1}$) on days $t_1$ and $t_0$, respectively (Morais and Costa, 2007).

The carbon dioxide biofixation rate $R_{CO2}$ (g $L^{-1}$ $d^{-1}$) was calculated using the following equation:

$$R_{CO2} = C_C P\left(\frac{M_{CO_2}}{M_C}\right) \quad (3)$$

where $C_C$ was the carbon content of microalgal cells (%, w/w), $M_{CO2}$ was the relative molecular mass of carbon dioxide, $M_C$ was the relative molecular mass of carbon, and $P$ was the biomass productivity (g $L^{-1}$ $d^{-1}$) (Morais & Costa, 2007; Tang et al., 2011).

## 2.4 Measurement of Chlorophyll Fluorescence

The maximum quantum yield of photosystem (PS) II (*Fv/Fm*) was measured by Maxi-Imaging-PAM (Walz, Effeltrich, Germany). The algal solutions and parameter settings before measurement of chlorophyll fluorescence referred to Zhang et al. (2021). The maximum quantum yield (*Fv/Fm*) was calculated from the following equation:

$$Fv/Fm = (Fm - Fo)/Fm \quad (4)$$

where *Fv* was the variable fluorescence calculated from *Fv* = *Fm* - *Fo*, *Fm* was the maximum fluorescence yield produced by a saturated light pulse in the chlorophyll fluorescence induction curve, and *Fo* was the minimal fluorescence of microalgae after dark adaptation (Genty et al., 1989).

## 2.5 Determination of Carbon and Nitrogen Content

To draw a calibration curve, 40, 50, 60, 70, and 80 mg glutamic acid were weighed in a stainless-steel crucible, and the total carbon and total nitrogen of the samples were measured by using an element analyzer (Vario Max CN, Elementar, Langenselbold, Germany). Subsequently, a suitable amount of algal powder (50.0~50.1 mg) was weighed in a stainless-steel crucible and the total carbon and total nitrogen of the sample were determined by the element analyzer. The carrier gas pressure was He: 0.38 MPa, $O_2$: 0.25 MPa. The temperatures of the combustion tube, secondary combustion tube, and reduction tube were 900°C, 900°C, and 830°C, respectively.

## 2.6 Determination of Total Soluble Carbohydrate and Protein Content

The total soluble carbohydrate was determined from 0.1 g dry algal powder in distilled water at 95~100°C for 10 min using anthrone colorimetry (Liu et al., 1973). Total soluble protein content was measured by the bicinchoninic acid assay (BCA) using 0.1 g dry algal powder (Smith et al., 1985). The above biochemical compositions were determined by assay kits (Jiancheng, Nanjing, China).

## 2.7 Determination of Fatty Acid Composition

Methanol containing 2% $H_2SO_4$ (5 mL) was added in 10 mL flasks containing approximately 5~10 mg dry algal powder and incubated for 1 h at 70°C. Then 2 mL of hexane and 0.75 mL of distilled water were added after the flasks cooled to room temperature and mixed for 30 s on a vortex mixer. Extraction of fatty acid methyl esters (FAMEs) referred to a previous study by Liu et al. (2015). FAMEs analyses were carried out by using an Agilent 7890 gas chromatography (GC) instrument equipped with a flame-ionization detector and a DB-23 capillary column (Agilent Technologies, Santa Clara, CA, USA, 30 m × 0.32 mm × 0.25 μm). The injector temperature was 270°C with a split ratio of 10:1. The temperature-rise program was as described previously (Meng et al., 2015).

## 2.8 Determination of Algal Cell Surface pH

The pH of the algal cell surface was determined by using an algal solution in logarithmic phase. The treatment of the algal solution, fluorophore loading, and fluorescence ratio-pH calibration curve were based on a study described previously (Golda-VanEeckhoutte et al., 2018). Algal cells were harvested during the mid-logarithmic phase and concentrated by centrifugation at 12,000 g for 3 min, washed twice with PBS buffer solution, and resuspended in sterile PBS buffer. The washed algal cells were loaded with fluorophore by adding 3 μL of 1 mM 5-(and-6)-carboxy seminaphtharhodafluor (SNARF)-1 dissolved in anhydrous dimethyl sulfoxide (DMSO; ≥ 99.9%), together with 3 μL of 5% solution of the Pluronic F-127 dissolved in DSMO. The fluorophores were loaded into the cells by passive diffusion during an incubation period of 30~40 min. For the blank treatment, the procedure of fluorophore loading was the same as before (including adding Pluronic F-127) but avoiding the addition of the SNARF fluorescent probes. After incubation, the algal cells were centrifuged at 12,000× g for 3 min, washed twice as described above, and resuspended in PBS buffer for the measurement of fluorescence emission. Fluorescence emission was measured at two wavelengths: 585 nm (F1) and 630 nm (F2). The 520 nm was set as the optimal excitation wavelength for the fluorescence detection of SNARF in all subsequent measurements by spectrofluorometry (F-4600, Hitachi, Tokyo, Japan). The pH was calculated by using a calibration curve of the quotient (defined as R) of F1 divided by F2 at different PBS buffer pH levels in triplicate samples as follows:

$$R = F1/F2 \tag{5}$$

To establish the calibration curve, the fluorescently labeled cells were killed by adding 7.25 μL 6.7 mM nigericin dissolved in absolute ethanol and incubated for 10 min. Subsequently, PBS buffers with different pH gradients (5.88, 6.26, 6.57, 6.86, 7.16, 7.47, and 8.01) were added and resuspended.

## 2.9 RNA Extraction and Illumina Sequencing

After cultivation for 7 days, CK, ST, and LT cells were centrifuged at 12,000 g for 5 min in 4°C, respectively. The samples were frozen in liquid nitrogen and then stored at -80°C immediately. Total RNAs were extracted and purified from frozen *N. oceanica* cells with an RNA extraction kit (Omega, Norcross,GA, USA) according to the manufacturer's protocol. RNA purity was checked by using a NanoPhotometer Spectrophotometer (Implen, CA, USA). RNA concentration was measured by using a Qubit 3.0 Fluorometer (Life Technologies, CA, USA). RNA integrity was assessed by using a Bioanalyzer 2100 system RNA Nano 6000 Assay Kit (Agilent Technologies, CA, USA). RNA purification, library construction, and RNA-seq were performed by the Annoroad Gene Technology Co., Ltd. (Beijing, China).

Briefly, a library for each sample was generated from 3 μg of RNA and then sequenced using Illumina NovaSeq 6000. To obtain the high-quality data used in the analysis, raw reads were first subjected to preliminary processing by using custom Perl scripts to remove reads that contained adapter sequences, poly-N sequences (greater than 5%), low quality reads, and reads with lengths of less than 30 bp. The filtered clean reads were mapped to an *N. oceanica* reference genome (https://genome.jgi.doe.gov/portal/, JGI Project Id: 1143084) using HISAT2 v2.1.0 (Kim et al., 2015). The read counts of each gene in each sample were counted by HTSeq v0.6.0, and fragments per kilobase million mapped reads (FPKM) were used for gene expression level quantification (Trapnell et al., 2010). DESeq2 was used to estimate the expression level of each gene per sample by using linear regression and then the *p* value was calculated with the Wald test (Wang et al., 2010). Finally, the *p* value was corrected by the Benjamini and Hochberg method to obtain the *q* value.

Genes with $q < 0.05$ and $|\log_2(\text{Fold Change})| > 1.0$ were identified as differentially expressed genes (DEGs).

## 2.10 Function Enrichment Analysis

The Gene Ontology (GO, http://geneontology.org/) enrichment of DEGs was implemented by the hypergeometric test, in which the *p* value was calculated and adjusted as a *q* value, and data background was genes in the whole genome. GO terms with $q < 0.05$ were considered to be significantly enriched. GO enrichment analysis could exhibit the biological functions of the DEGs. Kyoto Encyclopedia of Genes and Genomes (KEGG, http://www.kegg.jp/) was a database resource containing a collection of manually drawn pathway maps representing our knowledge on the molecular interaction and reaction networks. The KEGG enrichment of DEGs was implemented by the hypergeometric test, in which the *p* value was adjusted by multiple comparisons as the *q* value. KEGG terms with $q < 0.05$ were considered to be significantly enriched.

## 2.11 Metabolite Extraction

Each sample was ground with liquid nitrogen, 100 mg was weighed and then added to 200 μL pre-cooled water and 800 μL pre-cooled methanol/acetonitrile (1:1, v/v). It was mixed thoroughly, sonicated in an ice bath for 60 min, and then incubated at -20°C for 1 h to precipitate proteins. After centrifugation at 16,000 × *g* for 20 min at 4°C, the supernatant was collected and then evaporated in a high-speed vacuum concentration centrifuge. For mass spectrometry detection, 100 μL of acetonitrile/water solution (1:1, v/v) was added to the sample for redissolution, it was centrifuged at 14,000 × *g* for 15 min in 4°C, and the supernatant was removed for analysis.

## 2.12 LC-MS/MS Analysis

Metabolite profiling was conducted using an LC-MS/MS ultra-performance liquid chromatography (UPLC) system (Agilent 1290 Infinity LC; MS/MS, Triple-TOF 5600+, AB SCIEX). Chromatographic separation was performed on an ACQUITY UPLC BEH Amide column (2.1 mm × 100 mm × 1.7 μm; Waters) using mobile phase A (water + 25 mM ammonium acetate + 25 mM ammonia) and mobile phase B (acetonitrile). The gradient elution procedure was as follows: 0–0.5 min, 95% B; 0.5–7 min, B changed linearly from 95% to 65%; 7–9 min, B changed linearly from 65% to 40%; 9–10 min, B maintained at 40%; 10–11.1 min, B changed linearly from 40% to 95%; 11.1–16 min, B maintained at 95%. The column temperature was set to 25°C and the flow rate was maintained at 0.3 mL $min^{-1}$. QC samples were inserted into the sample queue to monitor and evaluate the stability of the system and the reliability of the experimental data.

Mass data acquisition was performed in electrospray ionization (ESI) positive and negative mode using the following parameters: ion source gas1 (Gas1) of 60 psi; ion source gas2 (Gas2) of 60 psi; curtain gas (CUR) of 30 psi; source temperature of 600°C; ion spray voltage floating of ± 5.5 kV; TOF MS scan m/z range: 60–1200 Da, product ion scan m/z range: 25–1,200 Da, TOF MS scan accumulation time 0.15 s/spectra, product ion scan accumulation time 0.03 s/spectra; information-dependent acquisition (IDA) was used for secondary mass spectrometry and adopted high sensitivity mode; declustering potential of ± 60 V; collision energy of 30 eV. IDA settings were as follows: exclude isotopes within 4 Da, candidate ions to monitor per cycle: 6.

## 2.13 Identification of Significantly Different Metabolites

The original data were formatted, and the XCMS program in MSDIAL software was used for peak alignment, retention time correction, and extraction peak area. The structures of metabolites were identified by using accurate mass number matching (< 25 ppm) and secondary spectrum matching methods to search public databases such as HMDB, MassBank, and a self-built metabolite standard library. For the extracted data, the ion peaks with missing values of more than 50% were deleted, the positive and negative ion peaks were integrated, and the software SIMCA-P 14.1 (Umetrics, Umea, Sweden) was used for pattern recognition. After these data were preprocessed by Pareto scaling, multidimensional statistical analysis was carried out, including unsupervised principal component analysis (PCA), partial least squares-discriminant analysis (PLS-DA), and orthogonal projections for latent structures-discriminant analysis (OPLS-DA). Differential metabolites were filtered according to $|\log_2(\text{fold change})| > 1$ and $p$ value$< 0.05$. Metabolites with the variable importance for the projection (VIP) > 1 and *p* value< 0.05 were identified as significantly different metabolites (SDMs). Metabolites were identified by the Shanghai Bioprofile Technology Co., Ltd. (Shanghai, China).

## 2.14 Feeding Experiments

The rotifer *Brachionus plicatilis* was provided by Institute of Oceanology, Chinese Academy of Sciences. For the RC, rotifers were fed with CK in a plant growth chamber (400 ppm). For the RS and RL, rotifers were fed with ST and LT in a plant growth chamber (1,000 ppm), respectively. These culture parameters were the same as the previous algal culture conditions. The initial inoculation concentration of rotifers was 8 rot $mL^{-1}$ and was cultured in a 1 L glass beaker. On the 0, 2, 4, 5, and 6 days, the same concentration of the algal solution was fed to keep the bait concentration at $2.5 \times 10^9$ cells $L^{-1}$, and the concentration of rotifers was measured by a hemocytometer. On day 7, the rotifers were collected with a 200-mesh (74 μm) filter and washed twice with distilled water to remove algal fragments and salts. Then, the rotifers were dried in an oven at 60°C for 24 h. The dried rotifers were ground with liquid nitrogen to obtain a powder and stored at -80°C. The fatty acid composition of rotifers was measured as described previously. For each of the three cultures for each treatment three sample replicates were taken.

## 2.15 Statistical Analysis

One-way analysis of variance (ANOVA) with the least significant difference *post hoc* test and the *t*-test were used to analyze the significant differences among different treatments. The Spearman's method was used to analyze the correlation coefficients among

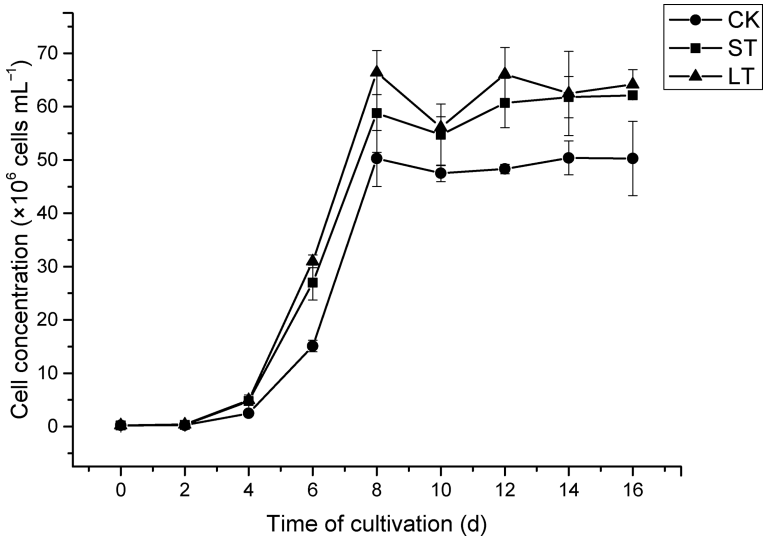


**FIGURE 1 |** The growth curve of *N. oceanica* cultivated at different cultivated conditions. The error bars represent the standard deviation (SD), n = 3.

replicated treatments, and the correlation coefficients among SDMs were calculated based on the Pearson's method (Hauke and Kossowski, 2011). R (3.5.3), and Adobe Illustrator CS6 was used to draw and modify graphics. Significant differences were assumed to be $p< 0.05$.

## 3 RESULTS

### 3.1 Cell Growth, Photosynthesis, and Carbon Dioxide Biofixation Rate in Response to Elevated $pCO_2$

The cell growth of *N. oceanica* was affected significantly under elevated $pCO_2$, as shown in **Figure 1**. Under the three conditions, cells all entered the logarithmic growth phase from the 2nd day and reached the highest cell concentration (CK, $5.03 \times 10^7$ cells $mL^{-1}$; ST, $5.88 \times 10^7$ cells $mL^{-1}$; LT, $6.64 \times 10^7$ cells $mL^{-1}$) around the 8th day to enter the stationary phase. According to equation (1), we calculated the growth rate of *N. oceanica* based on the cell density on the 2nd day and the 8th day: CK, 0.67275 ± 0.01725 $d^{-1}$; ST, 0.71645 ± 0.01075 $d^{-1}$($p$ =0.015); LT, 0.7169 ± 0.0188 $d^{-1}$ ($p$ =0.012). The results showed the growth of cells under ST and LT increased significantly compared with CK. ST and LT increased the *Fv/Fm* significantly ($p< 0.05$), whereas the CK had the lowest *Fv/Fm* value (**Figure 2A**). Moreover, high $CO_2$ conditions significantly increased the $CO_2$ biofixation rate compared with ambient conditions (**Figure 2B**). Briefly, consistent with other studies, we found that OA could enhance photosynthesis and $CO_2$ biofixation, promoting the growth of *N. oceanica*.

### 3.2 Biochemical Composition in Response to Elevated $pCO_2$

As shown in **Table 2**, the cells of ST and LT both significantly increased contents of total carbon and total nitrogen as well as the ratio of C/N when compared with CK. This indicated that high $CO_2$ concentration enhanced the contents of carbon and nitrogen to maintain rapid cell growth. The long-term elevated $pCO_2$ adaptation significantly decreased the total protein content, while the short-term elevated $pCO_2$ acclimation significantly increased the total soluble carbohydrate content when compared with the ambient conditions (**Table 2**).

The fatty acid profiles of *N. oceanica* grown under CK, ST, and LT conditions were detected by GC-MS. The proportion of unsaturated fatty acids (USFAs) were CK: 62.75 ± 3.17%; ST: 66.27 ± 0.87%; LT: 65.17 ± 0.50%, which were all above 60% (**Table 3**). This result is line in with previous study that *N. oceanica* was a type of microalga that is rich in USFAs (Sharma & Schenk, 2015), and was important to nutrient transfer in the marine food chain. Under the three conditions, the major fatty acid components of *N. oceanica* were C16 and C20 (> 87.86%). C14:0, C16:1n7, and C20:5n3 were significantly increased under elevated $pCO_2$ conditions, whereas C16:0 and C18:1n9 were significantly reduced (**Table 3**). Intriguingly, high $CO_2$ conditions significantly decreased the proportion of saturated fatty acids

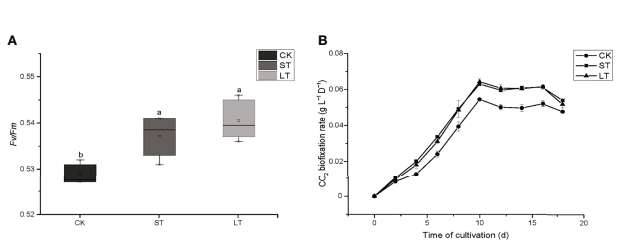


**FIGURE 2 |** The *Fv/Fm* **(A)** and $CO_2$ biofixation rate **(B)** of *N. oceanica* when subjected to different treatment conditions. The error bars represent the standard deviation (SD), n = 3. Different letters represent significant differences at $p< 0.05$. CK, control; ST, short-term acidification; LT, long-term acidification.

**TABLE 2 |** Biochemical components of *N. oceanica* when subjected to different treatments.

| Biochemical component content | CK | ST | LT |
|---|---|---|---|
| Carbon and nitrogen content (mg $L^{-1}$) | | | |
| Carbon | 45.58 ± 0.56$^b$ | 51.51 ± 0.07$^a$ | 51.74 ± 0.11$^a$ |
| Nitrogen | 7.47 ± 0.09$^b$ | 8.15 ± 0.03$^a$ | 8.13 ± 0.01$^a$ |
| C/N | 6.10 ± 0.04$^a$ | 6.45 ± 0.01$^b$ | 6.56 ± 0.03$^b$ |
| Total soluble carbohydrate content (mg $g^{-1}$) | 18.03 ± 2.21$^b$ | 30.57 ± 4.01$^a$ | 22.13 ± 1.47$^b$ |
| Total protein content (mg $mL^{-1}$) | 0.89 ± 0.03$^a$ | 0.96 ± 0.14$^a$ | 0.68 ± 0.01$^b$ |

*For each of the three cultures for each treatment three sample replicates were taken. Values are the averages of three replicates ± s.The different superscript letters indicate significant differences (p< 0.05). CK, control; ST, short-term acidification; LT, long-term acidification.*

**TABLE 3 |** Fatty acid composition (%) of *N. oceanica* when subjected to different treatments.

| Fatty acids | CK | ST | LT |
|---|---|---|---|
| Saturated fatty acid (%) | | | |
| C14:0 | 4.54 ± 0.21$^b$ | 5.49 ± 0.35$^a$ | 5.59 ± 0.00$^a$ |
| C16:0 | 32.60 ± 2.96$^a$ | 28.24 ± 0.53$^b$ | 29.05 ± 0.38$^b$ |
| Monounsaturated fatty acid (%) | | | |
| C16:1n7 | 26.25 ± 1.17$^b$ | 29.35 ± 0.24$^a$ | 28.45 ± 0.30$^a$ |
| C18:1n9 | 4.72 ± 0.21$^a$ | 3.08 ± 0.33$^b$ | 3.26 ± 0.17$^b$ |
| Polyunsaturated fatty acid (%) | | | |
| C18:2n6 | 1.87 ± 0.00$^a$ | 1.82 ± 0.21$^a$ | 1.44 ± 0.04$^b$ |
| C20:4n6 | 4.11 ± 0.38$^a$ | 4.29 ± 0.11$^a$ | 4.54 ± 0.31$^a$ |
| C20:5n3 | 24.90 ± 0.99$^b$ | 27.73 ± 1.48$^a$ | 27.67 ± 0.57$^a$ |
| ΣSFA | 38.14 ± 2.75$^a$ | 33.73 ± 0.87$^b$ | 34.64 ± 0.38$^b$ |
| ΣMUFA | 30.97 ± 1.37$^a$ | 32.43 ± 0.56$^a$ | 31.70 ± 0.47$^a$ |
| ΣPUFA | 30.89 ± 1.37$^b$ | 33.84 ± 1.42$^a$ | 33.65 ± 0.84$^a$ |
| ΣUSFA | 61.86 ± 2.75$^b$ | 66.27 ± 0.87$^a$ | 65.36 ± 0.38$^a$ |

*The different superscript letters indicate significant differences (p< 0.05). CK, control; ST, short-term acidification; LT, long-term acidification.*

(SFAs) but increased the proportion of unsaturated fatty acids (**Table 3**).

## 3.3 Algal Cell Surface pH in Response to Elevated $pCO_2$

According to the pH calibration curve using the fluorescence ratio (**Figure S3**), the cell surface pH of the three conditions were CK, 8.14 ± 0.01; ST, 7.83 ± 0.16; and LT, 7.84 ± 0.44. It was speculated that the carbonate system and pH of seawater were changed by OA. To adapt to changes in the environment, the surface pH of algal cells also changed, leading to significant changes in physiology and biochemistry.

## 3.4 Construction and Functional Analysis of the Transcriptome Library in Response to Elevated $pCO_2$

About 43.24~48.21 million raw reads were obtained in *N. oceanica* through the Illumina NovaSeq 6000 sequencing platform (**Table 4**). Subsequently, raw reads were filtered with the Trimmomatic ver. 0.32 (Bolger et al., 2014), resulting in over 41.12 million clean reads. In all nine *N. oceanica* libraries, more than 91.33% of the sequence quality scores were higher than Q30 (**Figure S4**), indicating that the libraries had high quality clean reads. Therefore, more than 36.27 million clean reads were compared to the reference genome, and the rate of matching

**TABLE 4 |** Summary statistics of the transcriptome of *N. oceanica* when subjected to different treatments.

| Sample Name | Raw Reads | Clean Reads | Q30 (%) | Mapped Reads | Mapping Rate (%) | Total Genes |
|---|---|---|---|---|---|---|
| **CK1** | 45247110 | 43308332 | 92.31 | 37185024 | 85.86 | 9344 |
| **CK2** | 43238672 | 41118394 | 92.42 | 35312473 | 85.88 | 9302 |
| **CK3** | 48211608 | 46292536 | 92.24 | 39684059 | 85.72 | 9352 |
| **ST1** | 48751542 | 46773438 | 92.55 | 40470445 | 86.52 | 9324 |
| **ST2** | 43547176 | 41994710 | 92.32 | 36267301 | 86.36 | 9359 |
| **ST3** | 46570054 | 44803422 | 92.07 | 38838988 | 86.69 | 9386 |
| **LT1** | 45036472 | 43014708 | 92.56 | 37569284 | 87.34 | 9334 |
| **LT2** | 46154424 | 44161292 | 91.33 | 38201646 | 86.50 | 9344 |
| **LT3** | 49239750 | 47236650 | 91.96 | 41003941 | 86.81 | 9338 |

*CK, control; ST, short-term acidification; LT, long-term acidification.*

ranged from 85.72 to 87.34% (**Table 4**). From FPKM calculations of the three types of libraries, 9332, 9356, and 9338 genes were obtained in CK, ST, and LT, respectively (**Table 4**).

## 3.5 Analysis of Gene Expression Patterns in Response to Elevated $pCO_2$

With the filter criteria of |log2(fold change)| > 1 and $q$< 0.05, 1692 DEGs were identified in LT when compared to the CK, of which 868 and 824 genes were upregulated and downregulated, respectively (**Figure 3A**). Likewise, 495 DEGs were identified in ST compared to the CK, of which 363 and 132 genes were upregulated and downregulated, respectively (**Figure 3A**). As shown in the volcano plots (**Figure S5**), the fold-change of upregulated and downregulated DEGs were the same in LT vs. CK, but the fold-change of upregulated DEGs were more than that of downregulated DEGs in ST vs. CK. In the relationships between different DEG groups displayed as a Venn diagram, there were 357 overlapping DEGs between LT vs. CK and ST vs. CK, 670 overlapping DEGs between LT vs. CK and LT vs. ST, and 141 overlapping DEGs between LT vs. ST and ST vs. CK, and the three groups of overlapping DEGs were 93 (**Figure 3B**). To compare the transcriptomes of the different conditions, a heat map was generated to show the transcript abundance of all DEGs. Hierarchical clustering analysis of DEGs showed that the expression patterns of the LT were highly distinct from those under normal conditions, whereas the expression patterns of the ST were similar to normal (**Figure 3C**). This result indicated that long-term elevated $pCO_2$ adaptation had a dramatic effect on gene expression, but short-term elevated $pCO_2$ acclimation was not particularly obvious.

## 3.6 Functional Analysis of Differential Expressed Genes in Response to Elevated $pCO_2$

As shown in **Figure 4**, GO analysis was conducted for the DEGs of LT vs. CK and ST vs. CK, and all DEGs were classified into cellular components, biological processes, and molecular function. GO analysis of these DEGs showed enrichment of six major cellular components, including membrane, macromolecular complex, organelle, organelle part, membrane part, and cell part. In biological processes, DEGs were enriched in metabolic process, cellular process, response to stimulus, localization, biological regulation, and cellular component organization or biogenesis. In molecular function, most of the DEGs were enriched in three categories including catalytic activity, transporter activity, and binding (**Figure 4**). KEGG pathway enrichment analysis revealed that these DEGs were mainly enriched in C- and N-related metabolic pathways (**Figure 5**). In the bubble chart of KEGG enrichment, DEGs were enriched in glycolysis/gluconeogenesis, fatty acid metabolism, fatty acid biosynthesis, carbon metabolism, carbon fixation in photosynthesis organisms, and biosynthesis of amino acid in the LT vs. CK (**Figure 5A**), and enriched in carbon metabolism, carbon fixation in photosynthetic organisms, and biosynthesis of amino acid in the ST vs. CK (**Figure 5B**). It could be hypothesized that these metabolic pathways were involved in the response of *N. oceanica* to OA and promoted its growth.

## 3.7 Metabolomic Analysis in Response to Elevated $pCO_2$

As shown in **Figure 6A**, in the unsupervised PCA analysis, the R2X value of PCA was 0.366, indicating that there were significant differences between the LT, ST, and CK groups. PLS-DA analysis

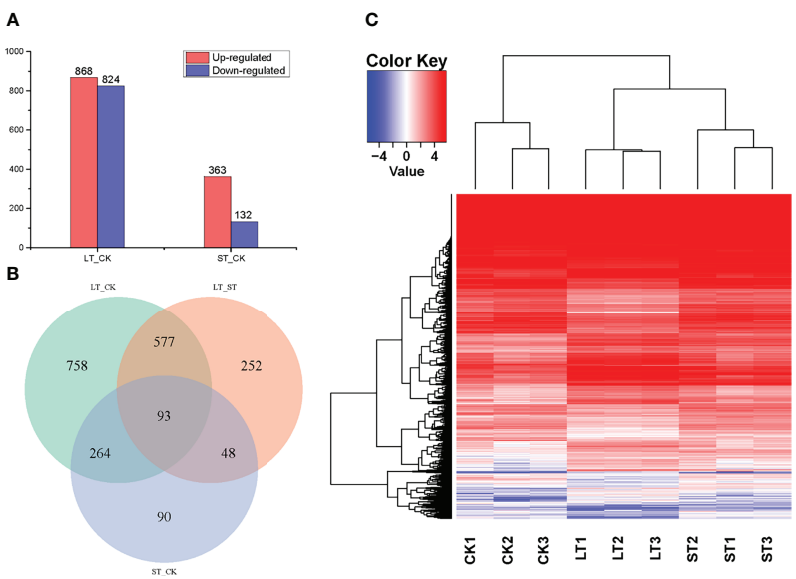


**FIGURE 3 |** Statistics and analysis of differentially expressed genes (DEGs) among the different treatments. **(A)** The number of DEGs between the different treatments. **(B)** Venn diagram shows the overlapping DEGs among of LT vs. CK, LT vs. ST, and ST vs. CK. **(C)** Heat map analysis of the DEGs among the different treatments; red represents upregulated, and blue represents downregulated. CK, control; ST, short-term acidification; LT, long-term acidification.

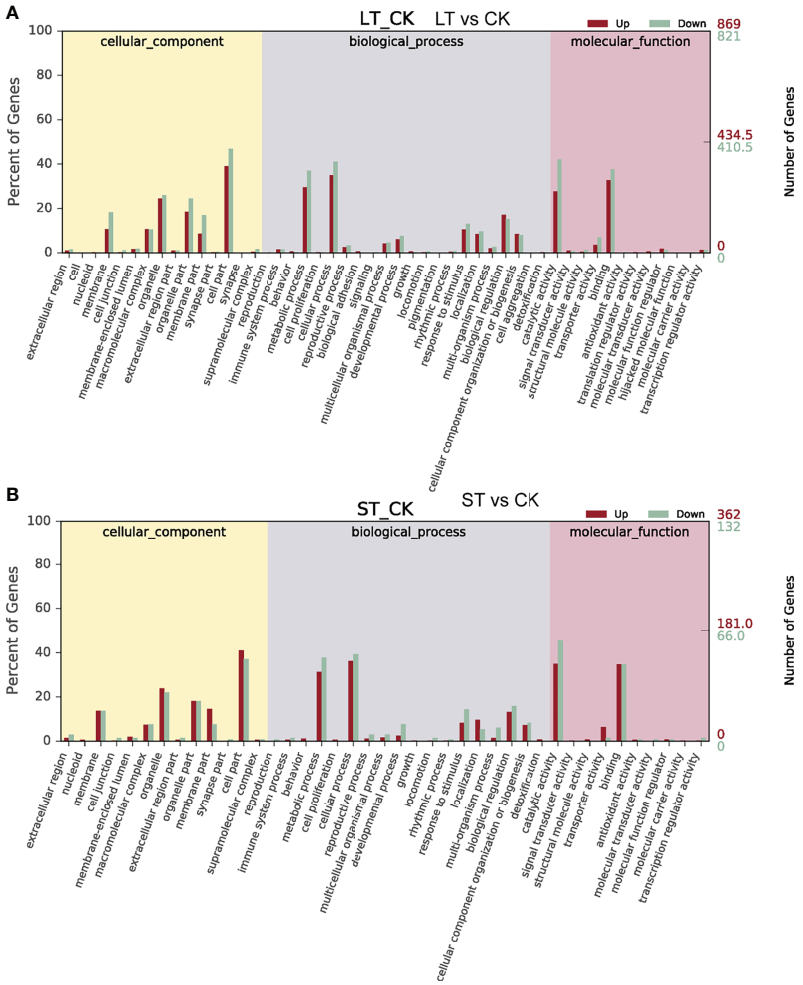


**FIGURE 4 |** Gene Ontology (GO) functional classification of differentially expressed genes (DEGs). **(A)** GO functional classification of DEGs in the LT vs CK. **(B)** GO functional classification of DEGs in the ST vs CK. CK, control; ST, short-term acidification; LT, long-term acidification.

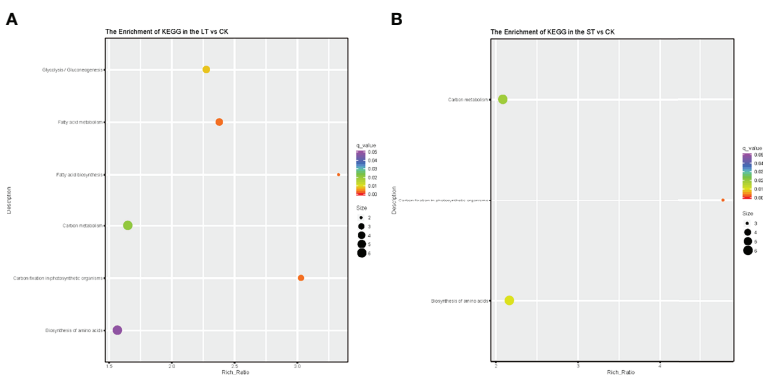


**FIGURE 5 |** Kyoto Encyclopedia of Genes and Genomes pathway enrichment of differentially expressed genes (DEGs) in the LT vs. CK **(A)** and ST vs. CK **(B)**. Number of DEGs was represented by the size of the circle. CK, control; ST, short-term acidification; LT, long-term acidification.

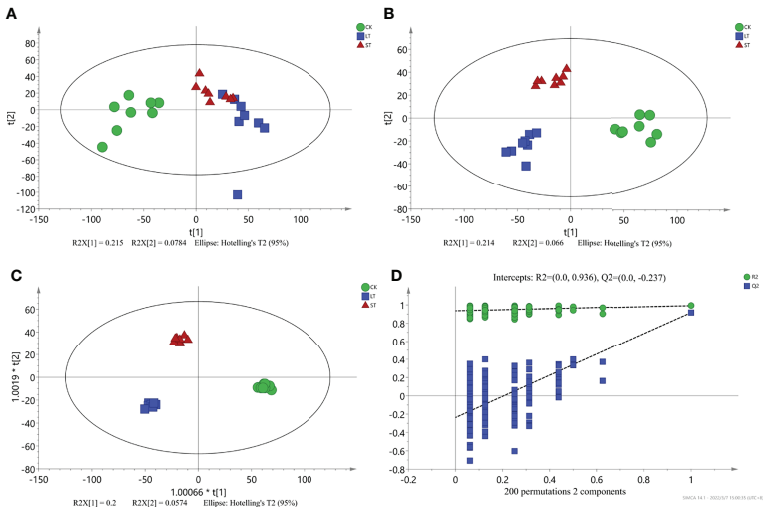


**FIGURE 6 |** Derived principal component analysis (PCA) score plot, partial least squares-discriminant analysis (PLS-DA) score plot, orthogonal projections for latent structures (OPLS-DA) score plot, and permutation test plot of OPLS-DA from the UPLC-Q-TOF-MS metabolite profiles. **(A)** PCA score plot of metabolite profiles from the LT, ST, and CK. **(B)** PLS-DA score plot in the LT vs. ST vs. CK. **(C)** OPLS-DA score plot in the LT vs. ST vs. CK. **(D)** Permutation test plot of OPLS-DA in the LT vs ST vs. CK. CK control; ST, short-term acidification; LT, long-term acidification.

showed that R2 and Q2 values were both close to 1.0, indicating that the model was very stable and effective (**Figure 6B**). In addition, OPLS-DA (modified PLS-DA) was used to clarify the metabolic patterns among different groups. To assist the screening of marker metabolites, VIP was calculated to measure the impact intensity and explanatory ability of each metabolite expression pattern on the classification discrimination of each group of samples (VIP > 1.0). In the LT vs. ST vs. CK, the parameters of the OPLS-DA model were R2X = 0.395, R2Y = 0.994, and Q2 = 0.754, the above data showed that the model was reliable and stable (**Figure 6C**). After 200 permutations, the R2 and Q2 intercepts of LT vs. ST vs. CK were 0.936 and −0.237. The intercept values of Q2 in both groups were less than 0.05, indicating a low risk of overfitting and the reliability of the model (**Figure 6D**).

With the filter criteria of $|\log_2(\text{fold change})| > 1$ and $p < 0.05$, the differential metabolites were presented by the volcano plots, and it was found that the metabolites of *N. oceanica* under OA conditions were significantly different from those under normal culture conditions. In the LT vs CK, upregulated and downregulated metabolites accounted for a half, while in the ST vs. CK, most of the metabolites were downregulated (**Figure S6**). The SDMs were used to mine the VIP obtained from the OPLS-DA model with biological significance. In the LT vs. CK and ST vs. CK, 321 and 303 SDMs were identified, and the hierarchical clustering analysis of these SDMs showed that the metabolic patterns of LT, ST, and CK were highly different (**Figures S7**, **S8**). Subsequently, Pearson's correlation was used to obtain the correlation coefficients between different groups of SDMs and display them in a matrix heatmap (**Figures S9**, **S10**). In addition, 14 out of 321 SDMs in the LT vs. CK and 9 out of 303 SDMs in the ST vs. CK were selected to analyze the changes in C- and N-related metabolic pathways combined with transcriptome, physiological, and biochemical data (**Table 5**).

## 3.8 Changes of Growth and Fatty Acid Profiles in *B. Plicatilis*

After feeding with *N. oceanica* under different acidification conditions, the growth curves of rotifers were measured as shown in **Figure 7**. The *B. plicatilis* in the RC group fed CK grew the fastest and remained in a stage of rapid growth, while the rotifers in the RS and RL groups fed ST and LT grew slowly.

Fatty acid profiles of *B. plicatilis* fed on algae powder grown with normal and high $CO_2$ concentration were analyzed by GC-MS, and three biological replicates were set for each condition. As shown in **Table 6**, the MUFA content of rotifers under different feeding conditions accounted for the largest proportion, RC: 47.32 ± 0.81%; RS: 49.62 ± 0.37%; RL: 48.89 ± 0.06%; The MUFAs of rotifers were significantly increased ($p < 0.05$) after they were fed powder from algae grown under acidified conditions. The EPA content of RS was increased and that of RL was significantly increased ($p < 0.05$), which was the same as that of *N. oceanica* under ST and LT conditions. However, the levels of arachidonic acid (C20:4N6, ARA) and C18:2N6 were significantly decreased in RS and RL, and at the same time, the levels of PUFAs in RS were significantly decreased. The insignificant change of PUFAs in RL might be caused by the large increase in EPA levels. The contents of C14:0 and C16:1N7 of rotifers were significantly increased ($p < 0.05$) by feeding algae powder grown with high $CO_2$ concentration, which was consistent with the change of *N. oceanica* under acidification. In particular, the content of C16:0 in rotifers was the same as that in *N. oceanica*, and both

**TABLE 5 |** Significantly different metabolites related to C and N metabolism.

| Metabolite | KEGG CID | Formula | LT_CK | | ST_CK | |
|---|---|---|---|---|---|---|
| | | | FC | Log2FC (LT_CK) | FC | Log2FC (ST_CK) |
| Glucose | C00031 | $C_6H_{12}O_6$ | 0.71 | – 0.49 | – | – |
| Fructose | C00095 | $C_6H_{12}O_6$ | 0.47 | – 1.08 | – | – |
| Mannose-6-phosphate | C00275 | $C_6H_{13}O_9P$ | 0.77 | – 0.38 | – | – |
| Melibiose | C05402 | $C_{12}H_{22}O_{11}$ | 1.78 | 0.83 | 1.72 | 0.78 |
| Glyceraldehyde | C02154 | $C_3H_6O_3$ | 0.62 | – 0.68 | 0.67 | – 0.57 |
| Aspartate | C16433 | $C_4H_7NO_4$ | 3.05 | 1.61 | – | – |
| Glutamine | C00303 | $C_5H_{10}N_2O_3$ | 1.44 | 0.52 | 0.71 | – 0.49 |
| Alanine | C01401 | $C_3H_7NO_2$ | – | – | 0.68 | – 0.56 |
| Asparagine | C00152 | $C_4H_8N_2O_3$ | 2.60 | 1.38 | 0.74 | – 0.43 |
| Leucine | C16439 | $C_6H_{13}NO_2$ | 6.40 | 2.68 | 1.76 | 0.82 |
| Glutamate | C00025 | $C_5H_9NO_4$ | 1.21 | 0.28 | – | – |
| Acetyl-CoA | C00024 | $C_{23}H_{38}N_7O_{17}P_3S$ | 0.79 | – 0.33 | – | – |
| Citrate | C00158 | $C_6H_8O_7$ | 0.85 | – 0.24 | 0.90 | – 0.15 |
| Malate | C00497 | $C_4H_6O_5$ | 0.38 | – 1.39 | 0.42 | – 1.26 |
| 2-Oxoglutarate | C00026 | $C_5H_6O_5$ | – | – | 0.42 | – 1.25 |
| Arachidonate | C00219 | $C_{20}H_{32}O_2$ | 1.75 | 0.80 | – | – |

*CK, control; ST, short-term acidification; LT, long-term acidification.*

LT and RL significantly reduced the proportion of C16:0 in SFAs. The variation in the trends of major fatty acids in *N. oceanica* and *B. plicatilis* were consistent (**Figure 8**), indicating that the changes of fatty acids in *N. oceanica* were transferred to rotifers after acidification.

## 4 DISCUSSION

In this study, the physiological and biochemical responses and regulation of *N. oceanica* to elevated $pCO_2$ were explored. By comparing transcriptome and metabonomics data, the changes of main metabolic pathways in *N. oceanica* under acidification were analyzed, and the molecular regulatory mechanism was explained. At the same time, the possible ecological effects were evaluated through animal feeding experiments, and the impact of changes in *N. oceanica* on the food chain during OA was analyzed.

### 4.1 Photosynthesis and Calvin Cycle

Similar to C3 higher plants, microalgae can absorb external inorganic carbon sources through the photosynthetic carbon fixation pathway, which can be converted into organic compounds to maintain cell energy metabolism (Spalding, 1989). In the

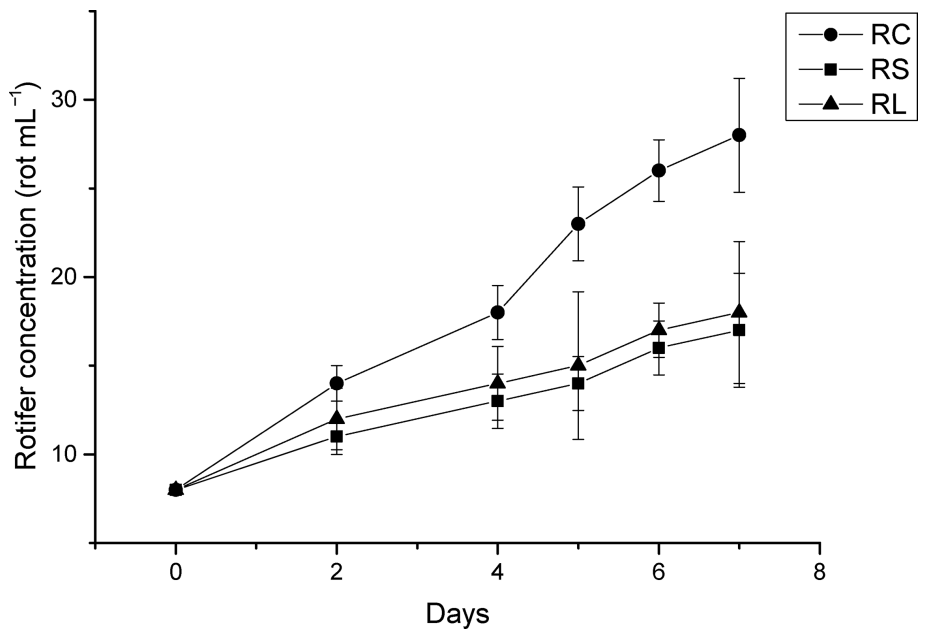


**FIGURE 7 |** The growth curve of rotifer *B. plicatilis* under different treatment treatments. RC, rotifer fed with CK; RS, rotifer fed with ST; RL, rotifer fed with LT.

**TABLE 6 |** Fatty acid composition (%) of ***B. plicatilis*** under different treatments (RC, RS and RL).

| Fatty acids | RC | RS | RL |
|---|---|---|---|
| Saturated fatty acid (%) | | | |
| C14:0 | 5.94 ± 0.06$^{b}$ | 7.99 ± 0.27$^{a}$ | 8.14 ± 0.14$^{a}$ |
| C16:0 | 25.56 ± 0.16$^{a}$ | 25.66 ± 0.59$^{a}$ | 24.41 ± 0.05$^{b}$ |
| C18:0 | 5.49 ± 0.08$^{a}$ | 3.74 ± 0.13$^{c}$ | 4.15 ± 0.06$^{b}$ |
| Monounsaturated fatty acid (%) | | | |
| C16:1n7 | 28.68 ± 0.05$^{c}$ | 32.16 ± 0.24$^{a}$ | 30.99 ± 0.01$^{b}$ |
| C18:1n9 | 14.89 ± 0.09$^{ab}$ | 14.21 ± 0.51$^{b}$ | 15.12 ± 0.50$^{a}$ |
| C20:1n9 | 3.76 ± 0.85$^{a}$ | 3.26 ± 0.26$^{a}$ | 2.78 ± 0.54$^{a}$ |
| Polyunsaturated fatty acid (%) | | | |
| C18:2n6 | 4.65 ± 0.37$^{a}$ | 2.79 ± 0.25$^{b}$ | 3.14 ± 0.39$^{b}$ |
| C20:4n6 | 2.83 ± 0.15$^{a}$ | 1.87 ± 0.57$^{b}$ | 1.79 ± 0.37$^{b}$ |
| C20:5n3 | 8.20 ± 0.27$^{b}$ | 8.34 ± 0.65$^{ab}$ | 9.48 ± 0.72$^{a}$ |
| ΣSFA | 37.00 ± 0.02$^{a}$ | 37.39 ± 0.73$^{a}$ | 36.70 ± 0.14$^{a}$ |
| ΣMUFA | 47.32 ± 0.81$^{b}$ | 49.62 ± 0.37$^{a}$ | 48.89 ± 0.06$^{a}$ |
| ΣPUFA | 15.68 ± 0.80$^{a}$ | 12.99 ± 0.78$^{b}$ | 14.41 ± 0.08$^{a}$ |
| ΣUSFA | 63.00 ± 0.02$^{a}$ | 62.61 ± 0.73$^{a}$ | 63.30 ± 0.14$^{a}$ |

*The different superscript letters indicate significant differences (**p**< 0.05). RC, rotifer fed with CK; RS, rotifer fed with ST; RL, rotifer fed with LT.*

photosynthetic pathway, only two DEGs were found under LT cells, namely photosystem II oxygen-enhancing protein 3 (*psbQ*) and ferredoxin-NADP$^{+}$ reductase (*FNR*), both of which were significantly downregulated, while no DEG was found in ST cells (**Table 7**; **Figure 9A**). Similarly, the expression of most light-capturing central protein genes in photosystems I and II was significantly inhibited after long-term acidification in *Chlamydomonas reinhardtii* (Zhang et al., 2021). Under short-term acidification, the photosynthesis-related light-trapping protein gene expression of microalgae *Coccomyxa subellipsoidea* C-169 was significantly downregulated (Peng et al., 2014).

Most genes involved in the Calvin cycle in LT and ST were also significantly downregulated, and the transketolase (tktA, Gene_5777) was the only gene significantly upregulated, by 2.25 times, under ST conditions (**Table 7**; **Figure 9B**). RuBisCO is a key enzyme in the initial phase of $CO_2$ fixation in the Calvin cycle, but no significant changes were observed under acidification conditions. In LT cells, three homologous genes of phosphoglycerate kinase (PGK), glyceraldehyde-3-phosphate dehydrogenase (GAPA), ribose 5-phosphate isomerase (rpiA), and tktA were significantly downregulated, as well as the transcript encoding ribulose-phosphate kinase (PRK) (**Table 7**). The study showed similar results that the RuBisCO of microalgae *Coccomyxa subbellipsoidea* C-169 did not change significantly during a short period of growth under high $CO_2$ concentrations (Peng et al., 2014). PGK and GAPA, the key enzymes in the Calvin cycle, can generate glyceraldehyde 3-phosphate through the consumption of photosynthesis NADPH and ATP catalytic glyceric acid-3-phosphate. Although we found that the carbon biofixation rate increased during acidification (**Figure 2**), the transcriptome

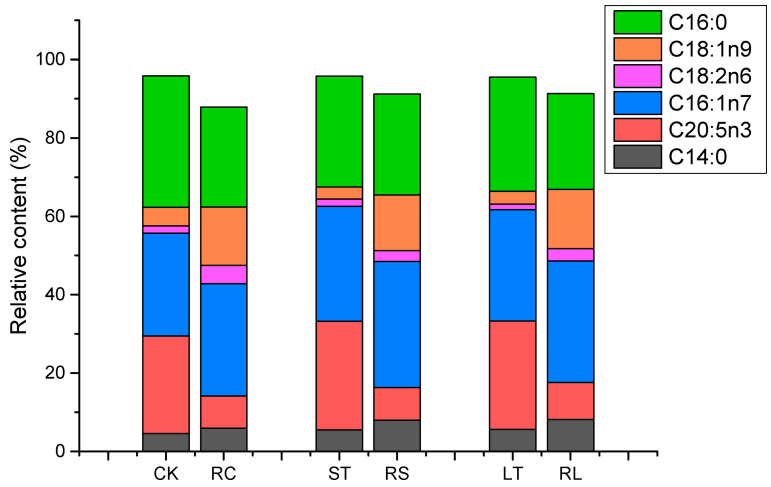


**FIGURE 8 |** Changes of main fatty acid profiles of *N. oceanica* (CK, ST and LT) and rotifer (*B*) *plicatilis* (RC, RS and RL) under different treatment treatments. CK, control; ST, short-term acidification; LT, long-term acidification. RC, rotifer fed with CK; RS, rotifer fed with ST; RL, rotifer fed with LT.

**TABLE 7 |** Differentially expressed genes related to C and N metabolism.

| Product | Gene ID | Gene name | EC number | Regulation (*padj*< 0.05) | |
|---|---|---|---|---|---|
| | | | | Log2FC[a] (LT_CK) | Log2FC (ST_CK) |
| **Photosynthesis** | | | | | |
| Photosystem II oxygen-evolving enhancer protein 3 | gene_6167 | psbQ | | -1.21 | – |
| Ferredoxin-NADP$^+$ reductase | gene_6155 | FNR | EC: 1.18.1.2 | -1.46 | – |
| **Calvin cycle** | | | | | |
| Phosphoglycerate kinase | gene_11697 | PGK | EC: 2.7.2.3 | -4.82 | -2.83 |
| Phosphoglycerate kinase | gene_6297 | PGK | EC: 2.7.2.3 | -2.11 | – |
| Phosphoglycerate kinase | gene_6744 | PGK | EC: 2.7.2.3 | -3.50 | -1.89 |
| Glyceraldehyde-3-phosphate dehydrogenase | gene_4207 | GAPA | EC: 1.2.1.13 | -2.72 | – |
| Transketolase | gene_3550 | tktA | EC: 2.2.1.1 | -1.74 | – |
| Transketolase | gene_5777 | tktA | EC: 2.2.1.1 | – | 1.17 |
| Ribose 5-phosphate isomerase A | gene_3706 | rpiA | EC: 5.3.1.6 | -1.68 | -1.07 |
| Phosphoribulokinase | gene_9029 | PRK | EC: 2.7.1.19 | -2.40 | -1.07 |
| **Glycolysis** | | | | | |
| Fructose-bisphosphate aldolase, class I | gene_318 | FBA | EC: 4.1.2.13 | -2.38 | -1.26 |
| Glyceraldehyde-3-phosphate dehydrogenase | gene_3483 | GAPDH | EC: 1.2.1.12 | -1.85 | – |
| Glyceraldehyde-3-phosphate dehydrogenase | gene_8679 | GAPDH | EC: 1.2.1.12 | 1.03 | – |
| Phosphoglycerate kinase | gene_6297 | PGK | EC: 2.7.2.3 | -2.11 | – |
| Phosphoglycerate kinase | gene_6744 | PGK | EC: 2.7.2.3 | -3.50 | -1.89 |
| Phosphoglycerate kinase | gene_11697 | PGK | EC: 2.7.2.3 | -4.82 | -2.83 |
| 2,3-bisphosphoglycerate-dependent phosphoglycerate mutase | gene_4647 | PGAM | EC: 5.4.2.11 | -1.13 | – |
| 2,3-bisphosphoglycerate-dependent phosphoglycerate mutase | gene_9748 | PGAM | EC: 5.4.2.11 | 1.08 | – |
| Enolase | gene_1499 | ENO | EC: 4.2.1.11 | -1.71 | -1.04 |
| Enolase | gene_1969 | ENO | EC: 4.2.1.11 | -2.21 | – |
| Pyruvate kinase | gene_1665 | PK | EC: 2.7.1.40 | -1.36 | – |
| Pyruvate kinase | gene_1740 | PK | EC: 2.7.1.40 | -1.71 | – |
| Pyruvate kinase | gene_3322 | PK | EC: 2.7.1.40 | -3.59 | – |
| Pyruvate kinase | gene_4717 | PK | EC: 2.7.1.40 | 1.61 | – |
| Pyruvate kinase | gene_10602 | PK | EC: 2.7.1.40 | -3.38 | – |
| Dihydrolipoamide acetyltransferase | gene_1161 | DLAT | EC: 2.3.1.12 | -1.60 | – |
| Dihydrolipoamide acetyltransferase | gene_8934 | DLAT | EC: 2.3.1.12 | -1.76 | – |
| Dihydrolipoamide dehydrogenase | gene_3601 | DLD | EC: 1.8.1.4 | -1.26 | – |
| Pyruvate carboxylase | gene_4579 | PC | EC 6.4.1.1 | – | 1.61 |
| **TCA cycle** | | | | | |
| ATP citrate (pro-S)-lyase | gene_11118 | ACLY | EC: 2.3.3.8 | -1.66 | – |
| ATP citrate (pro-S)-lyase | gene_118 | ACLY | EC: 2.3.3.8 | -2.06 | – |
| **Fatty acid biosynthesis** | | | | | |
| Acetyl-CoA carboxylase | gene_4535 | ACC | EC: 6.4.1.2 | -1.64 | – |
| Acetyl-CoA carboxylase | gene_8191 | ACC | EC: 6.4.1.2 | -1.15 | – |
| Acetyl-CoA carboxylase | gene_8192 | ACC | EC: 6.4.1.2 | -1.64 | – |
| Malonyl-CoA-[acyl-carrier-protein] transacylase | gene_2608 | MAT | EC: 2.3.1.39 | -1.21 | – |
| β-ketoacyl-[acyl-carrier-protein] synthase II | gene_2230 | KASII | EC: 2.3.1.179 | -3.11 | -1.26 |
| β-ketoacyl-[acyl-carrier-protein] synthase II | gene_9142 | KASII | EC: 2.3.1.179 | -1.47 | – |
| β-hydroxyacyl-[acyl-carrier-protein] dehydratase | gene_6107 | HAD | EC: 4.2.1.59 | -1.45 | – |
| Enoyl-[acyl-carrier-protein] reductase | gene_8401 | EAR | EC: 1.3.1.9 | -1.86 | – |
| **β-oxidation** | | | | | |
| Long-chain acyl-CoA synthetase | gene_738 | ACSL | EC: 6.2.1.3 | -1.71 | – |
| Long-chain acyl-CoA synthetase | gene_8558 | ACSL | EC: 6.2.1.3 | 1.39 | – |
| Acyl-CoA oxidase | gene_10606 | ACOX | EC: 1.3.3.6 | 1.61 | 1.32 |
| Acyl-CoA oxidase | gene_8528 | ACOX | EC: 1.3.3.6 | 1.11 | – |
| β-hydroxyacyl-CoA dehydrogenase | gene_4884 | HADH | EC: 1.1.1.35 | 3.42 | 2.04 |
| β-hydroxyacyl-CoA dehydrogenase | gene_5203 | HADH | EC: 1.1.1.35 | – | -1.14 |
| **Triacylglycerol biosynthesis** | | | | | |
| Glycerol-3-phosphate dehydrogenase (NAD$^+$) | gene_7684 | GPD1 | EC: 1.1.1.8 | -1.06 | – |
| Glycerol-3-phosphate acyltransferase | gene_9974 | GPAT | EC: 2.3.1.15 | -1.38 | – |
| Glycerol-3-phosphate acyltransferase | gene_9975 | GPAT | EC: 2.3.1.15 | -1.25 | – |
| **Nitrogen metabolism** | | | | | |
| Nitrate/nitrite transporter | gene_5827 | NRT | | -2.26 | – |
| Nitrate reductase | gene_5828 | NR | EC: 1.7.1.1 | - 2.34 | – |
| Carbamoyl-phosphate synthase (ammonia) | gene_3199 | CPS | EC: 6.3.4.16 | - 1.46 | – |

[a]$Log2FC = Log2(\frac{FPKM\,1000\,ppm}{FPKM\,400\,ppm})$, "–" no change, padj corrected p-value.

*CK, control; ST, short-term acidification; LT, long-term acidification.*

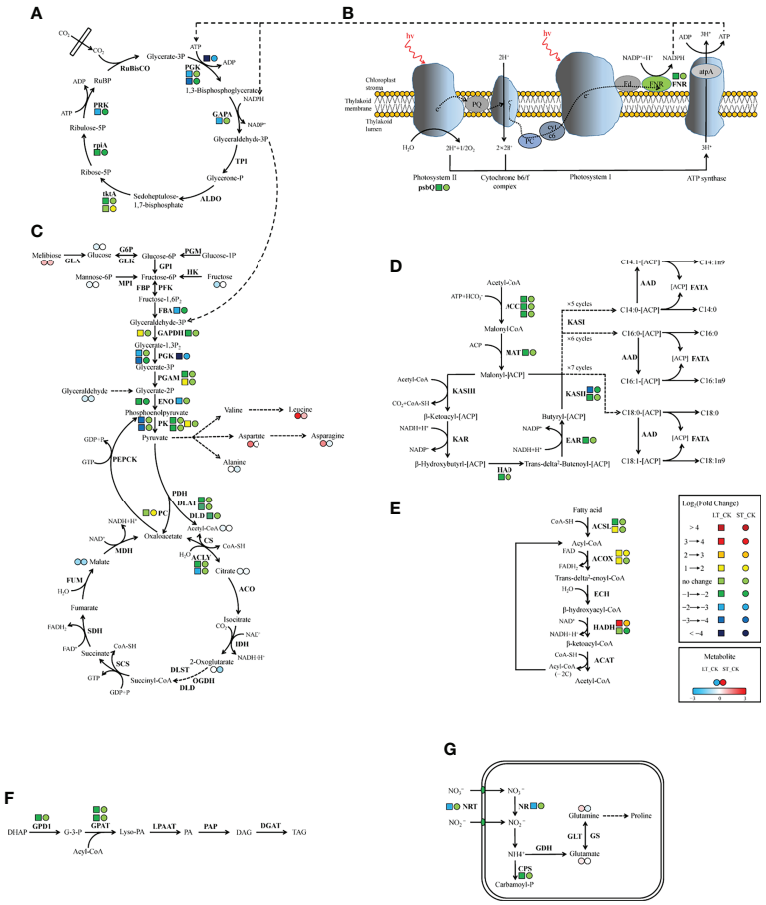

**FIGURE 9 |** Schematic representation of genes and metabolites changes in C and N metabolic pathways in *N. oceanica* under ocean acidification. **(A)** Calvin cycle. **(B)** Photosynthesis. **(C)** Glycolysis/gluconeogenesis and TCA cycle. **(D)** Fatty acid biosynthesis. **(E)** β-oxidation. **(F)** Triacylglycerol biosynthesis. **(G)** Nitrogen metabolism. Key enzymes and metabolites were included in the map. Next to the enzyme, left tetragon represents LT vs. CK; right circle represents ST vs. CK. Two adjacent circles next to the metabolite, left circle representsLT vs. CK and right circle represents ST vs. CK (red in upregulated, blue in downregulated). CK, control; ST, short-term acidification; LT, long-term acidification. RuBisCO, ribulose bisphosphate carboxylase; PGK, phosphoglycerate kinase; GAPA, glyceraldehyde-3-phosphate dehydrogenase; TPI, triosephosphate isomerase; ALDO, fructose-bisphosphate aldolase; tktA, transketolase; rpiA, ribose 5-phosphate isomerase A; PRK, phosphoribulokinase; psbQ, photosystem II oxygen-evolving enhancer protein 3; FNR, ferrdoxin-NADP+ reductase; PGM, phosphoglucomutase; GLA, galactosidase; G6P, glucose-6-phosphatase; GLK, glucokinase; GPI, glucose-6-phosphate isomerase; HK, hexokinase; MPI, mannose-6-phosphate isomerase; FBP, fructose-1,6-bisphosphatase; PFK, phosphofructokinase; FBA, fructose-bisphosphate aldolase; GAPDH, glyceraldehyde-3-phosphate dehydrogenase; PGAM, 2,3-bisphosphoglycerate-dependent phosphoglycerate mutase; ENO, enolase; PK, pyruvate kinase; PDH, pyruvate dehydrogenase; DLAT, dihydrolipoamide acetyltransferase; DLD, dihydrolipoamide dehydrogenase; PC, pyruvate carboxylase; PEPCK, phosphoenolpyruvate carboxykinase; CS, citrate synthase; ACLY, ATP citrate lyase; ACO, aconitate hydratase; IDH, isocitrate dehydrogenase; OGDH, 2-oxoglutarate dehydrogenase; DLST, dihydrolipoamide succinyltransferase; SCS, succinyl-CoA synthetase; SDH, succinate dehydrogenase; FUM, fumarate hydratase; MDH, malate dehydrogenase; ACC, acetyl-CoA carboxylase; MAT, malonyl-CoA-[acyl-carrier-protein] transacylase; KAS, β-ketoacyl-[acyl-carrier-protein] synthase; KAR, β-ketoacyl-[acyl-carrier protein] reductase; HAD, β-hydroxyacyl-[acyl-carrier-protein] dehydratase; EAR, enoyl-[acyl-carrier-protein] reductase; AAD, acyl-[acyl-carrier-protein] desaturase; FATA, fatty acyl-[acyl-carrier-protein] thioesterase A; ACSL, long-chain acyl-CoA synthetase; ACOX, acyl-CoA oxidase; ECH, enoyl-CoA hydratase; HADH, β-hydroxyacyl-CoA dehydrogenase; ACAT, acetyl-CoA C-acetyltransferase; DHAP, dihydroxyacetone phosphate; GPD1, glycerol-3-phosphate dehydrogenase (NAD+); G-3-P, glycerol-3-phosphate; GPAT, glycerol-3-phosphate acyltransferase; PA, phosphatidic acid; Lyso-PA, lysophosphatidic acid; LPAAT, Lyso-PA acyltransferase; PAP, PA phosphatase; DAG, diacyglycerol; DGAT, DAG acyltransferase; TAG, triacylglycerol; NRT, nitrate/nitrite transporter; NR, nitrate reductase; Fd-NiR, ferredoxin-dependent nitrite reductases; CPS, carbamoylphosphate synthase; GDH, glutamate dehydrogenase; GS, glutamine synthetase; GLT, glutamate synthase.

data suggested that the carbon biofixation pathway decreased. We guessed that the carbon fixation pathway was not always up-regulated, perhaps in the initial stage, but with the increase of carbon biofixation, the product inhibition effect was produced and the carbon biofixation pathway was down-regulated. The specific mechanism was worthy of future study.

Carbon is fixed through the Calvin cycle to form various carbon skeletons and other derivatives, such as carbohydrates, fatty acids, and amino acids. Although physiological and biochemical data showed that the total protein content of LT cells significantly decreased, the protein content of ST cells slightly increased but the carbohydrate content significantly increased (**Table 2**). According to metabonomics data, amino acid content significantly increased and most carbohydrates significantly decreased under LT conditions, whereas the levels of most amino acids significantly decreased under ST conditions (**Table 5**). We speculated that the downregulated *PGK* and *GAPA* significantly reduced the accumulation of carbohydrates in algal

cells under LT, which promoted a large amount of carbon source to flow to the synthesis of amino acids, and the consumption of carbohydrates promoted the rapid growth of algal cells under long-term acidification. However, under ST, due to the significant upregulation of *tktA*, the carbohydrate content was increased, and the increased $CO_2$ concentration promoted the photosynthetic carbon fixation pathway of *N. oceanica*, which in turn promoted the absorption of a large number of inorganic carbon sources that were then converted into carbohydrates as common energy materials for storage. This difference between LT and ST may be due to the adaptation of algal cells to different acidification time scales.

## 4.2 Glycolysis and TCA Cycle

Glycolysis/gluconeogenesis and the TCA cycle are important energy metabolic pathways in organisms. In particular, the TCA cycle is a central hub for the metabolism of sugars, lipids, and amino acids. Several key enzymes involved in glycolysis were significantly downregulated in LT. Including fructose diphosphate aldolase (FBA), phosphoglyceraldehyde dehydrogenase (GAPDH), PGK, phosphoglycerate mutase (PGAM), enolase (ENO), pyruvate kinase (PK), dihydrothioctyl transacetylase (DLAT), and dihydrothioctyl dehydrogenase (DLD) were significantly downregulated. However, the transcript of a homologous gene encoding PGAM (Gene_9748) and PK enzymes (Gene_4717) was significantly upregulated, and no significant changes were found in the gluconeogenesis pathway (**Table 7**; **Figure 9C**). In ST, two homologous genes *PGK* and *ENO* were significantly downregulated, while the pyruvate carboxylase (PC) gene was significantly upregulated by 3.05-fold in the gluconeogenesis pathway. Contrary to our findings, most of the glycolysis genes of *Chlorella sorokiniana* were significantly upregulated after short-term culture with a high concentration of $CO_2$ (Sun et al., 2016). Similarly, when *Haematococcus pluvialis* was grown at 15% $CO_2$ concentration, the expression of the transcription gene encoding PK was upregulated 3.5 times. In the metabolome results, the contents of glucose, fructose, and mannose-6-phosphate, the precursor metabolites of glycolysis, in LT decreased significantly, but the content of melibiose increased, and the content of glyceraldehyde, the intermediate metabolite of glycolysis, decreased significantly (**Table 5**). We hypothesized that *PGAM* (Gene_9748) and *PK* (Gene_4717), which were significantly upregulated, promoted glycolysis of LT, thus generating a large amount of energy to maintain rapid growth. During short-term acidification, significantly upregulated PC enzymes enhanced gluconeogenesis and thus promoted carbohydrate accumulation, which is consistent with the physiologically higher carbohydrate content finding in ST (**Table 2**).

The TCA cycle is a common metabolic pathway of aerobic organisms, in which intermetabolites are closely related to the synthesis and metabolism of amino acids (Li et al., 2014). Under LT conditions, most of the genes remained unchanged except for ATP-citrate lyase (ACLY) which was significantly downregulated. Citric acid and malic acid, intermediate metabolites of the TCA cycle, were also significantly decreased, while aspartic acid, asparagine, glutamine, leucine, and glutamate levels were significantly increased. In ST, the levels of citric acid, malic acid, and ketoglutaric acid were significantly decreased, while the levels of glutamine, asparagine, and alanine were significantly decreased but those of leucine were increased (**Table 5**). The significant reduction of TCA cycling-related metabolites in LT suggested that a large amount of carbon flow was directed to amino acid synthesis, whereas ST enhanced gluconeogenesis, resulting in carbon flow to carbohydrates and reduced amino acid content.

## 4.3 Lipid Metabolism

Biosynthesis of fatty acids in algal chloroplasts consists of a set of dissociated type II fatty acid synthases (FAS) adding two carbon units to the elongated fatty acid carbon chain in an iterative path (Ryall et al., 2003). Acetyl-CoA carboxylase (ACC) catalyzes the first step of *de novo* biosynthesis of fatty acids, using bicarbonate, ATP, acetyl-CoA, and biotin cofactors to produce malonyl-CoA, the cornerstone of fatty acid biosynthesis (Waite and Wakil, 1962; Alberts and Vagelos, 1968; Salie and Thelen, 2016). Under LT conditions, the expression of three ACC homologous genes was significantly downregulated. Transcripts encoding malonylmonoacyl-coenzyme A-ACP transferase (MAT), β-ketoalioyl-ACP synthase II (KASII), β-hydroxyl-ACP dehydrase (HAD), and enyl-ACp reductase (EAR) were significantly downregulated, while no significant changes were found in genes under ST (**Table 7**; **Figure 9D**). Contrary to our findings, the expression of several ACC genes in *H. pluvialis* growing at 15% $CO_2$ concentration was significantly upregulated (FC: 2.95–3.08 fold). As a precursor of *de novo* synthesis of fatty acids, acetyl-CoA content decreased by 21% under LT (**Table 5**), leading to the significant downregulation of genes related to fatty acid synthesis. In long-term acidification studies, 2020c; Liang et al. (2020b) found that there was no significant change in the expression of genes related to fatty acid synthesis in *Chlorella variabilis*, whereas ACC was significantly downregulated in *C. muelleri*, with species differences. In the fatty acid β-oxidation pathway, we found that acidification significantly upregulated gene expression of related enzymes (**Table 7**, **Figure 9E**), indicating that the acidified micrococcus could grow faster due to the energy supply of β-oxidation. According to the metabolome results, the level of polyunsaturated fatty acid arachidonic acid (ARA) was significantly increased by 1.75 times under LT conditions (**Table 3**). According to the results of the fatty acid profile, SFAs of *N. oceanica* under acidification significantly decreased while PUFA content significantly increased and EPA relative content of *N. oceanica* was significantly increased ($p<0.05$), indicating that acidification promoted the proportion of unsaturated fatty acids in algae cells (**Table 3**). Similar to our research results, Fan et al., (2015), Fan et al., (2016) found that algae cells exposed to a low carbon environment generally increased the content of SFAs, whereas algae cells exposed to a high carbon environment promoted the generation of PUFAs. While our result is inconsistent with that in *Chaetoceros muelleri* and *Cylindrotheca fusiformis* (Bermúdez et al., 2015; Liang et al., 2020c). The effects of high $pCO_2$ on algal fatty acid contents,

particularly on PUFA, were more diverse and species-specific, and the PUFA level may decline or increase in different microalga (Tsuzuki et al., 1990; Riebesell et al., 2000; Fiorini et al., 2010; Torstensson et al., 2013). In this study, the alga may also increase EPA levels to maintain membrane fluidity under elevated $pCO_2$.

However, under short-term acidification, most studies showed that the lipid accumulation of microalgae could be promoted (Wang et al., 2014; Patil & Kaliwal, 2016; Sabia et al., 2018). In *Chlorella vulgaris*, short-term acidification leads to the intracellular accumulation of acetyl-CoA and lipids (Jose and Suraishkumar, 2016). On the contrary, when *Chlorella sorokiniana* grew with elevated $CO_2$, most genes related to fatty acid synthesis were significantly downregulated, but lipid accumulation increased. Sun et al. (2016) speculated that the increase in substrate supply rather than the key enzymes of fatty acid biosynthesis play a more important role in the synthesis of triglycerides (TAG). In the pathway of triglyceride synthesis, GPD1 and two GPAT homologous genes were significantly downregulated under LT (**Table 7**; **Figure 9F**), indicating that the long-term acidification of *N. oceanica* may limit the accumulation of TAG by reducing the *de novo* synthesis of fatty acids, while the gene expression under ST conditions was not significant, and the related molecular regulation mechanism was difficult to explain, requiring further study by other methods.

## 4.4 Nitrogen Metabolism

Nitrogen is an essential nutrient for all living organisms and is required for the biosynthesis of large molecules such as proteins, nucleic acids, and chlorophyll. For *N. oceanica*, it is important to maintain the intracellular carbon and nitrogen balance. Although the level of total nitrogen increased with the increased the total carbon contens, the expression of related genes in the nitrogen assimilation pathway was significantly downregulated (*NRT*, *NR*, *CPS*) in LT cells, but in ST they were not significantly downregulated. Similar to our findings, Zhang et al. (2021) found that in *Chlamydomonas reinhardtii*, NRT and CPS gene expression was also significantly downregulated during long-term acidification. However, in *Synechococcus elongates*, elevated $CO_2$ promotes the upregulated expression of genes related to nitrogen assimilation, thus maintaining the C and N homeostasis of algal cells (Mehta et al., 2019). In the study by Liang et al., genes for nitrogen absorption and assimilation were found to be upregulated in *C.muelleri* (Liang et al., 2020c).Therefore, it could be hypothesized that the accumulation of a large number of nitrogen-containing compounds (glutamine, and glutamate) resulted in feedback inhibition of long-term acidified cells (**Table 5**), which significantly down-regulated the expression of genes related to nitrogen metabolism and enabled *N. oceanica* to maintain a relatively stable C/N balance for algal growth (**Figure 9G**). Some specific amino acid concentrations like Argpartate and Leucine increased since the total protein content decreased in LT cells. It is speculated that under LT, algae cells are possible to use decomposable proteins for energy supply, so as to maintain the rapid growth of algae cells in the long-term high carbon and low pH environment. The related molecular regulation mechanism needs to be further studied.

## 4.5 Growth and Effects of Fatty Acid Profiles in *B. Plicatilis*

Due to high protein content, polyunsaturated fatty acid content, and short growth cycle, *B. plicatilis* is the open bait of fish and crustaceans in the ocean. Therefore, it is an indispensable class of zooplankton in the marine ecosystem. It feeds on marine microalgae under natural conditions, so it also contains more polyunsaturated fatty acid EPA (Fu et al., 2016). Studies have shown that low pH seawater could induce oxidative stress and DNA damage, and reduce the growth rate, fertility, and longevity of parent ichthys, but the effect on offspring is not obvious (Lee et al., 2020). We speculated that the acidified environment may inhibit the feeding of rotifers and slow down the growth and development of the rotifer population under acidified culture conditions. Our results confirmed this theory. In addition, the total fatty acid profiles of microalgae changed when the $CO_2$ concentration was elevated compared with the 400 ppm $CO_2$, which may transfer at the trophic level. It was found that the growth and reproduction of the water flea *Acartia tonsa* were affected when the copepods were fed with acidified algae (Rossoll et al., 2012). Similarly, Meyers et al. (2019) also found that OA could affect the nutritional quality of planktonic microalgae and their reproduction after feeding copepods. Compared with the main fatty acid spectrum data of rotifers and *N. oceanica* (**Figure 9**), the variation trends were roughly the same, indicating that changes in nutrient quality generated by OA on *N. oceanica* could be transferred to rotifers through nutrient level transfer. Although PUFAs were increased in LT cells, they still had adverse effects on downstream consumers. More studies are therefore needed to understand the complex food chain effects induced by OA.

# DATA AVAILABILITY STATEMENT

The datasets presented in this study can be found in online repositories. The names of the repository/repositories and accession number(s) can be found below:
https://www.ncbi.nlm.nih.gov/, PRJNA719462.

# AUTHOR CONTRIBUTIONS

CL and NY designed the project. CL, YZ, ZG, YR, and DX performed the research. YZ, CL, DX and XZ analyzed the data. YZ and CL wrote the first draft. All authors contributed to interpreting the data and writing the manuscript. The manuscript was approved by all authors for publications. This work is the original works of the authors, and the manuscript

was not previously submitted to this journal. All authors contributed to the article and approved the submitted version.

## FUNDING

This research was supported by Special Funds of Shandong Province for Pilot National Laboratory for Marine Science and Technology (Qingdao) (2021QNLM050103-1), the National Natural Science Foundation of China (grants 31770393 and 41976110), the Taishan Scholars Funding of Shandong Province, and the Young Taishan Scholars Program (tsqn202103136).

## ACKNOWLEDGMENTS

We acknowledge Dr. Qingchun Zhang who provided *B. plicatilis* for this study.

## SUPPLEMENTARY MATERIAL

The Supplementary Material for this article can be found online at: https://www.frontiersin.org/articles/10.3389/fmars.2022.863262/full#supplementary-material

## REFERENCES

Alberts, A. W. and Vagelos, P. R. (1968). Acetyl CoA Carboxylase. I. Requirement for Two Protein Fractions. *Proc. Natl. Acad. Sci. U. S. A.* 59, 561–568. doi: 10.1073/pnas.59.2.561

Bermúdez, R., Feng, Y., Roleda, M. Y., Tatters, A. O., Hutchins, D. A., Larsen, T., et al. (2015). Long-Term Conditioning to Elevated $pCO_2$ and Warming Influences the Fatty and Amino Acid Composition of the Diatom Cylindrotheca Fusiformis. *PloS One* 10, e0123945. doi: 10.1371/ journal.pone.0123945

Caldeira, K. and Wickett, M. E. (2003). Anthropogenic Carbon and Ocean pH. *Nature* 425, 365. doi: 10.1038/425365a

Chen, X. A. and Gao, K. S. (2004a). Photosynthetic Utilization of Inorganic Carbon and Its Regulation in the Marine Diatom *Skeletonema Costatum*. *Funct. Plant Biol.* 31, 1027–1033. doi: 10.1071/FP04076

Chen, X. W. and Gao, K. S. (2004b). Characterization of Diurnal Photosynthetic Rhythms in the Marine Diatom *Skeletonema Costatum* Grown in Synchronous Culture Under Ambient and Elevated $CO_2$. *Funct. Plant Biol.* 31, 399–404. doi: 10.1071/FP03240

Chiu, S. Y., Kao, C. Y., Tsai, M. T., Ong, S. C., Chen, C. H. and Lin, C. S. (2009). Lipid Accumulation and $CO_2$ Utilization of *Nannochloropsis Oculata* in Response to $CO_2$ Aeration. *Bioresour. Technol.* 100, 833–838. doi: 10.1016/j.biortech.2008.06.061

Cripps, G., Flynn, K. J. and Lindeque, P. K. (2016). Ocean Acidification Affects the Phyto-Zoo Plankton Trophic Transfer Efficiency. *PloS One* 11, e0151739. doi: 10.1371/journal.pone.0151739

Das, P., Lei, W., Aziz, S. S. and Obbard, J. P. (2011). Enhanced Algae Growth in Both Phototrophic and Mixotrophic Culture Under Blue Light. *Bioresour. Technol.* 102, 3883–3887. doi: 10.1016/j.biortech.2010.11.102

Falkowski, P. (2012). Ocean Science: The Power of Plankton. *Nature* 483, 17–20. doi: 10.1038/483S17a

Fan, J., Xu, H., Luo, Y., Wan, M., Huang, J., Wang, W. (2015). Impacts of $CO_2$ Concentration on Growth, Lipid Accumulation, and Carbon-Concentrating-Mechanism-Related Gene Expression in Oleaginous *Chlorella*. *Appl. Microbiol. Biotechnol.* 99, 2451–2462. doi: 10.1007/s00253-015-6397-4

Fan, J., Xu, H. and Li, Y. (2016). Transcriptome-Based Global Analysis of Gene Expression in Response to Carbon Dioxide Deprivation in the Green Algae *Chlorella Pyrenoidosa*. *Algal Res.* 16, 12–19. doi: 10.1016/j.algal.2016.02.032

Field, C. B., Behrenfeld, M. J., Randerson, J. T., Falkowski, P. (1998). Primary Production of the Biosphere: Integrating Terrestrial and Oceanic Components. *Science* 281, 237–240. doi: 10.1126/science.281.5374.237

Fiorini, S., Gattuso, J. P., van Rijswijk, P., Middelburg, J. (2010). Coccolithophores Lipid and Carbon Isotope Composition and Their Variability Related to Changes in Seawater Carbonate Chemistry. *J. Exp. Mar. Bio. Ecol.* 394, 74–85. doi: 10.1016/j.jembe.2010.07.020

Fu, R., Zhang, X., Xu, Z., Qiu, H., Jiang, X. (2016). The Effect of Amino Acids, Fatty Acid Composition of Different Bait on *Brachionus Plicatilis*. *Funct. Plant Biol.* 41, 449–459. Journal of Zhejiang Ocean University (Natural Science) 35, 372-377.

Gao, K., and Campbell, D. A. (2014). Photophysiological Responses of Marine Diatoms to Elevated $CO_2$ and Decreased pH: A Review. *Funct. Plant Biol.* 41, 449-459. doi: 10.1071/FP13247

Gattuso, J. P., Magnan, A., Bille, R., Cheung, W. W., Howes, E. L., Joos, F., et al. (2015). Contrasting Futures for Ocean and Society From Different Anthropogenic $CO_2$ Emissions Scenarios. *Science* 349 (6243), aac4722. doi: 10.1126/science.aac4722

Genty, B., Briantais, J. M. and Baker, N. R. (1989). The Relationship Between the Quantum Yield of Photosynthetic Electron Transport and Quenching of Chlorophyll Fluorescence. *Biochim. Biophys. Acta-Gen. Subj.* 990, 87–92. doi: 10.1016/S0304-4165(89)80016-9

Glencross, B. (2009). Exploring the Nutritional Demand for Essential Fatty Acids by Aquaculture Species. *Rev. Aquac.* 1, 71–124. doi: 10.1111/j.1753-5131.2009.01006.x

Golda-VanEeckhoutte, R. L., Roof, L. T., Needoba, J. A. and Peterson, T. D. (2018). Determination of Intracellular pH in Phytoplankton Using the Fluorescent Probe, SNARF, With Detection by Fluorescence Spectroscopy. *J. Microbiol. Methods* 152, 109–118. doi: 10.1016/j.mimet.2018.07.023

Hauke, J. and Kossowski, T. (2011). Comparison of Values of Pearson's and Spearman's Correlation Coefficients on the Same Sets of Data. *Quaest. Geogr.* 30, 87–93. doi: 10.2478/v10117-011-0021-1

Hopkins, F. E., Suntharalingam, P., Gehlen, M., Andrews, O., Archer, S. D., Bopp, L., et al. (2020). The Impacts of Ocean Acidification on Marine Trace Gases and the Implications for Atmospheric Chemistry and Climate. *Proc. Mathematical. Physical Eng. Sci.* 476 (2237), 20190769. doi: 10.1098/rspa.2019.0769

Hu, H. and Gao, K. (2003). Optimization of Growth and Fatty Acid Composition of a Unicellular Marine Picoplankton, *Nannochloropsis* Sp., With Enriched Carbon Sources. *Biotechnol. Lett.* 25, 421–425. doi: 10.1023/A:1022489108980

Hurd, C. L., Lenton, A., Tilbrook, B. and Boyd, P. W. (2018). Current Understanding and Challenges for Oceans in a Higer-$CO_2$ World. *Nat. Clim. Change* 8, 686–694. doi: 10.1038/s41558-018-0211-0

*IPCC.* (2013) Climate Change 2013: The Physical Science Basis. Working Group I Contribution to the Fifth Assessment Report of the Intergovernmental Panel on Climate Change. *Cambridge University Press.*

Jin, P., Gao, K. and Beardall, J. (2013). Evolutionary Responses of a Coccolithophorid *Gephyrocapsa Oceanica* to Ocean Acidification. *Evolution* 67, 1869–1878. doi: 10.1111/evo.12112

Jin, P., Hutchins, D. A. and Gao, K. (2020). The Impacts on Ocean Acidification on Marine Food Quality and its Potential Food Chain Consequences. *Front. Mar. Sci.* 7, 543979. doi: 10.3389/fmars.2020.543979

Jin, P., Wang, T., Liu, N., Dupont, S., Beardall, J., Boyd, P. W., (2015). Ocean Acidification Increases the Accumulation of Toxic Phenolic Compounds Across Trophic Levels. *Nat. Commun.* 6, 8714. doi: 10.1038/ncomms9714

Jose, S. and Suraishkumar, G. K. (2016). High Carbon ($CO_2$) Supply Leads to Elevated Intracellular Acetyl CoA Levels and Increased Lipid Accumulation in *Chlorella Vulgaris*. *Algal Res.* 19, 307–315. doi: 10.1016/j.algal.2016.08.011

Lee, Y. H., Kang, H. M., Kim, M. S., Lee, J. S., Wang, M., Hagiwara, A., (2020). Multigenerational Mitigating Effects of Ocean Acidification on *In Vivo* Endpoints, Antioxidant Defense, DNA Damage Response, and Epigenetic Modification in an Asexual Monogonont Rotifer. *Environ. Sci. Technol.* 54, 7858–7869. doi: 10.1021/acs.est.0c01438

Liang, C., Wang, L., Zhang, Y., Zhang, J., Zhang, X. and Ye, N. (2020a). The Effects of Elevated $CO_2$ Concentrations on Changes in Fatty Acids and Amino Acids of Three Species of Microalgae. *Phycologia* 59, 208–217. doi: 10.1080/00318884.2020.1732714

Liang, C., Yang, X., Wang, L., Fan, X., Zhang, X., Xu, D., (2020b). Different Physiological and Molecular Responses of the Green Algae *Chlorella Variabilis* to Long-Term and Short-Term Elevated $CO_2$. *J. Appl. Phycol.* 32, 951–966. doi: 10.1007/s10811-019-01943-1

Liang, C., Zhang, Y., Wang, L., Shi, L., Xu, D., Zhang, X., (2020c). Features of Metabolic Regulation Revealed by Transcriptomic Adaptions Driven by Long-Term Elevated $pCO_2$ in *Chaetoceros Muelleri*. *Phycol. Res.* 68, 236–248. doi: 10.1111/pre.12423

Liu, J., Liu, Y., Wang, H. and Xue, S. (2015). Direct Transesterification of Fresh Microalgal Cells. *Bioresour. Technol.* 176, 284–287. doi: 10.1016/j.biortech.2014.10.094

Liu, D., Wong, P. and Dutka, B. J. (1973). Determination of Carbohydrate in Lake Sediment by a Modified Phenol-Sulfuric Acid Method. *Water Res.* 7, 741–746. doi: 10.1016/0043-1354(73)90090-0

Li, Y., Xu, J. and Gao, K. (2014). Light-Modulated Responses of Growth and Photosynthetic Performance to Ocean Acidification in the Model Diatom *Phaeodactylum Tricornutum*. *PloS One* 9, e96173. doi: 10.1371/journal.pone.0096173

Ma, X. N., Chen, T. P., Yang, B., Liu, J., Chen, F. (2016). Lipid Production From *Nannochloropsis*. *Mar. Drugs* 14, 61. doi: 10.3390/md14040061

Mehta, K., Jaiswal, D., Nayak, M., Prasannan, C. B., Wangikar, P. P. Srivastava, S. (2019). Elevated Carbon Dioxide Levels Lead to Proteome-Wide Alterations for Optimal Growth of a Fast-Growing Cyanobacterium, *Synechococcus Elongatus* PCC 11801. *Sci. Rep.* 9, 6257. doi: 10.1038/s41598-019-42576-1

Meng, Y., Jiang, J., Wang, H., Cao, X., Xue, S., Yang, Q., et al. (2015). The Characteristics of TAG and EPA Accumulation in *Nannochloropsis Oceanica* IMET1 Under Different Nitrogen Supply Regimes. *Bioresour. Technol.* 179, 483–489. doi: 10.1016/j.biortech.2014.12.012

Meyers, M. T., Cochlan, W. P., Carpenter, E. J., Kimmerer, W. J. (2019). Effect of Ocean Acidification on the Nutritional Quality of Marine Phytoplankton for Copepod Reproduction. *PloS One* 14, e0217047. doi: 10.1371/journal.pone.0217047

Morais, M. and Costa, J. A. V. (2007). Biofixation of Carbon Dioxide by *Spirulina* Sp. And *Scenedesmus Obliquus* Cultivated in a Three-Stage Serial Tubular Photobioreactor. *J. Biotechnol.* 129, 439–445. doi: 10.1016/j.jbiotec.2007.01.009

Müler-Navarra, D. C., Brett, M. T., Park, S., Chandra, S., Ballantyne, A. P., Zorita, E., et al. (2004). Unsaturated Fatty Acid Content in Seston and Tropho-Dynamic Coupling in Lakes. *Nature* 427, 69–72. doi: 10.1038/nature02210

Patil, L. and Kaliwal, B. (2016). Effect of $CO_2$ Concentration on Growth and Biochemical Composition of Newly Isolated Indigenous Microalga *Scenedesmus Bajacalifornicus* BBKLP-07. *Appl. Biochem. Biotechnol.* 182, 335–348. doi: 10.1007/s12010-016-2330-2

Peng, H., Wei, D., Chen, G., Chen, F. (2016). Transcriptome Analysis Reveals Global Regulation in Response to $CO_2$ Supplementation in Oleaginous Microalga *Coccomyxa Subellipsoidea* C-169. *Biotechnol. Biofuels* 9, 151. doi: 10.1186/s13068-016-0571-5

Pierrot, D., Lewis, E. and Wallace, D. W. R. (2006). *MS Excel Program Developed for $CO_2$ System Calculations* (Oak Ridge, Tennessee: Carbon Dioxide Information Analysis Center, Oak Ridge National Laboratory Vol.3 US Department of Energy).

Razzak, S. A., Ilyas, M., Ali, S. A. M., Hossain, M. M. (2015). Effects of $CO_2$ Concentration and pH on Mixotrophic Growth of *Nannochloropsis Oculata*. *Appl. Biochem. Biotechnol.* 176, 1290–1302. doi: 10.1007/s12010-015-1646-7

Riebesell, U., Revill, A., Holdsworth, D. and Volkman, J. (2000). The Effects of Varying $CO_2$ Concentration on Lipid Composition and Carbon Isotope Fractionation in *Emiliania Huxleyi*. *Geochim. Cosmochim. Acta* 64, 4179–4192. doi: 10.1016/S0016-7037(00)00474-9

Rocha, J. M. S., Garcia, J. E. C. and Henriques, M. H. F. (2003). Growth Aspects of the Marine Microalga *Nannochloropsis Gaditana*. *Biomol. Eng.* 20, 237–242. doi: 10.1016/S1389-0344(03)00061-3

Rossoll, D., Bermudez, R., Hauss, H., Schulz, K. G., Riebesell, U., Sommer, U., et al. (2012). Ocean Acidification-Induced Food Quality Deterioration Constrains Trophic Transfer. *PloS One* 7, e34737. doi: 10.1371/journal.pone.0034737

Ryall, K., Harper, J. T. and Keeling, P. J. (2003). Plastid-Derived Type II Fatty Acid Biosynthetic Enzymes in Chromists. *Gene* 313, 139–148. doi: 10.1016/S0378-1119(03)00671-1

Sabia, A., Clavero, E., Pancaldi, S., and Rovira, J. S. (2018). Effect of Different $CO_2$ Concentrations on Biomass, Pigment Content, and Lipid Production of the Marine Diatom *Thalassiosira Pseudonana*. *Appl. Microbiol. Biotechnol.* 102, 1945–1954. doi: 10.1007/s00253-017-8728-0

Salie, M. J. and Thelen, J. J. (2016). Regulation and Structure of the Heteromeric Acetyl-CoA Carboxylase. *Biochim. Biophys. Acta Mol. Cell Biol. Lipids* 1861, 1207–1213. doi: 10.1016/j.bbalip.2016.04.004

Smith, P. K., Krohn, R. I., Hermanson, G. T., Mallia, A. K., Gartner, F. H., Provenzano, M. D., et al. (1985). Measurement of Protein Using Bicinchoninic Acid. *Anal. Biochem.* 150, 76–85. doi: 10.1016/0003-2697(85)90442-7

Spalding, M. H. (1989). Photosynthesis and Photorespiration in Freshwater Green Algae. *Aquat. Bot.* 34, 181–209. doi: 10.1016/0304-3770(89)90056-9

Sun, Z., Chen, Y. F. and Du, J. (2016). Elevated $CO_2$ Improves Lipid Accumulation by Increasing Carbon Metabolism in *Chlorella Sorokiniana*. *Plant Biotechnol. J.* 14, 557–566. doi: 10.1111/pbi.12398

Tang, D., Han, W., Li, P., Miao, X., Zhong, J., (2011). $CO_2$ Biofixation and Fatty Acid Composition of *Scenedesmus Obliquus* and *Chlorella Pyrenoidosa* in Response to Different $CO_2$ Levels. *Bioresour. Technol.* 102, 3071–3076. doi: 10.1016/j.biortech.2010.10.047

Torstensson, A., Hedblom, M., Andersson, J., Andersson, M. X., Wulff, A. (2013). Synergism Between Elevated $pCO_2$ and Temperature on the Antarctic Sea Ice Diatom *Nitzschia Lecointei*. *Biogeosciences* 10, 6391–6401. doi: 10.5194/bg-10-6391-2013

Torstensson, A., Hedblom, M., Mattsdotter, , Bjork, M., Chierici, M., Wulff, A. (2015). Long-Term Acclimation to Elevated $pCO_2$ Alters Carbon Metabolism and Reduces Growth in the Antarctic Diatom *Nitzschia Lecointei*. *Proc. R. Soc B-Biol. Sci.* 282, 20151513. doi: 10.1098/rspb.2015.1513

Trapnell, C., Williams, B. A., Pertea, G., Mortazavi, A., Kwan, G., van Baren, M. J., et al. (2010). Transcript Assembly and Quantification by RNA-Seq Reveals Unannotated Transcripts and Isoform Switching During Cell Differentiation. *Nat. Biotechnol.* 28, 511–515. doi: 10.1038/nbt.1621

Trimborn, S., Thoms, S., Brenneis, T., Heiden, J. P., Beszteri, S., Bischof, K. (2017). Two Southern Ocean Diatoms Are More Sensitive to Ocean Acidification and Changes in Irradiance Than the Prymnesiophyte *Phaeocystis Antarctica*. *Physiol. Plant* 160, 155–170. doi: 10.1111/ppl.12539

Tsuzuki, M., Ohnuma, E., Sato, N., Takaku, T. and Kawaguchi, A. (1990). Effects of $CO_2$ Concentration During Growth on Fatty Acid Composition in Microalgae. *Plant Physiol.* 93, 851–856. doi: 10.1104/pp.93.3.851

Waite, M. and Wakil, S. J. (1962). Studies on the Mechanism of Fatty Acid Synthesis. XII. Acetyl Coenzyme A Carboxylase. *J. Biol. Chem.* 237, 2750–2757. doi: 10.1016/S0021-9258(18)60223-6

Wang, L., Feng, Z., Wang, X., Wang, X., Zhang, X. (2010). DEGseq: An R Package for Identifying Differentially Expressed Genes From RNA-Seq Data. *Bioinformatics* 26, 136–138. doi: 10.1093/bioinformatics/btp612

Wang, X. W., Liang, J. R., Luo, C. S., Chen, C. P., Gao, Y. H. (2014). Biomass, Total Lipid Production, and Fatty Acid Composition of the Marine Diatom *Chaetoceros Muelleri* in Response to Different $CO_2$ Levels. *Bioresour. Technol.* 161, 124–130. doi: 10.1016/j.biortech.2014.03.012

Zhang, Y., Gu, Z., Ren, Y., Wang, L., Zhang, J., Liang, C., et al. (2021). Integrating Transcriptomics and Metabolomics to Characterize Metabolic Regulation to Elevated $CO_2$ in *Chlamydomonas Reinhardtii*. *Mar. Biotechnol.* 23, 255–275. doi: 10.1007/s10126-021-10021-y

**Conflict of Interest:** The authors declare that the research was conducted in the absence of any commercial or financial relationships that could be construed as a potential conflict of interest.

**Publisher's Note:** All claims expressed in this article are solely those of the authors and do not necessarily represent those of their affiliated organizations, or those of the publisher, the editors and the reviewers. Any product that may be evaluated in this article, or claim that may be made by its manufacturer, is not guaranteed or endorsed by the publisher.

frontiers | Frontiers in Marine Science

ORIGINAL RESEARCH
published: 25 July 2022
doi: 10.3389/fmars.2022.887909

# Variability in the Carbon and Nitrogen Uptake Rates of Phytoplankton Associated With Wind Speed and Direction in the Marian Cove, Antarctica

*Bo Kyung Kim[1], Misa Jeon[1], Sang-Jong Park[2], Hyun-Cheol Kim[3], Jun-Oh Min[1], Jisoo Park[1] and Sun-Yong Ha[1]**

*[1] Division of Ocean Sciences, Korea Polar Research Institute, Incheon, South Korea, [2] Division of Atmospheric Sciences, Korea Polar Research Institute, Incheon, South Korea, [3] Center of Remote Sensing and Geographic Information System, Korea Polar Research Institute, Incheon, South Korea*

OPEN ACCESS

**Edited by:**
*Mi Sun Yun, Tianjin University of Science and Technology, China*

**Reviewed by:**
*Ya-Wei Luo, Xiamen University, China*
*Andrew Mcminn, University of Tasmania, Australia*

***Correspondence:**
*Sun-Yong Ha*
*syha@kopri.re.kr*

**Specialty section:**
*This article was submitted to Aquatic Microbiology, a section of the journal Frontiers in Marine Science*

**Received:** *02 March 2022*
**Accepted:** *16 June 2022*
**Published:** *25 July 2022*

**Citation:**
*Kim BK, Jeon M, Park S-J, Kim H-C, Min J-O, Park J and Ha S-Y (2022) Variability in the Carbon and Nitrogen Uptake Rates of Phytoplankton Associated With Wind Speed and Direction in the Marian Cove, Antarctica. Front. Mar. Sci. 9:887909. doi: 10.3389/fmars.2022.887909*

Quantifying the temporal variability in phytoplankton productivity is essential for improving our understanding of carbon (C) and nitrogen (N) dynamics and energy flows in natural aquatic ecosystems. Samples were collected at three-day intervals from December 2018 to January 2019 from fixed station in Marian Cove, Antarctica to determine the C and N ($NO_3^-$ and $NH_4^+$) uptake by phytoplankton. Considerable fluctuations in the total C and N productivities were observed, which led to dynamic changes in the phytoplankton communities and a stronger coupling between the phytoplankton biomass. The increased rate of $NO_3^-$ uptake coincided with an enhanced C uptake mainly by microphytoplankton (>20 μm), followed by an increase in $NH_4^+$ uptake towards the end of sampling period. However, the <2 μm fraction (picophytoplankton) showed little variation in C and $NO_3^-$ uptake, and the proportions of assimilated $NH_4^+$ contributed to more than half of the total assimilated inorganic N. The increased $NH_4^+$ did not increase the total phytoplankton biomass and C production. Interestingly, after January 9 (maximum chlorophyll a, C, and N uptake) there was a shift to a predominantly easterly wind (>6 m $s^{-1}$), which rapidly decreased the total chl-a, C and N uptake rate to ~4% of the highest values (0.6 mg $m^{-3}$, 1.0 mg C $m^{-3}$ $h^{-1}$, 0.1 mg N $m^{-3}$ $h^{-1}$, respectively) on January 12. The phytoplankton community was also replaced by neritic and ice-related species. These findings suggest that strong temporal shifts in phytoplankton C and N assimilation are strongly influenced by external forces (wind stress).

**Keywords: phytoplankton, carbon, nitrogen, stable isotope, Marian Cove, Antarctica**

## INTRODUCTION

The Southern Ocean plays a critical role in Earth's carbon cycle as a significant carbon sink, accounting for ~43% of the total oceanic inventory of anthropogenic $CO_2$ south of 30° S (Frölicher et al., 2015). This is a region of seasonal extremes, with large fluctuations in phytoplankton productivity. Coastal Antarctic is considered to have high productivity, with large summer blooms

phytoplankton representing the most important annual input to pelagic food webs (Kang et al., 1997; Fiala et al., 1998; Kang et al., 2002; Arrigo et al., 2008; Vernet et al., 2012; Biggs et al., 2019).

Phytoplankton bloom dynamics in coastal Antarctic waters are governed by irradiance, temperature, stratification, anticyclones, and nutrient supply (Saba et al., 2014; Schloss et al., 2014; Höfer et al., 2019, and references therein). They consists of a series of sequential blooms of different phytoplankton species and sizes that utilize different forms of dissolved inorganic N (DIN) for optimal growth, depending on the ambient nutrient concentration and cell phases. Usually, high primary productivity (C uptake) phytoplankton blooms are seasonal in ice-covered regions and occur after sea ice melts. These blooms are composed of large phytoplankton cells (>20 μm, e.g., diatoms) that utilize nitrate ($NO_3^-$; so-called "new") as their nitrogen (N) source. Smaller cells and haptophytes, which use regenerated forms of N compounds, e.g., ammonium ($NH_4^+$) to sustain growth, become important under post-bloom conditions (Dugdale and Goering, 1967; Kanda et al., 1990; Kristiansen et al., 1994; Bode et al., 2002; Clarke et al., 2008). Therefore, changes in the productivity and size classes of marine phytoplankton reflect environmental conditions and affect the flow of dietary energy from lower to upper trophic levels.

The coastal ecosystems of Antarctica on the western Antarctic Peninsula (WAP), where significant changes in sea ice and terrestrial ice sheet dynamics, temperature, nutrients, and salinity have been observed, are more vulnerable to climate change than other regions (Prézelin et al., 2000; Cook et al., 2005; Martinson et al., 2008; Stammerjohn et al., 2008; Annett et al., 2015; Cook et al., 2016; Llanillo et al., 2019). These changes are directly linked to observed changes in coastal ecosystems (Atkinson et al., 2004; Moline et al., 2004; Moon et al., 2015; Arrigo et al., 2017; Höfer et al., 2019; Plum et al., 2020; Gutt et al., 2021). In particular, Marian Cove is one of the fastest glacier retreat fronts in the WAP (Rückamp et al., 2011), and is a marine biological hotspot, as it is a fjord experiencing ecosystem changes due to global warming-induced glacier retreat and ice-melt (Gutt et al., 2021). Most studies in the area have focused primarily on benthic genera and bacterial community structures (Moon et al., 2015; Ahn et al., 2016; Ha et al., 2019; Kim et al., 2020; Bae et al., 2021), with numerous studies dealing with phytoplankton in the Marian Cove (Kang et al., 1997; Kang et al., 2002; Lee et al., 2015). However, limited phytoplankton productivity data are available from the same area (Yang, 1990; Kim et al., 2021). Studies on $^{15}N$-based uptake of phytoplankton have not been conducted in the Marian Cove till date. Therefore, the temporal pattern of phytoplankton succession in the Marian Cove, as influenced by their C and N uptake dynamics were undertaken to better understand the ecosystem structures and functions. The aim of this study was to describe the temporal variations in the C and N (new and regenerated) uptake rates of phytoplankton and associated chlorophyll a (chl-a) during summertime in the Marian Cove. The present study also constitutes the first measurement of *in-situ* N productivity in the study area and mainly focuses on the mechanisms controlling C and N dynamics related to environmental conditions.

# MATERIALS AND METHODS

## Study Site and Field Sampling

The Marian Cove is 4.5 km long, 1.5 km wide, ~110 m deep, and is located in the Maxwell Bay, southwest of the King George Island, WAP. The area has experienced ~1.7 km of glacial retreat for 50 years (Park et al., 1998; Lee et al., 2008; Rückamp et al., 2011). Recent (1956–1957 and 2020–2021) glacier retreat velocity was ~27.2 m/yr in the Marian Cove (**Figure 1**). The phytoplankton biomass (chl-a) in the area started to increase from October to November peaking (i.e., a "bloom") around January, whereas the lowest values occurred during winter (June–August) (Kang et al., 2002; Lee et al., 2015; Jeon et al., 2021). Marian Cove is characterized by intense summer blooms with high primary production in January (Kim et al., 2021). The general pattern of seasonal phytoplankton succession is that diatoms (>20 μm) dominate in summer and, pico- and nanophytoplanktons (<20 μm) dominate in winter (Kang et al., 1997; Kang et al., 2002; Lee et al., 2015; Jeon et al., 2021).

The study site was conducted from a fixed-point coastal monitoring site for marine ecosystem near King Sejong Station (62°13' S, 58°47' W; KSS), Korea (**Figure 1**). Experiments for C and N uptake by phytoplankton were conducted from December 19, 2018, to January 26, 2019, and results were compared with the environmental parameters (water temperature, salinity, chl-a, nutrients, and phytoplankton taxonomy). The water depth at the site is between 5 and 10 m, and is vertically well-mixed owing to wind- and tide-induced currents (Lee et al., 2015 and references therein). Surface water samples were collected every third day around solar noon at a depth of 0.5 m using a sampler. Average three–hour meteorological data (wind speed and wind direction) were collected during the sampling period from the automatic meteorological observation system (AMOS-3) of the KSS. The wind vane was located 10 m above ground (Park et al., 2013). Ten-minute interval data were averaged into hourly and daily data.

## Surface Seawater Temperature, Salinity, Macronutrient, and Chl-a Analyses

Water temperature and salinity were measured using a YSI Model 30 (Yellow Springs Inc. Ohio, USA). For dissolved inorganic nutrient ($NO_2^-$ + $NO_3^-$, $NH_4^+$, $PO_4^{3-}$, and $SiO_2$) concentrations, the seawater was filtered through GF/F filters (pre-combusted at 450°C for 4 h, nominal 0.7 μm, Whatman, UK). The filtered seawater samples were preserved at approximately -20°C until analysis. Major inorganic nutrients were measured using a 4-channel continuous autoanalyzer (QuAAtro, SEAL Analytical, UK), according to the manufacturer's instructions. Standard curves were run for each sample batch using freshly prepared standards

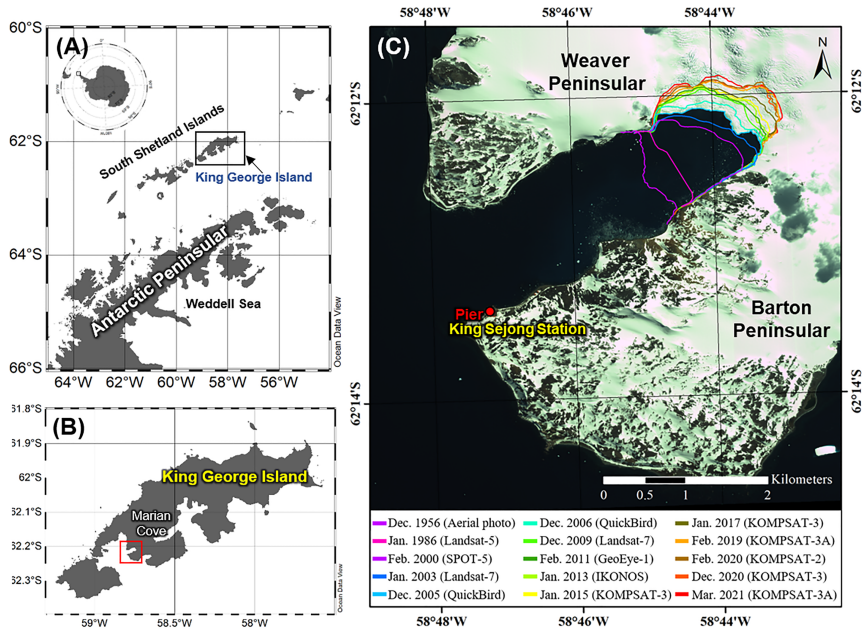


**FIGURE 1 |** Map showing the location of the **(A)** South Shetland Islands, **(B)** King George Island, and **(C)** Marian Cove. Glacier termini overlaid on remote sensing images and aerial photographs acquired in 1956-2021. The maps **(A**, **B)** were generated by using Ocean Data View v. 5.3.0 (https://odv.awi.de) (AWI, Bremerhaven, Germany, Schlitzer, R.).

with concentrations in the range of that of the samples. For total chl-a analysis, seawater was filtered through GF/F filters (pre-combusted at 450°C for 4 h). For size-fractionated chl-a analysis, water was passed sequentially through a nucleopore membrane filter (20 μm and 2 μm) and GF/F filters. All filters were extracted overnight with 90% acetone, and the extracts were analyzed using a fluorometer (Trilogy, Turner Designs, Sunnyvale, CA, USA) (Parsons et al., 1984).

## Experiments for Carbon and Nitrogen Uptake Rate

The sampled seawater was prefiltered through a 200 μm mesh to remove zooplankton. $^{13}$C-labeled sodium bicarbonate (Cambridge Isotope Laboratories, USA), $^{15}$N-labeled potassium nitrate and sodium ammonium (Sigma–Aldrich, USA) were added to the surface water samples in 1 L polycarbonate bottles. The $^{13}$C and $^{15}$N levels were ~4–20% of the total dissolved inorganic C and ambient nitrogenous nutrient concentrations. The bottles were incubated for 4–5 h in ambient seawater. The incubated seawater was filtered (0.3 L) through 450°C pre-combusted GF/F filters (25 mm). A fraction of the picophytoplankton and water passed through 2 μm nucleopore filters (47 mm) and the filtrate was passed through GF/F filters (25 mm). The filters were immediately stored at -80°C until further analysis. The C and N (nitrate and ammonium) uptake rates of the phytoplankton were measured according to the protocol described by Kim et al. (2021). The samples were placed overnight in an acid fume to remove carbonates. C and N isotope abundances were determined using Elemental Analysis (Euro EA3028, EuroVector, Milan, Italy) - Isotope Ratio Mass Spectrometry (Isoprime 100, EIementar, Manchester, UK) in a stable isotope laboratory at Hanyang University, Korea. Carbonate alkalinity of the water sample was determined by titration with 0.01 N HCl, and the total $CO_2$ content was calculated according to the method of Parson et al. (1984). The C or N uptake rates (mg C (or N) $m^{-3}$ $h^{-1}$) of phytoplankton were calculated based on Hama et al. (1983) and Dugdale and Goering (1967), respectively, using the following formula (1):

$$\text{Uptake rate}\left(\rho(t)\right) = \frac{\Delta POC\left(or\ PON\right)(t)}{t} = \frac{a_{is} - a_{ns}}{a_{ic} - a_{ns}} \times \frac{POC\left(or\ PON\right)(t)}{t} \quad (1)$$

where $\Delta POC(or\ PON)(t)$ is the increase in particulate organic C or N concentration during incubation (mg C (or N) $m^{-3}$), respectively, t is the incubation time, $a_{is}$ is the atomic % of $^{13}$C (or $^{15}$N) in the incubated sample, $a_{ns}$, is the atomic % of $^{13}$C (or $^{15}$N) in the natural sample, $a_{ic}$ is the atomic % of $^{13}$C (or $^{15}$N) in the total inorganic C (or N). The specific uptake rate can be defined as the rate of uptake or transport of the product ($h^{-1}$). Unlike the C uptake samples (duplicates), single samples were analyzed for the N uptake rates.

## Data Analysis

Pearson's correlation was used to investigate the relationship between environmental variables and C and N uptake rates. In

this study, we estimated the time series of temporally cumulative zonal wind stress ($\tau_x$, in N $m^{-2}$) from December 19, 2018 to January 26, 2019, to identify cumulative force exerted on the surface. The cumulative zonal wind stress at a particular time is calculated as the sum of the wind stresses over the previous days (1-day to 5-day in this study). Positive and negative values indicate eastward and westward wind stress, respectively.

# RESULTS

## Temporal Patterns of Temperature, Salinity, Chl-a, and Inorganic Macronutrients

The surface water temperature at the sampling site in the Marian Cove was the highest (2.2°C) and lowest (0.3°C) on December 19, 2018 and January 26, 2019, respectively (**Figure 2A**). With the exception of a few days (≤0.6°C) in December to January, most recorded temperatures were above >1°C. The surface salinity ranged from 29.6 to 34.5. Salinity was stable throughout the study period, except a low salinity period in January 12–20. Salinity was positively correlated with the water temperature ($r = 0.615$, $p < 0.05$; **Table 1**).

**Figure 2B** shows the temporal variability of the total chl-a content and the relative contribution of size-fractionated phytoplankton (micro-, nano-, and picophytoplankton). The highest total phytoplankton biomass (chl-a) was recorded on January 6 and 9, 2019 (14.6 and 20.0 mg $m^{-3}$, respectively). Average chl-a was 4.4 mg $m^{-3}$ (SD = ± 6.0 mg $m^{-3}$) during the period from December 19, 2018 to January 26, 2019 (**Figure 2B**). Microphytoplankton constituted the dominant size fraction during the sampling period, accounting for 16.5-93.6% of the total chl-a content, with a mean of 57.2% (± 26.2%), followed by nano- (30.3%), and picophytoplankton (12.5%). At peak chl-a content, microphytoplankton (>20 μm) contributed >90% of the total chl-a. In comparison, the contribution of picophytoplankton (<2 μm) to the total biomass was always low, reaching peak values (28%) on December 25, 2018. The total chl-a concentration was positively correlated with microphytoplankton ($p < 0.05$, $r = 0.748$) and negatively correlated with picophytoplankton ($p < 0.05$, $r = -0.651$) (**Table 1**).

The daily concentrations of $NO_2^-$+$NO_3^-$ and $SiO_2$ were 11.4–26.2 μM and 41.6–73.5 μM, respectively, although they differed widely on each sampling date. $PO_4^{3-}$ displayed the same pattern as $NO_2^-$+$NO_3^-$ (**Figure 2C**). However, the $PO_4^{3-}$ concentration was relatively lower (0.8-1.8 μM). Decrease in nutrient concentrations during sampling were common with substantially increased chl-a concentration, such as from early to mid-January. The largest decrease in nutrient concentration in the surface water from the initial values was observed during January 12–20. $NO_2^-$+$NO_3^-$ and $PO_4^{3-}$ concentrations decreased from 19.2 to 11.4 μM and 1.7 to 0.8 μM, respectively (**Figure 2C**). Similarly, low $NH_4^+$ was observed (<1 μM) at peak chl-a. Interestingly, $SiO_2$ concentrations further decreased between January 9 and 23, which was not observed for other inorganic nutrients (**Figure 2D**). Overall, the $NO_2^-$ +$NO_3^-$+$NH_4^+$:$PO_4^{3-}$ (N:P) and $NO_2^-$+$NO_3^-$+$NH_4^+$:$SiO_2$ (N:Si) molar ratios ranged from 11.7 to 15.4 (average ± SD = 13.2 ± 1.1) and 0.2 to 0.7 (average ± SD = 0.3 ± 0.1), respectively (**Figure 2E**).

## Wind Speed and Direction

**Figure 3** shows the three-hourly average wind speed and direction. The average wind speed during the study period was 6 m $s^{-1}$. A large change was observed in the average wind speed in the Marian Cove during the sampling period, reaching 14.4 m $s^{-1}$. The overall wind direction was WNW during the sampling period. Meanwhile, an easterly wind prevailed from January 10 and 13, with highest wind speeds (>6 m $s^{-1}$) (**Figures 3A, B**). The colored curve in **Figure 3C** shows the accumulated $\tau_x$ values, there were two strong eastward episodes. The pulses of accumulated $\tau_x$ match well with the wind speed through December 19, 2018 to January 26, 2019 (**Figures 3A, C**). It exhibits clearly that the overall intensity of the eastward in 2-day is the strongest from 1-day to 5-day (see red curve in **Figure 3C**). The accumulated intensity of easterly wind in 2-day between January 11 and 13 is the most prominent.

## Time Series in Surface-Water Uptake of Total C and N

The total C and N (sum of $NO_3^-$ and $NH_4^+$ uptake) uptake rates (mg C (or N) $m^{-3}$ $h^{-1}$) by phytoplankton in the surface water were measured during summer (December–January) (**Figures 4**, **5**), and were 0.3–24.5 mg C $m^{-3}$ $h^{-1}$ and 0.06–3.27 mg N $m^{-3}$ $h^{-1}$, respectively. The average C and N uptake rates were 6.8 mg C $m^{-3}$ $h^{-1}$ (SD = ± 7.9 mg C $m^{-3}$ $h^{-1}$) and 1.0 mg N $m^{-3}$ $h^{-1}$ (SD = ± 1.1 mg N $m^{-3}$ $h^{-1}$), respectively, with the highest rates observed on January 9 and the lowest on January 26 (**Figures 4A**, **5A**). The temporal pattern of N uptake was very similar to that of C uptake and chl-a content (**Figures 4A**, **5A**). Moreover, the specific uptakes ($h^{-1}$) of total C and $NO_3^-$ were the highest on January 6, after which they gradually decreased, peaked on January 17, and then steadily decreased until the end of the observation period (**Figures 4B**, **5C**). Relative contributions of the different N compounds to the measured total N uptake varied for on each sampling date (**Figure 5D**). Compared to total N, proportion of the $NO_3^-$ uptake fraction was 15.2% at the beginning (in the middle of December) but increased gradually to 64.7% on January 3.

Although both $NO_3^-$ and $NH_4^+$ were taken up by phytoplankton, the C and dominant N sources varied between the growth phases and blooms. During the sampling period, the 31-fold change in biomass was lower than the 84-fold change in total C uptake, and growth acceleration was much faster in this region. Simultaneously, a more substantial (462-fold) change in the total $NO_3^-$ uptake rate was observed, whereas the total $NH_4^+$ uptake (31-fold) was similar to that of the chl-a content. The total and specific C uptake rates were inversely correlated with DIN ($NO_2^-$+$NO_3^-$+$NH_4^+$, $p < 0.05$, $r = -0.595$, and $r = -0.601$, respectively) but positively

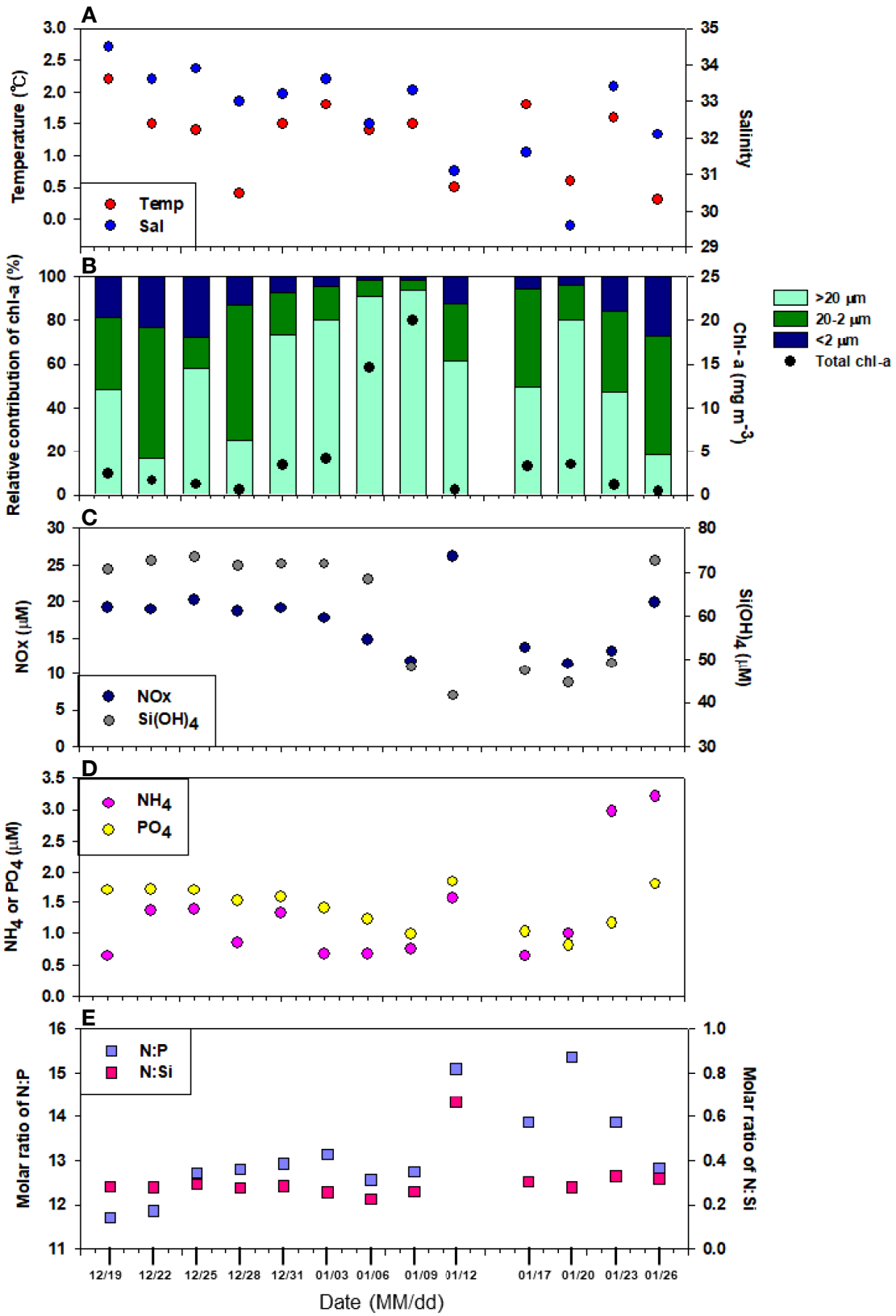


**FIGURE 2 |** Temporal variability of **(A)** water temperature and salinity, **(B)** total chlorophyll a concentration and percentage contribution of size-fractionated chlorophyll a, concentration of **(C)** $NO_x$ ($NO_2^-$+$NO_3^-$) and $SiO_2$, **(D)** $PO_4^{3-}$ and $NH_4^+$, **(E)** molar ratio of N:P and N:Si at surface water during sampling period.

**TABLE 1 |** Pearson correlation coefficients between the environmental parameters on productivity.

| | **Temp** | **Sal** | **Chl** | **T_C** | **Sp_T_C** | **P_C** | **Sp_P_C** | **T_Ni** | **T_Am** | **P_Ni** | **P_Am** | **$NO_2^-$+$NO_3^-$$NH_4^+$** | **$PO_4^{3-}$** | **$SiO_2$** | **DIN** | **Micro** | **Nano** | **Pico** |
|---|---|---|---|---|---|---|---|---|---|---|---|---|---|---|---|---|---|---|
| Temp | 1 | | | | | | | | | | | | | | | | | |
| Sal | 0.615* | 1 | | | | | | | | | | | | | | | | |
| Chl | | | 1 | | | | | | | | | | | | | | | |
| T_C | | | 0.973** | 1 | | | | | | | | | | | | | | |
| Sp_T_C | | | 0.859** | 0.930** | 1 | | | | | | | | | | | | | |
| P_C | 0.769** | 0.623* | | | | 1 | | | | | | | | | | | | |
| Sp_P_C | 0.748** | 0.640* | | | | 0.957** | 1 | | | | | | | | | | | |
| T_Ni | | | 0.939** | 0.987** | 0.943** | | | 1 | | | | | | | | | | |
| T_Am | | | 0.880** | 0.923** | 0.905** | | | 0.927** | 1 | | | | | | | | | |
| P_Ni | | | | | | | | | | 1 | | | | | | | | |
| P_Am | | | | | | | | | | 0.836** | 1 | | | | | | | |
| $NO_2^-$+$NO_3^-$ | | | | | | | | | | | | 1 | | | | | | |
| $NH_4^+$ | | | | | -0.567* | | | | | | | | 1 | | | | | |
| $PO_4^{3-}$ | | | | | -0.586* | | | | | | | 0.929** | | 1 | | | | |
| $SiO_2$ | | 0.746** | | | | | | | | | | | 0.577* | 1 | | | | |
| DIN | | | -0.616* | -0.595* | -0.601* | | | | | | | 0.982** | | 0.938** | | 1 | | |
| Micro | | | 0.748** | 0.771** | 0.831** | | | 0.784** | 0.688** | | | | | -0.553* | | | 1 | |
| Nano | | | -0.678* | -0.672* | -0.693** | | | -0.684** | -0.605* | | | | | | | | -0.953** | 1 |
| Pico | | | -0.651* | -0.724** | -0.849** | | | -0.736** | -0.637* | | | | 0.588* | 0.718** | | 0.614* | -0.769** | | 1 |

*The r-values shown in this table indicate statistical signifiificance when p-values are< 0.05 (*) and< 0.001 (**). Blanks indicate that r-values are not signifiificant. Temp; temperature, Sal; salinity, Chl; chlorophyll a, T_C; total carbon uptake rate, P_C; picophytoplankton carbon uptake rate, Sp_T_C; specifiific total carbon uptake rate, Sb_P_C; specifiific picophytoplankton carbon uptake rate, T_Ni; total nitrate uptake rate, T_Am; total ammonium uptake rate, P_Ni; picophytoplankton nitrate uptake rate, P_Am; picophytoplankton ammonium uptake rate, DIN; sum of NO3-+NO2-+NH4+; Micro; microphytoplankton (%), Nano; nanophytoplankton (%), Pico; picophytoplankton contribution (%) of total chl-a.*

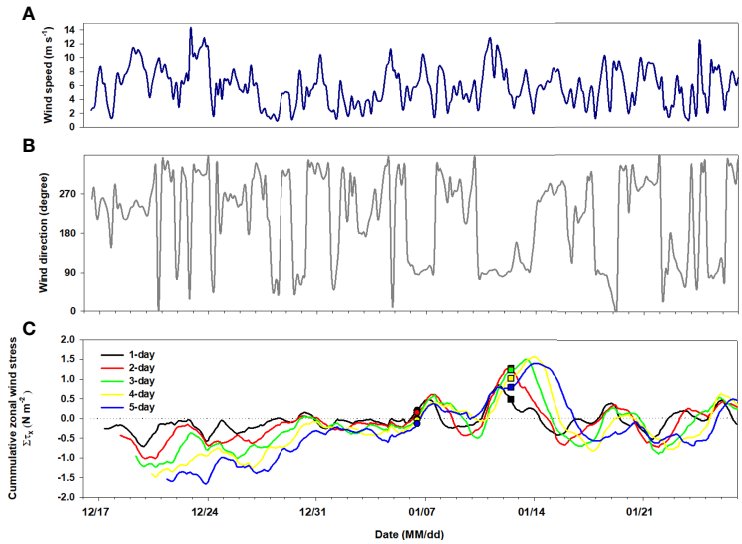


**FIGURE 3 |** Time series of **(A)** wind direction, **(B)** wind speed and **(C)** cumulative zonal wind stress during sampling period. In (**C**), the black line indicates the prescribed climatological wind stress ($\tau_x$) for the 1-day. The red, green, yellow, and blue lines are cumulative wind stress forcing for 2-, 3-, 4-, and 5-day, respectively. The circle and square symbols represent the sampling time of January 6 and 12, respectively.

correlated with phytoplankton biomass (chl-a, $p < 0.05$, $r = 0.973$, and $r = 0.859$, respectively) (**Table 1**). This suggests that the nutrients were alomost simultaneously used by the Marian Cove phytoplankton.

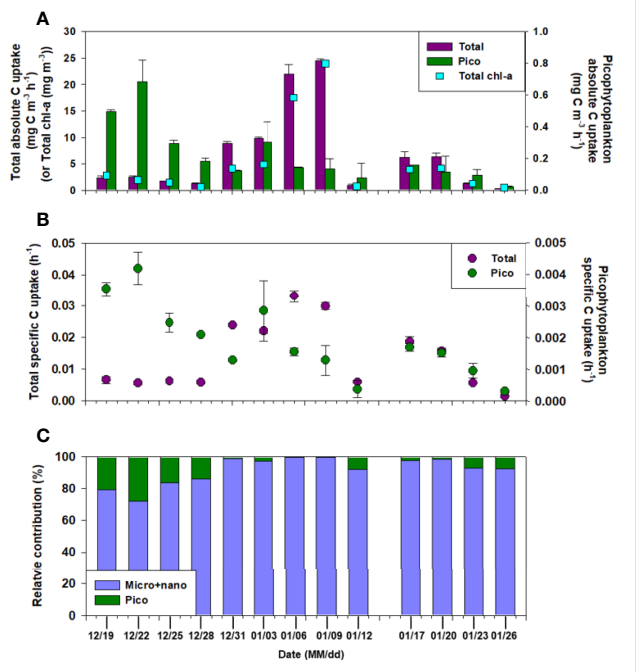


**FIGURE 4 |** Hourly **(A)** carbon and **(B)** specific uptake rates for total and picophytoplankton, and **(C)** the relative contribution of size-fractionated phytoplankton each sampling date.

## Relative Contribution of the Picophytoplankton (< 2 μm) Fraction to the Total Productivity

Decrease in the C uptake rate was mainly due to the decline in chl-a values for the total phytoplankton; however, the picophytoplankton fraction showed little variation in chl-a. We found that picophytoplankton productivity remained relatively constant during the sampling period compared to the total uptake, even with nutrient fluctuations (**Figure 4A**). The average surface C uptake by picophytoplankton was 0.2 mg C $m^{-3}$ $h^{-1}$ (SD = ± 0.2 mg C $m^{-3}$ $h^{-1}$), the highest being on December 22 (0.7 mg C $m^{-3}$ $h^{-1}$), and the lowest (0.02 mg C $m^{-3}$ $h^{-1}$) at the end of the observation period. The contribution of picophytoplankton to the total phytoplankton C uptake ranged from a minimum of 0.6% to a maximum of 27.9% on January 9 (**Figure 4C**). However, the average C uptake by picophytoplankton was up to 8.6% (SD = ± 8.7%) of the total measured C uptake. The specific uptake rate ($h^{-1}$) of picophytoplankton showed a similar trend to the uptake rate of C, and decreased with decreasing surface C uptake (**Figure 4B**). A positive relationship was observed between the picophytoplankton C uptake, temperature, and salinity ($p < 0.05$), while a negative relationship was found between the picophytoplankton relative contribution to total biomass an the total C uptake (**Table 1**).

$NO_3^-$ uptake by picophytoplankton in the surface waters varied from<0.01 to up to 0.04 mg N $m^{-3}$ $h^{-1}$, with a mean of 0.01 mg N $m^{-3}$ $h^{-1}$ (SD = ± 0.01 mg N $m^{-3}$ $h^{-1}$) (**Figure 5E**). The surface $NH_4^+$ uptake rates varied from 0.005 to 0.257 mg N $m^{-3}$ $h^{-1}$, whereas the $NO_3^-$ uptake rates showed a relatively narrow range (0.001-0.035 mg N $m^{-3}$ $h^{-1}$) (**Figure 5E**). The $NH_4^+$ uptake rate was higher than the $NO_3^-$ uptake rate in

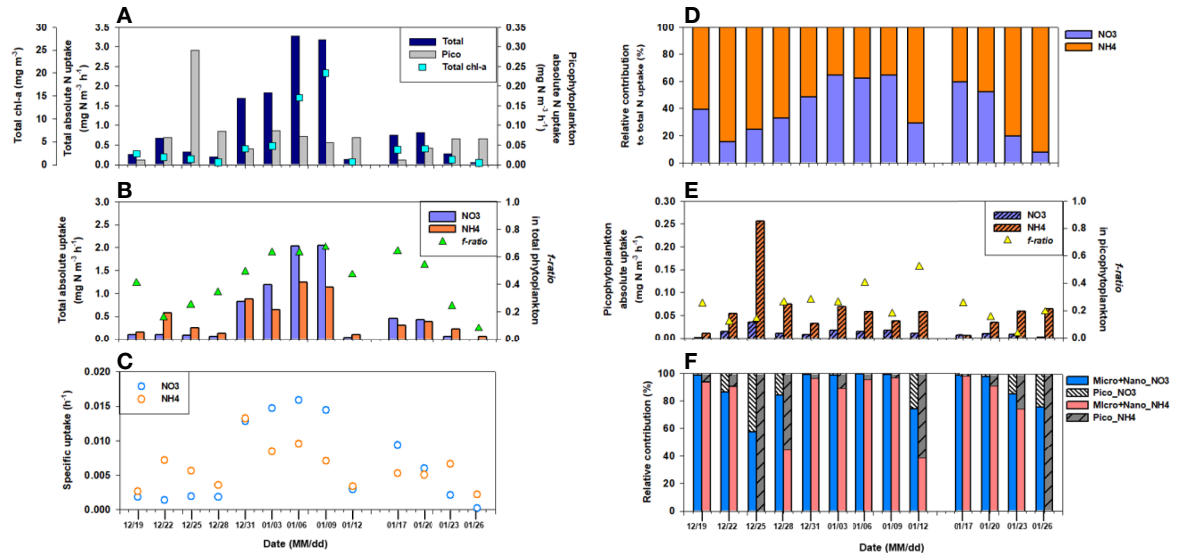


**FIGURE 5 |** Hourly rates of **(A)** nitrogen, **(B)** nitrate ($NO_3^-$) and ammonium ($NH_4^+$) uptake, **(C)** specific nitrate ($NO_3^-$) and ammonium ($NH_4^+$) uptake, and **(D)** the relative contribution of different N forms in total phytoplankton, **(E)** nitrate ($NO_3^-$) and ammonium ($NH_4^+$) uptake in picophytoplankton, **(F)** the relative contribution of size-fractionated phytoplankton for different N forms on each sampling date. The blue squares in **(A)** and triangles in **(B, E)** represent total chl-a concentration and *f*-ratio, respectively.

picophytoplankton, suggesting that it preferred $NH_4^+$ over $NO_3^-$ (average $NH_4^+$ to $NO_3^-$ uptake ratio of 9.1). Unlike the C uptake, neither $NO_3^-$ nor $NH_4^+$ uptake showed any trend (data not shown). No statistical relationship was observed between picophytoplankton N productivity and hydrography and/or dissolved inorganic nutrient concentrations (**Table 1**).

## DISCUSSION

We measured the *in-situ* C and N uptake rates of phytoplankton at a fixed monitoring site during the summer of 2018–2019 using a dual-stable isotope method. The Marian Cove is a semi-enclosed water body that has a tidal, turbid, wind-induced circulation current with high nutrient concentrations, water temperature, and organic matter load (Ahn et al., 1997; Yoo et al., 2003; Jeon et al., 2021). Freshwater discharge from glacier melt is an important control of phytoplankton production, and the accompanying high input of suspended particulate matter (SPM) in the inner Cove changes the optical conditions (Kim et al., 2021). During the study period, SPM concentration did not show any correlation with chl-a, C, or N uptake ($p > 0.05$, data not shown). However, phytoplankton C and N uptake rates and dominant species may be affected by the form of N supplied, nutrient levels, and wind-driven transport processes, such as glacial outflow in the cove. For the present study, we assumed a negligible influence of tidal forces because all sampling was conducted during flood tides.

### Phytoplankton Bloom and the Highly Variable C Uptake in Summer 2018

Relatively high phytoplankton biomass (up to 45 mg $m^{-3}$ near-shore waters adjacent to Palmer station; Goldman et al., 2014) and productivity have been observed in coastal and shelf areas (Garibotti et al., 2003; Arrigo et al., 2008; Ducklow et al., 2012b; Mendes et al., 2012). Particularly during the summer growing period, the phytoplankton species composition varied seasonally, with species abundance related to changes in environmental conditions based on 15 years of monitoring data (1996–2011) (Jeon et al., 2021). For example, seasonal nutrient depletion reflects diatom-dominated phytoplankton communities in regions where blooms are common, with a significant contribution of diatoms to the total phytoplankton biomass in the WAP (Clarke et al., 2008; Vernet et al., 2008; reviewed in Ducklow et al., 2012a; Höfer et al., 2019, and references therein).

Similarly, we observed massive phytoplankton blooms (chl-a up to 20 mg $m^{-3}$), which were mainly composed of microphytoplankton (>20 μm) and large diatoms (>40 μm, e.g., *Thalassiosira* spp.; **Supplementary Figure 1**). There was a strong relationship between microphytoplankton fraction and the total chl-a concentration ($p < 0.05$, $r = 0.748$, $n = 13$), where microphytoplankton contributed >90% of the total chl-a when the latter exceeded ~14 mg $m^{-3}$. When the chl-a concentration was<2 mg $m^{-3}$, nanophytoplankton was occasionally the dominant size class (**Figure 2B**). This is consistent with Jeon et al. (2021), who reported that centric and pennate diatoms comprised a substantial part of phytoplankton biomass in the Marian Cove, with an ~58% contribution to the total microphytoplankton abundance during summer blooms. Therefore, seasonal blooms result primarily from increases in microphytoplankton and diatoms.

We observed similar trends in the C uptake data and chl-a concentrations. During the peak bloom, the C uptake rate was much higher (24.5 mg C $m^{-3}$ $h^{-1}$) and the macronutrient concentrations declined considerably, implying a much more

active nutrient intake by the phytoplankton. Variability in macronutrient consumption is reflected in the phytoplankton biomass in the Antarctic coastal waters during summer (Clarke et al., 2008; Zhang et al., 2019, and references therein). The dominance of microphytoplankton is consistent with the total primary production, and also positively correlates with the chl-a in various coastal waters (Varela et al., 2002; Marañón et al., 2012; Kim et al., 2021). Previous studies have documented a markedly high chl-a and C uptake rate in the coastal ice-edge zone in Antarctic waters adjoining the Indian Ocean (up to 4.0 mg $m^{-3}$ and 3.3 mg C $m^{-3}$ $h^{-1}$, respectively; Verlencar et al., 1990), Marguerite Bay (>10 mg $m^{-3}$ and >4.2 mg C $m^{-3}$ $h^{-1}$, respectively; Ducklow et al., 2012b), Marian Cove (up to 19.5 mg $m^{-3}$ and 31.1 mg C $m^{-3}$ $h^{-1}$, respectively; Kim et al., 2021), and South Bay (>15 mg $m^{-3}$ and >50 mg C $m^{-3}$ $h^{-1}$, respectively; Höfer et al., 2019). This is consistent with observations from the Antarctic coastal waters, and supports the theory that this is one of the most important global "biological hotspots". The development of phytoplankton blooms is also an important factor affecting primary production.

However, the observed temporal variability (0.3–24.5 mg C $m^{-3}$ $h^{-1}$) probably reflects a combination of changes in light availability due to turbidity and water stability (Schloss et al., 2002; Kim et al., 2021), as well as water movement (Höfer et al., 2019). Although various environmental factors affected the C uptake rate, no statistically significant differences were observed in the direct light intensity, SPM, water temperature, and salinity during the sampling period. Low macronutrient contents were observed during the peak bloom, but the N/P ratio remained similar regardless of the growth phase and was unlikely to act as a limiting factor for phytoplankton growth. Earlier studies reported that macronutrient values in the Marian Cove are generally a non-limiting factor for phytoplankton growth (Lee et al., 2015; Jeon et al., 2021), both due to inflow from the Maxwell Bay and the penguin colonies (Pruszak, 1980; Nędzarek, 2008), where turbulent mixing and wind-driven upwelling cause continuous and abundant nutrient flow into the photic layer. Additionally, lateral iron inputs from glacial meltwaters and terrestrial sources are sufficient to sustain large-scale phytoplankton blooms on the King George Island (Schloss et al., 2014; Kim et al., 2015; Höfer et al., 2019), and phytoplankton growth is not limited, even during intense blooms (Bown et al., 2017).

Nevertheless, the significant reduction in biomass and total C uptake immediately after peak chl-a (on January 12) may have enhanced other phytoplankton losses, such as zooplankton predation and other loss rates (i.e., viral lysis, sinking, and aggregation) (Petrou et al., 2016). Grazing effects, phytoplankton sinking, and mortality rates were not explored in this study. Instead, heterotrophic activity and the physiological status of phytoplankton were estimated based on the $NH_4^+$ concentration and specific C uptake by phytoplankton. For example, being its main contributor, zooplankton excretion can boost ambient $NH_4^+$ concentrations (Corner and Davies, 1971). Bacterial degradation of organic matter may also result in summertime $NH_4^+$ accumulation (Koike et al., 1986). $NH_4^+$ and $NO_3^-$ concentrations in the area showed a rapid increase under lower C uptake on January 12 (**Figures 3D** and **4A**). Simultaneously, the specific C uptake rates by phytoplankton were approximately 1/6 of the peak value (0.03 $h^{-1}$). These results imply a physiological limitation of phytoplankton growth on January 12, which may have temporarily enhanced nutrient concentrations in the surface water due to less consumption by phytoplankton. This suggests the increased possibility of the influence of external forces (i.e., bottom-up control) rather than biointeractions (i.e., top-down control).

## N Uptake Dynamics of Phytoplankton and *f*-Ratio

Utilisation of inorganic N by phytoplankton was observed to be highly variable in the Marian Cove during summer. The total $NO_3^-$ uptake was higher than the $NH_4^+$ uptake in the bloom phase, while primary production in the system evolved from $NO_3^-$-based to $NH_4^+$-based at the end of sampling. This evolution is in agreement with earlier studies that reported rise in $NH_4^+$ levels during summers, when zooplankton and microbial metabolism provide regenerated N (Clarke et al., 2008; Mosseri et al., 2008). The high ambient $NH_4^+$ concentrations in conjunction with increased $NH_4^+$ uptake are indicative of an active regeneration process in the Marian Cove and are attributed to the late summer sampling. Thus, we hypothesized that $NH_4^+$ uptake occurs in relation to changes in its concentration and phytoplankton species/size composition.

Dependence of the $NH_4^+$ concentration on $NO_3^-$ uptake has been described in previous studies (Dortch, 1990; L'Helguen et al., 2008; Dugdale et al., 2012; Glibert et al., 2016). For example, $NH_4^+$ concentrations >1 μM (Dortch, 1990) or over a certain threshold (0.2–100 μM; Varela and Harrison, 1999; Dugdale et al., 2012; Glibert et al., 2016) inhibit $NO_3^-$ uptake rates. Our data also support that a relatively higher uptake of $NH_4^+$ than that of $NO_3^-$ was observed in the presence of >1 μM $NH_4^+$ in ambient waters, which might be influenced by the inhibition of assimilated $NO_3^-$ by phytoplankton. However, the elevated $NH_4^+$ uptake did not enhance the total phytoplankton C uptake or biomass. The observed rapid $NO_2^-$+$NO_3^-$ drawdown and uptake rate of $NO_3^-$ in January, coupled with increases in chl-a and C uptake, indicate high productivity. These results clearly suggest that $NO_3^-$ is the preferred growth- and biomass-promoting N source for the studied phytoplankton community. Notably, the $NH_4^+$ uptake by phytoplankton was higher despite the high $NO_3^-$ concentrations. Consequently, inhibition of $NO_3^-$ uptake by $NH_4^+$ (>1 μM) may be one of the factors that led to the low *f*-ratio (0.08–0.24, **Figure 5B**) in the total phytoplankton (*f*-ratio= $NO_3^-$ uptake/total N uptake ($NO_3^-$ + $NH_4^+$ uptake), Eppley and Peterson, 1979).

Another possible cause of the lower *f*-ratio could be the increasing contribution of the smaller cells (<20 μm). Microphytoplankton levels were higher during relatively high biomass and C and $NO_3^-$ uptake rates, reaching an *f*-ratio of up

to 0.67 on January 9 (**Figure 5B**). The $NH_4^+$ uptake rates were the highest in the picophytoplankton fraction throughout the sampling period, resulting in an *f*-ratio<0.5, which decreased to 0.03 at the end of the sampling period (**Figure 5E**). In picophytoplankton, $NH_4^+$ is preferentially assimilated over $NO_3^-$ because $NO_3^-$ assimilation is more energy consuming than $NH_4^+$ assimilation. Once $NO_3^-$ is transported into the cell, it must be further reduced to $NH_4^+$ before it can be assimilated (Mulholland and Lomas, 2008).

More importantly, *f*-ratio values show that planktonic diatoms (larger cells) are replaced by small phytoplankton in surface water, causing decreased primary production and C export. This is because $NO_3^-$-fueled new production at steady state is equivalent to the organic C that can be exported from total production in the euphotic layer (Eppley and Peterson, 1979). In this regard, phytoplankton species shifts toward smaller values could substantially lower C export efficiency as well as primary production (Montes-Hugo et al., 2008; Montes-Hugo et al., 2009; Lee et al., 2015, Mendes et al., 2012; Rozema et al., 2017; Schofield et al., 2017). The undergoing reductions in diatom silica production in response to ocean acidification and shifts toward smaller cells could reduce the vertical fluxes of diatoms and diminish C export efficiency before the end of this century (Petrou et al., 2019). Therefore, in the neritic area of Marian Cove, nutrient utilization in the surface layer during the summer induced variations in phytoplankton size composition in terms of chl-a and C and N uptake, from summer blooms (early January) skewed toward the microsized fraction (>20 μm) undergoing a gradual shift toward the pico sized fraction (<2 μm) through the nanosized fraction (2–20 μm) in late January. This shift in the size of the phytoplankton community probably involved the prevailing wind direction associated with physiological and morphological properties (e.g., nutrient uptake and export rate), as mentioned above.

## Role of Wind

Surface wind, meltwater dynamics, and currents, as key drivers of the upper water layer structure, strongly influence nutrient availability and phytoplankton growth (Deppeler and Davidson, 2017). Wind speed and direction may influence the strength and duration of phytoplankton blooms (Schloss et al., 2014; Deppeler and Davidson, 2017, and references therein). High-frequency (HF) wind forcing is important for the residence time of water (Kohut et al., 2018). The major component of HF zonal wind forcing was the so-called easterly wind events, which played a critical role in modulating water movement. Previous, studies on the Marian Cove (Yoo et al., 1999 and Yoo et al., 2015; Jeon et al., 2021) and the adjacent Potter Cove (Klöser et al., 1994) and Admiralty Bay (Nowosielski, 1980) have suggested that the prevailing easterly wind can generate outflow and upwelling near the cove head or deter the flow rate of surface influents from the Maxwell Bay. Pruszak (1980) observed the drift ice movement and reported that, surface water circulation can be controlled with a wind speed of >4 m $s^{-1}$ in the adjacent Admiralty Bay. There is also a study result that surface water flows out of the Marian Cove within one day when the east wind blows with an average wind speed of over 8 m $s^{-1}$ (Yoo et al., 1999).

Similarly, in our study, the wind direction changed from west to east, and continued for approximately three days. Additionally, strong winds (>6 m $s^{-1}$) blew simultaneously, which is believed to have caused low biomass and C and N uptake rates. Although easterly winds occurred on January 6, their speed was low compared to that during January 10–12. In detail, **Figure 3C** shows the evolution of zonal wind stress during sampling period. As a result of the analysis of cumulative wind stress from Day 1 to Day 5, the wind forcing was higher when 2 days were considered. Overall, negative $\sum \tau_x$ values with low wind speeds led to high chl-a, C, and N uptakes from January 2 to 9. This is because factors, such as outflowing water from the Marian Cove to the Maxwell Bay, also play a role in transporting particulate matter, including algae, near the ice wall and resuspending it (Brandini and Rebello, 1994; Yoo et al., 1999). This surface circulation influenced by the easterly wind can deliver surface water and suspended particles to the Maxwell Bay because the Coriolis effect is not important for a small bay width (~1.5 km for the Marian Cove) (Yoo et al., 2015). Resuspension of sediments and benthic diatoms in the inner Admiralty Bay induced by wind-driven upwelling (<20 m water depth) increases surface turbidity and nutrient concentrations (Brandini and Rebello, 1994); however, the effect of resuspension was not significant in the present study. As the $SiO_2$ concentration was lower than that at peak bloom, benthic diatom species (*Cocconei*s spp.) accounted for 8.5% of total diatom abundance (**Supplementary Figure 1**). On January 12, the dominant species were small (<20 μm) *Navicula* spp. and *Fragilariopsis* spp., accounting for 72.2% to the total diatom abundance that lives mainly on the ice walls and in low-salinity coastal waters (Kang et al., 1999; Fernandes and Procopiak, 2003; Jeon et al., 2021). More specifically, a change in the structure of the phytoplankton community was observed during the sampling period in microscope-based phytoplankton observation (**Supplementary Figure 1**). Phytoplankton communities were dominated by bacillariophytes (diatoms), which comprised >60% (up to 96.3%) of the total C biomass over the sampling period. *Thalassiosira* spp., accounting for 67.7% of total diatom abundance at peak bloom, decreased to 1/4 of its peak bloom value on January 12 (**Supplementary Figure 1**).

Water column stratification and relatively weak wind speed are favorable for initiating seasonal blooms, and the presence of sea ice and glacial meltwaters influences primary production patterns (Saba et al., 2014; Rozema et al., 2017; Höfer et al., 2019; Kim et al., 2021). In this regard, the relatively weak wind speeds observed at the beginning of January seem to enable water column stabilization, favoring an increase in the residence times of cells in the photic layer and providing more light for photosynthesis, allowing high phytoplankton accumulation in the cove.

# CONCLUSIONS

In this study, we examined the C and N uptake regimes in the Marian Cove during the austral summers of 2018–19 using $^{13}C$ and $^{15}N$ dual isotope tracer assays. During phytoplankton blooms, the study area was generally characterized by high *f*-ratios

(>0.5), suggesting that $NO_3^-$ plays a dominant role in phytoplankton nutrition. Low *f*-ratios were observed at the end of the sampling period, and microphytoplankton and planktonic diatoms were replaced by nanophytoplankton and sympagic (sea-ice-associated) diatoms, causing decreased primary production and C export. Our results highlight the influence of wind on the changes in C and N uptake regimes and physical–biological coupling in the Marian Cove. Increased regenerated production was not observed as the total phytoplankton biomass increased.

However, we assumed that the bacterial uptake rate was negligible in the present study. It is possible that the N uptake rate of heterotrophic bacteria may contribute to the N uptake rate in the study area. Phytoplankton and bacterial N uptake have been studied in various ecosystems (Bronk et al., 2007). Few records are available for the direct measurements of inorganic N uptake by bacteria in the Southern Ocean. The bacterial $NH_4^+$ demand in the coastal waters of the northern Gerlache Strait region of the Antarctic Peninsula during summer is 8~25% (mean 17%) of the total community $NH_4^+$ uptake rate (Tupas et al., 1994). Cochlan and Bronk (2001) reported similar mean value of 17% for the potential $NH_4^+$ uptake by heterotrophic bacteria in the Ross Sea during summer. The lower *f*-ratio could reflect more available $NH_4^+$ compared to $NO_3^-$. However, accurately determining the contributions to bacterial N uptake using the GF/F filter method, as in this study, to distinguish them by size is still challenging. Therefore, further research is needed to clarify the contribution of bacteria to the primary production of the Marian Cove and the trophic linkages between phytoplankton assemblages and associated consumers. More observations with a longer timescale are required to better understand the C and N dynamics in the Sothern Ocean, particularly in coastal waters where rapid changes in glacial retreat and vigorous meteorological conditions take place owing to the effects of climate change.

## DATA AVAILABILITY STATEMENT

The original contributions presented in the study are included in the article/**Supplementary Material**. Further inquiries can be directed to the corresponding author.

## AUTHOR CONTRIBUTIONS

S-YH conceived of the study, participated in its design and helped to draft the manuscript. BK drafted the manuscript and performed the field and laboratory experiments. MJ carried out the analysis of the chl-a and phytoplankton community. S-JP provided meteorological data. H-CK processed and analyzed satellite imagery for glacier change detection. J-OM contributed to writing the manuscript. JP was the leader of the Korean Antarctic Research Program and provided scientific advice. All authors contributed to the article and approved the submitted version.

## FUNDING

This study was supported by the Korea Polar Research Institute (KOPRI) and undertaken as part of "Carbon cycle change and ecosystem response under the Southern Ocean warming (PE22110)".

## ACKNOWLEDGMENTS

We take the opportunity to thank the colleagues and 32nd King Sejong Station Overwintering Team assistance during work.

## SUPPLEMENTARY MATERIAL

The Supplementary Material for this article can be found online at: https://www.frontiersin.org/articles/10.3389/fmars.2022.887909/full#supplementary-material

**Supplementary Figure 1 |** Temporal variations of the **(A)** relative C biomass (%) of each phytoplankton group and **(B)** the relative cell abundance of major dominant phytoplankton species in diatoms (%) among six sampling dates (December 22 and January 6, 9,12, 23, and 26).

## REFERENCES

Ahn, I.-Y., Chung, H., Kang, J.-S. and Kang, S.-H. (1997). Diatom Composition and Biomass Variability in Nearshore Waters of Maxwell Bay, Antarctica, During the 1992/1993 Austral Summer. *Polar. Biol.* 17, 123–130. doi: 10.1007/s003000050114

Ahn, I.-Y., Moon, H.-W., Jeon, M. and Kang, S.-H. (2016). First Record of Massive Blooming of Benthic Diatoms and Their Association With Megabenthic Filter Feeders on the Shallow Seafloor of an Antarctic Fjord: Does Glacier Melting Fuel the Bloom? *Ocean. Sci. J.* 51, 273–279. doi: 10.1007/s12601-016-0023-y

Annett, A. L., Skiba, M., Henley, S. F., Venables, H. J., Meredith, M. P., Statham, P. J., et al. (2015). Comparative Roles of Upwelling and Glacial Iron Sources in Ryder Bay, Coastal Western Antarctic Peninsula. *Mar. Chem.* 176, 21–33. doi: 10.1016/j.marchem.2015.06.017

Arrigo, K. R., van Dijken, G. L., Alderkamp, A.-C., Erickson, Z. K., Lewis, K. M., Lowry, K. E., et al. (2017). Early Spring Phytoplankton Dynamics in the Western Antarctic Peninsula. *J. Geophys. Res. Oceans.* 122, 9350–9369. doi: 10.1002/2017JC013281

Arrigo, K. R., van Dijken, G. L. and Bushinsky, S. (2008). Primary Production in the Southern Ocean 1997-2006. *J. Geophys. Res. Oceans.* 113, C8. doi: 10.1029/2007JC004551

Atkinson, A., Siegel, V., Pakhomov, E. and Rothery, P. (2004). Long-Term Decline in Krill Stock and Increase in Salps Within the Southern Ocean. *Nature* 432, 100–103. doi: 10.1038/nature02996

Bae, H., Ahn, I.-Y., Park, J., Song, S. J., Noh, J., Kim, H., et al. (2021). Shift in Polar Benthic Community Structure in a Fast Retreating Glacial Area of Marian Cove, West Antarctica. *Sci. Rep.* 11, 241. doi: 10.1038/s41598-020-80636-z

Biggs, T. E. G., Alvarez-Fernandez, S., Evans, C., Mojica, K. D. A., Rozema, P. D., Venables, H. J., et al. (2019). Antarctic Phytoplankton Community Composition and Size Structure: Importance of Ice Type and Temperature as Regulatory Factors. *Polar. Biol.* 42, 1997–2015. doi: 10.1007/s00300-019-02576-3

Bode, A., Castro, C. G., Doval, M. D. and Varela, M. (2002). New and Regenerated Production and Ammonium Regeneration in the Western Bransfield Strait Region (Antarctica) During Phytoplankton Bloom Conditions in Summer. . *Deep. Sea. Res. Part II* 49, 787–804. doi: 10.1016/S0967-0645(01)00124-2

Bown, J., Laan, P., Ossebaar, S., Bakker, K., Rozema, P. and de Baar, H. J. W. (2017). Bioactive Trace Metal Time Series During Austral Summer in Ryder Bay, Western Antarctic Peninsula. *Deep. Sea. Res. Part II* 139, 103–119. doi: 10.1016/j.dsr2.2016.07.004

Brandini, F. and Rebello, J. (1994). Wind Field Effect on Hydrography and Chlorophyll Dynamics in the Coastal Pelagial of Admiralty Bay, King George Island, Antarctica. *Antarct. Sci.* 6 (4), 433–442. doi: 10.1017/S0954102094000672

Bronk, D. A., See, J. H., Bradley, P. and Killberg, L. (2007). DON as a Source of Bioavailable Nitrogen for Phytoplankton. *Biogeosciences* 4, 283–296. doi: 10.5194/bg-4-283-2007

Clarke, A., Meredith, M. P., Wallace, M. I., Brandon, M. A. and Thomas, D. N. (2008). Seasonal and Interannual Variability in Temperature, Chlorophyll and Macronutrients in Northern Marguerite Bay, Antarctica. *Deep. Sea. Res. Part II* 55 (18-19), 1988–2006. doi: 10.1016/j.dsr2.2008.04.035

Cochlan, W. P. and Bronk, D. A. (2001). Nitrogen Uptake Kinetics in the Ross Sea, Antarctica. *Deep. Sea. Res. Part II* 48, 4127–4153. doi: 10.1016/S0967-0645(01)00083-2

Cook, A. J., Fox, A. J., Vaughan, D. G. and Ferrigno, J. G. (2005). Retreating Glacier Fronts on the Antarctic Peninsula Over the Past Half-Century. *Science* 308, 541–544. doi: 10.1126/science.1104235

Cook, A. J., Holland, P. R., Meredith, M. P., Murray, T., Luckman, A. and Vaughan, D. G. (2016). Ocean Forcing of Glacier Retreat in the Western Antarctic Peninsula. *Science* 353, 283–286. doi: 10.1126/science.aae0017

Corner, E. D. S. and Davies, A. G. (1971). Plankton as a Factor in the Nitrogen and Phosphorus Cycle in the Sea. *Adv. Biol.* 9, 101–204. doi: 10.1016/S0065-2881(08)60342-9

Deppeler, S. L. and Davidson, A. T. (2017). Southern Ocean Phytoplankton in a Changing Climate. *Front. Mar. Sci.* 4. doi: 10.3389/fmars.2017.00040

Dortch, Q. (1990). The Interaction Between Ammonium and Nitrate Uptake in Phytoplankton. Mar. *Ecol. Prog. Ser.* 61, 183–201. doi: 10.3354/meps061183

Ducklow, H. W., Clarke, A., Dickhut, R., Doney, S. C., Geisz, H., Kuan, H., et al. (2012a). The Marine System of the Western Antarctic Peninsula. *Antarct. Ecosyst. Extrem. Environ. Change World*, 121–159. doi: 10.1002/9781444347241.ch5

Ducklow, H. W., Schofield, O., Vernet, M., Stammerjohn, S. and Erickson, M. (2012b). Multiscale Control of Bacterial Production by Phytoplankton Dynamics and Sea Ice Along the Western Antarctic Peninsula: A Regional and Decadal Investigation. *J. Mar. Syst.* 98-99, 26–39. doi: 10.1016/j.jmarsys.2012.03.003

Dugdale, R. C. and Goering, J. J. (1967). Uptake of New and Regenerated Forms of Nitrogen in Primary Productivity. *Limnol. Oceanogr.* 12, 196–206. doi: 10.4319/lo.1967.12.2.0196

Dugdale, R. C., Wilkerson, F. P., Parker, A. E., Marchia, A. and Taberski, K. (2012). River Flow and Ammonium Discharge Determine Spring Phytoplankton Blooms in an Urbanized Estuary. *Estuar. Coast. Shelf. Sci.* 115, 187–199. doi: 10.1016/j.ecss.2012.08.025

Eppley, R. W. and Peterson, B. J. (1979). Particulate Organic Matter Flux and Planktonic New Production in the Deep Ocean. *Nature* 28, 677–680. doi: 10.1038/282677a0

Fernandes, L. F. and Procopiak, L. K. (2003). Observations on Valve Structures of *Navicula Directa* (Wm. Smith) Ralfs *in* Pritchard and *Navicula Glaciei* V. Heurck From Rocky Substrates in Antarctic Peninsula. *Hoehnea* 30 (1), 1–10.

Fiala, M., Kopczynsk, E. E., Jeandel, C., Oriola, L. and Vetion, G. (1998). Seasonal and Interannual Variability of Size-Fractionated Phytoplankton Biomass and Community Structure at Station Kerfix, Off the Kerguelen Islands, Antarctica. *J. Plankton. Res.* 20, 1341–1356. doi: 10.1093/plankt/20.7.1341

Frölicher, T. L., Sarmiento, J. L., Paynter, D. J., Dunne, J. P., Krasting, J. P. and Winton, M. (2015). Dominance of the Southern Ocean in Anthropogenic Carbon and Heat Uptake in CMIP5 Models. *J. Climate* 28 (2), 862–886. doi: 10.1175/JCLI-D-14-00117.1

Garibotti, I. A., Vernet, M., Ferrario, M. E., Smith, R. C., Ross, R. M. and Quetin, L. B. (2003). Phytoplankton Spatial Distribution Patterns Along the Western Antarctic Peninsula (Southern Ocean). *Mar. Ecol. Prog. Ser.* 261, 21–39. doi: 10.3354/meps261021

Glibert, P. M., Wilkerson, F. P., Dugdale, R. C., Raven, J. A., Dupont, C. L., Leavitt, P. R., et al. (2016). Pluses and Minuses of Ammonium and Nitrate Uptake and Assimilation by Phytoplankton and Implications for Productivity and Community Composition, With Emphasis on Nitrogen-Enriched Conditions. *Limnol. Oceanogr.* 61 (1), 165–197. doi: 10.1002/lno.10203

Goldman, J. A. A., Kranz, S. A., Young, J. N., Tortell, P. D., Stanley, R. H. R., Bender, M. L., et al. (2014). Gross and Net Production During the Spring Bloom Along the Western Antarctic Peninsula. *New Phytol.* 205 (1), 182–191. doi: 10.1111/nph.13125

Gutt, J., Isla, E., Xavier, J. C., Adams, B. J., Ahn, I.-Y., Cheng, C.-H. C., et al. (2021). Antarctic Ecosystems in Transition – Life Between Stresses and Opportunities. *Biol. Rev.* 96, 798–821. doi: 10.1111/brv.12679

Ha, S.-Y., Ahn, I.-Y., Moon, H.-W., Choi, B. and Shin, K.-H. (2019). Tight Trophic Association Between Benthic Diatom Blooms and Shallow-Water Megabenthic Communities in a Rapidly Deglaciated Antarctic Fjord. *Estuar. Coast. Shelf. Sci.* 218, 258–267. doi: 10.1016/j.ecss.2018.12.020

Hama, T., Miyazaki, T., Ogawa, Y., Iwakuma, T. and Takahashi, M. (1983). Measurement of Photosynthetic Production of a Marine Phytoplankton Population Using a Stable $^{13}C$ Isotope. *Mar. Biol.* 73, 31–36. doi: 10.1007/BF00396282

Höfer, J., Giesecke, R., Hopwood, M. J., Carrera, V., Alarcón, E. and González, H. E. (2019). The Role of Water Column Stability and Wind Mixing in the Production/Export Dynamics of Two Bays in the Western Antarctic Peninsula. *Prog. Oceanogr.* 174, 105–116. doi: 10.1016/j.pocean.2019.01.005

Jeon, M., Iriarte, J. L., Yang, E. J., Kang, S.-H., Lee, Y., Joo, H. M., et al. (2021). Phytoplankton Succession During a Massive Coastal Diatom Bloom at Marian Cove, King George Island, Antarctica. *Polar. Biol.* 44, 1993–2010. doi: 10.1007/s00300-021-02933-1

K1öser, H., Ferreyra, G., Schloss, I., Mercuri, G., Laturnus, F. and Curtosi, A. (1994). Hydrography of Potter Cove, a Small Fjord-Like Inlet on King George Island (South Shetlands). *Estuar. Coast. Shelf. Sci.* 38, 523–537. doi: 10.1006/ecss.1994.1036

Kanda, J., Ziemann, D. A., Conquest, L. D. and Bienfang, P. K. (1990). Nitrate and Ammonium Uptake by Phytoplankton Populations During the Spring Bloom in Auke Bay, Alaska. *Estuar. Coast. Shelf. Sci.* 30, 509–524. doi: 10.1016/0272-7714(90)90070-8

Kang, S.-H., Kang, J.-S., Chung, K.-H., Lee, M.-Y., Lee, B.-Y., Chung, H., et al. (1997). Seasonal Variation of Nearshore Antarctic Microalgae and Environmental Factors in Marian Cove, King George Island, 1996. *J. Polar. Res.* 8, 9–27.

Kang, J.-S., Kang, S.-H. and Lee, J. H. (1999). Cryophilic Diatoms *Navicula Glaciei* and *N. Perminuta* in Antarctic Coastal Environment. I. Morphology and Ecology. *Algae* 14 (3), 169–179.

Kang, J.-S., Kang, S.-H., Lee, J. H. and Lee, S. (2002). Seasonal Variation of Microalgal Assemblages at a Fixed Station in King George Island, Antarctic. *Mar. Ecol. Prog. Ser.* 229, 19–32. doi: 10.3354/meps229019

Kim, B. K., Jeon, M., Joo, H. M., Kim, T.-W., Park, S.-J., Park, J., et al. (2021). Impact of Freshwater Discharge on the Carbon Uptake Rate of Phytoplankton During Summer (January–February 2019) in Marian Cove, King George Island, Antarctica. *Front. Mar. Sci.* 8. doi: 10.3389/fmars.2021.725173

Kim, I., Kim, G. and Choy, E. J. (2015). The Significant Inputs of Trace Elements and Rare Earth Elements From Melting Glaciers in Antarctic Coastal Waters. *Polar. Res.* 34, 24289. doi: 10.3402/polar.v34.24289

Kim, S., Kim, J.-H., Lim, J.-H., Jeong, J.-H., Heo, J.-M. and Kim, I.-N. (2020). Distribution and Control of Bacterial Community Composition in Marian Cove Surface Waters, King George Island, Antarctica During the Summer of 2018. *Microorganisms* 8, 1115. doi: 10.3390/microorganisms8081115

Kohut, J. T., Winsor, P., Statscewich, H., Oliver, M. J., Fredj, E., Couto, N., (2018). Variability in Summer Surface Residence Time Within a West Antarctic Peninsula Biological Hotspot. *Phil. Trans. R. Soc* A376, 20170165. doi: 10.1098/rsta.2017.0165

Koike, I., Holm-Hansen, O. and Biggs, D. C. (1986). Inorganic Nitrogen Metabolism by Antarctic Phytoplankton With Special Reference to Ammonium Cycling. *Mar. Ecol. Prog. Ser.* 30, 105–116. doi: 10.3354/meps030105

Kristiansen, S., Farbrot, T. and Wheeler, P. A. (1994). Nitrogen Cycling in the Barents Sea—seasonal Dynamics of New and Regenerated Production in the Marginal Ice Zone. *Limnol. Oceanogr.* 39, 1630–1642. doi: 10.4319/lo.1994.39.7.1630

L'Helguen, S., Maguer, J.-F. and Caradec, J. (2008). Inhibition Kinetics of Nitrate Uptake by Ammonium in Size-Fractionated Oceanic Phytoplankton Communities: Implications for New Production and F-Ratio Estimates. *J. Plankton. Res.* 10, 1179–1188. doi: 10.1093/plankt/fbn072

Lee, J., Jin, Y. K., Hong, J. K., Yoo, H. J. and Shon, H. (2008). Simulation of a Tidewater Glacier Evolution in Marian Cove, King George Island, Antarctica. *Geosci. J.* 12, 33–39. doi: 10.1007/s12303-008-0005-x

Lee, S. H., Joo, H. M., Joo, H., Kim, B. K., Song, H. J., Jeon, M., et al. (2015). Large Contribution of Small Phytoplankton at Marian Cove, King George Island, Antarctica, Based on Long-Term Monitoring From 1996 to 2008. *Polar. Biol.* 38, 207–220. doi: 10.1007/s00300-014-1579-6

Llanillo, P. J., Aiken, C. M., Cordero, R. R., Damiani, A., Sepúlveda, E. and Fernández-Gómez, B. (2019). Oceanographic Variability Induced by Tides, the Intraseasonal Cycle and Warm Subsurface Water Intrusions in Maxwell Bay, King George Island (West-Antarctica). *Sci. Rep.* 9, 18571. doi: 10.1038/s41598-019-54875-8

Marañón, E., Cermeño, P., Latasa, M. and Tadonléké, R. D. (2012). Temperature, Resources, and Phytoplankton Size Structure in the Ocean. *Limnol. Oceanogr.* 57 (5), 1266–1278. doi: 10.4319/lo.2012.57.5.1266

Martinson, D. G., Stammerjohn, S. E., Iannuzzi, R. A., Smith, R. C. and Vernet, M. (2008). Western Antarctic Peninsula Physical Oceanography and Spatio-Temporal Variability. *Deep. Sea. Res. Part II* 55, 1964–1987. doi: 10.1016/j.dsr2.2008.04.038

Mendes, C. R. B., de Souza, M. S., Garcia, V. M. T., Leal, M. C., Brotas, V. and Garcia, C. A. E. (2012). Dynamics of Phytoplankton Communities During Late Summer Around the Tip of the Antarctic Peninsula. *Deep. Sea. Res. Part I* 65, 1–14. doi: 10.1016/j.dsr.2012.03.002

Moline, M. A., Claustre, H., Frazer, T. K., Schofield, O. and Vernet, M. (2004). Alteration of the Food Web Along the Antarctic Peninsula in Response to a Regional Warming Trend. *Glob. Change Biol.* 10, 1973–1980. doi: 10.1111/j.1365-2486.2004.00825.x

Montes-Hugo, M., Doney, S. C., Ducklow, H. W., Fraser, W., Martinson, D., Stammerjohn, S. E., et al. (2009). Recent Changes in Phytoplankton Communities Associated With Rapid Regional Climate Change Along the Western Antarctic Peninsula. *Science* 323, 1470–1473. doi: 10.1126/science.1164533

Montes-Hugo, M. A., Vernet, M., Smith, R. and Carder, K. (2008). Phytoplankton Size-Structure on the Western Shelf of the Antarctic Peninsula: A Remote-Sensing Approach. *Int. J. Remote Sens.* 29 (3), 801–829. doi: 10.1080/01431160701297615

Moon, H.-W., Wan Hussin, W. M. R., Kim, H.-C. and Ahn, I.-Y. (2015). The Impacts of Climate Change on Antarctic Nearshore Mega-Epifaunal Benthic Assemblages in a Glacial Fjord on King George Island: Responses and Implications. *Ecol. Indic.* 57, 280–292. doi: 10.1016/j.ecolind.2015.04.031

Mosseri, J., Quéguiner, B., Armand, L. K. and Cornet, V. (2008). Impact of Iron on Silicon Utilization by Diatoms in the Southern Ocean: A Case Study of Si/N Cycle Decoupling in a Naturally Iron-Enriched Area. *Deep. Sea. Res. Part II* 55, 801–819. doi: 10.1016/j.dsr2.2007.12.003

Mulholland, M. and Lomas, M. (2008). "Nitrogen Uptake and Assimilation, in: *Nitrogen in the Marine Environment, 2nd Edition*,". Eds. Capone, D. G., Bronk, D. A., Mulholland, M. and Carpenter, E. J. (San Diego: Elsevier), 303–385.

Nędzarek, A. (2008). Sources, Diversity and Circulation of Biogenic Compounds in Admiralty Bay, King George Island, Antarctica. *Antarct. Sci.* 20 (2), 135–145. doi: 10.1017/S0954102007000909

Nowosielski, L. (1980). Meteorological Conditions at Arctowski Station in 1978 (King George Island, South Shetland Islands). *Pol. Polar. Res.* 1 (1), 83–93.

Park, B. K., Chang, S. K., Yoon, H. I. and Chung, H. (1998). Recent Retreat of Ice Cliffs, King George Island, South Shetland Islands, Antarctic Peninsula. *Ann. Glaciol.* 27, 633–635. doi: 10.3189/1998AoG27-1-633-635

Park, S.-J., Choi, T.-J. and Kim, S.-J. (2013). Heat Flux Variations Over Sea Ice Observed at the Coastal Area of the Sejong Station, Antarctica. *Asia-Pacific. J. Atmos. Sci.* 49, 443–450. doi: 10.1007/s13143-013-0040-z

Parsons, T. R., Maita, Y. and Lalli, C. M. (1984). *A Manual of Chemical and Biological Methods for Seawater Analysis* (Oxford: Pergamon Press), 173.

Petrou, K., Baker, K., Nielsen, D., Hancock, A., Schulz, K. and Davidson, A. (2019). 'Acidification Diminishes Diatom Silica Production in the Southern Ocean'. *Nat. Clim. Change* 9, 781–786. doi: 10.1038/s41558-019-0557-y

Petrou, K., Kranz, S. A., Trimborn, S., Hassler, C. S., Ameijeiras, S. B., Sackett, O., et al. (2016). Southern Ocean Phytoplankton Physiology in a Changing Climate. *J. Plant Physiol.* 20 (203), 135–150. doi: 10.1016/j.jplph.2016.05.004

Plum, C., Hillebrand, H. and Moorthi, S. (2020). Krill vs Salps: Dominance Shift From Krill to Salps is Associated With Higher Dissolved N:P Ratios. *Nature* 10, 5911. doi: 10.1038/s41598-020-62829-8

Prézelin, B. B., Hofmann, E. E., Mengelt, C. and Klinck, J. M. (2000). The Linkage Between Upper Circumpolar Deep Water (UCDW) and Phytoplankton Assemblages on the West Antarctic Peninsula Continental Shelf. *J. Mar. Res.* 58, 165–202. doi: 10.1357/002224000321511133

Pruszak, Z. (1980). Current Circulation in the Water of Adrniralty Bay (Region of Arctowski Station on King George Island). *Pol. Polar. Res.* 1, 55–74.

Rozema, P. D., Venables, H. J., van de Poll, W. H., Clarke, A., Meredith, M. P. and Buma, A. G. J. (2017). Interannual Variability in Phytoplankton Biomass and Species Composition in Northern Marguerite Bay (West Antarctic Peninsula) is Governed by Both Winter Sea Ice Cover and Summer Stratification. *Limnol. Oceanogr.* 62, 235–252. doi: 10.1002/lno.10391

Rückamp, M., Braun, M., Suckro, S. and Blindow, N. (2011). Observed Glacial Changes on the King George Island Ice Cap, Antarctica, in the Last Decade. *Glob. Planet. Change* 79, 99–109. doi: 10.1016/j.gloplacha.2011.06.009

Saba, G. K., Fraser, W. R., Saba, V. S., Iannuzzi, R. A., Coleman, K. E., Doney, S. C., et al. (2014). Winter and Spring Controls on the Summer Food Web of the Coastal West Antarctic Peninsula. *Nat. Commun.* 5, 4318. doi: 10.1038/ncomms5318

Schloss, I. R., Ferreyra, G. A. and Ruiz-Pino, D. (2002). Phytoplankton Biomass in Antarctic Shelf Zones: A Conceptual Model Based on Potter Cove, King George Island. *J. Mar. Syst.* 36, 129–143. doi: 10.1016/S0924-7963(02)00183-5

Schloss, I. R., Wasilowska, A., Dumont, D., Almandoz, G. O., Hernando, M. P., Michaud-Tremblay, C.-A., et al. (2014). On the Phytoplankton Bloom in Coastal Waters of Southern King George Island (Antarctica) in January 2010: An Exceptional Feature? *Limnol. Oceanogr.* 59, 195–210. doi: 10.4319/lo.2014.59.1.0195

Schofield, O., Saba, G., Coleman, K., Carvalho, F., Couto, N., Ducklow, H., et al. (2017). Decadal Variability in Coastal Phytoplankton Community Composition in a Changing West Antarctic Peninsula. *Deep. Sea. Res. Part I* 124, 42–54. doi: 10.1016/j.dsr.2017.04.014

Stammerjohn, S. E., Martinson, D. G., Smith, R. C., Yuan, X. and Rind, D. (2008). Trends in Antarctic Annual Sea Ice Retreat and Advance and Their Relation to El Niño–Southern Oscillation and Southern Annular Mode Variability. *J. Geophys. Res. Oceans.* 113, C3. doi: 10.1029/2007JC004269J

Tupas, L. M., Koike, I., Karl, D. M. and Holm-Hansen, O. (1994). Nitrogen Metabolism by Heterotrophic Bacterial Assemblages in Antarctic Coastal Waters. *Polar. Biol.* 14, 195–204. doi: 10.1007/BF00240524

Varela, M., Fernandez, E. and Serret, P. (2002). Size-Fractionated Phytoplankton Biomass and Primary Production in the Gerlache and South Bransfield Straits (Antarctic Peninsula) in Austral Summer 1995–1996. *Deep. Sea. Res. Part II* 49, 749–768. doi: 10.1016/S0967-0645(01)00122-9

Varela, D. E. and Harrison, P. J. (1999). Effect of Ammonium on Nitrate Utilization by Emiliana Huxleyi, a Coccolithophore From the Oceanic Northeastern Pacific. *Mar. Ecol. Prog. Ser.* 186, 67–74. doi: 10.3354/meps186067

Verlencar, X. N., Somasunder, K. and Qasi, S. Z. (1990). Regeneration of Nutrients and Biological Productivity in Antarctic Waters. *Mar. Ecol. Prog. Ser.* 61, 41–59. doi: 10.3354/meps061041

Vernet, M., Kozlowski, W. A., Yarmey, L. R., Lowe, A. T., Ross, R. M., Quetin, L. B., et al. (2012). Primary Production Throughout Austral Fall, During a Time of Decreasing Daylength in the Western Antarctic Peninsula. *Mar. Ecol. Prog. Ser.* 452, 45–61. doi: 10.3354/meps09704

Vernet, M., Martinson, D., Iannuzzi, R., Stammerjohn, S., Kozlowski, W., Sines, K., et al. (2008). Primary Production Within the Sea-Ice Zone West of the Antarctic Peninsula: I—Sea Ice, Summer Mixed Layer, and Irradiance. *Deep. Sea. Res. Part II* 55, 2068–2085. doi: 10.1016/j.dsr2.2008.05.021

Yang, J. S. (1990). Nutrients, Chlorophyll-A and Primary Productivity in Maxwell Bay, King George Island, Antarctica. *J. Polar. Res.* 1, 11–18.

Yoo, K.-C., Lee, M. K., Yoon, H. I., Lee, Y. I. and Kang, C. Y. (2015). Hydrography of Marian Cove, King George Island, West Antarctica: Implications for Ice-Proximal Sedimentation During Summer. *Antarct. Sci.* 27, 185–196. doi: 10.1017/S095410201400056X

Yoo, K.-C., Yoon, H. I., Oh, J.-K., Kang, C. Y., Kim, Y. and Bae, S.-H. (2003). Wind- and Rain-Induced Variations of Water Column Structures and Dispersal Pattern of Suspended Particulate Matter (SPM) in Marian Cove, the South Shetland Islands, West Antarctica During the Austral Summer. *Sea.* 8, 357–368.

Yoo, K.-C., Yoon, H. I., Oh, J.-K., Kim, Y. and Kang, C. Y. (1999). Water Column Properties and Dispersal Pattern of Suspended Particulate Matter (SPM) of Marian Cove During Austral Summer, King George Island, West Antarctica. *Sea.* 4, 266–274. [Korean]

Zhang, R., Ma, Q., Chen, M., Zheng, M., Cao, J. and Qiu, Y. (2019). Nitrogen Uptake Regime Regulated by Ice Melting During Austral Summer in the Prydz Bay, Antarctica. *Acta Oceanol. Sin.* 38 (8), 1–7. doi: 10.1007/s13131-019-1434-2

**Conflict of Interest:** The authors declare that the research was conducted in the absence of any commercial or financial relationships that could be construed as a potential conflict of interest.

**Publisher's Note:** All claims expressed in this article are solely those of the authors and do not necessarily represent those of their affiliated organizations, or those of the publisher, the editors and the reviewers. Any product that may be evaluated in this article, or claim that may be made by its manufacturer, is not guaranteed or endorsed by the publisher.

frontiers | Frontiers in Marine Science

TYPE Original Research
PUBLISHED 19 August 2022
DOI 10.3389/fmars.2022.930690



OPEN ACCESS

EDITED BY
Patrick J. Neale,
Smithsonian Environmental Research Center (SI), United States

REVIEWED BY
Sarat Chandra Tripathy,
National Centre for Polar and Ocean Research (NCPOR), India
Willem Hendrik Van De Poll,
University of Groningen, Netherlands

*CORRESPONDENCE
Jae Joong Kang
jaejung@pusan.ac.kr
Sang Heon Lee
sanglee@pusan.ac.kr

SPECIALTY SECTION
This article was submitted to Aquatic Microbiology, a section of the journal Frontiers in Marine Science

RECEIVED 28 April 2022
ACCEPTED 25 July 2022
PUBLISHED 19 August 2022

CITATION
Lee CH, Kang JJ, Min J-O, Bae H, Kim Y, Park S, Kim J, Kim D and Lee SH (2022) Physiological characteristics of phytoplankton in response to different light environments in the Philippine Sea, Northwestern Pacific Ocean. *Front. Mar. Sci.* 9:930690. doi: 10.3389/fmars.2022.930690



# Physiological characteristics of phytoplankton in response to different light environments in the Philippine Sea, Northwestern Pacific Ocean

Chang Hwa Lee[1], Jae Joong Kang[2,3]*, Jun-Oh Min[1], Hyeonji Bae[2], Yejin Kim[2], Sanghoon Park[2], Joonmin Kim[2], Dongseon Kim[4] and Sang Heon Lee[2]*

[1]Department of Marine Sciences and Convergent Technology, Hanyang University, Ansan, South Korea, [2]Department of Oceanography, Pusan National University, Busan, South Korea, [3]Oceanic Climate & Ecology Research Division, National Institute of Fisheries Science, Busan, South Korea, [4]Marine Environmental Research Center, Korea Institute of Ocean Science and Technology, Busan, South Korea

The physiological status of phytoplankton, used to determine the quantity and quality of basic food sources in marine ecosystems, can change rapidly due to ambient environmental conditions (e.g., light, temperature, and nutrients). To understand the physiological characteristics of phytoplankton, the phytoplankton community composition, pigment concentration, primary production, and pigment production rate were estimated at 100% and 1% light depths in the Philippine Sea during the summer of 2019. The predominant phytoplankton classes at both light depths were *Prochlorococcus* and *Synechococcus* during the study period. Pigment concentrations, except for photoprotective pigment concentrations (i.e., diadinoxanthin and zeaxanthin), were significantly higher (*t*-test, $p<0.05$) at 1% light depth to increase the light-harvesting efficiency. The production rates of these pigments had a weak correlation with primary production at 100% light depth, whereas they showed a strong positive relationship at 1% light depth. Moreover, all photosynthetic pigments had a significantly faster turnover rate at 100% light depth compared with 1% light depth to obtain light energy to repair PSII subunits damaged by strong light. This suggests that the phytoplankton community, especially cyanobacteria (*Prochlorococcus* and *Synechococcus*), could use light energy absorbed by newly produced photosynthetic pigments for repairing photoinhibition-damaged PSII as well as for production activity. A further study on photosynthetic pigments responding to light conditions must be conducted for a better understanding of the physiological conditions of phytoplankton.

KEYWORDS

**photosynthetic pigment, physiological state, primary production, pigment production rate, light harvesting, PSII replacement, *Prochlorococcus***

## Introduction

In marine ecosystems, phytoplankton, as the primary producers, play a key role in supporting upper trophic organisms by providing basic food sources through their photosynthesis. Phytoplankton respond sensitively to ambient environmental conditions, causing variations in their physiological characteristics that determine the quality and quantity of food materials available for upper trophic organisms (Kang et al., 2017; Lee et al., 2020). Among various environmental factors, light, essential for photosynthesis, is one of the important factors that control the physiological status of phytoplankton. Phytoplankton pigments absorb light energy for their photosynthesis, and these pigments perform another physiological function called "photoprotection," protecting them from strong light and ultraviolet radiation (Ting et al., 2002; Eisner et al., 2003; Descy et al., 2009; Kirk, 2011; Croce and Van Amerongen, 2014). Generally, phytoplankton produce photoprotective pigments to protect their cells during photosynthesis under high light intensity, whereas they accumulate photosynthetic pigments for light-harvesting in low light conditions (Falkowski and Owens, 1980; Moore et al., 1995; Lutz et al., 2003; Roy et al., 2011). Thus, investigating variations in phytoplankton pigments under different light conditions provides useful information on the phytoplankton physiological responses that may be closely related to photosynthesis.

The Philippine Sea is located on the edge of the Northwestern Pacific Ocean and belongs to the east marginal sea of the Philippines. The Philippine Sea is an oligotrophic ocean, which is affected by a Pacific warm pool that is an oligotrophic water mass with a high sea-surface temperature (>29 °C) and low sea-surface salinity (<34.5) (Mackey et al., 1995; Messié and Radenac, 2006; Zhao et al., 2010). The predominant phytoplankton group in warm oligotrophic oceans is mostly pico-cell-sized, less than 2 μm, and mainly comprises *Prochlorococcus*, *Synechococcus*, and picoeukaryotes (Zhao et al., 2010). These small phytoplankton groups have distinct vertical distributions within the euphotic layer (Partensky et al., 1996; Hickman et al., 2009; Hickman et al., 2010; Zhao et al., 2010). *Synechococcus* mainly inhabits near-surface waters, whereas *Prochlorococcus* and picoeukaryotes are observed throughout the euphotic layer, with maximal biomass near the subsurface (Partensky et al., 1996; Hickman et al., 2009; Hickman et al., 2010; Zhao et al., 2010).

In oligotrophic oceans, including the Philippine Sea, light may be an important factor in determining the vertical distribution of phytoplankton, including *Prochlorococcus* and *Synechococcus*, along with the light gradient (Claustre and Marty, 1995; Partensky et al., 1999; Ting et al., 2002; Agustí, 2004). To investigate the influence of light on phytoplankton vertical distributions, the relationships between light gradients and phytoplankton community structures have been examined using various models and field observations (Sathyendranath and Platt, 2007; Hickman et al., 2009; Hickman et al., 2010; Luimstra et al., 2020). According to these previous studies, the photosynthetic pigment composition contributes to determining the phytoplankton community compositions in different light environments (Sathyendranath and Platt, 2007; Hickman et al., 2009; Hickman et al., 2010; Luimstra et al., 2020). Additionally, Ting et al. (2002) described how *Prochlorococcus* is particularly efficient in absorbing enriched blue light at depth compared with *Synechococcus*, and this light absorption ability gives *Prochlorococcus* a competitive advantage under low light conditions. Although nutrients are also an important factor in the survival and competition of phytoplankton, Yun et al. (2020) observed a weak impact of nutrient supplies in mesoscale eddies on phytoplankton community composition in the Philippine Sea. This light adaptation in photosynthetic pigments determines the competitive advantages of each phytoplankton group, and it may contribute to the phytoplankton community structure at different depths in oligotrophic oceans. While our understanding of the relationship between photosynthetic pigments and the community structure of phytoplankton is improving, the correlation between these pigments and photosynthetic activity depending on light conditions remains unclear. However, understanding this correlation is essential in the context of projected warming oceans that would possess significantly stratified water conditions, like the Philippine Sea. In this context, light conditions would be the most important environmental factor controlling the physiological properties of phytoplankton in warm oceans. Therefore, our research question is how the variation in light conditions affects the photosynthetic activity and photophysiological characteristics of phytoplankton. We investigated the phytoplankton community composition, pigment concentration, primary production, and pigment production rate in different light environments in the Philippine Sea during the summer of 2019. The specific objectives of this study are (1) to estimate the phytoplankton community composition, pigment concentration, primary production, and pigment production rate in different light environments; and (2) to investigate the relationships between primary production and pigment production rate to discuss the light adaptation strategies and physiological states of phytoplankton.

## Materials and methods

### Seawater sampling

Our study was conducted in the Philippine Sea, in the Northwestern Pacific Ocean, during the Korean R/V "ISABU" cruise from 27 August to 16 September 2019. Seawater samples

were collected at a total of five stations (Figure 1, Table 1) using a CTD (Conductivity–Temperature–Depth) mounted rosette sampler with 12 L Niskin bottles. Seawater samples for phytoplankton pigments and pigment production rates were collected at two light depths [(100 and 1% of surface PAR (photosynthetically active radiation)]. Temperature and salinity within the euphotic layer depth, defined as the depth with 1% intensity of surface PAR, were measured using CTD at the five stations. Surface PAR for determining the two light depths was measured using a PAR sensor (LI-COR underwater 4π light sensor) connected to a CTD-mounted rosette sampler. The mixed layer depth (MLD) was defined as the depth where the temperature difference from the reference depth was more than 0.2 °C, and the reference depth was 10 m in this study (de Boyer Montégut et al., 2004).

## Phytoplankton pigment analysis

Each seawater sample (4 L) for phytoplankton pigments (hereafter, "pigments") was filtered through 47 mm GF/F filters (Whatman) under low vacuum (<20 KPa) conditions. The filters were wrapped with aluminum foil and stored at −80 °C in the dark until pretreatment. In the laboratory, the extraction of the filtered pigment samples was conducted using 4 ml of 100% acetone and 100 µl of internal standard (IS, cantaxanthin) at 4 °C overnight. To eliminate floating matter, the extracts were passed through a 0.2 µm syringe filter (Advantec, hydrophobic). Then, 300 µl of distilled water (DW) was added to the filtrates to achieve optimal resolution during pigment analysis. In this study, we analyzed eleven phytoplankton pigments: fucoxanthin (Fuco), peridinin (Peri), 19'-hexanoloxyfucoxanthin (Hex-fuco),

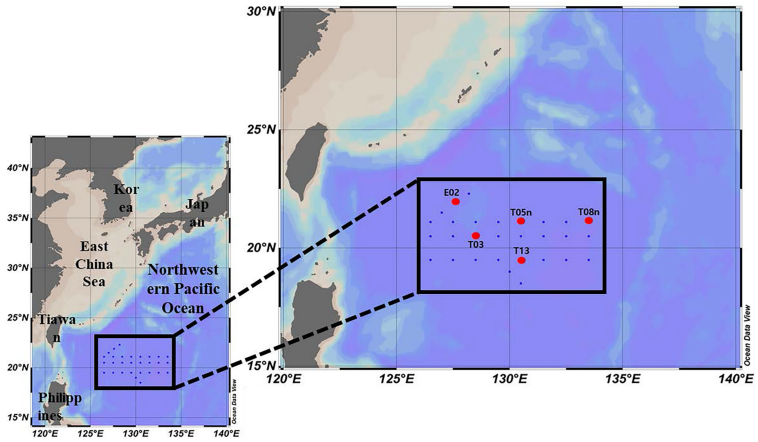


FIGURE 1
Sampling locations in the Philippine Sea, Northwestern Pacific Ocean (red circle: production station).

TABLE 1 Station information in the study area (Philippine Sea) during 2019.

| Station | Date (2019) | Location | | Light depth (%) | Water depth (m) | Temperature (°C) | Salinity | MLD (m) | SCM (m) |
|---|---|---|---|---|---|---|---|---|---|
| | | Latitude | Longitude | | | | | | |
| **E02** | 30 August | 21°54.08N | 127°36.03E | 100 | 0 | 29.85 | 34.51 | 23 | 130 |
| | | | | 1 | 130 | 23.89 | 34.99 | | |
| **T05n** | 01 September | 21°5.97N | 130°29.86E | 100 | 0 | 29.33 | 34.47 | 34 | 120 |
| | | | | 1 | 120 | 21.15 | 34.9 | | |
| **T08n** | 02 September | 21°06.03N | 133°29.91E | 100 | 0 | 29.37 | 34.46 | 45 | 140 |
| | | | | 1 | 65 | 26.60 | 34.94 | | |
| **T13** | 04 September | 19°30.02N | 130°30.02E | 100 | 0 | 28.97 | 34.28 | 44 | 100 |
| | | | | 1 | 100 | 24.07 | 34.98 | | |
| **T03** | 05 September | 20°30.00N | 128°30.00E | 100 | 0 | 29.00 | 34.47 | 53 | 125 |
| | | | | 1 | 56 | 25.77 | 34.73 | | |

19'-butanoyloxyfucoxanthin (But-fuco), chlorophyll *b* (Chl *b*), monovinyl chlorophyll *a* (MVChl *a*), divinyl chlorophyll *a* (DVChl *a*), diadinoxanthin (Diadino), violaxanthin (Viola), prasinoxanthin (Pras), and zeaxanthin (Zea). The concentrations of all pigments were measured using a high-performance liquid chromatography (HPLC) system (Agilent Infinite 1260, Santa Clara, CA, USA), following the method of Zapata et al. (2000). The biomarker pigments were identified by comparing their retention times with those of eleven standards (DHI Water and Environment, Hørsholm, Denmark).

## Phytoplankton community structure

The relative chlorophyll *a* (Chl *a*) biomass of eight phytoplankton communities (diatoms, dinoflagellates, prymnesiophytes, chrysophytes, chlorophytes, prasinophytes, *Synechococcus*, and *Prochlorococcus*) was estimated using the chemotaxonomy program CHEMTAX, described by Mackey et al. (1996). To separate the eight phytoplankton communities using CHEMTAX, we used initial pigment ratios (the ratios of pigment to MVChl *a* or DVChl *a*) in line with that of Miki et al. (2008), who conducted a study on phytoplankton dynamics in the Northwestern Pacific Ocean (Table S2). CHEMTAX analyses were performed separately for samples from 100% and 1% light depths.

## Primary production of phytoplankton

To measure the primary production of phytoplankton, we used a carbon stable isotope ($^{13}C$) tracer technique (Hama et al., 1983). The seawater samples collected at each depth were transferred to 1 L polycarbonate bottles covered with a screen filter (LEE filters; Garneau et al., 2007) to match each light condition. Then, labeled carbon ($NaH^{13}CO_3$, 99%, Cambridge Isotope Laboratories, Inc.) substrate, which corresponded to approximately 10% of the ambient dissolved inorganic carbon concentration (DIC), was added. After inoculating the substrate, one bottle collected from each depth was incubated in an acrylic incubator at a constant temperature maintained by continuously circulating underway seawater on deck under natural light for 4 to 5 h before noon. The incubated water samples were passed through pre-combusted 25 mm GF/F filters (Whatman) and stored at −20 °C until further pretreatment. In the laboratory, the filter samples for primary production were treated with HCl (36.5%–38.0%), fuming overnight to remove inorganic carbon (Hama et al., 1983). The particulate organic carbon (POC) concentrations and isotope abundances of the carbon were measured using the mass spectrometer (Finnigan Delta+XL) at the Stable Isotope Laboratory of the University of Alaska, Fairbanks, USA. The hourly primary production of phytoplankton was determined using an equation reported by Hama et al. (1983).

## Pigment production rate

Studies on the pigment labeling method using $^{14}C$ were conducted more than 20 years ago (Redalje and Laws, 1981; Goericke and Welschmeyer, 1993a; Goericke and Welschmeyer, 1993b), the main purpose being to estimate the phytoplankton growth rate. Goericke and Welschmeyer (1993a; 1993b) emphasized that labeling experiments should last 24 h to resolve the imbalance between the rates of pigment synthesis and cell growth of phytoplankton under a natural photocycle; whereas, Redalje and Laws (1981) determined that a balance between the specific activity of chl *a* carbon and total phytoplankton carbon appeared in incubations lasting 6 to 12 h based on data from laboratory cultures. However, the main purpose of using the pigment labeling method in this study was not to estimate the growth rate of phytoplankton but to understand the *in situ* photophysiological characteristics of phytoplankton. According to previous studies, phytoplankton can adjust their cellular pigment pool within a few hours in response to fluctuations in the light environment (Hitchcock 1977; Redalje and Laws, 1981; Roy et al., 2011). The $^{13}C$-labeling method is widely used to estimate various physiological aspects of *in situ* phytoplankton (Hama et al., 1983; Ha et al., 2014; Min et al., 2019; Kang et al., 2021). Thus, a modified labeling method using $^{13}C$, with a relatively short incubation time (4–5 h), was adopted in this study.

For onboard incubation (4–5 h), labeled carbon ($NaH^{13}CO_3$) substrate was added to each seawater sample in 9 L polycarbonate bottles. Onboard incubation was performed using an acrylic incubator under natural light. After incubation, the samples were filtered through pre-combusted 47 mm GF/F filters (Whatman) and kept at −80°C in the dark until further pretreatment.

In the home laboratory, to extract the biomarker pigments, 100% acetone (4 ml) and IS (100 µl), as used for HPLC pigment analysis (section *Phytoplankton pigment analysis*), were added to the filter samples and stored at 4 °C in the dark overnight. The extracted biomarker pigments were purified using a 0.2 µm syringe filter (Advantec-hydrophobic). To obtain a detectable carbon isotope abundance when using the mass spectrometer (Finnigan Delta+XL), the pigments were analyzed using a 500 µl injection volume. The pigments were then collected separately based on their retention times from HPLC pigment analysis (section *Phytoplankton pigment analysis*) using a fraction collector (Agilent-G1364C, Santa Clara, CA, USA) connected to the HPLC system (Agilent Infinite 1260). These fraction processes were repeated three to four times for all pigments. The fractionated pigments were dried using nitrogen gas to remove the solvent, and their abundance of carbon was

determined using the mass spectrometer (Finnigan Delta+XL) at the Stable Isotope Laboratory of the University of Alaska, Fairbanks, USA. The pigment production rate was calculated using an equation reported by Ha et al. (2014); Kang et al. (2021):

$$\Delta PPR\ (t) = CCP \times \frac{a_{is} - a_{ns}}{a_{ic} - a_{ns}} \quad (1)$$

where ΔPPR is the amount of each carbon pigment photosynthetically produced during incubation, $a_{is}$ is the percentage of $^{13}C$ atoms in each pigment compound of the incubated sample, $a_{ns}$ is the percentage of $^{13}C$ atoms in each pigment compound of the natural sample, $a_{ic}$ is the percentage of $^{13}C$ atoms in the $^{13}C$ enriched inorganic carbon, and CCP is the carbon concentration of each pigment at the end of incubation.

To determine the relationship between the light conditions and the production rate for each pigment, excluding pigment concentration (i.e., phytoplankton biomass), the turnover rate of each pigment was calculated thus:

$$\text{Turnover rate}(t) = \frac{(a_{is} - a_{ns})}{(a_{ic} - a_{ns})} \times \frac{1}{\text{incubation time}\ (t)}$$

## Statistical analysis

A Student's *t*-test was performed to validate significant differences in the variables of phytoplankton physiological status (phytoplankton community structure, pigment concentration, ratio of pigment to carbon biomass, primary production, and pigment production rate) between 100% and 1% light depth. A Pearson's correlation coefficient analysis was conducted to determine the relationship among the variables. These statistical analyses were carried out using SPSS 12.0 for Windows.

# Results

## Physical characteristics

For all stations, the MLD was 34–53 m (mean ± S. D. = 43.4 ± 6.9 m) (Figure 2, Table 1). The MLD at St. T05n was the lowest whereas it was deepest at St. T03. The euphotic layer depth going from 100% to 1% light depth was 56–130 m (94.2 ± 32.8 m) in this study. The euphotic layer depths (<70 m) at St. T08n and St. T03 were shallower than those at other stations. The MLD was shallower than the euphotic layer depth at all stations, which equated to non-mixing of water masses between 100% and 1% light depth during the study period. The temperatures were 28.97–29.85 °C (29.31 ± 0.36 °C) at 100% light depth and 21.15–26.60 °C (24.29 ± 2.10 °C) at 1% light depth during the study period. The temperatures at 1% light depth were higher at St. T08n and St. T03 than at the other stations. In comparison with temperature, salinity did not vary over a large range. The salinity ranged from 34.28 to 34.51 at 100% light depth and 34.73 to 34.99 at 1% light depth. The average salinity (34.44 ± 0.09) at 100% light depth was slightly lower than that (34.91 ± 0.11) at 1% light depth in this study.

## Phytoplankton community structure

The phytoplankton community structure obtained from CHEMTAX analysis is shown in Figure 3. At all stations, the average contribution of *Prochlorococcus* to the total

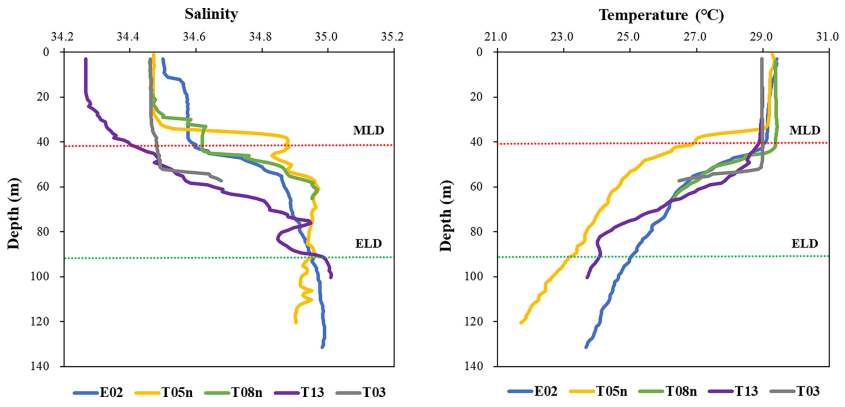


FIGURE 2
The profiles of salinity and temperature in the Philippines Sea, Northwestern Pacific Ocean. Red and green dash lines represent the average depths of mixed (MLD) and euphotic (ELD) layer, respectively.

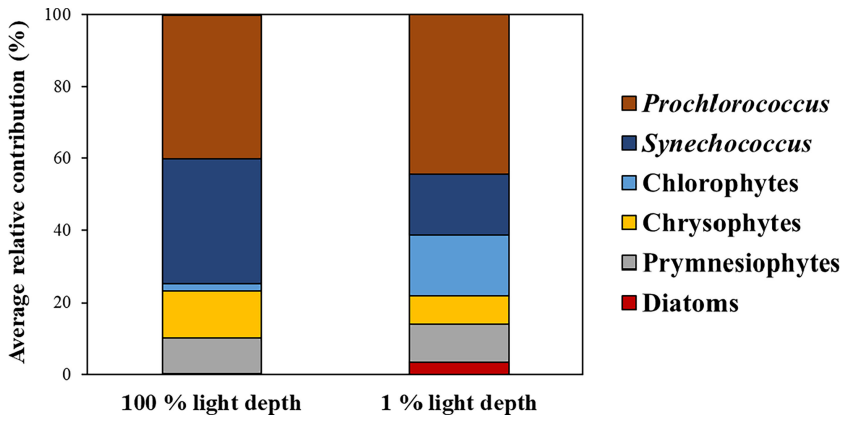


FIGURE 3
Average contributions of phytoplankton communities to total phytoplankton biomass between the two light depths.

phytoplankton biomass at both light depths was highest (42.3 ± 9.2%), followed by *Synechococcus* (25.8 ± 17.9%), and then the other groups (below 10%). *Prochlorococcus* was predominant at both light depths, with an average contribution to the total phytoplankton biomass of 40.0% (S. D. = ± 10.9%) and 44.4% (S. D. = ± 7.8%) at 100% light depth and 1% light depth, respectively (Figure 3). The contribution of *Synechococcus* was 23.2%–39.6% and 3.1%–43.9% at 100% light depth and 1% light depth, respectively. The average contribution of *Synechococcus* to the total phytoplankton biomass decreased from 100% light depth (34.5 ± 6.5%) to 1% light depth (17.1 ± 22.1%). Compared to *Synechococcus*, chlorophytes had a high average contribution (16.7 ± 15.6%) to the total phytoplankton biomass at 1% light depth compared to that (2.2 ± 2.01%) at 100% light depth. Meanwhile, the average contribution of chrysophytes was 13.1% (± 6.1%) and 7.7% (± 5.4%) at 100% light depth and 1% light depth, respectively. Other phytoplankton groups had slight differences in biomass contribution between the two light depths.

## Pigment concentration and the ratio of pigment to carbon biomass

In this study, Peri, Viola, and Pras were not detected between 100% and 1% light depth. Except for Zea and Diadino, the other pigments were significantly higher (*t*-test, $p<0.05$) at 1% light depth than at 100% light depth (Table 2). On average, the detected pigment concentrations ranged from 0.002–0.038 mg $m^{-3}$ at 100% light depth, and Zea, MVChl *a*, and DVChl *a* showed the highest concentrations among these pigments. At 1% light depth, the average concentration of these pigments was 0.003–0.121 mg $m^{-3}$, and Chl *b* had the highest concentration (0.121 ± 0.100 mg $m^{-3}$) among the pigments. Furthermore, the average concentration of Chl *b* changed significantly (*t*-test, $p<0.05$) between the two light depths (100% and 1%), the largest such change among the pigments. Similar to the case for the average pigment concentration, the average ratio of pigment to carbon biomass was significantly (*t*-test, $p<0.05$) higher at 1% light depth than at 100% light depth (Table S3). The average value of all the ratios changed more than three times between the two light depths. In particular, But-fuco and Chl *b* had the highest average ratio changes among the pigments.

## Primary production and pigment production rates

The magnitude of phytoplankton primary production varied between 100% and 1% light depth (Table 2). At 100% light depth, the primary production was 0.045–0.231 mg C $m^{-3}$ $h^{-1}$ (0.170 ± 0.074 mg C $m^{-3}$ $h^{-1}$). On the other hand, the primary production at 1% light depth was 0.002–0.071 mg C $m^{-3}$ $h^{-1}$ (0.027 ± 0.0027 mg C $m^{-3}$ $h^{-1}$), which was significantly lower (*t*-test, $p<0.05$) than that at 100% light depth. Meanwhile, the production rate of the photosynthetic pigments showed a different vertical distribution for each pigment (Figure 4). On average, the production rate of Chl *b* was 0.96–5.31 ng C $m^{-3}$ $h^{-1}$ (2.41 ± 1.72 ng C $m^{-3}$ $h^{-1}$) at 100% light depth and 0.67–29.75 ng C $m^{-3}$ $h^{-1}$ (12.67 ± 12.56 ng C $m^{-3}$ $h^{-1}$) at 1% light depth. The average production rate of DVChl *a* was 3.95 ng C $m^{-3}$ $h^{-1}$ (± 2.58 ng C $m^{-3}$ $h^{-1}$) at 100% light depth and 8.88 ng C $m^{-3}$ $h^{-1}$ (± 5.29 ng C $m^{-3}$ $h^{-1}$) at 1% light depth. The Chl *b* and DVChl *a* production rates were higher at 1% light depth than at 100% light depth, but these differences were not statistically significant (*t*-test, $p > 0.05$). Compared to these two pigments, the average production rate of MVChl *a* was slightly higher at 100% light depth than at 1% light depth

TABLE 2 Pigment concentrations, primary productions, pigment production rates, and pigment turnover rates between the 100% and 1% light depths in the Philippines Sea, Northwestern Pacific Ocean.

| Categorize | | Unit | 100% light depth | | 1% light depth | |
|---|---|---|---|---|---|---|
| | | | Avg. | Stdev. | Avg. | Stdev. |
| Pigment | Fuco* | mg $m^{-3}$ | 0.002 | 0.000 | 0.005 | 0.003 |
| | Peri | | – | – | – | – |
| | Hexfuco* | | 0.009 | 0.005 | 0.039 | 0.023 |
| | Butfuco* | | 0.002 | 0.001 | 0.026 | 0.021 |
| | Diadino | | 0.002 | 0.001 | 0.003 | 0.001 |
| | Viola | | – | – | – | – |
| | Pras | | – | – | – | – |
| | Zea | | 0.038 | 0.011 | 0.040 | 0.011 |
| | Chl *b** | | 0.009 | 0.008 | 0.121 | 0.100 |
| | MVChl *a** | | 0.031 | 0.012 | 0.098 | 0.053 |
| | DVChl *a** | | 0.025 | 0.022 | 0.082 | 0.051 |
| | TChl *a** | | 0.056 | 0.033 | 0.180 | 0.101 |
| Primary production | Carbon biomass* | mg C $m^{-3}$ | 76.7 | 16.7 | 55.9 | 7.85 |
| | Production rate** | mg C $m^{-3}$ $h^{-1}$ | 0.170 | 0.074 | 0.027 | 0.027 |
| Pigment turnover rate | Zea | $h^{-1}$ | 0.00009 | 0.00008 | 0.00003 | 0.00004 |
| | Chl *b** | | 0.00031 | 0.00014 | 0.00014 | 0.00009 |
| | MVChl *a*** | | 0.00040 | 0.00013 | 0.00010 | 0.00010 |
| | DVChl *a** | | 0.00028 | 0.00012 | 0.00013 | 0.00006 |

* and ** represent significant difference in the levels of $p<0.05$ and $p<<0.01$ between the two light depths, respectively. Fuco, fucoxanthin; Peri, peridinin: Hexfuco, 19'-hexanoyloxyfucoxanthin: Butfuco, 19'-butanoyloxyfucoxanthin; (Diadino, diadinoxanthin); Viola, violaxanthin; Pras prasinoxanthin; Zea, zeaxanthin; chlorophyll b; DVChl a, divinyl chlorophyll a; MVChl, a monovinyl chlorophyll a, Total Chl a (TChl a = MVChl a + DVChl a).

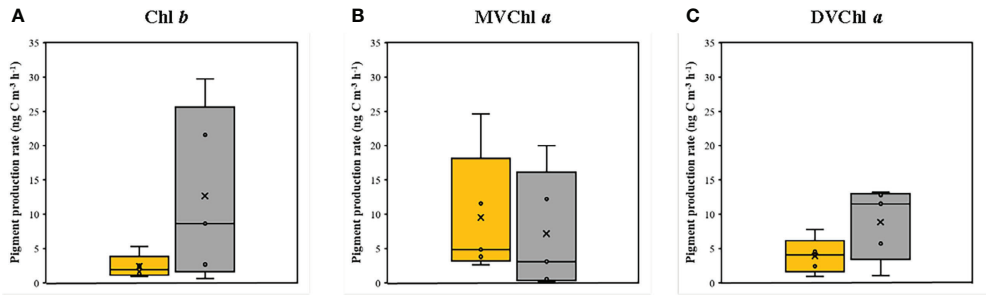


FIGURE 4
The production rates of **(A)** Chl b, **(B)** MVChl a and **(C)** DVChl a between the two light depths. Yellow and gray boxes represent 100 % and 1 % light depths, respectively. The abbreviations of pigment are shown in Table 2.

(Figure 4), with a vertical distribution similar to that of primary production. The MVChl *a* production rate was 2.69–24.66 ng C $m^{-3}$ $h^{-1}$ (9.53 ± 9.14 ng C $m^{-3}$ $h^{-1}$) and 0.13–20.02 ng C $m^{-3}$ $h^{-1}$ (7.20 ± 8.67 ng C $m^{-3}$ $h^{-1}$) at 100% light depth and 1% light depth, respectively. However, the difference in average MVChl *a* production rate between the two light depths was not significantly different (*t*-test, $p > 0.05$).

Unlike the distinct vertical distributions of each pigment production rate, the turnover rate of three photosynthetic pigments (Chl *b*, DVChl *a*, and MVChl *a*) was significantly higher at 100% light depth than at 1% light depth (Table 2). The turnover rate of Chl *b* ranged from 0.00018 to 0.00048 $h^{-1}$ (0.00031 ± 0.00014 $h^{-1}$) at 100% light depth and 0.00005 to 0.00022 $h^{-1}$ (0.00014 ± 0.00009 $h^{-1}$) at 1% light depth. In comparison, the turnover rate of MVChl *a* ranged from 0.00025 to 0.00054 $h^{-1}$ (0.00040 ± 0.00013 $h^{-1}$) at 100% light depth and 0.00000 to 0.00024 $h^{-1}$ (0.00010 ± 0.00010 $h^{-1}$) at 1% light depth. The DVChl *a* turnover rate was 0.00012–0.00024 $h^{-1}$ (0.00028 ±

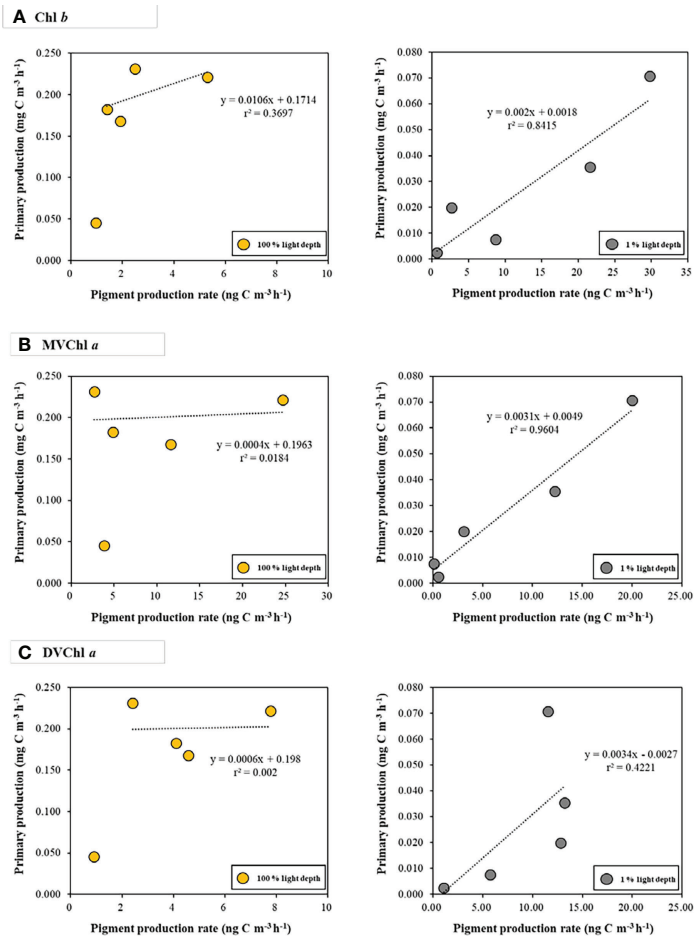


FIGURE 5
The relationships between photosynthetic pigment production rates **(A)** Chl b; **(B)** MVChl a; **(C)** DVChl a and primary production at the different light depths. Yellow and gray dots represent 100 % and 1 % light depths, respectively.

0.00012 $h^{-1}$) and 0.00007–0.00020 $h^{-1}$ (0.00013 ± 0.00006 $h^{-1}$) at 100% light depth and 1% light depth, respectively. Among these pigments, MVChl *a* had the largest difference (>4-fold) in the turnover rate between the different light depths.

The relationship between primary production and photosynthetic pigment production varied with light depth (Figure 5). At 100% light depth, the production rate of Chl *b*, MVChl *a*, and DVChl *a* had a weak correlation ($r^2$ = 0.3697, 0.0184, and 0.002 for Chl *b*, MVChl *a*, and DVChl a, respectively) with primary production. On the other hand, the production rate of these pigments had a positive correlation ($r^2$ = 0.8415, 0.9604, and 0.4221 for Chl *b*, MVChl *a*, and DVChl *a*, respectively) with primary production at 1% light depth. In particular, the Chl *b* and MVChl *a* production rates had significant relationships (Pearson correlation, $p<0.05$) with primary production compared with the DVChl *a* production rate.

# Discussion

## Vertical distribution characteristics of phytoplankton community

During the research period, strong stratification existed within the euphotic layer in the Philippine Sea, Northwestern Pacific Ocean (Figure 2). This suppressed vertical mixing between 100% and 1% light depth, causing phytoplankton at each depth to be constantly exposed to light. This affected the phytoplankton physiological characteristics (i.e., the phytoplankton community, pigment concentration, primary production, and pigment production rate). Thus, we focused on the two light depths (100% and 1% light depth) to determine the effects of different light levels on phytoplankton physiological characteristics.

For each light depth, we observed different vertical distributions of *Prochlorococcus*, *Synechococcus*, and chlorophytes. On average, *Prochlorococcus* was predominant at both light depths, whereas *Synechococcus* showed a relatively higher contribution at the surface layer compared to 1% light depth and chlorophytes showed the opposite trend to *Synechococcus* (Figure 3). These vertical distributions have also been observed in other oligotrophic regions (Claustre and Marty, 1995; Veldhuis et al., 2005; Zhao et al., 2010). Zhao et al. (2010) reported that *Prochlorococcus* and *Synechococcus* had different abundances between the two light depths in the Philippine Sea, western North Pacific. Their results showed that *Synechococcus* mainly existed at 100% light depth, whereas *Prochlorococcus* was predominant at 1% light depth. At each light depth, the change in group abundance was associated with phytoplankton adaptation ability resulting from a pigment composition response to light environments (Figure 3, Falkowski and Owens, 1980; Claustre and Marty, 1995). *Prochlorococcus* and chlorophytes have Chl *b*,which is well known for its high efficiency in light absorption, with blue light penetrating to 200 m (Table S1, Claustre and Marty, 1995; Ting et al., 2002). This pigment allows *Prochlorococcus* and chlorophytes to efficiently harvest light energy in deep water columns where blue light is enriched; thus they can adapt well to surface layers and to deep layers (Morel et al., 1993: Claustre and Marty, 1995; Ting et al., 2002). In contrast to *Prochlorococcus* and chlorophytes, *Synechococcus* has a pigment capable of absorbing green light, meaning it predominates in near-surface waters (i.e., above 30 m) (Ting et al., 2002). Additionally, *Synechococcus* has light-harvesting phycobiliproteins, such as phycocyanin and phycoerythrin, with an absorption maximum at 590–670 nm (yellow-red light) and 535–600 nm (green-yellow light), respectively (Grossman et al., 1993; Ruan et al., 2018). Hence, *Synechococcus* is more suited to 100% light depth than 1% light depth.

## Vertical distribution characteristics of primary production and pigment production

In addition to the phytoplankton community, pigment concentration and primary production also showed distinct vertical distributions between the two light depths (Table 2). Except for photoprotective pigments, the average concentration of photosynthetic pigments was significantly higher (*t*-test, $p<0.05$) at 1% light depth than at 100% light depth. In contrast, the average carbon biomass of phytoplankton was observed to be significantly higher (*t*-test, $p<0.05$) at 100% light depth than at 1% light depth. These results suggest that phytoplankton have distinct photophysiological states in different light environments. Falkowski and Owens (1980); Lutz et al. (2003), and Shibata et al. (2010) reported that phytoplankton adjust their pigment concentration depending on light conditions. Under low light conditions, phytoplankton increase their cellular photosynthetic pigment content to harvest light energy (Falkowski and Owens, 1980; Prezelin and Matlick, 1980; Richardson et al., 1983; Ramus, 1990; Falkowski and Raven, 2013), and this physiological response leads to an increase in pigment to carbon biomass ratio (Pig/C ratio) (Colijn et al., 1990; Veldhuis and Kraay, 1990; Moore et al., 1995; Lutz et al., 2003; Roy et al., 2011). Our results on Pig/C ratios are similar, depending on light conditions (Table S1). In addition, Chl *b*, DVChl *a*, and MVChl *a* were major photosynthetic pigments in the predominant phytoplankton groups (*Prochlorococcus*, *Synechococcus*, and chlorophytes) in this study; thus, the Pig/C ratios of these pigments can indicate their photophysiological states. Based on previous studies and our results, it can be inferred that the three major groups in the Philippine Sea increased their Pig/C ratios to harvest light energy under low light conditions. The average primary production was more than six times higher (*t*-test, $p<0.01$) at 100% light depth than at 1% light depth (Table 2). This large difference in primary production may be associated with environmental conditions such as light intensity and nutrients (Pabi et al., 2008; Tremblay et al., 2015; Lee et al., 2019; Zheng et al., 2021). Prior to this study, Yun et al. (2020) observed that picophytoplankton, the presence of which indicates a nutrient-deficient state, were the predominant phytoplankton groups despite the occurrence of mesoscale eddies supplying nutrients to the euphotic layer in the Philippine Sea. Our results on the phytoplankton community also indicated that picophytoplankton, containing *Prochlorococcus* and *Synechococcus*, was a major phytoplankton group in the Philippine Sea, suggesting that nutrients were limited at both light depths. Indeed, Pai and Chen (1994) did not detect significant concentrations of major nutrients (phosphate and nitrate) above the thermocline (approximately 250 m) at similar stations in the Philippine Sea. Moreover, Wong et al. (1995) reported that the Philippine Sea has characteristics of oligotrophic water, nearly devoid of nutrients at the top 200 m of the water column. Therefore, primary production between the two light depths is regulated by light intensity rather than nutrient conditions in the Philippine Sea during this research period.

Based on our results, light intensity seems to play a key role in determining the phytoplankton community, photosynthetic pigment concentration, and primary production. However, it remains unclear how phytoplankton produce their pigments for light energy absorption under different light conditions. We estimated the production rates for several major photosynthetic pigments in predominant phytoplankton groups at both light depths and investigated the relationships between pigment production rates and primary production. For each light depth, Chl *b* and DVChl *a* had high production rates at 1% light depth, whereas the MVChl *a* production rate was high at 100% light depth (Figure 4). Concerning the relationships between photosynthetic pigment production rate and primary

production, we observed positive correlations only for 1% light depth (Figure 5). The fact that, generally, the pigment concentration increases under low light conditions is well recognized as a physiological response of phytoplankton used to harvest light energy (Falkowski and Owens, 1980; Colijn et al., 1990; Veldhuis and Kraay, 1990; Moore et al., 1995; Lutz et al., 2003; Shibata et al., 2010; Roy et al., 2011; Falkowski and Raven, 2013). Additionally, Colijn et al. (1990) reported a positive linear correlation ($r^2$ = 0.81) between MVChl *a* and primary production within the euphotic layer in the German Bight. Liu X et al. (2019) observed that surface MVChl *a* concentrations had a significantly positive correlation (Spearman, r = 0.41, $p<0.01$) with integrated primary production in the East China Sea. These previous results imply that photosynthetic pigments may be involved in the production activity of phytoplankton *via* light energy absorption. In this regard, a relatively high MVChl *a* production rate at 100% light depth differs from the common physiological response of phytoplankton to light conditions. Moreover, the weak correlation between photosynthetic pigment production rate and primary production in this study suggests that phytoplankton do not utilize the light energy absorbed through photosynthetic pigments for primary production only (Figures 4, 5). During photosynthesis, under high light conditions, excess light energy absorbed by chlorophylls generates reactive oxygen species (ROS), resulting in damaged photosystem II (PSII), which is well known as photoinhibition (Liu J et al., 2019). Phytoplankton have mechanisms to protect their PSII from photoinhibition. The most important mechanism involves an increase in intracellular photoprotective pigment content (Siefermann-Harms, 1985; Roy et al., 2011; Falkowski and Raven, 2013). In general, phytoplankton exposed to high irradiance have a relatively high concentration of carotenoids, such as β-carotene and zeaxanthin, which do not transmit excitation energy to the reaction center of PSII, thus protecting the cell from excess light (Siefermann-Harms, 1985; Roy et al., 2011; Falkowski and Raven, 2013). Indeed, the concentration of zeaxanthin, the photoprotective pigment of the major phytoplankton groups (*Prochlorococcus* and *Synechococcus*), was similar between the surface layer and 1% light depth, unlike other pigments during the study period (Table 2), and the turnover rate of zeaxanthin in the surface layer (0.00009 $h^{-1}$) was higher than that at 1% irradiance (0.00003 $h^{-1}$) (Table 2). These results indicate the possibility that phytoplankton at 100% light depth may have been affected by photoinhibition during the study period. Another mechanism for photoinhibition is a replacement system that repairs the damaged PSII of phytoplankton (Figure S1, Komenda, 2000; Li et al., 2018; Liu J et al., 2019). Li et al. (2018) reviewed PSII photodamage mechanisms and showed that the turnover rate of PSII subunits, consisting of chlorophylls and proteins, increased above 0.02 $h^{-1}$ under high light conditions (Komenda, 2000; Li et al., 2018; Komenda and Sobotka, 2019; Liu J et al., 2019). Our results on the pigment turnover rate were similar to those of previous studies. During this study period, the surface phytoplankton might have been exposed to high light intensity due to the strong stratification within the euphotic layer (Figure 2). As a result, all photosynthetic pigment turnover rates were significantly higher (*t*-test, $p<0.05$) at 100% light depth than at 1% light depth. This implies that phytoplankton quickly produce the photosynthetic pigments needed to acquire additional energy for the restoration of photodamaged PSII subunits under high light intensity (Table 2). In particular, the turnover rate of surface MVChl *a* was more than four times higher compared to the 1% light depth. This large difference may result in a relatively high MVChl *a* production rate at 100% light depth (Figure 4). Therefore, phytoplankton might utilize light energy absorbed by newly produced photosynthetic pigments not only for production activity but also for PSII subunit repair under high light intensity.

The production rates of Chl *b* and MVChl *a* had strong positive correlations ($r^2$ = 0.8415 and $r^2$ = 0.9604, respectively) with primary production at 1% light depth (Figure 5). These results indicate that *Prochlorococcus* and chlorophytes produce Chl *b* and MVChl *a* for harvesting light energy under low light conditions—this is in accordance with the general physiological response of phytoplankton to light intensity (Colijn et al., 1990; Lutz et al., 2003; Shibata et al., 2010; Roy et al., 2011; Liu X et al., 2019). Unlike Chl *b* and MVChl *a*, DVChl *a* production rates did not have a significant correlation ($r^2$ = 0.4221, $p$ >0.05) with primary production, which may be because of the physiological characteristics of *Prochlorococcus* containing DVChl *a*. *Prochlorococcus* increases Chl *b* content over DVChl *a* for light absorption efficiency in low light conditions, and this photophysiological response creates a high ratio of Chl *b* to DVChl *a* (Claustre and Marty, 1995; Moore et al., 1995; Ting et al., 2002; Fujiki et al., 2013). Our CHEMTAX result also showed that *Prochlorococcus* had a high Chl *b* to DVChl *a* ratio (1.21) at 1% light depth, indicating that this group changed their pigment composition for light-harvesting under low light intensity (Table S2). In this regard, *Prochlorococcus* might have used Chl *b* as a more important photosynthetic pigment than DVChl *a* during this research period. This light-harvesting strategy could contribute to the relatively weak correlation between the DVChl *a* production rate and primary production (Figure 5).

## Summary and conclusions

In the Philippine Sea, phytoplankton had different relative abundances, pigment concentrations, and primary production between two light depths (100% and 1% light depths). This indicated that light intensity played a key role in determining phytoplankton physiological characteristics. For the different light depths, phytoplankton community composition may have been associated with the varying adaptability of

phytoplankton to various light conditions. Except for photoprotective pigments, the photosynthetic pigment concentration was significantly higher at 1% light depth than at 100% light depth. These vertical distributions represent the physiological response of phytoplankton to increase their light-harvesting efficiency. Primary production showed different vertical distributions of photosynthetic pigment concentration between the two light depths. This indicated that light intensity was an important factor in controlling primary production during this research period. In addition to the photosynthetic pigment concentration and the primary production, pigment production rates also had different vertical distribution with light depths. The Chl *b* and DVChl *a* production rates were relatively high at 1% light depth, whereas the MVChl *a* production rate was slightly high at 100% light depth. In addition, we observed significantly fast turnover rates for Chl *b*, MVChl *a*, and DVChl *a* at 100% light depth. These results suggest that phytoplankton would have utilized the light energy absorbed by newly produced photosynthetic pigments not only for production activity but also for the repair of photodamaged PSII subunits under high light intensity. This replacement mechanism could cause a weak correlation between the pigment production rates with the primary production. In other words, optimal photosynthetic activity (i.e., primary production) was not performed by the phytoplankton community at 100% light depth during this research period, especially by cyanobacteria (*Prochlorococcus* and *Synechococcus*), which were the predominant phytoplankton classes. Indeed, the negative effect of strong light and warm water on the primary production of cyanobacteria has been previously reported (Kehoe et al., 2015). This suggests that the influence of light conditions on phytoplankton, which is a fundamental marine food source, must be considered to understand variation in marine ecosystems in warming ocean scenarios—such scenarios are expected to expose phytoplankton to high light intensity and warm water temperature conditions. Therefore, our results provide a benchmark for studying the photosynthetic activity of phytoplankton associated with their photosynthetic pigments and dependent on changing light conditions.

## Data availability statement

The original contributions presented in the study are included in the article/Supplementary Material. Further inquiries can be directed to the corresponding authors.

## Author contributions

CL, JK, and SL conceived the ideas and designed methodology. CL, HB, and DK performed field experiments. CL, JK, HB, YK, SP, and J-OM conducted lab experiment. CL and KJ performed data analysis. CL, JK, and SL wrote the first draft of the manuscript. JK and SL reviewed and edited previous versions of the manuscript. All authors listed have made a substantial, direct, and intellectual contribution to the work and approved it for publication.

## Funding

This research was supported by the National Research Foundation of Korea (NRF) grant funded by the Korean government (MSIT; NRF-2019R1A2C1003515). Financial support for DK was provided by 'Study on Northwestern Pacific Warming and Genesis and Rapid Intensification of Typhoon', funded by the Ministry of Oceans and Fisheries (20220566). This research was supported by the "Development of assessment technology on the structure variations in marine ecosystem (R2022058)" funded by the National Institute of Fisheries Science (NIFS), Korea.

## Acknowledgments

We are grateful to the captain, all of the crew, and researchers for their outstanding assistance during the Korean R/V "*ISABU*" cruise.

## Conflict of interest

The authors declare that the research was conducted in the absence of any commercial or financial relationships that could be construed as a potential conflict of interest.

## Publisher's note



## Supplementary material

The Supplementary Material for this article can be found online at: https://www.frontiersin.org/articles/10.3389/fmars.2022.930690/full#supplementary-material

# References

Agustí, S. (2004). Viability and niche segregation of prochlorococcus and synechococcus cells across the central Atlantic ocean. *Aquat. Microb. Ecol.* 36, 53–59. doi: 10.3354/ame036053

Claustre, H., and Marty, J. C. (1995). Specific phytoplankton biomasses and their relation to primary production in the tropical north Atlantic. *Deep Res. Part I Oceanogr. Res. Pap.* 42, 1475–1493. doi: 10.1016/0967-0637(95)00053-9

Colijn, F., Villerius, L., Rademaker, M., Hammer, K. D., and Eberlein, K. (1990). Changes in spatial distribution of primary production, photosynthetic pigments and phytoplankton species composition during two surveys in the German bight. *Neth. J. Sea Res.* 25 (1-2), 155–164. doi: 10.1016/0077-7579(90)90016-A

Croce, R., and Van Amerongen, H. (2014). Natural strategies for photosynthetic light harvesting. *Nat. Chem. Biol.* 10, 492–501. doi: 10.1038/nchembio.1555

de Boyer Montégut, C., Madec, G., Fischer, A. S., Lazar, A., and Iudicone, D. (2004). Mixed layer depth over the global ocean: An examination of profile data and a profile-based climatology. *J. Geophys. Res. Ocean* 109, 1–20. doi: 10.1029/2004JC002378

Descy, J. P., Sarmento, H., and Higgins, H. W. (2009). Variability of phytoplankton pigment ratios across aquatic environments. *Eur. J. Phycol.* 44, 319–330. doi: 10.1080/09670260802618942

Eisner, L. B., Twardowski, M. S., Cowles, T. J., and Perry, M. J. (2003). Resolving phytoplankton photoprotective: Photosynthetic carotenoid ratios on fine scales using *in situ* spectral absorption measurements. *Limnol. Oceanogr.* 48, 632–646. doi: 10.4319/lo.2003.48.2.0632

Falkowski, P. G., and Owens, T. G. (1980). Light–shade adaptation: TWO STRATEGIES IN MARINE PHYTOPLANKTON. *Plant Physiol.* 66 (4), 592–595. doi: 10.1104/pp.66.4.592

Falkowski, P. G., and Raven, J. A. (2013). *Aquatic photosynthesis* (Princeton University Press).

Fujiki, T., Matsumoto, K., Saino, T., Wakita, M., and Watanabe, S. (2013). Distribution and photo-physiological condition of phytoplankton in the tropical and subtropical north pacific. *J. Oceanogr.* 69, 35–43. doi: 10.1007/s10872-012-0153-5

Garneau, M. È., Gosselin, M., Klein, B., Tremblay, J. É., and Fouilland, E. (2007). New and regenerated production during a late summer bloom in an Arctic polynya. *Mar. Ecol.-Prog. Ser.* 345, 13–26. doi: 10.3354/meps06965

Goericke, R., and Welschmeyer, N. A. (1993a). The chlorophyll-labeling method: Measuring specific rates of chlorophyll a synthesis in cultures and in the open ocean. *Limnol. Oceanogr.* 38 (1), 80–95. doi: 10.4319/lo.1993.38.1.0080

Goericke, R., and Welschmeyer, N. A. (1993b). The carotenoid-labeling method: measuring specific rates of carotenoid synthesis in natural phytoplankton communities. *Mar. Ecol.-Prog. Ser.* 98 (1), 157–171.

Grossman, A. R., Schaefer, M. R., Chiang, G. G., and Collier, J. L. (1993). The phycobilisome, a light-harvesting complex responsive to environmental conditions. *Microbiol. Rev.* 57, 725–749. doi: 10.1128/mmbr.57.3.725-749.1993

Ha, S. Y., La, H. S., Min, J. O., Chung, K. H., Kang, S. H., and Shin, K. H. (2014). Photoprotective function of mycosporine-like amino acids in a bipolar diatom (Porosira glacialis): Evidence from ultraviolet radiation and stable isotope probing. *Diatom Res.* 29, 399–409. doi: 10.1080/0269249X.2014.894945

Hama, T., Miyazaki, T., Iwakuma, T., Takahashi, M., Otsuki, A., and Ichimura, S. (1983). Measurement of photosynthetic production of a marine phytoplankton population using a stable $^{13}C$ isotope. *Mar. Biol.* 73 (1), 31–36. doi: 10.1007/BF00396282

Hickman, A. E., Dutkiewicz, S., Williams, R. G., and Follows, M. J. (2010). Modelling the effects of chromatic adaptation on phytoplankton community structure in the oligotrophic ocean. *Mar. Ecol. Prog. Ser.* 406, 1–17. doi: 10.3354/meps08588

Hickman, A. E., Holligan, P. M., Moore, C. M., Sharples, J., Krivtsov, V., and Palmer, M. R. (2009). Distribution and chromatic adaptation of phytoplankton within a shelf sea thermocline. *Limnol. Oceanogr.* 54, 525–536. doi: 10.4319/lo.2009.54.2.0525

Hitchcock, G. L. *The time course of photosynthetic adaptation, the growth response and variation in pigment, carbohydrate, and protein of Skeletonema costatum and Detonula confervacea to changes in light intensity*. (1977).

Kang, J. J., Joo, H., Lee, J. H., Lee, J. H., Lee, H. W., Lee, D., et al. (2017). Comparison of biochemical compositions of phytoplankton during spring and fall seasons in the northern East/Japan Sea. *Deep-Sea Res. Part II-Top Stud. Oceanogr.*, 143:73-81. doi: 10.1016/j.dsr2.2017.06.006

Kang, J. J., Min, J. O., Kim, Y., Lee, C. H., Yoo, H., Jang, H. K., et al. (2021). Vertical distribution of phytoplankton community and pigment production in the yellow sea and the east china sea during the late summer season. *Water* 13 (23), 3321. doi: 10.3390/w13233321

Kehoe, M., O'Brien, K. R., Grinham, A., and Burford, M. A. (2015). Primary production of lake phytoplankton, dominated by the cyanobacterium cylindrospermopsis raciborskii, in response to irradiance and temperature. *Inland Waters* 5 (2), 93–100. doi: 10.5268/IW-5.2.778

Kirk, J. T. (2011). *Light and photosynthesis in aquatic ecosystems* (Cambridge university press).

Komenda, J. (2000). Role of two forms of the D1 protein in the recovery from photoinhibition of photosystem II in the cyanobacterium synechococcus PCC 7942. *Biochim. Biophys. Acta-Bioenerg.* 1457, 243–252. doi: 10.1016/S0005-2728(00)00105-5

Komenda, J., and Sobotka, R. (2019). Chlorophyll-binding subunits of photosystem I and II: Biosynthesis, chlorophyll incorporation and assembly. *Adv. Bot. Res.* 91, 195–223. doi: 10.1016/bs.abr.2019.02.001

Lee, D., Jeong, J. Y., Jang, H. K., Min, J. O., Kim, M. J., Youn, S. H., et al. (2019). Comparison of particulate organic carbon to chlorophyll-a ratio based on the ocean color satellite data at the ieodo and socheongcho ocean research stations. *J. Coast. Res.* 90, 267–271. doi: 10.2112/SI90-033.1

Lee, J. H., Kang, J. J., Jang, H. K., Jo, N., Lee, D., Yun, M., et al. (2020). Major controlling factors for spatio-temporal variations in the macromolecular composition and primary production by phytoplankton in garolim and asan bays in the yellow Sea. *Reg. Stud. Mar. Sci.*, 36:101269. doi: 10.1016/j.rsma.2020.101269

Li, L., Aro, E. M., and Millar, A. H. (2018). Mechanisms of photodamage and protein turnover in photoinhibition. *Trends Plant Sci.* 23, 667–676. doi: 10.1016/j.tplants.2018.05.004

Liu, X., Laws, E. A., Xie, Y., Wang, L., Lin, L., and Huang, B. (2019). Uncoupling of seasonal variations between phytoplankton chlorophyll a and production in the East China Sea. *J. Geophys. Res. Biogeosci.* 124, 2400–2415. doi: 10.1029/2018JG004924

Liu, J., Lu, Y., Hua, W., and Last, R. L. (2019). A new light on photosystem II maintenance in oxygenic photosynthesis. *Front. Plant Sci.* 10. doi: 10.3389/fpls.2019.00975

Luimstra, V. M., Verspagen, J. M. H., Xu, T., Schuurmans, J. M., and Huisman, J. (2020). Changes in water color shift competition between phytoplankton species with contrasting light-harvesting strategies. *Ecology* 101 (3), e02951. doi: 10.1002/ecy.2951

Lutz, V. A., Sathyendranath, S., Head, E. J., and Li, W. K. (2003). Variability in pigment composition and opticalcharacteristics of phytoplankton in the LabradorSea and the central north Atlantic. *Mar. Ecol. Prog. Ser.* 260, 1–18. doi: 10.3354/meps260001

Mackey, M. D., Mackey, D. J., Higgins, H. W., and Wright, S. W. (1996). CHEMTAX-a program for estimating class abundances from chemical markers: application to HPLC measurements of phytoplankton. *Mar. Ecol. Prog. Ser.* 144, 265–283. doi: 10.3354/meps144265

Mackey, D. J., Parslow, J., Higgins, H. W., Griffithst, F. B., and O'sullivan, J. E. (1995). Plankton productivity and biomass in the western equatorial pacific: Biological and physical controls. *Deep Sea Res. Part II Top. Stud. Oceanogr.* 42, 49–533. doi: 10.1016/0967-0645(95)00038-R

Messié, M., and Radenac, M. H. (2006). Seasonal variability of the surface chlorophyll in the western tropical pacific from SeaWiFS data. *Deep Res. Part I Oceanogr. Res. Pap.* 53, 1581–1600. doi: 10.1016/j.dsr.2006.06.007

Miki, M., Ramaiah, N., Takeda, S., and Furuya, K. (2008). Phytoplankton dynamics associated with the monsoonin the sulu Sea as revealed by pigment signature. *J. Oceanogr.* 64, 663–673. doi: 10.1007/s10872-008-0056-7

Min, J. O., Ha, S. Y., Hur, J., and Shin, K. H. (2019). Primary productivity and photosynthetic pigment production rates of periphyton and phytoplankton in lake paldang using $^{13}C$ tracer. *Korean J. Ecol. Environ.* 52, 202–209. doi: 10.11614/ksl.2019.52.3.202

Moore, L. R., Goericke, R., and Chisholm, S. W. (1995). Comparative physiology of synechococcus and prochlorococcus: influence of light and temperature on growth, pigments, fluorescence and absorptive properties. *Mar. Ecol. Prog. Ser.* 116, 259–275.

Morel et al., 1993Morel, A., Ahn, Y. H., Partensky, F., Vaulot, D., and Claustre, H. (1993). Prochlorococcus and synechococcus: a comparative study of their optical properties in relation to their size and pigmentation. *J. Mar. Res.* 51, 617–649. doi: 10.1357/0022240933223963

Pabi, S., van Dijken, G. L., and Arrigo, K. R. (2008). Primary production in the arctic ocean 1998-2006. *J. Geophys. Res. Ocean* 113:C08005. doi: 10.1029/2007JC004578

Pai, S. C., and Chen, H. Y. (1994). Vertical distribution of cadmium in marginal seas of the western pacific ocean. *Mar. Chem.* 47 (1), 81–91. doi: 10.1016/0304-4203(94)90015-9

Partensky, F., Blanchot, J., Lantoine, F., Neveux, J., and Marie, D. (1996). Vertical structure of picophytoplankton at different trophic sites of the tropical northeastern Atlantic ocean. *Deep Sea Res. Part I Oceanogr. Res. Pap.* 43, 1191–1213. doi: 10.1016/0967-0637(96)00056-8

Partensky, F., Blanchot, J., and Vaulot, D. (1999). Differential distribution and ecology of prochlorococcus and synechococcus in oceanic waters: a review. *Bull. l'inst. Océanogr. Monaco* 19, 457–475.

Prezelin, B. B., and Matlick, H. A. (1980). Time course of photoadaptation in the photosynthesis irradiance relationship of a dinoflagellate exhibiting photosynthetic periodicity. *Mar. Biol.* 58, 85–96. doi: 10.1007/BF00396119

Ramus, J. (1990). A form-function analysis of photon capture for seaweeds. *Hydrobiologica* 204 (205), 65–71. doi: 10.1007/BF00040216

Redalje, D. G., and Laws, E. A. (1981). A new method for estimating phytoplankton growth rates and carbon biomass. *Mar. Biol.* 62 (1), 73–79. doi: 10.1007/BF00396953

Richardson, K., Beardall, J., and Raven, J. A. (1983). Adaptation of unicellular algae to irradiance: an analysis of strategies. *New Phycol.* 93, 157–191. doi: 10.1111/j.1469-8137.1983.tb03422.x

Roy, S., Llewellyn, C. A., Egeland, E. S., and Johnsen, G. (2011). *Phytoplankton pigments: characterization, chemotaxonomy and applications in oceanography* (Cambridge University Press).

Ruan, Z., Prášil, O., and Giordano, M. (2018). The phycobilisomes of synechococcus sp. are constructed to minimize nitrogen use in nitrogen-limited cells and to maximize energy capture in energy-limited cells. *Environ. Exp. Bot.* 150, 152–160. doi: 10.1016/j.envexpbot.2018.01.015

Sathyendranath, S., and Platt, T. (2007). Spectral effects in bio-optical control on the ocean system bio-optical properties of phytoplankton remote sensing of ocean colour species succession primary production phytoplankton functional types mixed-layer physics. *Oceanologia* 49, 5–39.

Shibata, T., Tripathy, S. C., and Ishizaka, J. (2010). Phytoplankton pigment change as a photoadaptive response to light variation caused by tidal cycle in ariake bay, Japan. *J. Oceanogr.* 66 (6), 831–843. doi: 10.1007/s10872-010-0067-z

Siefermann-Harms, D. (1985). Carotenoids in photosynthesis, I: location in photosynthetic membranes and light-harvesting function. *Biochim. Biophys. Acta* 811, 325–355. doi: 10.1016/0304-4173(85)90006-0

Ting, C. S., Rocap, G., King, J., and Chisholm, S. W. (2002). Cyanobacterial photosynthesis in the oceans: the origins and significance of divergent light-harvesting strategies. *Trends Microbiol.* 10 (3), 134–142. doi: 10.1016/S0966-842X(02)02319-3

Tremblay, J. É., Anderson, L. G., Matrai, P., Coupel, P., Bélanger, S., Michel, C., et al. (2015). Global and regional drivers of nutrient supply, primary production and $CO_2$ drawdown in the changing Arctic ocean. *Prog. Oceanogr.* 139, 171–196. doi: 10.1016/j.pocean.2015.08.009

Veldhuis, M. J. W., and Kraay, G. (1990). Vertical distribution and pigment composition of a picoplanktonic prochlorophyte in the subtropical north atlantic:a combined study of HPLC-analysis of pigments and flow cytometry. *Mar. Ecol. Prog. Ser.* 68, 121–127. doi: 10.3354/meps068121

Veldhuis, M. J. W., Timmermans, K. R., Croot, P., and van der Wagt, B. (2005). Picophytoplankton; a comparative study of their biochemical composition and photosynthetic properties. *J. Sea Res.* 53, 7–24. doi: 10.1016/j.seares.2004.01.006

Wong, G. T. F., Pai, S. C., and Chung, S. W. (1995). Cobalt in the western Philippine Sea. *Oceanol. Acta* 18 (6), 631–638.

Yun, M. S., Kim, Y., Jeong, Y., Joo, H. T., Jo, Y. H., Lee, C. H., et al. (2020). Weak response of biological productivity and community structure of phytoplankton to mesoscale eddies in the oligotrophic Philippine Sea. *J. Geophys. Res.-Oceans* 125 (12), e2020JC016436. doi: 10.1029/2020JC016436

Zapata, M., Rodríguez, F., and Garrido, J. L. (2000). Separation of chlorophylls and carotenoids from marine phytoplankton: A new HPLC method using a reversed phase C8 column and pyridine-containing mobile phases. *Mar. Ecol. Prog. Ser.* 195, 29–45. doi: 10.3354/meps195029

Zhao, S., Wei, J., Yue, H., and Xiao, T. (2010). Picophytoplankton abundance and community structure in the Philippine Sea, western pacific. *Chin. J. Oceanol. Limnol.* 28, 88–95. doi: 10.1007/s00343-010-9274-0

Zheng, Z., Wei, H., Luo, X., and Zhao, W. (2021). Mechanisms of persistent high primary production during the growing season in the chukchi Sea. *Ecosystems* 24, 891–910. doi: 10.1007/s10021-020-00559-8

frontiers | Frontiers in Marine Science

TYPE Original Research
PUBLISHED 25 October 2022
DOI 10.3389/fmars.2022.979998



OPEN ACCESS

EDITED BY
Connie Lovejoy,
Laval University, Canada

REVIEWED BY
Emmanuel Devred,
Fisheries and Oceans Canada (DFO), Canada
Heather Bouman,
University of Oxford, United Kingdom

*CORRESPONDENCE
Jisoo Park
jspark@kopri.re.kr

SPECIALTY SECTION
This article was submitted to Aquatic Microbiology, a section of the journal Frontiers in Marine Science

RECEIVED 28 June 2022
ACCEPTED 11 October 2022
PUBLISHED 25 October 2022

CITATION
Ko E, Gorbunov MY, Jung J, Lee Y, Cho K-H, Yang EJ and Park J (2022) Phytoplankton photophysiology varies depending on nitrogen and light availability at the subsurface chlorophyll maximum in the northern Chukchi Sea.
*Front. Mar. Sci.* 9:979998.
doi: 10.3389/fmars.2022.979998



# Phytoplankton photophysiology varies depending on nitrogen and light availability at the subsurface chlorophyll maximum in the northern Chukchi Sea

Eunho Ko[1], Maxim Y. Gorbunov[2], Jinyoung Jung[1], Youngju Lee[1], Kyoung-Ho Cho[1], Eun Jin Yang[1] and Jisoo Park[1*]

[1]Division of Ocean Sciences, Korea Polar Research Institute, Incheon, South Korea, [2]Department of Marine and Coastal Science, Rutgers University, New Brunswick, NJ, United States

Vertical distributions of phytoplankton in the Arctic Ocean are characterized by a very narrow subsurface chlorophyll maximum (SCM) layer formed every summer after the sea ice retreats. Despite the prevalence of this narrow SCM layer, phytoplankton photosynthetic response to climate change remains to be elucidated. Here, we examined the photophysiological properties of phytoplankton in the SCM layer in the northern Chukchi Sea during the summers of 2015–2018. There was a significant difference in the SCM depth between the northwestern and northeastern Chukchi Sea determined by the distribution of Pacific Summer Water (PSW) around the SCM layer (34 $\pm$ 14 m vs. 49 $\pm$ 10 m, respectively). The maximum quantum yield of photochemistry in photosystem II ($F_v/F_m$) in the SCM phytoplankton was high ($F_v/F_m \geq 0.54$) and similar in both regions until 2016; however, since then, $F_v/F_m$ in the northeastern Chukchi Sea has decreased by approximately 10%. This decrease was accompanied by a marked decrease in the fraction of microplankton, which are known to be susceptible to nutrient limitation. This result suggests a reduction in nitrogen availability in the SCM layer in the northeastern Chukchi Sea. Meanwhile, the maximum electron transfer rate ($ETR^{max}$) did not have a significant relationship with the nitrogen availability and phytoplankton community size structure in the SCM layer; however the improved light conditions (with an approximately two-fold increase in the relative ratio of surface PAR reaching the SCM layer) increased $ETR^{max}$ by up to

30% in the SCM phytoplankton in the northwestern Chukchi Sea. Therefore, these results provide a better understanding of how changes in nitrogen and light availability could affect phytoplankton photosynthesis and primary production in the Arctic Ocean.

KEYWORDS

photochemical efficiency, phytoplankton, nitrogen availability, maximum electron transfer rate, subsurface chlorophyll maximum, Arctic Ocean

## Introduction

Phytoplankton in the Arctic Ocean have been exposed to rapid changes in the marine environment, including sea ice reduction and warming (Wassmann et al., 2011; Tremblay et al., 2012). Observations in the Arctic Ocean showed that surface water temperature continued to rise from 1982 to 2018 (Carvalho and Wang, 2020), and the Arctic warming resulted in a drastic decline in sea ice (Comiso et al., 2017). For instance, the sea ice extent in September decreased by approximately 40% from 1981 to 2010 (Serreze and Stroeve, 2015). This reduction in sea ice led to an increase in fresh water content, which strengthened the stratification of the upper water column (Stroeve et al., 2007; Wang et al., 2019). The early retreat and thinning of sea ice allowed early light to penetrate into the water column, thus leading to the early development of spring phytoplankton bloom or developing massive under-ice phytoplankton bloom, which would have consumed nutrients in the surface layer (Wassmann et al., 2011; Arrigo et al., 2012). In addition, fall blooms have begun to be observed in the Arctic Ocean, and changes have occurred in the seasonal dynamics of phytoplankton (Ardyna et al., 2014; Ardyna and Arrigo, 2020). Changes in the marine environments due to climate change have been linked to nutrient availability and light conditions, which are a major factors affecting phytoplankton growth, community composition, and primary production in the Arctic Ocean (Lewis et al., 2020; Sugie et al., 2020; Song et al., 2021). However, only a few studies have comprehensively investigated how variations in these major factors affect the photosynthetic properties of phytoplankton estimated by variable fluorescence in the Arctic Ocean.

Recent studies on the variability of primary production have mainly been conducted based on ocean color data in the Arctic Ocean (Arrigo et al., 2008; Lewis et al., 2020). Satellite data is a powerful technology for remote and inaccessible marine environments, such as the Arctic Ocean; however, it does not include information on the vertical distribution of phytoplankton (Hill and Cota, 2005; Martin et al., 2010). It is well known that a distinct subsurface chlorophyll maximum (SCM) forms in the Arctic Ocean during the summer months (Martin et al., 2010). Arrigo and van Dijken (2011) have reported that the primary production in the SCM layer accounts for 0.2 to 16% of the annual primary production in the Arctic Ocean. In contrast, it has also been reported that by ignoring the presence of an SCM layer, integrated primary production can be underestimated by as much as 40–75% in the summer months (Hill et al., 2013), with potentially greater errors occurring in daily estimates when sharp SCM peaks are situated within the photic zone (Bouman et al., 2020). Therefore, in order to understand the changes in primary productivity in the Arctic Ocean, the growth conditions and the photosynthetic properties of phytoplankton at the SCM should be investigated.

Changes in the photosynthetic response of phytoplankton to environmental conditions are essential for determining phytoplankton growth and primary production. In a previous study, we investigated phytoplankton photosynthetic properties in the surface layer of the Arctic Ocean and revealed that severe nitrogen limitation leads to decrease in the photosynthetic rates and growth rates with the reduction in the fraction of microphytoplankton (e.g. > 20 μm) communities (Ko et al., 2020). Although phytoplankton in the SCM layer are generally known to have a relatively higher light-harvesting capability, photosynthetic efficiency, and growth rate than the surface phytoplankton (Coupel et al., 2012; Palmer et al., 2013), data on their photosynthetic response to environmental variation around the SCM layer are limited. Recently, the nutrient supply to the surface layer was confirmed to be influenced by the Atlantic-origin water in the northwestern Chukchi Sea, and this change affected the SCM depth and phytoplankton biomass (Jung et al., 2021). The SCM layer is usually formed below the pycnocline and is controlled by the vertical distribution of nitrogen, and thus Change in water column structure has affected the nutrient supply and environmental variables, which, in turn, affected phytoplankton photosynthesis in the SCM layer (Martin et al., 2010; Baldry et al., 2020). Therefore, we compared data by region to understand how changes in environmental variables (e.g. nitrogen availability and light conditions) affect the photophysiological properties of phytoplankton in the SCM layer.

The photosynthetic properties of the phytoplankton were identified using variable chlorophyll-a fluorescence. This method is useful for elucidating the spatial distribution of the photophysiological properties of phytoplankton because it is non-destructive, sensitive, and rapid for sampling in an extensive hydrographic region at higher spatial resolution than conventional $^{14}C$ experiments (Behrenfeld and Kolber, 1999; Moore et al., 2008). High-resolution data of variable fluorescence are evaluated to have the potential to reveal large-scale patterns and trends in photosynthetic rate and primary production (Schuback et al., 2021). In particular, the photochemical efficiency of photosystem II (PSII) in phytoplankton cells has been used to diagnose nutrient limitations in the ocean, including coastal areas, ocean gyres, upwelling systems, and polar regions (Kolber et al., 1994; Cheah et al., 2013; Park et al., 2017). In addition, the maximum electron transfer rate ($ETR^{max}$) has been should be more useful for evaluating nitrogen limitation because it is more sensitive to nitrogen stress than photochemical efficiency alone (Gorbunov and Falkowski, 2020; Ko et al., 2020). Thus, the photophysiological properties derived using this method are suitable for investigating phytoplankton photosynthesis in relation to environmental conditions, such as nutrient limitation and photoacclimation.

The objectives of this work were to (1) examine the spatial distribution of the photophysiological properties of phytoplankton at the SCM depth in the northern Chukchi Sea and (2) investigate the response of the photophysiological properties in relation to the changes in nutrient availability and light conditions at the SCM depth. In addition, we analyzed photosynthetic parameters derived from the electron transfer rate versus irradiance (ETR-E) curve. To achieve these goals, we analyzed the phytoplankton photophysiology in the SCM layer through field surveys in the Chukchi Sea from 2015 to 2018. This study identified the effect of nitrogen availability and light conditions on biomass, community size fraction, and photophysiological properties of phytoplankton in the SCM layer of the Chukchi Sea.

# Materials and methods

## Water sampling and study area

Water samples were collected onboard the Korean icebreaker R/V *Araon* every August, from 2015 to 2018, in the northern Chukchi Sea (Figure 1). Water samples were obtained from 5 to 6 depths ranging from the surface to 100 m using 10L Niskin bottles mounted on a conductivity, temperature, and depth rosette system (CTD; SBE 911 plus). In detail, the two samples were collected in the mixed layer including the surface layer, and 3–4 samples were collected from the SCM depth and the upper and lower layers based on the SCM depth. Fluorescence and photosynthetically active radiation (PAR) profiles were obtained from chlorophyll fluorescence (ECO FL, WET Labs) and PAR sensor (SBE PAR sensor) mounted on the CTD frame. Temperature and salinity profiles were used to calculate the stratification index ($\Delta\sigma_t$), freshwater content (FWC) and mixed layer depth (MLD). $\Delta\sigma_t$ was calculated as the difference in density between the surface layer and 100 m (Codispoti et al., 2005), and MLD was determined as the depth at which the difference in density of 0.05 kg $m^{-3}$ from the surface layer (Coupel et al., 2015). The salinity profile was used to quantify the amount of freshwater in the upper layer as described by Coupel et al. (2015). The FWC was calculated by integrating the ratio of the reference salinity (34.8, Aagaard and Carmack, 1989) to the salinity profile and the detailed method was described by Ko et al. (2020). After estimating the vertical attenuation coefficient obtained from the slope of the regression of the natural log-transformed PAR profile, the euphotic depth was estimated as the depth at which the PAR was 1% of the surface values (Kirk, 1994). The ratio of PAR at the SCM depth to the surface PAR (PAR_ratio) was calculated from the PAR profile for each station. Daily sea ice concentrations were obtained from the National Snow and Ice Data Center (https://nsidc.org/). The sea ice concentration for each station was calculated by averaging the pixels around the stations. The upper layer (~ 150 m) of the western Arctic is mainly composed of Pacific-origin water and is classified into two types based on the seasonal modification: Pacific Summer Water (PSW; $T > -1$°C, $31 \leq S \leq 32$ psu) and Pacific Winter Water (PWW; $T < -1$°C, $S > 31.5$ psu) (Gong and Pickart, 2015). Considering that the structure of the water column around the SCM layer is related to environmental factors, the study area was divided into two regions based on the distribution of PSW within 100 m depth. The PSW was mainly distributed in the eastern side of the northern Chukchi Sea, and it was named the northeastern Chukchi Sea (NEC). Conversely, the western side of the northern Chukchi Sea, where the PSW did not appear was expressed as the northwestern Chukchi Sea (NWC). A total of 84 stations were investigated over 4 years (2015 to 2018), with 40 stations in the NEC region and the remaining 44 stations in the NWC region (Table 1).

## Nutrients, nitracline and chlorophyll-a concentration

Nutrient distribution, including nitrite + nitrate ($NO_2$ + $NO_3$), phosphate ($PO_4$), silicate ($SiO_2$), and ammonium ($NH_4$) concentrations, were measured using a four-channel continuous auto-analyzer (QuAAtro, Seal Analytical) following the Joint Global Ocean Flux Study (JGOFS) protocols (Gordon et al., 1993). To evaluate accuracy and reproducibility, nutrient reference materials for seawater (Lot. No. BV, KANSO Techno) were measured with standards in all batches; the detailed methods are described by Jung et al. (2021). Nitracline

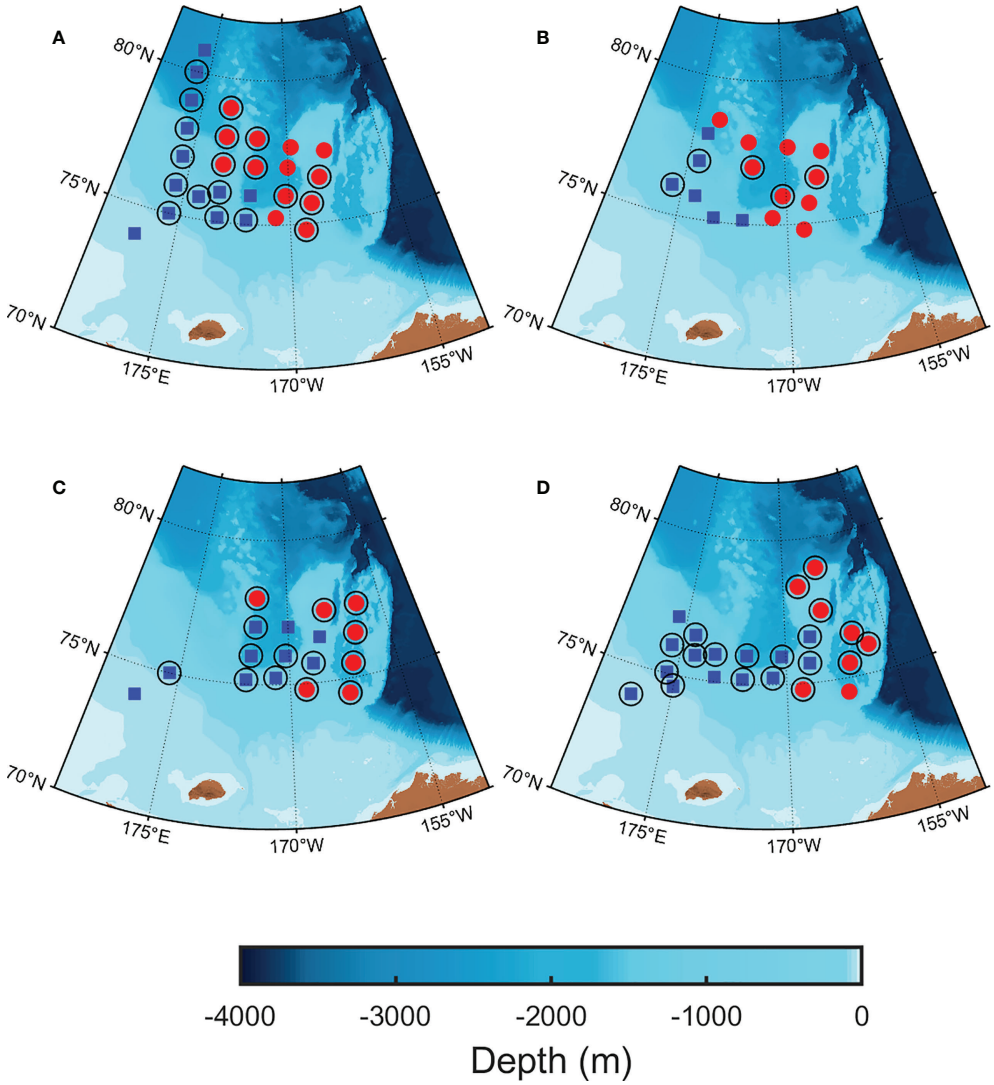


FIGURE 1
Maps of oceanographic stations in the northern Chukchi Sea. **(A)** 5–20 August, 2015; **(B)** 9–19 August, 2016; **(C)** 10–25 August, 2017; **(D)** 7–24 August, 2018. The study area was classified based on the distribution of Pacific Summer Water (PSW, T > –1°C, 31 ≤ S ≤ 32 psu) within 100 m of water depth. The blue square represents the northwestern Chukchi Sea (NWC) without PSW and the red circles represents the northeastern Chukchi Sea (NEC) with PSW, respectively. The empty circles represent the stations of the electron transfer rate versus irradiance curve.

depths were determined as the median of the shallowest depths where the gradient of $NO_2$ + $NO_3$ was greater than 0.1 μM $m^{-1}$ (Coupel et al., 2015).

Chlorophyll-a (Chl-a) samples were filtered with 500 mL of seawater through a glass fiber filter (Whatman GF/F), and extracted in the dark for 24 h with 90% acetone. Chl-a concentration was measured using a fluorometer (Trilogy, Turner Designs) calibrated using a purified Chl-a standard solution (Sigma) (Parsons et al., 1984). In addition, size-fractionated Chl-a was measured using a cascade connection filtration system composed of a 20 μm nylon mesh and a nuclepore filter with a pore size of 2 μm (Whatman). Using this system, the micro (≥ 20 μm), nano (2–20 μm), and pico (≤ 2 μm) Chl-a concentration were obtained. The SCM depth was determined as the depth, which was the highest fluorescence from the chlorophyll fluorescence profile. The profile of Chl-a concentration was obtained by correcting the chlorophyll fluorescence profile with Chl-a concentration, the SCM layer was identified as a depth where the gradient of Chl-a concentration was ± 0.01 ug $l^{-1}$ $m^{-1}$ and above the threshold of Chl-a concentration (0.11 ug $l^{-1}$) to calculate the contribution of the Chl-a concentration in the SCM layer (Martin et al., 2013).

TABLE 1 Regional environmental variables at the subsurface chlorophyll maximum (SCM) in the northwestern Chukchi Sea (NWC) and northeastern Chukchi Sea (NEC). Temperature (T; °C); Salinity (S; psu); Stratification index ($\Delta\sigma_t$, kg $m^{-3}$); Euphotic depth ($Z_{eu}$; m); Mixed layer depth (MLD; m), Fresh water content (FWC; m), Stratification index ($\Delta\sigma_t$; kg $m^{-3}$); nitrite + nitrate ($NO_2$+$NO_3$; μM); phosphate ($PO_4$; μM); silicate ($SiO_2$; μM); nitracline (m).

| Region | Year | ST | SCM depth | T | S | $\Delta\sigma_t$ | Zeu | MLD | FWC | $NO_2$+$NO_3$ | $PO_4$ | $SiO_2$ | Nitracline |
|---|---|---|---|---|---|---|---|---|---|---|---|---|---|
| NWC | 2015 | 13 | 45 ± 13 | -1.32 ± 0.20 | 31.69 ± 0.43 | 4.29 ± 1.14 | 45 ± 13 | 9 ± 3 | 14 ± 5 | 5.80 ± 2.81 | 1.19 ± 0.22 | 12.08 ± 5.51 | 33 ± 12 |
| | 2016 | 6 | 36 ± 8 | -1.46 ± 0.10 | 31.56 ± 0.25 | 2.67 ± 0.59 | 37 ± 7 | 12 ± 6 | 13 ± 2 | 4.30 ± 2.27 | 1.10 ± 0.18 | 10.74 ± 4.70 | 31 ± 8 |
| | 2017 | 10 | 32 ± 9 | -1.33 ± 0.18 | 30.58 ± 0.45 | 2.94 ± 0.63 | 41 ± 6 | 15 ± 8 | 12 ± 4 | 2.55 ± 2.08 | 1.07 ± 0.20 | 12.97 ± 3.62 | 24 ± 8 |
| | 2018 | 15 | 26 ± 15 | -1.45 ± 0.14 | 31.22 ± 0.49 | 2.96 ± 0.78 | 33 ± 16 | 8 ± 2 | 10 ± 3 | 4.68 ± 3.33 | 1.18 ± 0.21 | 12.51 ± 5.60 | 21 ± 9 |
| NEC | 2015 | 13 | 54 ± 8 | -0.52 ± 0.62 | 31.24 ± 0.31 | 5.34 ± 0.99 | 52 ± 8 | 9 ± 2 | 20 ± 2 | 3.11 ± 2.63 | 0.99 ± 0.17 | 9.62 ± 6.98 | 41 ± 13 |
| | 2016 | 10 | 49 ± 9 | -0.60 ± 0.46 | 31.10 ± 0.18 | 3.47 ± 0.57 | 57 ± 12 | 19 ± 5 | 19 ± 3 | 1.90 ± 1.08 | 0.86 ± 0.12 | 5.93 ± 1.96 | 35 ± 7 |
| | 2017 | 7 | 40 ± 11 | -0.54 ± 0.79 | 30.60 ± 0.57 | 3.59 ± 0.53 | 52 ± 8 | 14 ± 7 | 18 ± 3 | 1.58 ± 1.56 | 0.91 ± 0.17 | 7.95 ± 3.46 | 34 ± 9 |
| | 2018 | 8 | 50 ± 12 | -0.54 ± 0.41 | 31.00 ± 0.25 | 3.91 ± 0.39 | 61 ± 9 | 9 ± 2 | 18 ± 4 | 3.07 ± 1.65 | 0.97 ± 0.12 | 4.29 ± 3.52 | 36 ± 8 |

## Photophysiological properties of phytoplankton

The variable fluorescence of phytoplankton was determined using a new miniaturized fluorescence induction and relaxation (mini-FIRe) instrument (Gorbunov et al., 2020). The sensitivity and signal-to-noise ratio of this new instrument, which is suitable for use in oligotrophic waters, is approximately ca. 20 times better than the previous model (Gorbunov and Falkowski, 2004). For accurate measurements of quantum yields and functional absorption cross-sections, the FIRe instrument provides single photosynthetic turnover measurement within ca. 100 μs (Gorbunov et al., 1999).

For the measurement of variable fluorescence, seawater samples were kept at *in situ* temperature and under low-light conditions (~10 μmol quanta $m^{-2}$ $s^{-1}$) for approximately 60 min, which was necessary for recovery from photoinhibition and non-photochemical quenching. Then, each sample was measured to obtain the photophysiological properties of PSII, including minimal fluorescence yield ($F_o$; when all reaction centers are open), maximal fluorescence yield ($F_m$; all reaction centers are closed), photochemical efficiency ($F_v/F_m$), and functional absorption cross-section ($\sigma_{PSII}$), as described by Kolber et al. (1998). To calibrate the fluorescence parameters by depth, the blank signals were measured at two depths (ca. 0 and 100 m) after filtering the seawater with a syringe filter (0.2 μm), using the method described by Bibby et al. (2008). After subtracting the blank signal, $F_v/F_m$ was calculated using the ratio of variable fluorescence ($F_v = F_m - F_o$) to the maximum fluorescence ($F_m$).

Photosynthetic parameters were obtained by applying the electron transfer rate versus irradiance curve. The electron transfer rate (ETR) of the sample obtained from the SCM layer was measured using a programmable actinic light source mounted on the mini-FIRe. The ETR for each PSII reaction center was calculated as described by Gorbunov et al. (2000, 2001). The detailed method for calculating ETR has been described by Ko et al. (2020). The photosynthetic rates as a function of irradiance can be calculated using the hyperbolic tangent equation (Jassby and Platt, 1976) as follows:

$$ETR(E) = ETR^{max} \tanh\left(\frac{E}{E_k}\right) \quad (1)$$

where $ETR^{max}$ is the maximum electron transfer rate achievable at saturating light and $E_k$ is the light saturation parameter. The light utilization efficiency ($\alpha$) was estimated using $ETR^{max}/E_k$. To deduce the photosynthetic rates in absolute units (i.e., electrons per second per reaction center), cross-sections must be measured for the same spectral quality as the ambient irradiance. Therefore, both excitation and actinic light were kept in blue light range (455 nm, with a 20 nm half bandwidth) during the measurement of the photosynthesis versus irradiance curves.

## Statistical analysis

Analysis of variance was performed using MATLAB (R2020a) to confirm the difference in parameters by region. Principal component analysis was performed to understand the relationship between environmental variables and the photophysiological properties of phytoplankton using the *factoextra* package (v1.0.6) in the R software.

# Results

## Physical and chemical environments of the water-column

The physical and chemical properties differed between the NWC and NEC regions. These two regions were identified by the distribution of PSW around the SCM layer, as described previously (Table 1, Figure 2). The water temperature of the SCM depth in the NWC region, where the PWW was mainly located below the SCM layer, was 0.84°C lower than that in the

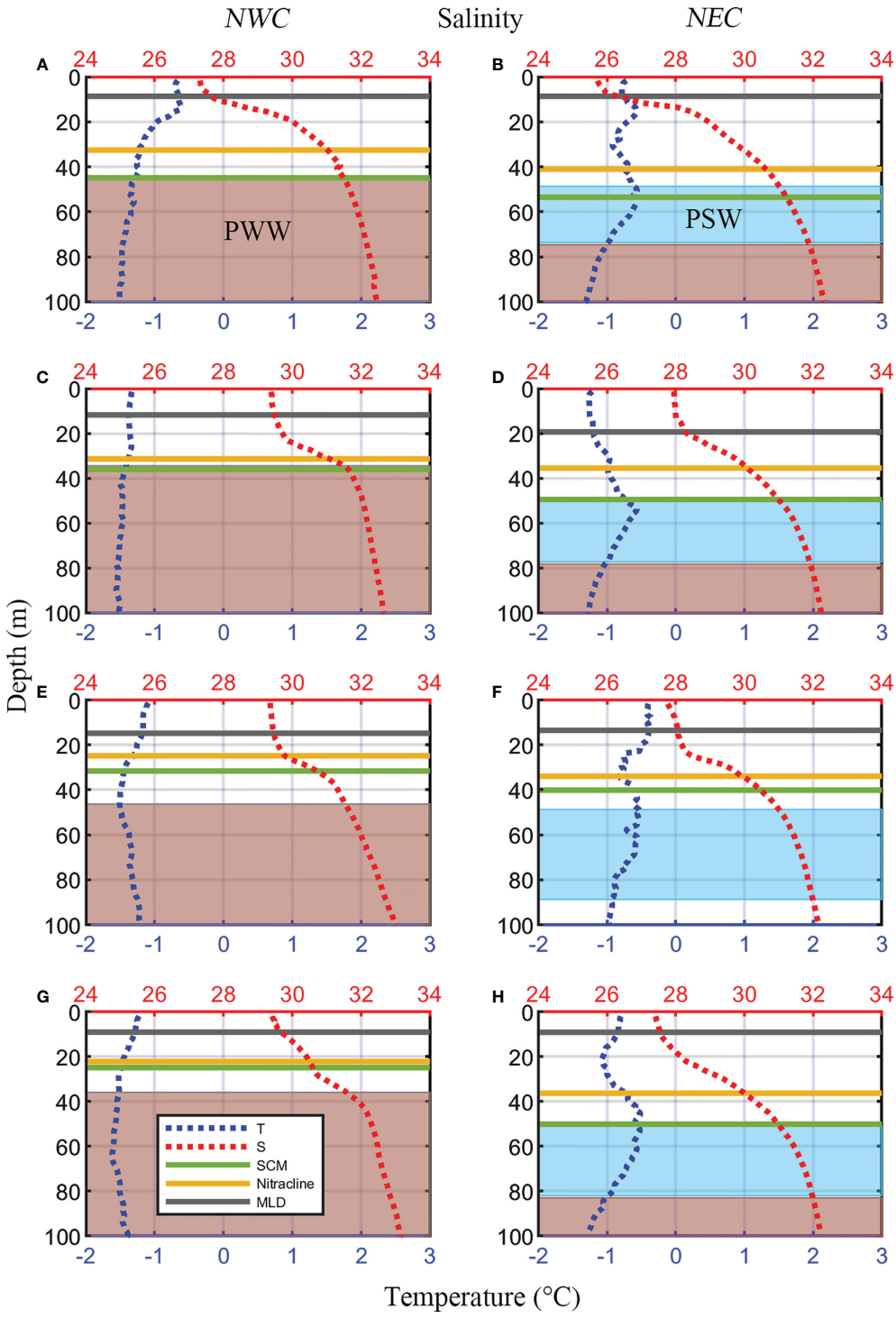


FIGURE 2
Vertical profiles of average temperature (blue dotted lines) and salinity (red dotted lines) by year in the northwestern Chukchi Sea (NWC, Left panels) and the northeastern Chukchi Sea (NEC, Right panels). Two horizontal dark gray, green and yellow lines indicate the mixed layer depth (MLD), subsurface chlorophyll maximum (SCM) layer and nitracline on average, respectively. The red and cyan shading represent the Pacific Winter Water (PWW, T > −1°C, S > 31.5 psu) and the Pacific Summer Water (PSW, T > −1°C, 31 ≤ S ≤ 32 psu) respectively. **(A, B)** 2015; **(C, D)** 2016; **(E, F)** 2017; **(G, H)** 2018.

NEC region, where the PSW was located around the SCM layer (−1.39 ± 0.17°C and −0.55 ± 0.56°C, respectively; $p< 0.01$) (Figure 2 and Table 1). The salinity was similar at the SCM depth in both regions (31.26 ± 0.59 psu and 31.04 ± 0.39 psu, respectively), and the lowest value was observed in 2017 (30.57 ± 0.42 psu and 30.60 ± 0.53 psu, respectively). The mixed layer depth (MLD) was similar in these two regions (10 ± 6 m and 12 ± 6 m, respectively) (Table 1). The MLD was the deepest in 2017 in the NWC region (15 ± 6 m) and in 2016 in the NEC region (19 ± 5 m; $p< 0.05$). The FWC in the NEC region was 19 ± 3 m on average, which was 58% higher than that in the NWC region (12 ± 4 m; $p< 0.01$). The FWC maintained a similar range each year in the NEC region, whereas it gradually decreased from 2015 to 2018 in the NWC region (Table 1). The $\Delta\sigma_t$ in the NEC region (4.23 ± 1.08 kg $m^{-3}$) recorded higher values than that in the NWC region (3.31 ± 1.05 kg $m^{-3}$, $p< 0.01$). The SCM depth was 49 ± 10 m in the NEC region, which was 15 m deeper than the 34 ± 14 m depth in the NWC region ($p< 0.05$, Table 1 and Figure 2). In addition, SCM depth showed a tendency to become shallower from 2015 to 2018 in the NWC region ($p< 0.01$). Although the SCM depth of the NEC region was the shallowest in 2017 (40 ± 11 m), it increased again in 2018 (Figures 2F, H). The nitracline of the two regions was also distinctly different (27 ± 10 m and 37 ± 10 m, respectively); in particular, that in the NWC region became shallow from 2015 to 2018 ($p< 0.05$). The euphotic depth ($Z_{eu}$) also differed significantly between the two regions (39 ± 13 m and 55 ± 10 m, respectively; $p< 0.01$), but there was no significant linear trend by region such as the SCM depth and nitracline (Table 1). However, $Z_{eu}$ showed a significant negative correlation with Chl-a concentration at the SCM depth ($r = -0.63$, $p< 0.01$). The PAR of the SCM depth was similar between the two regions (5.69 ± 6.98 μmol $m^{-2}$ $s^{-1}$ and 4.40 ± 5.82 μmol $m^{-2}$ $s^{-1}$, respectively). Also, the PAR_ratio in the NWC region was slightly higher than that in the NEC region (4.94 ± 8.99 and 2.81 ± 1.49, respectively), there was no statistically significant difference (Supplementary Figure 1).

In the case of nutrient distribution, the nutrient concentration at the SCM depth in the NWC region was relatively higher than that in the NEC region (Figure 3). There was a significant difference in the nitrate + nitrate concentration ($NO_2$ + $NO_3$) between the two regions (4.47 ± 2.92 μM and 2.49 ± 1.92 μM, respectively; $p< 0.01$) (Figure 3A), except in 2017. Regional differences in phosphate concentration ($PO_4$) were also distinct (1.14 ± 0.20 and 0.94 ± 0.15 μM, respectively; $p< 0.01$) (Figure 3B), with a little interannual variation. In 2015, there was no statistically significant difference in silicate concentration ($SiO_2$) between the two regions (12.08 ± 5.51 μM and 9.62 ± 6.98 μM, respectively), but regional differences have become clear since then (12.32 ± 4.79 μM and 5.97 ± 3.18 μM, respectively; $p< 0.01$) (Figure 3C). Ammonium concentration was almost depleted in the SCM layer of both regions during the study period (data not shown). Most environmental variables showed distinct regional differences, and the SCM layer and nitracline tended to gradually become shallow in the NWC region.

## Regional distribution of phytoplankton Chl-a concentration and community size structure at the SCM

Chl-a concentration and phytoplankton size structure showed distinct regional characteristics. The Chl-a concentration in the NWC region was higher than that in the NEC region (2.76 ± 3.08 mg $m^{-3}$ and 0.88 ± 0.74 mg $m^{-3}$, respectively; $p< 0.01$) (Figure 4 and Table 2). High Chl-a concentration (> 3 mg $m^{-3}$) was observed in the NWC region in 2015 and 2018, and in the NEC region in 2015. However, Chl-a concentrations in 2017 were lowest in both regions (0.49 ± 0.26 mg $m^{-3}$ and 0.48 ± 0.16 mg $m^{-3}$, respectively) (Figure 4C). The ratio of the Chl-a concentration in the SCM layer to the depth-integrated Chl-a concentration in the water column (0 – 100 m) was calculated. In the NWC region, the ratio of Chl-a concentration in the SCM layer was approximately 80 ± 18%, slightly higher than 70 ± 19% in the NEC region ($p< 0.01$), indicating that the contribution of the SCM layer was high in both regions (Supplementary Figure 2). Excluding 2017, the microphytoplankton community size structure prevailed, with an average of 75% in the NWC region (Figure 5A). The fractions of nano and picophytoplankton were very low at 15% and 10%, respectively. In 2017, the fraction of nano and picophytoplankton communities were 27% and 46%, respectively, and that of the microphytoplankton community decreased to 28% in the NWC region. In the NEC region, the microphytoplankton community fraction decreased significantly from 55% in 2015 to 6% in 2018 (Figure 5B). Meanwhile, the picophytoplankton community fraction more than double on average, from 21% in 2015 to 59% in 2018. The nanophytoplankton community fraction also increased slightly from 25% to 35%. Taken together, phytoplankton communities showed high Chl-a concentrations and were dominated by large-cells in the SCM layer of the NWC region. Conversely, in the SCM layer of NEC, phytoplankton had a relatively low Chl-a concentration, and small-sized communities tended to increase during this study.

## Regional distribution of phytoplankton photophysiological properties at the SCM

The regional distribution of the maximum photochemical efficiency ($F_v/F_m$), functional absorption cross-section ($\sigma_{PSII}$), and P-E parameters are shown in Figures 6 and 7, and Table 2. $F_v/F_m$ was higher than 0.5 at the SCM depth in most stations, and showed similar ranges in both regions when four-year data were combined (0.54 ± 0.07 and 0.53 ± 0.06, respectively).

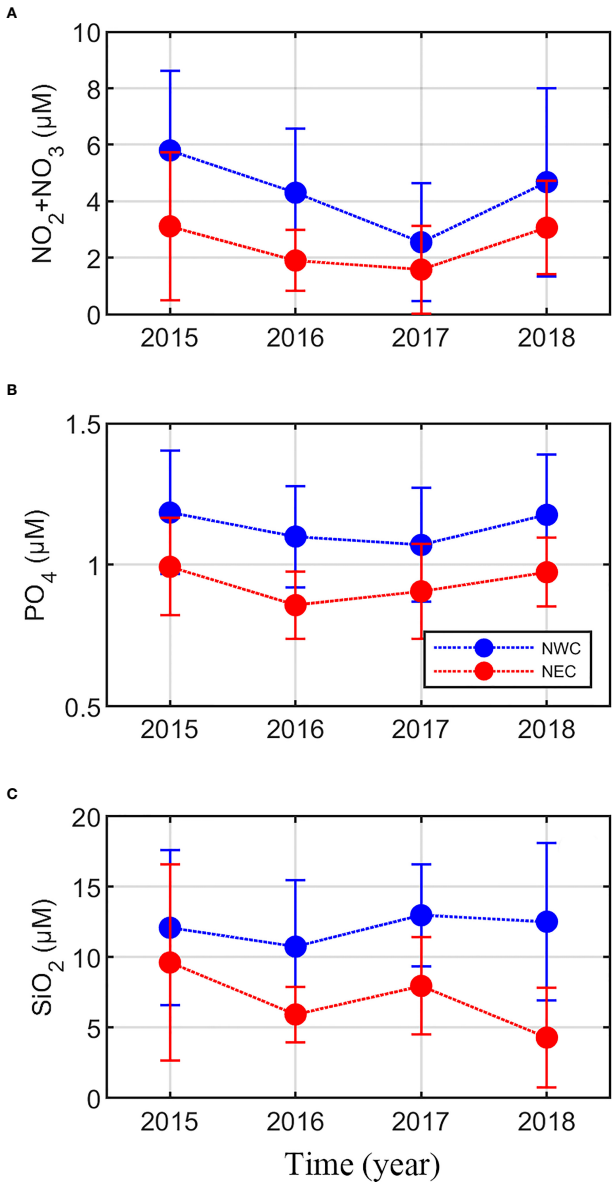


FIGURE 3
Regional distribution of nutrient concentration at the subsurface chlorophyll maximum by year (mean ± standard deviation). **(A)** nitrite + nitrate ($NO_2$ + $NO_3$; μM), **(B)** phosphate ($PO_4$; μM), **(C)**, and silicate ($SiO_2$; μM). The blue and red lines represent the northwestern Chukchi Sea (NWC) and the northeastern Chukchi Sea (NEC), respectively.

However, since 2017, the $F_v/F_m$ of the NEC region has been significantly lower than that of the NWC region (0.49 ± 0.07 and 0.54 ± 0.09, respectively; $p< 0.05$), showing a clear difference between the East and West regions (Figures 6 and 7A). The $\sigma_{PSII}$ in the NEC region was larger than that in the NWC region (710 ± 143 × $10^{-20}$ $m^{-2}$ $photons^{-1}$ and 607 ± 111 × $10^{-20}$ $m^{-2}$ $photons^{-1}$, respectively; $p< 0.05$) (Figure 7B and Table 2). $\sigma_{PSII}$ maintained a similar range by year in the NWC region, whereas it increased by 17% in the NEC region from 2017 (655 ± 112 × $10^{-20}$ $m^{-2}$ $photons^{-1}$ and 772 ± 140 × $10^{-20}$ $m^{-2}$ $photons^{-1}$, respectively; $p< 0.01$) (Figure 7B). The photosynthetic parameters obtained from the P-E curve also differed by region. The maximum electron transfer rate ($ETR^{max}$) of the NWC region was higher than that of the NEC region (53 ± 26 $e^{-1}$ $s^{-1}$ $R^{-1}$ and 36 ± 23 $e^{-1}$ $s^{-1}$ $R^{-1}$, respectively; $p< 0.01$) (Figure 7C). This was similar in both regions before 2016 (39 ± 24 $e^{-1}$ $s^{-1}$ $R^{-1}$ and 33 ± 24 $e^{-1}$ $s^{-1}$ $R^{-1}$, respectively). However, the $ETR^{max}$ of the NWC region has increased by approximately 36% compared to the NEC region since 2017, resulting in a significant difference between the two regions (61 ±

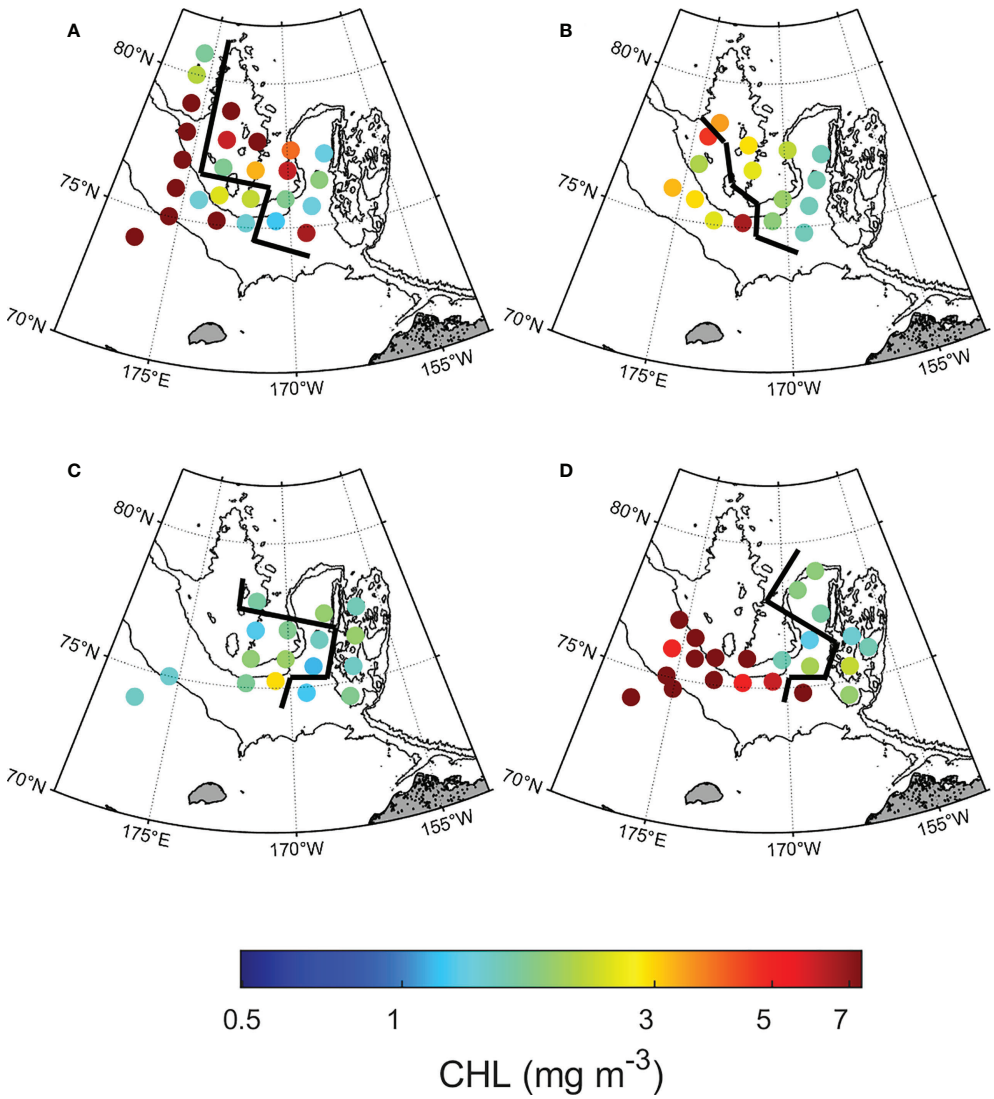


FIGURE 4
Spatial distribution of chlorophyll-a concentration (mg $m^{-3}$) at the subsurface chlorophyll maximum by year. **(A)** 2015, **(B)** 2016, **(C)** 2017, and **(D)** 2018. The left side of the black line shows the northwestern Chukchi Sea; the right side shows the northeastern Chukchi Sea.

24 $e^{-1}$ $s^{-1}$ $R^{-1}$ and 38 ± 23 $e^{-1}$ $s^{-1}$ $R^{-1}$, respectively; $p < 0.01$). The light saturation ($E_k$) of the NWC region was slightly higher than that of the NEC region, but the difference was not significant (27 ± 21 µmol photons $m^{-2}$ $s^{-1}$ and 18 ± 21 µmol photons $m^{-2}$ $s^{-1}$, respectively; $p = 0.08$) (Figure 7D). The light utilization efficiency coefficient ($\alpha$) showed distinct differences by region (2.43 ± 1.12 µmol electrons (µmol photons)$^{-1}$ and 3.30 ± 1.97 µmol electrons (µmol photons)$^{-1}$, respectively; $p < 0.05$) (Figure 7E). In particular, the $\alpha$ between the two regions was similar in 2015, but since then the $\alpha$ of the NEC region has become higher than that in the NWC region (4.44 ± 1.48 µmol electrons (µmol photons)$^{-1}$ and 3.03 ± 0.76 µmol electrons (µmol photons)$^{-1}$, respectively; $p < 0.01$). Overall, the photosynthetic parameters, excluding $E_k$, showed similar ranges in the two regions until 2016, but regional differences have become clear since 2017.

# Discussion

## What determines the SCM depth in the northern Chukchi Sea?

The water mass structure, characterized by water temperature and salinity, affects the vertical distribution and flux of nutrients, which in turn controls the SCM depth (Ardyna

TABLE 2 Regional phytoplankton size fraction and photophysiology variables at the subsurface chlorophyll maximum in the northwestern Chukchi Sea (NWC) and the northeastern Chukchi Sea (NEC).

| Region | Year | ST (P-E curve) | Chl-a | Micro | Nano | Pico | $F_v/F_m$ | $\sigma_{PSII}$ | $ETR^{max}$ | $E_k$ | α |
|---|---|---|---|---|---|---|---|---|---|---|---|
| NWC | 2015 | 10 | 3.52 ± 3.49 | 67 ± 32 | 14 ± 10 | 19 ± 23 | 0.54 ± 0.04 | 652 ± 128 | 31 ± 16 | 36 ± 33 | 1.14 ± 0.41 |
| | 2016 | 2 | 1.22 ± 0.42 | 77 ± 5 | 16 ± 5 | 7 ± 4 | 0.54 ± 0.03 | 566 ± 30 | 82 ± 5 | 31 ± 2 | 2.89 ± 0.33 |
| | 2017 | 7 | 0.49 ± 0.26 | 28 ± 24 | 27 ± 12 | 45 ± 20 | 0.52 ± 0.06 | 638 ± 117 | 57 ± 31 | 17 ± 11 | 3.84 ± 0.83 |
| | 2018 | 13 | 4.24 ± 3.33 | 80 ± 21 | 14 ± 11 | 5 ± 11 | 0.56 ± 0.10 | 563 ± 97 | 63 ± 20 | 25 ± 11 | 2.76 ± 0.56 |
| NEC | 2015 | 9 | 1.30 ± 1.04 | 55 ± 25 | 24 ± 12 | 21 ± 16 | 0.56 ± 0.02 | 636 ± 124 | 21 ± 5 | 28 ± 31 | 0.92 ± 0.56 |
| | 2016 | 3 | 0.70 ± 0.30 | 30 ± 22 | 25 ± 6 | 45 ± 20 | 0.55 ± 0.01 | 683 ± 92 | 78 ± 5 | 17 ± 4 | 4.84 ± 0.56 |
| | 2017 | 7 | 0.48 ± 0.16 | 12 ± 12 | 35 ± 6 | 53 ± 12 | 0.50 ± 0.04 | 718 ± 113 | 43 ± 26 | 10 ± 10 | 4.73 ± 1.25 |
| | 2018 | 8 | 0.77 ± 0.61 | 6 ± 3 | 35 ± 7 | 59 ± 9 | 0.48 ± 0.10 | 827 ± 150 | 33 ± 19 | 14 ± 14 | 3.40 ± 1.11 |

Chl-a concentration (Chl-a; $mg^{-3}$); Micro, nano, and picophytoplankton fraction (%), Maximum photochemical efficiency ($F_v/F_m$); functional absorption cross-section ($\sigma_{PSII}$; $10^{-20}$ $m^{-2}$ $photons^{-1}$); maximum electron transfer rate ($ETR^{max}$; $e^{-1}$ $s^{-1}$ $RC^{-1}$); minimum saturating irradiance ($E_k$; µmol photons $m^{-2}$ $s^{-1}$); light utilization efficiency (α; µmol electrons [µmol photons] $^{-1}$).

et al., 2013; Brown et al., 2015). The upper layer (0–150m) of the western Arctic Ocean was mainly composed of a relatively fresh surface mixed layer and Pacific-origin water entering the Arctic *via* Bering Strait, which was a high nutrient and low dissolved oxygen water (Codispoti et al., 2005). The Pacific-origin water was divided into relatively warm and fresh PSW and cold and saline PWW, and the PSW lay directly above PWW (Nishino et al., 2013; Gong and Pickart, 2016). A warm and saline Atlantic-origin water layer was located below the Pacific-origin water layer (Korhonen et al., 2013; Alkire et al., 2019). In the NWC region, PWW was distributed below the SCM layer, and in the NEC region, PSW mainly existed around the SCM layer and PWW was distributed below it. In other words, the water masses around the SCM layer differ between these two regions (Figure 2). These differences in the water mass distribution contributed to the difference in water temperature and salinity at the SCM in these two regions, and thus, affected nutrient budget (Figure 3 and Table 1). In 2017, the intrusion of Atlantic-origin cold water caused by cyclonic atmospheric circulation raised the PWW, supplying nutrients to the upper layer of the northwestern Chukchi Sea (Jung et al., 2021). This variability in water masses has influenced the expansion of PWW in the northern Chukchi Sea since 2017, which can be related to the reduction in the spatial distribution of PSW to the Chukchi borderlands towards 2018 (Figures 1C, D). Therefore, the difference in physicochemical conditions (temperature, salinity, and nutrients) of the water layer would affect the variability of SCM depth by region.

We found a significant correlation between nitracline and SCM depth ($r = 0.80$, $p < 0.01$; Figure 8A), indicating that

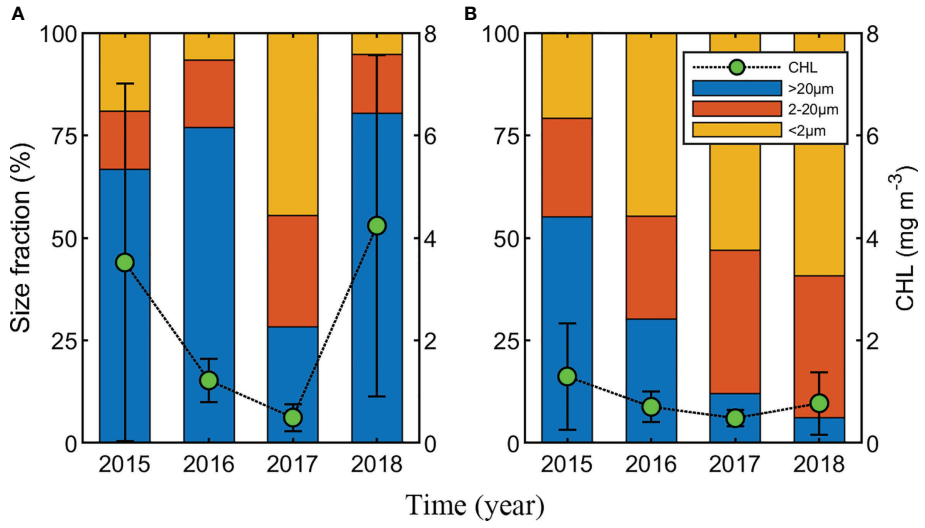


FIGURE 5
Distribution of phytoplankton Chlorophyll-a (Chl-a) concentration (mg $m^{-3}$) and average phytoplankton community size fraction (%) by region. **(A)** The northwestern Chukchi Sea, **(B)** The northeastern Chukchi Sea. Green circles and black vertical lines represent Chl-a concentration (mean ± standard deviation). Phytoplankton community size consisted of > 20 µm, 2–20 µm, and< 2 µm, respectively.

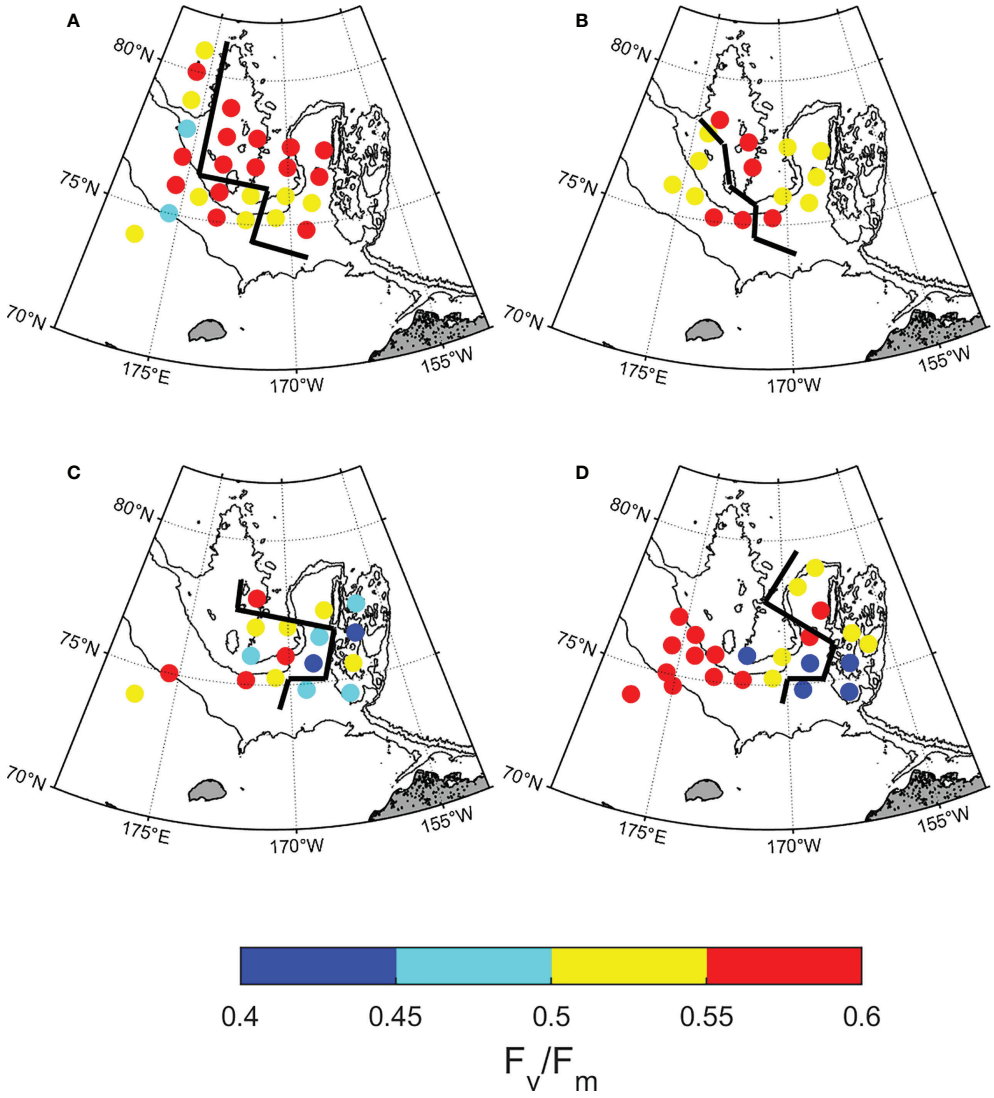


FIGURE 6
Spatial distribution of photochemical efficiency ($F_v/F_m$) at the subsurface chlorophyll maximum by year. **(A)** 2015, **(B)** 2016, **(C)** 2017, and **(D)** 2018. Based on the black line, the left side is the northwestern Chukchi Sea and the right side is the northeastern Chukchi Sea.

nitrogen availability is the key factor for the formation of the SCM layer in the Arctic Ocean. In addition, the nitracline position was significantly correlated with FWC ($r = 0.72$, $p < 0.01$; Figure 8B). This relationship suggests that the increased thickness of the freshwater surface layer deepens the sub-surface nutrients reservoir of PWW (Coupel et al., 2015). Freshwater produced by melting sea ice was one of the main factors controlling the FWC (Serreze et al., 2006). In our study, the FWC had a statistically significant negative correlation with sea ice concentration in the two regions ($r = -0.59$, $p < 0.01$; Figure 8C). Specifically, the period from the sea ice retreat to measurement in the NEC region was 44 days on average, and there was no significant difference by year. But, the averaged period was 35 days in the NWC region, which was the shortest in 2018 with 30 days. ($p < 0.01$, Supplementary Figure 3). The period in the two regions showed a positive correlation with FWC, suggesting that the sea ice melting was affecting the FWC ($r = 0.50$, $p < 0.01$, Figure 8D). The period of sea ice retreat was also related to the difference in the stability of the water column (stratification index) between both regions ($r = 0.36$, $p < 0.05$, Table 1). Furthermore, the position of the lower halocline between the Pacific-origin water and Atlantic-origin water in both regions was confirmed by another study (Alkire et al., 2019); in the NWC region, the lower halocline became shallower after 2016, meaning that the Pacific-origin waters have risen (Supplementary Figure 4). Thus, as mentioned earlier, the PWW

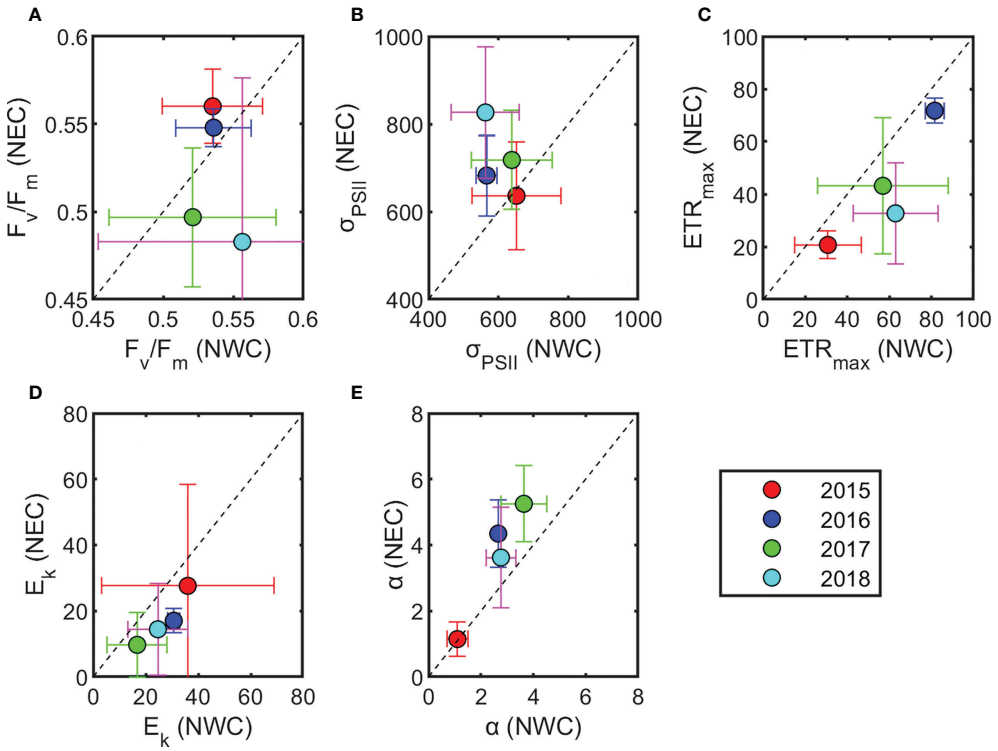


FIGURE 7
Distribution of phytoplankton photophysiological characteristics (mean ± standard deviation) by year. **(A)** Maximum photochemical efficiency ($F_v/F_m$), **(B)** functional absorption cross-section ($\sigma_{PSII}$; $10^{-20}$ $m^{-2}$ $photons^{-1}$), **(C)** maximum electron transfer rate ($ETR^{max}$; $e^{-1}$ $s^{-1}$ $RC^{-1}$), **(D)** minimum saturating irradiance ($E_k$; µmol photons $m^{-2}$ $s^{-1}$), and **(E)** light utilization efficiency (α; µmol electrons [µmol photons] $^{-1}$). For each variable, the x-axis and y-axis indicate the northwestern Chukchi Sea (NWC) and the northeastern Chukchi Sea (NEC), respectively.

uplift eventually increased the salinity and nutrients in the upper layer, which led to a decrease in FWC and shallower nitracline towards 2018 in the NWC region (Figure 2). Although the fluctuation of nitracline was not significant in the NEC region, the nutrient supply to the surface layer shallowly formed the position of the nitracline in the NWC region, resulting in a shallow SCM depth.

## Effects of nitrogen availability on phytoplankton photophysiology at the SCM

In the summer of the Arctic, phytoplankton in the SCM layer were reported to exhibit high nitrogen availability through assessment of nitrogen assimilation (Martin et al., 2012). We aimed at determining the effect of high nitrogen availability in the SCM layer on the photophysiological properties of phytoplankton. The variation in nitrogen availability may have contributed to regional differences in Chl-a concentration (2.76 mg $m^{-3}$ vs.< 1 mg $m^{-3}$) and dominant phytoplankton community size (micro vs. nano + pico), as well as the photosynthetic activity of phytoplankton (Figures 4 and 5). In the NWC region, the phytoplankton $F_v/F_m$ at the SCM depth was high during the entire study period (Figure 6). This result suggests that phytoplankton in the SCM layer exhibited the highest photosynthetic activity because the nitrogen availability was not limited. Meanwhile, in the NEC region, $F_v/F_m$ in the SCM layer remained high until 2016, and since then, it has decreased by approximately 10% (Figures 6C, D). $F_v/F_m$ of the two regions showed a significant difference since 2017 (Figures 6C, D, 7A). The reduced $F_v/F_m$ in the SCM layer was similar to that of surface phytoplankton (0.46 ± 0.09) in the Arctic Ocean, which was subject to severe nitrogen limitation (Mills et al., 2018; Ko et al., 2020). This result meant that the photosynthetic activity of phytoplankton decreased in the SCM layer because nutrient availability was lower than the cellular demands for photosynthesis (Parkhill et al., 2001). That is, the nitrogen availability in the SCM layer was probably inhibited, as the NEC region has shifted to the Chukchi borderlands since 2017. Therefore, our results revealed that the degree of nitrogen availability in the SCM layer was highly variable in the Arctic Ocean, which could be responsible for changes in the photosynthetic activity of phytoplankton.

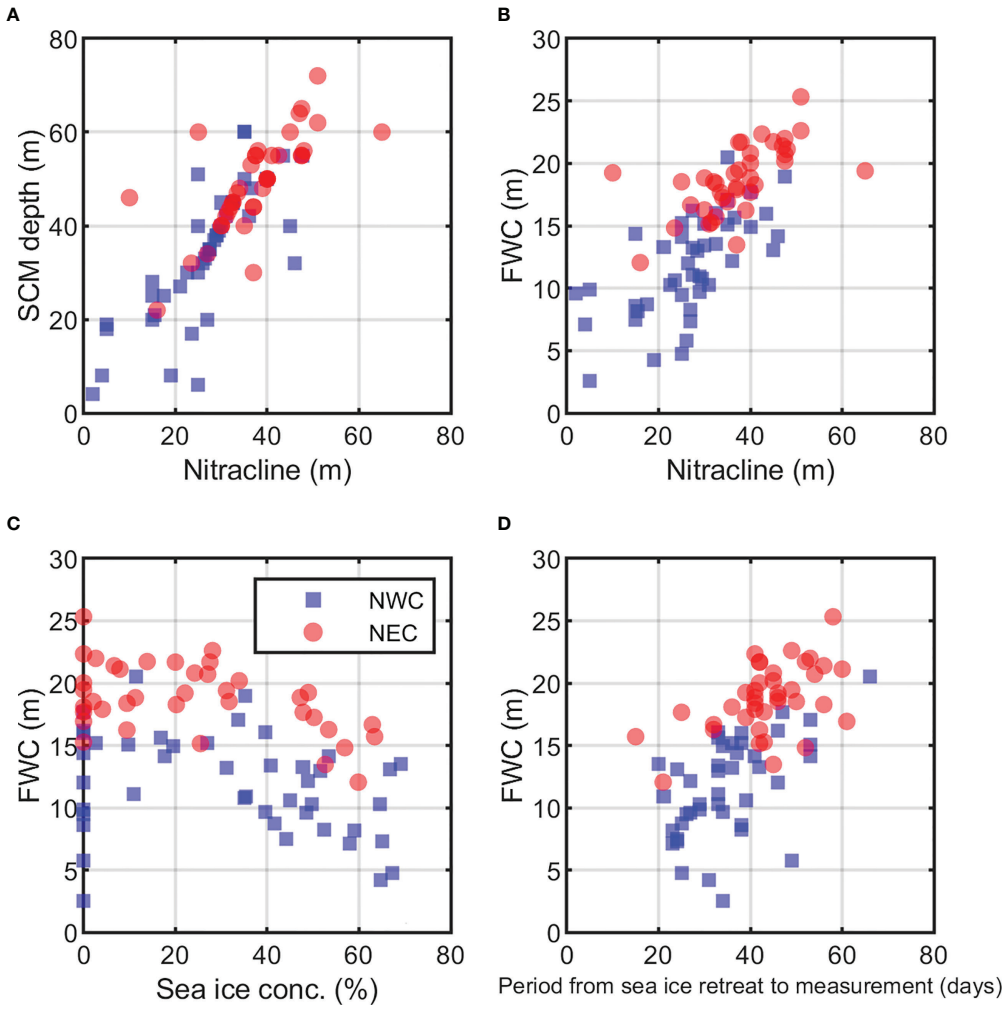


FIGURE 8
Variables related to the depth of subsurface chlorophyll maximum (SCM) by region from 2015 to 2018. **(A)** Relationship between nitracline and the SCM depth (r = 0.80, p< 0.01), **(B)** Relationship between nitracline and freshwater content (FWC; r = 0.72, p< 0.01), and **(C)** Sea ice concentration (%) and FWC (NWC: r = −0.61, p<0.01; NEC: r = −0.59, p< 0.01, Excluding 0% sea ice concentration). **(D)** FWC and the period from the sea ice retreat to measurement (days) (NWC: r = 0.53, p< 0.01; NEC: r = 0.50, p< 0.01). The blue squares and red circle represent the northwestern Chukchi Sea (NWC) and the northeastern Chukchi Sea (NEC), respectively.

In the first principal component (PC1: 39%), each photophysiological property of phytoplankton ($F_v/F_m$, $E_k$ vs. $\sigma_{PSII}$, $\alpha$) was negatively correlated with the dominant phytoplankton community size structure by region (r = −0.31 ~ −0.43, p< 0.01, Figure 9). $\sigma_{PSII}$ refers to the ability to absorb light (i.e., the physical size of PSII antennae) and the efficiency of electron conversion in PSII (Falkowski et al., 2004). In particular, an inverse relationship between $F_v/F_m$ and $\sigma_{PSII}$ was evident in both regions, which is known to be associated with high $\sigma_{PSII}$ and low $F_v/F_m$ as light-harvesting strategies for smaller cells (Suggett et al., 2009). In the Chukchi Sea, diatoms and small flagellates were dominant (Lee et al., 2019), and large diatoms were known to show high $F_v/F_m$ (≥ 0.5) and low $\sigma_{PSII}$ (400 to 600 × $10^{-20}$ $m^{-2}$ $photon^{-1}$) (Moore et al., 2005; Suggett et al., 2009). We expected that large-sized phytoplankton communities with high Chl-a concentrations in the NWC region would exhibit low light absorption (i.e., $\sigma_{PSII}$ and $\alpha$) owing to the package effect (Kirk, 1975; Lavergne and Joliot, 2000). Therefore, phytoplankton in the NWC region would have shown high $F_v/F_m$ and low $\sigma_{PSII}$ by dominant large diatoms (Figures 7B and 10A). In addition, the $E_k$ of the NWC region was relatively higher than that of the NEC region because large diatoms adapted to high light (Figures 7D and 10B) (Qiao et al., 2021). Along with the reduction in $F_v/F_m$ since 2017, the large-sized phytoplankton community fraction decreased by 34% compared with that before 2016 in the NEC region (Figures 7E and 10C). At this time, $\sigma_{PSII}$ and $\alpha$ increased, indicating an increase in antenna size in the NEC region. This could increase the probability of heat dissipation by increasing the lifetime of an exciton within the

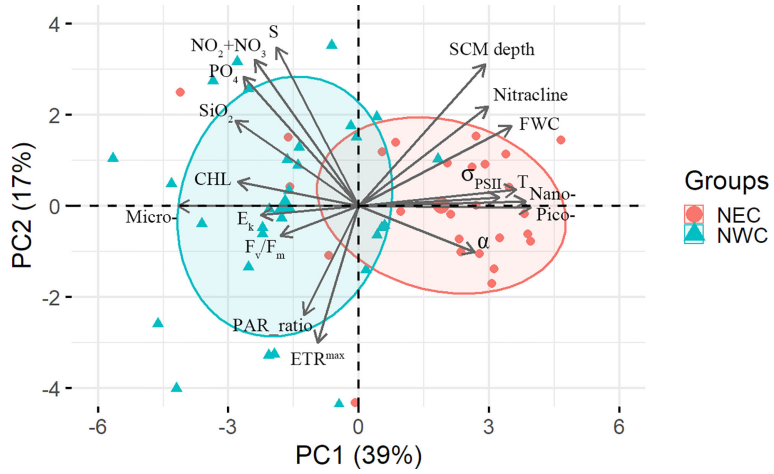


FIGURE 9
Biplot of the first and second principal components (PC1: 39%, PC2: 17%) between the environmental variables and phytoplankton photophysiological parameter in the subsurface chlorophyll maximum (SCM) grouped by regions. Terms and abbreviations: temperature (T); salinity (S); the SCM depth (SCM depth); nitracline; freshwater content (FWC); Chlorophyll-a concentration (Chl-a); size fraction (micro, nano, pico; %); photochemical efficiency ($F_v/F_m$); functional absorption cross-section ($\sigma_{PSII}$); maximum electron transfer rate ($ETR^{max}$); light saturation for photosynthesis ($E_k$); light utilization efficiency ($\alpha$); nitrite + nitrate ($NO_2$ +$NO_3$); phosphate ($PO_4$); and silicate ($SiO_2$); The ratio of photosynthetically available radiation (PAR) in the SCM layer to the surface layer (PAR_ratio).

antenna. Hence, the photochemical efficiency of phytoplankton with high $\sigma_{PSII}$ would have been reduced in the NEC region (Lavergne and Joliot, 2000). $ETR^{max}$ did not show a correlation with nitrogen availability or phytoplankton community size structure (Figures 9 and 10D). Finally, the inhibition of nitrogen availability in the SCM layer contributed to a decrease in the photosynthetic activity of phytoplankton, with an increase in picophytoplankton communities in the NEC region (Almazán-Becerril et al., 2012; Kulk et al., 2018). Therefore, this analysis suggests that the extent of nitrogen availability in the SCM layer was a major factor regulating the photosynthetic activity and light absorption ability of the regionally dominant phytoplankton communities.

## Change in maximum electron transfer rate depending on light condition at the SCM

Nitrogen availability appeared to affect the distribution of $F_v/F_m$ in the SCM layer, but did not show a significant relationship with $ETR^{max}$. Thus, we analyzed the factors that influenced the distribution of $ETR^{max}$ by region. In the second principal component (PC2: 17%), $ETR^{max}$ showed a positive correlation with PAR_ratio ($r = 0.33$, $p = 0.07$) and a negative correlation with the SCM depth ($r = -0.56$, $p < 0.01$, Figure 9). Arctic phytoplankton are well known for their adaptation to low-light conditions, resulting in high $\alpha$ and low $E_k$. (Platt et al., 1982; Gallegos et al., 1983; Palmer et al., 2011). The PAR_ratio in the Arctic Ocean is generally reported to be at a 1–5% level (Martin et al., 2012). This was similar to our results (~4.0%), with no regional differences in PAR_ratio. However, the PAR_ratio continued to increase from 2.7% in 2015 to 8.5% in 2018 as the SCM depth in the NWC region became shallow owing to the uplift of the nitracline described above. In fact, the PAR of the two years (2015 vs 2018) was not significantly different (4.6 ± 3.8 vs 7.0 ± 8.2 µmol photons $m^{-2}$ $s^{-1}$) in the NWC region (Supplementary Figure 1), but the increase in the PAR ratio considered that the light availability was improved in the SCM layer. For example, doubling of the average PAR_ratio between 2015 and 2018 resulted in a difference of approximately 30% in the $ETR^{max}$ in the NWC region (41 $e^{-1}$ $s^{-1}$ $RC^{-1}$ and 60 $e^{-1}$ $s^{-1}$ $RC^{-1}$, respectively) (Figure 11A). In the surface layer, severe nitrogen limitation reduced the $ETR^{max}$ by approximately 40% in the Chukchi Sea (Ko et al., 2020), which suggests a very strong reduction (ca. 80%) in net primary production (Gorbunov and Falkowski, 2020). In contrast to the surface layer, it was shown that the improvement in light conditions (e.g. a two-fold increase in the PAR ratio) increased $ETR^{max}$ in the presence of sufficient nitrogen availability within the SCM layer (Palmer et al., 2013). This result suggests that the position of the SCM layer associated with light availability affects the photosynthetic rate (Bouman et al., 2020). Similarly, the maximum rate of photosynthesis measured by the $^{14}C$ method was also regulated under a physical environment such as light (Harrison and Platt, 1986; Huot et al., 2013). Meanwhile, PAR_ratio was similar in the NEC region during the study period; thus, $ETR^{max}$ did not change significantly (Figure 11B). We found that the

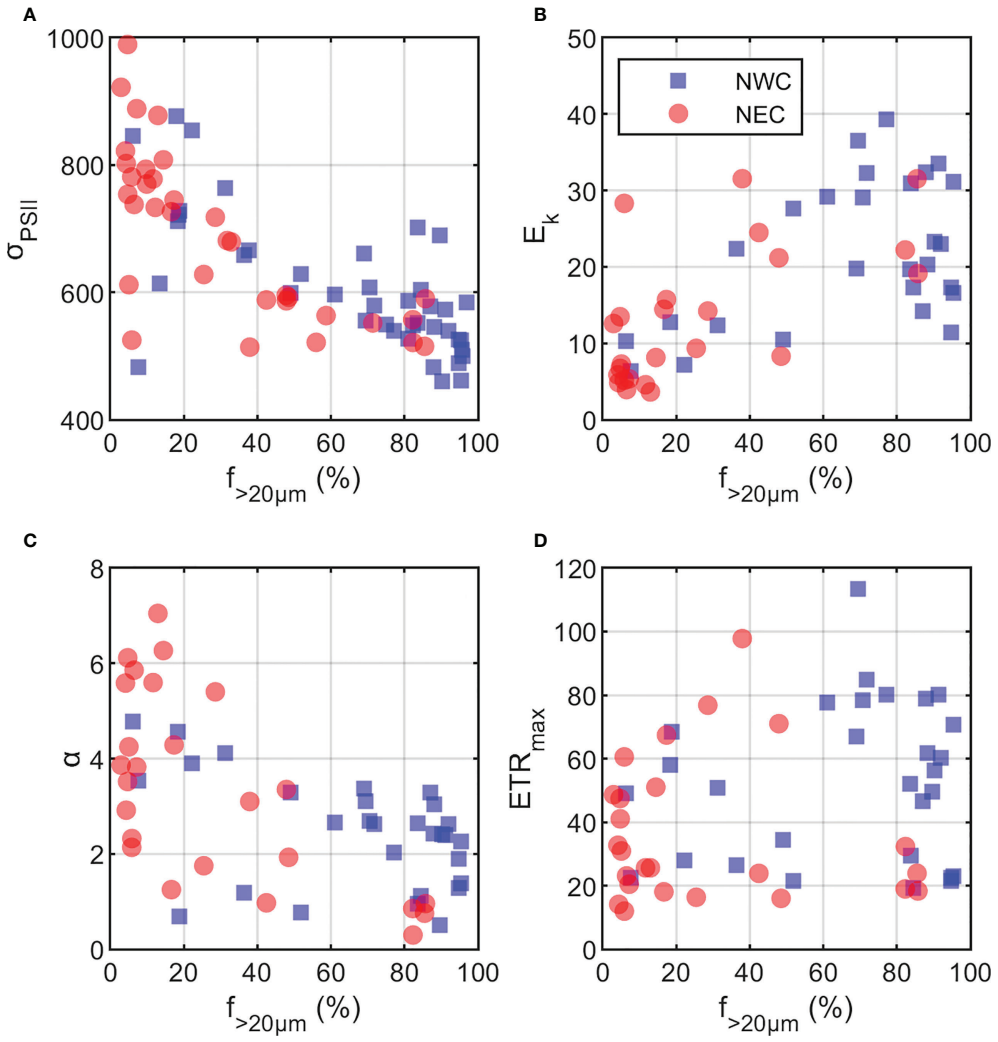


FIGURE 10
Relationships between microphytoplankton fraction ($f_{>20\mu m}$; %) and photosynthetic variables. **(A)** functional absorption cross-section ($\sigma_{PSII}$; $10^{-20}$ $m^{-2}$ photons$^{-1}$), **(B)** minimum saturating irradiance ($E_k$; µmol photons $m^{-2}$ $s^{-1}$), and **(C)** light utilization efficiency (α; µmol electrons [µmol photons] $^{-1}$), **(D)** maximum electron transfer rate ($ETR^{max}$; $e^{-1}$ $s^{-1}$ $RC^{-1}$). The red circle and blue square represent the northeastern Chukchi Sea (NEC) and the northwestern Chukchi Sea (NWC), respectively.

photophysiological properties of phytoplankton at the SCM depth depending on the light and nitrogen availability could greatly contribute to the primary production in the water column. Since the contribution of Chl-a concentration in the SCM layer was high in the summer of the Arctic Ocean, understanding the photophysiological properties of phytoplankton at the SCM depth would be essential to confirming changes in primary production in the Arctic Ocean.

Our study describes the responses of phytoplankton photophysiology to nitrogen availability and light conditions at the SCM in the Arctic Ocean in summertime. The extent of nitrogen availability in the SCM layer affects the photochemical activity (e.g. $F_v/F_m$) and light absorption ability (e.g. $\sigma_{PSII}$ and α) depending on the phytoplankton community structure by region. Similar to the effect of nitrogen limitation on surface phytoplankton in the Arctic Ocean, the reduced nitrogen availability in the SCM layer decreased $F_v/F_m$ by approximately 10% and also decreased the fraction of large phytoplankton in the NEC region. Despite the reduction in nitrogen availability in the NEC region, there was no significant change in $ETR^{max}$. Meanwhile, large phytoplankton in the NWC region, which showed sufficient nitrogen availability in the SCM layer, retained high photochemical efficiency but resulted in low light absorption ability due to the package effect. In addition, the improvement of the light conditions in the SCM layer caused by

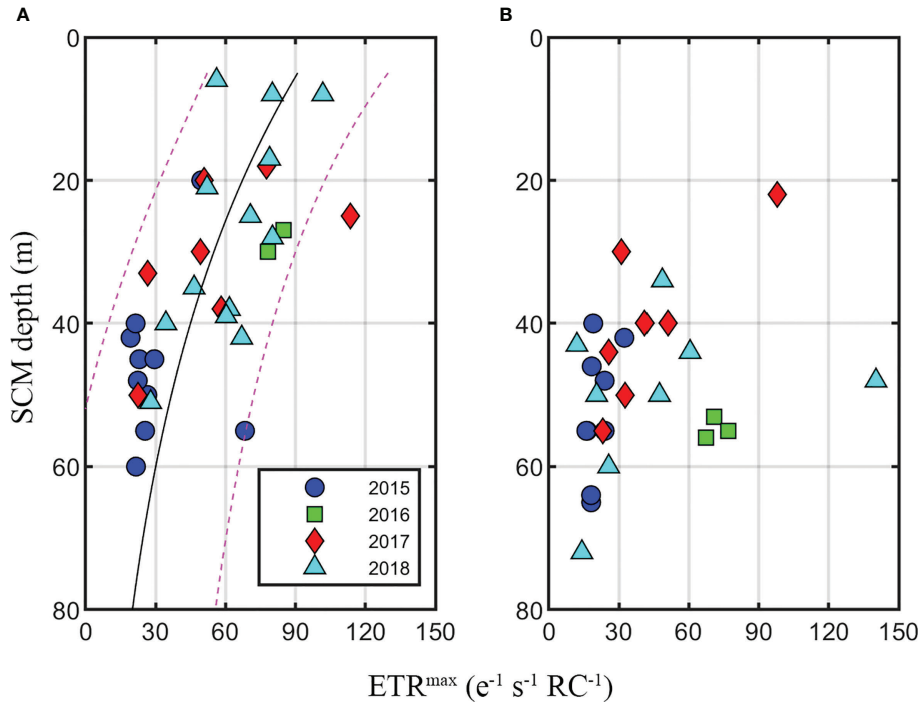


FIGURE 11
Regional distribution of maximum electron transfer rate ($ETR^{max}$) at the subsurface chlorophyll maximum (SCM) by year. **(A)** The northwestern Chukchi Sea and **(B)** the northeastern Chukchi Sea. The black line and blue dotted line represent a non-linear regression line and a 90% confidence interval.

the shallower SCM depth contributed to an increase in $ETR^{max}$ by up to 30%, which was similar to the increase in $ETR^{max}$ of surface phytoplankton by the alleviation of nitrogen limitation. In other words, fluctuations in light conditions could have a greater effect on phytoplankton photosynthetic capacity and primary production, based on sufficient nitrogen availability in the SCM layer. The recent inflows of the Atlantic-origin and Pacific-origin waters have delivered additional nutrient fluxes to the Arctic Ocean, which has caused the increase in primary production in the Arctic Ocean (Lewis et al., 2020). The amount and duration of light transmitted to the water layer has increased owing to the reduced sea ice extent and thickness in the Arctic Ocean (Ardyna and Arrigo, 2020). Therefore, our findings have important implications for understanding how changes in light conditions and nutrient fluxes might affect phytoplankton photosynthesis and primary production in the subsurface layer of the Arctic Ocean.

## Data availability statement

The datasets presented in this study can be found in online repositories. The names of the repository/repositories and accession number(s) can be found in the article/Supplementary Material.

## Author contributions

EK performed a field survey and data analysis and wrote the manuscript. MG contributed instrumentation and corrected the manuscript. JJ provided and analyzed chemical data. YL processed and provided biological data. K-HC processed and provided physical data. EY was the leader of the Korea-Arctic Ocean Warming and Response of Ecosystem Program and provided scientific advice. JP conceived the study, participated in the design, and helped to draft the manuscript. All authors contributed to the article and approved the submitted version.

## Funding

This research was a part of the project titled 'Korea-Arctic Ocean Warming and Response of Ecosystem (K-AWARE, KOPRI, 20210605)', funded by the Ministry of Oceans and Fisheries, Korea. MYG was in part funded by NASA Ocean Biology and Biogeochemistry Program (grants NNX16AT54G and 80NSSC18K1416).

## Acknowledgments

We thank the captain and the crew of the R/V Araon for assistance with field data collection, as well as members of the division of polar ocean science, KOPRI. We would like to thank Editage (www.editage.co.kr) for English language editing. The editor and reviewers for constructive comments.

## Conflict of interest

The authors declare that the research was conducted in the absence of any commercial or financial relationships that could be construed as a potential conflict of interest.

## Publisher's note

All claims expressed in this article are solely those of the authors and do not necessarily represent those of their affiliated organizations, or those of the publisher, the editors and the reviewers. Any product that may be evaluated in this article, or claim that may be made by its manufacturer, is not guaranteed or endorsed by the publisher.

## Supplementary material

The Supplementary Material for this article can be found online at: https://www.frontiersin.org/articles/10.3389/fmars.2022.979998/full#supplementary-material

## References

Aagaard, K., and Carmack, E. C. (1989). The role of Sea ice and other fresh-water in the Arctic circulation. *J. Geophysical Research-Oceans* 94 (C10), 14485–14498. doi: 10.1029/JC094iC10p14485

Alkire, M. B., Rember, R., and Polyakov, I. (2019). Discrepancy in the identification of the Atlantic/Pacific front in the central Arctic ocean: NO versus nutrient relationships. *Geophysical Res. Lett.* 46 (7), 3843–3852. doi: 10.1029/2018gl081837

Almazán-Becerril, A., Rivas, D., and García-Mendoza, E. (2012). The influence of mesoscale physical structures in the phytoplankton taxonomic composition of the subsurface chlorophyll maximum off western Baja California. *Deep Sea Res. Part I: Oceanographic Res. Papers* 70, 91–102. doi: 10.1016/j.dsr.2012.10.002

Ardyna, M., and Arrigo, K. R. (2020). Phytoplankton dynamics in a changing Arctic ocean. *Nat. Climate Change* 10 (10), 892–903. doi: 10.1038/s41558-020-0905-y

Ardyna, M., Babin, M., Gosselin, M., Devred, E., Belanger, S., Matsuoka, A., et al. (2013). Parameterization of vertical chlorophyll a in the Arctic ocean: impact of the subsurface chlorophyll maximum on regional, seasonal, and annual primary production estimates. *Biogeosciences* 10 (6), 4383–4404. doi: 10.5194/bg-10-4383-2013

Ardyna, M., Babin, M., Gosselin, M., Devred, E., Rainville, L., and Tremblay, J. E. (2014). Recent Arctic ocean sea ice loss triggers novel fall phytoplankton blooms. *Geophysical Res. Lett.* 41 (17), 6207–6212. doi: 10.1002/2014gl061047

Arrigo, K. R., Perovich, D. K., Pickart, R. S., Brown, Z. W., Dijken, G., Lowry, K. E., et al. (2012). Massive phytoplankton blooms under Arctic Sea ice. *Science* 336 (6087), 1408–1408. doi: 10.1126/science.1215065

Arrigo, K. R., and van Dijken, G. L. (2011). Secular trends in Arctic ocean net primary production. *J. Geophysical Research-Oceans*. 116, C09011. doi: 10.1029/2011JC007151

Arrigo, K. R., van Dijken, G., and Pabi, S. (2008). Impact of a shrinking Arctic ice cover on marine primary production. *Geophysical Res. Lett.* 35 (19), 1–6. doi: 10.1029/2008GL035028

Baldry, K., Strutton, P. G., Hill, N. A., and Boyd, P. W. (2020). Subsurface chlorophyll-a maxima in the southern ocean. *Front. Mar. Sci.* 7. doi: 10.3389/fmars.2020.00671

Behrenfeld, M. J., and Kolber, Z. S. (1999). Widespread iron limitation of phytoplankton in the south pacific ocean. *Science* 283 (5403), 840–843. doi: 10.1126/science.283.5403.840

Bibby, T. S., Gorbunov, M. Y., Wyman, K. W., and Falkowski, P. G. (2008). Photosynthetic community responses to upwelling in mesoscale eddies in the subtropical north Atlantic and pacific oceans. *Deep-Sea Res. Part Ii-Topical Stud. Oceanography* 55 (10-13), 1310–1320. doi: 10.1016/j.dsr2.2008.01.014

Bouman, H. A., Jackson, T., Sathyendranath, S., and Platt, T. (2020). Vertical structure in chlorophyll profiles: influence on primary production in the Arctic ocean. *Philos. Trans. A Math Phys. Eng. Sci.* 378 (2181), 20190351. doi: 10.1098/rsta.2019.0351

Brown, Z. W., Lowry, K. E., Palmer, M. A., van Dijken, G. L., Mills, M. M., Pickart, R. S., et al. (2015). Characterizing the subsurface chlorophyll a maximum in the chukchi Sea and Canada basin. *Deep-Sea Res. Part Ii-Topical Stud. Oceanography* 118, 88–104. doi: 10.1016/j.dsr2.2015.02.010

Carvalho, K. S., and Wang, S. (2020). Sea Surface temperature variability in the Arctic ocean and its marginal seas in a changing climate: Patterns and mechanisms. *Global Planetary Change* 193, 103265. doi: 10.1016/j.gloplacha.2020.103265

Cheah, W., McMinn, A., Griffiths, F. B., Westwood, K. J., Wright, S. W., and Clementson, L. A. (2013). Response of phytoplankton photophysiology to varying environmental conditions in the Sub-Antarctic and polar frontal zone. *PloS One* 8 (8), e72165. doi: 10.1371/journal.pone.0072165

Codispoti, L. A., Flagg, C., Kelly, V., and Swift, J. H. (2005). Hydrographic conditions during the 2002 SBI process experiments. *Deep-Sea Res. Part Ii-Topical Stud. Oceanography* 52 (24-26), 3199–3226. doi: 10.1016/j.dsr2.2005.10.007

Comiso, J. C., Meier, W. N., and Gersten, R. (2017). Variability and trends in the Arctic Sea ice cover: Results from different techniques. *J. Geophysical Research-Oceans* 122 (8), 6883–6900. doi: 10.1002/2017jc012768

Coupel, P., Jin, H. Y., Joo, M., Horner, R., Bouvet, H. A., Sicre, M. A., et al. (2012). Phytoplankton distribution in unusually low sea ice cover over the pacific Arctic. *Biogeosciences* 9 (11), 4835–4850. doi: 10.5194/bg-9-4835-2012

Coupel, P., Ruiz-Pino, D., Sicre, M. A., Chen, J. F., Lee, S. H., Schiffrine, N., et al. (2015). The impact of freshening on phytoplankton production in the pacific Arctic ocean. *Prog. Oceanography* 131, 113–125. doi: 10.1016/j.pocean.2014.12.003

Falkowski, P. G., Koblfzek, M., Gorbunov, M., and Kolber, Z. (2004). "Development and application of variable chlorophyll fluorescence techniques in marine ecosystems," in *Chlorophyll a fluorescence*. Eds. G. C. Papageorgiou and Govindjee, (Dordrecht: Springer Netherlands), 757–778.

Gallegos, C. L., Platt, T., Harrison, W. G., and Irwin, B. (1983). Photosynthetic parameters of arctic marine phytoplankton: Vertical variations and time scales of adaptation. *Limnology Oceanography* 28 (4), 698–708. doi: 10.4319/lo.1983.28.4.0698

Gong, D. L., and Pickart, R. S. (2015). Summertime circulation in the eastern chukchi Sea. *Deep-Sea Res. Part Ii-Topical Stud. Oceanography* 118, 18–31. doi: 10.1016/j.dsr2.2015.02.006

Gong, D. L., and Pickart, R. S. (2016). Early summer water mass transformation in the eastern chukchi Sea. *Deep-Sea Res. Part Ii-Topical Stud. Oceanography* 130, 43–55. doi: 10.1016/j.dsr2.2016.04.015

Gorbunov, M. Y., and Falkowski, P. (2004). Flourescence induction and relaxation (FIRE) technique and instrumentation for monitoring photosynthetic processes and primary production in aquatic ecosystems. *Photosynthesis: Fundam. Aspects to Global Perspect. 13th International congress of photosynthesis*. Montreal: Allen Press , 1029-1031.

Gorbunov, M. Y., and Falkowski, P. G. (2020). Using chlorophyll fluorescence kinetics to determine photosynthesis in aquatic ecosystems. *Limnology Oceanography* 66 (1), 1–13. doi: 10.1002/lno.11581

Gorbunov, M. Y., Falkowski, P. G., and Kolber, Z. S. (2000). Measurement of photosynthetic parameters in benthic organisms *in situ* using a SCUBA-based fast repetition rate fluorometer. *Limnology Oceanography* 45 (1), 242–245. doi: 10.4319/lo.2000.45.1.0242

Gorbunov, M. Y., Kolber, Z. S., and Falkowski, P. G. (1999). Measuring photosynthetic parameters in individual algal cells by fast repetition rate fluorometry. *Photosynthesis Res.* 62 (2-3), 141–153. doi: 10.1023/A:1006360005033

Gorbunov, M. Y., Kolber, Z. S., Lesser, M. P., and Falkowski, P. G. (2001). Photosynthesis and photoprotection in symbiotic corals. *Limnology Oceanography* 46 (1), 75–85. doi: 10.4319/lo.2001.46.1.0075

Gorbunov, M. Y., Shirsin, E., Nikonova, E., Fadeev, V. V., and Falkowski, P. G. (2020). A multi-spectral fluorescence induction and relaxation (FIRe) technique for physiological and taxonomic analysis of phytoplankton communities. *Mar. Ecol. Prog. Ser.* 644, 1–13. doi: 10.3354/meps13358

Gordon, L., Jennings, J., Ross, A., and Krest, J. (1993). A suggested protocol for continuous flow automated analysis of seawater nutrients (Phosphate, nitrate, nitrite and silicic acid) in the WOCE hydrographic program and the joint global ocean fluxes study. *Methods Manual WHPO*, 68/91, 1–52.

Harrison, W. G., and Platt, T. (1986). Photosynthesis-irradiance relationships in polar and temperate phytoplankton populations. *Polar Biol.* 5 (3), 153–164. doi: 10.1007/Bf00441695

Hill, V., and Cota, G. (2005). Spatial patterns of primary production on the shelf, slope and basin of the Western Arctic in 2002. *Deep-Sea Res. Part Ii-Topical Stud. Oceanography* 52 (24-26), 3344–3354. doi: 10.1016/j.dsr2.2005.10.001

Hill, V. J., Matrai, P. A., Olson, E., Suttles, S., Steele, M., Codispoti, L. A., et al. (2013). Synthesis of integrated primary production in the Arctic ocean: II. *In situ* and remotely sensed estimates. *Prog. Oceanography* 110, 107–125. doi: 10.1016/j.pocean.2012.11.005

Huot, Y., Babin, M., and Bruyant, F. (2013). Photosynthetic parameters in the Beaufort Sea in relation to the phytoplankton community structure. *Biogeosciences* 10 (5), 3445–3454. doi: 10.5194/bg-10-3445-2013

Jassby, A. D., and Platt, T. (1976). Mathematical formulation of the relationship between photosynthesis and light for phytoplankton. *Limnology Oceanography* 21 (4), 540–547. doi: 10.4319/lo.1976.21.4.0540

Jung, J., Cho, K. H., Park, T., Yoshizawa, E., Lee, Y., Yang, E. J., et al. (2021). Atlantic-Origin cold saline water intrusion and shoaling of the nutricline in the pacific Arctic. *Geophysical Res. Lett.* 48 (6), e2020GL090907. doi: 10.1029/2020GL090907

Kirk, J. T. O. (1975). A theoretical analysis of the contribution of algal cells to the attenuation of light within natural waters ii. spherical cells. *New Phytol.* 75 (1), 21–36. doi: 10.1111/j.1469-8137.1975.tb01367.x

Kirk, J. T. O. (1994). *Light and photosynthesis in aquatic ecosystems* (Cambridge: Cambridge University Press).

Ko, E., Gorbunov, M. Y., Jung, J., Joo, H. M., Lee, Y., Cho, K. H., et al. (2020). Effects of nitrogen limitation on phytoplankton physiology in the Western Arctic ocean in summer. *J. Geophysical Research-Oceans* 125 (11), e2020JC016501. doi: 10.1029/2020JC016501

Kolber, Z. S., Barber, R. T., Coale, K. H., Fitzwater, S. E., Greene, R. M., Johnson, K. S., et al. (1994). Iron limitation of phytoplankton photosynthesis in the equatorial pacific-ocean. *Nature* 371 (6493), 145–149. doi: 10.1038/371145a0

Kolber, Z. S., Prasil, O., and Falkowski, P. G. (1998). Measurements of variable chlorophyll fluorescence using fast repetition rate techniques: defining methodology and experimental protocols. *Biochim. Et Biophys. Acta-Bioenergetics* 1367 (1-3), 88–106. doi: 10.1016/S0005-2728(98)00135-2

Korhonen, M., Rudels, B., Marnela, M., Wisotzki, A., and Zhao, J. (2013). Time and space variability of freshwater content, heat content and seasonal ice melt in the Arctic ocean from 1991 to 2011. *Ocean Sci.* 9 (6), 1015–1055. doi: 10.5194/os-9-1015-2013

Kulk, G., van de Poll, W. H., and Buma, A. G. (2018). Photophysiology of nitrate limited phytoplankton communities in kongsfjorden, spitsbergen. *Limnology Oceanography.* 63 (6), 2606–2617. doi: 10.1002/lno.10963

Lavergne, J., and Joliot, P. (2000). Thermodynamics of the excited states of photosynthesis. *Biophysics textbook onLine. Biophys. Society Bethesda MD*, 1–12.

Lee, Y., Min, J. O., Yang, E. J., Cho, K. H., Jung, J., Park, J., et al. (2019). Influence of sea ice concentration on phytoplankton community structure in the chukchi and East Siberian seas, pacific Arctic ocean. *Deep-Sea Res. Part I-Oceanographic Res. Papers* 147, 54–64. doi: 10.1016/j.dsr.2019.04.001

Lewis, K. M., van Dijken, G. L., and Arrigo, K. R. (2020). Changes in phytoplankton concentration now drive increased Arctic ocean primary production. *Science* 369 (6500), 198–202. doi: 10.1126/science.aay8380

Martin, J., Dumont, D., and Tremblay, J. E. (2013). Contribution of subsurface chlorophyll maxima to primary production in the coastal Beaufort Sea (Canadian arctic): A model assessment. *J. Geophysical Research-Oceans* 118 (11), 5873–5886. doi: 10.1002/2013jc008843

Martin, J., Tremblay, J. E., Gagnon, J., Tremblay, G., Lapoussiere, A., Jose, C., et al. (2010). Prevalence, structure and properties of subsurface chlorophyll maxima in Canadian Arctic waters. *Mar. Ecol. Prog. Ser.* 412, 69–84. doi: 10.3354/meps08666

Martin, J., Tremblay, J. E., and Price, N. M. (2012). Nutritive and photosynthetic ecology of subsurface chlorophyll maxima in Canadian Arctic waters. *Biogeosciences* 9 (12), 5353–5371. doi: 10.5194/bg-9-5353-2012

Mills, M. M., Brown, Z. W., Laney, S. R., Ortega-Retuerta, E., Lowry, K. E., van Dijken, G. L., et al. (2018). Nitrogen limitation of the summer phytoplankton and heterotrophic prokaryote communities in the chukchi Sea. *Front. Mar. Sci.* 5 (362). doi: 10.3389/fmars.2018.00362

Moore, C. M., Lucas, M. I., Sanders, R., and Davidson, R. (2005). Basin-scale variability of phytoplankton bio-optical characteristics in relation to bloom state and community structure in the northeast Atlantic. *Deep-Sea Res. Part I-Oceanographic Res. Papers* 52 (3), 401–419. doi: 10.1016/j.dsr.2004.09.003

Moore, C. M., Mills, M. M., Langlois, R., Milne, A., Achterberg, E. P., La Roche, J., et al. (2008). Relative influence of nitrogen and phosphorous availability on phytoplankton physiology and productivity in the oligotrophic sub-tropical north Atlantic ocean. *Limnology Oceanography* 53 (1), 291–305. doi: 10.4319/lo.2008.53.1.0291

Nishino, S., Itoh, M., Williams, W. J., and Semiletov, I. (2013). Shoaling of the nutricline with an increase in near-freezing temperature water in the makarov basin. *J. Geophysical Research-Oceans* 118 (2), 635–649. doi: 10.1029/2012jc008234

Palmer, M. A., Arrigo, K. R., Mundy, C. J., Ehn, J. K., Gosselin, M., Barber, D. G., et al. (2011). Spatial and temporal variation of photosynthetic parameters in natural phytoplankton assemblages in the Beaufort Sea, Canadian Arctic. *Polar Biol.* 34 (12), 1915–1928. doi: 10.1007/s00300-011-1050-x

Palmer, M. A., van Dijken, G. L., Mitchell, B. G., Seegers, B. J., Lowry, K. E., Mills, M. M., et al. (2013). Light and nutrient control of photosynthesis in natural phytoplankton populations from the chukchi and Beaufort seas, Arctic ocean. *Limnology Oceanography* 58 (6), 2185–2205. doi: 10.4319/lo.2013.58.6.2185

Parkhill, J. P., Maillet, G., and Cullen, J. J. (2001). Fluorescence-based maximal quantum yield for PSII as a diagnostic of nutrient stress. *J. Phycology* 37 (4), 517–529. doi: 10.1046/j.1529-8817.2001.037004517.x

Park, J., Kuzminov, F. I., Bailleul, B., Yang, E. J., Lee, S., Falkowski, P. G., et al. (2017). Light availability rather than fe controls the magnitude of massive phytoplankton bloom in the amundsen Sea polynyas, Antarctica. *Limnology Oceanography* 62 (5), 2260–2276. doi: 10.1002/lno.10565

Parsons, T. R., Maita, Y., and Lalli, C. M. (1984). *A manual of chemical and biological methods for seawater analysis* (Oxford, UK: Pergamon Press). doi: 10.25607/OBP-1830.

Platt, T., Harrison, W. G., Irwin, B., Horne, E. P., and Gallegos, C. L. (1982). Photosynthesis and photoadaptation of marine phytoplankton in the arctic. *Deep Sea Res. Part A. Oceanographic Res. Papers* 29 (10), 1159–1170. doi: 10.1016/0198-0149(82)90087-5

Qiao, H., Zang, S., Yan, F., Xu, Z., Wang, L., and Wu, H. (2021). Physiological responses of the diatoms thalassiosira weissflogii and thalassiosira pseudonana to nitrogen starvation and high light. *Mar. Environ. Res.* 166, 105276. doi: 10.1016/j.marenvres.2021.105276

Schuback, N., Tortell, P. D. D., Berman-Frank, I., Campbell, D. A. A., Ciotti, A., Courtecuisse, E., et al. (2021). Single-turnover variable chlorophyll fluorescence as a tool for assessing phytoplankton photosynthesis and primary productivity: Opportunities, caveats and recommendations. *Front. Mar. Sci.* 8. doi: 10.3389/fmars.2021.690607

Serreze, M. C., Barrett, A. P., Slater, A. G., Woodgate, R. A., Aagaard, K., Lammers, R. B., et al. (2006). The large-scale freshwater cycle of the Arctic. *J. Geophysical Research-Oceans* 111, C11010. doi: 10.1029/2005JC003424

Serreze, M. C., and Stroeve, J. (2015). Arctic Sea ice trends, variability and implications for seasonal ice forecasting. *Philos. Trans. A Math Phys. Eng. Sci.* 373 (2045), 20140159. doi: 10.1098/rsta.2014.0159

Song, H. J., Ji, R. B., Jin, M. B., Li, Y., Feng, Z. X., Varpe, O., et al. (2021). Strong and regionally distinct links between ice-retreat timing and phytoplankton production in the Arctic ocean. *Limnology Oceanography* 66 (6), 2498–2508. doi: 10.1002/lno.11768

Stroeve, J., Holland, M. M., Meier, W., Scambos, T., and Serreze, M. (2007). Arctic Sea ice decline: Faster than forecast. *Geophysical Res. Lett.* 34 (9), L09501. doi: 10.1029/2007GL029703

Suggett, D. J., Moore, C. M., Hickman, A. E., and Geider, R. J. (2009). Interpretation of fast repetition rate (FRR) fluorescence: signatures of phytoplankton community structure versus physiological state. *Mar. Ecol. Prog. Ser.* 376, 1–19. doi: 10.3354/meps07830

Sugie, K., Fujiwara, A., Nishino, S., Kameyama, S., and Harada, N. (2020). Impacts of temperature, CO2, and salinity on phytoplankton community composition in the Western Arctic ocean. *Front. Mar. Sci.* 6. doi: 10.3389/fmars.2019.00821

Tremblay, J. E., Robert, D., Varela, D. E., Lovejoy, C., Darnis, G., Nelson, R. J., et al. (2012). Current state and trends in Canadian Arctic marine ecosystems: I. primary production. *Climatic Change* 115 (1), 161–178. doi: 10.1007/s10584-012-0496-3

Wang, Q., Wekerle, C., Danilov, S., Sidorenko, D., Koldunov, N., Sein, D., et al. (2019). Recent Sea ice decline did not significantly increase the total liquid freshwater content of the Arctic ocean. *J. Climate* 32 (1), 15–32. doi: 10.1175/jcli-d-18-0237.1

Wassmann, P., Duarte, C. M., Agusti, S., and Sejr, M. K. (2011). Footprints of climate change in the Arctic marine ecosystem. *Global Change Biol.* 17 (2), 1235–1249. doi: 10.1111/j.1365-2486.2010.02311.x

# Frontiers in Microbiology

**Explores the habitable world and the potential of microbial life**

The largest and most cited microbiology journal which advances our understanding of the role microbes play in addressing global challenges such as healthcare, food security, and climate change.

---

## Discover the latest Research Topics

See more →


**Frontiers**

Avenue du Tribunal-Fédéral 34
1005 Lausanne, Switzerland
frontiersin.org

**Contact us**

+41 (0)21 510 17 00
frontiersin.org/about/contact